ZHENG CUI

PRINTED ELECTRONICS

MATERIALS, TECHNOLOGIES AND APPLICATIONS

Higher Education Press

WILEY

VISIT…

LANZAROTE
Caliente.com

PRINTED ELECTRONICS

PRINTED ELECTRONICS

MATERIALS, TECHNOLOGIES AND APPLICATIONS

Zheng Cui
Suzhou Institute of Nano-Tech and Nano-Bionics (SINANO),
Chinese Academy of Sciences, China

With contributions from

Chunshan Zhou
Song Qiu
Zheng Chen
Jian Lin
Jianwen Zhao
Changqi Ma
Wenming Su
Suzhou Institute of Nano-Tech and Nano-Bionics (SINANO),
Chinese Academy of Sciences, China

WILEY

Higher
Education
Press

This edition first published 2016

© 2016 Higher Education Press. All rights reserved.

Published by John Wiley & Sons Singapore Pte. Ltd., 1 Fusionopolis Walk, #07-01 Solaris South Tower, Singapore 138628, under exclusive license granted by Higher Education Press for all media and languages excluding Simplified and Traditional Chinese and throughout the world excluding Mainland China, and with non-exclusive license for electronic versions in Mainland China.

For details of our global editorial offices, for customer services and for information about how to apply for permission to reuse the copyright material in this book please see our website at www.wiley.com.

All Rights Reserved. No part of this publication may be reproduced, stored in a retrieval system or transmitted, in any form or by any means, electronic, mechanical, photocopying, recording, scanning, or otherwise, except as expressly permitted by law, without either the prior written permission of the Publisher, or authorization through payment of the appropriate photocopy fee to the Copyright Clearance Center. Requests for permission should be addressed to the Publisher, John Wiley & Sons Singapore Pte. Ltd., 1 Fusionopolis Walk, #07-01 Solaris South Tower, Singapore 138628, tel: 65-66438000, fax: 65-66438008, email: enquiry@wiley.com.

Wiley also publishes its books in a variety of electronic formats. Some content that appears in print may not be available in electronic books.

Designations used by companies to distinguish their products are often claimed as trademarks. All brand names and product names used in this book are trade names, service marks, trademarks or registered trademarks of their respective owners. The Publisher is not associated with any product or vendor mentioned in this book. This publication is designed to provide accurate and authoritative information in regard to the subject matter covered. It is sold on the understanding that the Publisher is not engaged in rendering professional services. If professional advice or other expert assistance is required, the services of a competent professional should be sought.

Limit of Liability/Disclaimer of Warranty: While the publisher and author have used their best efforts in preparing this book, they make no representations or warranties with respect to the accuracy or completeness of the contents of this book and specifically disclaim any implied warranties of merchantability or fitness for a particular purpose. It is sold on the understanding that the publisher is not engaged in rendering professional services and neither the publisher nor the author shall be liable for damages arising herefrom. If professional advice or other expert assistance is required, the services of a competent professional should be sought.

Library of Congress Cataloging-in-Publication data applied for

ISBN: 9781118920923

Set in 10/12pt Times by SPi Global, Pondicherry, India

1 2016

Contents

Preface **xii**

1 Introduction **1**
Zheng Cui
1.1 What is Printed Electronics? 1
1.2 The Importance of Developing Printed Electronics 11
1.3 Multidisciplinary Nature of Printed Electronics 15
1.4 Structure and Content of the Book 17
References 19

2 Organic Printable Electronic Materials **21**
Song Qiu and Chunshan Zhou
2.1 Introduction 21
2.2 Organic Conductive Materials 22
  2.2.1 Characteristics of Organic Conductive Materials 22
  2.2.2 History of Organic Conductive Materials 23
  2.2.3 Conductive Polymer 23
    2.2.3.1 Structural Conductive Polymer 23
    2.2.3.2 Composite Conductive Polymer 25
  2.2.4 PEDOT 25
2.3 Printable Organic Small Molecular Semiconductors 27
  2.3.1 Fused Aromatic Compounds 28
  2.3.2 Heterocyclic Sulfur Compounds and Oligothiophenes 30
  2.3.3 Other Materials with High Mobility 33
2.4 Printable Polymeric Semiconductor 34
  2.4.1 P-type Polymer Semiconductors 35
    2.4.1.1 Sulfur-containing Heterocyclic Polymeric Semiconductors 35
    2.4.1.2 Phenyl-containing Polymeric Semiconductors 37
    2.4.1.3 Other p-type Polymeric Semiconductors 39

2.4.2 N-type Polymer Semiconductors 39
2.4.3 Ambipolar Transistor and Related Polymer Materials 41
2.4.4 Outlook 43
2.5 Other Printable Organic Electronic Materials 44
2.5.1 Organic Insulating Materials 44
2.5.2 Organic Materials for Sensors 47
2.6 Summary 49
References 49

3 Inorganic Printable Electronic Materials 54
Zheng Chen
3.1 Introduction 54
3.2 Metallic Materials 56
3.2.1 Metallic Ink 56
3.2.2 Post-printing Process 63
3.2.3 Metal Nanowire 64
3.3 Transparent Oxide 66
3.3.1 Transparent Oxide Semiconductor and Conductor 66
3.3.2 Low Temperature Solution Processing 68
3.3.3 Doped Transparent Oxide Nanoparticles 71
3.4 Single-wall Carbon Nanotube 72
3.4.1 Preparation and Selective Chemistry of SWNT 72
3.4.2 Purification of SWNT 76
3.4.3 Metallic SWNT Thin Film 77
3.4.4 Semiconducting SWNT Thin Film 79
3.5 Graphene 83
3.6 Silicon and Germanium 86
3.7 Metal Chalcogenides Semiconductor and Quantum Dots 90
3.7.1 Metal Chalcogenides Semiconductor 90
3.7.2 Quantum Dots 90
3.8 Nanoparticle/Polymer Dielectric Composites 92
3.9 Summary 95
References 96

4 Printing Processes and Equipments 106
Jian Lin
4.1 Introduction 106
4.2 Jet Printing 108
4.2.1 Inkjet Printing 108
4.2.1.1 Working Principles 108
4.2.1.2 Pattern Preparation 108
4.2.1.3 Application in Printed Electronics 110
4.2.2 Aerosol Jet Printing 111
4.2.2.1 Working Principle 112
4.2.2.2 Pattern Preparation 112
4.2.2.3 Advantages and Challenges 113

4.2.3 Electrohydrodynamic Jet Printing 114
4.2.4 Advantages and Disadvantages 114
4.3 Direct Replicate Printing 115
4.3.1 Screen Printing 116
4.3.1.1 Working Principle 116
4.3.1.2 Screen Mask 117
4.3.1.3 Advantages and Disadvantages 118
4.3.1.4 Applications 118
4.3.2 Gravure Printing 118
4.3.2.1 Principle and System 118
4.3.2.2 Gravure Plate 120
4.3.2.3 Advantages and Disadvantages 120
4.3.2.4 Applications in Printed Electronics 121
4.3.3 Flexographic Printing 122
4.3.3.1 Principle and System 122
4.3.3.2 Printing Plate 123
4.3.3.3 Advantages and Disadvantages 123
4.3.3.4 Applications in Printed Electronics 125
4.4 Indirect Replicate Printing 125
4.4.1 Offset Printing 125
4.4.2 Gravure Offset Printing 126
4.4.3 Pad Printing 128
4.5 Pre-printing Processes 129
4.5.1 Pattern Design 129
4.5.2 Modification of Surface Energy 130
4.5.3 Surface Coating 131
4.5.4 Embossing and Nanoimprinting 131
4.6 Post-printing Processes 134
4.6.1 Sintering 134
4.6.2 UV Curing 135
4.6.3 Annealing 135
4.7 Summary 136
References 137

5 Printed Thin Film Transistors 145
Jianwen Zhao
5.1 Introduction 145
5.2 Types of Transistors 146
5.3 Working Principles of Transistors 147
5.3.1 Basic Mechanism of MOSFETs 147
5.3.2 Charge Carriers and Carrier Mobility 149
5.3.3 Basic Parameters of TFT 149
5.3.3.1 Effective Mobility 149
5.3.3.2 Operating Voltage 151
5.3.3.3 Device Capacitance 151
5.3.3.4 Threshold Voltage (V_t) 153

5.3.3.5 *Subthreshold Swing (SS)* 155
5.3.3.6 *On/off Current Ratio (I_{on}/I_{off})* 155
5.3.3.7 *Hysteresis* 156
5.3.3.8 *Transconductance (g_m)* 157
5.3.3.9 *Stability* 157
5.4 Structures and Fabrication of TFTs 157
5.4.1 *Structures of TFTs* 157
5.4.2 *Characteristics of TFTs* 159
5.4.3 *Fabrication of TFTs* 160
5.4.3.1 *Fabrication of Electrodes* 160
5.4.3.2 *Fabrication of Active Layer* 163
5.4.3.3 *Fabrication of Dielectric Layers* 167
5.5 Fully Printed TFTs 172
5.5.1 *Printability of Electronic Materials* 172
5.5.2 *Influence of Surface Morphology* 173
5.5.3 *Interface Effect of Printed TFTs* 173
5.5.3.1 *Effect of Semiconductor/Dielectric Interface* 175
5.5.3.2 *Effect of Semiconductor/Semiconductor Interface* 176
5.5.3.3 *Effect of Semiconductor/Electrode Interface* 177
5.5.4 *Effect of Channel Length* 178
5.5.5 *Summary of Issues in Printing TFTs* 179
5.5.5.1 *Printable Inks and Printing Processes* 179
5.5.5.2 *Printed Electrodes* 180
5.5.5.3 *Printed Dielectric Thin Films* 180
5.6 Advances in Printed TFTs 180
5.6.1 *Printed Inorganic TFTs* 181
5.6.1.1 *SWCNT TFTs* 181
5.6.1.2 *Metal Oxide TFTs* 182
5.6.1.3 *Metal Dichalcogenide and Graphene TFTs* 184
5.6.2 *Printed Organic TFTs* 187
5.7 Basics of Printed Logic Circuits 189
5.7.1 *NAND and NOR Gates* 190
5.7.2 *Inverter* 190
5.7.3 *Ring Oscillator* 190
5.7.4 *Flip-flop* 193
5.7.5 *Backplane Driving Circuits for Display* 194
5.8 Summary 196
References 197

6 Printed Organic Thin Film Solar Cells 201
Changqi Ma
6.1 Introduction 201
6.1.1 *Solar Energy and its Utilization* 201
6.1.2 *Classification of Solar Cells* 202
6.1.3 *A Brief History of Organic Thin-Film Solar Cells* 203
6.2 Working Principles and Characterization of Organic Solar Cells 205
6.2.1 *Physical Processes* 205

6.2.2 *Basic Structure* 206
6.2.3 *Characterization* 208
6.2.3.1 *I-V Characteristics* 208
6.2.3.2 *Spectrum Response* 209
6.2.4 *The Main Factors Influencing Device Performance* 209
6.2.4.1 *Photon Absorption Ability of Organic Semiconductors* 210
6.2.4.2 *Energy Level Arrangement of Donor and Acceptor* 210
6.2.4.3 *Morphology of Photoactive Layer* 212
6.3 Materials for Organic Solar Cells 213
6.3.1 *Transparent Substrate* 214
6.3.2 *Transparent Conductive Electrode* 214
6.3.2.1 *Metal Oxide Film* 214
6.3.2.2 *Conductive Polymer Film* 215
6.3.2.3 *Thin Metal Film and Metal Grid* 215
6.3.2.4 *Carbon-rich Materials* 217
6.3.3 *Organic Semiconductor Materials* 218
6.3.3.1 p-*Type Organic Semiconductors* 218
6.3.3.2 n-*Type Organic Semiconductors* 223
6.3.4 *Inorganic Semiconductors* 227
6.3.5 *Other Functional Materials* 229
6.4 Inverted and Tandem Organic Solar Cells 229
6.4.1 *Inverted Organic Solar Cells* 229
6.4.2 *Tandem Organic Solar Cells* 231
6.4.3 *Inverted Tandem Organic Solar Cells* 231
6.5 Fabrication Methods 232
6.5.1 *Spin Coating* 233
6.5.2 *Doctor Blading* 235
6.5.3 *Screen Printing* 235
6.5.4 *Inkjet Printing* 237
6.5.5 *Other Thin Film Deposition Techniques* 237
6.6 Roll-to-roll Processing 237
6.7 Printable Perovskite Solar Cells 239
6.8 Summary and Outlook 239
References 240

7 Printed Organic Light Emission and Display 251
Wenming Su
7.1 Introduction 251
7.1.1 *Overview of Lighting and Display* 252
7.1.2 *Overview of Organic Light Emitting Diodes (OLEDs)* 253
7.2 Mechanism of Organic Light Emission 254
7.2.1 *Charge Injection and Transport* 255
7.2.2 *Exciton Formation and Light Emission* 256
7.2.3 *Characterization of OLED Performance* 256
7.2.3.1 *Luminous Efficacy* 256
7.2.3.2 *Quantum Efficiency* 257

- *7.2.3.3 Color* 257
- *7.2.3.4 Three Primary Colors* 258
- 7.3 Structures and Materials of OLED 259
  - *7.3.1 Small Molecular OLED* 259
    - *7.3.1.1 Typical Structure* 259
    - *7.3.1.2 Electrode Materials* 259
    - *7.3.1.3 Fabrication Process* 260
  - *7.3.2 Polymer OLEDs* 262
  - *7.3.3 General OLED Materials* 262
    - *7.3.3.1 Charge Injection Materials* 263
    - *7.3.3.2 Charge Transport Materials* 263
    - *7.3.3.3 Emitter Materials* 264
  - *7.3.4 Soluble OLED Materials* 265
    - *7.3.4.1 Printable Polymer OLEDs* 266
    - *7.3.4.2 Printable Small Molecular OLEDs* 266
    - *7.3.4.3 Cross-linking Materials for Printable OLEDs* 267
- 7.4 White Lighting OLEDs 267
  - *7.4.1 White Light Emission Mechanism* 267
  - *7.4.2 Important Parameters* 272
    - *7.4.2.1 CRI* 272
    - *7.4.2.2 Efficiency and Light Extraction* 273
    - *7.4.2.3 Lifetime* 275
  - *7.4.3 Investment in OLED Lighting* 275
- 7.5 Fabrication of OLED by Printing 277
  - *7.5.1 Spin and Slot Die Coating* 277
  - *7.5.2 Inkjet Printing* 278
  - *7.5.3 Screen Printing* 278
  - *7.5.4 Roll-to-roll Printing* 279
  - *7.5.5 Current Status of the Printed OLED Industry* 280
- 7.6 Summary 281
- References 282

8 Encapsulation Technology for Organic Electronic Devices 287

Wenming Su

- 8.1 Introduction 287
- 8.2 Aging of Organic Electronic Devices 288
  - *8.2.1 Characteristics and Mechanisms of Aging* 288
  - *8.2.2 Requirements for Organic Electronics Encapsulation* 290
- 8.3 Principle of Encapsulation 291
  - *8.3.1 Water/oxygen Penetration Mechanism through Thin Films* 291
  - *8.3.2 Organic/inorganic Multilayer Encapsulation* 292
  - *8.3.3 Measurement of Encapsulation Property* 293
- 8.4 Thin-film Encapsulation Technology 296
  - *8.4.1 History of Thin-film Encapsulation* 297
  - *8.4.2 Single Layer Thin-film Encapsulation* 298
  - *8.4.3 Multilayer Thin-film Encapsulation* 298

8.4.4 Barix^{TM} Thin-film Encapsulation 300
8.4.5 Thin Film Deposition Methods 301
8.4.5.1 PECVD 301
8.4.5.2 ALD 303
8.4.5.3 Parylene Deposition 303
8.4.6 Flexibility of Encapsulation Thin Film 304
8.4.7 Trends of Thin-film Encapsulation 306
8.5 Applications of Thin-film Encapsulation 307
8.5.1 Encapsulation of Flexible OLED 307
8.5.2 Encapsulation of Flexible OPV 309
8.6 Summary 313
References 314

9 Applications and Future Prospects of Printed Electronics 316
Zheng Cui
9.1 Introduction 316
9.2 Application Areas of Printed Electronics 317
9.2.1 Organic Photovoltaic 317
9.2.2 Flexible Display 321
9.2.3 Organic Lighting 324
9.2.4 Electronics and Components 326
9.2.5 Integrated Smart Systems 331
9.3 Challenges for Printed Electronics 333
9.3.1 Materials 333
9.3.2 Printing Process and Equipment 335
9.3.3 Encapsulation 335
9.3.4 Design Methodology and Standardization 336
9.4 Summary and Outlook 336
References 337

Index 339

Preface

My involvement in printed electronics started in 2009 when I returned to China, after 20 years of working in the UK. My previous career was centered around the development and application of microfabrication and nanofabrication technologies. Going back to China gave me the opportunity to do something different. I joined the Suzhou Institute of Nano-Tech and Nano-Bionics, which is one of the research institutes within the Chinese Academy of Sciences, and set up the Printable Electronics Research Center (PERC) there with the help of start-up funds from the Institute and from the Administration of Suzhou Industrial Park where the Institute is located. Six years ago, printed electronics was quite a new field, particularly in China. The PERC that I set up was then the first research center dedicated to printed electronics R&D in China. Although I started on printed electronics from scratch, my previous years of experience on micro-nanofabrication helped me to understand printed electronics from the manufacturing perspective, which is different from those with a background in materials science. Printing is, after all, an additive fabrication similar to lithography-based micro-nanofabrication.

Over the last six years, PERC has built up a multidisciplinary research team and well-equipped laboratories. We decided to develop the technology from all directions, including synthesis and formulation of electronic inks, development of printing processes, printable thin-film transistors, photovoltaic, and organic light emission. We have even worked on encapsulation technology for organic electronic devices which are known to be susceptible to water and oxygen. The ultimate goal of PERC is to develop those technologies that could be useful and practical, eventually leading to some products that the market needs. With our efforts, we have achieved a great deal in the last six years. We developed a range of electronic inks from inorganic materials such as carbon nanotubes, metal oxides, copper and aluminum, and dielectrics, to organic photovoltaic and organic light-emitting materials. We developed a range of printing processes including inkjet printing, aerosol jet printing, gravure printing, gravure offset printing and screen printing. We succeeded in making thin-film transistors on flexible substrates using inorganic inks, making gravure and inkjet-printed organic solar cells, and making flexible organic light emitting diodes, as well as barrier films for encapsulation of organic devices. An innovative hybrid printing technique we developed has been implemented by industry to realize mass production of transparent conductive films for touch panels. We are very proud of what we have achieved in this new and exciting field.

When we started working on printed electronics, we were very much aware that the field was not only new to us but also new to the majority of other scientists and engineers. This was particularly the case in China. We felt from very early on that more people should know about printed electronics and more researchers should get involved in the development, which is the only way to push the technology forward. So we began to plan a book. With the diligent work of my team, the Chinese book, *Printed Electronics: Materials, Technologies and Applications,* was published by the Chinese Higher Education Press in March 2012. This was the first book on printed electronics ever published in China. Three years have passed since this book was published. On the one hand, technology has moved on with new advances in the last three years. On the other hand, the authors of the first Chinese book have gained more experience by working directly in the field. It was time to update the book and we decided to write an English version to share the knowledge and information about printed electronics not only with readers in China but also with readers around the world. This English book is not simply a translation of the previously published Chinese book, but has newly updated information including some of our own work carried out at PERC in the past three years.

This book is written with members of my own research team, which is a multidisciplinary team with diverse backgrounds from physics to chemistry and to electronic engineering. Dr. Chunshan Zhou (author of Chapter 2 – the Chinese version of this chapter was written by Dr. Song Qiu who used to work at PERC) is an organic chemist at PERC working on organic semiconductor materials synthesis; Dr. Zheng Chen (author of Chapter 3) is leading the research at PERC on inorganic nanomaterials for electronic inks and printable inorganic thin-film transistors; Dr. Jian Lin (author of Chapter 4) is the expert on printing processes at PERC; Dr. Jianwen Zhao (author of Chapter 5) has been working on printed carbon nanotubes thin-film transistors since he was a postdoctoral researcher in Singapore six years ago. He has developed a range of techniques to purify and formulate single-walled semiconductor carbon nanotube inks and successfully printed high performance thin-film transistors; Dr. Changqi Ma (author of Chapter 6) is the leader of the organic photovoltaic group at PERC. With organic chemistry training during his Ph.D studies and a number of years of working in Germany, he has developed some new organic photovoltaic materials and is recently working on perovskite solar cells; Dr. Wenming Su (author of Chapters 7 and 8) is the expert on organic light-emitting diodes (OLED) and thin-film encapsulation at PERC, and is leading the engineering group at PERC. Since the authors themselves are directly practicing in their relevant topic area, they are well qualified to write on the topics. We put into the book not only the information and knowledge published by others, but also our own research experience and results. As the leader of PERC and the organizer of this book, I myself contributed Chapters 1 and 9, which reflect my understanding of printed electronics and my observation of the technological progress in the last six years with my deep involvement in the field. I also took charge of the English editing of all chapters.

There are already books published on organic electronics and flexible electronics. Printing as an alternative manufacturing technology gives organic electronics and flexible electronics extra dimensions and new application possibilities. We tried not to have too much overlap with organic electronics and flexible electronics. We organized the information we gathered specifically on printing and printed aspects of making electronics with or without organic materials and with or without flexible substrates. Printed electronics is still a growing field. The technology is still in its early stage of development. We hope that we have put together a comprehensive set of information and knowledge so that readers of the book will gain a general understanding of printed electronics, the materials and technologies that are involved in this field and the potential applications. The contents have been organized and presented in a logical way so that people with a general knowledge of physics, chemistry and electronics will be able to comprehend. We hope that this book will serve as a guide for anyone who is interested in printed electronics and that useful information may be found in the book. Due to the limitations of our own experience and knowledge, there may inevitably be errors and inaccuracy of information in this book; we sincerely welcome comments and criticisms on the book from experts in the field.

Finally, I would like to give my sincere thanks to my team members at the Printable Electronics Research Center (PERC), Suzhou Institute of Nano-Tech and Nano-Bionics (SINANO), Chinese Academy of Sciences (CAS). This book is truly the fruit of team effort. My acknowledgement also goes to the funding bodies that have provided major financial supports to my research team in the last five years under the National Key Basic Research Program of China (2015CB351900), the Strategic Priority Research Program of the Chinese Academy of Sciences (XDA01020304) and the National Natural Science Foundation of China (91123034).

崔铮

Zheng Cui

1

Introduction

Zheng Cui

1.1 What is Printed Electronics?

Printed electronics, as the name implies, is a type of electronics that are created by printing technology. To be more specific, it is an electronic science and technology based on conventional printing techniques as the means to manufacture electronics devices and systems. To most people, “printed electronics” is an unfamiliar phrase. Even experts in electronics may not have heard it. Many people may have it confused with conventional printing technology or mixed up with electronic printing. Conventional printing is for printing paper media, such as books, newspapers, and magazines. Even electronic printing is not printed electronics. Electronic printing is still conventional media printing but with more use of computers and electronic typesetting. A closer analogy to printed electronics would be electronics or integrated circuit (IC)-based electronics, rather than conventional printing. The aim of printed electronics is to make integrated electronic systems using printing technology instead of much more expensive and complex IC manufacturing technology.

Silicon-based IC technology has been in use for nearly 60 years. Modern silicon microelectronics and its manufacturing technology have evolved into an extremely complicated process. There are several hundreds of steps involved in producing a silicon IC chip, from the preparation of single crystal silicon substrates to making billions of transistors and getting these transistors interconnected, including repeated thin film deposition, lithography, etching, and packaging [1]. IC manufacturing has become so expensive that the latest deep UV photolithography system can cost tens of millions of dollars, whereas an extreme UV lithography system for making silicon chips at below 32 nm feature size has a price tag of more than $120 million [2]. The IC industry has become so investment intensive that only a handful companies in the world can afford to play in the field. On the other hand, printing is a very simple process compared to the IC manufacturing process, as illustrated in Figure 1.1 In order to turn a functional material into a functional structure

---

Printed Electronics: Materials, Technologies and Applications, First Edition. Zheng Cui, Chunshan Zhou, Song Qiu, Zheng Chen, Jian Lin, Jianwen Zhao, Changqi Ma and Wenming Su.
© 2016 Higher Education Press. All rights reserved. Published 2016 by John Wiley & Sons Singapore Pte. Ltd.

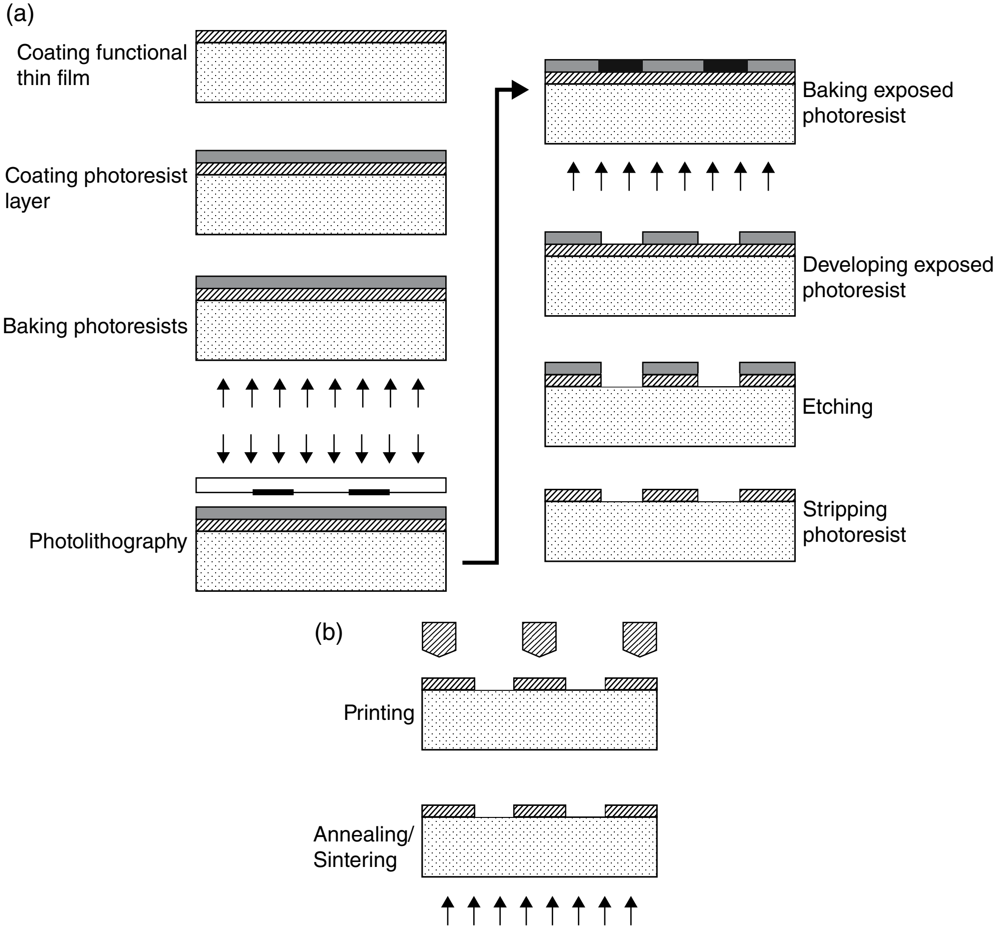
(a)
Coating functional thin film
Coating photoresist layer
Baking photoresists
Photolithography
Baking exposed photoresist
Developing exposed photoresist
Etching
Stripping photoresist
(b)
Printing
Annealing/ Sintering

Figure 1.1 Comparison of IC manufacturing and printing processes. (a) Conventional IC manufacturing; and (b) printing process

or pattern on a silicon substrate, IC manufacturing has to go through thin film deposition, spin-coating photoresist layer, baking, photolithography, baking, developing, etching, and stripping of the photoresist masking layer. If printing is employed, the functional material can be directly printed as patterns onto the substrate. Only a subsequent annealing/sintering process is needed.

Printing is an additive manufacturing process, similar to the deposition process in micro- and nanofabrication [3] but combined with patterning. In printed electronics, the components of an electronic device or a system can be made by printing in additive fashion. For example, for a field-effect transistor, the source, drain, and gate electrodes, as well as semiconductor and insulating layers, can all be printed in ink forms and layer by layer onto a substrate. It is very much like color printing in a conventional printing press, where each color ink is printed sequentially and several color layers are overlaid to form the final color print. Because of its similarity to the printing process, the machine to print electronics is not much different from a conventional media printer. Figure 1.2 compares a conventional roll-to-roll paper media

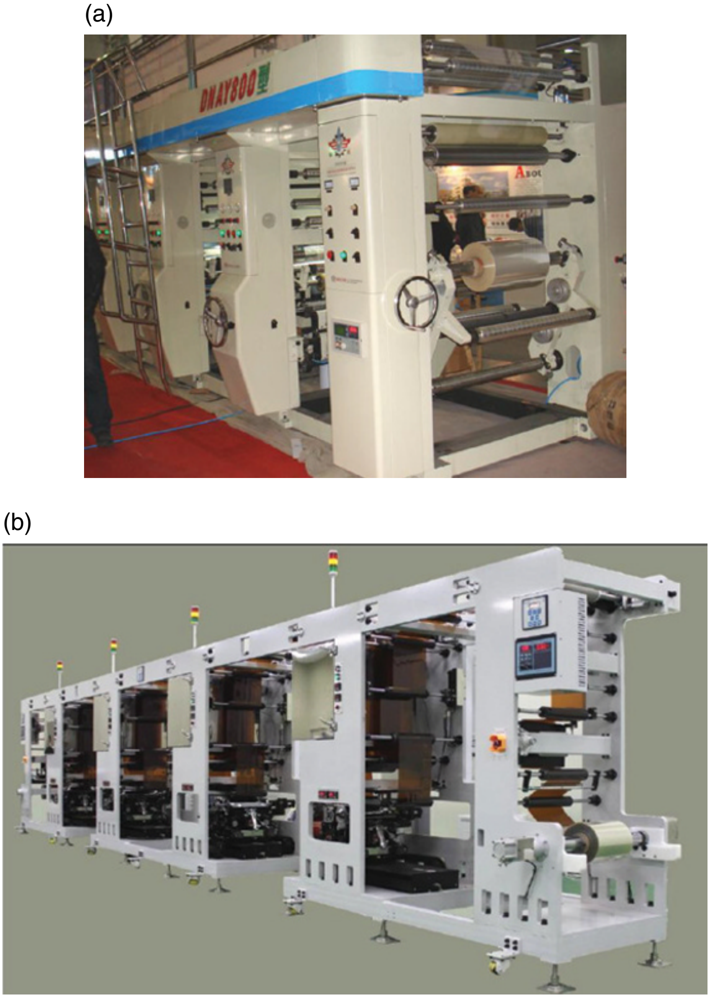

Figure 1.2 Comparison of (a) conventional paper media printer; and (b) electronics printer. (Courtesy of iPEN Co. Ltd.)

printer and an electronics printer. They look almost the same. The only difference is the inks they use. The inks for printing electronics have conducting, semiconducting, or dielectric properties. They are electronic materials, not pigment, which is the key for printing to be used for printed electronics.

Printed electronics originated from organic electronics. In 1977, Alan Heeger, together with Alan G. MacDiarmid and Hideki Shirakawa, discovered that polymer could be conductive by doping certain molecules [4], which earned them the Nobel Prize in Chemistry in 2000. This discovery completely overthrew the conventional wisdom that organic polymer materials are always insulators. Following the discovery of conductive polymers, organic semiconductor materials were developed in 1983 [5] and organic field-effect transistors (OFETs) were first

Table 1.1 Charge mobility of organic and inorganic semiconductor materials

Semiconductor materials	Charge mobility ($cm^2v^{-1}s^{-1}$)
GaAs	10^4
Single-crystal silicon	10^3
Poly silicon	10
Amorphous silicon	0.1–1
Organic semiconductor	10^{-4}–1

made in 1986 [6]. In the same period, Dr. C.W. Tang at Kodak developed organic photovoltaic (OPV) materials [7] and later invented the organic light-emitting diode (OLED) [8], from which organic electronics as a field of scientific interest started.

The reason the scientific community got interested in organic electronics was not only due to scientific curiosity but more importantly that they foresaw the prospect of printing electronic devices from organic polymers that could be naturally made into ink forms. Once they could be printed, electronic devices could be made on a massive scale at low cost, very much like printing newspapers. So from the early stage of development, people made attempts to process organic electronic materials in solution forms to make transistors [9]. In 1994, a research group led by Francis Garnier first reported OFETs made on plastic substrates [10]. Although only electrodes were printed and the organic semiconductors were deposited by vacuum evaporation, the significance of the work was that it proved transistors could be made on plastic substrates, opening the era of plastic electronics. Fully printed transistors were reported in 1997 when Dr. Zhenan Bao, working at Bell Labs, printed all layers including conductor, semiconductor, and dielectrics onto polyester (PET) film by a screen printing technique [11]. More recently, Professor Sirringhaus at Cambridge University made fully printed organic transistors by the inject printing technique [12].

It is apparent that organic electronics had its eye on low cost printing electronics from the beginning of its development. However, for a very long period, printing did not become the mainstream fabrication means for making organic electronic devices. The main reason lies in the fact that the charge mobility, which is a key property of semiconductor material, for the solution form of organic semiconductors is always lower than those small molecular organic semiconductors that cannot be made into solution form and have to be deposited by vacuum evaporation. In other words, transistors made by printable organic materials are not as good as those made by vacuum evaporated organic materials.

Charge mobility is the speed of electronic charge (electrons for n-type semiconductor or holes for p-type semiconductor) movement in semiconductor materials. It determines how fast a transistor switches at an applied external electric field. Table 1.1 lists the charge mobility of commonly used inorganic semiconductor materials, in comparison with organic semiconductor. It shows that the charge mobility of organic semiconductor materials is far lower than inorganic semiconductors.

The research in organic electronics in its over 3 decades of development history has been mainly focused on how to improve the charge mobility, as it is obvious that only high mobility organic semiconductors have value in any practical applications. The last 25 years have indeed seen the steady improvement of charge mobility in organic semiconductors, as shown in

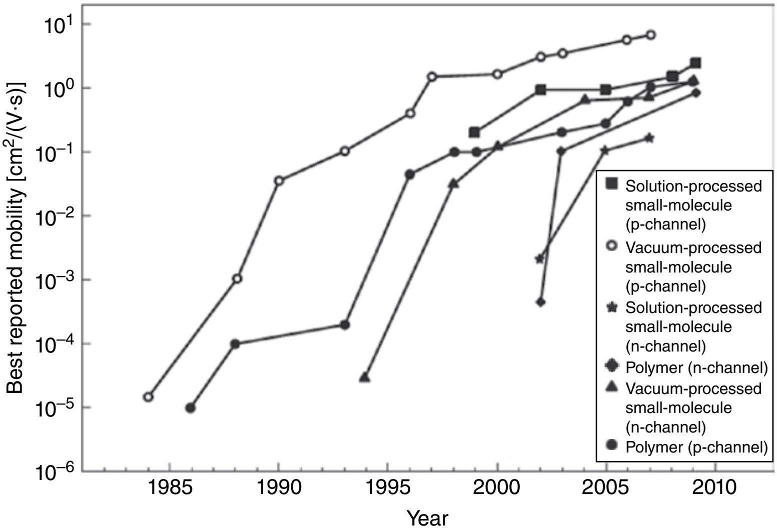

Figure 1.3 Evolution of charge mobility for organic semiconductor materials. (Adapted from [13] with permission from the Royal Society of Chemistry.)

Figure 1.3, which indicates the evolution of charge mobility from 1985 to 2010 for three different types of organic p-channel and n-channel semiconductor materials: vacuum-deposited small molecular organic materials, solution-processed small molecular organic materials, and solution-processed polymer materials [13].

The evolution curves reveal two things: first, there has been tremendous progress in improving the charge mobility of organic semiconductor materials. The mobility has increased 6 orders of magnitudes in the last 25 years. Second, the charge mobility of solution-processed polymeric organic semiconductor materials, though continuously improved, was always an order of magnitude lower than that of vacuum-deposited small molecular materials throughout the 25 years of development. Though the gap became smaller in the last few years due to the efforts in solution forms of organic semiconductors, small molecular organic semiconductor materials are still far better in terms of charge mobility [14]. As the ability to process organic semiconductor in solution form is the prerequisite of printing fabrication, low performance has prevented printing from becoming the preferred means of making organic electronic devices, although to be able to print electronic devices was originally the goal of organic electronics development.

Comparing the charge mobility of organic electronic materials in Figure 1.3 with that of inorganic semiconductor materials in Table 1.1, one can see that the mobility of organic semiconductors only barely catches up with that of amorphous silicon and is 3 orders of magnitude lower than single crystal silicon, which is the most common semiconductor material in IC microelectronics. According to the roadmap of organic semiconductors published in 2013 by the Organic Electronics Association (OE-A), as shown in Figure 1.4, the charge mobility of organic semiconductor materials may increase an order of magnitude higher than the current level in the next 10 years. Beyond that, organic semiconductors may reach their limits and inorganic or nanomaterials may come into play [15]. Besides, it would be difficult to change

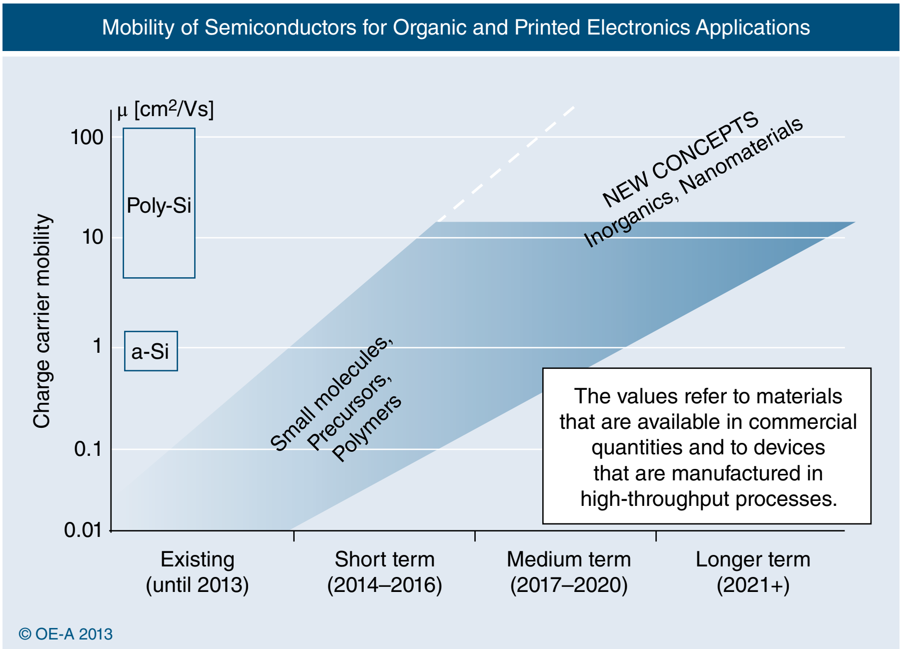

Figure 1.4 OE-A roadmap for the charge carrier mobility of organic semiconductors. (Reprinted from [15] with permission of OE-A.)

the fact that vacuum deposited small molecular organic semiconductors are always better than the printed solution form of organic semiconductors. The most obvious example is OLEDs. The best-performing OLED devices, no matter for lighting or for display, are still manufactured by vacuum deposition instead of printing. Printing has not succeeded in becoming the mainstream manufacturing technology for organic electronic devices, though some promising developments have been reported recently in printed OLEDs.

Printed electronics gained attention only in the last 8 years or so, largely due to the development and maturity of inorganic nanomaterials. Nanoscale inorganic materials (nanoparticles, nanowires, nanotubes, etc.) can be made into ink forms that can then be printed into patterns. The properties of those nanomaterials give the printed patterns and structures the conducting, semiconducting, dielectric, and optoelectronic properties that form a variety of electronic, optoelectronic, or photovoltaic devices, demonstrating that printing can be truly a low cost electronic manufacturing technology. Printed electronics began to establish itself as an independent scientific discipline and technology field. Scientific publications related to printed electronics started to increase, as indicated by the number of papers listed in the Web of Science database in the 10-year period up to 2013 (Fig. 1.5). International conferences and trade fairs in the theme of printed electronics began to appear. The first International Exhibition and Conference for the Printed Electronics Industry (LOPE-C) was held in 2009 in Germany. In the same year, South Korea hosted the first International Conference on Flexible and Printed Electronics (ICFPE). These conferences have become the focus of the printed electronics research community and industry. The 2015 LOPE-C drew more than 2,300 visitors from 42 countries.

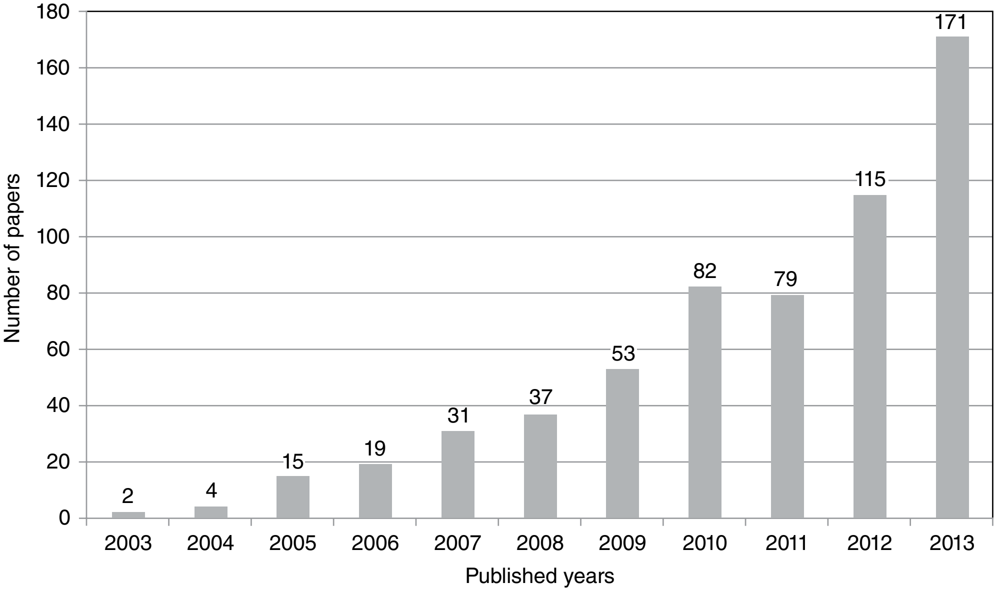

Figure 1.5 Published papers with "printed electronics" as key words. (Statistics from Web of Science database.)

An article published in *+Plastic Electronics* magazine in 2011, titled "Nanomaterials Are Becoming Synonymous with Printed Electronics" [16], reflected the view that inorganic nanomaterials have revived printed electronics.

The earliest adopted inorganic nanomaterial in printed electronics is nanosilver. It is known that silver is the best conductive material, far better than organic conductive polymers. Silver nanoparticles can be made into paste or ink and printed. After sintering, the printed silver patterns become solid silver, which serves as a conductive track in a variety of electronic circuits. In fact, silver paste has long been used in silicon solar cell manufacturing. Figure 1.6 shows a silicon solar cell where those bright tracks are silver electrodes made by screen printing of silver paste. Although printed, the silver paste used in silicon solar cell manufacturing is not made of silver nanoparticles but microsize particles. The difference between nansilver and microsilver is the sintering temperature. For microsilver, the sintering temperature needs to be more than 400°C in order to turn the silver paste into solid silver. Such high temperature is, however, not applicable to plastic substrates. Silver paste or ink made from nanosilver with particle size below 100 nm, on the other hand, can be sintered at below 150°C, which is the temperature most plastic film substrates can bear.

Nanosilver inks can be printed by a variety of printing methods such as inkjet printer, screen printer, gravure printer, or flexographic printer. Figure 1.7 shows a flexible circuit made by printing nanosilver ink on PET substrate. The emergence of nanosilver inks opens the route to printing conductive patterns onto plastic or even paper substrates with performance near or better than conventional copper-based conductive circuits. The electronics industry has already been testing the feasibility of printing electronic circuit boards, antennas of radio frequency identification (RFID) tags. Recently, inks made of silver nanoparticles or silver nanowires have

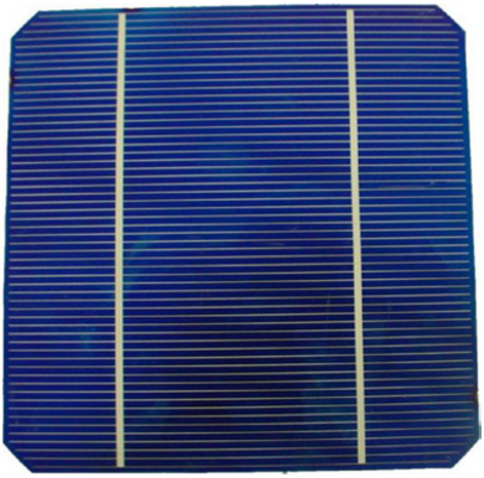

Figure 1.6 Picture of silicon solar cell where the front conductive electrodes are made by screen printing silver paste

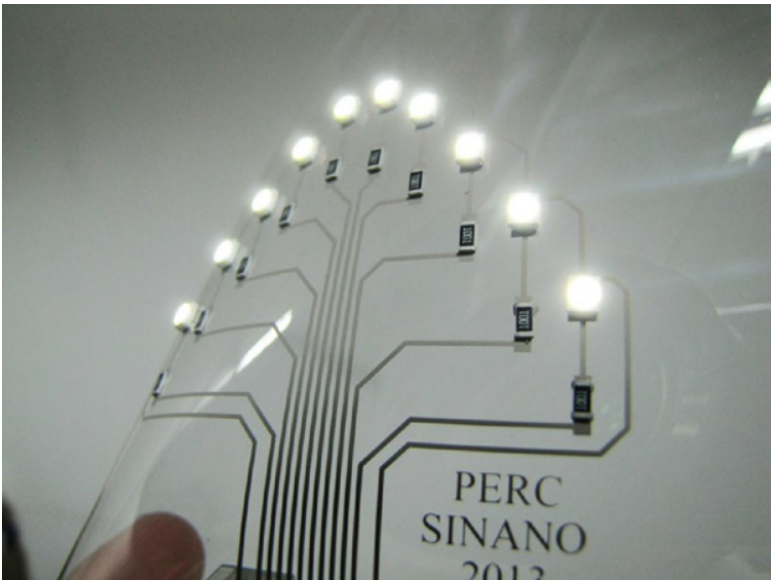

Figure 1.7 Flexible circuits on transparent plastic film made by inkjet printing of nanosilver ink

been applied to make transparent conductive films that can replace indium tin oxide (ITO) to be used in touch panels for mobile phones and tablet computers. These are the products conventionally made by photolithography and etching processes that are wasting large quantities of materials and polluting the environment.

In addition to conductive nanomaterials, inorganic semiconducting nanomaterials also demonstrated their superior performance in printed electronics. Although organic semiconductor materials have advanced considerably in the last 5 years with charge mobility approaching 10 $cm^2v^{-1}s^{-1}$ [17], single-walled semiconducting carbon nanotubes can have charge mobility exceeding 10^4 $cm^2v^{-1}s^{-1}$. Such high charge mobility has been proved in field-effect transistors made of single carbon nanotube. They have also been made into ink forms and printed to make field-effect transistors. Though not as high as that of single carbon nanotube, the charge mobility of printed transistors using carbon nanotube ink can easily get to more than 30 $cm^2v^{-1}s^{-1}$ [18]. Inks made of nanosilicon have been successfully printed to make fully functional 128 bits RFID with effective charge mobility exceeding 100 $cm^2v^{-1}s^{-1}$ [19]. Another family of inorganic semiconductor inks based on doped InO or ZnO has also found applications in printed transistors and demonstrated high charge mobility [20, 21].

Besides charge mobility, another critical issue concerning organic semiconductor materials is the environmental stability. Most organic semiconductors are very sensitive to oxygen and water vapor, which can kill their charge transportation ability. For OPV materials, the water vapor transmission rate (WVTR) should not exceed 10^{-4} g/day/m^2. For OLED, the WVTR should be less than 10^{-6} g/day/m^2, which is equivalent to less than a drop of water on a 50 × 100 m football pitch for a month. With such a strict requirement, any devices employing the organic materials have to be made in an oxygen-free and moisture-free environment and tightly encapsulated. For devices made on glass substrates, this requirement is relatively easy to realize because the sealing only needs to be implemented at the edges between two glass panels. For devices made on flexible plastic substrates, it is difficult to fulfill the requirement, and barrier layers have to be applied to the entire surface of plastic substrates. Effective barrier materials and coating techniques should meet the 10^{-6} g/day/m^2 WVTR requirement. Therefore, one of the intensively studied areas in organic electronics is to develop environmentally stable organic electronic materials as well as effective barrier-coating techniques. In contrast to organic electronic materials, inorganic materials do not have the environmental stability issue. Printing of inorganic nanomaterial inks can be done in an ambient environment and printed devices do not need special care for encapsulation. Therefore, printed electronics is relatively easy to implement with inorganic nanomaterials. It is fair to say that the use of inorganic nanomaterials has brought printed electronics closer to market.

Organic electronic materials have their own merits when applied to printed electronics, despite the above-mentioned problems. Though inorganic nanomaterials have their distinctive advantages over organic materials, they have their own issues when applied to printed electronics. The advantages and disadvantages of both categories of materials are summarized in Table 1.2 and 1.3. Detailed explanation for the tables will be given in Chapters 2 and 3 of this book. One can see from the tables that these materials are far from perfect and mature for printed electronics. A lot of research and development needs to be done in printable electronic materials, as well as in printing technologies and in various applications.

Table 1.2 Pros and cons of organic materials for printed electronics

Advantages	Disadvantages
Designability of organic molecules	Low charge mobility
Low annealing temperature	Poor environment stability
Flexibility	Poor printability of small molecular materials
Better printability of polymer materials	Batch to batch inconsistency

Table 1.3 Pros and cons of inorganic nanomaterials for printed electronics

Advantages	Disadvantages
Inherently high charge mobility	Difficulty in ink formulation (separation and dispersion issues)
Environmental stability	Impurity due to surfactants
Mature manufacturing technology	High post-processing temperature
Abundantly available	"Coffee-ring" effect
Batch to batch consistency	Inferior property compared to their bulk form

Table 1.4 New classes of electronics and their key features

Terms	Active materials	Substrate materials	Fabrication methods
Organic electronics	Organic polymers or small molecules	Any rigid or flexible materials	Thermal evaporation, coating, or printing
Plastic electronics	Organic polymers	Plastics	Coating or printing
Flexible electronics	Organic or inorganic materials	Flexible metals, plastics, or glass	Coating, printing, or surface mounting
Paper electronics	Organic or inorganic inks or pastes	Paper	Coating or printing
Transparent electronics	Transparent organic or inorganic materials	Transparent rigid or flexible materials	Printing or photolithograpy
Textile electronics	Organic or inorganic inks or pastes	Textile or fabric materials	Printing or weaving
Wearable electronics	Organic or inorganic inks or pastes	Flexible and stretchable materials	Coating, printing, or surface mounting
Printed electronics	Organic or inorganic inks or pastes	Any rigid or flexible materials	Coating or printing

When defining printed electronics, one should be aware of a few other newly emerged electronics; for example, organic electronics, plastic electronics, flexible electronics, paper electronics, transparent electronics, textile electronics, and wearable electronics. They all represent a new class of electronic technologies that are different from the silicon-based microelectronics. Table 1.4 gives a rough guide on what the key features are for each category of the new electronics.

Organic electronics refers to those electronic devices whose active materials, that is, the materials enabling electronic charge transport in a device, are organic in nature, whether they are organic polymers or organic small molecules. Organic electronic devices are not necessarily flexible. They can be made on glass or silicon substrates as well. Plastic electronics, though almost the same as organic electronics, refers exclusively to organic electronics on plastic substrates. The key feature of flexible electronics is the flexibility. To be flexible does not have to be on plastics. Thin sheet of metals or glass can be flexible. The reason that metals or glass are used as the substrates is their ability to withstand high annealing or sintering temperature. As one will learn from the rest of this book, some electronic inks, especially inks made of inorganic materials, require high temperature to sinter. To make electronics flexible, one can also simply mount silicon chips onto plastic substrates. Though not flexible microscopically, the whole electronic system can be flexible macroscopically [22]. Paper electronics is quite straightforward to understand. No matter what materials are used to make the devices, they have to be on paper substrate. Transparent electronics requires not only transparent substrates but all the electronic materials have to be transparent. Textile electronics is electronic devices or systems on cloth, either weaved into a cloth with electronically functionalized fabrics or printed/mounted onto the surface of cloth. Wearable electronics generally refers to electronic devices that are small and lightweight and can be wearable, for example, the Google Glass and the Apple Watch. Compared to all the aforementioned electronics, printed electronics differs from all the others only in the way the electronic devices are fabricated. Printed electronics encompasses the other electronics, because both organic and inorganic electronic materials can be printed and electronic devices can be printed either on rigid substrates or flexible substrates, whether on papers, plastics, textiles, or glass.

1.2 The Importance of Developing Printed Electronics

Why are organic electronics, flexible electronics, or printed electronics being developed? It is because these electronics are different from the familiar silicon microelectronics with two distinctive features: one is the additive fabrication process in which electronic materials are added layer by layer to make a device; the other is that the functionality of a device is independent of substrate materials. The first feature enables printing as a means of device fabrication, which is less waste of materials and less energy consumption compared to thermal evaporation or sputtering deposition. The second feature enables many cheap materials other than silicon to be used as substrates. The combination of these two features makes it possible to manufacture large-area, flexible, green manufacturing, and low cost electronic products. For example, the largest size of silicon wafer by far in IC manufacturing is 12 inch (300 mm), whereas printing can work with sheet size of easily over meters; using plastic films as substrates, whether information displays or solar cells or lighting panels, can be flexible, lightweight, or even transparent; printing manufacturing, with its high throughput capability and low cost of equipment and ink materials, can significantly lower the cost of final products. In addition, the additive manufacturing process is green, meaning no subtractive etching involved, no high temperature processes needed, hence low in energy consumption, material waste, and environment pollution.

Can printed electronics replace silicon microelectronics? The answer is no. There is no doubt that printing is a simpler and faster manufacturing technique than lithographic patterning for silicon microelectronics, as illustrated in Figure 1.1. However, printing does not have the accuracy and resolution capability of modern lithography techniques widely used in the IC industry. Modern IC chips have minimum circuit feature size less than 20 nm, whereas modern printing machines can only print features of a few micrometers at best, which is a thousand times larger. The best organic or inorganic semiconductor materials that are printable are still 2 orders of magnitude poorer than the basic semiconductor materials used in IC chips. Therefore, the performance of printed electronic devices is nowhere near the performance of silicon microelectronics. Performance versus cost when comparing printed electronics with silicon microelectronics could be shown as in Figure 1.8. Though the performance of printed electronics is poorer, it is cheaper. In addition, printed electronics can offer large size and flexibility that silicon microelectronics cannot. They are not to replace each other but complementary to each other.

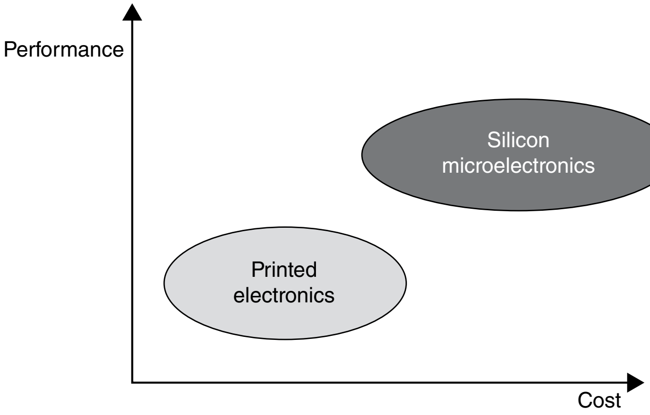

Figure 1.8 Printed electronics vs. silicon microelectronics

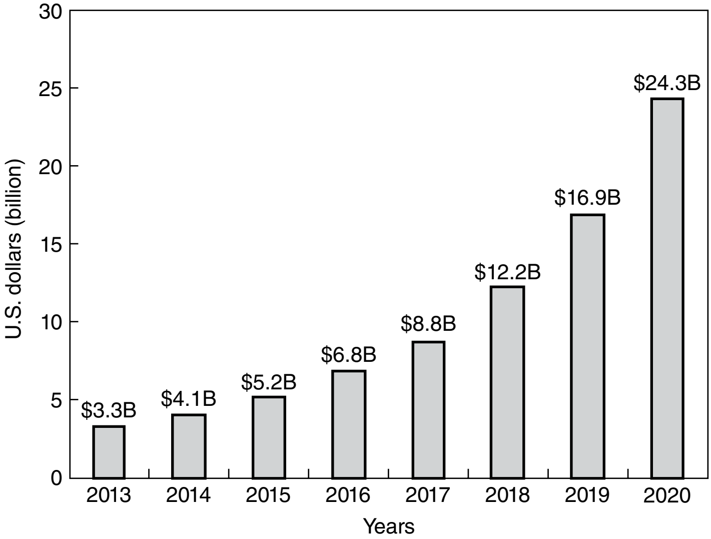

Figure 1.9 Market forecast for printed electronics. (Data from IHS market report with permission.)

It is those unique features that earn printed electronics a place in the vast electronic application market. Some market research firms have been tracking the growth of printed electronics over the years. For example, IDTechEx, a British market research firm, started charting and forecasting the market growth of printed, organic, and flexible electronics in 2008. Their latest market report showed the combined market for printed, organic, and flexible electronics will be $80 billion by 2023 [23]. In the combined market, printed electronics will take a 25% share by 2023, which is around $20 billion. Another market research firm, Display Bank, published their report in June 2013, which specifically targets the printed electronics market, forecasting that the printed electronics market will grow to $24.3 billion by 2020 [24]. Figure 1.9 is the chart of year-to-year growth from the report.

The forecasted growth rate is not surprising because printed, organic, and flexible electronics are already around us. Samsung and LG, the Korean electronics giants, are already shipping OLED TVs to customers. Panasonic in Japan and AUO in Taiwan have both demonstrated OLED TVs using inkjet printing as one of the manufacturing techniques. Wall size, transparent, and interactive touch-controlled displays are no longer only seen in the movie *Avatar* but commercially available. There will be more of these products in the market, as printing enables a large volume of them to be produced at lower cost. With the Internet of Things (IoT) gaining more widespread use, it is estimated the world will need a trillion sensors by 2023 to connect most things around us [25]. Current manufacturing technologies for silicon microelectronics would be prohibitively high cost. Printed electronics could offer an alternative solution to meet the demand for trillion sensors.

Developing printed electronics is important not only because it represents a fast-growing market but also because it represents a paradigm shift in electronic manufacturing. Conventional subtractive manufacturing takes away materials, which involves lithographic patterning and acidic etching. A perfect example is the manufacturing of printed circuit boards (PCBs). A PCB is not made by printing but by lithographic patterning and acidic etching of copper-coated sheets. Acidic etching not only produces highly polluting waste solutions but also wastes 90% of copper material. China is the world’s largest producer of PCBs. The price China pays for such a production capacity is the widespread pollution of soil and water. If the additive printing method can partly replace the subtractive etching, not only the pollution and waste of materials can be reduced—the cost of manufacturing also can be lowered because of simplified manufacturing processes. Printing can potentially make finer lines, which can increase the circuit connection density. The concept of green manufacturing is already being heavily promoted in China. Printing is beginning to be used for making RFID antennas, which are traditionally made by acidic etching.

Like 3D printing, which is hotly pursued worldwide, printed electronics can change the face of many conventional electronic manufacturing processes. Some industries already employed printing to replace some existing manufacturing steps; for example, to print color filters in LCD panel manufacturing and to print e-ink in e-paper manufacturing. Panasonic unveiled their printed 55” high definition colored polymer OLED TV in 2013, and AU Optronics Corp. in Taiwan demonstrated their printed 65” OLED TV in 2014 [26], as shown in Figure 1.10. Though still a prototype, it demonstrated that a TV can be manufactured by printing. The silicon solar cell industry already widely uses screen printing for front electrode manufacturing. Other industries are beginning to consider printing as an alternative manufacturing technology.

The importance of printed electronics gained notice in recent years both in the academic community and the electronic industry. The OE-A, which was established in 2004 in Germany and initially focused on organic electronics, has expanded rapidly in recent years because printed electronics is a main area of focus. OE-A now has 223 members across the globe from 31 countries, covering both academic institutions and industries. Scientific publications in the area of printed electronics started to appear in 2003 and increased significantly in the last few years, as shown in Figure 1.5. The similar trend is seen for patent applications, as shown in Figure 1.11 which is the search results from the Derwent Innovation Index database. The search key words are “organic electronics,” “plastic electronics,” “printed electronics,” and “large-area electronics.”

Figure 1.10 Inkjet printed 65" OLED TV demonstrated by AU Optronics Corp. (Taiwan) in 2014

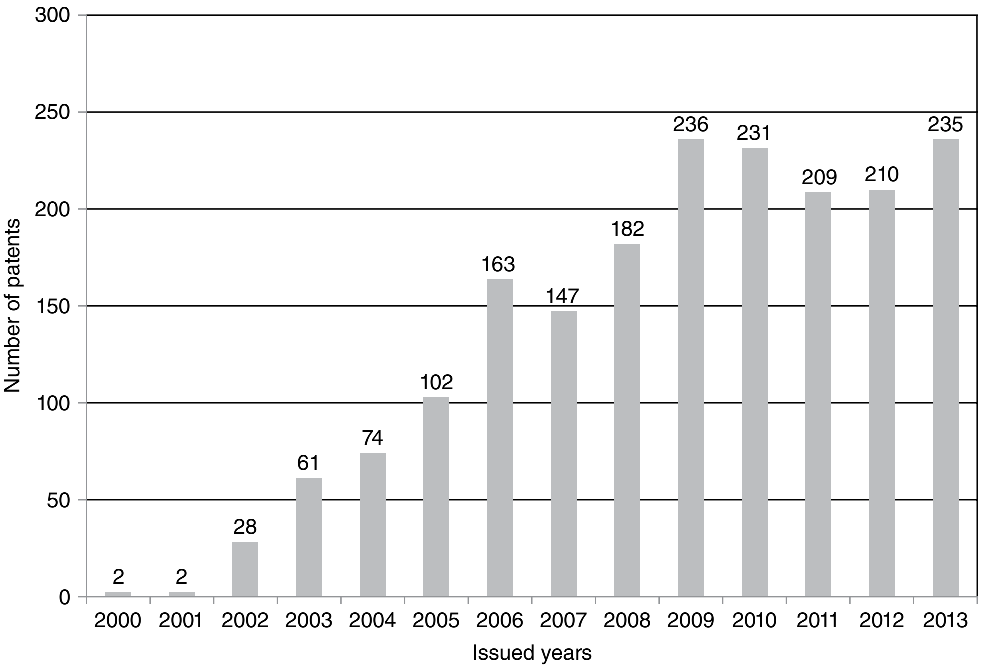

Figure 1.11 Patent applications by years related to organic, large-area, and printed electronics

1.3 Multidisciplinary Nature of Printed Electronics

Can printed electronics be on its own as a scientific and technological discipline? To answer this question, one has to examine what is included in printed electronics. As seen in Table 1.4, printed electronics is closely related to organic electronics, plastic electronics, flexible electronics, or paper electronics, but they are not the same. Organic electronic devices can be fabricated by printing but also by thermal evaporation. So organic electronics is different from printed electronics. Electronic inks can be printed either on rigid substrates or flexible substrates. So printed electronics is different from flexible electronics. Printed electronics can stand on its own because applying printing to electronic device fabrication brings out a series of unique scientific and technological issues and problems that need to be studied and investigated. Yet, to study these issues requires multidisciplinary knowledge and expertise.

First, printed electronics is based on inks, requiring a wide range of materials, such as conductors, semiconductors, dielectrics, or light-emitting or photovoltaic materials to be printable. They can be organic or inorganic materials. How to make these materials into ink forms requires high level expertise in both chemistry and physics. For organic electronic inks, the quest is to find the materials that are of high electric charge transport mobility and environmentally stable, as well as printable. The long history of organic electronics development has been to find these magic materials through molecular design and synthesis. For inorganic electronic inks, the choices are fewer because one can only choose the materials from the Periodic Table of the Elements plus their compounds. Fortunately, the success of nanomaterials development in recent years made the task much easier. The available nanomaterials, such as carbon nanotubes, graphene, a variety of nanowires, metallic and semiconducting nanoparticles, and metal oxides, all have desirable electronic properties. The key issue is to make the nanomaterials into inks. Making them into ink forms entails dispersing the fine powders of nanomaterials either in a solvent or in an aqueous solution. Alternatively, inorganic inks can be produced through some redox reactions of inorganic compound precursors. There will be detailed descriptions of these techniques in the following chapters of this book. To disperse inorganic powders is relatively easy compared to finding a magical organic molecule. The rapid development of printed electronics in recent years is in large part due to the application of nanomaterials to printable electronic inks.

Making electronic inks is only half of the story. Any inks have to match with the printing methods to be used and with the substrates to be printed on. One of the basic requirements is the viscosity. An inkjet printer requires ink with a very narrow range of viscosity, typically between 10 cp and 20 cp (1 cp = 1mPa.s). Too viscous of an ink will clog the inkjet nozzle. Too thin of an ink and its flow cannot be controlled. A gravure printer requires viscosity of a few hundreds of cp, whereas a screen printer needs the ink to be more than 10,000 cp in viscosity, which can no longer be called an ink but is instead a paste. The ink viscosity directly influences the thickness of printed materials. The more viscous the ink is, the thicker the printed layer will be. As for the matching with substrate, one of the basic properties of substrate is the surface energy. High surface energy means high surface hydrophilicity. Printed ink will have strong adhesion to the surface. Low surface energy means high surface hydrophobicity. Printed ink will have less lateral spread, resulting in high printing resolution. Both hydrophilic surfaces and hydrophobic surfaces have good and bad influences on printing quality. Whether the ink is solvent based or aqueous based also influences the final printing quality.

Though the above-mentioned issues are also common issues in the printing industry, for printed electronics, the final printing result is not its visual effect but the performance of printed electronic devices. Similar to printing colors in conventional printing where different colors are formed by printing and superimposing three primary colors, an electronic device is made in printed electronics by printing different electronic materials layer by layer and overlapping them. These electronic materials function as conductors, semiconductors, insulators, or emitting lights or absorbing lights. They must be able to function as they are intended after printed onto a substrate. So printed electronics is not a simple printing but involves physics, chemistry, and electronics.

It must be pointed out that printing is not an ideal method to fabricate electronic devices. The fundamental drawbacks are

1. The resolution of printed features is far poorer than that made by the common fabrication methods used in the silicon microelectronic industry. For example, screen printing can print features no less than 50 μm; the best resolution of inkjet printing is about 20 μm; an aerosol jet printer, which is a variation of the inkjet printing method [27], can print minimum features of about 5 μm; the latest development in inkjet printing is to introduce an electrostatic field to pull out fine inkjet, called super inkjet, which can produce line features approaching 1 μm [28]. Even so, printing resolution is nowhere near the resolution capability of current extreme UV lithography for IC manufacturing, which is under 20 nm.
2. The materials deposited by printing do not have the surface smoothness as those done by thermal evaporation, sputtering, chemical vapor deposition, or any other methods used in IC manufacturing. The high roughness can cause serious problems at the interface where different materials are overlapped to each other. Electric breakdown or charge leakage often happens due to the surface roughness.
3. Though printing can potentially be done in roll-to-roll (R2R) fashion with very high throughput, it does not have the alignment and overlay accuracy as in optical lithography for IC manufacturing. The overlay accuracy is required when different patterns are printed onto each other, which is vital to device function. The current optical lithography has overlay accuracy of a few nanometers, whereas the overlay accuracy for R2R printing is about 10 μm at best. An inkjet printer has better overlay accuracy but still no better than 1 μm. Poor overlay can cause degradation of device uniformity and yield in high throughput printing.

There are also other issues, such as the compatibility of solvents used in different inks and the necessity of drying/annealing/sintering of printed inks. These are the problems the printed electronics community has to face. On one hand, continuous research and development are being carried out to overcome the problems or to improve the performance of printing by improving inks, process technology, and printing equipment. An example of such improvement is the development of the super inkjet printer, which is considered a big step forward in traditional inkjet printing technology. On the other hand, one should find the applications which can utilize the strength of printed electronics, i.e. large size, flexible and low cost and play down its drawbacks. As is illustrated in Figure 1.6, printed electronics is not to compete with but to be complementary to silicon microelectronics.

Traditional printing is already a mature industry. Printed electronics, however, is a new scientific discipline whose advances need joint effort from many different scientific disciplines, such as organic and inorganic chemistry, solid state physics, surface physics, electronics, and mechanics. Being a new and developing field, academic researchers in the existing scientific disciplines can find new and exciting research topics in printed electronics. The history of organic electronics development has proved the point. Originated from organic chemistry, organic electronics has in the last 20 years developed into an independent field that combines chemistry, physics, and electronics. One can foresee that printed electronics would create new space and opportunity for the development of information technology, in which printed smart cards and flexible displays can certainly stimulate new applications. Electronic design would have to change to accommodate printed transistors and circuits. Many traditional industries would have more application ideas when flexible, wearable, or transparent materials are combined with printed electronics. In the process, printed electronics will become a more sophisticated and established scientific discipline.

1.4 Structure and Content of the Book

Printed electronics is still in its infancy stage. Though having been talked about since the early days of organic electronics, the interest in printing as a means of electronic manufacturing was renewed only in the last few years, when inorganic nanomaterials started to be made into inks for printed electronics. Although neither printing nor electronics is a new field, the combination of the two is new and unfamiliar to most academic researchers and technology developers, particularly to university students and graduates. This book is written with the purpose of presenting a comprehensive picture about what printed electronics is. The structure of the book is designed to cover all aspects of knowledge about printed electronics, from materials to technologies to applications.

There are 9 chapters in the book, including the introduction (Chapter 1), organic printable electronic materials (Chapter 2), inorganic printable electronic materials (Chapter 3), printing processes and equipment (Chapter 4), printable thin-film transistors (Chapter 5), printable organic thin-film solar cells (Chapter 6), printable light-emitting devices (Chapter 7), encapsulation for printed electronics (Chapter 8), and applications of printed electronics (Chapter 9). The contents of each chapter are so highly cross-disciplinary that experts in different fields may find it familiar as well as unfamiliar. There is plenty of basic information and knowledge in the book, necessary to understand printed electronics, and the latest developments are discussed, bringing readers to the forefront of this field.

Printable materials are the foundation of printed electronics. Chapters 2 and 3 focus on the materials aspects of printed electronics. In Chapter 2, organic electronic materials are introduced according to whether they are conductors, semiconductors, or dielectrics. There are two types of organic materials that have electronic properties, small molecules and polymers. The study of organic electronic materials is mainly the design and synthesis of small molecules or polymeric molecules so that they possess certain electronic or optoelectronic functions. The possibility of design and synthesis of new organic molecules is unlimited, as is the study of organic electronic materials. The over 2 decades of organic electronics research has been the history of searching for the wonder materials that could have higher electronic charge mobility or higher efficiency of photoelectronic conversion. A literature search has shown that so far 726 chemical compounds have been studied and tested. Over 350 of them are of organic semiconductor properties and 55 of them have charge mobility $> 1\ \mathrm{cm^2 v^{-1} s^{-1}}$ [29]. However, not all of the organic semiconductor materials can be printable. Chapter 2 mainly describes those printable organic electronic materials and how to make them printable. As most of the organic materials are susceptible to oxygen and water molecules, how to improve their environmental stability as well as their electronic properties is also the subject of this chapter.

As mentioned earlier, printed electronics originated from organic materials but has thrived because of inorganic materials. The key to the successful application of inorganic materials in printed electronics is the maturity of inorganic nanomaterials development in recent years. Those inorganic nanomaterials, such as carbon nanotubes, graphene, and a variety of nanowires and nanoparticles, can be made into ink forms and become printable. The electronic devices made by printing inorganic nanomaterial inks are of better performance and better environmental stability than most printed organic electronic devices. Nanomaterials have been the subject of many books and scientific publications. How to make nanomaterials printable is the topic of Chapter 3. Most inorganic nanomaterials that can be made into inks have been discussed, including metals, transparent oxide, carbon nanotubes and graphene, silicon and germanium, and inorganic/organic composites. Different methods for ink formulation are introduced.

The key feature of printed electronics is printing. Chapter 4 focuses on a wide variety of printing methods that can be used for printed electronics. Although printing is an old and mature technology, printing a newspaper is fundamentally different from printing a transistor. While introducing the basic principles of printing, Chapter 4 places much of the emphasis on differences between conventional printing and printing electronic devices. One of the special issues in printing nanomaterials-based inks is the “coffee ring” effect. As the ink is formulated by dispersing nanoparticles in aqueous or solvent solutions, the nanoparticles will spontaneously aggregate at the edge of ink drops on a substrate after drying, causing non-uniform distribution of material. Pre-and post-treatment of substrates also play a vital role in the final printing quality, hence the performance of printed devices. As the criteria of judging the printing quality are no longer the visual effects, the contents introduced in Chapter 4 will be useful not only for novices in printing but also for technical professionals who are familiar with traditional paper media printing.

The most important applications of printed electronics are in three groups: transistors, solar cells, and light-emitting devices. They are introduced in Chapters 5, 6, and 7, respectively. Transistors (Chapter 5) are the basic building block for many electronic systems, typically for information processing (logic and memory circuits) or for switching pixels in information display (backplane). In printed electronics, transistors can be either OFETs or inorganic based on semiconducting carbon nanotubes or transparent oxide semiconductors. Printed solar cells (Chapter 6) can be OPV or inorganic photovoltaic, such as copper indium gallium selenide (CIGS) or the recently thriving perovskite compounds. Light-emitting devices (Chapter 7) are mainly OLEDs. Most OLEDs are fabricated by a vacuum evaporation process. There are some light-emitting materials, particularly polymeric light-emitting materials as well as specially formulated organic small molecular materials, that can be printed. The three chapters focus on working principles of relevant devices, their materials requirements, and fabrication processes.

As mentioned earlier, one of the serious drawbacks for organic electronic devices is the environmental stability. Most organic electronic molecules tend to react with water and oxygen molecules and lose their charge transport ability. The device will be dead when water vapor and oxygen penetrate inside. For example, OLEDs can only tolerate a water vapor transmission rate (WVTR) of 10^{-6} grams per square meter per day (g/m^2/day). The WVTR for OPV is

10^{-4} g/m^2/day. Therefore, OLED and OPV devices must be protected from water and oxygen. It is less of an issue for OLED and OPV made on glass substrates, as glass can naturally stop the penetration of water and oxygen molecules. One only needs to take care of the sealing at the edges of glass panels. It will be a big issue when OLEDs and OPVs are made on flexible plastic substrates. Plastics are naturally porous to water and oxygen molecules. Chapter 8 deals with this issue. The decay characteristics of OLEDs and OPVs under the influence of water vapor and oxygen is analyzed. Different sealing and encapsulation techniques are introduced, particularly about barrier layer formation on plastic surfaces, which is vital for flexible OLED and OPV applications.

Printed electronics is not about basic science but is very much application oriented. The main driving force to develop printed electronics comes from the expectation of its great market potential. Printing enables large-size and flexible electronics, photovoltaics, and displays to be produced at low cost, which differs from silicon microelectronics and has its unique place in the electronics market. The last chapter of the book (Chapter 9) focuses on the applications of printed electronics. The chapter describes the applications in five categories—organic photovoltaic, organic lighting, flexible display, electronic devices and circuits, and integrated smart systems. In each category, the state of the art is introduced and future trends are predicted. As the last chapter of the book, it also summarizes the main challenges lying ahead and gives the outlook.

Considering the multidisciplinary nature of printed electronics and that readers may come from very diverse backgrounds, each chapter of the book mainly describes the principles of technology, aided by ample pictures and illustrations and without much mathematics. The book serves both as an advanced introduction to the topic and as an aid for professionals to explore the new field. Senior-leval undergraduates, post-graduates, academic researchers, and engineering professionals with basic training in physics, chemistry, or electronics will all be able to learn printed electronics from the book and find it a useful professional reference. References and web links are provided at the end of each chapter so that readers can discover more information on the subject.

References

[1] Zant PV. *Microchip Fabrication*. 5th ed. New York: McGraw-Hill, 2004.

[2] LaPedus M. EUV tool costs hit $120 million. EE Times, November 19, 2011.

[3] Cui Z. *Micro-Nanofabrication Technologies and Applications*. 3rd ed. Beijing: Chinese Higher Education Press, 2013.

[4] Shirakawa HL, Edwin J, MacDiarmid AG, Chiang CK, Heeger AJ. Synthesis of electrically conducting organic polymers: halogen derivatives of polyacetylene. J. Chemical Society, Chemical Communications 1977;16:578.

[5] Ebisawa F, Kurokawa T, Nara S. Electrical properties of polyacetylene/polysiloxane interface. J. Appl. Phys. 1983;54(6):3255–3259.

[6] Tsumura A, Koezuka H, Ando T. Macromolecular electronic device: field-effect transistor with a polythiophene thin film. Appl. Phys. Lett. 1986;49(18):1210–1212.

[7] Tang CW. Two-layer organic photovoltaic cell. Appl. Phys. Lett. 1986;48(2):183–185.

[8] Tang CW, VanSlyke SA. Organic electroluminescent diodes. Appl. Phys. Lett. 1987;51:913.

[9] Assadi A, et al. Field effect mobility of poly(3-hexylthiophene). Appl. Phys. Lett. 1988;53(5):195–197.

[10] Garnier F, Gilles Horowitz XP, Fichou D. Organic-based field-effect transistors: critical analysis of the semiconducting characteristics of organic materials. Molecular Engineering 1991;1(2):131–139.

[11] Bao Z, et al. High-performance plastic transistors fabricated by printing techniques. Chem. Mater. 1997;9: 1299–1301.

[12] Sirringhaus H, et al. High-resolution inkjet printing of all-polymer transistor bircuits. Science 2000;290: 2123–2126.

[13] Klauk H. Organic thin-film transistors. Chem. Soc. Rev. 2010;39:2643–2666.

[14] *Organic and Printed Electronics: Applications, Technologies and Suppliers*. 6th ed. Frankfurt: Organic Electronics Association, 2015.

[15] *Organic and Printed Electronics: Applications, Technologies and Suppliers*. 5th ed. Frankfurt: Organic Electronics Association, 2013.

[16] Rogers D. Nanomaterials are becoming synonymous with printed electronics. +Plastic Electronics 2011;3(6):35.

[17] Li J, Zhao Y, Liu Y. A stable solution-processed polymer semiconductor with record high-mobility for printed transistors. Scientific Report 2012;2:754.

[18] Wang C, Zhao J, Cui Z. High performance thin film transistors based on regioregular poly(3-dodecylthiophene)-sorted large diameter semiconducting single-walled carbon nanotubes. Nanoscale 2013;5:4156.

[19] O'Connor MC. Kovio unveils printed-silicon HF RFID chip tag. RFID J. http://www.rfidjournal.com/article/view/4389, 2008.

[20] Schneider JJ, et al. A printed and flexible field-effect transistor device with nanoscale zinc oxide as active semiconductor material. Advanced Materials 2008;20(18):3383–3387.

[21] Noh YY, et al. Inkjet printed ZnO nanowire field effect transistors. Appl. Phys. Lett. 2007;91:043109.

[22] *Flexible Electronics: Materials and Applications*, ed. W.S. Wong and A. Salleo. New York: Springer, 2009.

[23] IDTechEX. Printed, organic & flexible electronics: forecasts, players & opportunities 2013–2023. http://www.idtechex.com/, 2013.

[24] DisplayBank. Printed electronics technology and market outlook. http://www.displaybank.com/, 2013.

[25] Summit T. Trillion sensors roadmap. www.tsensorssummit.org/, 2013.

[26] Peng-Yu C, et al. 65-inch inkjet printed organic light-emitting display panel with high degree of pixel iniformity. SID Digest 2014;30(1):396.

[27] Aersol jet printer. Available from: http://www.optomec.com.

[28] Super inkjet printing technology. http://www.sijtechnology.com/.

[29] Wang CDH, Hu W, Liu Y, Zhu D. Semiconducting π-conjugated systems in field-effect transistors: a material odyssey of organic electronics. Chem. Soc. Rev. 2012;112:2208–2267.

2

Organic Printable Electronic Materials

Song Qiu and Chunshan Zhou

2.1 Introduction

Organic and printed electronics are closely related because of the widely used conductive polymers, organic semiconductors, and plastic thin films that are the base materials for many thin, light, and flexible electronic devices. Printable organic electronics enable a wide range of electronic components to be made through low cost roll-to-roll printing or coating processes, opening up the possibility of a range of new products and applications, including organic photovoltaics (OPVs), organic light-emitting diodes (OLEDs), and organic thin-film transistors (OTFTs), which can be integrated into radio frequency identification (RFID) tags, display backplanes, memory and sensor devices, and so forth.

Organic electronic materials are the basis for all organic electronic devices. They can be divided into conductors, semiconductors, dielectric, and optoelectronic materials. Semiconductor materials are at the core of organic electronic devices. Their conductivity, charge carrier mobility, and energy band gap are similar to conventional inorganic semiconductor materials, but they have their own characteristics:

1. A much wider range of organic compounds and molecular structures than inorganic materials is available to make electronic devices. The possibilities for design of new organic compounds or molecules are almost infinite. In fact, the discovery of new organic electronic materials has never stopped in the four decades since organic conductive materials were invented.
2. Organic materials can be processed in a variety of ways to make an electronic device. They can be solution processed, vacuum evaporated, self-assembled, and so forth. Most of these processing methods are simple and low cost, compared to those for inorganic electronic materials.
3. Organic materials are naturally compatible with flexible polymeric substrates. Therefore, organic electronics are also called plastic electronics. Use of plastic substrates means low temperature processes and flexible and low cost manufacturing.

Printed Electronics: Materials, Technologies and Applications, First Edition. Zheng Cui, Chunshan Zhou,
Song Qiu, Zheng Chen, Jian Lin, Jianwen Zhao, Changqi Ma and Wenming Su.
© 2016 Higher Education Press. All rights reserved. Published 2016 by John Wiley & Sons Singapore Pte. Ltd.

Table 2.1 Pros and cons of organic electronic materials

Advantages	Disadvantages
Designability of organic molecules	Low charge mobility
Low annealing temperature	Poor environment stability
Flexibility	Poor printability of small molecular materials
Better printability of polymer materials	Batch to batch inconsistency

To meet the demands of large-scale printing processes, the small organic molecules or polymers should be treated or dispersed, to be made into ink or slurry forms. They should have not only good intrinsic performance but also suitable solubility and film-forming ability. Therefore, solution processability is an important precondition to select organic printable electronic materials. The pros and cons of organic electronic materials are summarized in Table 2.1.

The rest of this chapter will give detailed descriptions and explanations for the above advantages and disadvantages for different types of organic electronic materials. A variety of organic printable electronic materials will be introduced, from the structural design and synthesis to the relationship between structure and performance of materials, with particular emphasis on organic semiconductors, including small molecules and polymers.

2.2 Organic Conductive Materials

2.2.1 Characteristics of Organic Conductive Materials

According to Ohm's law, when both ends of a sample are applied with a DC voltage (V) and an electric current flows through the sample (I), the resistance (R) is $R=\frac{V}{I}$. The reciprocal of resistance is called conductance (G): $G=\frac{I}{V}$. The unit of resistance is ohm (Ω); the unit of conductivity is siemens (S). The resistance of a material sample is inversely proportional to the cross-sectional area and proportional to the thickness: $R=\rho\frac{d}{s}$. Similarly, conductivity is $G=\sigma\frac{s}{d}$.

In the above two formulas, ρ is the resistivity in the unit of (Ω • cm), and σ is the conductivity in the unit of (Ω^{-1} • cm^{-1} or S• cm^{-1}). Clearly, the resistivity and conductivity are no longer relevant to the volume of material but only depend on their intrinsic properties. They are the parameters to characterize conductive materials. Table 2.2 lists the scale of conductivity for superconductors, conductors, semiconductors, and insulators.

Table 2.2 Range of material conductivity

Classification	Conductivity (S• cm^{-1})	Typical examples
Insulator	$<10^{-10}$	Quartz, polyethylene, polystyrene, sapphire
Semiconductor	10^{-10}–10^{2}	Silicon, germanium, polyacetylene
Conductor	10^{2}–10^{8}	Silver, copper, graphite
Superconductor	$>10^{8}$	Niobium (9.2 K), $LaBaCuO_4$ (35 K), Bechgaard salt

2.2.2 History of Organic Conductive Materials

Organic compounds have been used as insulators for a long time. In the early twentieth century, McCoy and Moore predicted that "it would be possible to prepare metal-free organic metal conductor elements." Since then, scientists working in the field of organic semiconductor research have made significant progress.

- 1954: Pyrene and bromine were found to form charge transfer complexes [1]. They were the first conductive molecules and had a relatively high conductivity, $\sigma_{rt} = 1\ \text{S} \bullet \text{cm}^{-1}$, but poor stability. The discovery made a huge impact in the understanding of organic compounds.
- 1977: Hideki Shirakawa, with A. J. Heeger and M. MacDiarmid, found that the conductivity of polyacetylene film could be greatly improved by doping and could become a good conductor, which led to the discovery of conductive polymers [2].
- 1986: A. Tsulnura et al. [3] fabricated the first organic thin-film transistor with an electrochemically prepared polythiophene thin film.
- 1987: C.W. Tang [4] from Kodak Laboratories developed the first organic light-emitting diodes with organic molecular thin film.
- 1989: Camier for the first time prepared organic thin-film transistor with oligothiophene [5].
- 1990: J.H. Burroughes [6] successfully developed the first polymer organic light-emitting diode.
- 1996: Ambipolar transistors consisting of α-6T and C_{60} were successfully prepared by Dodabalapur [7]. In the same year, the first single crystal organic transistors were successfully fabricated using single crystals of sexithiophene by Horowitz [8], with the mobility up to $0.1\ \text{cm}^2 \cdot \text{V}^{-1} \cdot \text{s}^{-1}$.

From the late 1990s, research institutions and industrial enterprises have paid great attention to organic conductors and organic semiconductors. Both scientific research and commercial applications were then entering a rapid development era, with organic conductors and semiconductors eventually becoming an established scientific discipline and an industrial sector.

2.2.3 Conductive Polymer

According to structural features and conductive mechanisms, conductive polymer materials can be divided into the following categories. Conductive polymers of the *structural type* are mainly prepared by chemical synthesis or electrochemical methods. The conductivity of these polymers depends directly on the chemical structure and doped state. Conductive polymers of the *composite type* are prepared by adding carbon black or conductive filler such as metal powder in the polymer; common products include conductive rubber, conductive paint, resistors, conductive electromagnetic shielding, and conductive adhesives.

2.2.3.1 Structural Conductive Polymer

Among the structural conductive polymers that have been studied, such as polyacetylene, polyaniline, polypyrrole, and polythiophene, doped polyacetylene has the highest electrical conductivity. Since the discovery of doped polyacetylene, its conductivity has been improved by 12 orders of magnitude to reach 5×10^3–10^4 S·cm^{-1}, and doped polyacetylene film with aligned crystalline orientation can even get the conductivity as high as 10^5 S • cm^{-1}, almost comparable to copper.

Generally, there are four types of conductive polymers: polymer electrolyte, conjugated polymers, charge transfer complexes, and organic metal chelate. Among them, conjugated polymers have been the most extensively researched and most practical for applications. According to the structure of conductive carriers, conductive polymers have two forms of conduction mechanisms: electronic conduction and ionic conduction.

1. Electron conduction in conjugated polymer. The conjugated polymer refers to the main chain of polymer having alternating carbon-carbon single and multiple bonds, connecting p-orbital with delocalized electrons in main chain of polymers, which in general may lower the overall energy and increase stability. A typical example is polyacetylene with carbon bonds structure as ─CH = CH─.

   In order to be conductive, a conjugated polymer must meet two conditions. First, there are strongly delocalized molecular orbits; second, there are overlapped molecular orbits. The conjugated polymer satisfying these two conditions can transport electrical currents by its own charge carriers.

   In conjugated polymers, the ease with which an electron leave a molecular orbit depends on the number of π electrons in a conjugate chain and their activation energy. Theory and practice have shown that the longer the molecular chains of a conjugated polymer, the more π electrons it has, and the lower the activation energy of electrons, the more easily these electrons can be delocalized, hence the better the electrical conductivity.
2. Doping and conductivity of conjugated polymer. Although conjugated polymers have a strong tendency to be conductive, the conductivity is not high. In the example of polyacetylene, if completely free of impurities, the conductivity of polyacetylene would be very small. The addition of iodine or arsenic oxide (AsO_5) as electron acceptor in polyacetylene facilitates the π electrons of polyacetylene to transfer to receptors, and the conductivity can be increased to 10^4 Ω^{-1} • cm^{-1}, almost reaching the level of conductive metal. On the other hand, because of the strong electron affinity of polyacetylene, it can accept electrons from electron donors such as alkali metal to increase the conductivity. The method of adding electron donor or acceptor to improve the electrical conductivity of conjugated polymer is called "doping." Different from doping in inorganic semiconductors, the doping concentration in conjugated polymers can be very high, up to the maximum of 0.1 dopant molecule per node of a polymer chain. With increasing doping concentration, the conductivity of doped polymers can change from semiconductor to metal.

   Doping can be implemented by chemical and physical methods. Chemical doping includes gas phase doping, liquid phase doping, electrochemical doping, and photon-induced doping. Physical doping is mainly ion implantation. There are many types of dopants; here are some commonly used species:
   (a) Electron acceptor
   Halogen: Cl_2,Br_2,I_2,ICl,ICI_3,IBr,IF_5
   Lewis acid: PF_5,As,SbF_5,BF_3,BCI_3,BBr_3,SO_3
   Proton acid: HF,HCl,HNO_3,H2SO_4,$HCIO_4$,FSO_3H,$ClSO_3H$,$CFSO_3H$
   Metal compounds: TaF_5, WFs, BiF_5, $TiCl_4$, $ZrCl_4$, $MoCl_5$, $La(NO_3)_3$, $Ce(NO_3)_3$
   Organic compounds: TCNE, TCNQ, DDQ

   (b) Electron donor
      Alkaline metal: Li, Na, K, Rb, Cs
      Electrochemical doping agent: R_4N^+,R_4P^+ (R = CH_3, C_6H_5)
3. Application of conductive polymers
   (a) Making transparent conductive films, either colored or colorless, for touchscreen sensors, transparent electrodes, transparent switches, and other applications.
   (b) As the electrode material in batteries to replace metal or graphite electrodes. It is easy to process, lightweight, and of high specific energy.
   (c) For electromagnetic shielding.
   (d) As an antistatic additive to avoid electrostatic charge accumulation.

Though they are widely used in the above applications, structural conductive polymers are generally unstable in air. Their conductivity degrades with time. There are also other issues, such as the manufacturing costs, material inconsistencies, toxicity, poor solubility in solvents, and inability to melt. However, recent research in structural conductive polymers has made considerable progress, with better electrical and physical properties and lower costs.

2.2.3.2 Composite Conductive Polymer

Composite conductive polymer is a class of polymers that incorporates a large amount of conductive materials through dispersion or lamination. Dispersion is the most used method of making composite conductive polymers.

Unlike structural conductive polymers, in a composite conductive polymer the polymer material itself is not conductive; it only serves as an adhesive. Conductivity is realized by the blended conductive materials, such as carbon black or metal powder. Because of the simplicity and low cost to prepare, composite conductive polymers are widely used in conductive rubber, conductive coating, conductive adhesive, electromagnetic wave shielding material, and antistatic material, and they play an important role in many fields.

Theoretically, any polymer materials can be used as a matrix for making composite conductive polymer. The commonly used polymers include polyethylene, polypropylene, PVC, polystyrene, ABS, epoxy resin, acrylic resin, phenolic resin, unsaturated polyester, polyurethane, polyimide, silicone resin. In addition, the matrices of butyl rubber, styrene butadiene rubber, ad acrylonitrile butadiene rubber are also used to make conductive rubbers.

Common conductive fillers are gold, silver, copper, nickel, aluminum, cobalt powder, silver-coated silicon oxide powder, silver-coated glass beads, carbon black, graphite, tungsten carbide, and carbide. In recent years, conductive nanomaterials such as silver nanoparticles, silver nanowires, carbon nanotubes, and graphene have also been used to make composite conductive polymers. Silver is widely used because it has the best conductivity. Carbon black is also widely used, not because of its conductivity, which is not very high, but because of its low cost.

2.2.4 PEDOT

The most well-known and widely used conductive polymer is poly(3,4-ethylenedioxythiophene) or PEDOT, which is based on 3,4-ethylenedioxythiophene monomer. The advantages of this polymer are optical transparency in its conducting state, high stability, moderate band gap, and

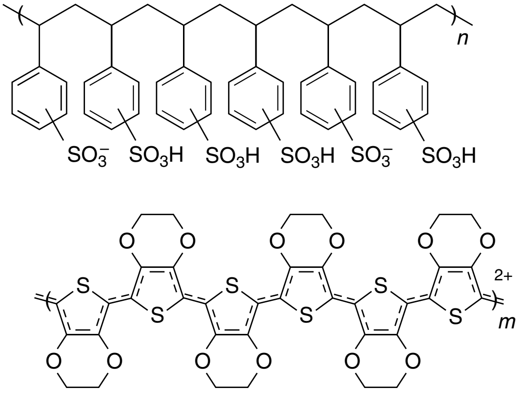

Figure 2.1 Structure of PEDOT:PSS

low redox potential. The main disadvantage is its poor solubility, though this can be partly circumvented by the PEDOT:PSS composite (poly(3,4-ethylenedioxythiophene):polystyrene sulfonate); its structure is shown in Figure 2.1. PEDOT:PSS is a mixture of two ionomers. One component is made of sodium polystyrene sulfonate. Part of the sulfonyl groups are deprotonated and carry a negative charge. PEDOT is the other component, which is a conjugated polymer and carries positive charges.

PEDOT:PSS is a transparent conductive polymer with high ductility. AGFA used to coat 200 million photographic films per year with a thin, extensively stretched layer of virtually transparent and colorless PEDOT:PSS as an antistatic agent to prevent electrostatic discharges and humidity conditions during production and normal film use.

If organic compounds, including high boiling solvents like methylpyrrolidone, dimethyl sulfoxide, sorbitol, ionic liquids, and surfactants, are added, the conductivity of PEDOT:PSS can be increased by 2–3 orders of magnitudes [9]. This makes it suitable as a transparent electrode for use in touchscreens, OLEDs, and electronic paper to replace the traditional indium tin oxide (ITO), the popular inorganic transparent electrode material. Due to the high conductivity—up to 1000 S/cm is possible—it can be used as a cathode material in capacitors to replace manganese dioxide or liquid electrolytes.

The conductivity of PEDOT:PSS can also be significantly improved by post-treatment with various compounds such as ethylene glycol, dimethyl sulfoxide (DMSO), salts, zwitterions, cosolvents, acids, geminal diols, and amphiphilic fluoro-compounds. Recently, conductivity of more than 3000 S was observed on PEDOT:PSS treated with sulfuric acid. This conductivity is comparable to that of ITO.

PEDOT:PSS is generally applied as a dispersion of gelled particles in water. A conductive layer is obtained by spin coating a layer of the dispersion on the surface of glass and driving out the water by heat. Special PEDOT:PSS inks and formulations were developed for different coating and printing processes. Water-based PEDOT:PSS inks are mainly used in slot die coating, flexography, rotogravure, and inkjet printing. If a high viscous paste and slow drying is required, like in screen printing, PEDOT:PSS can be supplied in high boiling solvents like propanediol. Dry PEDOT: PSS pellets, which are redispersable in water and solvents such as ethanol to increase drying speed during printing, can be produced with a freeze-drying method.

Finally, to overcome degradation to ultraviolet light and high temperature or humidity conditions, UV stabilizers for PEDOT:PSS are also available. Commercially available PEDOT:PSS is produced by Heraeus with the trade name Clevios and by AGFA with the trade name Orgacon.

2.3 Printable Organic Small Molecular Semiconductors

Organic semiconductor materials can be divided into two categories according to their molecular weights: one is organic small molecules, including conjugated oligomers and some fused ring molecules; the other is polymers, mainly the amorphous conjugated polymers. They can also be divided into p-type materials, mainly with hole carriers, and n-type materials, mainly with electron carriers. According to their energy level structures, p-type organic semiconductors have low ionization potential (IP) and the highest occupied molecular orbit (HOMO) in order to facilitate hole injection, and n-type organic semiconductors have high electron affinity (EA) and the lowest unoccupied molecular orbit (LUMO) in order to facilitate electron injection.

The charge transport mobility of organic semiconductor materials is influenced by the following factors:

1. The band structure of molecules in solid state should have enough molecular orbital overlap to ensure that the charge transferring between adjacent molecules does not have to overcome a high energy barrier.
2. Organic molecules in the solid state can form compact, orderly stacking, which facilitates the charge transport between molecules.
3. Molecule energy level matches that of electrode material to facilitate charge injection from electrodes.
4. In order to reduce the leakage current and to improve the on/off ratios of the device current, the intrinsic conductivity of the semiconductor should be as low as possible.

The organic materials that can meet the above requirements are basically plane-conjugated small molecules composed of an aromatic unit, and most are fused aromatic compounds and oligomers containing conjugated structure.

Organic small molecules can be easily purified, which reduces the damage of impurities to the integrity of crystal and can reach the required purity to fabricate devices. The plane structure greatly reduces the energy barrier between molecules, which is beneficial to the high speed transport of charge carriers. It can easily form self-assembled polycrystalline film or single crystals, and the mobility of field-effect transistors made from organic small molecules can be greatly improved.

When making transistors by printing, the organic small molecules must be processed in solutions and should be able to form high quality film as well as be environmentally stable. However, the solution form of organic small molecules is generally of low viscosity. They are not easily processed into high quality films and most of the organic small molecular semiconductors are sensitive to environment. It is a great challenge to design and synthesize printable organic small semiconductor molecules. In the following sections, three types of small molecular semiconductors will be introduced: the fused aromatic compounds, heterocyclic sulfur compounds, and oligothiophenes, together with some other high mobility materials.

2.3.1 Fused Aromatic Compounds

Fused ring compounds have rigid plane conjugate structure, lower energy of ground state to excited state, and can easily form compact and ordered thin films, which enables strong electronic interaction between the molecules. Acenes (e.g., anthracene, tetracene, pentacene, and rubrene) are the representative materials (Fig. 2.2).

Rubrene (3 in Fig. 2.2), that is 5, 6, 11, 12-tetraphenyl tetracene, is an important acene and has very high carrier mobility. In 2004, Sundar et al. [10] successfully prepared organic field-effect transistors (OFETs) from rubrene crystals and achieved mobility of 15.4 $cm^2 \cdot V^{-1} \cdot s^{-1}$ along the *b* axis and 4.4 $cm^2 \cdot V^{-1} \cdot s^{-1}$ along the *a* axis, which represents the best OFET at that time. However, due to the presence of phenyl substituent, the crystalline structure of rubrene tends to be in random and poor repeatability; it is difficult to prepare highly ordered rubrene thin film through common solution processing or vacuum evaporation. In 2005, Stingelin-Stutzmann et al. [11] dissolved rubrene, polystyrene of ultrahigh relative molecular weight, and diphenyl anthracene in toluene and obtained high quality rubrene polycrystalline thin films with spin coating and subsequent heat treatment. The fabricated organic transistor had mobility reaching 0.7 $cm^2 \cdot V^{-1} \cdot s^{-1}$. This method provided a new approach to fabricate high mobility organic transistors through solution processing of organic small molecules.

Pentacene (2 in Fig. 2.2), a polycyclic aromatic compound consisting of five linearly fused benzene rings, is the most widely studied organic semiconductor material. As a single crystal, pentacene molecules present a herringbone packing motif, with vertical distance of about 0.259 nm between adjacent parallel molecules, which results in strong intermolecular electronic interactions. As early as 1997, Lin et al. [12] prepared organic field-effect transistors with pentacene and achieved mobility over 1.5 $cm^2 \cdot V^{-1} \cdot s^{-1}$. The performance of pentacene transistors has since been improved progressively by optimization of the dielectric layer, thin-film growth conditions, and the device structure. Through reducing the surface roughness of the dielectric layer and optimization of polycrystalline thin-film growth conditions, organic transistors with mobility approaching 5 $cm^2 \cdot V^{-1} \cdot s^{-1}$ was achieved, and RFIDs were successfully made for microwave frequency identification [13]. In 2004, Jurchescu et al. [14] made single crystal pentacene with ultrahigh purity and achieved mobility as high as 35 $cm^2 \cdot V^{-1} \cdot s^{-1}$.

However, the poor solubility of pentacene in common organic solvents, as well as its poor environmental stability in air, hindered its practical application. Considerable research effort was focused on functionalizing the compounds, such as introducing thiophene or selenium ring to pentacene to increase its stability, as summarized in Figure 2.3. Laquindanum et al. [15] synthesized ADT with thiophene instead of benzene at both ends of pentacene (4 in Fig. 2.3),

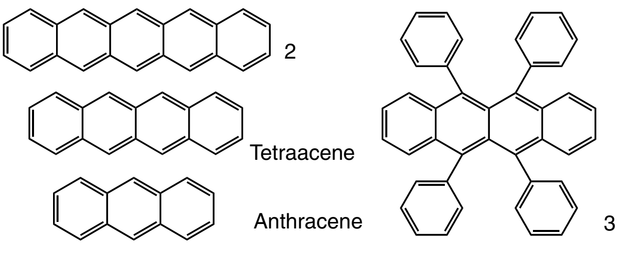

Figure 2.2 Molecule structure of acenes and rubrene

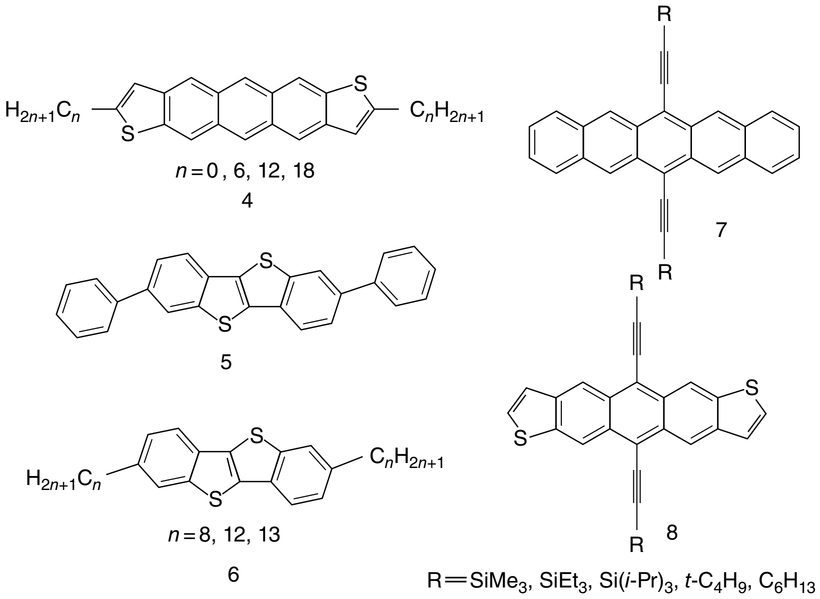
$H_{2n+1}C_n$
C_nH_{2n+1}
S
n = 0, 6, 12, 18
4
5
n = 8, 12, 13
6
R
7
8
R = SiMe$_3$, SiEt$_3$, Si(i-Pr)$_3$, t-C$_4$H$_9$, C$_6$H$_{13}$

Figure 2.3 Pentacene derivatives 4–8

and the structure can be added as functional groups to improve the solubility of pentacene. The resulting hole mobility reached 0.15 $cm^2 \cdot V^{-1} \cdot s^{-1}$. In 2006, Takimiya et al. [16] synthesized diphenyl substituted BTBT (5 in Fig. 2.3), and its thin-film transistors exhibited mobility up to 2 $cm^2 \cdot V^{-1} \cdot s^{-1}$ and were fairly stable in air. In 2007, Ebata et al. [17] synthesized a series of soluble materials, Cn-BTBT (6 in Fig. 2.3), with high mobility of 3.9 $cm^2 \cdot V^{-1} \cdot s^{-1}$ [18], which opened a new direction to improve solubility and stability of ancene materials.

Anthony et al. [19] synthesized a series of substituted acene compounds (7, 8 in Fig. 2.3) by introducing silicon alkynyl at the C6/C13 positions of ADT and pentacene. They adjusted the molecular packing motifs in the crystals through changing the sizes of different substituted groups, in order to improve the carrier's transport and solubility (Fig. 2.4). This attempt was very successful, and one of the materials with the best performance was TIPS-pentacene. Different from a herringbone or lamellar arrangement in previous acenes, a 2D "brick-wall" arrangement of pentacene molecules was found in the crystals of TIPS-pentacene, which resulted in the highest mobility. TIPS-pentacene has good solubility, and the hole mobility of transistors prepared by solution process reached 1.42 $cm^2 \cdot V^{-1} \cdot s^{-1}$ [20], which was very close to that prepared by vacuum deposition. Although this material exhibited poor photon stability, easy photo isomerization, and other problems, it is one of the printable organic semiconductor materials with the best overall performance at present and has been widely used to benchmark the performance of new printable organic electronic materials and for printed transistors.

Naphthalene diimides and perylene diimides (Fig. 2.5) are currently the most stable n-type semiconductor materials with high mobility, and the introduction of alkyl or fluorinated alkyl on the N atom can effectively improve both the solubility of materials and the stability of devices. The devices based on this type of material are fairly stable in air, whereas most other n-type organic transistors can only work in a high vacuum or inert atmosphere. Therefore,

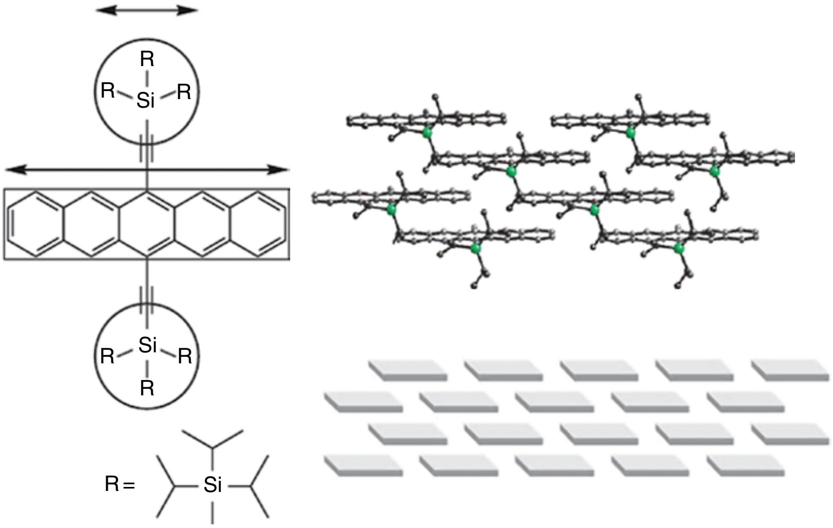

Figure 2.4 The molecular structure of TIPS-pentacene and its molecular packing motifs

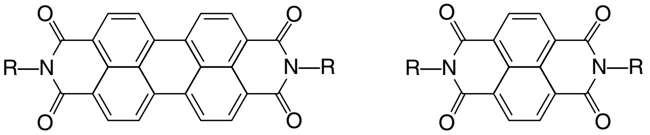

9a R=C_8H_{17}

9b R=$C_{13}H_{27}$

9c R=$CH_2C_2F_7$

10a R=cyclohexyl

10b R=C_6H_{13}

Figure 2.5 N-type semiconductor materials: perylene diimides and naphthalene diimides

these two materials were studied the most among all n-type materials. Under optimized process conditions, the electron mobility of thin films for 9a [21], 9b [22], and 9c [23] all reached over 1.0 $cm^2 \cdot V^{-1} \cdot s^{-1}$.

2.3.2 Heterocyclic Sulfur Compounds and Oligothiophenes

Because of the five ring units of thiophene, the neighboring molecules in oligothiophenes present a zigzag inverse arrangement. Because the H atoms between the adjacent units have almost no steric interaction, oligothiophenes in the solid phase are more likely to form high intramolecular planar structure and intermolecular close packing (shown in Fig. 2.6). In addition, the S atom of thiophene has high electronic polarization and is able to induce various interactions, such as van der Waals forces, weak hydrogen bonds, and S-S interactions, which could change the packing motifs or enhance intermolecular interactions. Therefore, the compounds containing thiophene in the solid state usually have high carrier mobility and

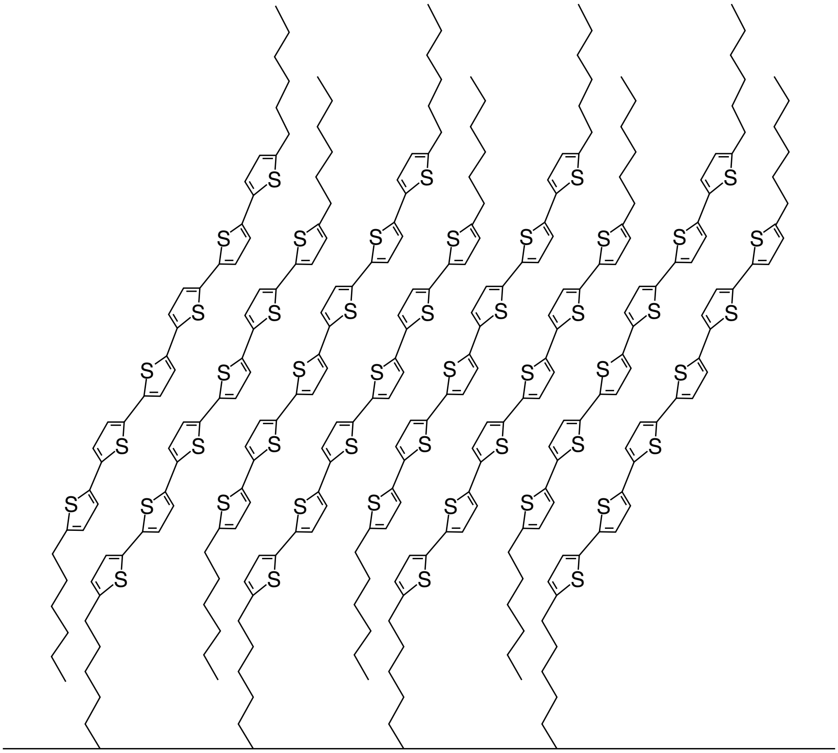

Figure 2.6 Structure of oligothiophene and its packing motif on the surface of substrate

are widely used in devices that require high carrier mobility, such as organic thin-film transistors and organic solar cells.

The oligothiophenes commonly used to make organic transistors are mostly tetramers and hexamers (shown in Fig. 2.7). It has been found that the introduction of alkyl at the end of thiophene can improve the orderliness of thiophene films and significantly increase the field-effect mobility. For instance, the μ_h of sexithiophene (α-6T) is generally in the order of 10^{-2} $cm^2 \cdot V^{-1} \cdot s^{-1}$. By adjusting the length of the alkyl chains, the structure of devices, and the growth conditions of thin films through the introduction of alkyl, it can be increased to 1.1 $cm^2 \cdot V^{-1} \cdot s^{-1}$ [24].

Due to the narrow gap (Eg) and the high HOMO energy level, the oligothiophenes can be easily oxidized in air, which leads to a decrease in device stability. For this reason, researchers adopted diphenyl and phenanthrene instead of oligothiophenes as end-capped groups, which regulated the energy level of molecules and improved the thermal stability of materials. Organic transistors with good stability and high mobility were obtained [25]. For example, the films of dithiophenes with phenanthrene end-capped rings exhibited mobility over 0.1 $cm^2 \cdot V^{-1} \cdot s^{-1}$. Moreover, no obvious degradation for the device was observed after 1 month of storage in air. Thiophene derivative (13 in Fig. 2.7) [26] can be obtained from oligothiophenes with anthracene as end-capped groups, having hole mobility of 0.5 $cm^2 \cdot V^{-1} \cdot s^{-1}$.

Generally, oligothiophenes are p-type materials. By introduction of fluorine-containing alkyl chains or aromatic groups, they can be converted into n-type materials and show electron

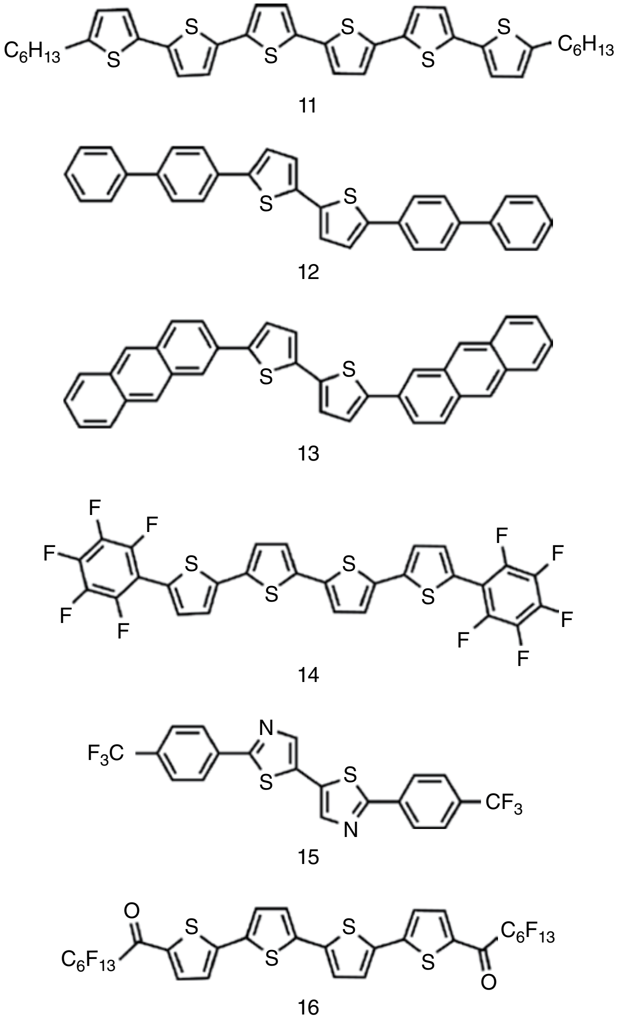

Figure 2.7 Heterocyclic sulfur compounds and oligothiophenes

transfer properties. However, the devices made by this kind of material are more sensitive to air, and the electron mobility measured in air is only 1/5–1/10 of that in vacuum. Compound 14 in Figure 2.7 is relatively stable in air, with its electron mobility of 0.5 $cm^2 \cdot V^{-1} \cdot s^{-1}$. The study found that only those molecules with end-fluoroarene groups were resistant to water and oxygen and resulted in relatively stable devices. In 2005, Yoon et al. [27] successfully achieved bipolar charge transport from a single material with the introduction of carbonyl at the end of thiophene tetramers (16 in Fig. 2.7), and its electron mobility could reach 0.6 $cm^2 \cdot V^{-1} \cdot s^{-1}$ in vacuum. Sulfur and nitrogen containing heterocyclic have a good effect on the stability and mobility of n-type semiconductors, and the electron mobility of trifluoromethylphenyl-substituted dithiazole (15 in Fig. 2.7) [28] can reach 1.83 $cm^2 \cdot V^{-1} \cdot s^{-1}$ at room temperature.

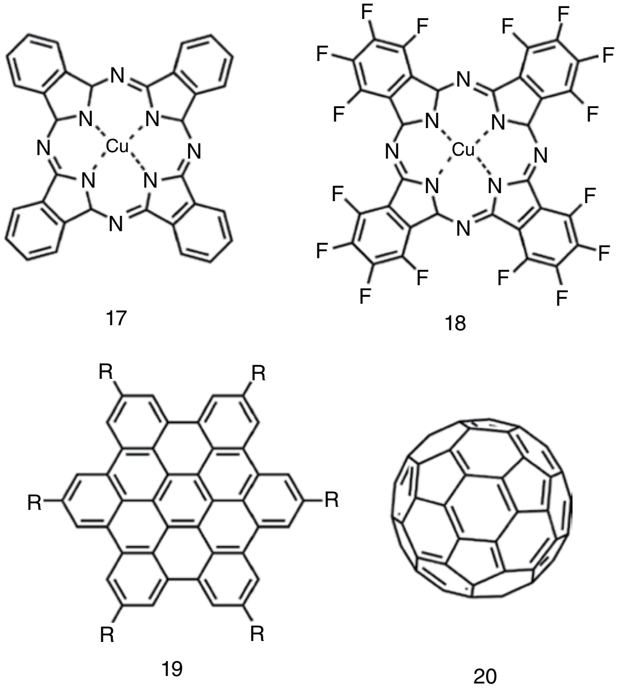

17

18

19

20

Figure 2.8 Molecular structures of high mobility discotic compounds

2.3.3 Other Materials with High Mobility

The copper phthalocyanines (shown in Fig. 2.8) are important materials for organic transistors with high mobility. The maximum mobility of single crystal copper phthalocyanine [29] could reach up to 1 $cm^2 \cdot V^{-1} \cdot s^{-1}$. Copper phthalocyanine and perfluorinated copper phthalocyanine are representative molecules. Through dielectric layer modification, thin-film growth control, and double layers of phthalocyanine, organic transistors with mobility at over 0.1 $cm^2 \cdot V^{-1} \cdot s^{-1}$ were fabricated and worked in air for more than 10,000 h [30]. In addition to perylene diimides, perfluorinated copper phthalocyanine is also a stable n-type organic semiconductor material, with electron mobility of 0.05 $cm^2 \cdot V^{-1} \cdot s^{-1}$ or so [31].

Alkyl-substituted hexabenzocoronenes are important discotic fused ring compounds that can form a stable hexagonal liquid crystalline phase; their mobility is very high along the direction of cylindrical stacking. Recently, through continuous optimization of film-forming conditions, device structure, and control of molecular orientation, Pisula et al. [32] successfully made organic transistors with hole mobility of over 0.01 $cm^2 \cdot V^{-1} \cdot s^{-1}$ based on hexabenzocoronene derivatives.

Fullerene (C_{60}) and its derivatives are important n-type organic semiconductors, with extraordinarily high electron mobility. OFETs with fullerene as the active layer showed mobility as high as 6 $cm^2 \cdot V^{-1} \cdot s^{-1}$ [33] but degraded rapidly when exposed to air, hence are not practical to organic transistors.

2.4 Printable Polymeric Semiconductor

The discovery of conductive polymers has opened up a new research field. One of the most remarkable research directions is polymer field-effect transistors (PFETs). The mobility of PFETs has exceeded $1\,cm^2{\cdot}V^{-1}{\cdot}s^{-1}$ with an on/off ratio more than 10^6, comparable to that of amorphous silicon.

The main reasons that PFETs have attracted so much attention are, first, polymers are of good flexibility, which renders them the most promising materials for flexible devices (such as plastic circuits and electronic papers); and second, polymers are suitable for low temperature large-area solution processing. In addition, polymers are richly available with wide varieties, and the properties of polymer semiconductors can be adjusted conveniently through appropriate chemical modification. Developments in recent years showed that polymer-based transistors have huge potential application in smart labels, identification cards, memory, sensors, flat-panel displays, and so forth.

Generally, if polymer transistors are to be practical in electronic circuits, their mobility and on/off ratio should be at least in the range of 0.1–$1\ cm^2 \bullet V^{-1} \bullet s^{-1}$ and 10^6–10^8, respectively. At present, the mobility and on/off ratio of polymer semiconductor materials can meet those requirements. Certainly, it is still a main focus in this field to further improve the mobility and on/off ratio of polymer transistors.

From the polymer design point of view, a suitable polymer semiconductor for transistors should have the following properties:

1. In order that charge carriers can effectively inject into polymer material at the applied voltage, the molecular orbital energy should match the work function of the electrode to achieve better ohmic contact.
2. In polymer semiconductors, the charge transport generally occurs by a molecule-to-molecule hopping mechanism; consequently, an activation barrier is associated with each intermolecular carrier transfer. Therefore, the molecular outer orbits should have enough overlap, so as to reduce the energy barrier when charges transfer between adjacent molecules. If the molecular outer orbits have no or little overlap, the carrier is almost impossible to transport in this system due to the high energy barrier.
3. The orientation (conjugate direction) of polymer molecules in PFETs should be in the same direction as the current flow. In fact, the conjugate direction of polymer relative to substrates has great influence on the mobility; the π-π stacking parallel to substrates is favorable to carrier transport [34].

As for practical semiconductors, electrical, optical, and chemical stability must be considered. Good solubility and film-forming ability are also required for the large-area and low cost solution process.

A major problem that restrains the development of PFETs is the difficulty in purification of polymers; they cannot be purified using the same methods as for small molecules, such as sublimation and chromatography. In addition, most polymers tend to form amorphous films (poor intermolecular π-π overlap) and find it difficult to form ordered crystalline films. In general, the mobility of PFETs is about 10^{-6}–$10^{-4}\ cm^2{\cdot}V^{-1}{\cdot}s^{-1}$, which is several order of magnitude lower than that of organic small molecules.

2.4.1 P-type Polymer Semiconductors

P-type polymer semiconductors are the materials with holes as the majority of carriers. For p-type materials, the HOMO energy needs to match the work function of electrodes to reduce the hole injection barrier. At present, the most studied p-type materials are polythiophenes and polyfluorenes (PFs) (Fig. 2.9).

2.4.1.1 Sulfur-containing Heterocyclic Polymeric Semiconductors

The first PFETs were prepared using polythiophene (PT) as the active layer [35]. In fact, as early as 1982, the electrical properties of polymers such as PT had drawn a lot of attention [36]. Subsequently, poly(3-alkylthiophene) (P3AT) compounds became a focus due to their good solubility and stability [37]. In 1993, McCullough et al. [38] studied the relationship between structure and photoelectric properties of P3AT compounds in detail. According to the positions of the alkyl substituents in P3AT, three random couplings exist (Fig. 2.10): head to head (HH), tail to tail (TT), and head to tail (HT). The most notable one is HT-P3AT, namely, regioregular P3AT. For regioregular P3ATs all the substituents are on the 3 positions, while a regiorandom polymer can have substituents on both the 3 and 4 positions [39]. As a result, regiorandom P3AT does not have well-ordered morphology, and its mobility is usually in the range of 10^{-7}–10^{-4} cm^2·V^{-1}·s^{-1} [40]. The mobility of P3HT field-effect transistors was only 10^{-5}–10^{-4} cm^2·V^{-1}·s^{-1} [41], while that of regioregular poly(3-hexaylthiophene) (RR-P3HT)

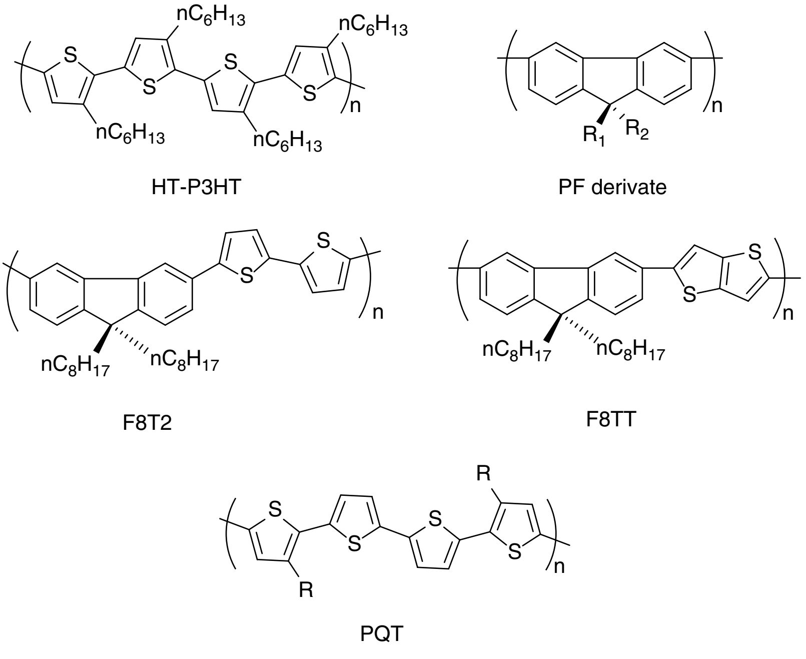

HT-P3HT

PF derivate

F8T2

F8TT

PQT

Figure 2.9 Structure of typical p-type materials HT-P3HT, PF derivative, F8T2, F8TT, and PQT

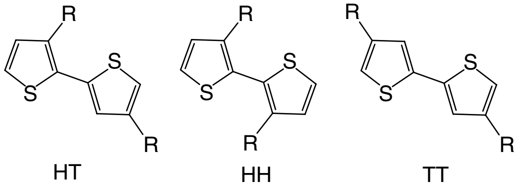

Figure 2.10 Couplings of 3-alkylthiophene in P3ATs

[42] and poly (3, 3’-dialkyltetrathiophene) (PQT) [43] based devices reached or exceeded 0.1 $cm^2 \cdot V^{-1} \cdot s^{-1}$, with on/off ratio > 10^6 [44], which is close to that of amorphous silicon transistors.

Extensive research on PTs has played a positive role in the development of both theory and practice of PFETs. P3ATs as organic semiconductors for OFETs have many advantages; the most important one is their good crystallinity. As early as 1992, people found P3ATs tended to form planar microcrystalline, whereby stacks of planar thiophene main chains are spaced by the alkyl side chains [45]. Furthermore, it was found that the crystalline of P3ATs was related to the regioregularity of PT backbone. The higher the HT content in molecules, the more crystallinity of polymer [46]. Subsequently, Babel and Jenekhe [47] found that the RR-P3ATs and RR-P3HT (hexyl side chain) showed the best mobility. They believed this was because of better self-organization in poly(3-hexylthiophene) compared to other polymers in the series, which is beneficial to carrier transport. For RR-P3HT with high HT content (HT > 91%), when thin film of this polymer is cast onto an SiO_2 or PMMA substrate, the polymer backbone and the alkyl chains in the resulting film tend to be parallel to the substrate, with the π-stacking direction also parallel to the substrate, which facilitates charge carrier transport in the PT main chains, and the mobility can reach as high as 0.1 $cm^2 \cdot V^{-1} \cdot s^{-1}$. For P3HTs with lower regioregularity, the π-stacking direction in the film is perpendicular to the substrates, and the mobility is only 2×10^{-4} $cm^2 \cdot V^{-1} \cdot s^{-1}$.

A problem that has been troubling the development of polymer transistors is that polymers are difficult to purify. Residual impurities can either dope the polymer, which leads to low on/off ratio, or act as traps that result in low mobility. P3ATs are easily soluble in common organic solvents (chloroform, etc.), and impurities and low molecular weight fractions (with low mobility) are easily removable, which is one of the attractions of P3ATs.

It has been found that the performance of P3ATs is influenced by the following factors:

1. Average molecular weight (M_w). Initially, Trznadel et al. [48] found that the average conjugate length of RR-P3HT increased with the increase of M_w. When studying the relationship between field-effect mobility of RR-P3HT and average molecular weight, Kline et al. [49] found that M_w has a substantial effect on the way the chains pack on each other; in turn, this causes the mobility to vary by at least 4 orders of magnitude. They believed that some of the variations in mobility observed in previous studies were at least in part due to variations in M_w instead of some variables that were reported. After that, Zen et al. [50] found that P3HTs with high M_w have higher mobility. The study on annealing at high temperature confirmed that, at room temperature, the high molecular weight fractions adopt a planar backbone conformation that allows a close interchain contact and an efficient interchain carrier transport, so the field-effect mobility is higher.

2. The length and chemical property of side chains. If the alkyl chain is too long the film matrix can be dominated by the insulating alkyl substituents, resulting in low mobility. In contrast, if the alkyl chain is too short, the polymer has low solubility and poor film-forming ability, resulting in worse performance.
3. The size of side chains. Bulky side chains can lead to poor molecular ordering and low crystallinity and the distance between the PT backbones increases, resulting in lower mobility ($< 10^{-4}$ $cm^2 \cdot V^{-1} \cdot s^{-1}$) [51].
4. The solvents used during film formation. Bao et al. [52] found a mobility close to 0.1 $cm^2 \cdot V^{-1} \cdot s^{-1}$ was obtained using chloroform as solvent when using P3HT as the active layer, while the mobility is only 6×10^{-4} $cm^2 \cdot V^{-1} \cdot s^{-1}$ if THF is used. It might be due to the difference in film quality when different solvents are used [53]. Park et al. [54] used polymer as insulator and also found that a solvent with a solubility parameter closer to that of polymer insulator caused more roughening of PHEMA surface and as a result led to a poorer device performance. Therefore, in their opinion, the solvent with the solubility parameter that is the furthest away from that of polymer insulator should be used for the best device performance.

Another key parameter is the on/off ratio of P3HT devices. For devices prepared and measured in air the on/off ratio is at most several hundred. However, with various sample treatments an on/off ratio can be greatly increased. The useful treatments include (1) thermal annealing under vacuum [52]; (2) protection measures (inert gas, etc.)—for example, the on/off ratio of OFET with P3HT as active layer can reach as high as 10^6–10^8 when prepared under nitrogen atmosphere and coated with a reducing layer; and (3) surface treatment to suppress doping caused by impurity or surface reactive groups from the dielectric layer. When SiO_2 substrates were treated with hexamethyldisilazane (HMDS), the mobility of P3HT (in nitrogen atmosphere) increased from 0.01–0.04 $cm^2 \cdot V^{-1} \cdot s^{-1}$ to 0.05–0.1 $cm^2 \cdot V^{-1} \cdot s^{-1}$, with the on/off ratio also increasing from 10^2–10^4 to $> 10^6$.

OFETs generally have poor stability. The PT semiconductor can possess a relatively low IP and it is easily doped by oxygen, leading to a low on/off ratio caused by high off currents [55]. It is generally believed that photo-oxidation of the thiophene ring by singlet oxygen, which breaks apart the conjugated backbone of PT, results in the degradation of device performance [56]. However, it is also thought that the stability of P3AT devices seems sufficient for applications [57]. Proper encapsulation should prevent or slow down the degradation from oxidation, leading to a long lifetime of devices. Another available approach is chemical modification to PT backbones or the design of more stable compounds (Fig. 2.11) [58]. Ong et al. [43] fabricated stable OTFTs with PQT 12 (in PQT, $R = nC_{12}H_{25}$) under ambient conditions. After annealing at 120–140°C, the mobility reached as high as 0.14 $cm^2 \cdot V^{-1} \cdot s^{-1}$ with an on/off ratio over 10^7. The PQT-12 devices also showed only a slight decrease in performance after being stored under ambient conditions in the dark for 1 month, which is in sharp contrast to the drastic degradation in performance of the RR-P3HT devices under identical conditions. The study demonstrated the ionization potential of PQT is higher than RR-P3HT, which means PQT-12 has significantly greater stability against oxidative doping by atmospheric oxygen than that of P3AT.

2.4.1.2 Phenyl-containing Polymeric Semiconductors

Polymers using fluorine as the building block are widely studied. The most promising PF is based on dioctyl-fluorene copolymerized with thiophene units F8T2, possessing thermotropic

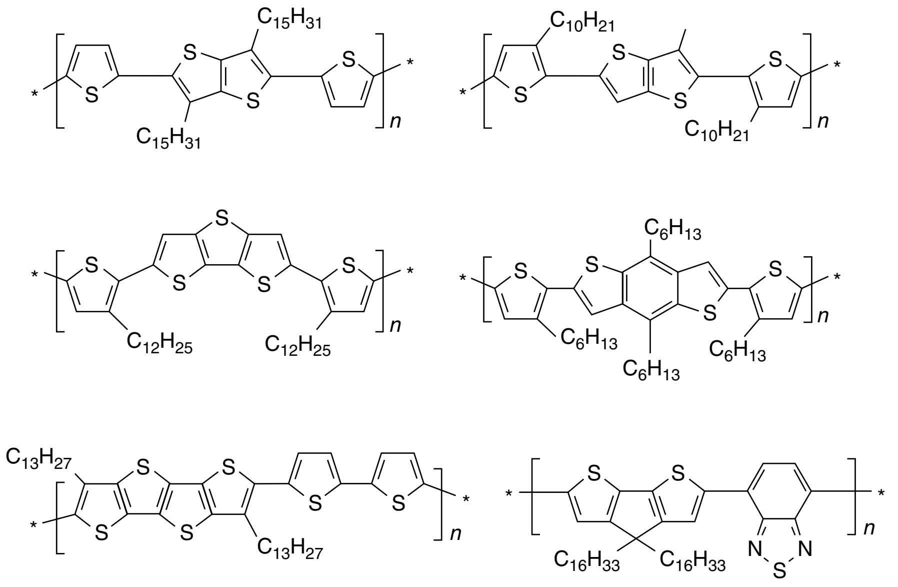

Figure 2.11 Sulfur-containing polymeric semiconductors with high mobility

and nematic liquid-crystalline (LC) phase above 265°C [59]. F8T2 has similar molecular configuration to that of P3HT and is a good material for OFETs. Sirringhaus et al. [60] fabricated OFETs in which the F8T2 chains were aligned parallel to the substrates by annealing at 275–285°C under inert N_2 atmosphere and depositing on mechanically rubbed polyimide. During the quenching step the alignment of polymer chains was preserved and the OFETs showed good stability, with mobility reaching 0.01–0.02 $cm^2 \cdot V^{-1} \cdot s^{-1}$ and on/off ratio > 10^5. This provided an effective way to control polymer microstructure.

Subsequently, Salleo et al. [61] used trichlorosilanes such as octadecyltrichlorosilane (OTS) to chemically modify the SiO_2 surface to form self-assembled monolayers (SAMs) and then deposited F8T2 at room temperature (at this time, F8T2 is in its non-LC phase and does not show any in-plane long range order). The highest mobility of 0.015 $cm^2 \cdot V^{-1} \cdot s^{-1}$ was obtained by treating the dielectric with OTS, which was similar to the highest reported mobility of oriented LC F8T2. Compared with the former method, the films deposited on OTS-treated SiO_2 do not require deposition on a rubbed polyimide alignment layer and high temperature anneal.

Lim et al. [62] conducted additional studies on PF. They hypothesized that high crystallinity can be obtained by introducing thieno [2, 3, 3–108] thiophene group with a high degree of planarity and rigidity instead of bithiophene, which may result in improvement of device performance. The hypothesis was proved by experiment. In contrast to F8T2, the new copolymer F8TT with rigid thieno[2, 3, 3–108]thiophene exhibited more ordered morphology and mobility 3 times higher than that of F8T2 devices. This implicates that better field-effect semiconductor materials may be obtained by improving the planarity and rigidity of molecules. Recently, they synthesized a new copolymer F8Se2, using Se instead of S in F8T2. The study showed F8Se2 is also a thermotropic LC polymer, and the FET device exhibited a hole mobility of 0.012 $cm^2 \cdot V^{-1} \cdot s^{-1}$ and a low threshold voltage of −4 V. They believed that the improved performance of F8Se2 is because of the electron-donating properties of selenium and the resulting in stronger chain interactions between neighboring chains [63]. An outstanding advantage of F8T2 is its good stability. Comparable to P3HT, F8T2 possesses higher ionization potential, therefore greater stability against doping (atmospheric oxygen or other residue impurities).

There are many other FET devices based on PF [64], but the performance (such as mobility of 10^{-5}–10^{-4}cm^2·V^{-1}·s^{-1}) is not ideal. Recently, Chen et al. [65] synthesized a novel soluble and stable poly(9, 9'-dioctylfluorene) (PFO), with mobility of 0.03 cm^2·V^{-1}·s^{-1}. This indicates that there is still much room for improvement of PF materials.

2.4.1.3 Other p-type Polymeric Semiconductors

P3AT and PFO can both easily form microcrystalline, which is probably the reason they exhibit high mobility. The emergence of amorphous polytriarylamine (PTAA) with high mobility overthrew the conventional thinking. PTAA [66] showed good stability and mobility of 10^{-3}–10^{-2} cm^2·V^{-1}·s^{-1}, which suggests that exploration of amorphous materials cannot be ignored while studying microcrystalline materials.

In 2005, Wenping Hu at the Institute of Chemistry, Chinese Academy of Sciences, in cooperation with NTT Corporation in Japan, synthesized a type of polyphenylacetylene (TA-PPE) having not only a certain rigidity but also self-assembled end groups. They prepared Au nanogap electrodes (gap width ≈ 40 nm), combined with electric field-induced self-assembled technology, and successfully fabricated nanodevices based on the conjugated polymers. The nanodevice worked well not only as a nanometer-scale photon switch but also as a p-type transistor. Strong oscillation similar to single-electron charging oscillations was observed in this self-assembled transistor under low temperature. This represented another development direction of polymer transistors—a molecular device [67].

In addition to the materials discussed above, there are many other p-type semiconductors for polymer transistors, such as polyphenazine [68], polyphenothiazine [69], poly 2-methoxy aniline [70], polythienylenevinylene (PTV) [71], and poly(*p*-phenylene vinylene) (PPV) [72]. In addition, the device performance may be improved by blend or copolymerization of several polymers [73, 74]. These polymeric semiconductors showed improvement in stability, or solubility, or other aspects. However, generally speaking, their mobility is still 2–3 orders of magnitude lower than that of P3HT, and the on/off ratio is not ideal. Exploration of new polymeric semiconductors is still a major task ahead.

2.4.2 N-type Polymer Semiconductors

The n-type materials are those in which the majority of carriers are electrons. An essential component of CMOS circuits is n-type FET. The design principle for p-type and n-type semiconductor materials is the same. The only difference is that the energy level of n-type material should facilitate electron injection into the LUMO. In addition, the LUMO level of good n-type semiconductors must be close to the work function of the source and drain electrodes in order to facilitate the electron transport from source to drain in a transistor.

The progress of n-type FETs has lagged far behind p-type FETs. The main reasons include (1) the normally used electrode materials, such as Au and Ag, all have high work function,

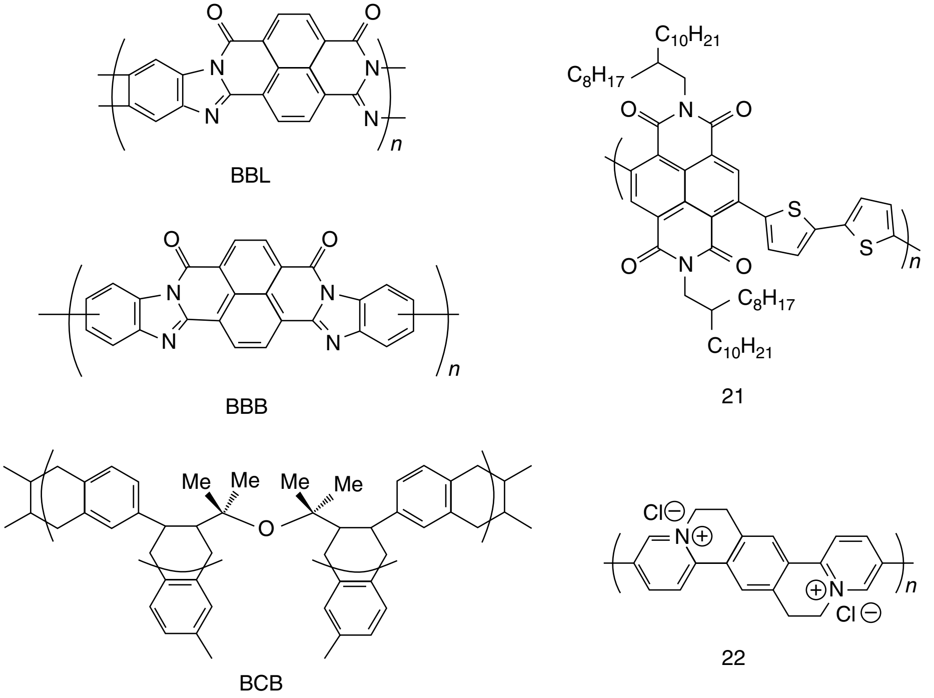

Figure 2.12 Representative n-type polymer semiconductors

which is favorable for the injection of holes instead of electrons. Those materials with low work function, such as Ca, Al, and Mg, are easily oxidized and unstable in ambient conditions. (2) Most n-type organic semiconductors are sensitive to oxygen and water in air and easily form electron traps, leading to the degradation in device performance in air.

Based on a study by de Leeuw et al. [75], only the material with proper electron affinity (in general > 3eV) may be thermodynamically stable for an n-type device. The introduction of hydrophobic groups, thereby reducing water doping in the polymer, can also build stable devices.

Reports on n-type polymer semiconductors are much fewer than those on p-type polymer semiconductors. The intrinsic n-type polymer semiconductors BBL and BBB (Fig. 2.12) were reported by Babel and Jenekhe. Ladder polymer BBL has an extremely high glass transition temperature (T_g > 500°), high thermal stability in air, and forms nematic LC phase in the solid [76], insoluble in aprotic organic solvents and soluble in Lewis acid-forming complex [77]. The rich nitrogen and oxygen heteroatoms (high electronegative elements) in BBL molecules give rise to high electron affinity of ~4.0–4.4 eV, which is potentially a good n-type material.

Babel and Jenekhe fabricated n-type FET from BBL [78] in 2002. They fabricated BBL films from the solution in methanesulfonic acid (MSA) by spin coating or drop casting, because prior studies of charge transport in BBL thin films prepared from Lewis acid/nitromethane solutions showed rather low electron mobility (10^{-6}–10^{-4} cm^2·V^{-1}·s^{-1}). X-ray diffraction (XRD) studies exhibited that the BBL chains in the films were arranged in a layered structure in which the molecular plane is perpendicular to the substrate. The n-channel OTFTs fabricated by spin coating showed an electron mobility of up to 5×10^{-4} $cm^2 \cdot V^{-1} \cdot s^{-1}$ and on/off ratio of 150 (the highest electron mobility in a conjugated polymer at that time). They found the field-effect mobility of electrons in BBL thin films varied by 2 orders of magnitude depending on the thin-film processing method used. Further study showed BBL thin films prepared from MSA had a higher degree of crystallinity than those from Lewis acid solutions. BBL thin films were spin coated from MSA solutions and annealed in air. An electron mobility as high as 0.1 $cm^2 \cdot V^{-1} \cdot s^{-1}$ was realized, with typical n-channel FET output characteristics observed [79]. This demonstrated that electron transport can be as facile as hole transport in conjugated polymer semiconductors. The study also found that carrier mobility in BBL with ladder architecture was enhanced about 10^5 as compared to its nonladder analog BBB, which is instructive to develop semiconductor materials with high electron mobility. Babel and Jenekhe [80] also studied the properties of blends of BBL and another polymer (with low electron mobility). Relatively high mobility (2 orders of magnitude higher than that of the component with lower mobility) was observed with proper proportions of both components.

The main drawback of BBL as an n-type semiconductor is that it is insoluble in common organic solvent, but only soluble in strong protonic acids or Lewis acid, which has limited its practical application. Other than BBL, some new polymers with possible n-type characteristics were also reported [81]. They are potentially good materials for polymer transistors and can overcome the disadvantage of poor solubility of BBL.

Yan et al. [82] developed a promising naphthalene-based polymer (21 in Fig. 2.12) that exhibited an unprecedented high mobility up to 0.85 $cm^2 \cdot V^{-1} \cdot s^{-1}$, on/off ratio of 10^6, and excellent stability in ambient conditions. Interestingly, a water-processed conjugated polymer (22 in Fig. 2.12) was recently developed by Izuhara et al. [83] that demonstrated mobility as high as 3.4 $cm^2 \cdot V^{-1} \cdot s^{-1}$ for gate voltages of 15–20 V, opening a new direction to develop environmentally friendly water-soluble conjugated polymers for electronics.

Chua et al. [84] found that the reason the n-type OFET is difficult to fabricate is because of the effect of insulating materials. The trapping of electrons at the semiconductor-dielectric interface by hydroxyl groups can result in quenching of n-type FET activity; for example, hydroxyl groups present in the form of silanols in the case of commonly used SiO_2 dielectrics. Based on this analysis, they designed compound BCB without hydroxyl groups (Fig. 2.12) and found that most conjugated polymers showed n-type FET characteristics with BCB as gate dielectrics. The electron mobility of polymers such as PFO, PPV, and P3HT were ~10^{-4}–10^{-2} $cm^2 \cdot V^{-1} \cdot s^{-1}$, comparable to those of holes, which breaks the long-held view that the field-effect mobility of electrons is always 10–100 times lower than that of holes. Further study showed other polymers, including polyethylene, poly(methyl methacrylate), and parylene, can also be used as dielectrics for n-type FET.

2.4.3 Ambipolar Transistor and Related Polymer Materials

Ambipolar OFET and its semiconductors with high mobility have been an important field of research. The carrier of ambipolar OFET can be either holes or electrons. By alternating gate bias voltage, an ambipolar OFET can show either p-type FET characteristics (negative gate bias) or n-type FET characteristics (positive gate bias). However, polymer transistors are generally unipolar, that is, either in favor of hole transport or in favor of electron transport. The main difficulty in achieving ambipolar transistor operation is the injection of holes and electrons into

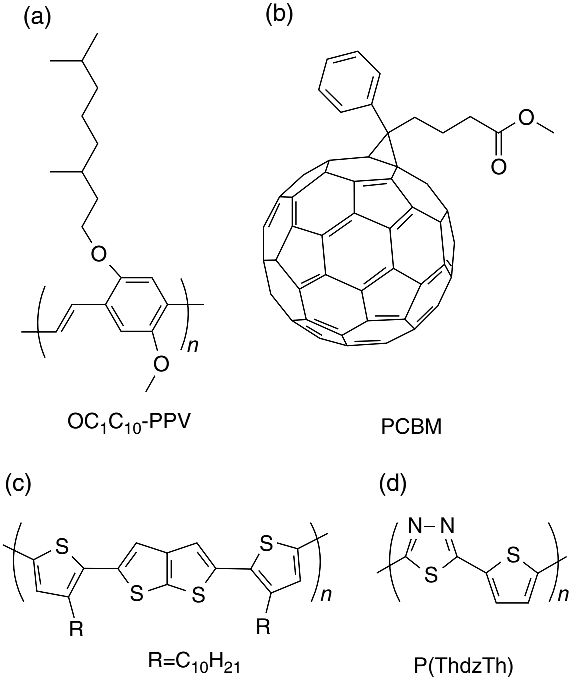

Figure 2.13 Structure of some materials used for ambipolar transistors

a single semiconductor from the same electrode, which needs to have a work function that allows injection of holes in HOMO of the semiconductor and the injection of electrons in LUMO. For an ambipolar device, this will result in an injection barrier of at least half of the band gap energy for one of the carriers. Consequently, matching of the work function of electrodes with energy levels of the semiconductors is crucial to achieve ambipolar transport.

Ambipolar polymer FET is typically achieved with blends of p-type polymers and n-type small molecules (Fig. 2.13). Meijer et al. [85] prepared ambipolar transistors based on heterogeneous blends, consisting of interpenetrating networks of OC_1C_{10}-PPV (p-type semiconductor) and PCBM (n-type semiconductor), in combination with Au electrodes, exhibiting a hole and electron mobility of 3×10^{-5} $cm^2 \cdot V^{-1} \cdot s^{-1}$ and 7×10^{-4} $cm^2 \cdot V^{-1} \cdot s^{-1}$, respectively. The energy levels are as follows: the difference between the HOMO level of OC_1C_{10}-PPV and the work function of Au is only 0.1eV, which will result in an ohmic contact for the hole injection. The difference between the LUMO level of PCBM and the work function of Au is 1.4 eV; however, due to the formation of a strong interface dipole layer at the Au/PCBM interface, this value can be significantly reduced to 0.76 eV, leading to a matched energy level. The authors believed that ambipolar transport is a generic property of organic semiconductors and it is crucial to achieve the matching of the work function of electrodes with the energy levels of semiconductors.

The compound used by Meijer et al. can be solution processed. However, the mobility is low and there is an imbalance between hole and electron transport; in addition, the n-type characteristics must be measured under vacuum conditions. Shkunov et al. [86] made an improvement and prepared ambipolar transistors based on the blend of p-type polymer incorporating thieno[2,3-*b*]thiophene units and PCBM. The highest mobility had been achieved on OTS-treated SiO_2 substrates in the saturation regime, with electron mobility reaching 9×10^{-3} $cm^2 \cdot V^{-1} \cdot s^{-1}$ and hole mobility reaching 4×10^{-3} $cm^2 \cdot V^{-1} \cdot s^{-1}$, higher than that reported by Meijer et al. and with a balance between hole and electron transport.

Ambipolar charge transport was also observed for FETs with an air-stable binary blend of n-type polymer BBL and p-type small molecule copper phthalocyanine, with hole mobility up to 2×10^{-4} $cm^2 \cdot V^{-1} \cdot s^{-1}$ and electron mobility up to 3×10^{-5} $cm^2 \cdot V^{-1} \cdot s^{-1}$ [87].

Recently, Yamamoto et al. [88] reported ambipolar transport of charge transfer (CT)-type copolymer of thiophene and thiadiazole, P(ThdzTh), which contains the electron-donating thiophene unit and the highly electron-accepting thiadiazole unit. A cyclic voltammetry (CV) test showed that the polymer was susceptible to both electrochemical p-doping and n-doping. The measurement of a FET device demonstrated that this polymer can work in either p-type or n-type mode.

2.4.4 Outlook

Polymer field-effect transistors have great potential in the field of low cost, large-area flexible electronics and displays. The performance of PFET has constantly been improved, with some close to that of amorphous silicon. However, the following issues must be resolved if the polymer transistors are to compete with their inorganic counterparts.

1. Improving mobility. Although the mobility of some polymer transistors has reached 0.1 $cm^2 \cdot V^{-1} \cdot s^{-1}$, it is still too low compared with high performance small molecule materials such as pentacene.
2. Developing n-type devices. Regardless of the great progress of n-type devices, they are still lagging far behind p-type in performance. Slow progress in n-type devices will hinder the commercialization of polymer transistors.
3. Understanding the relationship between the structure and performance of PFETs. Currently, the relationship between the mobility and the structure of polymer semiconductor remains undefined; the understanding of the carrier transport mechanism of polymer in PFET is not thorough enough; some phenomena cannot be explained by existing theories and the understanding of the structure-property relationship is still in the early stages.
4. Improving the stability of the device. The stability of polymer transistors is one of the key deciding factors as to whether they can be commercialized. The device stability is not ideal at present; outstanding performance of many devices can only be achieved in an inert atmosphere (even in vacuum), which cannot meet the requirements of practical applications.

There remains great room for development of polymer transistors in materials, manufacturing technology, and theory. Molecular structure optimization of the existing materials or synthesis of new materials is an urgent task for chemists.

The advantage of polymer FET lies in low temperature, large area, and solution processing. The corresponding preparation techniques of PFET are different from that of inorganic materials, which rely on traditional microfabrication, and from small molecular materials, which rely on vacuum deposition. The development of polymer materials for PFETs has to combine with low cost solution-process techniques in order to take full advantage of PFETs.

The techniques for fabrication of polymer transistors have progressed rapidly in recent years. Besides common drop casting and spin coating, many printing techniques have been developed, such as screen printing, inkjet printing, micromolding in capillaries, and microcontact printing. Manufacturing technologies and equipment for printed electronics will be introduced in Chapter 4 of this book. With the advances in manufacturing technologies, polymer transistors will eventually be widely used in printed electronics.

2.5 Other Printable Organic Electronic Materials

2.5.1 Organic Insulating Materials

In OTFTs, insulating materials to form the insulating layer between the semiconductor and metal electrode are of great importance. This is because the carriers in OTFTs mainly transport in the 2–6 molecular layers of organic semiconductor close to the side of the insulating layer. The properties of the insulating layer that influence the OTFT performance are as listed below.

1. The morphology, orientation, and surface roughness of the insulating layer have great influence on the thin-film morphology of semiconductors, crystal size of semiconductors, molecular arrangement, and charge transport [89, 90].
2. The interface properties of the insulating layer (such as hydroxyl, surface energy, and UV irradiation) have great influence on the stability of OTFTs and carrier transport [91, 92].
3. The dielectric constant of the insulating layer is closely linked to threshold voltage and operating voltage of transistors. The threshold voltage can be effectively reduced with high dielectric constant insulating layer materials.
4. The interface of insulating layer to organic semiconductor layer will also affect the carrier injection from the semiconductor layer to electrode. The contact resistances between electrode and the semiconductor layer may vary by more than 10 times at different dielectric/semiconductor interfaces [93]. Therefore, many researchers now believe that research and preparation of insulation materials with good performance, matching with organic semiconductors, is an important direction for the development of OTFTs in the future.

Currently, the organic insulating materials applied in OTFTs include the following categories: polymethyl metharcylate [94], polyimide [95], polyvinylphenol [96], polystyrene [97], polyvinylalcohol [98], and benzocyclobutene [99]. Compared with inorganic insulating materials, they have the following advantages: wide variety of materials, low surface roughness, low surface trap density, low impurity concentration, good compatibility with organic semiconductor, low cost and low temperature solution processing, and compatibility with flexible substrate, thus, the organic insulating materials show great potential in flexible electronics. The formulas of some organic insulation materials are listed in Figure 2.14. OTFTs made from those materials have been reported in literature.

In 1990, Peng et al. [100] first prepared organic OTFTs of α-sexithiophene with organic polymer as the insulating layer. In that paper, the authors pointed out that carrier mobility was

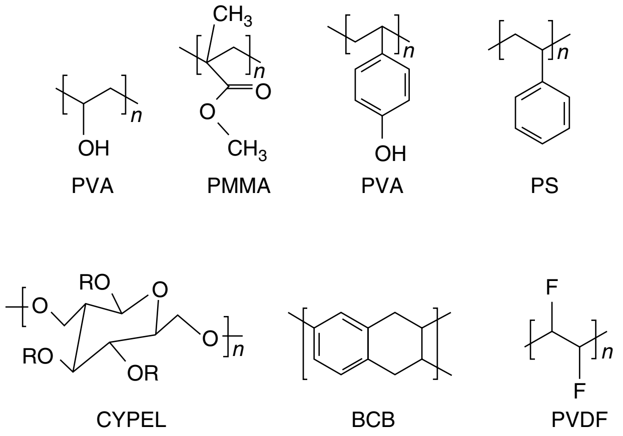

Figure 2.14 Structures of some polymer dielectric materials

reliant on the dielectric of the insulating materials. When using low dielectric polymers such as PMMA and PS for the insulating layer, no field enhancement current was found; when using high dielectric constant polymers such as CYEPL and PVC for the insulating layer, the field current was higher than that of SiO_2. Inspired by this work, they prepared all-organic transistors with CYEPL as the insulating layer and α-sexithiophene as the active layer; the carrier mobility was 0.43 $cm^2{\cdot}V^{-1}{\cdot}s^{-1}$.

In 1997, Bao's group [101] prepared poly(3-hexaylthiophene) transistors by printing on plastic substrates with polyimide as the insulating layer, and the carrier mobility was 0.01–0.03 $cm^2{\cdot}V^{-1}{\cdot}s^{-1}$. A few years later, Gelinck et al. [102] prepared all-organic integrated circuits by printing photoresist as the insulating layer and pentacene and poly(3-hexaylthiophene) as organic semiconductors, with bottom-gate configuration. The carrier mobility was 1×10^{-2} and 3×10^{-3} $cm^2{\cdot}V^{-1}{\cdot}s^{-1}$, respectively.

In 2002, Klauk et al. [103] prepared all-organic thin-film transistors where the contact electrode, insulating layer, and active layer were all deposited by spin coating, and the device showed carrier mobility 0.1 $cm^2{\cdot}V^{-1}{\cdot}s^{-1}$ and on/off ratio 10^3. The researchers then fabricated the devices using the same process, with cross-linked polyethylene phenol as the insulating layer, and the carrier mobility reached up to 3 $cm^2{\cdot}V^{-1}{\cdot}s^{-1}$ [103], which is higher than that of the transistors (1 $cm^2{\cdot}V^{-1}{\cdot}s^{-1}$) with OTS-modified SiO_2 as the insulating layer under the same conditions. Since then many articles on cross-linked polymers, such as photo-crosslinking and thermal-crosslinking (Fig. 2.15) [104], as the insulating layer have been published.

For most of the polymer insulating layers, there exists the hysteresis phenomenon. In order to solve the problems, many researchers adopted high dielectric constant soluble polymers as the insulating layer, or double insulating layers [105]. In 2009, Lee et al. [105] reported the preparation of pentacene transistors, with double insulating layers using high and low dielectric constant materials; the carrier mobility reaches to 1.22 $cm^2{\cdot}V^{-1}{\cdot}s^{-1}$ and the operating voltage is only 5V. From the data reported in literature, the method described above solved the problems to some extent. The performance of organic OTFTs with polymer insulation layer reported in recent years is summarized in Table 2.3.

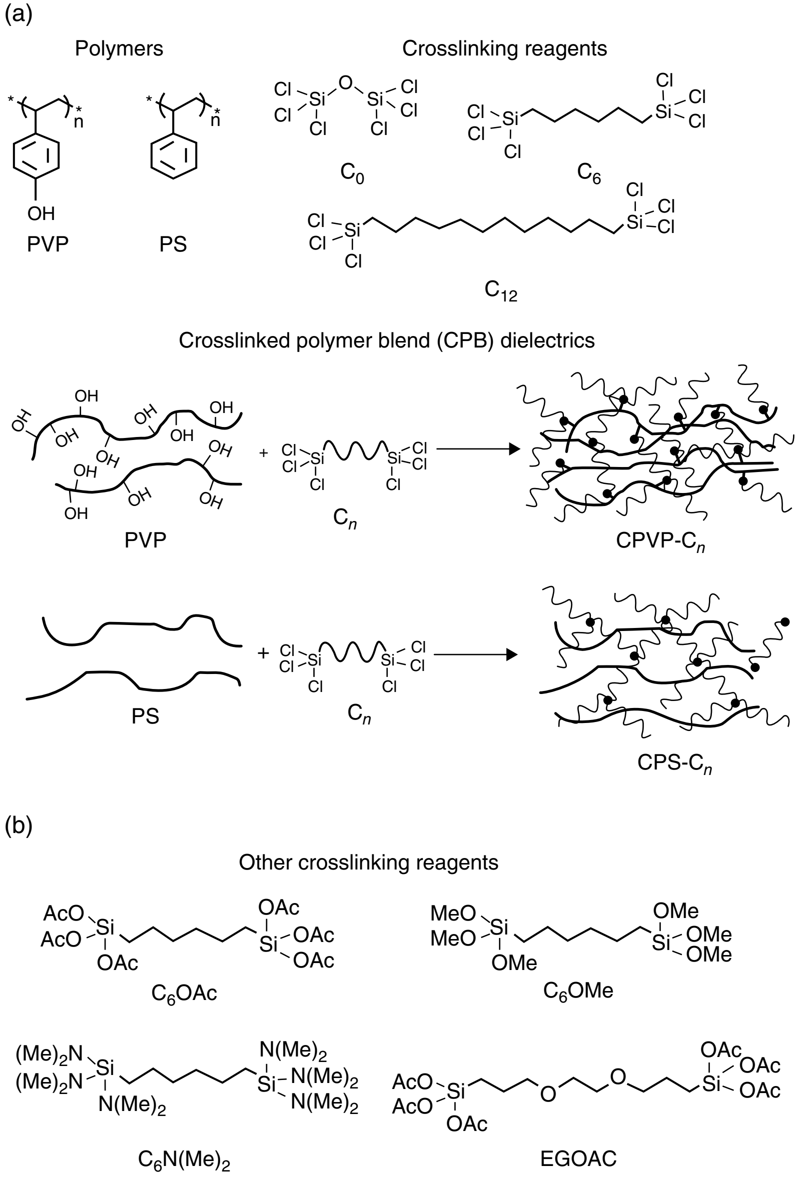
(a)
Polymers
Crosslinking reagents
PVP
PS
C0
C6
C12
Crosslinked polymer blend (CPB) dielectrics
PVP
Cn
CPVP-Cn
PS
Cn
CPS-Cn
(b)
Other crosslinking reagents
C6OAc
C6OMe
C6N(Me)2
EGOAC

Figure 2.15 Schematic diagram of preparation of dielectric layer with cross-linked polymer, cross-linking reaction conditions, and the molecular structure of cross-linking agent

When polymers are used as gate insulating layers, relatively thick layers with thickness exceeding 100 nm are usually formed, resulting in high drive voltage of at least 10 V. However, thinning the gate insulating layers will increase the current that tunnels or leaks through, which may increase power consumption. In 2008, Roberts et al. [106] successfully fabricated OTFTs with a poly(vinyl phenol)-based layer as the gate insulating layer, which

Table 2.3 Performance of OTFTs with polymer insulation

Organic insulating materials	Dielectric constant	Preparation method	Organic semiconductor	μ (cm^2/Vs)	Year
CYEPL	18.5	Casting	α-6T	0.034	1990
	18.5	Casting	α-6T	0.43	1990
	12	Spin coating	P3HT	0.04	2004
	13.3	Casting	pentacene	0.18	2006
	13.3	Casting	F8T2	5.4×10^{-3}	2006
PVA	7.8	Casting	α-6T	9.3×10^{-4}	1990
	5.1	Spin casting	pentacene	0.9	2003
	10	Spin coating	P3HT	0.03	2004
	8	Spin coating	pentacene	0.2	2005
	/	Spin coating	pentacene	1.1	2006
	5	Spin coating	PCBM	0.05–0.2	2005
	6.1	Spin coating	C_{60}	0.16	2008
PI		Printing	α, ω-6T	0.07	1994
		Casting	α-6T	0.01	2000
		In situ reaction	CuPc	0.011	2008
		In situ reaction	pentacene	0.36	2009
		In situ reaction	pentacene	1	2004
BCB		Spin coating	TFB	0.0003	2004
PS	2.5	Spin coating	P(NDI2OD-T$_2$)	0.4	2009
PVP		Spin coating	F8T2	0.02	2000
	4.2	Spin coating	pentacene	0.1	2002
	3.6	Spin coating	pentacene	3	2002
	3.1	Spin coating	pentacene	2.59	2005
		Spin coating	P3HT	0.09	2008
		Inkjet printing	TIPS-pentacene	1	2009
PMMA		Spin coating	α-6T	0.02	1996
	3.2	Printing	P3HT	0.1	1999
	3.5	Spin coating	pentacene	0.241	2007
	3.6	Spin coating	P(NDI2OD-T$_{2)}$	0.45	2009

has a uniform thickness of a few nanometers, and the OTFTs were reported to have drive voltage of 1 V and mobility of 0.4 cm^2·V^{-1}·s^{-1}.

2.5.2 *Organic Materials for Sensors*

Sensors are mainly divided into three categories: (1) physical sensors, which are used to measure physical quantity, such as temperature, humidity, and pressure; (2) chemical sensors, which are used to detect chemicals or monitor chemical reactions with the responses of chemical and physical changes; and (3) biosensors, which as a branch of chemical sensors are used to detect certain chemicals or reflect certain physiological processes through biologically sensitive components.

Compared with inorganic semiconductor and metal oxide sensing materials, organic materials for sensors have the following advantages: (1) freedom of design and synthesis of new materials with new functions for diverse and specific sensing targets; (2) capability of specific molecular recognition especially for chemical and biological sensing; and (3) low cost process especially in regard to printing over a large area.

Organic polymer materials for sensing materials were developed in the 1960s, with electrical, optical, thermal, mechanical, chemical, and biological characteristics, greatly expanding the field of sensor technology. Since optical, electrical, and electrochemical properties of conjugated polymers are sensitive to the external environment, such as temperature, solvent, pH, the state of aggregation, and changes in the chemical environment, they are very suitable as high sensitivity sensor materials. For example, polyvinylidene fluoride (PVDF) and its copolymer materials have excellent radioresistance, electrical insulation, chemical stability, and thermal stability. They can be processed as film by stretching, polarization, and plating electrodes, showing strong piezoelectric effect, electrostriction effect, and pyroelectric effect, which shows a remarkable prospect in sensor applications.

In recent years, scientists have found that a trace of analyte can significantly change the photoelectric properties of conjugated polymers that can be utilized as sensors. Conjugated polymer sensors can be divided into four categories: electrical conductivity sensors, electrochemical potential sensors, light-absorbing sensors, and fluorescence sensors. The first three types are mostly based on conductive conjugated polymers, such as polyacetylene, polyaniline, polythiophene, and polypyrrole, which are widely used to detect metal ions, gas, steam, and other compounds; the conjugated polymers used as fluorescence sensors are photoluminesence materials, such as PPV, polyparaphenylene (PPP), PF, and polyphenylene acetylene (PPE). Currently, the organic fluorescence sensor is one of the most widely used fluorescence sensors and has the fastest response. The main advantage of conjugated polymer fluorescence sensors is that the high conjugacy of the polymer chain can make electrons and energy flow freely within the polymer chain, so that the local perturbation can be amplified within the whole polymer chain, or even the whole system. This amplification mechanism is unique for conjugate polymers and is difficult for small molecular fluorescence sensors to achieve.

The development of conjugated polymer for fluorescence sensors has been incremental. It was initially only for detection of metal ions in inorganic small molecules, then for some organic molecules, and now it has been developed to detect biological macromolecules, such as DNA and protein. As for the detection mechanism, the detection was initially realized by the interaction between simple water-soluble conjugated polymer and quenching with opposite charge, then using specific binding of trap and analyte, by which the selectivity and sensitivity of detection are greatly improved. For the example of sensing biological macromolecules, Dr. Whitten's group [107] and Bazan's group [108] realized the detection of DNA single strands with a specific sequence of base pairs and also detected them with neutral RNA, which is the most advanced study in this area. In their method, the energy transfer mechanism can make the luminous intensity of fluorescein reach up to 25 times the initial signal, which enables the detection limit of target DNA down to 10 picomoles (10^{-11} M).

The emergence of fluorescent sensors is closely related to the progress of supramolecular science in recent years, such as molecular assembly, molecular recognition, host-guest chemistry, the structure of intramolecular conjugated charge-transfer compounds, and the improvement of luminescent performance. On the other hand, their development is also closely linked to many demands from wide disciplines, such as biochemistry, clinical medicine, pharmaceutical chemistry, and many issues encountered in environmental science, which has greatly pushed the development of organic fluorescent sensing technology forward. However, it should be pointed out that the research and development is still in the early stages and there remain many issues and problems to be studied further.

2.6 Summary

Organic electronic materials have attracted much attention in academia and industry in the last few decades. Numerous new organic/polymeric materials along with a large number of new sciences, new manufacturing technologies, and new applications have emerged. However, this is not a mature field yet, as there are many issues remaining to be solved when dealing with practical applications of organic electronics. Some of the key issues include

1. Difficulties in preparing high quality and orderly structured thin films. Organic electronic materials in electronics devices are basically in the form of ultra-thin films. How the organic molecules stack in the film has greater impact on device performance than the material itself. However, the conventional methods for preparing thin film are still costly, slow, and of poor precision. The film quality and the control of molecule stacking are not high enough and precise enough.
2. Stability issue of organic material. The nature of organic materials makes them susceptible to environmental influences such as water, oxygen, or photon irradiation that cause the organic electronic devices to be less stable and repeatable in normal working conditions. To design and synthesize high stability material is still a huge task facing the organic electronics research community. Another possible solution is to develop effective and low cost encapsulation and packaging technologies.

Nevertheless, organic electronic materials, with their simple and low cost manufacturing processes, especially for printing and potentially for large-area flexible electronics, optoelectronics, and sensing applications, are still hotly pursued by many scientific disciplines and industrial sectors. With more R&D efforts pouring into this area, one is reasonably confident to predict that the remaining issues will be solved and the organic electronic industry will grow. Many new and fascinating applications will emerge in the future.

References

[1] Akamatsu H, Inokvchi H, Matsunaga Y. Electrical conductivity of the perylene–bromine complex. Nature 1954;173:168.
[2] Chiang CK, Shirakawa H, Frineher CR. Electrical conductivity in doped polyacetylene. Phys. Rev. Lett. 1977;39:1098.
[3] Tsulnura A, Koezuka H, Ando T. Macromolecular electronic device: field-effect transistor with a polythiophene thin-film. Appl. Phys. Lett. 1986;49:1210.
[4] Tang CW, Vanslyke SA. Organic electroluminescent diodes. Appl. Phys. Lett. 1987;51:913.
[5] Horowitz G, Fichou D, Peng X, Xu Z, Garnier F. A field-effect transistor based on conjugated alpha-sexithienyl. Solid State Commun. 1989;72:381.
[6] Burroughes JH, Bradley DDC, Brown AK. Light-emitting-diodes based on conjugated polymers. Nature 1990;347:539.
[7] Laquindanum JG, Katz HE, Lovinger AJ, Dodabalapur A. Morphological origin of high mobility in pentacene thin-film transistors. Chem. Mater. 1996;8:2542.

[8] Horowitz G, Gamier F, Yassar A, Hajlaoui R, Kouki F. Field-effect transistor made with a sexithiophene single crystal. Adv. Mater. 1996;8:52.

[9] Seung HE, Senthilarasua S, et al. Polymer solar cells based on inkjet-printed PEDOT:PSS layer. Org. Electron. 2009;10:536.

[10] Sundar VC, Zaumseil J, Podzorov V, et al. Elastomeric transistor stamps: reversible probing of charge transport in organic crystals. Science 2004;303:1644.

[11] Stingelin-Stutzmann N, Smits E, Wondergem H, et al. Organic thin-film electronics from vitreous solution-processed rubrene hypereutectics. Nat. Mater. 2005;4:601.

[12] Lin YY, Gundlach DJ, Nelson S, et al. Stacked pentacene layer organic thin-film transistors with improved characteristics. IEEE Electron Dev. Lett. 1997;18:606.

[13] Kelley TW, Muyres DV, Baude PF, et al. High performance organic thin film transistors. Mat. Res. Soc. Symp. Proc. 2003;771;L6.5.1.

[14] Jurchescu OD, Baas J, Palstra TTM. Effect of impurities on the mobility of single crystal pentacene. Appl. Phys. Lett. 2004;84:3061.

[15] Laquindanum JG, Lovinger AJ, Katz HE. Synthesis, morphology, and field-effect mobility of anthradithiophenes. J. Am. Chem. Soc. 1998;120(4):664.

[16] Takimiya K, Kunugi Y, Konda Y, Ebata H, et al. 2,7-diphenyl [1] benzoselenopheno [3, 2-b][1] benzoselenophene as a stable organic semiconductor for a high-performance field-effect transistor. J. Am. Chem. Soc. 2006;128:3044.

[17] Ebata H, Izawa T, Miyazaki E, et al. Highly soluble [1]benzothieno [3, 2-b] benzothiophene (BTBT) derivatives for high-performance, solution-processed organic field-effect transistors. J. Am. Chem. Soc. 2007;129:15732.

[18] Izawa T, Miyazaki E, Takimiya K. Molecular ordering of high-performance soluble molecular semiconductors and re-evaluation of their field-effect transistor characteristics. Adv. Mater. 2008;20:3388.

[19] Anthony JE, Brooks JS, Eaton DL, Parkin SR. Functionalized pentacene: improved electronic properties from control of solid-state order. J. Am. Chem. Soc. 2001;123:9482.

[20] (a)Park SK, Jackson TN, Anthony JE, et al. High mobility solution processed 6, 13-bis(triisopropyl-silylethynyl) pentacene organic thin film transistors. Appl. Phys. Lett. 2007;91:063514. (b)Kim DH, Lee DY, Lee HS, et al. High-mobility organic transistors based on single-crystalline microribbons of triisopropylsilylethynyl pentacene via solution-phase self-assembly. Adv. Mater. 2007;19:678.

[21] Chesterfield RJ, McKeen JC, Newman CR, et al. Organic thin film transistors based on N-alkyl perylene diimides: charge transport kinetics as a function of gate voltage and temperature. J. Phys. Chem B 2004;108:19281.

[22] Tatemichi S, Ichikawa M, Koyama T, Taniguchi T. High mobility n-type thin-film transistors based on N, N′-ditridecyl perylene diimide with thermal treatments. Appl. Phys. Lett. 2006;89:112108.

[23] Gsänger M, Hak Oh J, Könemann M, et al. A crystal-engineered hydrogen-bonded octachloroperylene diimide with a twisted core: an n-channel organic semiconductor. Angew. Chem. Int. Ed. 2010;49:740.

[24] Halik M, Klauk H, Zschieschang U, et al. Relationship between molecular structure and electrical performance of oligothiophene organic thin film transistors. Adv. Mater. 2003;15:917.

[25] Mohapatra S, Holmes BT, Newman CR, et al. Organic thin-film transistors based on tolyl-substituted oligothiophenes. Adv. Funct. Mater. 2004;14:605.

[26] Merio JA, Newman CR, Gerlach CP, et al. p-Channel organic semiconductors based on hybrid acene-thiophene molecules for thin-film transistor applications. J. Am. Chem. Soc. 2005;127: 3997.

[27] Yoon MH, DiBenedetto SA, Facchetti A, et al. Organic thin-film transistors based on carbonyl-functionalized quaterthiophenes: high mobility n-channel semiconductors and ambipolar transport. J. Am. Chem. Soc. 2005;127:1348.

[28] Ando S, Murakami R, Nishida J, et al. N-type organic field-effect transistors with very high electron mobility based on thiazole oligomers with trifluoromethylphenyl groups. J. Am. Chem. Soc. 2005;127:14996.

[29] Zeis R, Ziegrist T, Kloc C. Single-crystal field-effect transistors based on copper phthalocyanine. Appl. Phys. Lett. 2005;86:022103.

[30] Zhang J, Wang J, Wang H, et al. Organic thin-film transistors in sandwich configuration. Appl. Phys. Lett. 2004;84:142.

[31] Bao Z, Lovinger AJ, Brown J. New air-stable n-channel organic thin film transistors. J. Am. Chem. Soc. 1998;120:207.

[32] Pisula W, Menon A, Stepputat M, et al. A zone-casting technique for device fabrication of field-effect transistors based on discotic hexa-*peri*-hexabenzocoronene. Adv. Mater. 2005;17(6):684.

[33] Anthopoulos TD, Singh B, Marjanovic N, et al. High performance n-channel organic field-effect transistors and ring oscillators based on C_{60} fullerene films. Appl. Phys. Lett. 2006;89:213504.

[34] Sirringhaus H, Brown PJ, Friend RH, et al. Two-dimensional charge transport in self-organized, high-mobility conjugated polymers. Nature 1999;401:685.

[35] Forrest SR. The path to ubiquitous and low-cost organic electronic appliances on plastic. Nature 2004;428:911.

[36] Baughman RH, Bredas JL, Chance RR, et al. Structural basis for semiconducting and metallic polymer dopant systems. Chem. Rev. 1982;82:209.

[37] Patil AO, Heeger AJ, Wudl F. Optical properties of conducting polymers. Chem. Rev. 1988;88:183.

[38] McCullough RD, Tristram-Nagle S, Williams SP, et al. Self-orienting head-to-tail poly(3-alkylthiophenes): new insights on structure-property relationships in conducting polymers. J. Am. Chem. Soc. 1993;115:4910.

[39] Bao ZN, Rogers JA, Katz HE. Printable organic and polymeric semiconducting materials and devices. J. Mater. Chem. 1999;9:1895.

[40] Kobashi M, Takeuchi H. Inhomogeneity of spin-coated and cast non-regioregular poly(3-hexylthiophene) films, structures and electrical and photophysical properties. Macromolecule, 1998;31:7273.

[41] Assadi A, Svensson C, Willander M, et al. Field-effect mobility of poly (3-hexylthiophene). Appl. Phys. Lett. 1988;53:195.

[42] Sirringhaus H, Tessler N, Friend RH. Integrated optoelectronic devices based on conjugated polymers. Science 1998;280:1741.

[43] Ong BS, Wu Y, Liu P, et al. High-performance semiconducting polythiophenes for organic thin-film transistors. J. Am. Chem. Soc. 2004;126:3378.

[44] Wu YO, Liu P, Ong BS, et al. Controlled orientation of liquid-crystalline polythiophene semiconductors for high-performance organic thin-film transistors. Appl. Phys. Lett. 2005;86:142102.

[45] Prosa TJ, Winokur MJ, Moulton J, Smith P, Heeger AJ. X-ray structural studies of poly(3-alkylthiophenes): an example of an inverse comb. Macromolecules 1992;25:4364.

[46] Yang C, Orfino FP, Holdcroft SA. Phenomenological model for predicting thermochromism of regioregular and nonregioregular poly(3-alkylthiophenes). Macromolecules 1996;29:6510.

[47] Babel A, Jenekhe SA. Alkyl chain length dependence of the field-effect carrier mobility in regioregular poly(3-alkylthiophene)s. Synth. Met. 2005;148:169.

[48] Trznadel M, Pron A, Zagorska M, et al. Effect of molecular weight on spectroscopic and spectroelectrochemical properties of regioregular poly(3-hexylthiophene). Macromolecules 1998;31:5051.

[49] Kline RJ, McGehee MD, Kadnikova EN, et al. Controlling the field-effect mobility of regioregular polythiophene by changing the molecular weight. Adv. Mater. 2003;15:1519.

[50] Zen A, Pflaum J, Hirschmann S, et al. Effect of molecular weight and annealing of poly(3-hexylthiophene)s on the performance of organic field-effect transistors. Adv. Funct. Mater. 2004;14:757.

[51] Bao Z, Lovinger AJ. Soluble regioregular polythiophene derivatives as semiconducting materials for field-effect transistors. Chem. Mater. 1999;11:2607.

[52] Bao Z, Dodabalapur AD, Lovinger AJ. Soluble and processable regioregular poly(3-hexylthiophene) for thin film field-effect transistor applications with high mobility. Appl. Phys. Lett. 1996;69:4108.

[53] Brown AR, de Leeuw DM, Havinga EE, et al. A universal relation between conductivity and field-effect mobility in doped amorphous organic semiconductors. Synth. Met. 1994;68:65.

[54] Park J, Park SY, Shim SO, et al. A polymer gate dielectric for high-mobility polymer thin-film transistors and solvent effects. Appl. Phys. Lett. 2004;85:3283.

[55] McCulloch I, Bailey C, Giles M, et al. Influence of molecular design on the field-effect transistor characteristics of terthiophene polymers. Chem. Mater. 2005;17:1381.

[56] Abdou MSA, Orfino FP, Son Y, et al. Interaction of oxygen with conjugated polymers: charge transfer complex formation with poly(3-alkylthiophenes). J. Am. Chem. Soc. 1997;119:4518.

[57] Ficker J, von Seggern H, Rost H, et al. Influence of intensive light exposure on polymer field-effect transistors. Appl. Phys. Lett. 2004;85:1377.

[58] (a)Li YN, Wu YL, Liu P, et al. Poly(2,5-bis(2-thienyl)-3,6-dialkylthieno[3,2-b]thioph ene)s-high-mobility semiconductors for thin-film transistors. Adv. Mater. 2006;18:3029. (b)Heeney M, Bailey C, Genevicius K, et al. Stable polythiophene semiconductors incorporating thieno[2,3-b]thiophene. J. Am. Chem. Soc. 2005;127:1078. (c)Li J, Qin F, Li CM, et al. High-performance thin-film transistors from solution-processed dithienothiophene polymer semiconductor nanoparticles. Chem. Mater. 2008:20:2057. (d)Pan H, Wu Y, Li Y, et al. Benzodithiophene copolymer: a low-temperature, solution-processed high-performance semiconductor for thin-film transistors. Adv. Funct. Mater. 2007;17:3574. (e)Fong HH, Pozdin VA, Amassian A, et al. Tetrathienoacene copolymers as high mobility, soluble organic semiconductors. J. Am. Chem. Soc. 2008;130:13202.

[59] Grell M, Redecker M, Whitehead KS, et al. Monodomain alignment of thermotropic fluorene copolymers. Liq. Cryst. 1999;26:1403.

[60] Sirringhaus H, Wilson RJ, Friend RH, et al. Mobility enhancement in conjugated polymer field-effect transistors through chain alignment in a liquid-crystalline phase, Appl. Phys. Lett. 2000;77:406.

[61] Salleo A, Chabinyc ML, Yang MS, Street RA. Polymer thin-film transistors with chemically modified dielectric interfaces. Appl. Phys. Lett. 2002;81:4383.

[62] Lim E, Jung BJ, Lee J, Shim HK, et al. Thin-film morphologies and solution-processable field-effect transistor behavior of a fluorene–thieno[3,2-b]thiophene-based conjugated copolymer. Macromolecules 2005;38:4531.

[63] Kim YM, Lim E, Kang IN, et al. 2D NMR observation of strain-induced β-form in poly[(R)-3-hydroxybutyrate]. Macromolecules 2006;39:4081.

[64] Wang F, Luo J, Yang KX, et al. Conjugated fluorene and silole copolymers: synthesis, characterization, electronic transition, light emission, photovoltaic cell, and field effect hole mobility. Macromolecules 2005;38:2253.

[65] Chen MX, Crispin X, Perzon E, et al. High carrier mobility in low band gap polymer-based field-effect transistors. Appl. Phys. Lett. 2005;87:252105.

[66] Veres J, Ogier S, Lloyd G, et al. Gate insulators in organic field-effect transistors. Chem. Mater. 2004;16:4543.

[67] Hu WP, Nakashima H, Furukawa K, et al. A self-assembled nano optical switcher and transistor based on a rigid conjugated polymer, thioacetyl-end-functionalized poly(para-phenylene ethynylene)s. J. Am. Chem. Soc. 2005;127:2804.

[68] Zhu Y, Babel A, Jenekhe SA. Phenoxazine-based conjugated polymers: a new class of organic semiconductors for field-effect transistors. Macromolecules 2005;38:7983.

[69] Hwang DH, Kim SK, Park MJ, et al. Conjugated polymers based on phenothiazine and fluorene in light-emitting diodes and field effect transistors. Chem. Mater. 2004;16:1298.

[70] Graeff CFO, Onmori RK, Guimaraes FEG, et al. Field effect transistor using poly(o-metoxyaniline) films. Synth. Met. 1999;105:151.

[71] Fuchigami H, Tsumura A, Koezuka H. Polythienylenevinylene thin-film transistor with high carrier mobility. Appl. Phys. Lett. 1993;63:1372.

[72] Hulea IN, Brom HB, Houtepen AJ, et al. Wide energy-window view on the density of states and hole mobility in poly(p-phenylene vinylene). Phys. Rev. Lett. 2004;9316:166601.

[73] Zen A, Saphiannikova M, Neher D, et al. Comparative study of the field-effect mobility of a copolymer and a binary blend based on poly(3-alkylthiophene)s. Chem. Mater. 2005;17:781.

[74] Crouch DJ, Skabara PJ, Lohr JE, et al. Thiophene and selenophene copolymers incorporating fluorinated phenylene units in the main chain: synthesis, characterization, and application in organic field-effect transistors. Chem. Mater. 2005;17:6567.

[75] De Leeuw DM, Simenon MMJ, Brown AR, et al. Stability of n-type doped conducting polymers and consequences for polymeric microelectronic devices. Synth. Met. 1997;87:53.

[76] Song HH, Fratini AV, Chabinyc M, et al. Crystal structure and thin film morphology of BBL ladder polymer. Synth. Met. 1995;69:533.

[77] Jenekhe SA, Johnson PO. Complexation-mediated solubilization and processing of rigid-chain and ladder polymers in aprotic organic solvents. Macromolecules 1990;23:4419.

[78] Babel A, Jenekhe SA. Electron transport in thin-film transistors from an n-type conjugated polymer. Adv. Mater. 2002;14:371.

[79] Babel A, Jenekhe SA. High electron mobility in ladder polymer field-effect transistors, J. Am. Chem. Soc. 2003;125:13656

[80] Babel A, Jenekhe SA. n-Channel field-effect transistors from blends of conjugated polymers. J. Phys. Chem. B 2002;106:6129.

[81] Zhu Y, Alam MM, Jenekhe SA. Regioregular head-to-tail poly(4-alkylquinoline)s: synthesis, characterization, self-organization, photophysics, and electroluminescence of new n-type conjugated polymers. Macromolecules 2003;36:8958.

[82] Yan H, Chen Z, Zheng Y, Newman C, Quinn JR, Dotz F, Kastler M, Facchetti A. A high-mobility electron-transporting polymer for printed transistors. Nature 2009;457:679.

[83] Izuhara D, Swager TM. Poly(pyridinium phenylene)s: water-soluble n-type polymers. J. Am. Chem. Soc. 2009;131:17724.

[84] Chua LL, Zaumseil J, Chang JF, et al. General observation of n-type field-effect behavior in organic semiconductors. Nature 2005;434:194.

[85] Meijer EJ, de Leeuw DM, Setayesh S, et al. Solution-processed ambipolar organic field-effect transistors and inverters. Nat. Mater. 2003;2:678.

[86] Shkunov M, Simms R, Heeney M, et al. Ambipolar field-effect transistors based on solution-processable blends of thieno [2,3-b] thiophene terthiophene polymer and methanofullerenes. Adv. Mater. 2005;17:2608.

[87] Babel A, Wind JD, Jenekhe SA. Ambipolar charge transport in air-stable polymer blend thin-film transistors. Adv. Funct. Mater. 2004;14:891.

[88] Yamamoto T, Yasuda T, Sakai Y, et al. Ambipolar field-effect transistor (FET) and redox characteristics of a π-conjugated thiophene/1, 3, 4-thiadiazole CT-type copolymer. Macromol. Rapid Comm. 2005;26:1214.

[89] Yang SY, Shin K, Park CE. The effect of gate-dielectric surface energy on pentacene morphology and organic field-effect transistor characteristics. Adv. Funct. Mater. 2005;15:1806.

[90] Umeda T, Kumaki D, Tokito S. Surface-energy-dependent field-effect mobilities up to 1 cm^2/Vs for polymer thin-film transistor. J. Appl. Phys. 2009;105: 024516-1.

[91] Yildirim FA, Schliewe RR, Bauhofer W, et al. Spin-cast composite gate insulation for low driving voltages and memory effect in organic field-effect transistors. Org. Electron. 2008;9:70.

[92] Mao LF. Investigating the effects of the interface defects on the gate leakage current in MOSFETs. Appl. Sur. Sci. 2008;254:6628.

[93] Blanchet GB, Fincher CR, Lefenfeld M. Contact resistance in organic thin film transistors. Appl. Phys. Lett. 2004;84:296.

[94] Huang TS, Su YK, Wang PC. Study of organic thin film transistor with polymethylmethacrylate as a dielectric layer. Appl. Phys. Lett. 2007;91:106092116-1.

[95] Ahn T, Choi YJ, Jung HM, et al. Fully aromatic polyimide gate insulators with low temperature processability for pentacene organic thin-film transistors. Org. Electron. 2009;10:12.

[96] Sethuraman K, Ochiai S, Kojima K, et al. Performance of poly (3-hexylthiophene) organic field-effect transistors on cross-linked poly (4-vinyl phenol) dielectric layer and solvent effects. Appl. Phys. Lett. 2008;92:183302.

[97] Sirringhaus H, Kawase T, Friend RH, et al. High-resolution inkjet printing of all-polymer transistor circuits. Science 2000;290:2123.

[98] Egginger M, Vladu MI, Sariciftci NS, et al. Mobile ionic impurities in poly(vinyl alcohol) gate dielectric: possible source of the hysteresis in organic field-effect transistors. Adv. Mater. 2008;20:1018.

[99] Chua LL, Ho PKH, Sirringhaus H, Friend RH. High-stability ultrathin spin-on benzocyclobutene gate dielectric for polymer field-effect transistors. Appl. Phys. Lett. 2004;84:3400.

[100] Peng X, Horowitz G, Fichou D, Garnier F. All-organic thin-film transistors made of alpha-sexithienyl semiconducting and various polymeric insulating layers. Appl. Phys. Lett. 1990;57:2013.

[101] Bao Z, Feng Y, Dodabalapur A, Raju VR, Lovinger AJ. High-performance plastic transistors fabricated by printing techniques. Chem. Mater. 1997;9:1299.

[102] Gelinck GH, Geuns TCT, de Leeuw DM. High-performance all-polymer integrated circuits. Appl. Phys. Lett. 2000;77:1487.

[103] Klauk H, Halik M, et al. High-mobility polymer gate dielectric pentacene thin film transistors. J. Appl. Phys. 2002;92:5259.

[104] (a)Yoon MH, Yan H, Facchetti A, Marks TJ. Low-voltage organic field-effect transistors and inverters enabled by ultrathin cross-linked polymers as gate dielectrics. J. Am. Chem. Soc. 2005;127:10388. (b)Kim C, Wang Z, Choi HJ, Ha YG, Facchetti A, Marks TJ. Printable cross-linked polymer blend dielectrics. design strategies, synthesis, microstructures, and electrical properties, with organic field-effect transistors as testbeds. J. Am. Chem. Soc. 2008;130:6867.

[105] Lee KE, Oh MS, Choi JM, et al. Flexible high mobility pentacene transistor with high-k/low-k double polymer dielectric layer operating at -5V. Org. Electron. 2009;10:194.

[106] Roberts ME, Mannsfeld SCB, Bao Z. et al. Water-stable organic transistors and their application in chemical and biological sensors. Proc. Natl. Acad. Sci. U.S.A, 2008;105:12134.

[107] (a)Chen L, McBranch DW, Whitten DG, et al. Highly sensitive biological and chemical sensors based on reversible fluorescence quenching in a conjugated polymer. Proc. Natl. Acad. Sci. U.S.A. 1999;96:12287. (b)Kumaraswamy S, Bergstedt S, Whitten DG, et al. Fluorescent-conjugated polymer superquenching facilitates highly sensitive detection of proteases. Proc. Natl. Acad. Sci. U.S.A. 2004;101:7511. (c)Achyuthan KE, Bergstedt TS, Whitten DG, et al. Fluorescence superquenching of conjugated polyelectrolytes: applications for biosensing and drug discovery. J. Mater. Chem. 2005;15:2648.

[108] (a)Wang D, Gong X, Bazan GC. Biosensors from conjugated polyelectrolyte complexes. Proc. Natl. Acad. Sci. U.S.A. 2002;99:49. (b)Gaylord BS, Heeger AJ, Bazan GC. DNA detection using water-soluble conjugated polymers and peptide nucleic acid probes. Proc. Natl. Acad. Sci. U.S.A. 2002;99:10954. (c)Fan C, Wang S, Bazan GC, et al. Beyond superquenching: hyper-efficient energy transfer from conjugated polymers to gold nanoparticles. Proc. Natl. Acad. Sci. U.S.A. 2003;100:6297.

3

Inorganic Printable Electronic Materials

Zheng Chen

3.1 Introduction

Inorganic electronic materials have been dominating microelectronics in the last 50 years. Many inorganic electronic materials have been developed and successfully used in logic circuitry, memory, display, lighting, sensors, solar cells, and so forth, due to their high performance and environmental stability. A considerable amount of knowledge and a great deal of technology have been accumulated about inorganic electronic materials. Therefore, it is natural to utilize them for printed electronics. However, it is well known that making inorganic materials printable is more difficult than for soluble organic materials. In addition, the requirement of post-treatments, such as high temperature annealing and sintering, for inorganic nanomaterial inks hinders their widespread applications. Now, after over a decade of efforts, some printable inorganic electronic materials emerged and have been successfully used in some niche applications.

Conductor is the essential component in electronics and also the earliest developed printable electronic material. The most widely used printable conducting formulation is conductive paste, where metal or carbon particles are mixed with resins to form pastes. These pastes are screen printed for applications in electrical interconnection in such things as printed circuit boards. Despite their long history of use in industry, these conductive pastes suffered from low conductivity, high sintering temperature, and thick printed film. In recent years, the progress in nanomaterials development, namely silver nanoparticles or nanowires and copper nanoparticles, enabled better conductive inks. Different from the conventional conductive pastes, these inks are made of metallic nanoparticles mixed with some volatile solvents and a small amount of surfactants. Because there is no resin used, the printed metallic films have high conductivity, only a few times lower than their bulk forms. Their post-treatment temperature is also lower than the resin-containing pastes.

Metal oxides are a unique class of materials that are both transparent and of excellent electron transport property. They are either semiconductors or conductors, depending on the level of

---

Printed Electronics: Materials, Technologies and Applications, First Edition. Zheng Cui, Chunshan Zhou, Song Qiu, Zheng Chen, Jian Lin, Jianwen Zhao, Changqi Ma and Wenming Su.
© 2016 Higher Education Press. All rights reserved. Published 2016 by John Wiley & Sons Singapore Pte. Ltd.

doping of additional elemental materials. The transparent oxide semiconductors (TOSs) are seen as the next-generation semiconductors for making thin-film transistors (TFTs) used to drive flat-panel displays. Their heavily doped forms are transparent conductive oxide (TCO), of which indium tin oxide (ITO) is the most well-known transparent conductor. Although the conductivity of TCO is far lower than metallic conductors such as silver, it is still widely used in various electronic devices that require optical transparency and matching work function. Both TOS and TCO are normally deposited by vacuum sputtering. However, they can also be made printable. The main challenges of printable TOS and TCO are their high annealing temperature and low charge mobility.

Carbon nanotube and graphene are the two most studied nanomaterials. They can be used as either semiconductors or conductors. Since the discovery of carbon nanotubes in the 1990s, though considerable research has been carried out, they are still not in large-scale use in electronics. One of the major hurdles is the difficulty in obtaining a bulk quantity of carbon nanotubes with high purity of specific electronic properties. In recent years, substantial improvements have been made on its synthesis, dispersion, purification, and printing deposition of film, which is a step closer to practical application. A similar story is true for graphene as well. At present, graphene's performance as conductive ink is poor, and it does not have enough band gap as semiconductor. The only potential application for graphene is to make transparent conductive film by chemical vapor deposition (CVD) growth for touch-panel applications.

Silicon is the core material for conventional microelectronics. However, silicon can also be printable and silicon inks have found applications in solar cells, sensors, and TFTs. Metal chalogenides are another group of inorganic semiconductors that have excellent photoelectronic properties, originating from their direct band-gap structure. Metal chalogenide inks include soluble precursors, dispersed quantum dots, or nanoparticles. The printable metal chalogenides can potentially be used in solar cells, lighting, displays, sensors, and so forth.

Dielectric ink is also needed for printed electronics applications. It serves as an insulation layer as well as a capacitance layer. Dielectric ink is far more difficult to make and to print than conductor and semiconductor inks. So far few dielectric inks are reported and successfully used in printed electronics.

In principle, any inorganic materials that are stable in ambient environment can potentially be made into nanoparticles, dispersed in liquid to make inks, and printed. They have some key advantages over their organic counterparts. However, they have some challenging issues when used for printed electronics as well. The key advantages and disadvantages of inorganic materials for printed electronics are summarized in Table 3.1.

In this chapter, the above advantages and disadvantages will be explained for different material categories, together with methods of ink formulation and main application areas.

Table 3.1 The pros and cons of inorganic materials for printed electronics

Advantages	Disadvantages
Inherently high charge mobility	Difficulty in ink formulation (separation and dispersion issues)
Environmental stability	Impurity due to surfactants
Mature manufacturing technology	High post-processing temperature
Abundantly available	Inferior property compared to their bulk form
Batch-to-batch consistency	

3.2 Metallic Materials

3.2.1 Metallic Ink

Metals are widely used in electronic devices as connectors, inductors, electrodes, and antennas because of their high conductivity. The choice of a particular metal as printable conductor, besides conductivity, depends on cost, processing temperature, ink production in volume, and long-term reliability [1]. The top four metals that have been used as printable conductors are silver (Ag), copper (Cu), gold (Au), and aluminum (Al), ranking in conductivity of 1.59, 1.72, 2.44, and 2.65 $\mu\Omega\cdot$cm, respectively. As their conductivities only differ slightly, other parameters become deciding factors, such as chemical inertness and cost. Gold seems a perfect conductor, as it is easy to prepare the ink, to print, environmentally stable, and the printed conductor has conductivity close to its bulk form at low processing temperature [2]. However, the price of gold is too high for low cost printed electronics. The most important and successful printable metal is silver because of its relatively low price compared to gold, its high conductivity, and its relatively high chemical inertness. Silver ink can be easily produced and activated in ambient to achieve conductivity close to its bulk form at sintering temperature lower than 200°C, or even at near room temperature [1]. Copper is a promising conductive material. It is significantly cheaper (100 times) than Ag. However, preparing copper ink is difficult because of its high tendency of oxidation. Aluminum has the same problem, except it is more chemically active than copper. As for other useful metals, there are far more serious challenges in ink preparation and printing processes that restrict them only for some niche applications [3–5].

Metals cannot be dissolved in commonly used aqueous or organic solvents. To make metals printable, the conventional way is to mix metal particles with high viscosity polymer solutions, especially thermosetting resins, to form pastes [6]. The conductive pastes can provide good mechanical interconnection and excellent reliability but poor electrical conductivity with resistivity in the range of about 10^{-3} to 10^{-4} $\Omega\cdot$cm, which is 2–3 orders higher than that of bulk metal (10^{-6} $\Omega\cdot$cm). The recent progress in nanomaterials and surface modification techniques enables metallic nanoparticles to be well dispersed in an organic solvent or water with only a small amount of surfactants or lubricants and no resins added. These are normally called "inks," different from the aforementioned "paste" [6]. After printing the ink and drying the solvent, the metal nanoparticles contact closely with each other to form a self-supported continuous film, with little residue of surfactants or lubricants. The printed metallic films are able to provide excellent electrical conductivity, but the mechanical property and reliability are not as good as metal pastes. Similar to a soluble compound, such nanoparticle-based solutions have the lowest viscosity, which enables high resolution printing and thin-film formation through inkjet printers.

Metal compounds can be dissolvable and form solution-type inks, which are particle-free and often called metal-organic decomposition (MOD) ink [1]. They are considerably different from those aforementioned nanoparticle-type inks in terms of ink properties and film formation process. In the case of metal compound ink, the conductive thin films are obtained through converting the deposited metal compound film into metal film by post-treatments. The particle-free characteristic of MOD ink can reduce nozzle clogging, exclude colloidal stabilizers, and form more compact film than that from nanoparticle-type ink. The downside of MOD inks is that the solubility of metal compound limits the maximum metal content in the ink, which is always lower than that of nanoparticle-type inks [1]. In order to achieve high electrical conductivity film at low post-process temperature, metal compound should be, among other things, of high conversional ratio, high solubility, high stability in solvent, low cost, and low deposition temperature.

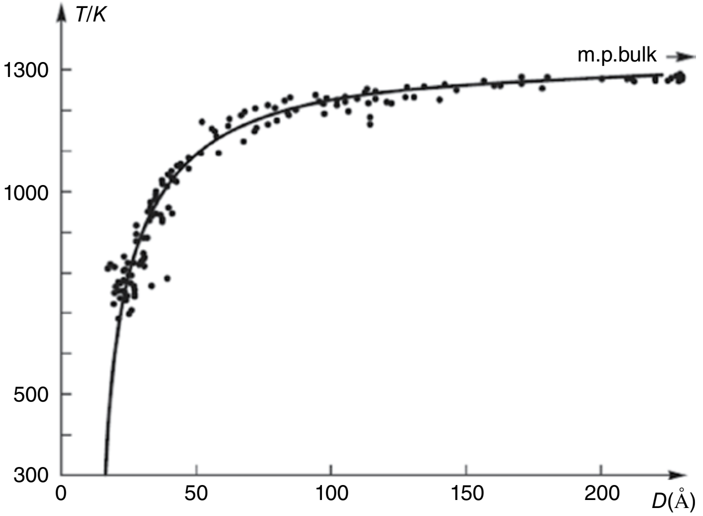

Figure 3.1 Experimental and theoretical melting point temperature of gold particles. (Reprinted from [7] with permission from American Physical Society.)

The small size of metallic nanoparticles can reduce the melting point and facilitate the sintering of such particles at low temperatures. As shown in Figure 3.1, the melting temperature of gold nanoparticles of less than 5 nm in diameter is below 300°C, whereas bulk gold melts at over 1000°C [7]. Moreover, small size, spherical shape, and uniform size distribution of nanoparticles facilitate the formation of dense film. Among various methods explored to prepare metal nanoparticle-based inks, the solution phase synthesis method is the most popular method due to its simplicity, low cost, and scalability to high volume production.

The solution phase synthesis is primarily based on the oxidation-reduction reaction of metal ions, invariably involving organic solvents and ligands [8]. An earlier work for preparing metal nanoparticles is the Turkevich method, where Au nanoparticles with narrow size distribution were prepared utilizing sodium citrate to reduce the $AuCl^{4-}$ [9]. More recently, the Brust method, which was a modification of the Turkevich method, was widely used for gold nanoparticle synthesis, where $AuCl^{4-}$ is transferred into toluene or chloroform using tetraalkylammonium bromide and is reduced with sodium borohydride in the presence of alkylthiols. The synthesized gold nanoparticles are covered with strongly bound ligands that render them well dispersed in organic solvent [10].

Two of the most prominent synthesis methods to produce Ag nanoparticles are the Lee–Meisel method [11] and the Creighton method [12]. Similar to the Turkevich method, the Lee–Meisel method utilizes the reduction of silver nitrate ($AgNO_3$) by sodium citrate to prepare Ag nanoparticles [11]. Narrow size distribution in Ag nanoparticles was achieved using a stronger reducing agent (sodium borohydride, $NaBH_4$) instead of sodium citrate to reduce $AgNO_3$ in the Creighton method [12]. Based on these classic methods, other similar solution synthesis has been explored using modified reactive reagents, solvents, capping agents, and other parameters in reaction to prepare not only Au and Ag but also other metal nanoparticles such as Pt [13], Pd [14], Cu [15], and Ni [16] with specific shapes and size distributions.

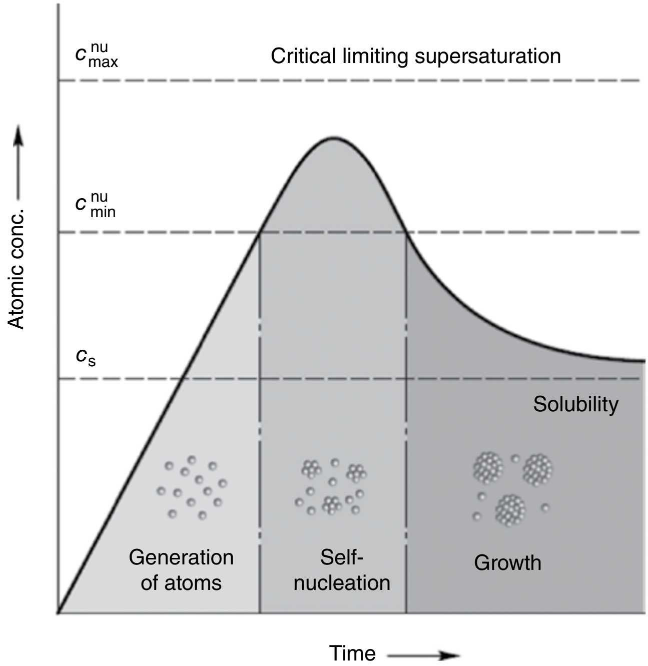

Figure 3.2 Plot of atomic concentration against time, illustrating the generation of atoms, nucleation, and subsequent growth. (Reprinted with permission from [18], copyright 1950 American Chemical Society.)

Although successful synthesis of metal nanocrystals in a variety of shapes and controllable size distribution has been frequently reported in the last two decades and the chemical reactions involved often appear to be fairly simple, the nucleation and growth mechanisms behind the simple chemistry are extremely complicated. In general, the growth process of nanocrytals can be divided into three stages: (1) nucleation, (2) evolution of nuclei into seeds, and (3) growth of seeds into nanocrystals. In principle, any one of the experimental parameters could be used to control the growth process so as to fine-tune the properties of metal nanoparticles [17].

In the first stage of nanoparticle growth, the nucleation process of metal nanocrystals may take completely different pathways, depending on the specific route of either decomposition or reduction of precursor to zero-valent atoms [17]. For the decomposition route, the atoms start to aggregate into small clusters (i.e. nuclei) via self-nucleation when the concentration of atoms reaches the point of supersaturation, and then the concentration of metal atoms in solution is reduced [18]. Nucleation will stop if the concentration of atoms drops below the level of minimum supersaturation. With a continuous supply of atoms via ongoing precursor decomposition, the nuclei will grow into nanocrystals of increasingly larger size until an equilibrium state is reached between the atoms on the surface of the nanocrystal and the atoms in the solution. The evolution process with time is illustrated in Figure 3.2. Besides growth via atomic addition, the nuclei and nanocrystals can directly aggregate into larger clusters [19]. For the reduction route, it is unclear if the precursor compound is reduced into zero-valent atoms first, which aggregate into nuclei and then grow into nanocrystals, or if the unreduced

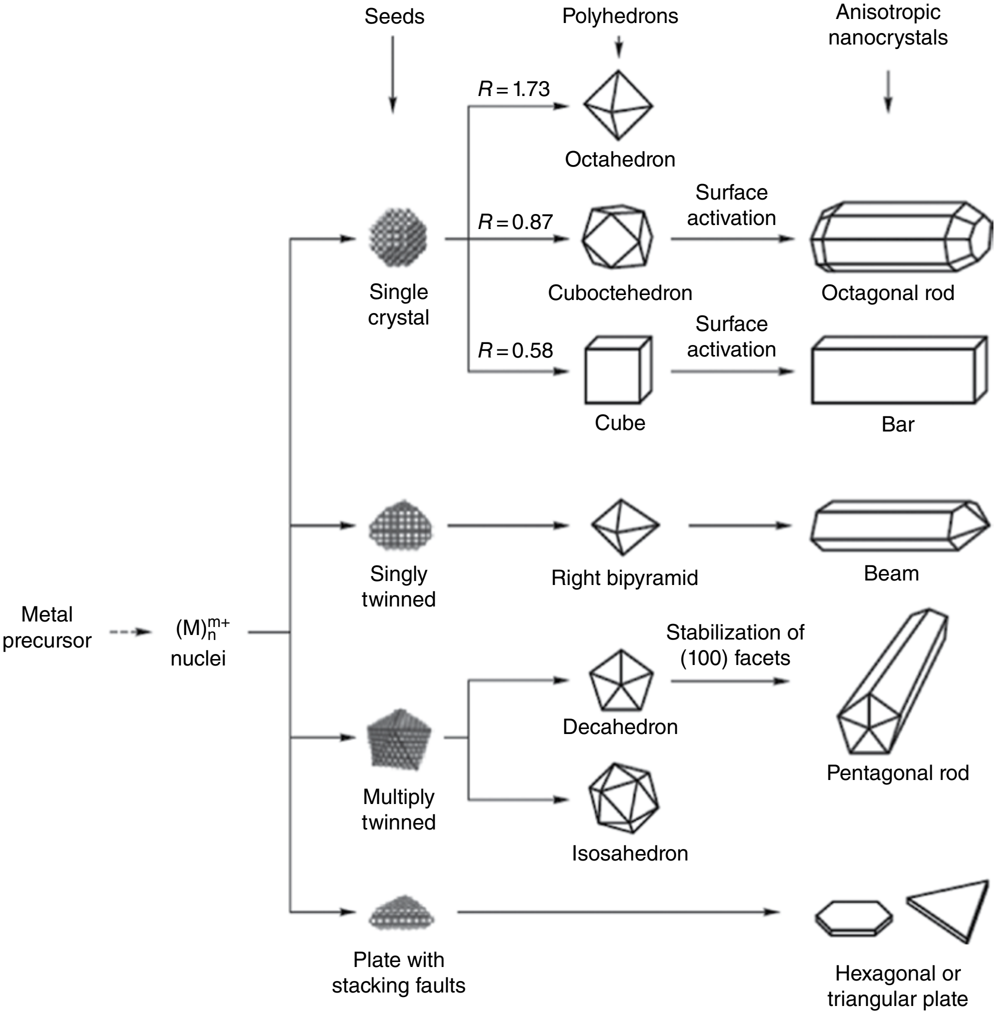
Seeds
Polyhedrons
Anisotropic nanocrystals
R = 1.73
Octahedron
R = 0.87
Surface activation
Cuboctehedron
Octagonal rod
Single crystal
R = 0.58
Surface activation
Cube
Bar
Singly twinned
Right bipyramid
Beam
Metal precursor
(M)$_n^{m+}$ nuclei
Stabilization of (100) facets
Decahedron
Pentagonal rod
Multiply twinned
Isosahedron
Plate with stacking faults
Hexagonal or triangular plate

Figure 3.3 Reaction pathways that lead to fcc metal nanocrystals with different shapes. (Reprinted from [17] with permission from Wiley.)

metal species begin forming nuclei prior to reduction. Simulation investigations based on first-principle molecular dynamics indicate that precursor compounds can be directly converted into nuclei without going through a zero-valent state [20–23].

The emergence of a seed from a nucleus is marked by a critical size, beyond which structural fluctuations become so energetically costly that the cluster becomes locked into a well-defined structure. The seeds may take a single-crystal, singly twinned, or multiply twinned structure, and all of these may coexist in solution. Up to now, a one-to-one correlation between the initial seeds and final nanocrystals has been established for a number of noble metals. Figure 3.3 shows some reaction pathways that lead to fcc (face-centered cubic) metal nanocrystals with different shapes. In order to obtain uniform nanocrystal shape, the key is to control the population of seeds with different internal structures. They are history dependent, and their formation is determined by both the statistical thermodynamics of the free energies of different species and kinetic factors regarding the generation and addition of metal atoms to a nucleus. Through the further addition of metal atoms, seeds can grow in size and evolve into nanocrystals. The overall evolution of a crystal is dictated by the competition between decrease in bulk energy (which favors growth) and increase in surface energy (which favors dissolution). Benefiting from the understanding in growth mechanism of nanocrytals, some rules have been established and proven to be effective as synthetic protocols. More detailed information about how to control the size and shape of metal nanoparticles is discussed in [17].

Nanoparticles have the tendency to aggregate and flocculate, due to their high surface energy. In general, addition of capping agents is necessary to enhance the dispersion and stability of nanoparticles in a solvent, as well as to control the size and shape of a nanocrystal during the synthesis of nanoparticles. In order to avoid instability of the capping process, there should be high binding energy enabling strong interaction between the nanoparticle and the capping agent. On the other hand, the high binding energy results in the requirement of high thermal energy (high annealing temperature) to strip the capping agent from the surface of a nanoparticle after printing the ink. It has been found that the functional groups with O, N, and S atoms can usually interact well with metals such as Au, Ag, and Cu [24]. In addition to the functional group, the length of hydrocarbon chain should also be selected to balance between dispersion and oxide-resistance stability of ink and conductivity of printed film, because long chain may lead to too much insulating residue in the final printed film. The solvent composition used in the ink is also crucial for ink characteristics and the quality of the printed patterns, such as ink stability and uniform surface morphology of the printed features. However, very little research has been done in this area so far.

Au and Ag inks are comparable regarding their high conductivities and thermal stabilities, but silver has a clear advantage over Au in terms of cost. Ag and Au inks with high solids content reaching to 50 wt% are easily purchased or homemade in the lab; the typical resistance of printed Ag and Au lines is only a few times that of bulk metal at curing temperature no more than 200°C [2, 25, 26]. Printed Au and Ag conductive lines have been successfully applied in some devices; for example, the metal mesh-based transparent conductive film, transistors, and solar cells [26–29].

Though Ag ink is mature in terms of properties such as high conductivity and stability, the relative high cost and electromigration of silver atoms, which often results in circuit failure under high humidity conditions, limit its widespread industrial application. Copper ink is a promising substitute for Ag and Au ink due to its much lower cost and comparable conductivity. However, oxidation of copper during synthesis, storage, and/or handling degrades its electrical properties. First, it is very difficult to obtain pure copper nanoparticles without copper oxide by the conventional reduction method when water and oxygen molecules exist in the reaction medium. At the same time, Cu particles require a high sintering temperature due to the high melting temperature of Cu and the presence of copper oxides. Cu particles are easily oxidized in air during the sintering process. Therefore, in order to avoid the oxidation during post-heat treatment, the copper film is in general annealed in a reductive/inert atmosphere (H_2 or N_2). It is critical to develop an economically feasible process to produce copper ink on a large scale and to avoid oxidation in post-processing.

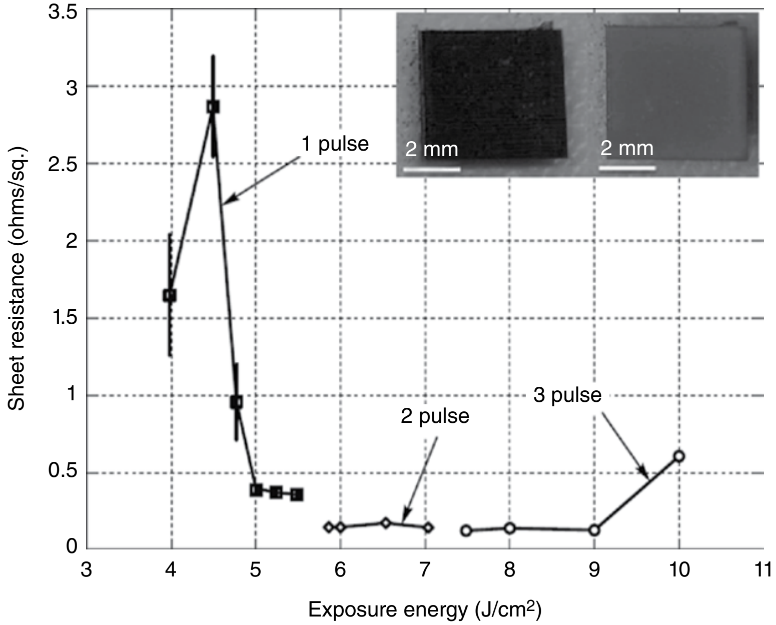

Figure 3.4 Sheet resistance of sintered Cu layer as function of IPL exposure energy and number of pulses. The inset shows a photograph of as-printed CuO (left, not conductive) and IPL sintered Cu (right, conductive). (Reprinted with permission from [33], copyright 2014 American Chemical Society.)

To address the oxidation issue, copper nanoparticles for use in conductive inks are usually synthesized in organic solvent under an inert atmosphere using capping agents to prevent aggregation and oxidation. Many passivation materials, including carbon-based materials (carbon and graphene), organic species (polymers and surfactants), and metals (Ag, Au, and Ni), have been employed to wrap the surface of Cu nanoparticles to provide sufficient protection against oxidation and at the same time not impair their electrical conductivity [30]. Other research has been carried out to investigate the oxidation-resistance ability of these passivation materials. Jeong et al. minimized the surface oxidation by adjusting the molecular weight of poly(N-vinylpyrrolidone) capping molecules, which were introduced during the synthesis of Cu nanoparticles. Cu granular films with good conductivity (~11 μΩcm) were obtained after heat treatment at 275°C under vacuum [5]. Deng et al. investigated the antioxidative effect of short chain carboxylic acids as capping agents in copper inks, which were then used to prepare high conductivity copper films (14 μΩcm) annealed in nitrogen ambient at temperatures as low as 200°C [31, 32]. In recent years, great progress has been made on ambient annealing of solution-processed copper film utilizing intensive pulsed light sintering (IPL). Wang et al. successfully obtained the resistivity of copper-based conductive films as low as 3–5 μΩcm after sintering using intense pulsed light from a xenon flash lamp, utilizing a Cu-ion ink with reductive formic acid [3]. Kang et al. also demonstrated the IPL air sintering of inkjet-printed CuO layers to convert the electrically insulating CuO into conductive Cu. Figure 3.4 shows the change in sheet resistance of the sintered Cu layer as a function of exposure energy and number of pulses. At the same time, the color of CuO film

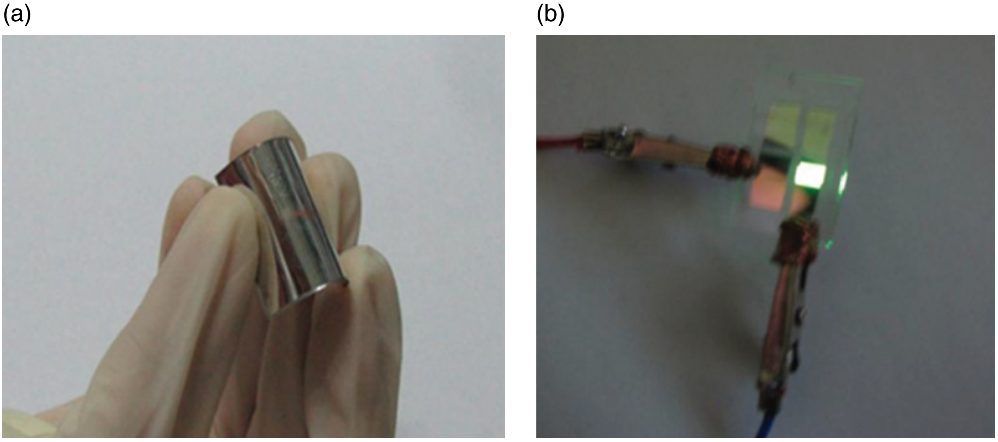

Figure 3.5 Printed flexible aluminum substrate (a) and lighting of OLED with printed aluminum cathode (b). (Reprinted from [37] with permission from the Royal Society of Chemistry.)

turned from black into the Cu red color, and the lowest resistivity of about 55.4 nΩ·m (about 30% conductivity of bulk Cu) was obtained [33].

In addition to Au, Ag, and Cu, other reactive metal inks, such as aluminum (Al) [34], tin (Sn) [35, 36], and indium (In) [36], have also been prepared and used under the protection of inert or reducing atmosphere. Lee et al. proposed a solution process to stamp Al cathodes using aluminum trihydridedibutyletherate ($AlH_3\{O(C_4H_9)_2\}$) precursor ink, which can decompose into Al at 150°C with $Ti(O\text{-}i\text{-}Pr)_4$ vapor as a catalyst in an argon (Ar) environment [34]. At the authors' Printable Electronics Research Center, Su et al. used a similar chemical process to synthesize Al ink and screen print it into Al film. With sintering temperature as low as 80°C for 30 s, the printed Al cathode with thickness of 50 nm showed a sheet resistance of 2.29 Ω/sq. and work function of 3.72 eV [37], which is suitable as cathodes for flexible organic light-emitting diodes (OLEDs). Figure 3.5 shows the Al film on a flexible plastic substrate (a) and the OLED employing the printed Al as cathode. Recently, Jo et al. fabricated a low cost, highly conductive Sn ink for inkjet printing by using a modified polyol process and printed Sn film with maximum resistivity of 64.27 μΩ·cm, which is 6 times higher than the bulk Sn resistivity (10.1 μΩ·cm) [35]. Metal indium and its alloy nanoparticle inks have been prepared and used to fabricate ITO nanoparticle conductive film and $CuInS_2$ film for solar cells [32, 36].

The rheological property and wettability of an ink, such as viscosity and surface tension, are also important in order to obtain good quality and repeatable printed patterns. The rheological property is related not only to the solvent but also to the solid content, dispersion, size, and shape of nanoparticles. It has been indicated that the viscosity of an ink is higher for smaller size nanoparticles and/or flaky-shaped nanoparticles if other parameters are the same. The contact angle of an ink on solid surface strongly depends on the surface tension of ink and the free energy of the solid substrate surface [38]. Therefore, it may be necessary to introduce additional agents into the ink system, including surfactant, wetting agent, reducing agent, anchoring agent, and defoaming agent [39].

3.2.2 Post-printing Process

For both compound-type and nanoparticle-type inks, it is critical to convert the printed precursor film into a conductive pattern by an additional process (typically heat treatment), which dries and sinters the ink, maximizing its electrical conductivity through improvement in interparticle connectivity. In addition to the drying and sintering of ink, the post-printing processes for MOD ink also include precipitation of metal, removing organic components, and generating nanoparticles in situ at relatively low temperatures [1].

The curing temperature is defined as the temperature at which the film starts showing conductance by direct physical contact of particles. Although evaporation of solvent in the drying process forces the particles close together, a thin organic layer between the metal particles may prevent electrons moving from one particle to another. The solvent needs to be removed with elevated temperature. At higher temperatures, sintering takes place when all the organic materials are burned off and necks begin to form between particles. Further increase in temperature results in the formation of large necks, and a metallic crystal structure is formed with a low number of grain boundaries. With additional increase of temperature, melting of metal nanoparticles occurs and the printed film becomes a denser solid film due to the low melting point of small size nanoparticles.

The sintering process of particles at low temperature is known as Ostwald ripening, which is one of the modes of particle growth wherein large particles grow at the expense of smaller ones. The driving force of Ostwald ripening is surface energy reduction, because smaller particles have a higher chemical potential than larger particles. Therefore, the Ostwald ripening process actually originates from the surface and grain boundary diffusion rather than bulk diffusion, which allows for neck formation and neck radii increase but leaves behind a porous structure, resulting in conductivity lower than the bulk material.

Conventional thermal annealing of printed conductive films is commonly performed in an oven, in a hot air flow, or on a hotplate. Selective heating methods such as scanned laser irradiation have also been employed to spare those substrates that cannot withstand high temperature. Ko et al. reported an up to 25% increase in conductivity using an Argon ion laser beam to sinter printed gold nanoparticle ink, without heating up the substrate. However, this approach is relatively slow and a following washing step is necessary to remove any unsintered materials [40]. Another approach is to utilize different absorption of microwaves between metal nanoparticles and thermoplastic substrate to selectively heat the printed metal line. Based on the Maxwell–Wagner polarization principle, microwave is heavily absorbed in metals but almost transparent in thermoplastic polymers. With microwave radiation, printed Ag tracks are sintered with conductivity of 60% of the bulk silver on low cost polymer foils [41]. Other selective sintering technologies, including low pressure argon plasma [42], UV radiation [43], high temperature plasma sintering [44], and electrical current sintering [45], were all demonstrated to yield resistivity values of a few times of the bulk metal, though each has its own advantages and disadvantages [1].

There are also some "magic" approaches that can activate the printed metal film without using heat. They are based on a chemical reaction or an aggregation mechanism [46]. One such technique is called reactive inkjet printing, where MOD inks and corresponding reducing agents are inkjet printed together to generate the conductive tracks in situ on a substrate. For example, Bidoki et al. produced silver lines, with conductivity of 0.3% of bulk silver, through sequentially printing ascorbic acid and silver nitrate solutions on paper [47]. A modified

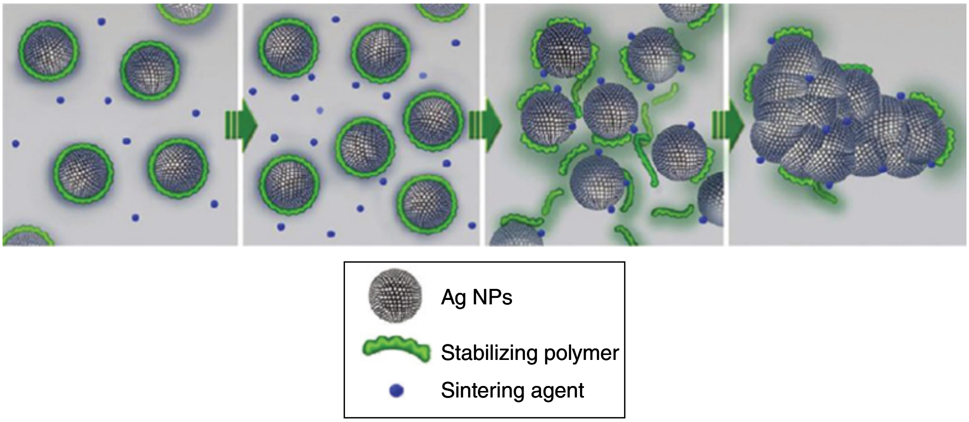

Figure 3.6 Schematic illustration of "built-in sintering": the stabilizer detachment, which leads to NP sintering (the grey circles represent the polymeric stabilizer; the small dots represent the sintering agent). (Reprinted with permission from [50], copyright 2011 American Chemical Society.)

method produced smooth and continuous silver lines with conductivity of 6% of bulk silver at room temperature [48]. Such technique was also utilized to prepare conductive copper lines through inkjet printing both copper salt and sodium borohydride ($NaBH_4$) as a reducing agent sequentially [49]. In the case of nanoparticle-based ink, conductivity can be achieved at room temperature through triggering the aggregation of nanoparticles and collapse of capping agent on the surface of nanoparticles. Magdassi et al. reported that conductive silver films were prepared by exposing the inkjet-printed silver ink to HCl vapor, which causes the neutralization of the stabilizer leading to aggregation of particles. They called the process "built-in sintering." Their special silver ink contains destabilizing agent with Cl^- ions, which can cause the detachment of anchored polymer stabilizer from the surface of nanoparticles during drying of printed pattern, and thus enable the coalescence and sintering of nanoparticles, as shown in Figure 3.6. Up to 41% of the bulk silver conductivity was achieved in a printed pattern at room temperature by a single printing step [50].

In the case of printed metal tracks undergoing a high temperature sintering process, the thermal stability of printed metal is critical. Perelaer et al. investigated the thermal stability of the printed lines with different silver inks. They found that some of the inks can withstand temperatures as high as 600°C without changing conductivity. Some inks may lose their conductivity suddenly at a certain temperature. Such loss of conductivity is probably attributed to the formation of cracks in the printed tracks [51, 52].

3.2.3 Metal Nanowire

In the last 2 decades, the synthesis of metal nanowire has been extensively investigated as part of nanomaterials development. The development has come to fruition, as in recent years they have been heavily used for, in the case of Ag nanowires (NW), making flexible transparent conductive films [53, 54]. Until now, several shape-controllable methods have been explored to make metal nanowires, including the hydrothermal process [55, 56], the microwave-assisted process [57, 58], the electrochemical process [59, 60], the template technique [61, 62], and chemical synthesis [63]. In the case of making Ag nanowires, the polyol process seems to be the most promising one due to low cost, high yield, and simplicity. In this process, Ag nanowires are typically synthesized by the reduction of silver nitrate in ethylene glycol in the presence of a stabilizing agent of poly(vinylpyrrolidone) (PVP), where ethylene glycol (EG) acted as both solvent and reducing agent. Similar processes have also been used to prepare Cu nanowires except that an additional stronger reducing agent is required to reduce Cu salt [53].

As mentioned in Section 3.2.1, the shape of metal nanoparticles depends on the thermodynamics and kinetics of each of the three steps: nuclei formation, evolution from nuclei to seeds, and evolution from seeds to nanocrystals [17]. Although the exact mechanism of Ag nanowire growth has not been entirely understood, it has been known that the nanowires are derived almost entirely from multiple-twinned decahedra particles bound to bound at the lower energy facet, which is most naturally abundant but also most reactive because of the presence of twin defects [2]. The crystalline defects provide active sites for growing the nanowires along their longitudinal axes, while the less-strained side surfaces of the nanowires are bound by facets due to lower reactivity toward the deposition of silver atoms [8]. PVP plays a key role to control the structure of silver nanoparticles, because it can prevent not only the aggregation of nanoparticles but also react preferentially with the {100} facets of silver nanoparticles through interactions between silver atoms and oxygen atoms of PVP carboxyl groups [64]. To trigger the formation of nanowire, Br ion was even added to form AgBr nanocrystals and to reduce the concentration of free cationic silver ions in the solution during initial seed formation, so as to enable the formation of the thermodynamically more stable multiple-twinned Ag seeds [65].

Although ordered metal nanowire arrays possess higher electric conductivity, random nanowire networks provide more homogeneous film and can be readily and cheaply prepared by low temperature solution deposition techniques such as spray coating, drop coating, spin coating, rod coating, and direct gravure printing. Figure 3.7 shows Ag NW ink, Meyer rod-coating setup, Ag NW film coating on PET substrate, and its SEM image [65]. Recently, solution-processed random networks of metal nanowires have been explored as a promising transparent conductive film with low sheet resistance at high transmittance (2 Ω/sq. at 90% transmittance) [54]. They have found application in touch panels for mobile phones and pad computers. Such solution-processed electrodes have also demonstrated their ability to be integrated into organic solar cells [66] and OLEDs [67].

The electro-optical properties of nanowire networks are dependent upon their diameter, length, density, orientation, and junction resistance. Bid et al. observed the increase of resistance for individual nanowires with decreasing wire diameter and attributed this phenomenon to surface scattering of electrons, as the diameter of the nanowire reduces close to or below the mean free path of electrons of the bulk material [68]. Due to the percolative nature of nanowire networks, the resistance of a network increases as the length of nanowires decreases. In the percolation model, fewer nanowires are required to make a conduction path across a given space if longer nanowires are used, thus there are fewer junctions between wires, resulting in lower resistances observed in networks [69].

Based on the same mechanism, the orientation of nanowires is also considered to determine the number of junctions required for electron transport in the network. Another effective method to decrease the electric resistance of a network is to increase the density of nanowires above the percolation threshold; however, this can also lead to a decrease in the optical transmission of the

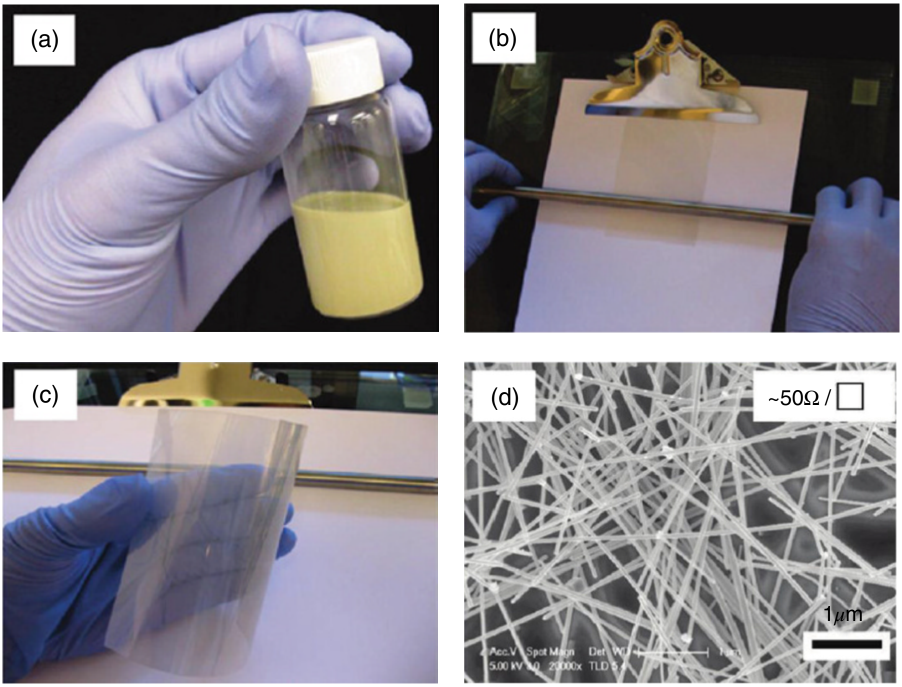

Figure 3.7 Photograph of (a) Ag NW ink, (b) Meyer rod coating setup for scalable Ag NW coating on plastic substrate, (c) finished Ag NW film coating on PET substrate, and (d) a SEM image of Ag NW coating shown in (c). (Reprinted with permission from [65], copyright 2010 American Chemical Society.)

network. As mentioned above, junction resistance between metal nanowires is one of the key factors in determining the resistance of a network. Some annealing techniques such as thermal annealing, high pressure annealing, electrical annealing, optical sintering and encapsulation, and high pressure mechanical press are commonly used in an attempt to reduce the junction resistance and hence the resistance of nanowire networks [70].

3.3 Transparent Oxide

3.3.1 Transparent Oxide Semiconductor and Conductor

Since Nomura et al. demonstrated the flexible In-Ga-Zn-O (IGZO) TFTs in 2004 [71], TOSs emerged because of their advantages of favorable field-effect mobility, high optical transparency, and good environmental stability [72]. The mobility in excess of 10 cm^2/Vs and the I_{on}/I_{off} current ratio over 10^7 for transparent oxide TFTs have been demonstrated by many research groups around the world [73]. Recently, metal oxide-based TFTs were reported to have reached electron mobility up to 160 cm^2/Vs [72]. In addition, other important issues such as reproducibility, stability, and uniformity have also been solved for large-area practical applications. The excellent properties of TOSs mainly originate from the metal ions in the oxide compound, which have a distinctive electron configuration of $(n-1)\ d^{10}\ ns^0\ (n \geq 4)$.

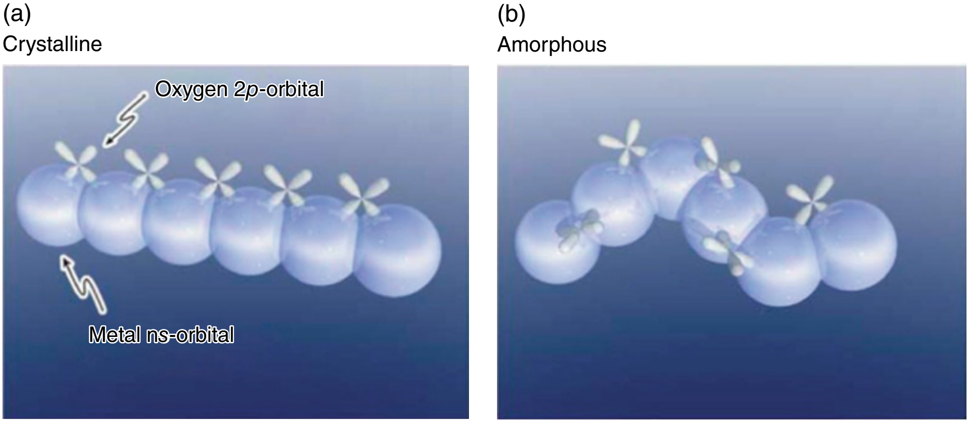

Figure 3.8 Amorphous oxide semiconductors composed of post-transition metal cations. Spheres denote metal s orbitals. The contribution of oxygen 2p orbitals is small. Direct overlap between neighbouring metal s orbitals is rather large and is not significantly affected even in an amorphous structure. (Reprinted from [71] with permission from Nature Publishing Group.)

In these oxide compounds, the bottom of the conducting band is mainly formed by direct spatial overlap between neighboring metal ns-orbital with spherical symmetrics, resulting in high mobility insensitive to structural deformation, as shown in Figure 3.8. Therefore, these oxide semiconductors maintain their electron mobility in the amorphous phase comparable to their crystalline counterpart, enabling uniform device properties over large areas and at low process temperature. In addition, $(n-1)d^{10}$ electron configuration avoids the d-d electron interband transition, which would induce visible light absorption [71].

Being a compound semiconductor, it is doubtless that its structural and electric characteristics depend heavily on its elemental composition [72]. For example, in the quaternary system of IGZO, indium ions can enhance the mobility by providing a primary conduction pathway but also can reduce the I_{on}/I_{off} current ratio, whereas Ga ions act as a carrier suppressor due to Ga's strong oxygen affinity. In addition, Zn ions introduce cation size variation in the structure, which helps to stabilize the amorphous phase [74]. Besides these metal cations, oxygen also influences the electronic performance of the oxide film, because oxygen vacancies are the major source of free electron. The elemental composition dependence causes the difficulty as well as provides the possibility of controlling the electronic performance in the oxide film. The metal elements commonly found in these compound semiconductors include indium (In), zinc (Zn), tin (Sn), gallium (Ga), and copper (Cu).

Apart from being semiconductors, transparent oxides can behave like conductors as well. The TCO is a heavily doped transparent oxide semiconductor that is conductor-like but has a limited conductivity of 4×10^{-7} Ωm [75]. Though 1–2 orders of magnitude lower than that of bulk metal material, these TCOs are still very important electrode materials, because they can provide optical transparency and an electronically functional interface for many devices. ITO has been the most widely used TCO and the benchmark of all transparent conductive films [76, 77]. Among the metal elements found in TOSs, indium is the most important element because its ns state provides a primary conduction pathway. However, indium is a rare earth element and its mineral reserve in earth is limited. Thus, various metal oxide compounds without indium, such as zinc-tin-oxide (ZTO), aluminum-doped zinc-oxide (AZO), and fluorine-doped tin-oxide (FTO), have been developed [76, 78].

Most of the TOSs and TCOs are dominantly electron transport (n-type). There is so far no report about p-type TOSs or TCOs with comparable performance. The problems of making p-type conductive wide band gap oxides were ascribed to the large electronegativity of oxygen, resulting in localization of the valence band holes on oxygen ions. In order to reduce the localization of holes, one way is to use a cation with closed shell levels such as Cu and Ag to degenerate with the O 2p states [79]. More detailed mechanisms can be found in [80]. Since NiO was found as a p-type oxide by Sato et al. in 1993 [81], one important event is the discovery of a series of Cu-based oxide p-type conducting films, such as $CuAlO_2$ and $SrCu_2O_2$ [79]. Although they exhibited considerable improvement over NiO, the conductivity and mobility were still several orders of magnitude lower than that of n-type materials [79]. Moreover, the amorphous phases of these oxides did not show p-type conduction, whereas to crystallize these oxides requires higher annealing temperatures than the n-type counterparts. Other attempts to develop p-type oxides include Zn-Rh-O and Zn-Co-O as p-type amorphous TCO film with resistivity near 0.5 Ωcm and 0.05 Ωcm [82–84]. Indium-doped molybdenum oxide (IMO) was also explored and synthesized, showing low resistivity. Individual single-crystal IMO nanowires demonstrated resistivity as low as 5.98×10^{-4} Ωcm and its amorphous films on glass exhibited resistivity of 2.5×10^{-3} Ωcm at optical transmittance of 80–88% [85]. A series of solution-processed p-type conductive amorphous films were reported at low processed temperatures, based on A-B-O (B = Ru, Ir and A = Bi, Pb, lanthanide element except Ce) having low resistivity (10^{-2}–10^{-3} Ωcm), although both Ru and Ir are more expensive than indium [86, 87]. In the case of TFT, breakthrough research regarding p-type TOS-TFTs is the tin monoxide (SnO) TFTs with record field-effect mobility of 6.75 cm^2/Vs fabricated at temperatures as low as 180°C; however, the transistors still suffer from low I_{on}/I_{off} ratio of 10^3–10^4 [88].

3.3.2 Low Temperature Solution Processing

It should be noted that all of the aforementioned oxide films or TFT devices were produced by vacuum deposition techniques. For printed electronics applications, solution-type metal oxides are needed. In recent years, research on solution-processed metal oxides has made great progress. Some TFTs exhibited excellent electronic characteristics with electron mobility in excess of 10 cm^2/Vs, high I_{on}/I_{off} ratio more than 10^6, and high environmental stability [89, 90]. However, the relatively high processing temperature requires the same high temperature tolerance for the substrate and earlier deposited functional layers in a device. Therefore, the main objective of research is to improve the electronic transport in the solution-processed metal oxide film prepared at lower temperature [91]. Great efforts have been made to achieve this goal by developing new chemical formulations and novel processing routes [91].

Employing nanocrystals and nanoparticles can avoid the high temperature required for conversion of chemical precursor into a metal-oxide-metal (M-O-M) bond and crystallization, which is necessary in the case of metal compounds. However, the TFTs employing nanoparticle-based metal oxide ink have exhibited modest electronic performance, because of the inherent high melting temperature of the metal oxide nanoparticle and the highly insulating surfactant, as well as the difficulty in forming dense films [91]. Yet the nanoparticle-based ink is still vital to preparation of solution-processed transparent conductive oxide film, mostly due to smaller contact resistance between particles and facilitating thick film, which will be introduced later.

In contrast to the nanoparticles-based ink, metal compound solutions are able to form continuous dense ultrathin film through controlling deposition and annealing processes. It has been reported the fabrication of high performance TOS-TFTs utilizing metal compound solution as the precursor ink [92]. The conventional chemical formulation of metal compound solution is to dissolve metal salts in 2-methoxyethanol with a small amount of ethanolamine for stability. This classic formulation has been used to prepare TOS-TFTs at annealing temperature of usually more than 400°C [89, 93]. A number of special chemical formulations, including ammine-hydroxo metal aqueous solution, combustion, and metal nitrate aqueous solution, were reported in recent years that could achieve low temperature solution-processed high performance TOS-TFTs [94–96].

Ammine-hydroxo metal aqueous solution is a carbon-free aqueous ink that is made by dissolving the as-prepared metal hydroxide in high concentration ammonium hydroxide solution. The ammine-hydroxo metal complex can decompose and release the ammonia gas well below 100°C, leaving the metal hydroxide without other residues. With further elevated annealing, metal hydroxide turns into metal oxide by dehydration reaction, condensation, and crystallization kinetic processes. The simplified dissolution and decomposition scheme may be expressed as in Equation (3.1):

$$\mathrm{M(OH)n(s)} + \mathrm{xNH_3(aq)} \rightarrow \mathrm{M(OH)n(NH_3)x(aq)} \rightarrow \mathrm{ZnO(s)} + \mathrm{xNH_3(g)} + \mathrm{H_2O(g)}, \quad (3.1)$$

where M represents metal atom. A widely used formulation is ammine-hydroxo zinc aqueous solution ($\mathrm{Zn(OH)_x(NH_3)_y}^{(2-x)+}$) for zinc oxide (ZnO) thin film, which is among the most important TOSs with low cost, high mobility, and prone to crystallization at low temperature. Benefiting from almost no impurity, high performance ZnO transistor with mobility about 1.8 $\mathrm{cm^2/Vs}$ was fabricated at the temperature of 150°C [94]. Furthermore, a special annealing process further enabled mobility more than 10 $\mathrm{cm^2/Vs}$ (measured in vacuum) at the temperature $\leq$ 180°C [97]. However, there are some drawbacks regarding this formulation: (1) it is highly corrosive due to a high concentration of ammonia; and (2) some important metal elements, especially indium and gallium, cannot be used in the formulation, which has hindered the application of such printable ink.

Very recently, metal nitrate aqueous solution, which has not been used recently, was demonstrated to be effective for fabrication of metal oxide film at low temperature. The mechanism is that metal hydrate formed by combining metal ions and water molecules instead of nitrate ions would evaporate in the form of $\mathrm{HNO_3}$ or thermally decompose at temperatures <200°C. TFTs using the spin-casted indium oxide film as active layer annealed at 200°C exhibited mobility >2 $\mathrm{cm^2/Vs}$ and $>10^6$ I_{on}/I_{off} ratio [96]. Similar to the above ammine-hydroxo formulation, some metal elements (e.g. Sn) are not compatible with this formulation, and the modest acidic pH would potentially damage printing apparatus.

In 2011, an intriguing formulation was introduced by Kim et al. for low temperature fabrication of high performance TOS film [95], taking advantage of the combustion chemistry that thereafter was widely used for energy-efficient synthesis of bulk ceramic material such as chalcogenides, III-V semiconductors, carbides, binary oxides, and intermetallics [98]. Figure 3.9 shows the principles of the combustion chemistry for low temperature processing

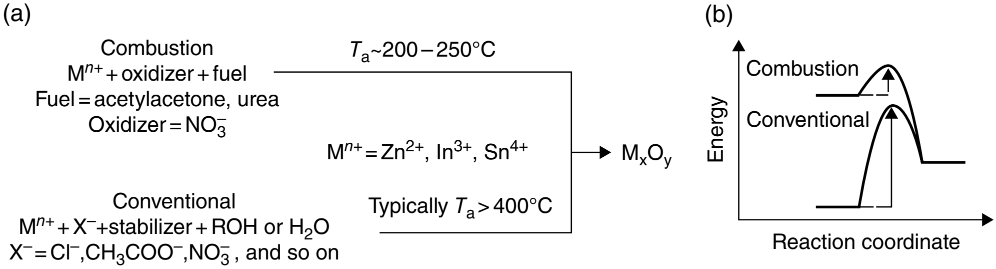
(a)
Combustion
M^{n+} + oxidizer + fuel
Fuel = acetylacetone, urea
Oxidizer = NO_3^-
T_a~200 – 250°C
M^{n+} = Zn^{2+}, In^{3+}, Sn^{4+}
M_xO_y
Conventional
M^{n+} + X^- + stabilizer + ROH or H_2O
X^- = Cl^-, CH_3COO^-, NO_3^-, and so on
Typically T_a > 400°C
(b)
Energy
Combustion
Conventional
Reaction coordinate

Figure 3.9 Combustion chemistry for low temperature processing of metal oxides. (a) Depiction of the two different synthetic approaches; (b) energy of combustion synthesis-based processes versus conventional processes. (Reprinted from [95] with permission from Nature Publishing Group.)

of metal oxide film. The self-generated heat originating from the "fuel" and "oxidizer" coexisting in the precursor can provide a localized energy supply for activating the metal oxide film at low processing temperature. In this formulation, nitrate (NO_3^-) usually is used as an "oxidizer" while acetyl-acetone or urea can act as "fuel." This chemical annealing route is in principle applicable to most metal elements, including In, Ga, Zn, and Sn, and therefore can be useful for many metal oxides such as indium oxide, indium zinc oxide, zinc-tin-oxide, and indium yttrium oxide [95, 99]. It is also possible for preparing high conductivity tin-doped indium oxide at temperatures as low as 200°C [95], which to the best of our knowledge has never been achieved with other compound-type ink. However, the combustion process is sensitive to too many factors to be controllable, such as the thickness, density, and pre-decomposition of the precursor [99].

Besides ink formulation, the annealing process is also crucial for the electronic performance of solution-processed metal oxide films. The main effects of annealing include chemical conversion, M-O-M formation, densification, and crystallization of film. Recently, special ambient annealing and some advanced annealing techniques were employed to improve the electronic performance of metal oxide films and lower the processing temperature.

Ambient annealing is crucial for the performance of solution-processed TOS films as well, because it can influence the chemical conversion of precursor and M-O-M configuration including O vacancy in the final film. High performance In_2O_3 TFTs were fabricated by annealing spin-casted metal halide precursor film in an O_2/O_3 environment. The In_2O_3 TFTs annealed in an O_2/O_3 atmosphere at temperatures of 200–300°C showed excellent n-type transistor behaviors with field-effect mobility of 0.85–22.14 cm^2/Vs and I_{on}/I_{off} ratio of 10^5–10^6. The annealing atmosphere of O_2/O_3 enhanced performance of solution-processed In_2O_3 TFTs at lower processing temperatures. Based on XPS results, it was suggested that the films annealed in O_2/O_3 contain more fully coordinated indium sites with six nearest-neighbor oxygen atoms and more oxygen-deficient sites. In contrast, conventional air-annealed films contain less fully coordinated indium sites and more hydroxyl groups [100]. In the case of ZnO film from the ammine-hydroxo zinc aqueous solution, devices annealed in N_2 exhibited 1 order of magnitude higher (maximum values ~11cm²/Vs) field-effect mobility than those annealed in air when the process temperature was 180°C, due to larger grains formed in the film [97].

An additional vacuum annealing was also applied to improve TOS-TFTs prepared using the formulation of metal nitrate aqueous solution [96]. There are at least two important impacts on the solution-processed oxide semiconductor film under vacuum annealing: (1) generating more electrons by creating oxygen vacancies in oxide film; (2) facilitating the forward chemical conversion of precursor film into oxide by effective removal of water molecules generated during the dehydration process. The excessive electrons can fill some trap sites so as to reduce carriers scattering, resulting in higher mobility [100].

A deep ultraviolet (DUV) photo-annealing method was adopted to achieve high degrees of sol–gel condensation and film densification in amorphous metal-oxide semiconductor systems including IGZO, indium zinc oxide (IZO), and indium oxide (In_2O_3) based on photochemical activation of sol–gel precursors. The mechanism is that high energy DUV photons induce photochemical cleavage of alkoxy groups and activate metal and oxygen atoms to facilitate formation of the M–O–M network. These photo-activated metal oxide semiconductors exhibited high bias stability with field-effect mobility of 14 and 7 cm^2/Vs on glass and polymer substrates, respectively. Seven-stage ring oscillators were fabricated with the TFTs on polymer substrates, achieving an oscillation frequency of more than 340 kHz [101].

By exposure to a wet environment, metal compounds can be transformed into metal hydroxide or M–O–M frameworks through hydrolysis and condensation at low temperature. However, if hydrolysis were to be induced by the addition of an aqueous catalyst (either acid or base) to the metal compound solution before thin-film processing, uncontrolled and undesirable precipitates would form easily. To overcome this problem, Banger et al. reported the formation of amorphous metal oxide semiconducting thin films by applying hydrolysis directly on the surface of film to produce the designated metal oxide skeleton framework from soluble metal alkoxide precursors at lower temperatures, called “sol–gel on chip.” Such in situ hydrolysis allowed for the fabrication of TOS-TFTs with high field-effect mobility of 10 cm^2/Vs, reproducible, and stable turn-on voltages V_{on}–0V and high operational stability at processed temperatures as low as 230°C [102].

Microwave irradiation can also assist low temperature annealing to improve the performance of ZnO TFTs, which were prepared utilizing ammine-hydroxo zinc aqueous solution. By microwave-assisted annealing, the ZnO TFTs exhibited a 3–6 times higher field-effect mobility and small hysteresis in comparison to TFTs processed by conventional hot plate annealing. It was also found that the microwave-assisted annealing can shorten the processing time from tens to a few minutes. Such an improvement was ascribed to accelerated dehydroxylation at low temperature by microwave irradiation, resulting in the shorter Zn–Zn distance, fewer hydroxyl groups, and better crystallization [103].

3.3.3 Doped Transparent Oxide Nanoparticles

A transparent conductive oxide is created by heavily doping a transparent oxide semiconductor. Its conductivity is proportional to its mobility and free electron concentration. For low temperature solution-processed transparent oxides described in Section 3.3.2, the maximum mobility is approximately 10 cm^2/Vs, which is significantly lower than 90 cm^2/Vs of ITO through the vacuum deposition process. On the other hand, the high free electron concentration cannot be acquired from oxygen vacancy alone but requires heavily hetero valent doping, which is limited by the solubility of the doping element. For example, the equilibrium solubility of Sn in bulk In_2O_3 has been reported to be no more than 6% (cation basis) depending on the temperature. Furthermore, high energy is critical for the doping atoms to overcome the energy barrier that occurs in the substitution sites. Thus it is challenging to obtain high doping concentration at low annealing temperature [104]. Doped transparent oxide nanoparticles provide the possibility of low temperature fabrication of solution-processed transparent conductive oxide film.

Controllable synthesis of metal oxide nanocrystals has long been extensively investigated through mainly the hydrolysis condensation route. The challenge is to introduce dopant atoms into nanocrystals, which is difficult due to the self-purify effect of nanocrystal [104]. In order for efficient dopant incorporation to occur, the key is to balance the growth of host crystal and deposition of dopant ions during crystal growth. One strategy reported in control of the final material stoichiometry is to use a single-source precursor (SSP), which is a metal-organic cluster containing all the elements required for multicomponent materials. It was not very successful in preserving the composition and stoichiometry of the SSP in the final nanocrystals. Another effective strategy is to decouple the doping process from the nanocrystal nucleation and growth reactions, including a nucleation-doping or growth-doping approach. In the nucleation-doping approach, the dopant nucleates first and the nuclei are then overcoated with a shell of the host material; in the case of growth doping, host nanocrystals are prepared to reach the desired size and dopant is then added dropwise to prevent homogeneous nucleation. In addition, to balance host and dopant precursor reactivity, an appropriate coordinating ligand can be attached to the metal cations depending on the intrinsic reactivity dictated by their relative Lewis acidity and the sizes of cations. More detailed chemistry can be found in [105].

Dispersions of doped transparent oxide nanoparticles have proved to be promising inks for low temperature fabrication of solution-processed transparent conductive oxide film. Lee et al. and Ito et al. reported 5.2×10^{-3} and 7×10^{-3} Ω·cm of resistivity, respectively, in their ITO films prepared with a simple solution-phase approach at 300°C annealing temperature, employing monodispersed ITO nanoparticles [106, 107]. An ITO-nanoparticle-based paste was utilized to deposit transparent conductive oxide film of 600 nm thickness by gravure printing and annealed at temperature less than 200°C on plastic substrate, which displayed a sheet resistance down to 400 Ω/sq. and visible light transmission of 85% [108]. Gaspera et al. reported Ga-doped ZnO film from coating of colloidal inks, which can be conductive after drying at 60°C following an additional UV irradiation [109]. In addition, some of the solution-processed nanoparticles-based ITO films were employed as electrodes in devices such as solar cells and electroluminescent lamps [110, 111].

3.4 Single-wall Carbon Nanotube

3.4.1 Preparation and Selective Chemistry of SWNT

A single-wall carbon nanotube (SWNT) can be envisioned as a seamless hollow cylinder formed through rolling a graphene sheet with a coincidence of two atoms (O and A) in the sheet, as shown in Figure 3.10. An SWNT can be uniquely defined by a chiral vector, $C = n\boldsymbol{a}_1 + m\boldsymbol{a}_2$, which is an OA vector represented in the unit vectors ($\boldsymbol{a}_1$ and $\boldsymbol{a}_2$) of the graphene lattice. If n or $m = 0$, the nanotubes are called zigzag nanotubes, and if $n = m$, the nanotubes are called armchair nanotubes. Otherwise, they are called chiral nanotubes. From the (n, m) indices, one can readily judge whether the SWNTs are metallic or semiconducting. When n = m, the nanotube is metallic; when $|n\text{-}m| = 3j$, where j is an integer, then the nanotube is semiconducting

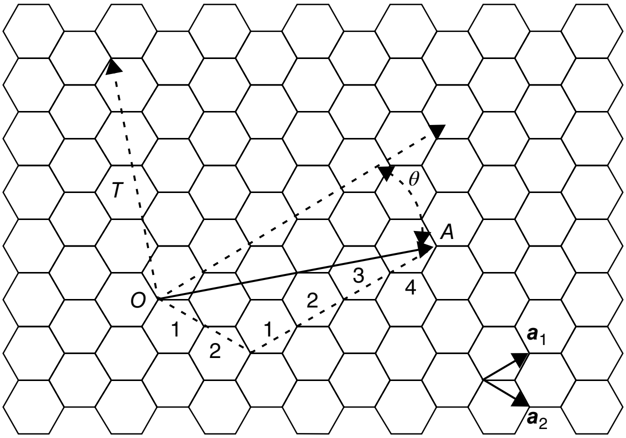

Figure 3.10 A SWNT can be considered a graphene sheet rolled up with a coincidence of two atoms (O and A) in the sheet. The OA vector is defined as chiral vector, $C_h = n\boldsymbol{a}_1 + m\boldsymbol{a}_2$, where $\boldsymbol{a}_1$ and $\boldsymbol{a}_2$ are the unit vectors of the graphene lattice

with a very small band gap, otherwise the nanotube is a semiconductor [112]. In addition, the diameter (d) and chiral angle (θ) of an ideal nanotube can be calculated from its (n, m) indices, as follows:

$$d = \frac{\sqrt{3}a}{\pi}\sqrt{n^2 + nm + m^2} \tag{3.2}$$

$$\theta = \tan^{-1}\left[\frac{\sqrt{3}m}{2n+m}\right] \tag{3.3}$$

where a (~0.142 nm) is the nearest neighbor C–C distance [113].

Owing to their small size (diameter around 1–2 nm), surface without dangling bonds, and superior optical electronics as well as their astonishing mechanical properties, SWNTs promise great potential for a wide range of applications in electronic devices, such as transparent conductive films, electric interconnects, transistors, and sensors. It has been found that an individual semiconductor SWNT (s-SWNT) has mobility of 10^5 cm^2/Vs [114], while an individual metallic SWNT (m-SWNT) has conductivity in excess of 200,000 S/cm [115] and a current carrying capacity of 10^9 A/cm^2 [116].

Though they can be either excellent conductors or semiconductors, SWNTs are always produced as a mixture of metallic and semiconducting nanotubes. To produce pure m-SWNTs or s-SWNTs with well-defined electronic properties, various methods have been employed including selective growth, selective removal, selective adsorption, and band structure modulation. For selective growth, there are three most commonly used synthesis methods: (1) CVD, (2) arc discharge, and (3) laser ablation. In each method, catalyst particles and carbon source, as well as growth temperature, substrates, and so forth, are the key parameters to control SWNT growth with specific diameter/chirality distribution [112]. Purity in more than 91% of metallic SWNTs was reported in 2009 [117], while growth of s-SWNTs with 95% purity was achieved as well [118]. Furthermore, selective growth of SWNTs with specific chirality has been developed [119]. Although the control of purity has been improved by the selective growth processes, post-synthesis sorting of s-SWNT or m-SWNT is still required in order to obtain samples with better purity and uniformity.

As-produced CNTs typically contain a mixture of various materials including catalyst particles, catalyst support, amorphous or non-tubular carbon, and a mixture of nanotubes of various lengths, diameters, chiralities, and bundles of tubes. Those amorphous carbon and carbon particles can be eliminated through a selective oxidative etching process due to their higher oxidation reaction rate than CNTs [120]. To further purify the CNTs, dispersing is usually required, which is also necessary for ink preparation. Carbon nanotubes can be directly dispersed in some organic solvents such as dimethyl formamide, N-methyl-2-pyrrolidone, chloroform, and dichlorobenzene without any dispersant. It is the simplest and most favorable method, which can exclude the influence of additional agents on the electronic performances of SWNTs [121]. Unfortunately, the concentrations of dispersed CNTs in these organic solvents are too low to be useful for industrial applications (>0.1g/L). Recently, Professor Coleman's group found that the solvent cyclohexyl pyrrolidone can disperse CNTs up to 2 g/L with high levels of individual tubes or small bundles, but the high boiling point of this solvent may be a problem in high speed printing [122]. In addition, CNTs can also be dispersed in super acids, which unfortunately are highly corrosive for printing equipment.

Just like the dispersion of any other nanoparticles, surfactants have been widely used to promote the dispersion of CNTs in various solvents [123]. It should be pointed out that the presence of large amounts of surfactants can lead not only to significantly lower electron transport levels in films but also to deterioration of electronic properties of individual SWNTs. Understanding the carbon nanotube chemistry is important for the selection of appropriate surfactant for dispersing/separation of SWNTs with specific characteristics. As illustrated in Figure 3.11 [124], the surface chemistry of SWNTs can be classified into five categories: (1) covalent exterior sidewall chemistry; (2) covalent chemistry at defect sites or open ends; (3) non-covalent surfactant encapsulation; (4) non-covalent polymer wrapping; and (5) molecular insertion into the SWNT interior [125]. Differences in the chemistry have been found for SWNTs with different diameter and chirality [126]. For example, it is believed that m-SWNTs have a higher electron density of states (DOS) at their Fermi levels [127] and a smaller ionization potential [128] than their semiconducting counterparts, resulting in higher reactivity of m-SWNTs than s-SWNTs.

Selective chemistry of exterior sidewalls has proven to be most important and has been widely employed to sort metallic and semiconductor SWNTs. Many reagents have shown reaction selectivity for m-SWNTs, such as diazonium salts [129], dichlorocarbene [130], hydroxyl (OH) radicals [131], nitronium ions (NO_2^+) [132], and OsO_4 [133], whereas H_2O_2 [134] and azomethineylides [135] mainly react with s-SWNTs. It was also found that such covalent interaction would significantly disrupt the conducting properties of single-wall carbon nanotubes [136]. For example, diazonium covalent functionalization on m-SWNTs caused saturation of the double bonds and selective decay of the transitions between the van Hove singularities of the metallic nanotubes [129]. By dichlorocarbene covalent functionalization, an energy gap at the Fermi level was opened in metallic SWNTs, converting metallic SWNTs to semiconductors [130]. Most of these reactions are reversible, but some are irreversible. For example, nitronium ions (NO_2^+) can attract those small-size m-SWNTs and turn them into amorphous carbon. Such selective influence on electronic performances in SWNTs has also been used to render

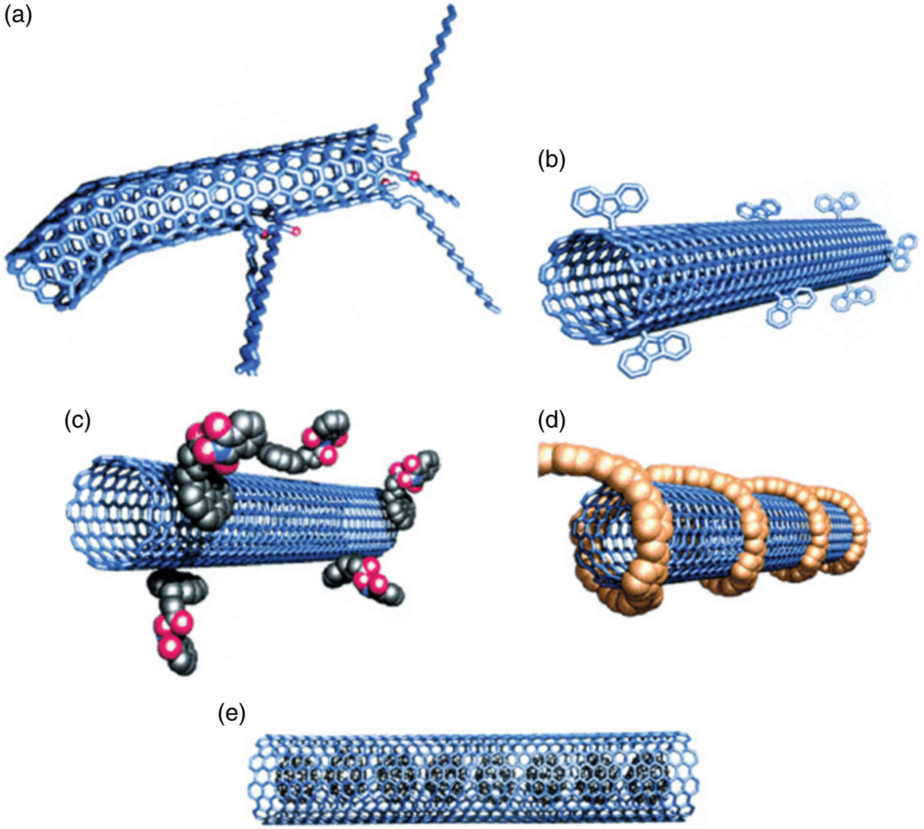

Figure 3.11 Chemistry on SWNTs: (a) covalent chemistry at defects or open ends; (b) covalent sidewall chemistry; (c) non-covalent surfactant encapsulation; (d) non-covalent polymer wrapping; and (e) molecular insertion into the SWNT interior. (Reprinted from [124] with permission from Wiley.)

metallic SWNTs inactive in thin-film electronic devices, yielding a purely semiconducting SWNT channel between source and drain electrodes of a TFT [137, 138].

In contrast to covalent chemistry, non-covalent adsorption can provide selective functionalization on SWNTs with less influence on their electronic properties. Selective adsorption of chemical agents on SWNTs with amine group has been extensively employed. For example, metallic SWNTs can be selectively functionalized by propylamine, isopropylamine, and intetrahydrofuran [139, 140]. Butoctadecylamine (ODA) possesses stronger physisorption on the sidewalls of s-SWNTs than m-SWNT if the SWNTs are acidicly treated beforehand [141]. Some other molecules such as bromine and charge-transfer aromatics have been confirmed to selectively attach to m-SWNTs rather than s-SWNT as well [128, 142]. In the case of s-SWNTs, selective non-covalent functionalization has been realized by taking advantage of porphyrin chemistry [143]. Furthermore, chiral dependent absorption was observed when chiral diporphyrin molecules were used [144]. With regard to diameter selectivity, some common surfactants such as sodium dodecylsulphate, sodium dodecylbenzenesulphonate, and sodium cholate have also been shown to be useful [145]. In addition, some polymers, including conjugated polymer and DNA, exhibited selective non-covalent interaction with certain chiralities of SWNTs [146–149].

3.4.2 Purification of SWNT

Based on the selective functionalization, SWNTs can be further sorted according to their different physical and electronic properties with separation techniques including electrophoresis, chromatography, and ultracentrifugation [126]. For example, SWNTs can be sorted according to their relative mobility through a gel, capillary, or solution in response to a DC electric field. It was found that the SWNTs with low molecular weight travel more quickly under the influence of the electrical field, thus leading to sorting SWNTs by length as well as by diameter in gel electrophoresis [150]. Similarly, high resolution capillary electrophoresis can be used not only for sorting but also for separating individual SWNTs from bundled SWNTs [150]. Electrophoresis has also been used for separating SWNTs by electronic type [129]. Another approach for electronic sorting of SWNTs is dielectrophoresis based on AC electric field, according to the differences in their dielectric constants. Figure 3.12 shows the typical experimental setup for dielectrophoresis of SWNT solution using a microelectrode array [151]. A drop of SWNTs suspended in solution is placed on a microelectrode array. In an AC electric field, metallic nanotubes are polarized much faster than their semiconducting counterparts, resulting in preferential polarization in metallic nanotubes. Finally, the polarized SWNTs are selectively deposited onto the substrate between the microelectrodes. The sorting can be accelerated by increasing the frequency of the AC field [151]. Furthermore, surface charges on semiconducting SWNTs can be neutralized by the use of cationic and anionic surfactants to improve the electronic separation [152]. To overcome the disadvantage of limited throughput in dielectrophoretic sorting with microelectrode arrays, larger electrodes or dielectrophoretic field-flow fractionation (FFF) were utilized to scale-up the process. The dielectrophoretic FFF approach exhibited the ability for not only electronic-type separation but also diameter-dependent sorting among semiconducting SWNTs [153].

Chromatography is one of the most commonly used methods for separation of organic compounds, so it is reasonable to consider the method for separating SWNTs is based on the difference in affinity with the stationary phase. Several chromatographic methods have been explored for sorting SWNTs. Different from conventional organic compounds, the functionalized SWNTs are usually hard to elute from the column. Therefore, one key technique is to promote an appropriate stationary phase during the functionalization of SWNTs, which depends on the

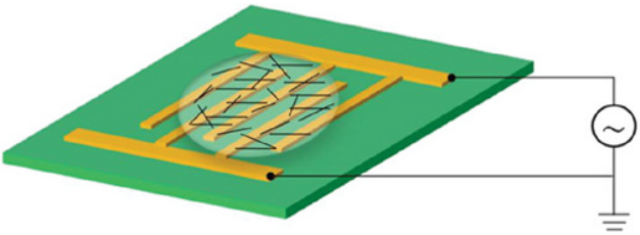

Figure 3.12 The original geometry used for dielectrophoretic sorting of SWNTs

surfactant [112]. Tanaka et al. developed a chromatography/electrophoretic hybrid approach to separate sodium dodecylsulphate (SDS) functionalized SWNTs with an agarose gel-filled column. However, only the m-SWNTs were separated from the starting gel in an electric field, whereas the s-SWNTs were left in the column [154]. In order to get both m-SWNTs and s-SWNTs, a continuous method was developed, in which the s-SWNTs were tightly bound to the gel and were eluted with 1% sodium deoxycholate solution after m-SWNTs were eluted with 1% SDS solution wash [155]. Similar to this approach, a simpler but effective method named the “gel-squeezing method” was developed as well [156].

Ion-exchange chromatography (IEX) of DNA-encapsulated SWNTs has shown the ability for separation of SWNT by diameter or electronic type [157, 158]. It was found that the sorting quality depends on DNA sequence, with a sequence of (GT)n where n is 10–45 leading to the best results [157]. Theoretical results indicated that the effective charge density of the DNA–SWNT hybrid was primarily governed by the DNA helical pitch [146]. Under the optimized DNA wrapping and IEX elution, a few small-diameter SWNTs with well-defined (n, m) values were isolated. Because the electronic type and diameter sorting are convoluted by SWNT length variations, sorting SWNTs by length first can improve the subsequent sorting of IEX [146]. Size-exclusion chromatography (SEC) and gel-permeation chromatography (GPC) have both been demonstrated for SWNT length separation [147].

One widely used separation technique is ultracentrifugation, which sorts SWNTs according to their sedimentation coefficient depending on several parameters including buoyant density and molecular weight. Conventional ultracentrifugation occurs in a constant density medium and typically suffers from convolution among multiple structural parameters. If coupled with corresponding selective chemistry, conventional ultracentrifugation would suffice for sorting SWNTs by diameter and particular electronic type as well [159]. Alternatively, density gradient ultracentrifugation (DGU) allows for sorting SWNTs by their buoyant density. In this approach, the SWNTs are loaded in the centrifuge tube where a density gradient has been intentionally formed. By ultracentrifugation, the SWNTs then sediment through the gradient until they reach their respective isopycnic points (that is, the point where the SWNT density matches the density of the gradient). Finally, the SWNTs will form layers in the centrifuge tube according to their buoyant density, which would depend on the SWNT diameter if the encapsulating surfactant layer was uniform for all SWNTs in solution. Actually, because SWNTs can only be dispersed in solutions with the aid of surfactants, the buoyant density of an SWNT in a DGU experiment will depend on both the geometry of the SWNT and surfactant coating. If SWNTs were functionalized as a function of their electronic structure, then DGU can sort SWNTs by their electronic properties. The first reported DGU approach used to sort SWNTs by diameter is for DNA–SWNT hybrids [160]. Subsequently, surfactants also were employed to enable sorting SWNTs by their electronic properties [126]. Figure 3.13 represents DGU diameter sorting of small-diameter (0.7–1.1 nm) SWNTs encapsulated with sodium cholate. In the centrifuge tube, the semiconducting tubes of SWNTs have been sorted into bands of various colors, corresponding to different band gaps of semiconducting tube [161].

3.4.3 Metallic SWNT Thin Film

As mentioned at the beginning of this section, individual metallic SWNTs (m-SWNT) have mobility in excess of 200,000 S/cm [115], while the highest conductivity of m-SWNT network is theoretically predicted at about 90,000 S/cm [162], which is almost an order of

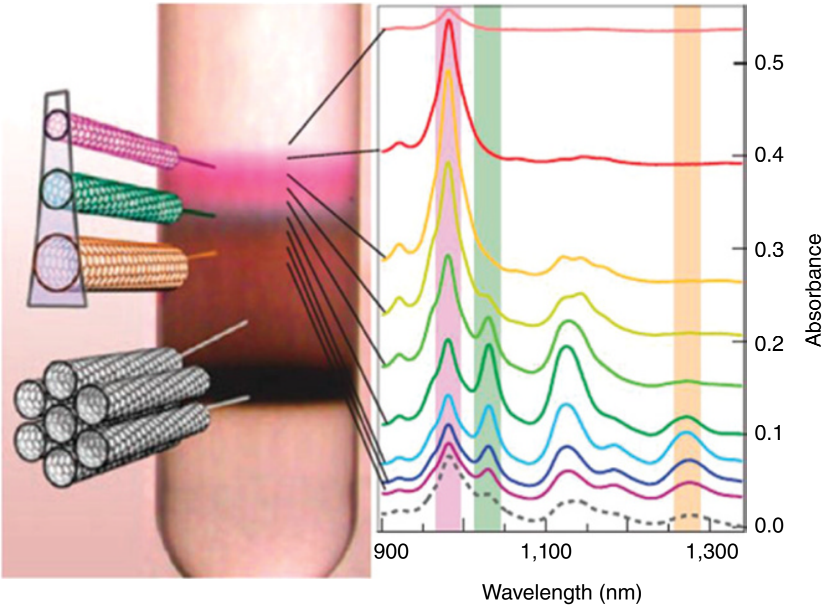

Figure 3.13 Photograph and optical absorbance spectra after the DGU separation of CoMoCAT-grown SWNTs (7–11 Å). (Reprinted from [161] with permission from Nature Publishing Group.)

magnitude greater than the highest value (12,825 S/cm) experimentally measured to date [163]. Similar to those metal nanowires, the m-SWNT network is considered as a promising material for transparent conductive film, and the optical-electronic dependence on length and other parameters depicted in Section 3.2.4 for metal nanowires is also applicable to the m-SWNT networks. Hecht et al. reported that the DC conductivity (σ_{dc}) of metallic CNT network films increases with the CNT length as a power law (σ_{dc}~$L^{1.46}$) [69]. The density (thickness) dependence of conductance can also be represented by a power law function with exponent ranging from 1 to 1.5 (1.33 for the ideal 2D case) above the percolation threshold, which is typically less than 1% surface coverage in the case of CNT network. Such increase of film conductivity with thickness continues until the film is about 100 times the density of percolation threshold, and then the conductivity approaches that of bulk material [77]. The width of CNT film would be critical for the CNT film conductivity if the film width became comparable to ~10 times the CNT length. A non-linear decrease of film conductivity was found with the decrease of film width and the conductivity drops dramatically as film width approaches tube length [164].

Broadly speaking, the conductivity of m-SWNT network can be enhanced through two strategies: (1) improving the conductivity of individual SWNT; and (2) decreasing the junction resistance. Because the conductivity of an individual m-SWNT depends on its mobility and carrier concentration, just like those doped transparent oxide conductors (e.g. ITO), the most straightforward method toward improving conductivity is to increase the carrier concentration by doping and use higher mobility SWNT. Experimental results indicated that both SWNT bundle and multiwall CNT network film have lower conductivity than that of m-SWNT. In addition, the presence of semiconductor SWNTs would also lead to higher resistance in CNT films, because the contact resistance at metallic-semiconducting junctions SWNTs is 3 orders of magnitude higher than that at the metallic-metallic junctions [113]. Therefore, the purity of m-SWNTs is crucial to obtain high conductivity in SWNT film [77].

Conductive m-SWNTs film can be made by using vacuum-assisted filtration, spin coating, spray coating, dip coating, and Mayer rod coating using m-SWNTs ink. Mayer rod coating is a simple and effective technique in which a metal bar with a wire wrapped around the outside is used to draw an aliquot of ink over a substrate surface. To some extent, the process in this technique is similar to some printing techniques such as gravure printing. Using the Mayer rod coating, Dan et al. reported CNT conductive film with sheet resistance of 100 Ω/sq. and 300 Ω/sq. at the visible transmittance of 70% and 90%, respectively [165].

3.4.4 Semiconducting SWNT Thin Film

Individual or aligned s-SWNTs possess many excellent properties such as ultrahigh mobility, transparency, and flexibility, the use of which as the channel material enables high performance TFTs. However, the manipulation toward an individual or aligned array of nanotubes is too complicated to realize on large-area substrates. For practical applications, a random SWNT network is better, though its electronic properties are inferior to those of individual or aligned SWNTs. In the pursuit of high performance electronics, one of the major challenges is to remove impurity in s-SWNTs network, especially those metallic CNTs. As discussed in the previous section, sorting CNTs by their electronic properties is done by dispersing them in solution. The solution can be directly used as ink for deposition of a random SWNT network, which enables a variety of solution-processed electronic devices. Semiconductor-enriched nanotube solutions are now commercially available, which makes it easy for researchers to explore device applications.

Because the percolation threshold is typically less than 1% of surface coverage in the case of a CNT network, a few metallic CNTs (including m-SWNT) can cause low I_{on}/I_{off} ratio and even loss of pinch-off. Consequently, as the nanotube density increases or channel length decreases, the mobility (or unit-width normalized transconductance) improves while the current I_{on}/I_{off} ratio decreases. Therefore, a trade-off needs to be taken into consideration when optimizing the device performance for different types of applications. Solution-processed SWNT TFTs had been suffering from low I_{on}/I_{off} ratio [166, 167] for a long time until Bao's work was published in 2011 [163]. They reported a convenient and effective approach to achieve highly selective dispersion of s-SWNTs, taking advantage of high sorting efficiency by regioregular poly (3-dodecylthiophene) (rr-P3DDT) wrapping. A geometric model was devised to illustrate such polymer wrapping around a smooth cylinder with a fixed diameter, as shown in Figure 3.14. Moreover, their s-SWNT solution deposition technique was the soaking method, in which the substrate was immersed into the s-SWNT solution for a certain period of time, allowing carbon nanotubes to settle onto the substrate. After that, solvent washing and annealing were used to remove impurities and to improve the electrical properties of printed SWNT TFTs. Therefore, the substrates need to be modified with 3-aminopropyltrimethoxysilane (APTES) to improve the interaction between s-SWNTs and the substrates. Finally, high mobility (~12 cm^2/Vs) TFTs with high I_{on}/I_{off} ratio ($>10^6$) were obtained with the SWNT networks [163].

Since then, other groups also demonstrated high performance s-SWNTs, using various polymers and different SWNT diameters and substrate treatment methods [169–176]. At the

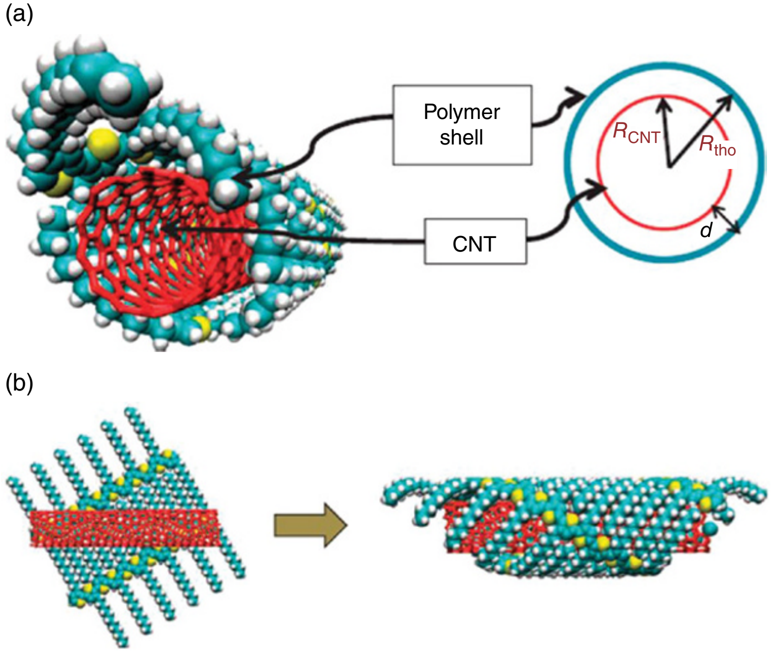

Figure 3.14 Geometric models of the polymer–SWNT supramolecular structure, where the polymer is regioregular poly(3-dodecylthiophene). (a) Schematics of a cross-sectional geometrical view of the polymer–SWNT supramolecular structure, in which d represents the gap between the radii of SWNT and the polymer tubular structure. (b) The interdigitation of the polymer's side chain causes the formation of a double-stranded polymer, which in turns proceeds to wrap around the SWNT. (Reprinted from [168] with permission from Nature Publishing Group.)

authors' Printable Electronics Research Center, a similar method was used to selectively sort large-diameter s-SWNTs using rr-P3DDT and (9, 9-dioctylfluorene-co-bithiophene) (F8T2). The sorted s-SWNT solutions by F8T2 were used directly for fabricating TFTs by aerosol jet printing, and the printed TFTs show effective mobility as high as 42.1 $cm^2\ V^{-1}s^{-1}$ (±1.2 $cm^2V^{-1}s^{-1}$) and on/off ratio up to 10^7 [171]. Furthermore, our center also investigated the effect of surface wettability properties on the electrical properties of printed s-SWNT TFTs on SiO_2/Si substrates. It was found that a simple oxygen plasma treatment of the substrate can significantly improve the electrical properties of transistors based on PFO-BT-sorted s-SWNTs. The mobility of printed TFTs treated with oxygen plasma for 1 min is 10-fold of that on substrate without any treatment [176]. Recently, large-area fully printed transistors with sorted SWNT inks have been demonstrated, which exhibited much-improved performance with mobility and I_{on}/I_{off} current ratio of up to ~9 cm^2/Vs and 10^5 [177].

Although electrons can transport as well as holes in s-SWNT in theory [178], most reported SWNT TFTs exhibited p-type characteristics, due to the doping of SWNTs by oxygen [179, 180] (oxygen in air and oxidizing acids during the solution process) and the relatively small Schottky barrier for the holes at the contacts of metal source/drain electrodes. For digital logic circuits, it is desirable to be able to generate both p-type and n-type SWNT transistors so as to construct pn-diodes and CMOS logic circuits. Many approaches have been used to switch

SWNT devices from p-type to n-type, including chemical doping, electrostatic doping, trap-charge-induced doping, metal work-function-induced doping, and ion implantation [181]. For example, the use of low work function metals such as Al and Ca, which reduce the barrier for electrons at the contacts, enable the n-type unipolar SWNT transistors. Another effective technique is passivation of the nanotube TFTs with high-k dielectric layer such as HfO_2 deposited by atomic layer deposition (ALD). It was attributed to the desorption of moisture and oxygen from the metal contacts during the vacuum baking process in the ALD chamber as well as positive fixed charges introduced at the interface between HfO_2 and the substrate [182]. More systematic review of the doping strategy on CNT devices can be found in the literature [181].

The solution-processed SWNT transistors have shown promise in a wide range of applications including integrated circuits, radio-frequency electronics, artificial skin sensors, and displays. Ha et al. constructed aerosol-jet-printed s-SWNT-based transistors on polyimide, combined with prepatterned Cr/Au electrodes, aerosol-printed ion gel as dielectric, and poly(3,4-ethylenedioxythiophene):polystyrene sulfonate (PEDOT:PSS) as gate electrode. The TFTs exhibited high field-effect mobility of 20 cm^2/Vs and high I_{on}/I_{off} ratios of ~10^5 even in short channel, due to the high purity of s-SWNTs. By using narrow source and drain electrodes, high operating frequency inverters (~1 MHz) and five-stage ring oscillators (>20 KHz) were successfully demonstrated at low voltages (<3 V) using these devices [183]. Some mechanically flexible integrated circuits have also been demonstrated [175]. Figure 3.15 shows the mechanically flexible s-SWNT-based logic gates such as an inverter, two-input NAND, and NOR. Owing to the excellent mechanical flexibility of the carbon nanotube networks, the fabricated inverter circuit is extremely bendable under various curvature radii (down to 1.27 mm) (Fig. 3.15c) and repeated bending tests (2000 cycles) (Fig. 3.15d).

On the other hand, high mobility and on/off ratio of s-SWNT TFTs provided a promising backplane technology for AMOLED (active-matrix organic light-emitting diode) display. In 2011, monolithically integrated AMOLED arrays with 500 pixels driven by 1000 s-SWNT TFTs were first demonstrated as shown in Figure 3.16 [184]. By combination of CNT TFT-based control circuits, AMOLEDs, and pressure-sensing elements, Wang et al. reported the first user-interactive e-skin that not only spatially maps the applied pressure but also provides an instantaneous visual response through a built-in active-matrix OLED display with red, green, and blue pixels [185]. When pressure is applied to a certain region on the continuous piece of pressure sensitive rubber (PSR), arrays of CNT TFTs located under the region will turn on the OLEDs connected to the corresponding CNT TFTs under the same region. Figure 3.17 illustrates the schematic diagram of an element in the user-interactive electronic skin arrays and the design mechanism and display under the pressure applied by C-, A- and L-shaped PDMS slabs [185]. Chen et al. reported full-printed s-SWNT-based transistors with mobility of 10–30 cm^2/Vs and I_{on}/I_{off} ratios of 10^4–10^7 and successfully used them to control OLEDs [186]. Noh and Jung et al. reported mass production of fully printed SWNT-based transistors by combining roll-to-roll gravure printing with inkjet printing on PET. A series of electronic systems such as inverters, ring oscillators, and 1-bit radio frequency identification (RFID) tags were demonstrated using these transistors, which exhibited moderate variation in the output and transfer characteristics attributed to the misalignment of printed source/drain electrodes and the variation in the roughness of the dielectric layer [187–190].

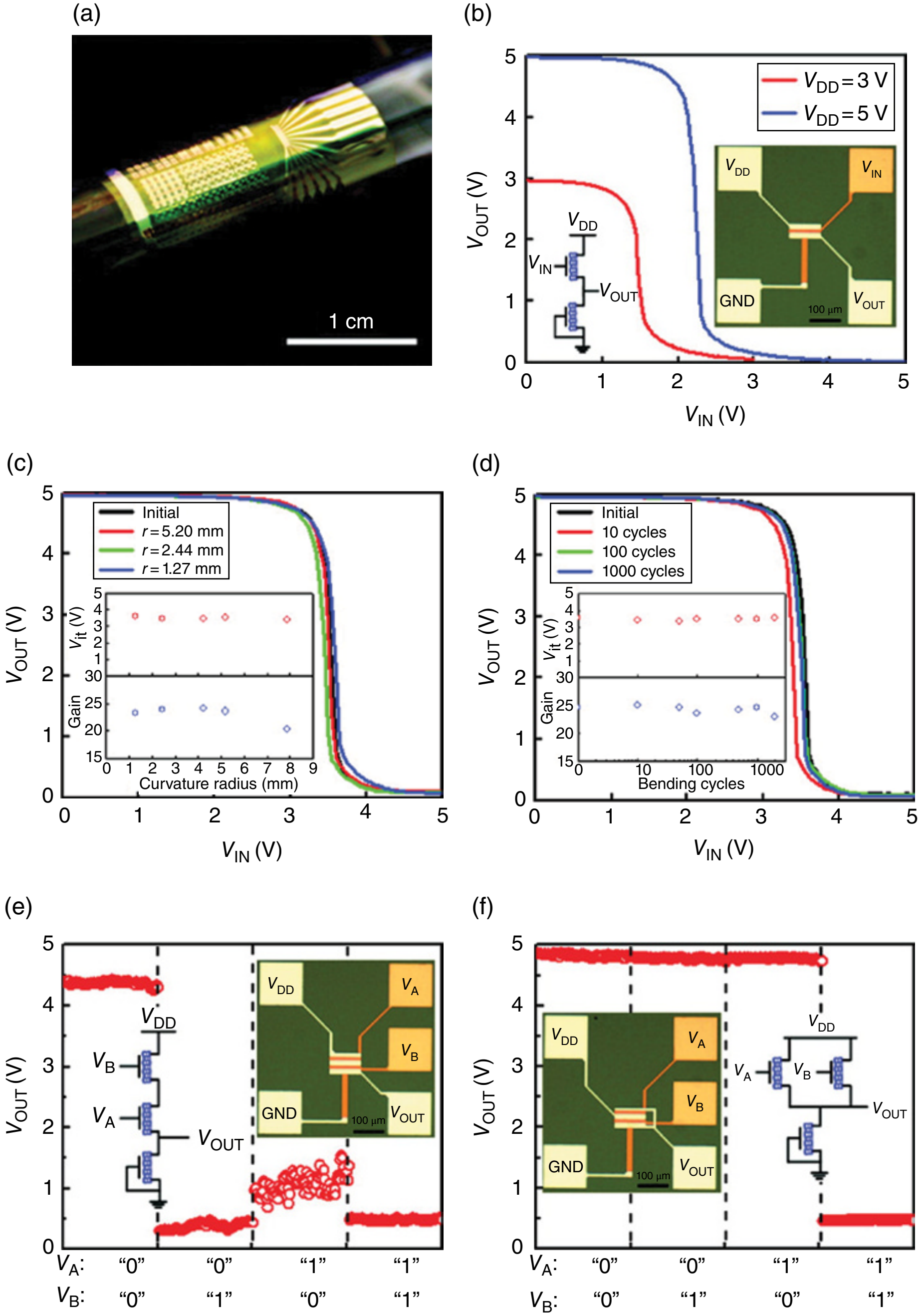

Figure 3.15 (a) Photograph of a flexible s-SWNT-based integrated circuit wrapped on a test tube with a curvature radius of 5 mm. (b) Flexible nanotube inverter measured with VDD of 3 or 5 V. (c) Inverter measured at various curvature radii. Inset: Inverter threshold voltage and gain as a function of curvature radius, showing minimal performance change even when bent down to 1.27 mm radius. (d) The inverter VTC is measured after various numbers of bending cycles, indicating good reliability after 2000 cycles. (e, f) Output characteristics of the diode-loaded two-input NAND (e) and NOR (f) logic gates. (Reprinted with permission from [175], copyright 2012 American Chemical Society.)

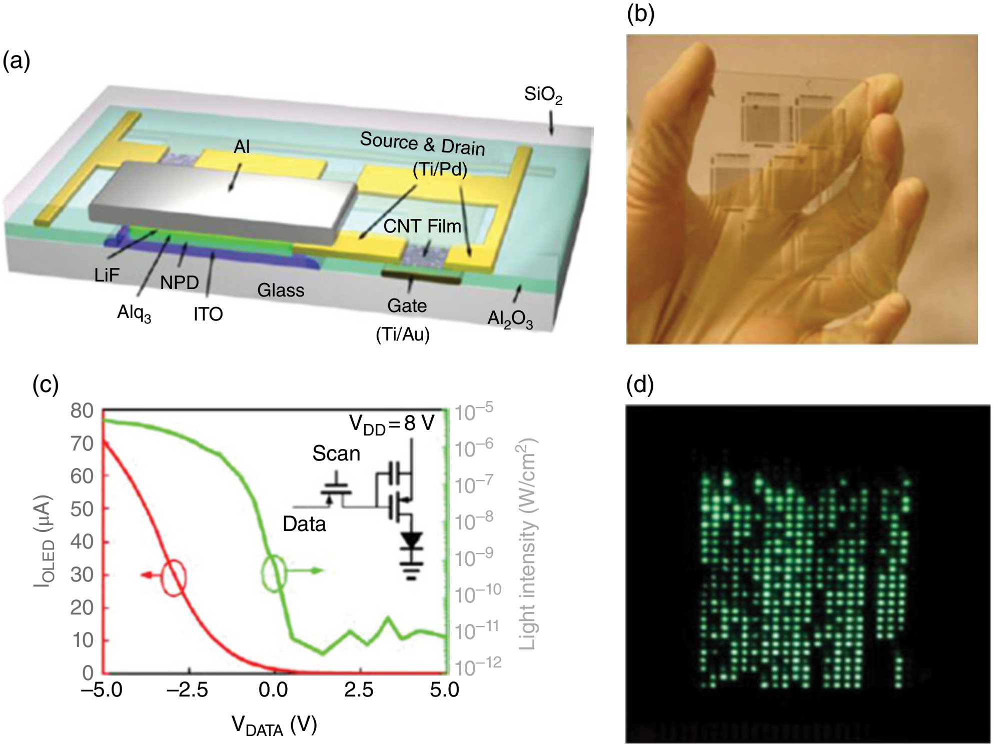

Figure 3.16 (a) Schematic diagram of one pixel of OLED controlled by s-SWNT-based driver circuitry. (b) Arrays of AMOLED-controlled CNT circuits fabricated on a transparent glass substrate. (c) Current and light intensity behavior of a pixel of the CNT-controlled OLED unit. (d) Arrays of AMOLED illuminating after being turned on by CNT network-based driver circuit. (Reprinted with permission from [184], copyright 2011 American Chemical Society.)

3.5 Graphene

An ideal single-layer graphene is zero band gap semiconductor with a width more than 10 μm and thickness of 0.34 nm (corresponding to the interlayer spacing of graphite) and that can be sufficiently isolated from its environment to be considered freestanding [191]. Figure 3.18 shows examples of multilayer and single-layer graphene [191]. Due to zero effective electron/hole mass in graphene, its charge carriers (both electron and hole) exhibit giant intrinsic mobility and can travel for micrometers without scattering at room temperature. Room temperature electron mobility of 2.5×10^5 cm^2/Vs was measured in experiments, which approaches to theoretically predicted limit (2×10^5 cm^2/Vs) [192, 193]. However, graphene has to be loaded on a substrate in practical applications, which leads to great degradation of electronic mobility [194]. The mobility for grahene on SiO_2 substrate is about 40,000 cm^2/Vs [194]. Similar to the heavily doped transparent conductive oxide, conductivity of graphene is proportional to both mobility and carrier density; however, its mobility would usually degrade with the increase of charge carrier concentration by doping. It was found that the mobility deceased from 10^5 cm^2/Vs to 10^4 cm^2/Vs when the charge carrier increased from 10^{12}/cm^2 to 10^{13}/cm^2 [195–197]. Wu et al. predicted that the sheet resistance of graphene will vary with the number of layers

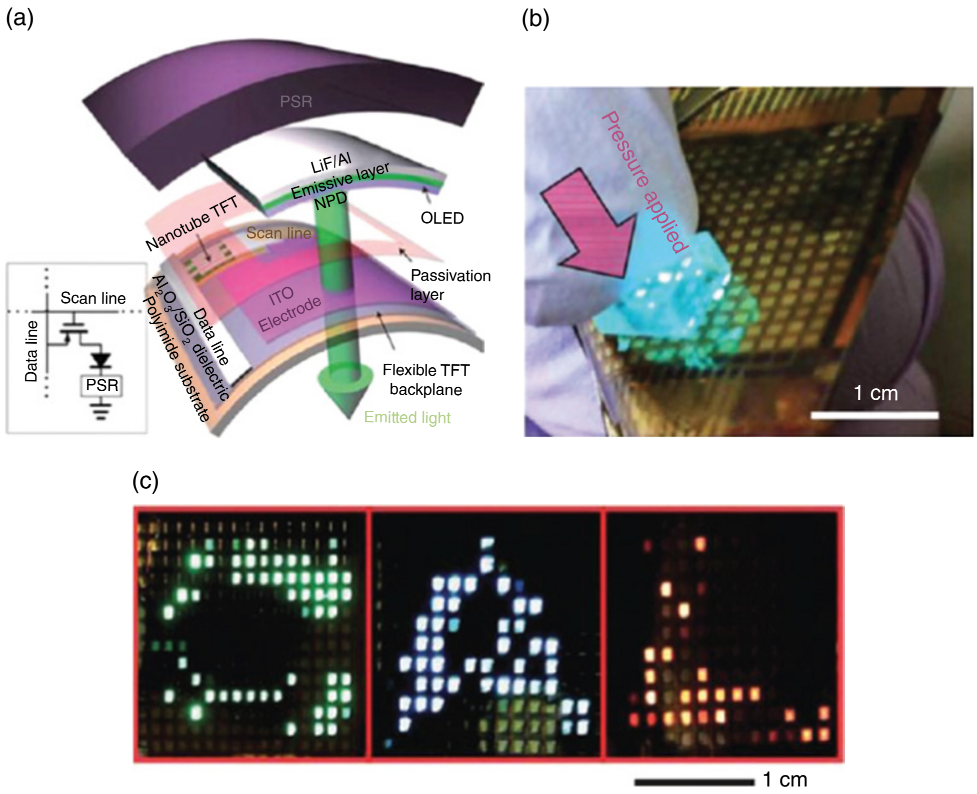
(a)
PSR
LiF/Al
Emissive layer
NPD
OLED
Nanotube TFT
Scan line
Passivation layer
ITO Electrode
Scan line
Data line
PSR
Al2O3/SiO2 dielectric
Data line
Polyimide substrate
Flexible TFT backplane
Emitted light
(b)
Pressure applied
1 cm
(c)
1 cm

Figure 3.17 (a) Schematic diagram of a pixel of PSR-based sensor integrated with an OLED in conjunction with a CNT thin-film-based driver. (b) Demonstration of lighting arrays of OLEDs under the region where pressure is applied on the e-skin. (c) Illustration of Lett. C, A, and L illuminated by the e-skin as pressure is applied to PDMS stamps formed in the letter shapes. (Reprinted from [185] with permission from Nature Publishing Group.)

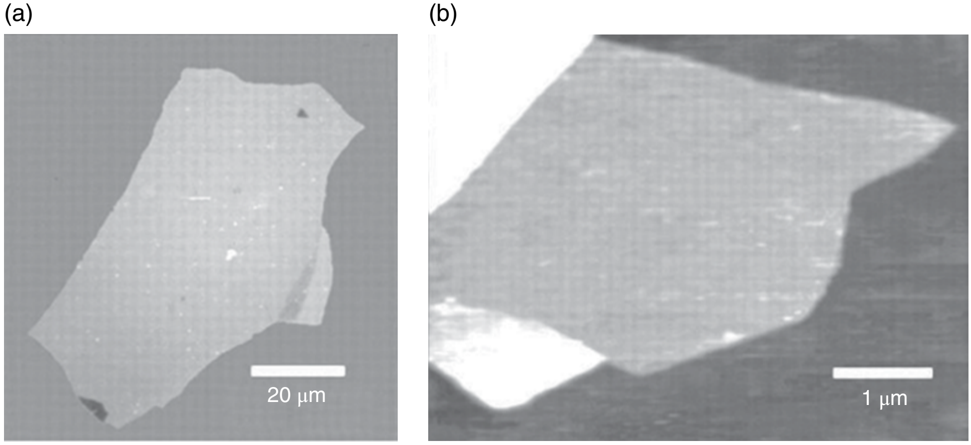

Figure 3.18 (a) Photograph of a relatively large multilayer graphene flake with thickness ~3 nm on top of an oxidized Si wafer. (b) AFM image of single-layer graphene on SiO_2 surface. (Reprinted with permission from [200], copyright 2008 American Chemical Society.)

as R s~62.4/N Ω/sq. for highly doped graphene [198]. Graphene also has high optical transmittance due to its atomic thinness, though graphene has a surprisingly high absorbance of ~2.3 N% (N is the number of layers) [199]. In addition, excellent mechanical strength and elasticity make graphene suitable in flexible electronics applications.

Many methods have been developed to prepare graphene with properties appropriate for specific applications, which can be categorized into mechanical exfoliation, solution-based and chemically assisted exfoliation, chemical synthesis, epitaxial growth through sublimated SiC surfaces, and pyrolysis of hydrocarbons on metal surfaces [201]. The mechanical exfoliation using tape, the so-called "Scotch tape method," is a process utilizing adhesive tape to repeatedly peel off layers of highly oriented pyrolytic graphite and press it onto an appropriate substrate. Although this mechanical exfoliation technique can produce the highest quality samples to provide an excellent platform for studying the fundamental transport and optical properties of individual graphene sheets, it is hard to scale up for practical applications [77]. Epitaxial growth on silicon carbide (SiC) surfaces is a process in which Si atoms are sublimated from SiC wafer and leave a graphitized surface. The quality of such graphene can be very high on wafer scale and suitable for applications concerning high frequency transistors [202]. There are two major drawbacks to this method: the high cost of SiC wafers and the high processed temperatures (above 1,000°C). A CVD method based on the pyrolysis of hydrocarbons on metal surfaces has emerged to be one of the most promising techniques for large-scale production of high quality graphene films on metal foils [203]. After the formation of graphene, it is required to transfer the graphene layer from the metal foil/film to a dielectric surface or other substrate of interest. The transfer process may be as complicated as the growth of graphene itself [204]. As shown in Figure 3.19, roll-to-roll production of 30-inch graphene films has been demonstrated through transfer of the graphene films grown by CVD from flexible copper substrates to polymer substrates. The transfer process includes adhesion of polymer supports, copper etching (rinsing), and dry transfer printing on a target substrate. The final films have sheet resistances as low as 125 Ω/sq. and 30 Ω/sq. at 97.4% and 90% optical transmittance, respectively [205].

Solution and chemical exfoliation is considered as the most promising approach to high volume production of printable graphene inks. In these processes, bulk graphite was intercalated by inserting chemical agents between layers that weaken the cohesive van der Waals force. Sometimes, one chemical intercalation cannot produce high quality single-layer graphene but multilayer graphene, thus reintercalation was used to enable high yield production of high quality single-layer graphene sheets [206]. Due to similar chemical structures, many techniques used in carbon nanotubes can be employed in the case of graphene. For example, Coleman et al. reported liquid-phase exfoliation of graphite in an organic solvent such as N-methyl-pyrrolidone (NMP), while it is widely known that NMP is an excellent solvent for CNTs [207, 208]. Graphite oxidation would happen in most chemical exfoliation processes and was also utilized intentionally to exfoliate graphene, in which graphite pellets are first oxidized and ultrasonically exfoliated in an aqueous solution, followed by chemical reduction to remove the oxygen groups [209]. However, it is essential that graphene films must be fully reduced from the graphite oxide because incomplete reduction will lead to relatively poor electrical quality when compared to pristine graphene [210]. To remove the oxygen from graphene oxide, many reduction methods have been developed including chemical, thermal, electrochemical techniques, but they generally resulted in inferior samples that are more precisely named as reduced graphene oxide (RGO) [201]. Homogeneous stable colloidal suspensions of electrically conducting graphene can be achieved in many organic solutions with the aid of polymer or surfactant [211]. It was also found that graphene can disperse in an alkaline condition without any extraneous surfactant agent [212].

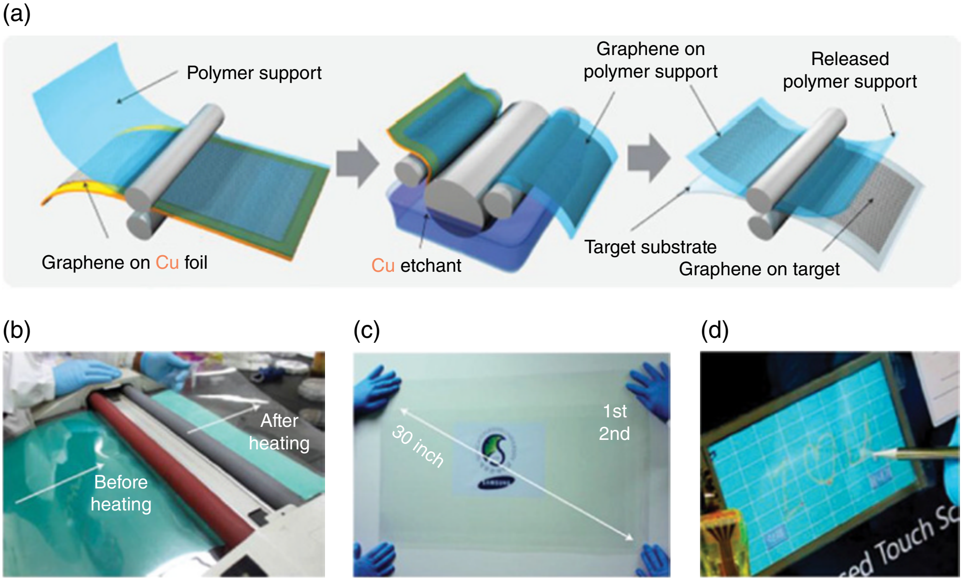

Figure 3.19 (a) Schematic of roll-based production of graphene films grown on a copper foil. The process includes adhesion of polymer supports, copper etching (rinsing), and dry transfer printing on a target substrate. A wet-chemical doping can be carried out using a setup similar to that used for etching. (b) Roll-to-roll transfer of graphene films from a thermal release tape to a PET film at 120°C. (c) A transparent ultralarge-area graphene film transferred onto a 35-inch PET sheet. (d) A graphene-based touch panel connected to a computer. (Reprinted from [205] with permission from Nature Publishing Group.)

Although 30 Ω/sq. sheet resistance with high optical transmittance (90%) has been obtained in large-area films with a CVD process as discussed above [205], solution-processed (potentially by printing) graphene films still suffer from high sheet resistance at high transmittance. RGO film reduced by hydroiodic acid exhibited a sheet resistance of 840 Ω/sq. and a transmittance of 78% [213]. Recently, Wang et al. reported large-area fabrication of uniform RGO films by rod coating, and the flexible conductive films displayed several kΩ/sq. sheet resistance at the transmittance of 80% [214]. Therefore, it may be realistic to consider applications whose conductivity requirement is relatively lower [204]. In the case of graphene used as a semiconductor, its zero band gap limits its practical use as channel material in graphene-based electronics. Some methods have been used to open a band gap in graphene: for example, patterning the sheet in nanoribbons form; deposition on special substrate; bilayer graphene under a dual gate; and chemical modification [215]. However, the opening of band gap would always result in the degradation of charge carrier mobility in graphene [216]. Currently, printing-based graphene transistors are not yet suitable for practical applications.

3.6 Silicon and Germanium

Silicon (Si) and germanium (Ge) are the most important semiconductors in the history of microelectronics, belonging to the same IVA group as those carbon allotrope materials. First germanium, then silicon became dominant as the core semiconductor material for transistors, which lasted over a half century till the present day. In recent years, SiGe alloy also emerged as a promising material in applications such as IR (infrared) detectors and waveguides. In addition to integrated circuits, silicon is also among the most important semiconductor materials used in such applications as solar cells and backplanes in flat panel displays.

The success of silicon is attributed to its many advantages. Silicon is the second-most abundant element in the earth's crust and can be prepared cheaply into large-size high quality single crystalline wafers with purity in excess of 99.9999999%. The native oxide on the silicon surface (silica) is an excellent dielectric material that prevents the further oxidation of silicon. In addition, silicon with appropriate doping exhibits very good electronics performance, including high mobility, proper band gap, high thermal conductivity, and large minor carrier lifetime. The worldwide industrial application and scientific research over a half century has made unparalleled accumulation in knowledge about silicon. Therefore, silicon cannot be ignored in printed electronics, though there is little literature about its printing aspect due to the high melt point and easy oxidation of silicon ink.

In 2008, a corporation named Kovio claimed that it had printed silicon-based RFIDs with their high performance silicon, dopant, metal, and insulator inks, where the transistors had mobility close to 100 cm^2/Vs. Innovalight Corp. has also developed silicon ink for solar cells. In the case of research, Shimoda *et al.* reported silicon TFTs using a polysilanes methylbenzene solution as "silicon ink" prepared by a UV light polymerization process of cyclopentasilane (CPS). The spin-casted and inkjet-printed silicon TFT exhibited mobility of 108 and 6.5 cm^2/Vs, respectively, though the preparation of ink and silicon film must be under inert ambient [217]. There have been a few other reports of nanoparticles-based inks that were printed to fabricate Si/Ge TFTs but did not exhibit very good performance [218–220].

Silicon and germanium nanoparticles have been synthesized by a variety of physical and chemical methods including electrochemical etching of bulk silicon, chemical etching, laser ablation, mechanical milling of bulk silicon, pyrolysis of silane, and wet chemistry approaches. Pyrolysis of silane can be triggered by high-temperature heating [221], laser heating [222], microdischarge [223], microwave [224], and plasma treatment [225] under different conditions to synthesize high quality silicon/germanium nanocrystals with controllable dimensions in large quantity. If borane or phosphine is added in the reactive gas flow, doped Si/Ge nanocrystals can be achieved [224, 226]. Furthermore, organic molecules can be grafted onto the surface of nanocrystals through thermally activated reactions [225]. Kortshagen's group reported production of Si/Ge nanocrystal inks utilizing a two-step plasma process (Fig. 3.20), where one is for nanocrystals formation and another is for further organic grafting [225]. They also fabricated Ge and Si TFTs using the plasma-synthesized nanocrystal inks, and the Ge-TFTs exhibited promising performance with electron and hole mobility in the order of 10^{-2} cm^2/Vs and I_{on}/I_{off} ratio better than 10^3 [219]. Similar to those metal nanoparticles, wet chemistry approaches have proven to be an effective strategy for the fabrication of Si nanoparticles based on redox of silicon compound such as silicon halides [227, 228] and metal silicide [229] using a standard Schlenk technique. Laser ablation of a silicon target leads to thermal vaporization of Si followed by nanocrystal growth. If the process takes place in a specific solution or gas ambient, Si nanocrystal dimensions can be controlled and organic capper can be grafted on the surface of nanocrystal in situ [230]. High energy mechanical ball milling of bulk silicon was also used to produce blue luminescent alkyl/alkenyl-passivated Si nanocrystal [231] and ink [220]. Silicon nanocrystals can also be produced by electrochemical etching of silicon

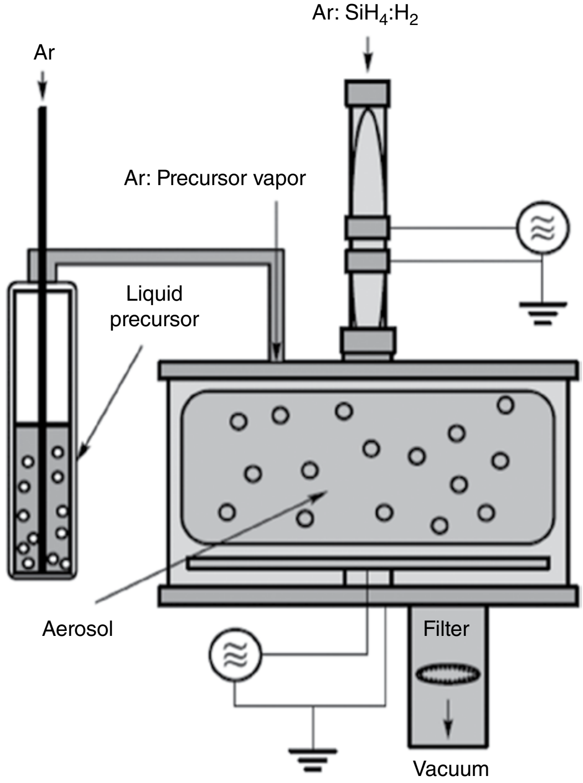

Figure 3.20 Two-step plasma experimental setup for the synthesis and in-flight functionalization of silicon nanocrystals. The surface functionalization is performed immediately after synthesis by plasma-assisted in-flight grafting of organic molecules in the second plasma chamber. (Reprinted from [225] with permission from Wiley.)

wafer taking place in an HF solution (in some cases, an additional treatment of etched wafers in H_2O_2 was applied) [232]. Another interesting method is based on SiO_x ($x < 2$) that has been produced commercially. In this method, SiO_x is first turned into the mixture of Si and SiO_2 through a phase separation in high temperature annealing. Silicon nanoparticles can then be obtained after immersing the mixture in HF or HF/HNO_3 solution [233].

The surface of silicon nanoparticles is prone to oxidize into Si—O—Si and Si—OH upon exposure to air. To improve both the dispersion and oxidation resistance, organic agents are required as cappers to be grafted on the surface of silicon nanocrystals, therefore the formation of the Si—C bond is crucial. The most important silicon surface states providing opportunity for the formation of Si—C bond are highly reactive Si fresh surface and hydride-terminated surface (Si—H or Ge—H). As-generated fresh silicon surfaces in some preparation processes of nanoparticles (such as high-energy mechanical ball milling of bulk silicon) are highly reactive due to the presence of dangling bonds and double bonds that can be used to form Si—C bond, as shown in Figure 3.21. In addition, some chemical reaction processes (Fig. 3.22) have been developed to turn Si—H into Si—C. Si—H surfaces can be generated during the preparation

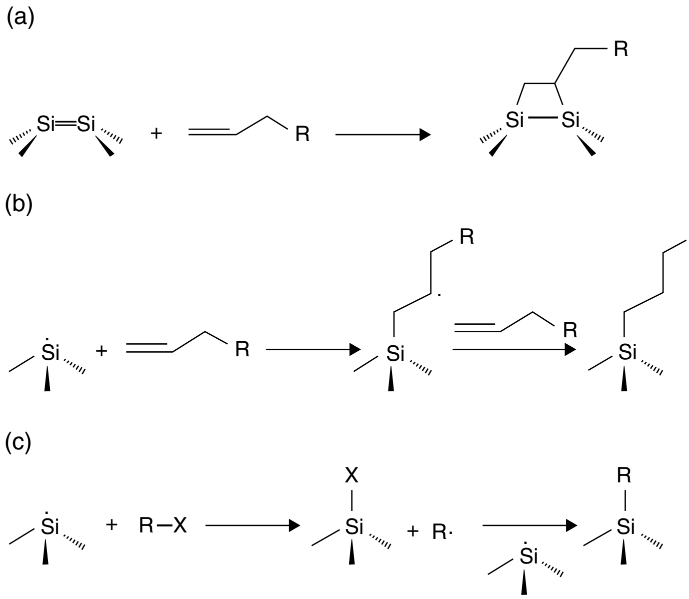
(a)
Si
Si
+
R
Si
Si
R
(b)
Si
+
R
Si
R
R
Si
R
(c)
X
R
Si
+
R–X
Si
+
R·
Si
Si

Figure 3.21 Possible reactive groups formed upon fresh silicon surfaces (Si = Si dimers and silicon radicals), where R is an organic radical and X is Cl or Br. Upon exposure to alkenes or alkyl halides, Si—C bond formation may occur through the pathways shown here

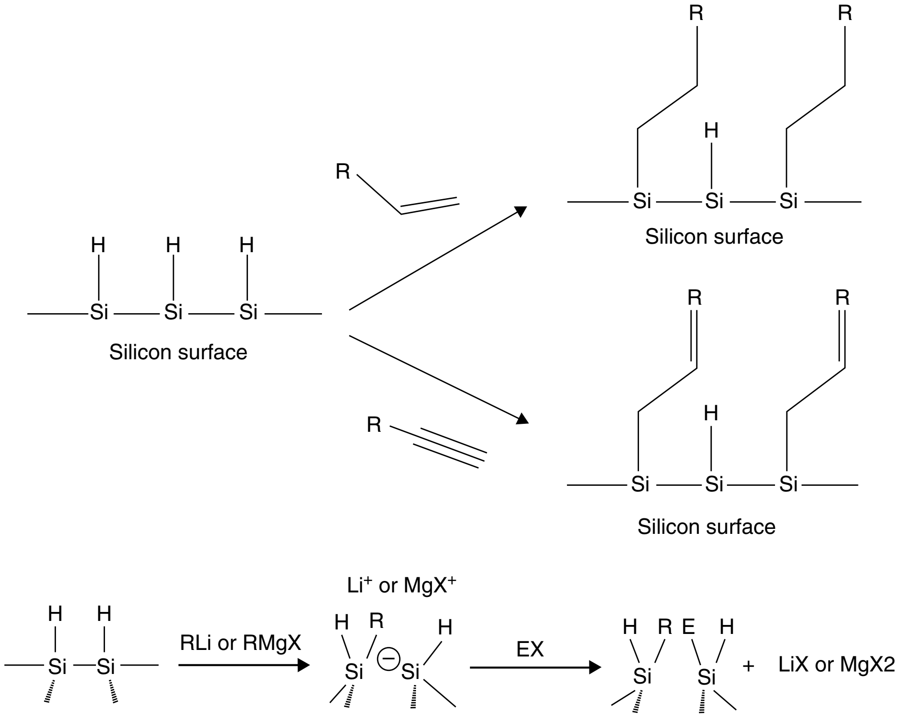
R
R
H
Si
Si
Si
Silicon surface
R
H
H
H
Si
Si
Si
Silicon surface
R
R
H
R
Si
Si
Si
Silicon surface
Li+ or MgX+
H
H
Si
Si
RLi or RMgX
H
R
H
Si
Si
EX
H
R
E
H
Si
Si
+
LiX or MgX2

Figure 3.22 Chemical reaction processes to turn Si—H into Si—C, where EX means an electrophile

process of nanoparticles or by post-treatment in HF or NH_4F solution. In addition, an Si—H surface is prone to transferring into an Si—X (X = Cl, Br) surface, which also can be further turned into Si—C by the Grignard reaction [234].

3.7 Metal Chalcogenides Semiconductor and Quantum Dots

3.7.1 Metal Chalcogenides Semiconductor

Metal chalcogenides (sulfides, selenides, and tellurides) semiconductors combine direct band gap with very high mobility and other characteristics, leading to successful applications in various electronic and optoelectronic devices such as photovoltaics, highly emissive electroluminescent devices, and sensors. In addition, metal chalcogenides are also the most important materials for quantum dots, due to, among other things, their high photoluminescent (PL) quantum yields, size-tunable band gap, and small exciton binding energy. As semiconductors, metal chalcogenides TFTs have demonstrated mobility more than 20 cm^2/Vs and $I_{on}/I_{off} > 10^6$ [235, 236].

Metal chalcogenides semiconductor films were achieved from deposition of metal salt precursor solution and subsequent annealing or from metal oxide precursor films in the corresponding chalcogen-contained reductive ambient. However, the annealing temperatures required are in excess of 300°C and even more than 500°C in some cases. Another more effective solution-based ink was reported by Mitzi et al. in which chalcogenides with excess chalcogens simply dissolve in hydrazine (N_2H_4) to form metal-chalcogenide anions stabilized by hydrazinium ($N_2H_5^+$) cations in solution [237, 238]. For example, SnS_2 with excess S dissolves in hydrazine to generate a solution of $(N_2H_5)_4Sn_2S_6$ that can crystallize upon evaporation of the hydrazine. At elevated temperatures (no more than 300°C), the precursor of $(N_2H_5)_4Sn_2S_6$ decomposes and then condenses into extended chalcogenide frameworks, yielding highly crystallized chalcogenide films [237]. Multicomponent metal chalcogenides such as SnS_xSe_{2-x} can also be prepared easily by taking advantage of this chemistry. Such metal chalcogenide semiconductor films have acted as active layers in high performance transistors (channel mobility > 10cm^2/Vs) and solar cells (power conversion efficiency of 12%) [239].

3.7.2 Quantum Dots

Quantum dots (QDs) are semiconductor particles with size approaching the Bohr radius of excitations within the corresponding bulk semiconductor, which can offer many intriguing properties such as size-tunable band gap, small exciton binding energy, and high PL quantum yields, due to the quantum size effect and their very high available surface area. The colloidal metal chalcogenides QDs have been successfully synthesized by a wide variety of wet chemical techniques to achieve a high degree of crystallinity, specific mean size, and size distribution. Ligands are usually used to stabilize the inorganic nanoparticles and can simultaneously result in relatively monodispersed suspensions in solution phase. Therefore, colloidal QDs are naturally suitable for printed electronics due to the combination of small size, monodispersity, distinctive properties, and low cost [240].

Colloidal QDs have been successfully prepared by a general method named the hot-injection technique. With good understanding of growth kinetics, the controls on size, size dispersity, and shape of nanoparticles can be well performed. In most cases, the metal precursor is initially held in the main reaction flask at a given temperature and chalcogenides precursors are injected. In some cases, the reverse procedure may be used, where the metal precursor is injected into a hot chalcogenide precursor solution. Volumes of literature have reported a variety of high quality metal chalcogenides QDs such as CdX, PbX, and ZnX (X = S, Se, Te) and even their core/shell QDs [241].

Despite advances in both the synthesis of QDs and the formation of high quality QD solid-state films, for a long time, field-effect transistors based on different colloidal QD films presented very poor carrier mobilities, mainly due to the long chain of dielectrically isolating ligand molecules and high number of surface defects that hinder the charge transport by trapping charge carriers in mid-gap states. Annealing and sintering have been used to improve the performance of a range of QD films, by means of reducing the distance between the particles in the film [242]. Romero and Drndic et al. showed improvements in field-effect transistor performance of annealed PbSe QD films, where the current increased from less than 10fA to several pA [243]. Kim et al. reported hole mobility up to 0.82 cm^2/Vs in a bottom-gate configuration and 2.38 cm^2/Vs in a top-gate configuration by sintering HgTe QD films [244]. To remove long-chain organic ligands, high temperatures are usually required, which adversely leads to the sintering of the QDs, resulting in elimination of quantum confinement [245]. Even so, the achieved mobilities are still rather limited by the annealing/sintering.

Ligand exchange processes are proven to be more effective and “soft,” where bulk organic ligands are replaced with shorter ligands in the solution or film. If the ligand exchange is performed after the formation of QD films, disorder and cracks may be observed in the treated film partly due to the volume shrink, as shown in Figure 3.23 [246]. In order to form a continuous, void-free, and crack-free film, a multilayer strategy is required where film deposition followed by chemical treatment to exchange the longer ligands with shorter ligands is repeated several times until the desired film thickness is reached. In contrast to the solid-state exchange process, the solution-exchange approach, which replaces the original, long organic ligands with shorter ones prior to film deposition, would enable the direct formation of close-packed QD films with short interdot separation and also allow a single-step process for large-scale industrial thin-film production [235, 247].

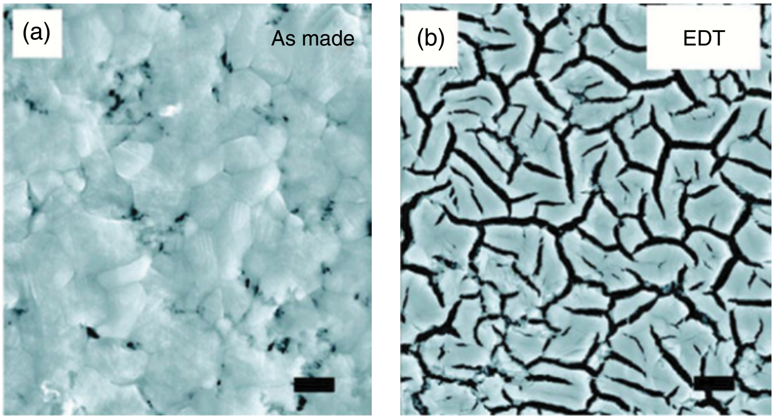

Figure 3.23 Microstructure of spin-cast PbSe QD films before and after EDT treatment. (a) An untreated film; and (b) a treated film. (Reprinted with permission from [246], copyright 2008 American Chemical Society.)

A variety of small ligand molecules have been extensively explored to replace the longer organic ligands and to improve interdot electronic coupling between adjacent QDs [240]. Liu et al. reported electron mobility in excess of 7 cm^2/Vs in ALD Al_2O_3 in-filled QD FETs with ethanedithiol as short ligand [248]. Talgorn et al. used 1,2-ethanediamine as the ligand and obtained PbSe QD films with mobility up to 3 cm^2/Vs [249]. On the other hand, since Kovalenko et al. first reported the passivation of QDs using molecular metal chalcogenide complexes (MCCs) in 2009 [247], short inorganic ligands have emerged as a more promising alternative to passivate the surface of QDs. Different MCCs ($Sn_2S_6^{4-}$, $Sn_2Se_6^{4-}$, $In_2Se_4^{2-}$, $Cu_7S_4^{-}$, and so on) have been prepared by this approach [240]. These inorganic surface ligands provide a negative charge to create strong electrostatic repulsion among the colloidal QDs, resulting in a stable colloidal QD solution in polar solvents. Their TFT based on CdSe QD films exchanged with $In_2Se_4^{2-}$ ligands exhibited a remarkable mobility about 15 cm^2/Vs [250]. With a rapid thermal annealing treatment after deposition of the QDs, they even achieved charge carrier mobility up to 38 cm^2/Vs [251]. Moreover, Nag et al. also developed inorganic ligand exchanges with metal-free inorganic ligands including S^{2-}, HS^-, Se^{2-}, HSe^-, Te^{2-}, TeS_3^{2-},OH^-, NH_2^- [252]. Kagan's group reported electron mobility more than 20 cm^2/Vs and I_{on}/I_{off} ratio > 10^6 in CdSe QD field-effect transistor at room temperature using thiocyanate surface ligands [235]. Employing these high performance transistors, flexible and low voltage complex integrated circuits were constructed [236].

3.8 Nanoparticle/Polymer Dielectric Composites

Besides conductors and semiconductors, dielectric materials are also important in electronics because they are indispensible for making capacitors and insulating layers. However, dielectric layers are rarely printed because of the lack of printable dielectric materials and the difficulty of printing a high quality dielectric layer [253]. In general, a dielectric layer must be thick enough (usually hundreds of nanometers or even a few micrometers) to prevent electrical leakage. On the other hand, large capacitance per unit area of printed dielectric layer is required in order to reduce the working voltage of a device. The large capacitance, which is directly proportional to the dielectric permittivity and inversely proportional to the film thickness, implies that the printed dielectric material must have high permittivity (high k) so that a thick layer can be tolerated.

Many solution-processable dielectric materials have been developed as gate dielectrics, including polymer [253], inorganic oxide [254], ion-gel [255], and solid-state electrolyte [256]. Ion gel [166, 167, 257, 258] and solid-state electrolytes have high dielectric constant but high conductivity at high frequency, which limits the switching speed of a transistor. Solution-processable inorganic materials such as ZrO_2 [254] have high permittivity and high frequency stability, but it is difficult to prevent the printed ceramic film from getting pinholes and cracks that can cause deadly short circuits in devices. In contrast, polymer dielectric materials are easy to print but of low permittivity. A composite combining high k inorganic nanoparticles with printable polymer may generate a new type of dielectric materials that would have high dielectric constant and high frequency stability as well as good printability. The permittivity of a composite depends on the permittivity of each component, its volume content, and its spatial arrangement in the composites [259, 260]. Some theoretical models have been developed to predict the composite permittivity [261]. Among these models, the Lichtenecker-Logarithmic (L-L) mixture model is the most used formula, shown as follows:

$$\log\varepsilon = \upsilon_p \log\varepsilon_p + \upsilon_c \log\varepsilon_c, \tag{3.4}$$

where ε, ε_p, and ε_c are the permittivities of polymer composite, polymer matrix, and filler particles, and ν_p and ν_c are the volume ratios of polymer matrix and filler, respectively. Although the L-L model is a semi-empirical model, it has been proven to be a useful formula for determining the effective permittivity of homogenized dielectric [262].

For a nanocomposite dielectric material, its dielectric constant generally increases with the loading of high k inorganic nanoparticles. However, the leakage current also increases with increased loading of nanoparticles due to the insufficient filling of polymer among nanoparticles and electromigration of metallic atoms through the gaps from electrode material. One early report presented the solution-processed TiO_2 nanoparticles/poly-4-vinylphenol (PVP) nanocomposites, which had been used as a dielectric layer to construct TFTs with mobility more than 0.2 cm^2/Vs. However, the relative dielectric constant was only 5.4 compared to 3.5 of PVP, with the maximum TiO_2 solid content (7 wt%). The increase in TiO_2 nanoparticles content led to increased leakage current simultaneously, which could be ascribed to nanoparticle agglomeration at higher concentrations [263].

Surface modification has been employed to improve inorganic nanoparticle solubility/dispersibility in both solution and polymer. These high-k inorganic materials usually are oxides, so the commonly used surfactants include phosphonates, silane coupling agents, and carbonates [264–267]. In 2005, Maliakal et al. reported the fabrication of TiO_2-polystyrene (PS) nanocomposites with TiO_2 volume content up to 18.2% via a ligand exchange reaction between oleic acid-stabilized titanium oxide nanoparticles and diethyl phosphonate terminated polystyrene. Pentacene TFTs incorporating the new TiO_2/polystyrene nanocomposite gate dielectric exhibited mobility approaching 0.2 cm^2/Vs [268].

The use of higher permittivity inorganic nanoparticle and/or polymer matrix is another possibility to increase the dielectric constant of nanocomposites. Kim et al. reported solution-processible high permittivity nanocomposite gate insulators by embedding $BaTiO_3$ nanoparticles whose surfaces were modified with a phosphoric acid into poly4-vinylphenol. Due to the effective surface modification, the volume fraction of $BaTiO_3$ was able to increase to 37 vol%, resulting in a dielectric constant of 14 and a low leakage current 10^{-8} A/cm^2 [269]. Yildirim et al. reported ferroelectric nanocomposites with dielectric constants up to 51.5 by combining $BaTiO_3$ nanoparticles and a high-k P(VDF-TrFE) copolymer [270]. Recently at the authors' Printable Electronics Research Center, solution-processed $BaTiO_3$ nanocomposites have been developed by taking advantage of the high-k albumen, demonstrating maximum relative permittivity of 52 and good dielectric stability over a wide range of frequencies [265]. In addition, many conductive materials such as metal [271] and carbon fiber [272] were also employed for preparation of high-k nanocomposites with the loading under the percolation thresholds.

In situ surface modification of nanoparticles has proven to be an effective strategy to enhance the efficiency of nanocomposite formation. Guo et al. reported the formation of isotactic polypropylene-$BaTiO_3$ and TiO_2 nanocomposites via in situ metallocene polymerization. The process is shown in Figure 3.24. In the first step, methylaluminoxane (MAO) was anchored onto the nanoparticles via surface hydroxyl group reaction to form covalent Al-O bonds. After washing away unbound MAO, the MAO-coated nanoparticles are subjected to reaction with the polymerization catalyst ($EBIZrCl_2$). Furthermore, the surface-anchored $EBIZrCl_2$-derived catalysts produce highly isotactic polypropylene. The achieved nanocomposite

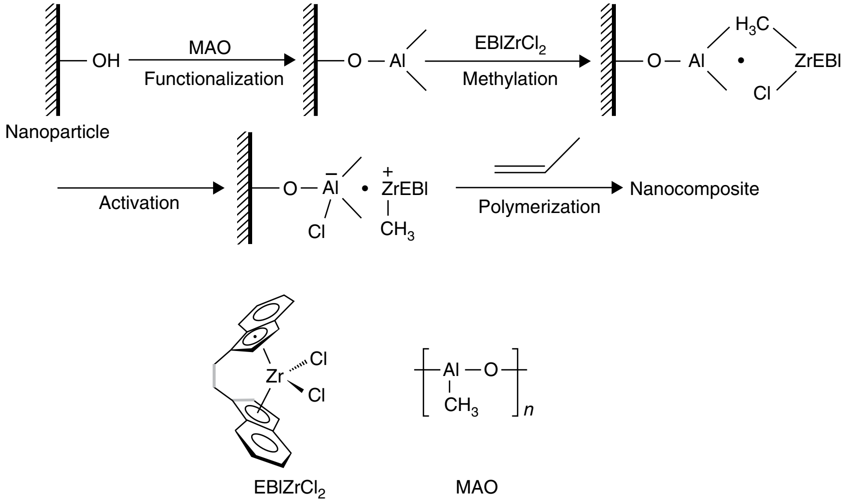
OH
MAO
Functionalization
Nanoparticle
O—Al
EBIZrCl2
Methylation
H3C
ZrEBI
Cl
Activation
Cl
CH3
Polymerization
Nanocomposite
Zr
Cl
Cl
Al—O
CH3
n
EBIZrCl2
MAO

Figure 3.24 Nanocomposites are synthesized via sequential nanoparticle MAO functionalization, catalyst immobilization/activation, and in situ isotactic propylene polymerization. (Reprinted with permission from [273], copyright 2007 American Chemical Society.)

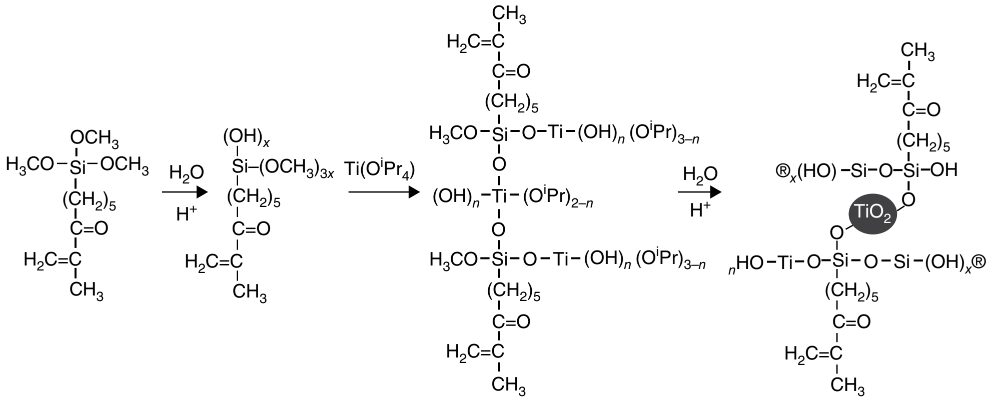
H2O
H+
Ti(OiPr4)
H2O
H+
TiO2

(MPTS) (1)

(Partially hydrolyzed MPTS) (2)

(–Si–O–Ti–hybrids) (3)

(TiO_2 nanocomposites) (4)

Figure 3.25 Schematic representation of the formation of inorganic–organic hybrid titania nanocomposites. (Reprinted from [274] with permission from Wiley.)

film showed very low leakage current densities (10^{-6}–10^{-9} A/cm^2 at 200 V) and high breakdown fields of 4 MV/cm [273]. Using in situ formation of inorganic nanoparticles, some special solution-processable inorganic/organic dielectric materials have also been synthesized. Kim et al. prepared a hybrid titania material by a process involving the phase separation of TiO_2 by hydrolysis and polycondensation from hybrids between titanium tetraisopropoxide (TTIP) and 3-(methacryloyloxy)propyl trimethoxysilane (MPTS) with excess acidic water at an elevated temperature, as shown in Figure 3.25 [274]. Utilizing similar strategy, high performance TiO_2/PVP [275] and ZrO_2-based nanocomposites [276] were prepared as dielectric layers for the construction of TFTs.

Although some solution-processed nanocomposites have been used as a dielectric layer in TFTs, few works are reported with respect to printing the dielectric layer in TFTs so far. Recently, a new nanocomposite dielectric ink formed by dispersing $Ca_2Nb_3O_{10}$ nanosheets in acetone-diluted poly(methyl methacrylate) (PMMA) solution was successfully printed as dielectric layers in IGZO TFTs with an aerosol jet printer at the authors' Printable Electronics Research Center. The solution-processed IGZO transistors exhibited electron mobility of 2.4 cm^2/Vs and I_{on}/I_{off} ratio of 10^4 [277]. Other work also demonstrated fully printed carbon nanotube TFTs, where PMMA/$BaTiO_3$ nanocomposite inks having dielectric constant of 14–17 were printed as the dielectric layers by roll-to-roll gravure printing [187–190].

3.9 Summary

In this chapter, some inorganic electronic materials including conductors, semiconductors. and dielectric materials that may be useful for printed electronics were briefly introduced with respect to their properties, ink preparation, and film formation by solution or printing.

In general, there are two types of inorganic "inks": compound solution ink and particle suspension ink. In the case of compound solution ink, the chemistry of the compound precursor is the most crucial factor for the quality of achieved film and the processed temperature. For the particle suspension ink, factors such as particle size and its distribution, shape of particles, dispersions, surfactant/capper, solvent, and other additional agents are all important for the ink formulation. Dispersion of particles in solution has been extensively studied and there are many classic theoretical models to describe the process. Two main stabilization mechanisms that prevent the particles from aggregating in solution are electrostatic repulsion and steric repulsion. To establish the repulsion forces, surface modification must be performed based on the surface chemistry of particles. The tremendous progress in nanomaterials in recent years has enabled the emergence of more and more nanoparticle-based inks and high performance inorganic electronic devices being made by solution process or printing. Furthermore, inks made from 1D/2D nanomaterials such as nanowires and graphene are able to produce film textures different from the isotropic nanoparticles with unexpected improvement in electronic properties.

However, it should be noted that there are differences between solution process and printing process. There are far fewer reports on printing than on solution processes such as spin coating for making high performance electronic film or devices. For some ink materials, solution process and printing are equally applicable. This may not be the case for some other inks. Process temperature is another ongoing concern. For most inorganic inks, high annealing temperature after film formation is necessary to achieve optimum performance. The high process temperature, however, may prevent using some flexible and low cost substrate materials such as plastics and papers. In general, for inorganic materials to be applicable in printed electronics the performance is only one aspect of material characteristics. Reproducibility, stability, feasibility in high throughout process, and cost are equally important factors that should be considered.

Although the development of inorganic materials for printed electronics is a relatively new field, the progress and advances are rapid. Many of the materials introduced in this chapter have exhibited their capabilities as high conductivity conductors, high mobility semiconductors, or high capacitance dielectrics. There are many more that have not been covered. The information provided in this chapter may serve as a guide to lead the way for exploration of new printable inorganic electronic materials, which would eventually lead to practical applications.

References

[1] Perelaer J, et al. Printed electronics: the challenges involved in printing devices, interconnects, and contacts based on inorganic materials. J. Mater. Chem. 2010;20:8446–8453.

[2] Anto BT, et al. Hydrophilic sparse ionic monolayer–protected metal nanoparticles: highly concentrated Nano-Au and Nano-Ag inks that can be sintered to near-bulk conductivity at 150 degrees C. Adv. Func. Mater. 2010;20:296–303.

[3] Wang BY, et al. Cu ion ink for a flexible substrate and highly conductive patterning by intensive pulsed light sintering. ACS Appl. Mater. Interfaces 2013;5:4113–4119.

[4] Kim I, et al. Synthesis of oxidation-resistant core-shell copper nanoparticles. Rsc Advances 2013;3: 15169–15177.

[5] Jeong S, et al. Controlling the thickness of the surface oxide layer on Cu nanoparticles for the fabrication of conductive structures by inkjet printing. Adv. Func. Mater. 2008;18:679–686.

[6] Yang C, et al. Printed electrically conductive composites: conductive filler designs and surface engineering. J. Mater. Chem. C 2013;1:4052–4069.

[7] Buffat P, Borel JP. Size effect on melting temperature of gold particles. Phys. Rev. A 1976;13:2287–2298.

[8] Alexandridis P. Gold nanoparticle synthesis, morphology control, and stabilization facilitated by functional polymers. Chem. Engineering & Technology 2011;34:15–28.

[9] Turkevich J, et al. A study of the nucleation and growth processes in the synthesis of colloidal gold. Discussions of the Faraday Soc.1951:55+.

[10] Brust M, et al. Synthesis of thiol-derivatized gold nanoparticles in a 2-phase liquid-liquid system. J. Chem. Soc.–Chem. Communications 1004:801–802.

[11] Lee PC, Meisel D. Adsorption and surface-enhanced raman of dyes on silver and gold sols. J. Physical Chem. 1082;86:3391–3395.

[12] Creighton JA, et al. Plasma resonance enhancement of raman-scattering by pyridine adsorbed on silver or gold sol particles of size comparable to the excitation wavelength. J. Chem. Soc.–Faraday Trans. 1979;75:790–798.

[13] Sastry M, et al. Organization of polymer–capped platinum colloidal particles at the air–water interface. Thin Solid Films 1998;324:239–244.

[14] Scott RWJ, et al. Synthesis, characterization, and stability of dendrimer–encapsulated palladium nanoparticles. Chem. Mater. 2003;15:3873–3878.

[15] Sinha A, et al. Synthesis of nanosized copper powder by an aqueous route. J. Mater. Synthesis Processing 1999;7:373–377.

[16] Hou Y, et al. Size–controlled synthesis of nickel nanoparticles. Appl. Surface Science 2005;241:218–222.

[17] Xia YN, et al. Shape–controlled synthesis of metal nanocrystals: simple chemistry meets complex physics? Angewandte Chemie–International Edition 2009;48:60–103.

[18] Lamer VK, Dinegar RH. Theory, production and mechanism of formation of monodispersed hydrosols. J. Amer. Chem. Soc. 1950;72:4847–4854.

[19] Watzky MA, Finke RG. Transition metal nanocluster formation kinetic and mechanistic studies. A new mechanism when hydrogen is the reductant: Slow, continuous nucleation and fast autocatalytic surface growth. J. Amer. Chem. Soc. 1997;119:10382–10400.

[20] Ciacchi LC, et al. Growth of platinum clusters via addition of Pt(II) complexes: a first principles investigation. J. Physical Chem. B 2003;107:1755–1764.

[21] Ciacchi LC, et al. Nucleation and growth of platinum clusters in solution and on biopolymers. Platinum Metals Review 2003;47:98–107.

[22] Mertig M, et al. DNA as a selective metallization template. Nano Lett. 2002;2:841–844.

[23] Ciacchi LC, et al. Initial nucleation of platinum clusters after reduction of K2PtCl4 in aqueous solution: a first principles study. J. Amer. Chem. Soc. 2001;123:7371–7380.

[24] Nath S, et al. Ligand-stabilized metal nanoparticles in organic solvent. J. Colloid Interface Science 2010;341:333–352.

[25] Ankireddy K, et al. Highly conductive short chain carboxylic acid encapsulated silver nanoparticle based inks for direct write technology applications. J. Mater. Chem. C 2013;1:572–579.

[26] Fukuda K, et al. Profile control of inkjet printed silver electrodes and their application to organic transistors. ACS Appl. Mater. & Interfaces 2013;5:3916–3920.

[27] Yu JS, et al. Silver front electrode grids for ITO-free all printed polymer solar cells with embedded and raised topographies, prepared by thermal imprint, flexographic and inkjet roll–to–roll processes. Nanoscale 2012;4:6032–6040.

[28] Na SI, et al. ITO-free flexible polymer solar cells with inkjet-printed Ag grids. Semiconductor Science Technology 2012:27.

[29] Wu YL, et al. High-performance organic thin-film transistors with solution-printed gold contacts. Adv. Mater. 2005;17:184–+.

[30] Magdassi S, et al. Copper nanoparticles for printed electronics: routes towards achieving oxidation stability. Mater. 2010;3:4626–4638.

[31] Deng DY, et al. Antioxidative effect of lactic acid-stabilized copper nanoparticles prepared in aqueous solution. J. Mater. Chem. 2012;22:23989–23995.

[32] Deng DY, et al. Copper nanoparticles: aqueous phase synthesis and conductive films fabrication at low sintering temperature. ACS Appl. Mater. Interfaces 2013;5:3839–3846.

[33] Kang H, et al. Direct intense pulsed light sintering of inkjet-printed copper oxide layers within six milliseconds. ACS Appl. Mater. Interfaces 2014;6:1682–1687.

[34] Lee HM, et al. A novel solution-stamping process for preparation of a highly conductive aluminum thin film. Adv. Mater. 2011;23:5524–+.

[35] Jo YH, et al. Synthesis and characterization of low temperature Sn nanoparticles for the fabrication of highly conductive ink. Nanotechnology 2011:22.

[36] Yarema M, et al. From highly monodisperse indium and indium tin colloidal nanocrystals to self-assembled indium tin oxide nanoelectrodes. ACS Nano 2012;6:4113–4121.

[37] Fei F, et al, A printed aluminum cathode with low sintering temperature for organic light-emitting diodes. Rsc Advances 2015;5:608–611.

[38] Kim D, et al. Direct writing of silver conductive patterns: improvement of film morphology and conductance by controlling solvent compositions. Appl. Phys. Lett. 2006:89.

[39] Kodas TT, et al. Metal precursor composition for use in fabricating transparent antenna, comprises metal precursor compound and conversion reaction inducing agent. WO2003032084-A; WO2003032084-A2; US2003180451-A1; EP1448725-A2; AU2002337822-A1; KR2005033513-A; JP2005537386-W; US2006001726-A1; AU2002337822-A8; US2006269824-A1; US2007096062-A1; US2007096064-A1; US2007096065-A1; US2007099330-A1; US2007096063-A1; US2007221887-A1; KR893564-B1; US7629017-B2; US2010034986-A1; US7713899-B2, 2003.

[40] Ko SH, et al. All-inkjet-printed flexible electronics fabrication on a polymer substrate by low-temperature high-resolution selective laser sintering of metal nanoparticles. Nanotechnology 2007:18.

[41] Perelaer J, et al. Plasma and microwave flash sintering of a tailored silver nanoparticle ink, yielding 60% bulk conductivity on cost-effective polymer foils. Adv. Mater. 2012;24:3993–3998.

[42] Reinhold I, et al. Argon plasma sintering of inkjet printed silver tracks on polymer substrates. J. Mater. Chem. 2009;19:3384–3388.

[43] Valeton JJP, et al. Room temperature preparation of conductive silver features using spin-coating and inkjet printing. J. Mater. Chem. 2010;20:543–546.

[44] Groza JR, et al. Plasma activated sintering of additive-free A1n powders to near-theoretical density in 5 minutes. J. Mater. Research 1992;7:2643–2645.

[45] Allen ML, et al. Electrical sintering of nanoparticle structures. Nanotechnology 2008:19.

[46] Smith PJ, Morrin A. Reactive inkjet printing. J. Mater. Chem. 2012;22:10965–10970.

[47] Bidoki SM, et al. Inkjet fabrication of electronic components. J. Micromechanics Microengineering 2007;17:967–974.

[48] Kao ZK, et al. Formation of conductive silver films via inkjet reaction system. J. Mater. Chem. 2011;21: 18799–18803.

[49] Li DP, et al. Conductive copper and nickel lines via reactive inkjet printing. J. Mater. Chem. 2009;19: 3719–3724.

[50] Grouchko M, et al. Conductive inks with a built-in mechanism that enables sintering at room temperature. ACS Nano 2011;5:3354–3359.

[51] Chen Z, Cui Z. Thin film transistors with printed semiconductive oxide channel and silver source-drain electrodes. in Nanotechnology Conference & Expo – Nanotech 2011, 2011:441–444.
[52] Perelaer J, et al. Inkjet-printed silver tracks: low temperature curing and thermal stability investigation. J. Mater. Chem. 2008;18:3209–3215.
[53] Rathmell AR, Wiley BJ. The synthesis and coating of long, thin copper nanowires to make flexible, transparent conducting films on plastic substrates. Adv. Mater. 2011;23:4798–+.
[54] Wu H, et al. A transparent electrode based on a metal nanotrough network. Nature Nanotechnology 2013;8:421–425.
[55] Xu J, et al. A simple approach to the synthesis of silver nanowires by hydrothermal process in the presence of gemini surfactant. J. Colloid Interface Science 2006;298:689–693.
[56] Wang ZH, et al. A simple hydrothermal route to large-scale synthesis of uniform silver nanowires. Chem. 2005;11:160–163.
[57] Kou JH, Varma RS. Speedy fabrication of diameter-controlled Ag nanowires using glycerol under microwave irradiation conditions. Chem. Communications 2013;49:692–694.
[58] Zhu YJ, Hu XL. Microwave-assisted polythiol reduction method: a new solid–liquid route to fast preparation of silver nanowires. Mater. Lett. 2004;58:1517–1519.
[59] Zheng XJ, et al. Growth of silver nanowires by an unconventional electrodeposition without template. Electrochemistry Communications 2007;9:629–632.
[60] Ni K, et al. Synthesis of silver nanowires with different aspect ratios as alcohol-tolerant catalysts for oxygen electroreduction. Electrochemistry Communications 2008;10:1027–1030.
[61] Pourahmad A, Sohrabnezhad S. Preparation and characterization of Ag nanowires in mesoporous MCM-41 nanoparticles template by chemical reduction method. J. Alloys Compounds 2009;484:314–316.
[62] Naderi N, Hashim MR. Synthesis of Cu nanowires with polycarbonate template. In Malaysia Annual Phys. Conference 2010. 1328, T. Y. Tou, et al. Eds. ed Melville: Amer Inst Phys., 2011:205–207.
[63] Kim SH, et al. Low temperature synthesis and growth mechanism of Ag nanowires. J. Alloys Compounds 2007;433:261–264.
[64] Sun YG, Xia YN. Large-scale synthesis of uniform silver nanowires through a soft, self–seeding, polyol process. Adv. Mater. 2002;14:833–837.
[65] Hu LB, et al. Scalable coating and properties of transparent, flexible, silver nanowire electrodes. ACS Nano 2010;4:2955–2963.
[66] Song M, et al. Highly efficient and bendable organic solar cells with solution-processed silver nanowire electrodes. Adv. Func. Mater. 2013;23:4177–4184.
[67] Coskun S, et al. Optimization of silver nanowire networks for polymer light emitting diode electrodes. Nanotechnology 2013:24.
[68] Bid A, et al. Temperature dependence of the resistance of metallic nanowires of diameter >= 15 nm: applicability of Bloch–Gruneisen theorem. Phys. Rev. B 2006:74.
[69] Hecht D, et al. Conductivity scaling with bundle length and diameter in single walled carbon nanotube networks. Appl. Phys. Lett. 2006:89.
[70] Langley D, et al. Flexible transparent conductive materials based on silver nanowire networks: a review. Nanotechnology 2013:24.
[71] Nomura K, et al. Room–temperature fabrication of transparent flexible thin–film transistors using amorphous oxide semiconductors. Nature 2004;432:488–492.
[72] Fortunato E, et al. Oxide semiconductor thin-film transistors: a review of recent advances. Adv. Mater. 2012;24:2945–2986.
[73] Kamiya T, et al. Present status of amorphous In-Ga-Zn-O thin-film transistors. Science Technology Adv. Mater. 2010:11.
[74] Jeong JK, et al. High performance thin film transistors with cosputtered amorphous indium gallium zinc oxide channel. Appl. Phys. Lett. 2007:91.
[75] Bellingham JR, et al. Intrinsic performance limits in transparent conducting oxides. J. Mater. Science Lett. 1992;11:263–265.
[76] Hoel CA, et al. Transparent conducting oxides in the ZnO-In2O3-SnO2 system. Chem. Mater. 2010;22: 3569–3579.
[77] Hecht DS, et al. Emerging transparent electrodes based on thin films of carbon nanotubes, graphene, and metallic nanostructures. Adv. Mater. 2011;23:1482–1513.
[78] Wager JF, et al. Transparent Electronics: New York:Springer, 2007.

[79] Kawazoe H, et al. Transparent p-type conducting oxides: design and fabrication of p-n heterojunctions. MRS Bulletin 2000;25:28–36.

[80] Sheng S, et al. p-Type transparent conducting oxides. Physica Status Solidi A 2006;203:1891–1900.

[81] Sato H, et al. Transparent conducting p-type NIO thin-films prepared by magnetron sputtering. Thin Solid Films 1993;236:27–31.

[82] Kamiya T, et al. Electrical properties and structure of p-type amorphous oxide semiconductor xZnO center dot Rh2O3. Adv. Func. Mater. 2005;15:968–974.

[83] Narushima S, et al. A p-type amorphous oxide semiconductor and room temperature fabrication of amorphous oxide p-n heterojunction diodes. Adv. Mater. 2003;15:1409–1413.

[84] Kim S, et al. Room temperature deposited oxide p-n junction using p-type zinc-cobalt-oxide. J. Appl. Phys. 2001:107.

[85] Chen HY, et al. Indium-doped molybdenum oxide as a new p-type transparent conductive oxide. J. Mater. Chem. 2011;21:5745–5752.

[86] Chen SP, et al. Silver conductive features on flexible substrates from a thermally accelerated chain reaction at low sintering temperatures. ACS Appl. Mater. Interfaces 2012;4:7063–7067.

[87] Yang WD, et al. One step synthesis of uniform organic silver ink drawing directly on paper substrates. J. Mater. Chem. 2012;22:23012–23016.

[88] Caraveo–Frescas JA, et al. Record mobility in transparent p-type tin monoxide films and devices by phase engineering. ACS Nano 2013;7:5160–5167.

[89] Kim MG, et al. High-performance solution-processed amorphous zinc-indium-tin oxide thin-film transistors. J. Amer. Chem. Soc. 2010;132:10352–10364.

[90] Lee CG, Dodabalapur A. Solution-processed zinc-tin oxide thin-film transistors with low interfacial trap density and improved performance. Appl. Phys. Lett. 2010:96.

[91] Jeong S, Moon J. Low-temperature, solution-processed metal oxide thin film transistors. J. Mater. Chem. 2012;22:1243–1250.

[92] Thomas SR, et al. Solution-processable metal oxide semiconductors for thin-film transistor applications. Chem. Soc. Rev. 2013;42:6910–6923.

[93] Song K, et al. Solution processed invisible all-oxide thin film transistors. J. Mater. Chem. 2009;19:8881–8886.

[94] Meyers ST, et al. Aqueous inorganic inks for low-temperature fabrication of ZnO TFTs. J. Amer. Chem. Soc. 2008;130:17603–17609.

[95] Kim MG, et al. Low-temperature fabrication of high-performance metal oxide thin-film electronics via combustion processing. Nature Mater. 2011;10:382–388.

[96] Hwang YH, et al. An "aqueous route" for the fabrication of low-temperature-processable oxide flexible transparent thin-film transistors on plastic substrates. Npg Asia Mater. 5, Apr 2013.

[97] Lin YH, et al. High–performance ZnO transistors processed via an aqueous carbon–free metal oxide precursor route at temperatures between 80–180 degrees C. (vol 25, pg 4340, 2013), Adv. Mater. 2013;25: 4689–4689.

[98] Merzhanov AG. The chemistry of self–propagating high–temperature synthesis. J. Mater. Chem. 2004;14: 1779–1786.

[99] Hennek JW, et al. Exploratory combustion synthesis: amorphous indium yttrium oxide for thin–film transistors. J. Amer. Chem. Soc. 2012;134:9593–9596.

[100] Han SY, et al. Low–temperature, high–performance, solution–processed indium oxide thin–filmtTransistor., J. Amer. Chem. Soc. 2011;133:5166–5169.

[101] Kim YH, et al. Flexible metal–oxide devices made by room–temperature photochemical activation of sol–gel films. Nature 2012;489:128.

[102] Banger KK, et al. Low–temperature, high–performance solution–processed metal oxide thin–film transistors formed by a "sol–gel on chip" process. Nature Mater. 2011:10:45–50.

[103] Jun T, et al. High–performance low–temperature solution–processable ZnO thin film transistors by microwave–assisted annealing. J. Mater. Chem. 2011;21:1102–1108.

[104] Dalpian GM, Chelikowsky, JR. Self–purification in semiconductor nanocrystals. Phys. Rev. Lett. 2006;96.

[105] Buonsanti R, Milliron DJ. Chem. of doped colloidal nanocrystals. Chem. of Mater. 2013;25:1305–1317.

[106] Lee J, et al. A facile solution–phase approach to transparent and conducting ITO nanocrystal assemblies. J. Amer. Chem. Soc. 2012;134:13410–13414.

[107] Ito D, et al. Convenient preparation of ITO nanoparticles inks for transparent conductive thin films. J. Nanoparticle Research 2012:14.

[108] Puetz J, Aegerter MA. Direct gravure printing of indium tin oxide nanoparticle patterns on polymer foils. Thin Solid Films 2008;516:4495–4501.

[109] Della Gaspera E, et al. Low–temperature processed Ga–doped ZnO coatings from colloidal inks. J. Amer. Chem. Soc. 2013;135:3439–3448.

[110] Straue N, et al. Tape casting of ITO green tapes for flexible electroluminescent lamps. J. Amer. Ceramic Soc. 2012;95:684–689.

[111] Jeong JA, et al. Ink–jet printed transparent electrode using nano–size indium tin oxide particles for organic photovoltaics, Solar Energy Mater. Solar Cells 2010;94:1840–1844.

[112] Zhang HL, et al. Separation and/or selective enrichment of single–walled carbon nanotubes based on their electronic properties. Chem. Soc. Rev. 2011;40:1324–1336.

[113] Lu FS, et al. Separated metallic and semiconducting single–walled carbon nanotubes: opportunities in transparent electrodes and beyond. Langmuir 2011;27:4339–4350.

[114] Durkop T, et al. Extraordinary mobility in semiconducting carbon nanotubes. Nano Lett. 2004;4:35–39.

[115] Ebbesen TW, et al. Electrical conductivity of individual carbon nanotubes. Nature 1996;382:54–56.

[116] Yao Z, et al. High–field electrical transport in single–wall carbon nanotubes. Phys. Rev. Lett. 2000;84:2941–2944.

[117] Harutyunyan AR, et al. Preferential growth of single–walled carbon nanotubes with metallic conductivity. Science 2009;326:116–120.

[118] Ding L, et al. Selective growth of well–aligned semiconducting single–walled carbon nanotubes. Nano Lett. 2009;9:800–805.

[119] Wang H, et al. Selective synthesis of (9,8) single walled carbon nanotubes on cobalt incorporated TUD–1 catalysts. J. Amer. Chem. Soc. 2010;132:16747–16749.

[120] Ismail AF, et al. A review of purification techniques for carbon nanotubes. Nano 2008;3:127–143.

[121] Zhang J, et al. Dispersion of single–walled carbon nanotubes by nafion in water/ethanol for preparing transparent conducting films. J. Physical Chem. C 2008;112:16370–16376.

[122] Bergin SD, et al. New solvents for nanotubes: approaching the dispersibility of surfactants. J. Physical Chem. C 2010;114:231–237.

[123] Wang H, Dispersing carbon nanotubes using surfactants. Current Opinion Colloid Interface Science 2009;14:364–371.

[124] Hirsch A. Functionalization of single–walled carbon nanotubes. Angewandte Chemie–International Edition 2002;41:1853–1859.

[125] Tasis D, et al. Chem. of carbon nanotubes. Chem. Rev. 2006;106:1105–1136.

[126] Hersam MC. Progress towards monodisperse single–walled carbon nanotubes. Nature Nanotechnology 2008;3:387–394.

[127] Strano MS, et al. Electronic structure control of single–walled carbon nanotube functionalization. Science 2008;301:1519–1522.

[128] Lu J, et al. Selective interaction of large or charge–transfer aromatic molecules with metallic single–wall carbon nanotubes: critical role of the molecular size and orientation. J. Amer. Chem. Soc. 2006;128:5114–5118.

[129] Kim WJ, et al. Selective functionalization and free solution electrophoresis of single–walled carbon nanotubes: separate enrichment of metallic and semiconducting SWNT. Chem. of Mater. 2007;19:1571–1576.

[130] Hu H, et al. Sidewall functionalization of single–walled carbon nanotubes by addition of dichlorocarbene. J. Amer. Chem. Soc. 2003;125:14893–14900.

[131] Wang Y, et al. Direct enrichment of metallic single–waited carbon nanotubes induced by the different molecular composition of monohydroxy alcohol homologues. Small 2007;3:1486–1490.

[132] An KH, et al. A diameter–selective attack of metallic carbon nanotubes by nitronium ions. J. Amer. Chem. Soc. 2005;127:5196–5203.

[133] Banerjee S, Wong SS. Selective metallic tube reactivity in the solution–phase osmylation of single–walled carbon nanotubes. J. Amer. Chem. Soc. 2004;126:2073–2081.

[134] Miyata Y, et al. Selective oxidation of semiconducting single–wall carbon nanotubes by hydrogen peroxide. J. Physical Chem. B 2006;110:25–29.

[135] Menard–Moyon C, et al. Separation of semiconducting from metallic carbon nanotubes by selective functionalization with azomethine ylides, J. Amer. Chem. Soc. 2006;128:6552–6553.

[136] Park H, et al. Effects of sidewall functionalization on conducting properties of single wall carbon nanotubes. Nano Lett. 2006;6:916–919.

[137] Wang CJ, et al. Electronically selective chemical functionalization of carbon nanotubes: correlation between Raman spectral and electrical responses. J. Amer. Chem. Soc. 2005;127:11460–11468.

[138] An L, et al. A simple chemical route to selectively eliminate metallic carbon nanotubes in nanotube network devices. J. Amer. Chem. Soc. 2004;126:10520–10521.

[139] Maeda Y, et al. Large–scale separation of metallic and semiconducting single–walled carbon nanotubes. J. Amer. Chem. Soc. 2005;127:10287–10290.

[140] Maeda Y, et al. Dispersion and separation of small–diameter single–walled carbon nanotubes. J. Amer. Chem. Soc. 2006;128:12239–12242.

[141] Chattopadhyay D, et al. A route for bulk separation of semiconducting from metallic single–wall carbon nanotubes. J. Amer. Chem. Soc. 2003;125:3370–3375.

[142] Park N, et al. Band gap sensitivity of bromine adsorption at carbon nanotubes. Chem. Phys. Lett. 2005;403: 135–139.

[143] Li HP, et al. Selective interactions of porphyrins with semiconducting single–walled carbon nanotubes. J. Amer. Chem. Soc. 2004;126:1014–1015.

[144] Peng X, et al. Optically active single–walled carbon nanotubes. Nature Nanotechnology 2007;2:361–365.

[145] McDonald TJ, et al. Kinetics of PL quenching during single–walled carbon nanotube rebundling and diameter–dependent surfactant interactions. J. Physical Chem. B 2006;110:25339–25346.

[146] Zheng M, et al. DNA–assisted dispersion and separation of carbon nanotubes. Nature Mater. 2003;2:338–342.

[147] Zheng M, Semke ED. Enrichment of single chirality carbon nanotubes. J. Amer. Chem. Soc. 2007;129: 6084–+.

[148] Tu XM, et al. DNA sequence motifs for structure–specific recognition and separation of carbon nanotubes. Nature 2009;460:250–253.

[149] Park S, et al. A review of fabrication and applications of carbon nanotube film–based flexible electronics. Nanoscale 2013;5:1727–1752.

[150] Doorn SK, et al. High resolution capillary electrophoresis of carbon nanotubes. J. Amer. Chem. Soc. 2002;124:3169–3174.

[151] Krupke R, et al. Separation of metallic from semiconducting single–walled carbon nanotubes. Science 2003;301:344–347.

[152] Hong S, et al. Electrical transport characteristics of surface–conductance–controlled, dielectrophoretically separated single–walled carbon nanotubes. Langmuir 2007;23:4749–4752.

[153] Shin DH, et al. Continuous extraction of highly pure metallic single–walled carbon nanotubes in a microfluidic channel. Nano Lett. 2008;8:4380–4385.

[154] Tanaka T, et al. High–yield separation of metallic and semiconducting single–wall carbon nanotubes by agarose gel electrophoresis. Appl. Phys. Express 2008:1.

[155] Fujii S, et al. Performance enhancement of thin–film transistors by using high–purity semiconducting single–wall carbon nanotubes. Appl. Phys. Express 2009:2.

[156] Tanaka T, et al. Simple and scalable gel–based separation of metallic and semiconducting carbon nanotubes. Nano Lett. 2009;9:1497–1500.

[157] Zheng M, et al. Structure–based carbon nanotube sorting by sequence–dependent DNA assembly. Science 2003;302:1545–1548.

[158] Strano MS, et al. Understanding the nature of the DNA–assisted separation of single–walled carbon nanotubes using fluorescence and Raman spectroscopy. Nano Lett. 2004;4:543–550.

[159] Wei L, et al. Selective enrichment of (6,5) and (8,3) single–walled carbon nanotubes via cosurfactant extraction from narrow (n,m) distribution samples. J. Physical Chem. B 2008;112:2771–2774.

[160] Arnold MS, et al. Enrichment of single–walled carbon nanotubes by diameter in density gradients. Nano Lett. 2005;5:713–718.

[161] Arnold MS, et al. Sorting carbon nanotubes by electronic structure using density differentiation. Nature Nanotechnology 2006;1:60–65.

[162] Pereira LFC, et al. Upper bound for the conductivity of nanotube networks. Appl. Phys. Lett. 2009:95.

[163] Hecht DS, et al. High conductivity transparent carbon nanotube films deposited from superacid. Nanotechnology 2011:22.

[164] Behnam A, et al. Resistivity scaling in single–walled carbon nanotube films patterned to submicron dimensions. Appl. Phys. Lett. 2006:89.

[165] Dan B, et al. Continuous and scalable fabrication of transparent conducting carbon nanotube films. ACS Nano 2009;3:835–843.

[166] Zhao, J et al. Printed thin–film transistors with functionalized single–walled carbon nanotube inks. J. Mater. Chem. 2012;22:2051–2056.

[167] Zhao J, et al. Fabrication and electrical properties of all–printed carbon nanotube thin film transistors on flexible substrate., J. Mater. Chem. 2012;22:20747–20753.

[168] Lee HW, et al. Selective dispersion of high purity semiconducting single–walled carbon nanotubes with regioregular poly(3–alkylthiophene)s. Nature Communications 2011:2.

[169] Wang C, et al. High performance thin film transistors based on regioregular poly(3–dodecylthiophene)–sorted large diameter semiconducting single–walled carbon nanotubes. Nanoscale 2013;5:4156–4161.

[170] Xu WY, et al. Sorting of large–diameter semiconducting carbon nanotube and printed flexible driving circuit for organic light emitting diode (OLED). Nanoscale 2014;6:1589–1595.

[171] Qian L, et al. Electrical and photoresponse properties of printed thin–film transistors based on poly(9,9–dioctylfluorene–co–bithiophene) sorted large–diameter semiconducting carbon nanotubes. J. Physical Chem. C 2013;117:18243–18250.

[172] Liu ZY, et al. SMALL–hysteresis thin–film transistors achieved by facile dip–coating of nanotube/polymer composite. Adv. Mater. 2012;24:3633–3638.

[173] Mesgari S, et al. High selectivity cum yield gel electrophoresis separation of single–walled carbon nanotubes using a chemically selective polymer dispersant. J. Physical Chem. C 2012;116:10266–10273.

[174] Bisri SZ, et al. High performance ambipolar field–effect transistor of random network carbon nanotubes. Adv. Mater.2012;24:6147–6152.

[175] Wang C, et al. Extremely bendable, high–performance integrated circuits using semiconducting carbon nanotube networks for digital, analog, and radio–frequency applications. Nano Lett. 2012;12:1527–1533.

[176] Liu Z, et al. Effect of surface wettability properties on the electrical properties of printed carbon nanotube thin–film transistors on SiO_2/Si substrates. ACS Appl. Mater. Interfaces 2014;6:9997–10004.

[177] Lau PH, et al. Fully printed, high performance carbon nanotube thin–film transistors on flexible substrates. Nano Lett. 2013;13:3864–3869.

[178] Martel R, et al. Ambipolar electrical transport in semiconducting single–wall carbon nanotubes. Phys. Rev. Lett. 2001:87.

[179] Collins PG, et al. Extreme oxygen sensitivity of electronic properties of carbon nanotubes.. Science 2000;287: 1801–1804.

[180] Martel R, et al. Single– and multi–wall carbon nanotube field–effect transistors. Appl. Phys. Lett. 1998;73: 2447–2449.

[181] Biswas C, Lee YH. Graphene versus carbon nanotubes in electronic devices. Adv. Func. Mater. 2011;21:3806–3826.

[182] Zhang JL, et al. Air–stable conversion of separated carbon nanotube thin–film transistors from p–type to n–type using atomic layer deposition of high–kappa oxide and its application in CMOS logic circuits. ACS Nano 2011;5:3284–3292.

[183] Ha MJ, et al. Aerosol jet printed, low voltage, electrolyte gated carbon nanotube ring oscillators with sub–5 mu s stage delays. Nano Lett. 2013;13:954–960.

[184] Zhang JL, et al. Separated carbon nanotube macroelectronics for active matrix organic light–emitting diode displays. Nano Lett. 2011;11:4852–4858.

[185] Wang C, et al. User–interactive electronic skin for instantaneous pressure visualization. Nature Mater. 2013;12:899–904.

[186] Chen PC, et al. Fully printed separated carbon nanotube thin film transistor circuits and its application in organic light emitting diode control. Nano Lett. 2011;11:5301–5308.

[187] Jung M, et al. All–printed and roll–to–roll–printable 13.56–mhz–operated 1–bit RF tag on plastic foils. IEEE Trans. Electron Devices 2010;57:571–580.

[188] Noh J, et al. Fully gravure–printed D flip-flop on plastic foils using single–walled carbon–nanotube–based TFTs. IEEE Electron Device Lett. 2011;32:638–640.

[189] Noh J, et al. Integrable single walled carbon nanotube (SWNT) network based thin film transistors using roll–to–roll gravure and inkjet. Organic Electronics 2011;12:2185–2191.

[190] Noh J, et al. All printed edge–triggered register using single walled carbon nanotube–based thin film transistor. J. Nanoscience Nanotechnology 2012;12:4261–4264.

[191] Novoselov KS, et al. Electric field effect in atomically thin carbon films. Science 2004;306:666–669.

[192] Mayorov AS, et al. Micrometer–scale ballistic transport in encapsulated graphene at room temperature. Nano Lett. 2011;11:2396–2399.

[193] Morozov SV, et al. Giant intrinsic carrier mobilities in graphene and its bilayer. Phys. Rev. Lett. 2008;100.

[194] Chen JH, et al. Intrinsic and extrinsic performance limits of graphene devices on SiO2. Nature Nanotechnology 2008;3:206–209.

[195] Bolotin KI, et al. Ultrahigh electron mobility in suspended graphene. Solid State Communications 2008;146: 351–355.

[196] Schedin F, et al. Detection of individual gas molecules adsorbed on graphene. Nature Mater. 2007;6:652–655.

[197] Fang T, et al. Carrier statistics and quantum capacitance of graphene sheets and ribbons. Appl. Phys. Lett. 2007:91.

[198] Wu JB, et al. Organic light–emitting diodes on solution–processed graphene transparent electrodes. ACS Nano 2010;4:43–48.

[199] Nair RR, et al. Fine structure constant defines visual transparency of graphene. Science 2008;320:1308–1308.

[200] Balandin AA, et al. Superior thermal conductivity of single–layer graphene. Nano Lett. 2008;8:902–907.

[201] Weiss NO, et al. Graphene: an emerging electronic material. Adv. Mater. 2012;24:5782–5825.

[202] Lin YM, et al. 100–GHz transistors from wafer–scale epitaxial graphene. Science 2010;327:662–662.

[203] Li XS, et al. Large–area synthesis of high–quality and uniform graphene films on copper foils. Science 2009;324:1312–1314.

[204] Novoselov KS, et al. A roadmap for graphene. Nature 2012;490:192–200.

[205] Bae S, et al. Roll–to–roll production of 30-inch graphene films for transparent electrodes. Nature Nanotechnology 2010;5:574–578.

[206] Li XL, et al. Highly conducting graphene sheets and Langmuir–Blodgett films. Nature Nanotechnology 2008;3:538–542.

[207] Hernandez Y, et al. High–yield production of graphene by liquid-phase exfoliation of graphite. Nature Nanotechnology 2008;3:563–568.

[208] Hwang JY, et al. Polymer structure and solvent effects on the selective dispersion of single-walled carbon nanotubes. J. Amer. Chem. Soc. 2008;130:3543–3553.

[209] Compton OC, Nguyen ST. Graphene oxide, highly reduced graphene oxide, and graphene: versatile building blocks for carbon–based materials. Small 2010;6:711–723.

[210] Mattevi C, et al. Evolution of electrical, chemical, and structural properties of transparent and conducting chemically derived graphene thin films. Adv. Func. Mater. 2009;19:2577–2583.

[211] Park S, et al. Colloidal suspensions of highly reduced graphene oxide in a wide variety of organic solvents. Nano Lett. 2009;9:1593–1597.

[212] Tung VC, et al. High–throughput solution processing of large–scale graphene. Nature Nanotechnology 2009;4:25–29.

[213] Zhao JP, et al. Efficient preparation of large–area graphene oxide sheets for transparent conductive films. ACS Nano 2010;4:5245–5252.

[214] Wang J, et al. Rod-coating: towards large-area fabrication of uniform reduced graphene oxide films for flexible touch screens. Adv. Mater. 2012;24:2874–2878.

[215] Sharma BK, Ahn JH. Graphene based field effect transistors: efforts made towards flexible electronics.. Solid–State Electronics 2013;89:177–188.

[216] Schwierz FSF. Graphene transistors. Nature Nanotechnology 2010;5:487–496.

[217] Shimoda T, et al. Solution–processed silicon films and transistors. Nature 2006;440:783–786.

[218] Weis S, et al. Conduction mechanisms and environmental sensitivity of solution-processed silicon nanoparticle layers for thin–film transistors. Small 2011;7:2853–2857.

[219] Holman ZC, et al. Germanium and silicon nanocrystal thin-film field-effect transistors from solution. Nano Lett. 2010;10:2661–2666.

[220] Harting M, et al. Fully printed silicon field effect transistors. Appl. Phys. Lett. 2009:94.

[221] Scriba MR, et al. Hot-wire synthesis of Si nanoparticles. Thin Solid Films 2008;516:844–846.

[222] Cannon WR, et al. Sinterable ceramic powders from laser–driven reactions.1. Process description and modeling. J. Amer. Ceramic Soc. 1982;65:324–330.

[223] Sankaran RM, et al. Synthesis of blue luminescent Si nanoparticles using atmospheric-pressure micro-discharges. Nano Lett. 2005;5:537–541.

[224] Lechner R, et al. Thermoelectric effect in laser annealed printed nanocrystalline silicon layers. Physica Status Solidi–Rapid Research Lett. 2007;1:262–264.

[225] Mangolini L, Kortshagen U. Plasma-assisted synthesis of silicon nanocrystal inks. Adv. Mater. 2007;19:2513.

[226] Holman ZC, Kortshagen UR. Plasma production of nanodevice-grade semiconductor nanocrystals. J. Phys. D–Appl. Phys. 2011:44.

[227] Baldwin RK, et al. Room temperature solution synthesis of alkyl-capped tetrahedral shaped silicon nanocrystals. J. Amer. Chem. Soc. 2002;124:1150–1151.

[228] Baldwin RK, et al. Solution reduction synthesis of surface stabilized silicon nanoparticles. Chem. Communications 2002:1822–1823.

[229] Pettigrew KA, et al. Solution synthesis of alkyl- and alkyl/alkoxy-capped silicon nanoparticles via oxidation of Mg2Si, Chem. of Mater. 2003;15:4005–4011.

[230] Shirahata N, et al. Laser–derived one–pot synthesis of silicon nanocrystals terminated with organic monolayers. Chem. Communications:2009:4684–4686.

[231] Heintz AS, et al. Mechanochemical synthesis of blue luminescent alkyl/alkenyl-passivated silicon nanoparticles. Adv. Mater. 2007;19:3984–+.

[232] Kusova K, et al. Brightly luminescent organically capped silicon nanocrystals fabricated at room temperature and atmospheric pressure. ACS Nano 2010;4:4495–4504.

[233] Liu SM, et al. Enhanced photoluminescence from Si nano-organosols by functionalization with alkenes and their size evolution. Chem. Mater. 2006;18:637–642.

[234] Buriak JM. Organometallic chemistry on silicon and germanium surfaces. Chem. Rev. 2002;102:1271–1308.

[235] Choi JH, et al. Bandlike transport in strongly coupled and doped quantum dot solids: a route to high-performance thin-film electronics. Nano Lett. 2012;12:2631–2638.

[236] Kim DK, et al. Flexible and low-voltage integrated circuits constructed from high-performance nanocrystal transistors. Nature Communications 2012:3.

[237] Mitzi DB, et al. High–mobility ultrathin semiconducting films prepared by spin coating. Nature 2004;428:299–303.

[238] Mitzi DB. Solution–processed inorganic semiconductors. J. Mater. Chem. 2004;14:2355–2365.

[239] Mitzi DB. Solution Processing of chalcogenide semiconductors via dimensional reduction. Adv. Mater. 2009;21:3141–3158.

[240] Hetsch F, et al. Quantum dot field effect transistors. Mater. Today 2013;16:312–325.

[241] Kershaw SV, et al. Narrow bandgap colloidal metal chalcogenide quantum dots: synthetic methods, heterostructures, assemblies, electronic and infrared optical properties. Chem. Soc. Rev. 2013;42:3033–3087.

[242] Drndic M, et al. Transport properties of annealed CdSe colloidal nanocrystal solids. J. Appl. Phys. 2002;92: 7498–7503.

[243] Romero HE, Drndic M. Coulomb blockade and hopping conduction in PbSe quantum dots. Phys. Rev. Lett. 2005:95.

[244] Kim H, et al. Bottom- and top-gate field-effect thin-film transistors with p channels of sintered HgTe nanocrystals. Appl. Phys. Lett. 2006:89.

[245] Wills AW, et al. Thermally degradable ligands for nanocrystals. ACS Nano 2010;4:4523–4530.

[246] Luther JM, et al. Structural, optical and electrical properties of self–assembled films of PbSe nanocrystals treated with 1,2–ethanedithiol. ACS Nano 2008;2:271–280.

[247] Kovalenko MV, et al. Colloidal nanocrystals with molecular metal chalcogenide surface ligands. Science 2009;324:1417–1420.

[248] Liu Y, et al. PbSe quantum dot field-effect transistors with air-stable electron mobilities above 7 cm(2) V-1 s(-1). Nano Lett. 2013;13:1578–1587.

[249] Talgorn E, et al. Unity quantum yield of photogenerated charges and band-like transport in quantum-dot solids. Nature Nanotechnology 2011;6:733–739.

[250] Lee JS, et al. Band-like transport, high electron mobility and high photoconductivity in all–inorganic nanocrystal arrays. Nature Nanotechnology 2011;6:348–352.

[251] Chung DS, et al. Low voltage, hysteresis free, and high mobility transistors from all-inorganic colloidal nanocrystals. Nano Lett. 2012;12:1813–1820.

[252] Nag A, et al. Metal–free inorganic ligands for colloidal nanocrystals: S2-, HS-, Se2-, HSe-, Te2-, HTe-, TeS32-, OH-, and NH2- as surface ligands. J. Amer. Chem. Soc. 2011;133:10612–10620.

[253] Ortiz RP, et al. High-k organic, inorganic, and hybrid dielectrics for low-voltage organic field-effect transistors. Chem. Rev. 2010;110:205–239

[254] Park JH, et al. Low-temperature, high-performance solution-processed thin-film transistors with peroxo-zirconium oxide dielectric. ACS Appl. Mater. Interfaces 2012;5:410–417.

[255] Cho JH, et al. High-capacitance ion gel gate dielectrics with faster polarization response times for organic thin film transistors. Adv. Mater. 2008;20:686–690.

[256] Braga D, et al. Ultralow contact resistance in electrolyte-gated organic thin film transistors. Appl. Phys. Lett. 2010;97:193311–193313.

[257] Lee J, et al. Ion gel-gated polymer thin-film transistors: operating mechanism and characterization of gate dielectric capacitance, switching speed, and stability. J. Physical Chem. C 2009;13:8972–8981.

[258] Hong K, et al. Printed, sub-2V ZnO electrolyte gated transistors and inverters on plastic. Adv. Mater. 2013;25:3413–3418.

[259] Choudhury A, Dielectric and piezoelectric properties of polyetherimide/BaTiO3 nanocomposites. Mater. Chem. and Phys. 2010;121:280–285.

[260] Choudhury A. Preparation, characterization and dielectric properties of polyetherimide nanocomposites containing surface-functionalized BaTiO3 nanoparticles. Polymer International 2012;61:696–702.

[261] Subodh G, et al. PTFE/Sr2Ce2Ti5O16 polymer ceramic composites for electronic packaging applications. J. European Ceramic Soc. 2007;27:3039–3044.

[262] Simpkin R. Derivation of Lichtenecker's logarithmic mixture formula from Maxwell's equations. IEEE Trans. Microwave Theory and Techniques 2010;58:545–550.

[263] Chen FT, et al. Organic thin-film transistors with nanocomposite dielectric gate insulator. Appl. Phys. Lett. 2004;85:3295–3297.

[264] Kim P, et al. Phosphonic acid-modified barium titanate polymer nanocomposites with high permittivity and dielectric strength. Adv. Mater. 2007;19:1001–+.

[265] Wu X, et al. Investigation of solution processable albumen-BaTiO3 nanocomposite and its application in high-k films. Composites Science and Technology 2013;81:48–53.

[266] Kobayashi Y, et al. Fabrication of barium titanate nanoparticles-polymethylmethacrylate composite films and their dielectric properties. Polymer Engineering and Science 2009;49:1069–1075.

[267] Noh HY, et al. Mechanically flexible low-leakage nanocomposite gate dielectrics for flexible organic thin-film transistors. Electrochemical and Solid State Lett. 2008;11:H218–H221.

[268] Maliakal A, et al. Inorganic oxide core, polymer shell nanocomposite as a high K gate dielectric for flexible electronics applications. J. Amer. Chem. Soc. 2005;127:14655–14662.

[269] Kim P, et al. Solution-processible high-permittivity nanocomposite gate insulators for organic field–effect transistors. Appl. Phys. Lett. 2008:93.

[270] Yildirim FA, et al. Spin-cast composite gate insulation for low driving voltages and memory effect in organic field-effect transistors. Appl. Phys. Lett. 2007:90.

[271] Dang ZM, et al. Dielectric behavior of three-phase percolative Ni-BaTiO3/polyvinylidene fluoride composites. Appl. Phys. Lett. 2002;81:4814–4816.

[272] Dang ZM, et al. Study on dielectric behavior of a three-phase CF/(PVDF+BaTiO3) composite. Chem. Phys. Lett. 2003;369:95–100.

[273] Guo N, et al. Supported metallocene catalysis for in situ synthesis of high energy density metal oxide nanocomposites. J. Amer. Chem. Soc. 2007;129:766–767.

[274] Kim H, et al. Preparation of inorganic-organic hyhrid titania sol-gel nanocomposite films, and their dielectric properties. Physica Status Solidi A 2006;203:1962–1970.

[275] Kim J, et al. Solution-based TiO2-polymer composite dielectric for low operating voltage OTFTs. J. Amer. Chem. Soc.. 2010;132:14721–14723.

[276] Ha YG, et al. Flexible Low-voltage organic thin-film transistors enabled by low-temperature, ambient solution-processable inorganic/organic hybrid gate dielectrics. J. Amer. Chem. Soc. 2010;132:17426–17434.

[277] Wu X, et al. A new nanocomposite dielectric ink and its application in printed thin-film transistors. Composites Science and Technology 2014;94:117–122.

4

Printing Processes and Equipments

Jian Lin

4.1 Introduction

Printing is a replication process in which printable ink is applied to a substrate in order to transmit information (images, graphics, text, and so forth.) in a repeatable manner using an image-carrying medium [1]. Several important features of printing technology can be derived from the this definition:

- Printing can produce specific patterns on substrate, which is different from a blanket-coating process.
- Printed patterns consist of additional materials added onto the substrate, which is also called an additive process.
- Printing produces patterns repeatedly, rather than a one-only creation.
- There is always a pattern carrier (analog or digital) involved in printing.
- Traditional printing provides visual information.

In printed electronics, printing is a manufacturing technology that is derived from traditional media printing industry. Therefore, all of the aforementioned features except the last one are also applicable to printing electronic devices. The goal of printed electronics, however, is to manufacture electronic product rather than to produce visual information. Therefore, the key difference between printing electronics and printing visual information lies in the ink materials, which must be able to function as conductors, semiconductors, resistors, dielectrics, sensors or photoelectric convertors. It is not only the inks and the printing that are essential parts of printing electronics; the ink drying process after printing is also essential for a printed ink pattern to acquire specific electronic property. To meet the requirements of printing electronics, new research and development on traditional printing technologies are needed, which

Printed Electronics: Materials, Technologies and Applications, First Edition. Zheng Cui, Chunshan Zhou, Song Qiu, Zheng Chen, Jian Lin, Jianwen Zhao, Changqi Ma and Wenming Su.

© 2016 Higher Education Press. All rights reserved. Published 2016 by John Wiley & Sons Singapore Pte. Ltd.

include the selection of materials, preparation of inks, printing methods and equipments, as well as various pre-printing and post-printing treatments.

Electronic ink preparation is the most critical part of printed electronics. The composition of the material is the first consideration when selecting a material for electronic ink. Materials dispersed in pure liquid phase may have perfect electrical properties but may not be suitable for printing, or the film quality is poor through the printing process. It is often necessary to add other constituents to make the ink printable. Those additives are usually detrimental to the final electric property of printed films or patterns. Achieving trade-offs between improving printability and keeping electrical performance are important topics of research in electronic inks. The formulations of functional inks have been introduced in Chapters 2 and 3 of this book.

The film properties (crystalline type, purity, doping uniformity, surface morphology, contact interface, and so on) in electronic devices strongly influence device performance. As a liquid, ink moves on substrate before drying. The spontaneous movements of ink during and after printing can bring changes to the dimension of printed structures, which makes a huge difference in the electrical performance of a device and should be controlled to ensure the printed patterns meet the design specification. When printing multilayer structure, the interactions between printed layers, for example, diffusion, intermixing, contamination or damage, also need to be effectively controlled. Chemical reactions may occur in electronic ink during printing, drying and post-processing, which complicates the relationship between the properties of the ink and the final printed structures.

Printing can be divided into two categories, according to whether a template is employed or not. The only printing method available without using a template is inkjet printing. For printing that relies on a template, there are four different types: screen printing, gravure printing, letterpress printing, and offset printing. Different printing methods require different ink properties. It is possible to match a particular ink with a suitable printing method without changing the ink property too much. For example, the viscosity of some laboratory-made ink is very low (less than 5 cp). It is hard to increase the viscosity while keeping the same electrical properties. This type of ink is difficult to print by a screen printer but easy with an inkjet printer or gravure printing. Some inorganic materials can only be made into inks with their microparticle or nanoparticle forms. The viscosities of these types of inks are usually high, such as some conductive and dielectric pastes. These pastes are suitable only for screen printing of thick films.

Printing resolution and speed are the other two key parameters for printed electronics. High-resolution printing produces small size printed devices, high integration density, and with less materials consumption. However, most printing methods have resolutions between 50–100 μm, though 20 μm resolution is possible with optimized process conditions for some printing methods. Some new concepts of printing have been developed in recent years, such as aerosol jet printing and electrohydrodynamic jet printing, which have pushed printing resolution to less than 10 μm, or even approaching 1 μm. Thanks to the adoption of flexible substrates that enables roll-to-roll printing process in a manufacturing environment, the printing speed can be significantly fast and is expected to rival traditional media printing.

Given the vast wealth of literature on traditional printing, this chapter will not cover every aspect of printing but only give a brief introduction to printing principles and equipment. The focus is to analyze the advantages and disadvantages of various printing technologies when they are applied to printed electronics and how they are applied. The "inks" mentioned in this chapter refer to printable liquid phase materials, whether they are conductors, semiconductors, or dielectrics, and the "substrates" refer to any surfaces bearing the printed materials.

4.2 Jet Printing

4.2.1 Inkjet Printing

Inkjet printing refers to individual ink droplets precisely controlled by computer to jet out an ink nozzle, forming a digital pattern by ink droplet matrix. Such inkjet printers are already widely used in offices, homes, and factories.

4.2.1.1 Working Principles

Inkjet printing in principle can be divided into two modes of operation, continuous inkjet (CIJ) and drop on demand (DOD) inkjet. In a CIJ printer, ink droplets are produced and ejected continuously. The ink droplets, which are charged during the printing, are controlled by an electrostatic field. The imaging droplets pass through the electrostatic field to the substrate while other droplets are deflected to an ink catcher for re-use. A DOD printer ejects ink droplets when a pulse of voltage is applied, without any drop deflecting and catching. Generally speaking, the CIJ printer has higher jetting frequency and the DOD printer has a much simpler inkjet head structure. Their working principles are schematically shown in Figure 4.1.

There are two principal mechanisms of propelling ink drops in an inkjet printer head, piezoelectric propelling and thermal bubble propelling. In the piezoelectric inkjet head, a voltage is applied to the piezoelectric pressure transducer to make it bend or change shape, which repels the ink out of the nozzle, as schematically shown in Figure 4.1(b). In the thermal bubble inkjet head, an electrical current is passed through a heating element to make the ink vaporize rapidly. A bubble is then formed in the chamber to cause pressure increase, which propels a droplet of ink out of the nozzle, as schematically shown in Figure 4.2. In printed electronics, the most popular inkjet printers are based on piezoelectric DOD inkjet heads. Figure 4.3 shows some typical inkjet printers currently in use at the authors' Printable Electronics Research Center.

4.2.1.2 Pattern Preparation

Inkjet printing is a digital printing. There is no need for a master plate or template as the image carrier. The image to be printed is digitally stored in a computer. Software supplied by inkjet equipment manufacturers can create and edit the digital images. Monochrome bitmap format is the common image file type used in these inkjet printers. The black pixels in the bitmap file represent the printed ink droplet matrix and the white pixels represent the non-printed area. Any computer designed pattern files can be converted into monochrome bitmap digital files by software supplied with an inkjet printer. The printer control program converts the monochrome bitmap image into a string of electrical pulses, which drives the printer head to propel ink droplets. Alternatively, a printing pattern can be manually set by setting parameters

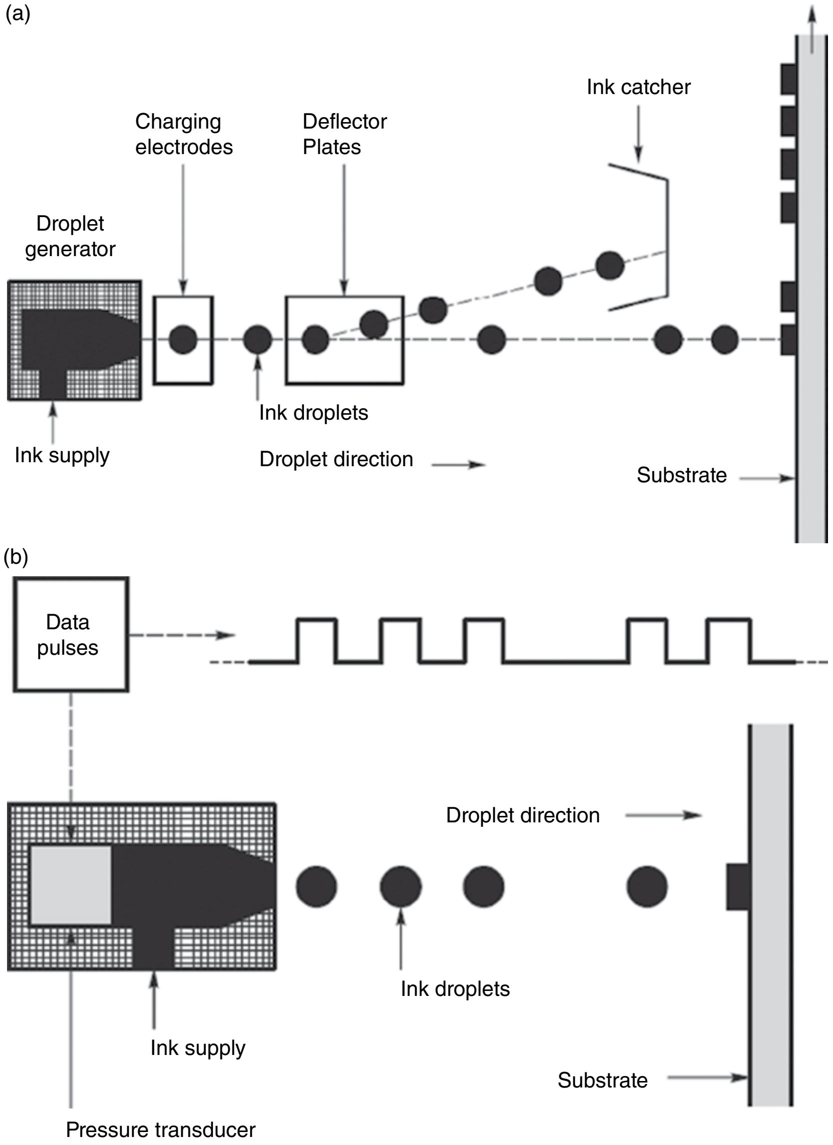
(a)
Ink catcher
Charging electrodes
Deflector Plates
Droplet generator
Ink supply
Ink droplets
Droplet direction
Substrate
(b)
Data pulses
Droplet direction
Ink droplets
Ink supply
Substrate
Pressure transducer

Figure 4.1 Working principles of CIJ (a) and DOD (b) inkjet printers. Reprinted from ref. [1] with permission from Springer

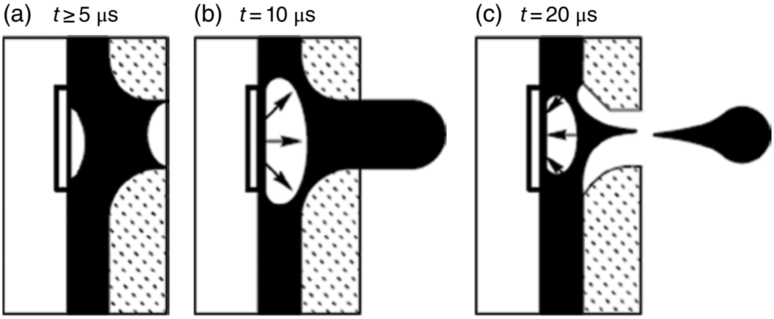
(a) $t \geq 5$ μs
(b) $t = 10$ μs
(c) $t = 20$ μs

Figure 4.2 Schematic principle of thermal inkjet. Reprinted from ref. [1] with permission from Springer

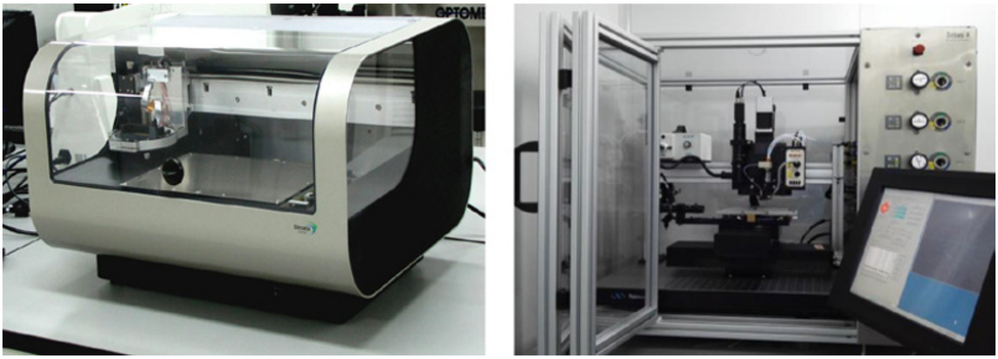

Figure 4.3 Typical inkjet printer for printed electronics, DMP-2831 (left) and Jetlab II (right)

(such as dot spacing, lines, arrays, and layers) directly using the manufacturer's software to form a drop matrix, which is convenient for printing simple patterns.

4.2.1.3 Application in Printed Electronics

Inkjet printing is most suitable for laboratory research in printed electronics. Many parameters in an inkjet printer, such as the volume, number, velocity, and direction of the ink droplets, as well as the temperatures of ink or substrate, can be observed and controlled precisely. The movement of ink droplets and their interaction with substrates can be easily studied. Inkjet printing is also very material-saving and substrates can be tailored in any sizes. Many electronic materials can be inkjet-printed including polymers, organic and inorganic materials, carbon materials. They work as conductor, semiconductor, dielectrics and insulator, which have been introduced in Chapters 2 and 3. The key requirements for inkjet-printed ink materials are low viscosity, fine size of particle if the ink is a colloid or a suspension liquid, and low volatility to avoid nozzle clogging.

The most reliable inkjet-printed inks containing electronic materials are metallic inks. It was reported in 1988 that soluble metal compounds including silver (Ag), titanium (Ti), bismuth (Bi), and niobium (Nb) were directly inkjet-printed for metal electrode fabrication [2]. At present, silver is the mainstream metal conductive ink because of its good conductivity, chemical stability and availability. Many types of silver inks are commercially available. As most of metallic inks require post-print heating process (including solvent removal, curing, or sintering), some thermal decomposable and vaporizable additives can be added to improve the viscosity, surface tension, or other physical properties of an ink, enabling these metallic inks more suitable for inkjet printing. This is particularly the case for silver inks, which can be easily formulated to fit to a specific application. Inks containing other metals such as gold, copper and nickel are also commercially available for some niche applications.

Polymeric ink is another big group of printable electronic materials. It covers almost all electronic functions such as conductor, semiconductor, optoelectronic materials, dielectric materials, and insulating materials. Typical polymeric inks include high work function conductive polymer PEDOT:PSS, semiconductor polymer such as P3HT and MEH-PPV, and dielectric

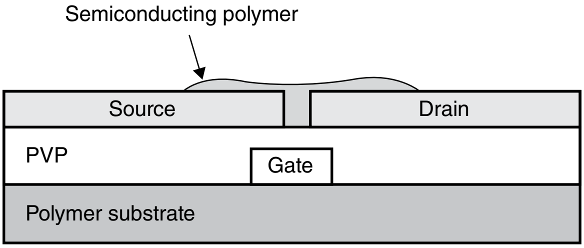

Figure 4.4 Schematics of an organic field-effect transistor (OFET)

or insulating polymer PMMA, and such [3–16]. There are wider choices for polymeric inks because polymers can be synthesized and modified by chemical or physical methods. For the properties of ink materials and formulation methods, the relevant information can be found in Chapters 2 and 3 of this book.

Thanks to the advantages of digital control and non-contact mode, inkjet printing is the most versatile printing method. Almost all electronic components can be inkjet printed. Reported examples of inkjet printed devices include field-effect transistors [17–22], sensors [23–26], solar cells [27–30], light emitting and displays [10, 31–35], memories [36–39], resistors [8, 40, 41], capacitors [42, 43], inductor [44], antennas [45–50], and so on. Electronic systems based on all printed functional components were also reported [44, 51, 52]. They can also be partially printed by inkjet printer. Figure 4.4 shows schematically an organic field-effect transistor which only has its semiconductor layer printed and other layers can be made by conventional microfabrication processes.

There are some challenges when applying inkjet printing in printed electronics. Firstly, the inkjet printable ink is difficult to formulate. The physical properties such as viscosity, surface tension and volatility of ink should be strictly controlled within a relatively narrow range. Secondly, the resolution of inkjet printing is poor, typically greater than 20 μm. Thirdly, the nozzles of an inkjet printer are relatively easy to clog when solids precipitate from ink, because solvents contained in the ink can volatilize quickly, or the ink contains particles that are too large, or the ink has poor stability. Fourthly, ink movement after jetting out of a nozzle is unavoidable because of its low viscosity and substrate surface conditions [4, 11, 53, 54]. The ink movement can have both positive and negative effects. In some cases, the negative effect may have positive outcome. For example, the “coffee ring” effect is a common phenomenon in inkjet printed patterns, which is unwanted if a uniform material deposition is required. However, this coffee ring effect has been utilized to obtain narrow conductive circle lines, which become the basis for a new type of transparent conductive film [55, 56]. Various pre-printing and post-printing processes have been developed to overcome the detrimental effects, which will be discussed later in this chapter (section 4.5 and 4.6).

4.2.2 Aerosol Jet Printing

Aerosol jet printing, developed by Optomec Inc., works on a different principle from inkjet printing and has advantages such as high resolution and suitability for a wide range of inks. So far, Optomec is the only provider of the commercial aerosol jet printer [57–62]. The aerosol jet printing technology introduced in this chapter is based on the information provided by Optomec and the author's own experience as a user of this printer.

4.2.2.1 Working Principle

The principle of the aerosol jet printing process is very different from inkjet printing. Ink is first turned into a dense aerosol of tiny droplets between 1–5 microns in size pneumatically or ultrasonically in an atomizer. The aerosol of ink is then carried by an air stream to the nozzle, which is aerodynamically focused by a ring-shaped compressed air sheath to form a fine and high velocity aerosol stream spraying onto a substrate. The principle is illustrated in Figure 4.5. The focused ink stream has a diameter as small as 5 μm and sprays continuously, with a shutter to stop the ink stream at non-printed areas. Figure 4.6 shows the actual aerosol jet printer and the close-up of the ink nozzle and the shutter.

4.2.2.2 Pattern Preparation

Unlike inkjet printing which forms a pattern by dot matrix, aerosol jet printing uses continuous lines to form a pattern. The printing nozzle is kept still while the sample stage moves. The system converts an AutoCAD design file into a series of lines and instructions according to the pattern area to control the stage movements, as well as opening and closing the shutter. Alternatively, the printing routes can be directly set by the system's built-in program for simple design patterns.

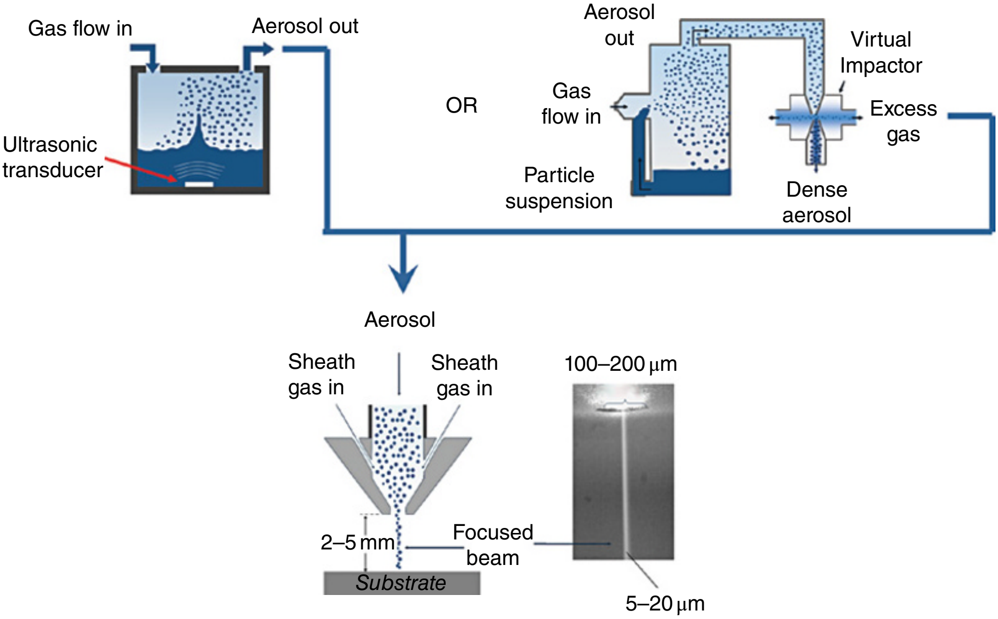
Gas flow in
Aerosol out
Ultrasonic transducer
OR
Aerosol out
Gas flow in
Particle suspension
Virtual Impactor
Excess gas
Dense aerosol
Aerosol
Sheath gas in
Sheath gas in
100–200 μm
2–5 mm
Focused beam
Substrate
5–20 μm

Figure 4.5 Principle of aerosol jet printing. Reprinted with permission from Optomec, Inc

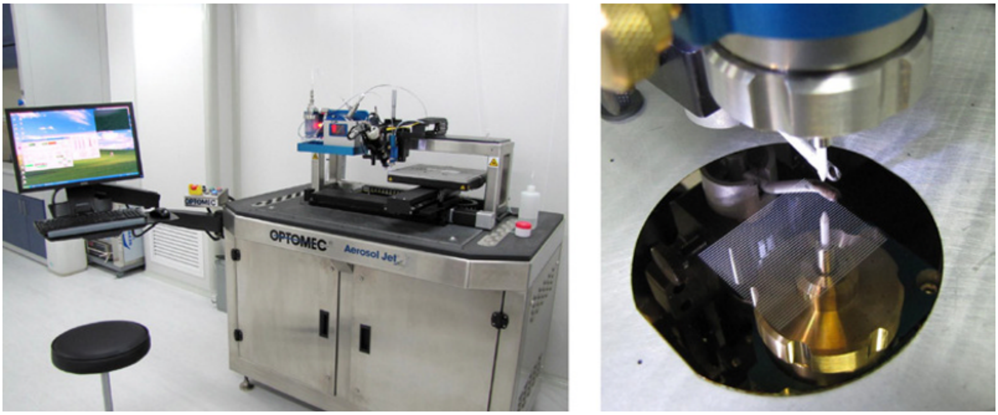

Figure 4.6 Aerosol jet printer (left) and the jet nozzle with the shutter (right)

Table 4.1 Comparison between inkjet printing and aerosol jet printing

Features	Inkjet printing	Aerosol jet printing
Line width	~50 µm	<5 µm
Layer Thickness	~0.1 µm	10 nm to 10 µm
Ink Viscosity	10–14 cP	0.7 – 2500 cP
Substrate Requirements	Planar print head above ~1 mm	Non-Planar print head above 1 to 5 mm
Droplet Size	10 pL (20–50 µm)	10 fL (1–5 µm)
Pattern Generation	Digital – Raster	Digital – Vector and/or Raster

4.2.2.3 Advantages and Challenges

Aerosol jet printing has a number of advantages over inkjet printing. The two printing methods are compared in Table 4.1. The most important advantage of aerosol jet over inkjet is that the range of printable ink is much wider (0.7–2500cP, according to the manufacturer's specification), because the diameter of aerosol jet nozzle is more than 200 µm, which is much larger than the nozzle of an inkjet printer. As a result, the aerosol jet printer is much more tolerable to various ink materials and much less likely to have nozzle clogging problems. Aerosol jet printing has been used to print front-side electrodes of silicon solar cells [63–65], transistors [60, 66] and biosensors [67]. The ink materials include metal inks, carbon nanomaterials inks, and polymeric inks. Figure 4.7 shows an array of thin-film transistors printed by aerosol jet printer, and a close-up look of a single printed transistor.

There are still some challenges when applying aerosol jet printing to printed electronics. The main challenge is that the aerosol jet printing relies on stable air flow, which means there will be a lagging effect when trying to adjust printing parameters. It will not happen instantly. This lagging effect also causes difficulty in studying spontaneous movements of printed ink because the large amount of atomized liquid droplets are harder to track than a single droplet in an inkjet printer. In addition, an aerosol jet printing system is much more expensive than a desktop inkjet printer. The multi nozzle system of aerosol jet printing is not as mature as that of inkjet printing, which makes the large area printing much slower and with low throughput.

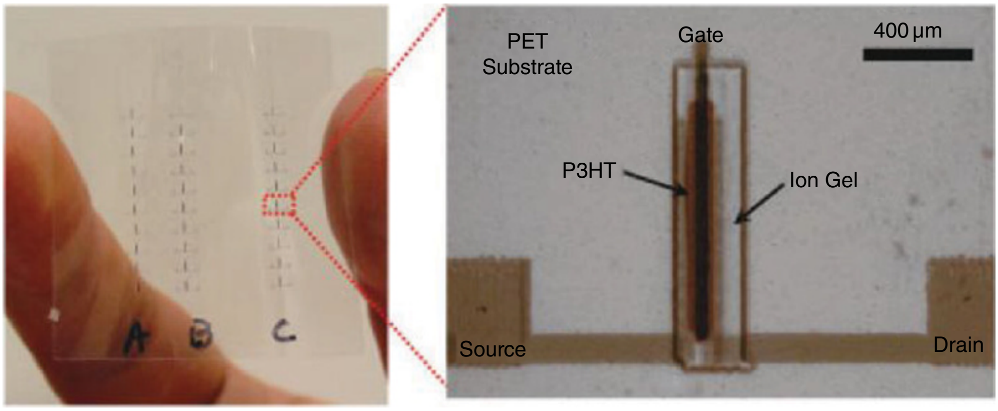

Figure 4.7 Optical image of a 30 transistor array printed by aerosol jet printing. The right image shows a magnified single transistor. (Reprinted from [60] with permission from John Wiley and Sons)

4.2.3 Electrohydrodynamic Jet Printing

For inkjet printers, the printing resolution is directly related to the size of ink droplets, which is in turn related to the size of printing nozzle. It becomes more difficult to jet out inks if the nozzle is too small, because of the viscosity and surface tension of ink liquid. In addition, a small nozzle diameter greatly increases the chance of clogging. This problem can be resolved by electrohydrodynamic (EHD) jet printing. EHD jet printing is a technique that uses an electric field to create the ink flow through a fine nozzle onto a substrate. Electrohydrodynamics is a field of fluid dynamics that studies the flow of electrically charged liquid under the influence of an external electrical field. In EHD jet printing, the ink is pumped through a nozzle and a strong electric field is applied between the nozzle and the substrate holder. A droplet much smaller than the nozzle diameter can be formed and ejected out if the electric field force is larger than the surface tension force. Figure 4.8 is a schematic setup of EHD jet printing. Fine nozzles as small as 300 nm in diameter were reported and printed lines at 240 nm width were achieved [68]. EHD jet printing has been used to print high resolution conductive components using metal-based or polymer inks to make short channel transistors [69], flexible memoristors [70] and polymer layer in resistive switching devices [71]. Commercial EHD jet printers are available from vendors in Japan and Korea [72, 73].

4.2.4 Advantages and Disadvantages

Jet printing, also called non-contact printing or digital printing, is popular in laboratories for printed electronics research, because it deposit inks directly on substrate with digital control and without any contact between the equipment and substrates. Its advantages in printed electronics are:

- Ink with very low viscosity can be used. As mentioned in Section 4.1, viscosities of some laboratory made inks are too low for traditional printing.
- The contact between printing equipment and substrate is avoided. The limitations due to substrate property such as roughness, brittleness and flexibility can be ignored. On the other hand, the damage and contamination are minimized because of its non-contact nature.
- There is no need for a master plate. The design patterns can be easily modified. This is particularly suitable for scientific research, small batch printing and fast prototyping.

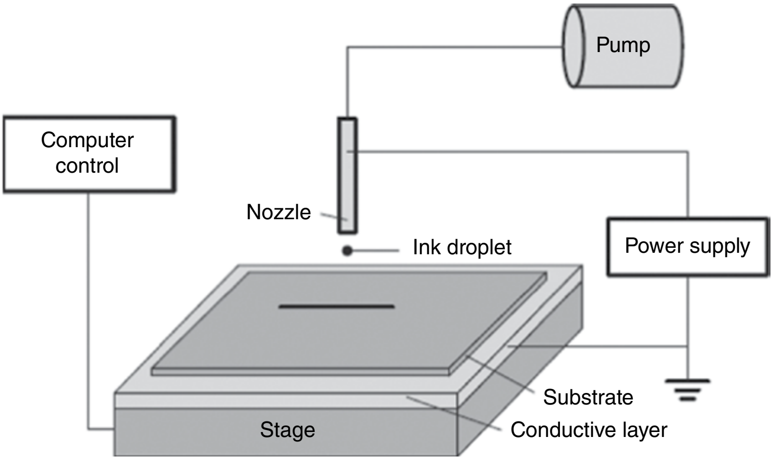

Figure 4.8 Schematic of an EHD printer. (Adopted from web with courtesy)

- Multi-material printing is more accurate and easier to implement, which is very similar to multicolor printing. As electronic devices are often composed of multi-materials and multi-layers, it is necessary to overlap different printed materials. Jet printing systems normally have better alignment and overlay accuracy than any other printing methods. A multiple nozzle configuration also facilitates several ink types to be printed simultaneously.
- Jet printing allows inks to be deposited only where they are needed. The materials waste is much less compared to other printing methods.

The primary disadvantage of jet printing is low throughput when printing large area and high volume. Although multiple nozzles and parallel printing can improve its throughput, the industrial scale jet printing is not as mature as those traditional replicate printing methods. However, large scale jet printing processes and equipment are being developed rapidly. They are likely to be used more and more in the industrial environment in future.

4.3 Direct Replicate Printing

The aforementioned jet printing is also called digital printing. “Digital” means the images or patterns to be printed are in digital format. They are electronic design files. In contrast, the replicate printing relies on a master or a template that carries the images or patterns. The printing process is basically a replication process, replicating the images or patterns from a master plate to other surfaces. Digital images can be easily altered and every printing can be different. A master plate, once made, cannot be altered. Every printing from the master plate is the same and it is best suited for a large number of printings with the same information. It is a high volume and high throughput printing process, suitable for printing newspapers or textiles. Depending on the nature of a template, the replicate printing can be divided into screen printing, gravure printing, flexographic printing, and such. Images can be directly or indirectly replicated from a master plate. This section will discuss the direct replicate printings, that is, screen printing, gravure printing and flexographic printing, which have found applications in printed electronics. The indirect replicated printing will be introduced in the next section.

4.3.1 Screen Printing

4.3.1.1 Working Principle

Screen printing is the most simple and the most widely used printing method in industry. Its working principle is illustrated in Figure 4.9. The master plate is a mesh (screen) with patterned and non-patterned areas as transparent and opaque respectively. The ink for screen

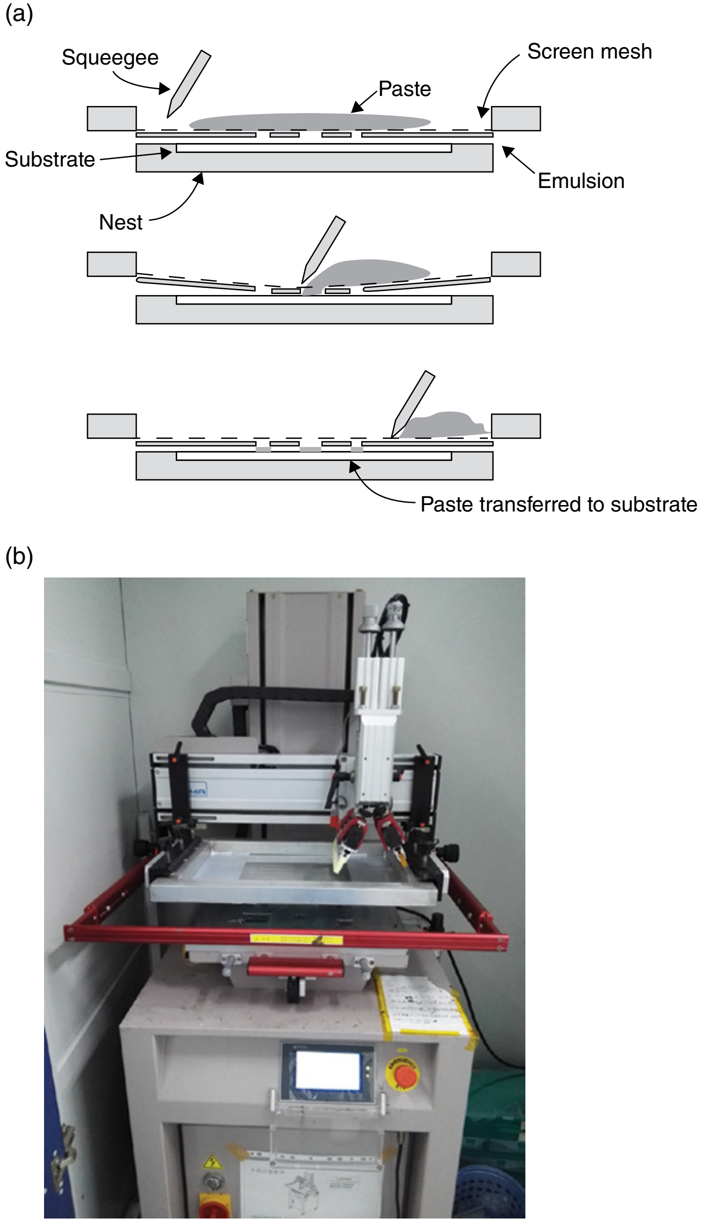
(a)
Squeegee
Screen mesh
Paste
Substrate
Emulsion
Nest
Paste transferred to substrate
(b)

Figure 4.9 (a) Working principle of a screen printer; and (b) an actual screen printer printing is of high viscosity and usually called paste. It allows for thick-film patterns to be manufactured. The printing starts by covering the screen with paste and placing a substrate under the screen. A squeegee (blade) moves across the screen, which applies a pressure to the paste-covered screen and forces the paste to penetrate through the patterned area to deposit on the substrate. The process is illustrated in Figure 4.9a. The printed paste on the substrate can replicate exactly the pattern of the screen. The highly viscous paste ensures it will not leak onto the substrate without the squeegee press. Figure 4.9b shows an actual screen printer where the application of paste and squeegee press can be performed automatically.

The most traditional screen printer has a flat screen and a flat substrate holder, which works in sheet to sheet feeding mode. Printers with flat screens can also work in roll feeding mode whereby a roll of flexible substrate is fed to the printer, although the printing is still performed on flat sheet. The printer should have accurate control of substrate feeding to ensure the synchronization between sheet printing and substrate feeding. Another type of screen printer employs a rotary screen that integrates squeegees and paste in a roller. When combined with the roll feeding of a flexible substrate, this type of screen printer works in true roll-to-roll mode, allowing high throughput printing.

4.3.1.2 Screen Mask

The screen mask is composed of a frame, a fabric mesh and the stencil on the fabric mesh. The fabric mesh is usually made of natural silk, plastic, or metal fibers. The stencil is made of patterned light-sensitive materials deposited on the fabric mesh. The patterning is done by optical lithography. A schematic diagram of fabric mesh is shown in Figure 4.10. The selection of frame, fabric mesh and stencil materials, as well as the stencil deposition method, all play important roles in controlling the final pattern resolution and film thickness[1]. Because of the fabric mesh structure, the printing resolution is generally low, normally over 100 μm. However, screen printed conductive patterns with thinner line width such as 50 μm [74] and 30 μm [75] were also reported. Using positive chemically amplified resists as the stencil material, printing Ag circuits of 13 μm feature size were reported [76].

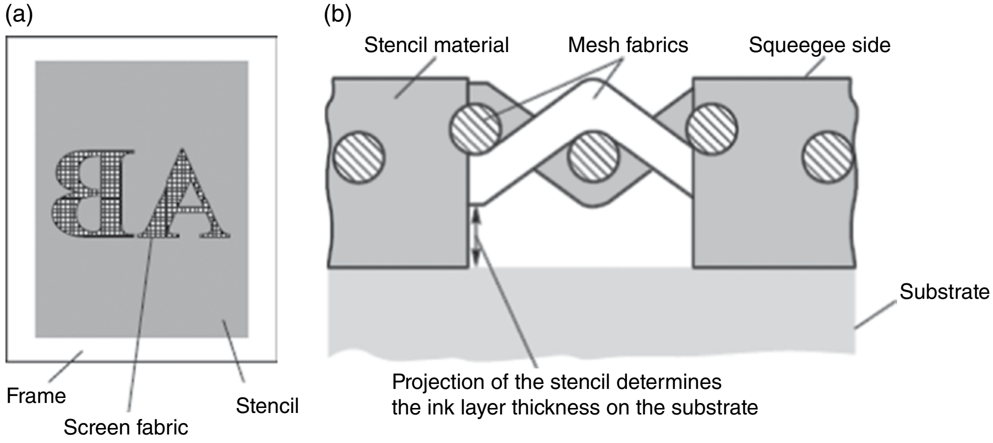

Figure 4.10 Schematic diagram of screen frame, fabric and stencil. (Reprinted from [1] with permission from Springer)

4.3.1.3 Advantages and Disadvantages

Compared with other printing methods, the advantages of screen printing are as follows.

- The paste can be formulated with micro-sized solid materials which are easier to obtain and use than nano-sized particles. There are various commercial pastes including metal, carbon, and polymers, which can be screen printed to make electrical components.
- It is able to print patterns on either flat or curved substrates because the screen can be soft. Different kinds of substrate, including fragile wafer, can be printed on.
- Screen printing can obtain thick film (more than 10 μm) more easily than other types of printing technology.
- It is much easier to control the paste movements during the printing operation, because the paste has high viscosity.
- The overall cost of screen printing is lower than other printing methods, both in equipment and in paste materials. For simple and low resolution structures, screen printing is adequate.

The primary disadvantage is that the printable paste must have high viscosity. Additives are necessary for most electric materials to be formulated into high viscosity paste, which usually decrease their electrical properties. Because of high viscosity, the pattern surface can be very rough. Another disadvantage is its low resolution, which limits its use in printing electronic devices with fine structures and requiring accurate overlays.

4.3.1.4 Applications

Screen printing is widely used for manufacturing components or devices in various conventional electronics such as electronic circuit boards, membrane switches and electronic display boards. [77–81]. The technology has been adopted in silicon solar cell manufacturing since the 1970s [82–88], mainly for printing front side electrodes using silver pastes. Figure 4.11 shows the silicon solar cells with bright grids on the front side, which are screen printed silver electrodes. With the improvement in resolution and emergence of new electronic pastes, screen printing has also found applications in organic solar cells [89–91], as well as transistors, sensors and other electronic components [92–113].

4.3.2 Gravure Printing

4.3.2.1 Principle and System

Gravure printing replicates patterns using a gravure plate that has engraved patterns in the form of dented dots. The dented plate is also called cliché. Inks are loaded into the dented dots, which are then transferred to substrate surface during printing process. A gravure printer consists of a gravure plate (or a gravure roller), ink supply unit, a doctor blade and an impression roller. Before printing, the gravure is immersed in the ink. Any excess ink not in the dented dots is removed using a doctor blade. The ink contained in the engraved area is transferred to a substrate surface by the impression roller in contact with the gravure at pressure (transfer occurs because of the adhesive forces between substrate and ink). This process is illustrated in Figure 4.12 where the gravure roller has its surface engraved.

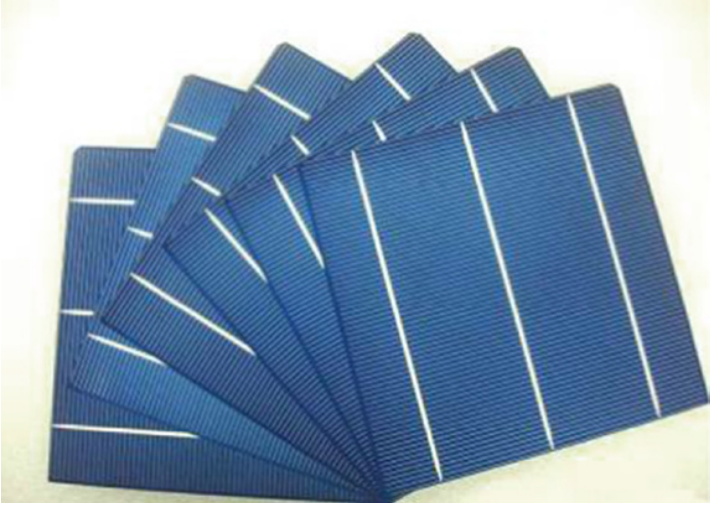

Figure 4.11 Front side electrodes made by screen printing on commercial silicon solar cells. Adopted from web with courtesy to its origin

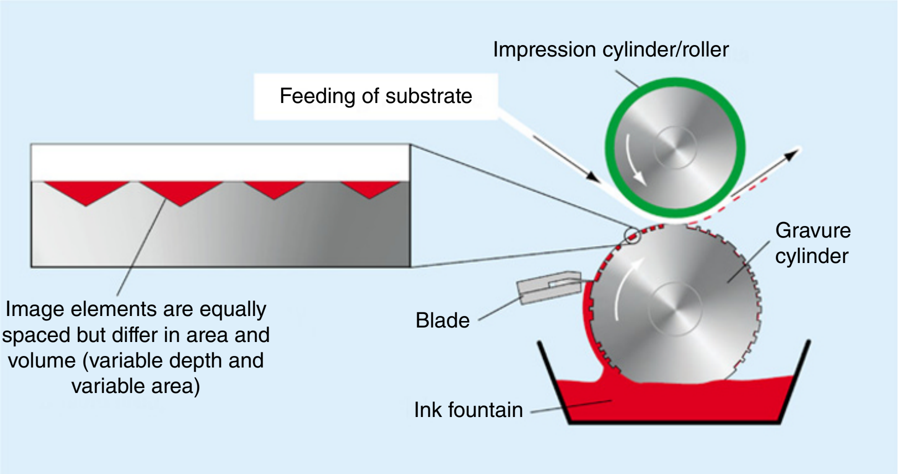
Impression cylinder/roller
Feeding of substrate
Gravure cylinder
Blade
Image elements are equally spaced but differ in area and volume (variable depth and variable area)
Ink fountain

Figure 4.12 Schematic principle of gravure printing. (Reprinted from [1] with permission from Springer)

Gravure printers have two modes of operations: web-fed printing and sheet-fed printing. The web-fed gravure printer has a gravure roller, like the one illustrated in Figure 4.12, which allows roll-to-roll high speed printing. Most of the gravure printers in industry are web-fed printers for mass production because the printing quality and stability is better at high speed. Sheet-fed gravure printers print in a sheet-to-sheet manner. This type of printer is best suited for small batch printing or laboratory use. Figure 4.13 is a photograph of a desktop gravure printer for laboratory use. It has a flat gravure plate and can print one sheet at a time only.

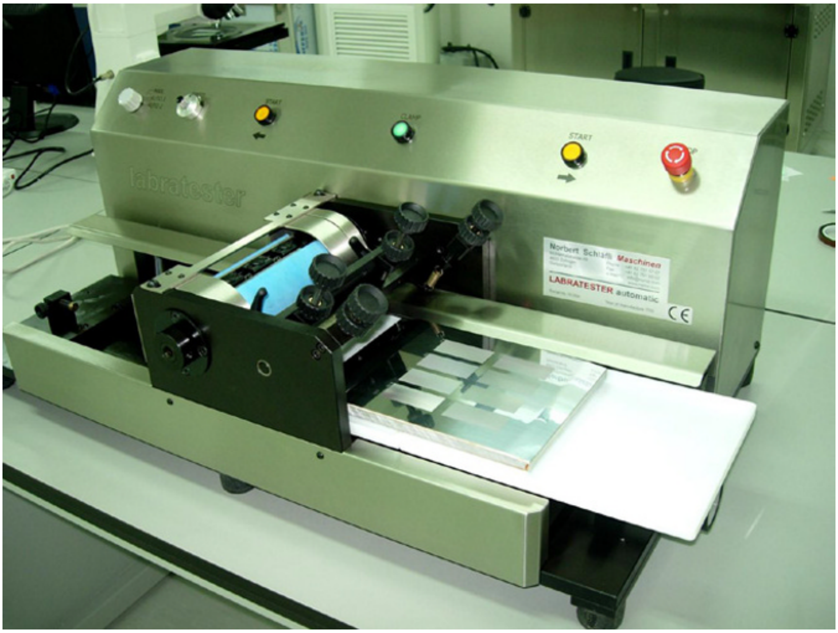

Figure 4.13 A desktop gravure printer (Labratester from Norbert Schlaefli)

4.3.2.2 Gravure Plate

A gravure plate typically comprises a steel base and a copper layer. A pattern is first decomposed into a matrix of dots. Each dot is engraved into the copper layer as a dent called a gravure cell. Each cell has walls around it, which prevent the cells from merging into each other and provide support for the doctor blade movement. Typically the gravure cells are electro-engraved into a diamond shape, or laser engraved into a spherical shape. The matrix of the diamond shaped gravure plate is shown in Figure 4.14. A thin layer of chrome is electroplated after engraving to protect the copper surface from the abrasion of the doctor blade during printing and to reduce the surface energy of plate.

The cell shape and depth on a gravure plate play key roles in controlling the quality of printed patterns. In a gravure printing process, the amount of ink that can be printed is controlled by the size and depth of the gravure cells. So gravure printing can precisely control pattern thickness and morphology. The drawback of the cell based gravure plate is that pattern edges show a “serrated teeth structure”.

4.3.2.3 Advantages and Disadvantages

The advantages of gravure printing are

- Low viscosity ink can be used, which means that high purity dispersion of inks is possible without additives. Inks consisting of dispersed micro-size particles can be printed.
- High throughput printing is possible through the roll-to-roll process.

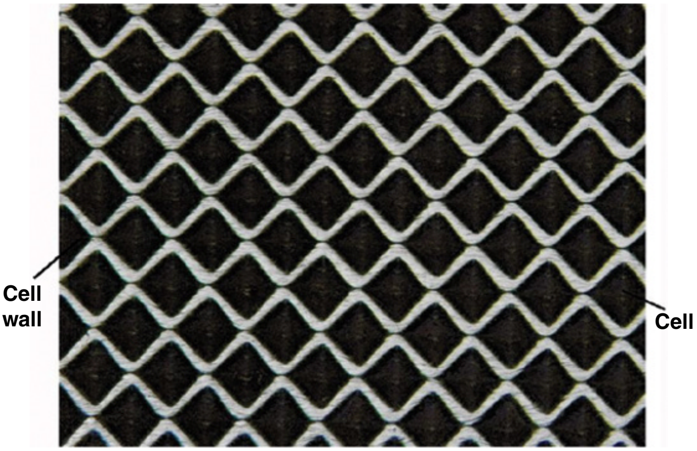

Figure 4.14 Optical microscopic image of typical diamond shaped gravure plate

- The engraved structure of a gravure plate makes it possible to control ink volume exactly. Different thicknesses in a pattern are possible by employing gravure cells of various sizes and depths. The printed layer thickness can be more than 5 μm.
- The metallic gravure plate usually has a long working life and can produce millions of prints without suffering pattern deterioration.

The primary disadvantage of gravure printing is the high cost of making a gravure plate. It is not suitable for prototyping or small batch production. Moreover, the rigid printing plate and requirement for high impression pressure make it only suitable for printing on flexible substrate, although this drawback can be overcome by indirect gravure printing, which will be introduced in Section 4.4.

Conventional gravure printing has a limited resolution of about 50 μm and cannot directly print patterns on rigid substrate because of the hard gravure plate. However, a direct gravure printing method using an elastic polymer plate was reported to print fine electrical circuits on ceramics with printed lines of 20 μm [114]. By controlling the ink volume to femtoliter scale, sub-10 μm resolution can be realized by gravure printing [115, 116].

Another issue in gravure printing is how to manage ink movement on the printed surface. Because the pattern area on a gravure plate is in the form of individual disconnected cells, ink transferred from individual cells onto a substrate surface must be able to move around to form a homogeneous film. Properties of ink and substrate surface play key roles in this process. It is reported that surfactants and additives in PEDOT:PSS ink and surface tension modification for substrate help to achieve better results. A wetting envelope was used to search the best match between ink and substrate [117, 118].

4.3.2.4 Applications in Printed Electronics

Electronic devices fabricated by gravure printing have been reported, including printing field-effect transistors [119–121], solar cells [122, 123], light-emitting devices [124, 125] and multi-function circuits [126–130]. Figure 4.15 shows printed rectennas on flexible

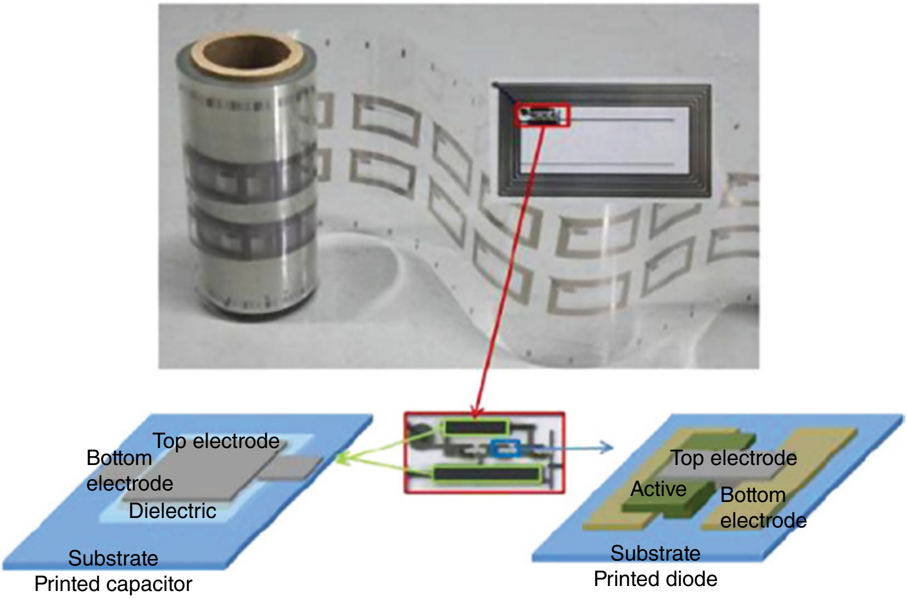

Figure 4.15 Gravure printed rectennas containing printed capacitor, diode, and electrodes. (Reprinted from [130] with permission from IOP Publishing)

substrates, which include capacitors, diodes and conductive tracks. There were also studies on process issues of gravure printing, such as resolution, film formation, use of low viscosity inks, printing on rigid substrates, and so on [131–135]. However, detailed study of gravure printing is difficult because the ink movement in this process is more difficult to trace than inkjet. Most published research results were on sheet-fed rather than web-fed gravure printers.

4.3.3 Flexographic Printing

4.3.3.1 Principle and System

Flexographic printing uses an elastic printing plate or a roller with pattern areas as surface reliefs protruding above non-pattern areas. The key component that controls the transfer of the precise amount of ink to the flexographic plate is the anilox cylinder, which is very similar to a gravure roller except that the engraved cells cover all the surface of the roller.

In the flexographic printing process, the anilox cylinder is first immersed in an ink tank and a doctor blade is used to remove excess ink from the non-engraved surface of anilox cylinder. The ink in the cells is then transferred evenly onto the flexographic printing plate, which is subsequently transferred to the substrate by contact force. The printing process is illustrated in Figure 4.16. It should be noted that the figure only shows some basic components. A real flexographic printer will have more rollers for tension control of flexible thin substrate and other functions.

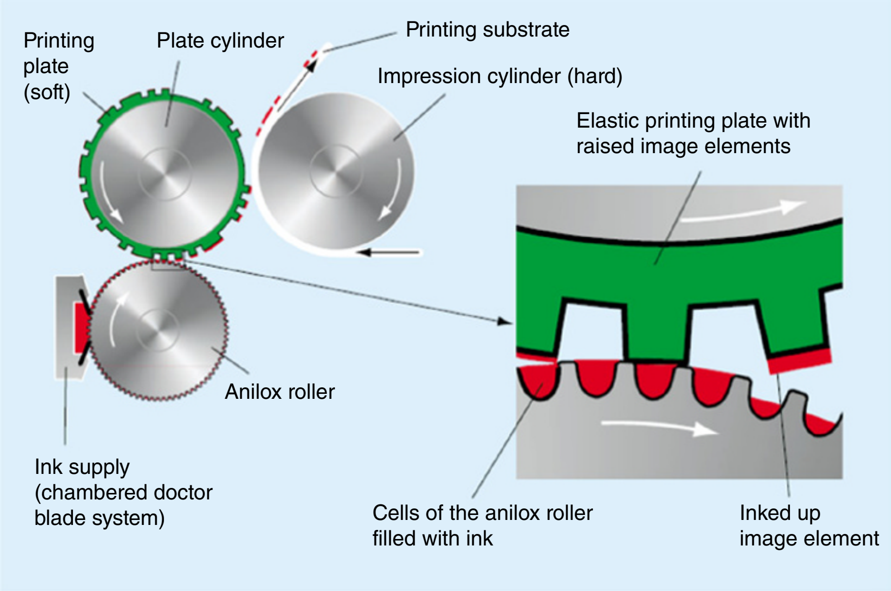
Printing plate (soft)
Plate cylinder
Printing substrate
Impression cylinder (hard)
Elastic printing plate with raised image elements
Anilox roller
Ink supply (chambered doctor blade system)
Cells of the anilox roller filled with ink
Inked up image element

Figure 4.16 Schematic diagram illustrating the principles of a typical flexography printing unit. (Reprinted from [1] with permission from Springer)

4.3.3.2 Printing Plate

Materials of flexographic printing plates are generally divided into rubber and photopolymer. For rubber plate, the oldest technology is hand engraved plate. Modern flexographic printing plates are usually made by molded rubber and laser engraved rubber. Alternatively, soluble photopolymer is patterned by UV light exposure. Patterned areas are solidified upon UV exposure through a mask. The unexposed areas, which retain their solubility, can be washed off. The final surface relieved printing plate looks like the one shown in Figure 4.17. The maximum ink transferred by surface relief type of printing plate is usually less than screen printing or gravure printing, so the film printed by flexography printing is thinner compared to the maximum thickness deposited by the other two methods.

4.3.3.3 Advantages and Disadvantages

The advantages of flexography printing are:

- The viscosity of the ink is usually in the range of 50–200 cP, which is easier for ink formulation.
- The flexographic plate is resilient, low cost and easy to make.
- Because of the elastic plate, it can print ink on wider range of substrates, including rigid or rough surface. The printing pressure used in flexography printing is lower than gravure printing.
- A thinner printed layer with a sharp edge and smooth surface is easy to obtain by flexographic printing.

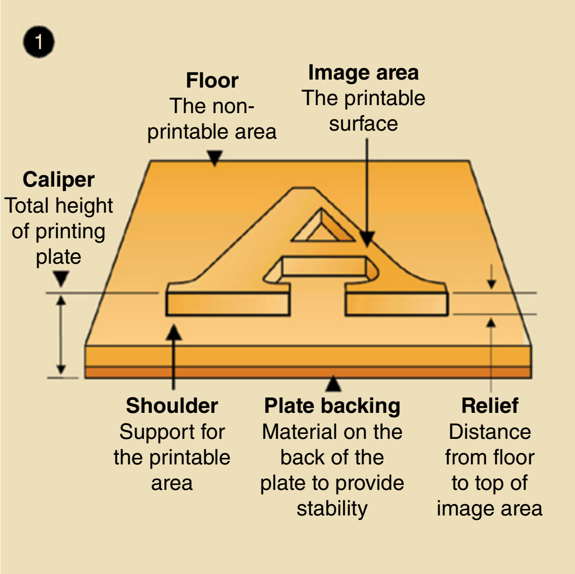
1
Floor
The non-printable area
Image area
The printable surface
Caliper
Total height of printing plate
Shoulder
Support for the printable area
Plate backing
Material on the back of the plate to provide stability
Relief
Distance from floor to top of image area

Figure 4.17 A schematic diagram of a flexographic printing plate. (Adopted from web with courtesy to its origin)

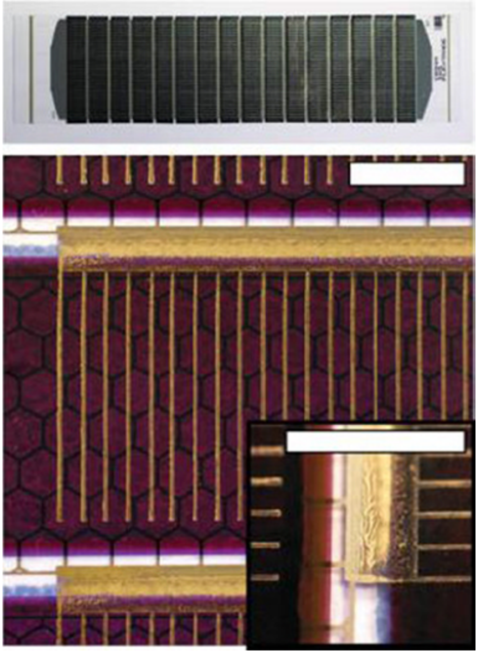

Figure 4.18 Silver back electrodes on ceramic substrate, printed by flexographic printer. (Reprinted from [139] with permission from John Wiley and Sons)

However, the flexographic plate has a short service life compared to gravure plate. Distortion may occur under printing pressure because of the elastic nature of printing plate. On the other hand, a flexographic printer is more complex than a screen printer or a gravure printer. One should pay more attention to the physical and chemical interactions between ink, anilox cylinder, plate, and substrate in order to achieve better printing quality.

4.3.3.4 Applications in Printed Electronics

The flexographic printing is an attractive method for printing electronics. But there are fewer reports on this method, and the existing reported works are usually about printing one or two thin functional layers rather than all the layers of a device. They also include printing conductive patterns such as source, drain and gate electrodes of a field-effect transistor [136–138], solar cell electrodes [139], RFID Tags [140], the display device [141], as well as other applications [142–144]. This technology can also print conductive patterns on a rigid ceramic surface, as is shown in Figure 4.18 [145].

4.4 Indirect Replicate Printing

Indirect Printing is a method by which the surface to be printed is not in direct contact with the printing plate. The ink pattern in indirect printing is printed on an elastic intermediate carrier (blanket) first and then transferred onto the substrate surface.

4.4.1 Offset Printing

Offset printing is an indirect printing. Its working principle is schematically shown in Figure 4.19 [1]. The ink in an offset printing process is first transferred from a printing plate onto a rubber blanket, and then to the substrate. As opposed to other printing technologies, the offset printing has a flat plate with a very tiny height difference between the pattern and non-pattern areas. The ink on the printing plate forms patterns because of the different interactions between the ink and the plate in the hydrophobic pattern area and the hydrophilic non-pattern area. There are two commonly used methods to achieve the ink-repellent effect on the printing plate.

In conventional offset printing technology, inking and dampening are the two key processes. The printing plate is first coated with dampening solution (usually water with additives) by dampening rollers. The water on the hydrophilic non-pattern area forms a very fine film and the hydrophobic pattern area is unreceptive to water. This film of dampening solution on the non-pattern area prevents any subsequent inking, enabling the ink staying only on pattern area.

Waterless offset printing technology is a new technology that does not require the dampening solution. The whole printing plate is coated with a thin ink-repellent silicone layer as a non-pattern area. In the pattern area the silicone layer is removed to make the surface ink-receptive. Therefore, there is no dampening unit in a waterless offset printer. The ink coated on the printing plate will stay in the pattern area, and be repelled from non-pattern area.

The offset printers can also be divided into sheet-fed mode and web-fed mode. For higher throughput, roll-to-roll web-fed offset printers are widely used in printing industry. However,

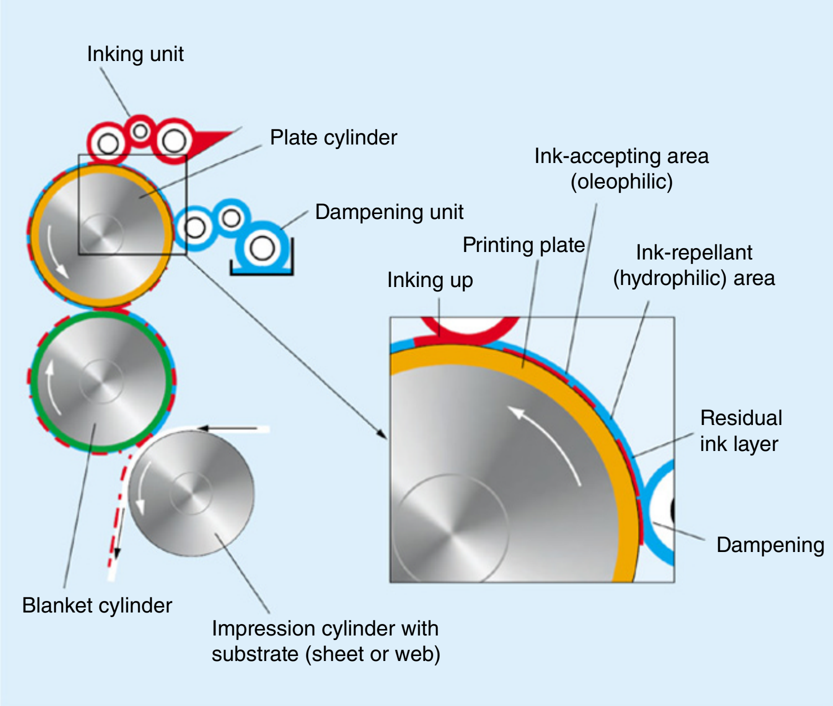
Inking unit
Plate cylinder
Ink-accepting area (oleophilic)
Dampening unit
Printing plate
Inking up
Ink-repellant (hydrophilic) area
Residual ink layer
Dampening
Blanket cylinder
Impression cylinder with substrate (sheet or web)

Figure 4.19 Schematic principle of an offset printing unit. (Reprinted from [1] with permission from Springer)

offset printing has seldom been used in printed electronics even though it is the most popular process in traditional printing industry. There was a report that PEDOT:PSS ink was offset printed as source and drain electrodes for organic field-effect transistors [146, 147]. The most important reason is that the inks used in conventional offset printer have viscosities more than 40000 cP [1]. It is difficult for most printed electrical materials to be formulated into such viscous ink. Moreover, an offset printer is mechanically more complex than other printers. Figure 4.20 shows an actual printing system used for printing the organic field-effect transistors.

4.4.2 *Gravure Offset Printing*

As discussed in Section 4.3, gravure printing is very suitable for printing electronics, but it cannot print on fragile substrate directly. Indirect gravure printing can solve this problem. Similar to offset printing, a gravure offset printer uses a blanket cylinder to transfer ink. In gravure offset printing, the ink is first printed by gravure plate onto a blanket cylinder, and then transferred to the substrate from the blanket cylinder. The principle of gravure offset printing is illustrated in Figure 4.21. Like gravure printing, gravure offset can use either a flat gravure plate, or a gravure cylinder. The process can be divided into sheet-fed and web-fed mode.

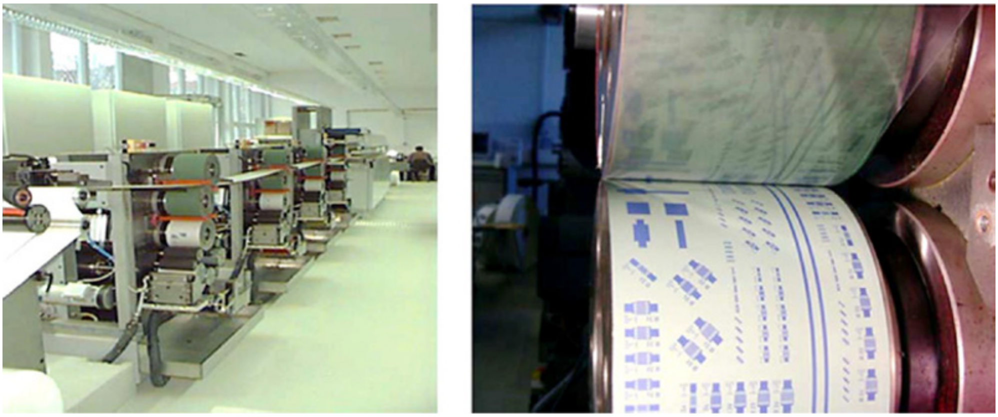

Figure 4.20 The reported offset printer and printed sample. (Reprinted from [146] with permission from AIP Publishing LLC)

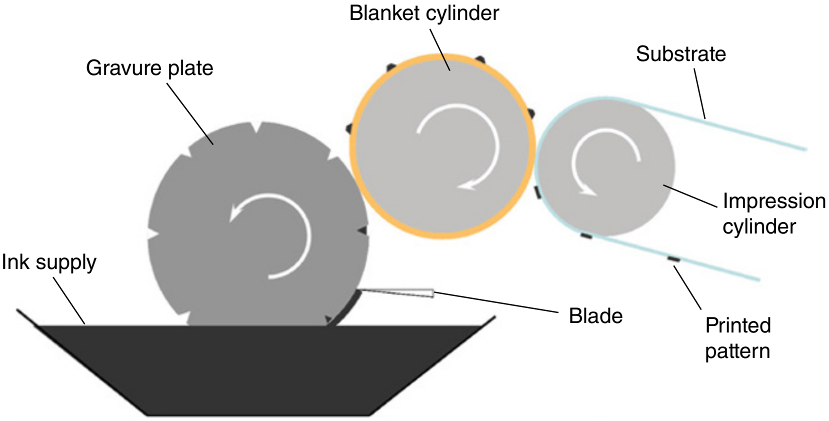

Figure 4.21 Schematic principle of gravure offset printing. (Adopted from web with courtesy to its origin)

Gravure offset printing is the most advantageous method of gravure printing because it employs the same inking unit as the direct gravure printing. In particular, the engraved cell structure of a gravure plate can meter the ink volume exactly, in order to obtain a pattern with different densities. Low viscosity ink can also be used. In addition to these merits, it can print on variety of substrates. During the ink transfer process, the ink can move on the blanket to smooth the pattern edge and absorb into the blanket after solvent evaporation. It is possible for gravure offset to achieve a narrower printed line than direct gravure without the serrated teeth edge. However, the gravure offset printer is mechanically more complex than a direct gravure machine and there are more interactions among the ink, plate, blanket, and substrate.

It has been reported that gravure offset printing has been used to print electronics since 1994 [148]. Most of the materials printed by this technology were metals [149, 150]. Using a

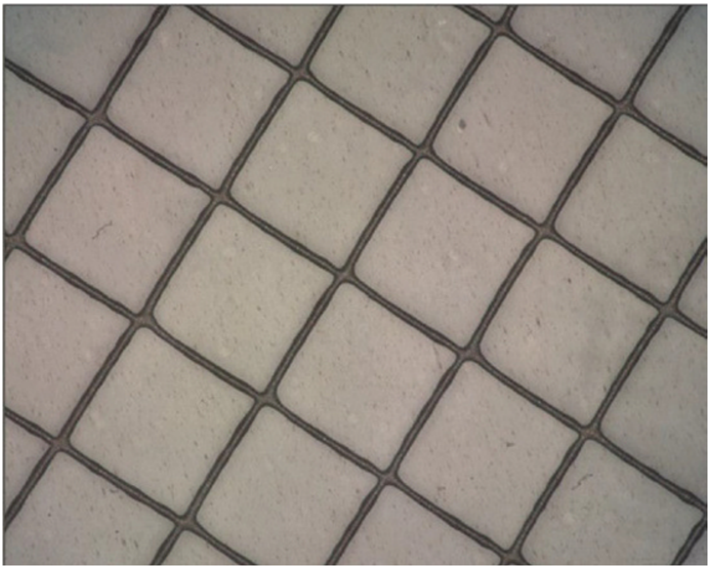

Figure 4.22 Reported 20 µm width silver lines printed by gravure offset printer. (Reprinted from [155] with permission from IOP Publishing)

soft rubber roller, the technology can print conductive components or devices on ceramic surfaces[151, 152]. Polymer was also printed [153]. The ink transfer process and reliability of gravure offset printing was studied [154, 155], and the resolution obtained by gravure offset was as small as 20 µm [155, 156], as is shown in Figure 4.22. Research for improving the gravure printing equipments was also reported [157, 158].

4.4.3 Pad Printing

Pad printing (or pad transfer printing) is also an indirect gravure printing technology. It employs a special silicone rubber stamp as the blanket and is suitable for transferring ink on uneven substrate. In a pad printing process, the ink is filled in the gravure plate and the excess ink is removed by doctor blade. The ink remaining in the cells is then transferred from gravure plate to substrate surface using an elastic silicone rubber stamp. The principle of pad printing is shown in Figure 4.23. To obtain better printing quality, the ink for pad printing is usually of high solid content, low viscosity, and quick drying. The gravure plate used in pad printing is usually flat. One problem with pad printing is the pattern distortion, which is related to the topography of substrate surface and pad deformation. The distortion has to be studied carefully and taken into account when making the gravure plate. For printed electronics, pad printing can transfer conductive inks on uneven or rough surfaces. It was reported to print solar cell [159, 160], disposable electrodes [161], RFID antennas [162], transducers, [163] and display devices [164] on uneven substrates.

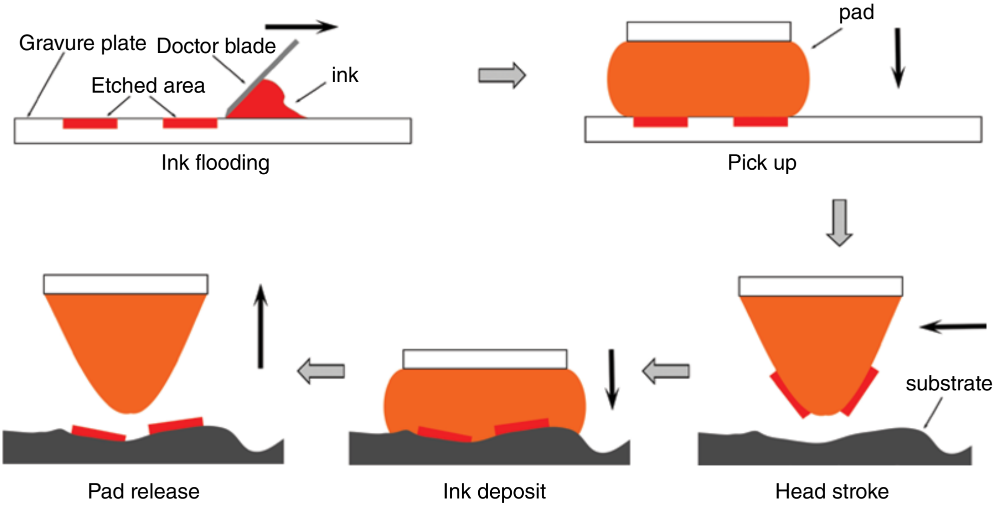

Figure 4.23 Schematic principle of pad printing. (Adopted from web with courtesy to its origin)

4.5 Pre-printing Processes

4.5.1 Pattern Design

Pattern preparation for individual printing method was introduced in Sections 4.2, 4.3, and 4.4; however, there are some generic issues that relate pattern design to final printed pattern quality. The main issue is the pattern distortions due to ink movements in the printing process. This distortion can be compensated for at the pattern design stage.

The patterns used for inkjet, gravure or screen printing are composed of matrix of dots. For example, in inkjet printing, the dot spacing should be determined based on the droplet volume and ink movement on the substrate surface in order to obtain a perfect printed film. Dot spacing that is too large will lead to individual printed drops, and spacing that is too small may cause bulging of printed lines or patterns. To control the droplet volume, proper nozzle diameter and waveform of applied voltage for propelling the droplets should be chosen. The ink movement during the printing process depends on ink properties, the working temperature of the nozzle, the temperature of the substrate, jetting frequency, and the substrate surface property. Dot spacing in pattern design should match with the above parameters.

A similar process is necessary to decide the structure of the cells and the width of the cell walls for direct gravure printing. Ink properties, movements of plate and substrate, and interactions among ink, plate, and substrate should be taken into account in pattern design. In indirect gravure printing, interactions among ink, plate, blanket and substrate are more complex compared to the direct gravure method. For screen printing, the mesh size and fabric diameter should be carefully chosen according to the paste property and interactions among paste, screen, and substrate in pattern design; while the paste movement is easier to control because of its high viscosity.

For flexography printing, there is also a distortion between the pattern on the plate and the printed pattern on the substrate because the elastic relief plate can deform under pressure.

The blanket in indirect printing is another possible reason for pattern distortion. The pattern distortion must be taken into account in plate pattern design for pad printing.

4.5.2 Modification of Surface Energy

Treatment to increase substrate surface energy, making the surface hydrophilic, is usually a critical step in printing aqueous ink, because the surface energy of the substrate directly affects the resolution, uniformity and adhesion of printed films, as seen in the example shown in Figure 4.24, where the surface property makes a significant difference in printing quality. The oxidation reactions, such as oxygen plasma, corona and UV irradiation, are the most used methods to create a hydrophilic surface. On the other hand, strong oxidizing liquid such as potassium dichromate solution can also be used for hydrophilic treatment. These solutions are usually highly corrosive, however, creating problems in safety and waste disposal.

For all the surface treatment methods mentioned above, corona treatment is widely used in industry. The principle of corona treatment is that atmospheric discharge created by high biased voltage produces plasma that oxidizes substrate surface. Compared with oxygen plasma treatment, no vacuum and oxygen are needed for corona treatment, which is more suitable for large scale industrial manufacturing. The oxidation reactions can also be used to clean substrate, creating uniform surface energy. In addition, oxidation reactions can increase the work function of electrode materials such as indium tin oxide (ITO) and silver.

Self-assembly method is another way to change the surface energy [165]. A self-assembled monolayer on the substrate will have the surface energy of self-assembled molecules, as

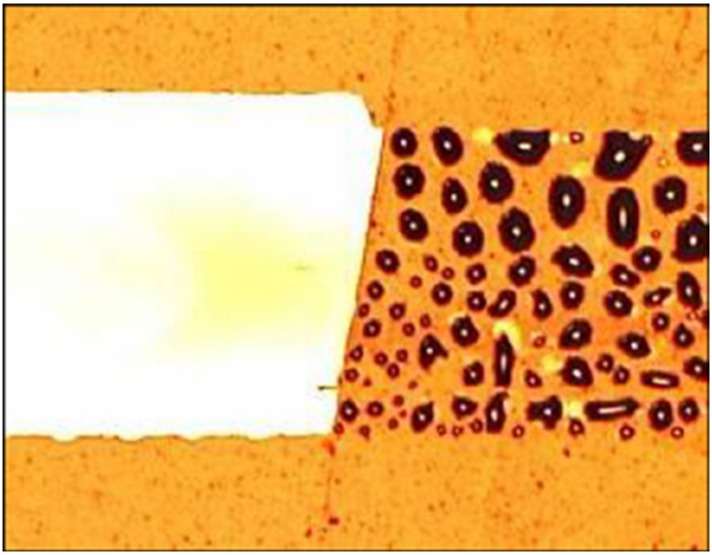

Figure 4.24 Comparison of a rectangle pattern silver inkjet printed on a hydrophilic surface (left) and a hydrophobic surface (right)

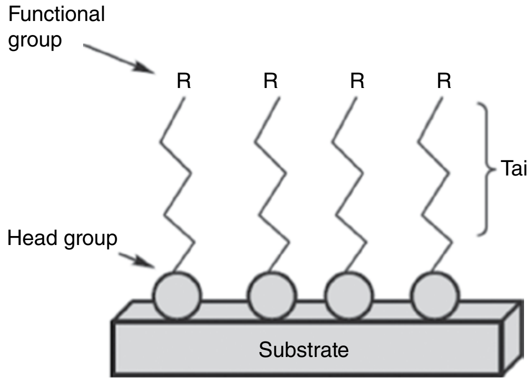

Figure 4.25 Schematic of molecular self-assembly to modify the surface energy of a substrate. (Adopted from web with courtesy to its origin)

shown in Figure 4.25. Most self-assembly treatments are applied to reduce the surface energy of a substrate. Typical examples of reported self-assembled monolayers are silanes (such as octadecyl trichlorosilane) on a silicon surface [166] and self-assembled thiols on a metal surface [167].

4.5.3 Surface Coating

It is difficult to print an electronic component directly on rough surface, especially on fiber-based substrates such as paper or textile, if the printed film has a thickness less than 1 μm [168, 169]. To make such surfaces suitable for printing, surface coating is necessary. With regard to paper substrates, there are several studies on the topic of coating paper for printed electronics [170–172]. Figure 4.26 shows four layers including a pre-coating layer, smoothing layer, barrier layer and a top coating layer on recycled papers [172].

Coating is a general name for depositing materials on substrate without patterns [173]. A simple and important coating method is spin coating, which is widely used in laboratories. Some printing technologies, such as gravure, screen, inkjet, or flexographic printing, can also be used for coating. Other typical coatings based on liquid materials include doctor blade, spray, plating, and slot die. Slot die coating, in which the liquid flow is controlled through a fine slit, is reported to be well suited for making multilayer solar cells [174, 175]. An example of slot die coating for making solar cells is shown in Figure 4.27. Besides these solution-processed methods, vapor deposition, sputtering, and atomic layer deposition (ALD) are also used for coating thin films [173].

4.5.4 Embossing and Nanoimprinting

Embossing methods, which can fabricate high precision plastic microstructures, have also been used for printed electronics. It was reported in 2003 that short channel field-effect transistors were fabricated by embossing with a channel length of less than 1 μm [176].

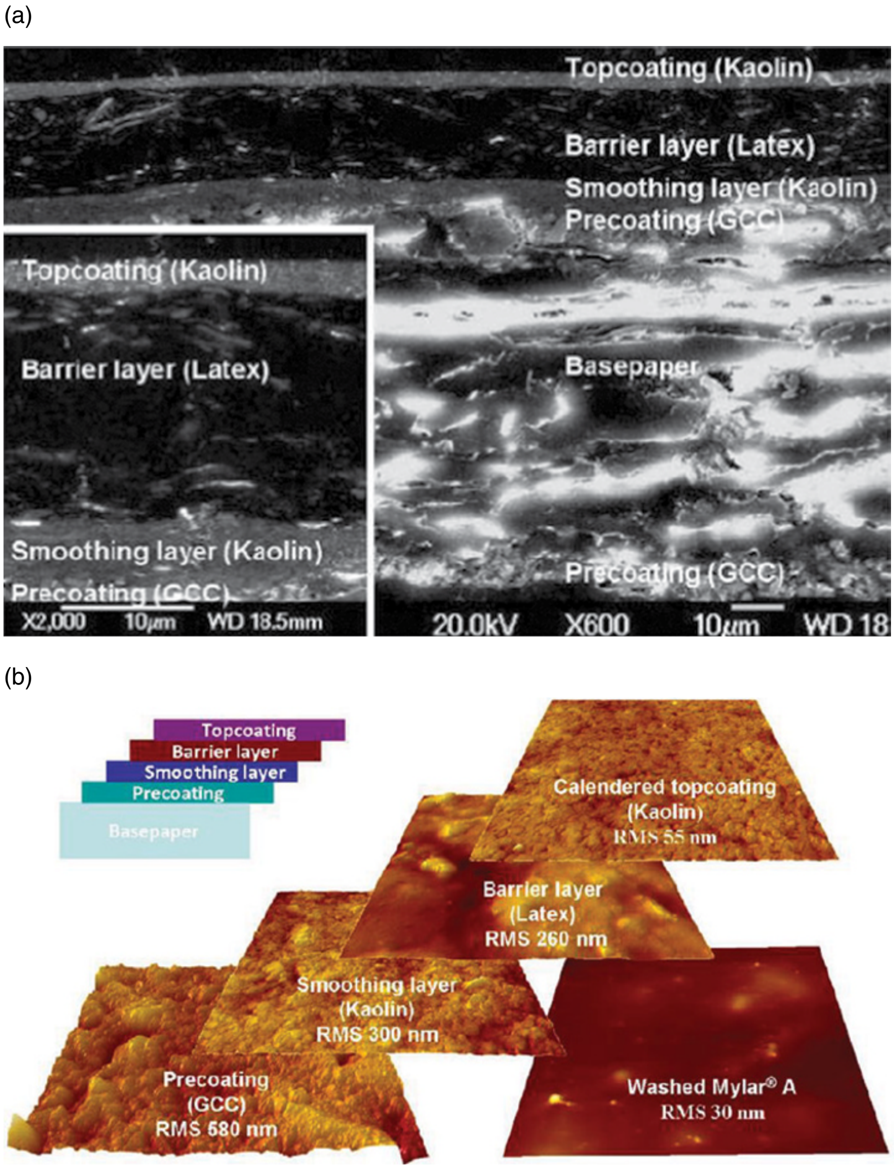
(a)
Topcoating (Kaolin)
Barrier layer (Latex)
Smoothing layer (Kaolin)
Precoating (GCC)
Topcoating (Kaolin)
Barrier layer (Latex)
Basepaper
Smoothing layer (Kaolin)
Precoating (GCC)
Precoating (GCC)
X2,000 10μm WD 18.5mm
20.0kV X600 10μm WD 18
(b)
Topcoating
Barrier layer
Smoothing layer
Precoating
Basepaper
Calendered topcoating
(Kaolin)
RMS 55 nm
Barrier layer
(Latex)
RMS 260 nm
Smoothing layer
(Kaolin)
RMS 300 nm
Precoating
(GCC)
RMS 680 nm
Washed Mylar® A
RMS 30 nm

Figure 4.26 Coating layers on paper as a substrate for printed electronics: (a) SEM images of coating layers cross-section; and (b) Atomic force microscope images of layer surfaces. (Reprinted from [172] with permission from Elsevier)

The Schubert group reported that they were able to reduce the minimum line width in inkjet printing with the aid of embossed grooves, as is illustrated in Figure 4.28. A hard master is placed on a thermoplastic polymer film at a certain temperature (mostly higher than the glass transition temperature of polymer) and pressure is applied on the master to form grooves.

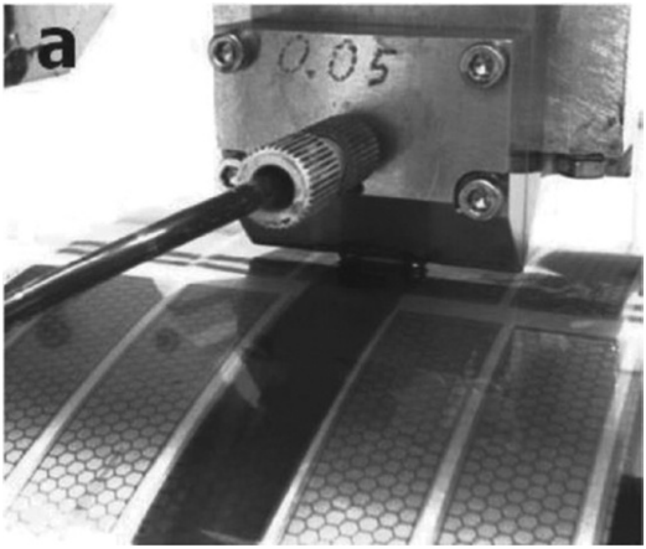

Figure 4.27 The active layer of solar cell made by slot die coating. (Reprinted from [175] with permission from John Wiley and Sons)

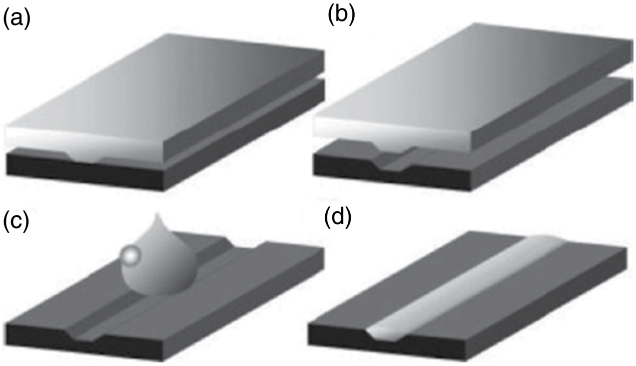

Figure 4.28 Schematic principle of substrate hot embossing and inkjet printing on previously embossed substrate. (Reprinted from [177] with permission from John Wiley and Sons)

Grooves of 5–15 μm were obtained on the substrate by hot embossing and most inkjet-printed ink stayed in the grooves to form a narrower line [177, 178].

Nanoimprint lithography (NIL) is very much the same as embossing, only that nanoimprint can create much finer features [179]. There are thermal NIL and UV NIL methods. The thermal NIL method has a very similar principle to the aforementioned hot embossing. The difference is that a layer of resist is coated on the substrate, and the patterned material is the resist layer rather than the substrate, as illustrated in Figure 4.29. In the UV NIL process, a UV curable liquid resist layer is applied on the substrate. The resist is then solidified by UV light exposure through a transparent master that is pressed into the resist layer.

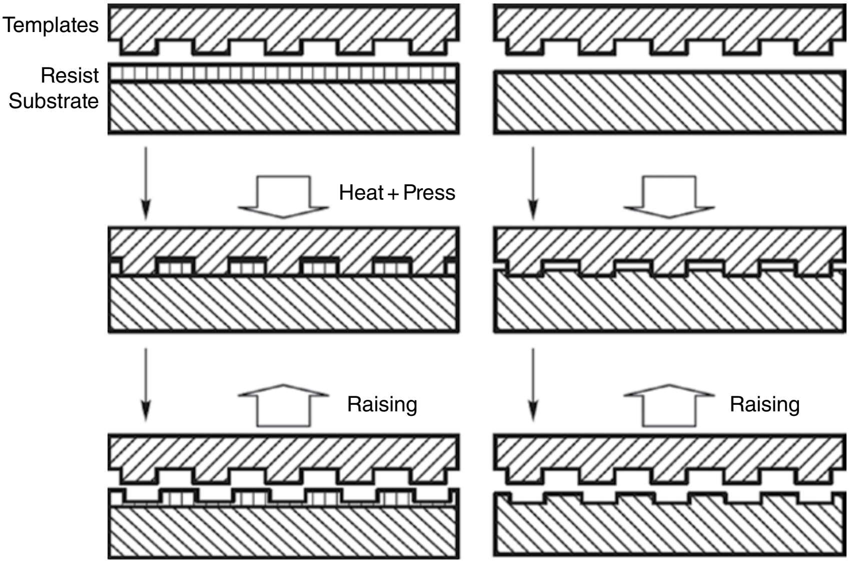

Figure 4.29 Schematic principle of the thermal nanoimprinting (left) and embossing (right)

4.6 Post-printing Processes

“Post-printing processes” refers to the necessary physical or chemical treatments after printing to improve electrical or other properties of printed materials. In contrast to the traditional printing industry, the post-printing processes introduced here are mainly focused on physical or chemical reactions in the printed ink components.

Typical treatments for accelerating reactions are sintering, UV curing, and annealing. These treatments are similar to “drying” in the traditional printing industry to make ink solidify either by chemical reaction, physical processes, or a combination of both. However, solidifying the printed electronic inks is not enough to make them work. Residual solvent or additives may affect the material properties and must be thoroughly removed. For example, the work function of a strictly dewatered PEDOT:PSS layer has a work function 0.5eV higher than the case of normal dry state [180]. Apart from removing the solvents and additives, theory and practice shows that these processes can improve morphology and microstructure of printed thin film, and ultimately determine the performance of electronic devices.

4.6.1 Sintering

The metal or oxide particles in printable ink are usually capped with organic materials, which are necessary for dispersion of nanoparticles and for ink formulation, but prevent electrons moving from one particle to another because of their insulating nature. The sintering operation, which is defined as a process of making particles lose their organic shell and having direct physical contact with each other [181], should be used in these particle-based inks. On the other hand, sintering is also a key process for improving the electrical property of particle-based inks, in which the powders are usually heated to a temperature below the melting point, and the atoms diffused across the boundaries of the powder to fuse the particles together [182].

The most widely used method for sintering is direct heating treatment at a specific temperature on a hot plate or in an oven. Such treatments can achieve an ideal sintering effect because of the precisely controlled temperature and even heating. However, they take longer time than other sintering methods. A long, hot air drying tunnel of several meters is necessary for a roll to roll printing system. It is also not suitable for thermally unstable substrate materials such as plastics because the substrate bears the same temperature during the process.

Photonic heating using UV or infrared light or laser is an alternative method for fast sintering [183]. A focused light beam is very suitable for selective heating that can protect substrate from high temperatures. Furthermore, flash UV light is used to improve the photonic heating for better selectivity, higher temperature, and uniform morphology [184–186]. Microwave is another selective sintering method for uniform, fast, and volumetric heating [187]. A combination of different heating methods already mentioned are also employed to achieve optimum effect [181]. More information for photonic sintering can be found in Chapter 2 of this book (Section 3.2.2).

4.6.2 UV Curing

Ultraviolet (UV) curable materials are usually insulating and chemically stable, and can be used as dielectrics, insulators or acid resistance layers. They are also conductive after adding metal particles and can be used as resistors [188]. UV curing is suitable to be equipped in a printer because its optical fiber and lens can be very small. A printer with a UV curing unit can solidify printed ink very quickly without heating and can control the spontaneous movement of ink on substrate. It is helpful to obtain sharp edge and smooth morphology of printed patterns without distortion. However, UV curable materials play limited roles in electronics at present. UV curing will be applied more widely if there are UV curable materials that can function as conductors or semiconductors.

4.6.3 Annealing

Annealing is an attractive technology for improving the material properties of solution-processed semiconductors used in transistors, solar cells, and other devices [189]. Different from fusing together isolated particles in a sintering process, annealing is mainly used to relieve internal stresses. For example, thermal annealing of P3HT:PCBM bulk heterojunction solar cells is a critical step for improving their efficiency. It has been demonstrated that thermal annealing can strongly affect the morphology of a nanocomposite layer. In some cases, the application of thermal annealing is constrained by the high temperature needed. Consequently, solvent vapor annealing at room temperature was developed [190, 191]. Figure 4.30 shows the AFM images of triethylsilylethynyl-anthradithiophene (TESADT) on an SiO_2 surface before and after the solvent vapor annealing process. [191] The annealing processes are typically employed for making field-effect transistors [192–196] and solar cells [197, 198].

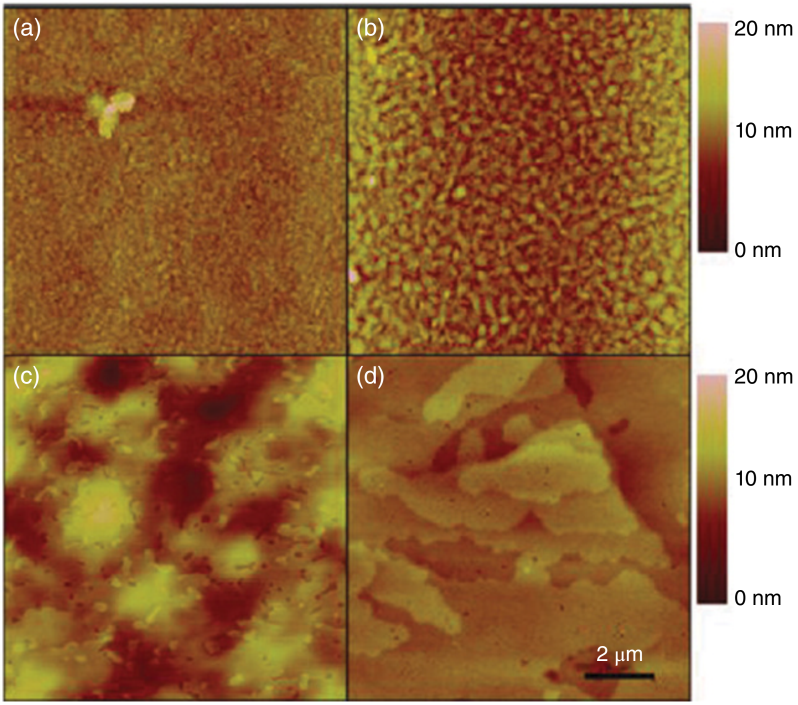

Figure 4.30 The AFM images of sample morphology before and after solvent vapor annealing process: (a) TESADT on SiO_2 surface; (b) TESADT on the SiO_2 modified with 4-phenylbutyltrichlorosilane (4-PBTS) SAM; (c) solvent vapor annealed TESADT on SiO_2 surface; and (d) solvent vapor annealed TESADT on SiO_2 surface with 4-PBTS SAM (Reprinted from [191] with permission from Elsevier)

4.7 Summary

Printing technologies suitable for printing electronics are introduced in this chapter, including their working principles, pattern carriers and printable ink properties. Their advantages and application areas are analyzed. One should choose the most appropriate printing method according to factors such as ink and substrate properties, application requirements, throughput requirement and production cost, and so forth. However, one should bear in mind that printing alone is rarely enough to make electronic devices. Other methods such as etching, coating and vacuum vapor deposition may also be used as supplementary means in printed electronics.

Pre-printing and post-printing processes are very important for the performance of printed electronics. The ink movements and interactions with substrate, template or transfer plate during the printing process should be taken into account at pattern design stage. Substrate treatments can change the surface energy, roughness, and other properties of a printed surface to obtain better film quality and resolution. In addition, post-printing operations are usually needed to improve the printed films for better electrical properties or longer device life.

References

[1] Kipphan H, ed. *Handbook of Print Media*. Berlin: Springer, 2001.

[2] Teng KF, Vest RW. Metallization of Solar-Cells with Ink Jet Printing and Silver Metallo-Organic Inks. IEEE Transactions on Components Hybrids Manufacturing Technology. 1988;11:291–297.

[3] Calvert P, Yoshioka Y, Jabbour GE. Inkjet printing of self-assembling polymers. Abstracts Papers, American Chemistry Society. 2002;224:U398–U398.

[4] Tekin E, Smith PJ, Schubert US. Inkjet printing as a deposition and patterning tool for polymers and inorganic particles. Soft Matter. 2008; 4:703–713.

[5] Liedenbaum CTHF, Haskal EI, Duineveld PC, Van der Weijer P. Progress in polymer light-emitting devices at Philips. Organic Light–Emitting Materials and Devices IV. 2000;4105:1–8.

[6] Sirringhaus H. High-resolution inkjet printing of all-polymer transistor circuits. Science. 2000;290:2123–2126.

[7] Kawase T, Sirringhaus H, Friend RH, Shimoda T. All-polymer thin film transistors fabricated by inkjet printing. Organic Field-Effect Transistors. 2001;4466:80–88.

[8] Chen B, Cui TH, Liu Y, Varahramyan K. All-polymer RC filter circuits fabricated with inkjet printing technology. Solid-State Electronics. 2003;47:841–847.

[9] Kawase T, Shimoda T, Newsome C, Sirringhaus H, Friend RH. Inkjet printing of polymer thin film transistors. Thin Solid Films. 2003;438:279–287.

[10] Shimoda T, Morii K, Seki S, Kiguchi H. Inkjet printing of light-emitting polymer displays. MRS Bulletin. 2003;28:821–827.

[11] de Gans BJ, Duineveld PC, Schubert US. Inkjet printing of polymers: State of the art and future developments. Advanced Materials. 2004;16:203–213.

[12] Schubert US. Digital Fabrication. Inkjet printing of functional polymers and nanoparticles. Digital Fabrication 2006, Final Program and Proceedings. 2006;4–4.

[13] Thompson BC, Frechet JMJ. Organic photovoltaics – Polymer-fullerene composite solar cells. Angewandte Chemie–International Edition. 2008;47:58–77.

[14] Yoon SC, Eom SH, Senthilarasu S, Uthirakumar P, Lim J, Lee C, Lim HS, Lee J, Lee SH. Polymer solar cells based on inkjet-printed PEDOT:PSS layer. Organic Electronics. 2009;10:536–542.

[15] Cho YW, Kim JD, Choi JS, Kim BS, Choi YC. Piezoelectric inkjet printing of polymers: Stem cell patterning on polymer substrates. Polymer. 2010;51:2147–2154.

[16] Hiromi Minemawari TY, Matsui H, Tsutsumi J, Haas S, Chiba R, Kumai R, Hasegawa T. Inkjet printing of single-crystal films. Nature. 2011; 435.

[17] Sirringhaus H. Device physics of Solution-processed organic field-effect transistors. Advanced Materials. 2005; 17:2411–2425.

[18] Lee SH, Choi MH, Han SH, Choo DJ, Jang J, Kwon SK. High-performance thin-film transistor with 6,13-bis(triisopropylsilylethynyl) pentacene by inkjet printing. Organic Electronics. 2008; 9:721–726.

[19] Lee DH, Han SY, Herman GH, Chang CH. J. Inkjet printed high-mobility indium zinc tin oxide thin film transistors. Journal of Materials Chemistry. 2009;19:3135–3137.

[20] Kyoohee Woo CB, Jeong Y, Kim D, Moon J. Inkjet-printed Cu source/drain electrodes for solution-deposited thin film transistors. Journal of Materials Chemistry. 2010;20.

[21] Tseng HY, Purushothaman B, Anthony J, Subramanian V. High-speed organic transistors fabricated using a novel hybrid-printing technique. Organic Electronics. 2011;12:1120–1125.

[22] Ko SH, Pan H, Grigoropoulos CP, Luscombe CK, Frechet JMJ, and Poulikakos D. All-inkjet-printed flexible electronics fabrication on a polymer substrate by low-temperature high-resolution selective laser sintering of metal nanoparticles. Nanotechnology 2007;18.

[23] Bietsch A, Zhang JY, Hegner M, Lang HP, Gerber C. Rapid functionalization of cantilever array sensors by inkjet printing. Nanotechnology. 2004;15:873–880.

[24] Li B, Santhanam S, Schultz L, Jeffries–El M, Iov MC, et al. Inkjet printed chemical sensor array based on polythiophene conductive polymers. Sensors and Actuators B–Chem. 2007;123:651–660.

[25] Loffredo F, Burrasca G, Quercia L, Della Sala D. Gas sensor devices obtained by ink-jet printing of polyaniline suspensions. Macromolecular Symposia. 2007; 247:357–363.

[26] Wang CT, Huang KY, Lin DTW, Liao WC, Lin HW, Hu YC. A Flexible Proximity Sensor Fully Fabricated by Inkjet Printing. Sensors. 2010;10:5054–5062.

[27] Hoth CN, Schilinsky P, Choulis SA, Brabec CJ. Printing highly efficient organic solar cells. Nano Letters. 2008;8:2806–2813.

[28] Eom SH, Senthilarasu S, Uthirakumar P, Yoon SC, Lim J, Lee C, Lim HS, Lee J, Lee SH. Polymer solar cells based on inkjet-printed PEDOT:PSS layer. Organic Electronics. 2009;10:536–542.

[29] Hoth CN, Choulis SA, Schilinsky P, Brabec CJ. J. On the effect of poly(3-hexylthiophene) regioregularity on inkjet printed organic solar cells. Materials Chemistry. 2009;19:5398–5404.

[30] Eom SH, Park H, Mujawar SH, Yoon SC, Kim SS, Na SI, Kang SJ, Khim D, Kim DY, Lee SH. High efficiency polymer solar cells via sequential inkjet-printing of PEDOT:PSS and P3HT:PCBM inks with additives. Organic Electronics. 2010;11:1516–1522.

[31] Bharathan J, Yang Y. Polymer electroluminescent devices processed by inkjet printing: I. Polymer light-emitting logo. Applied Physics Letters. 1998;72:2660–2662.

[32] Haverinen HM, Myllyla RA, Jabbour GE. Inkjet Printed RGB Quantum Dot-Hybrid LED. Journal of Display Technology. 2010;6:87–89.

[33] Chang SC, Bharathan J, Yang Y, Helgeson R, Wudl F, Ramey MB, Reynolds JR. Dual-color polymer light-emitting pixels processed by hybrid inkjet printing. Applied Physics Letters. 1998;73:2561–2563.

[34] Hebner TR, Wu CC, Marcy D, Lu MH, Sturm JC. Ink-jet printing of doped polymers for organic light emitting devices. Applied Physics Letters. 1998;72:519–521.

[35] Daniel J, Arias AC, Russo B, Krusor B. Flexible Electrophoretic Displays with jet-printed backplanes. 2009 Sidney International Symposium Digest of Technical Papers. 2009;Vol Xl, Books I–Iii:660–663.

[36] Voit W, Zapka W, Dyreklev P, Hagel O-J, Hagerstrom A, Sandstrom P. Inkjet printing of non–volatile rewritable memory arrays. NIP, Digital Fabrication Final Program and Proceedings. 2006;24–37(4).

[37] Ng TN, Russo B, Arias AC. Degradation mechanisms of organic ferroelectric field-effect transistors used as nonvolatile memory. Applied Physics. 2009;106.

[38] Sekitani T, Zaitsu K, Noguchi Y, Ishibe K, Takamiya M, Sakurai T, Someya T. Printed Nonvolatile Memory for a Sheet-Type Communication System. IEEE Transactions on Electron Devices. 2009;56:1027–1035.

[39] Leppaniemi J, Aronniemi M, Mattila T, Alastalo A, Allen M, Seppa H. Printed WORM Memory on a Flexible Substrate Based on Rapid Electrical Sintering of Nanoparticles. IEEE Transactions on Electron Devices. 2011;58:151–159.

[40] Lee KI, Lee DY, Kim SH, Lee CS, Shin KW, Han JH, Cho JW. Temperature Dependent Resistance of Multi Wall Carbon Nanotube By Inkjet Printing. NIP 25: Digital Fabrication 2009, Technical Program and Proceedings. 2009;623–626.

[41] Polzinger B, Willeck H, Ghabri R, Keck J, Muller P, Eberhardt W, Kuck H. Printing of resistors on polymer packages. 4m/Icomm 2009 – the Global Conference on Micro Manufacture. 2009;440:143–146.

[42] Kaydanova T, Miedaner A, Curtis C, Alleman J, Perkins JD, Ginley DS, Sengupta L, Zhang X, He S, Chiu L. J. Direct inkjet printing of composite thin barium strontium titanate films. Journal of Materials Research. 2003;18:2820–2825.

[43] Liu Y, Cui TH, Varahramyan K. All-polymer capacitor fabricated with inkjet printing technique. Solid-State Electronics. 2003;47:1543–1548.

[44] Bidoki SM, Nouri J, Heidari AA. Inkjet deposited circuit components. Journal of Micromechanics and Microengineering. 2010;20,5:55023–55030.

[45] Amin Y, Prokkola S, Shao BT, Hallstedt J, Chen Q, Tenhunen H, Zheng LR. Low cost paper based bowtie tag antenna for high performance UHF RFID applications. Nanotech Conference & Expo. 2009;Vol 1, Technical Proceedings:538–541.

[46] Mantysalo M, Mansikkamaki P. An inkjet-deposited antenna for 2.4 GHz applications. Aeu–International Journal of Electronics and Communications. 2009;63:31–35.

[47] Rida A, Yang L, Reynolds T, Tan E, Nikolaou S, Tentzeris MM. Inkjet-Printing UHF Antenna for RFID and Sensing Applications on Liquid Crystal Polymer. IEEE Antennas and Propagation Society International Symposium and Usnc/Ursi National Radio Science Meeting. 2009;Vols 1–6:820–823.

[48] Rida A, Yang L, Tentzeris MM. Design and characterization of novel paper-based inkjet-printed UHF antennas for RFID and sensing applications. IEEE Antennas and Propagation Society International Symposium. 2007;Vols 1–12:2510–2513.

[49] Shaker G, Tentzeris M, Safavi–Naeini S. Low-cost antennas for mm-wave sensing applications using inkjet printing of silver nano-particles on liquid crystal polymers. IEEE Antennas and Propagation Society International Symposium. 2010;1–4.

[50] Rida A, Yang L, Vyas R, Tentzeris MM. Conductive inkjet-printed antennas on flexible low-cost paper-based substrates for RFID and WSN applications. IEEE Antennas and Propagation Magazine. 2009;51:13–23.

[51] Yang L, Rida A, Vyas R, Tentzeris MM. RFID tag and RF structures on a paper substrate using inkjet-printing technology. IEEE Transactions on Microwave Theory and Techniques. 2007;55:2894–2901.

[52] Vyas R, Lakafosis V, Rida A, Chaisilwattana N, Travis S, Pan J, Tentzeris MM. Paper-based RFID-enabled wireless platforms for sensing applications. IEEE Transactions on Microwave Theory and Techniques. 2009;57:1370–1382.

[53] Soltman D, Subramanian V. Inkjet-printed line morphologies and temperature control of the coffee ring effect. Langmuir. 2008;24:2224–2231.

[54] Singh M, Haverinen HM, Dhagat P, Jabbour GE. Inkjet printing-process and its applications. Advanced Materials. 2010;22:673–685.

[55] Layani M, Gruchko M, Milo O, Balberg I, Azulay D, Magdassi S. Transparent conductive coatings by printing coffee ring arrays obtained at room temperature. Acs Nano. 2009; 3:3537–3542.

[56] Zhang ZL, Zhang XLY, Xin ZQ, Deng MM, Wen YQ, Song YL. Controlled inkjetting of a conductive pattern of silver nanoparticles based on the coffee-ring effect. Advanced Materials. 2013;25:6714–6718.

[57] King BH, Renn MJ, Essien M, Marquez GJ, Giridharan MG, Sheu J. Material depositing apparatus for depositing aerosol stream on planar/non–planar target, has deposition flowhead that combines aerosol with annular sheath gas flow and extended nozzle attached to output of flowhead. US2006008590–A1; US7938079–B2.

[58] Renn MJ, King BH, Essien M, Giridharan MG, Sheu J. Mask–less, non–contact direct printing of mesoscale structures of various materials onto heat–sensitive targets e.g. substrates, by laser–processing deposit of material at temperature as high as damage threshold temperature of target. US2007019028–A1.

[59] King BH, Ramahi DH, Woolfson K, Eichi B, Deibit Eichi RD, Beri US. Material deposition assembly comprises sheath inlets that performs fluid connection with sheath plenum enclosing exit of aerosol channel and entrance of anisotropic nozzle. WO2009029938–A2; US2009090298–A1; WO2009029938–A3; TW2009248 52–A; KR2010067098–A; IN201001759–P4; CN101842166–A; JP2010538277–W.

[60] Xia Y, Zhang W, Ha MJ, Cho JH, Renn MJ, Kim CH, Frisbie CD. Printed Sub-2 V gel-electrolyte-gated polymer transistors and circuits. Advanced Functional Materials. 2010;20:587–594.

[61] Brennan JD, Hossain SMZ, Luckham RE, Smith AM, Lebert JM, Davies LM, Pelton RH, Filipe CDM. Development of a bioactive paper sensor for detection of neurotoxins using piezoelectric inkjet printing of sol-gel-derived bioinks. Analytical Chemistry. 2009;81:5474–5483.

[62] Renn MJ, King BH, Paulsen JA. Aerosol jet deposition head for direct printing of aerosolized materials onto heat sensitive targets, has combination chamber where sheath gas flow and aerosol streams are combined. WO2006065978–A2; US2006175431–A1; EP1830927–A2; IN200703077–P4; KR2007093101–A; CN101098734–A; US2008013299–A1; JP2008522814–W; TW200626741–A; SG158137–A1; TW315355–B1; US2010173088–A1; US2010192847–A1; US7938341–B2.

[63] Mette A, Richter PL, Horteis M, Glunz SW. Progress in Photovoltaics. 2007;15:621–627.

[64] King BH, O'Reilly MJ, Barnes SM. 34th IEEE Photovoltaic Specialists Conference. 2009;Vols 1–3:2000–2004, 2491.

[65] Horteis M, Glunz SW. Metal aerosol jet printing for solar cell metallization. Progress in Photovoltaics. 2008; 16:555–560.

[66] Jones CS, Lu XJ, Renn M, Stroder M, Shih WS. Aerosol-jet-printed, high-speed, flexible thin-film transistor made using single-walled carbon nanotube solution. Microelectronic Engineering. 2010;87:434–437.

[67] Ingo G, Groth E, Wirth I, Schumacher J, Maiwald M, Zoellmer V, Busse M. Surface biofunctionalization and production of miniaturized sensor structures using aerosol printing technologies. Biofabrication. 2010;2:1.

[68] Park JU, Hardy M, Kang SJ, Barton K, Adair K, Mukhopadhyay DK, Lee CY, Strano MS, Alleyne AG, Georgiadis JG, Ferreira PM, Rogers JA. High-resolution electrohydrodynamic jet printing. Nature Materials. 2007;6:782–789.

[69] Someya T, Sekitani T, Noguchi Y, Zschieschang U, Klauk H. Organic transistors manufactured using inkjet technology with subfemtoliter accuracy. Proceedings of the National Academy of Sciences of the United States of America. 2008;105:4976–4980.

[70] Awais MN, Kim HC, Doh YH, Choi KH. ZrO2 flexible printed resistive (memristive) switch through electrohydrodynamic printing process. Thin Solid Films. 2013;536:308–312.

[71] Awais MN, Choi KH. Resistive Switching in a Printed Nanolayer of Poly(4-vinylphenol). Journal of Electronic Materials. 2013;42:1202–1208.

[72] Rahman K, Ali K, Muhammad NM, Hyun MT, Choi KH. Fine resolution drop-on-demand electrohydrodynamic patterning of conductive silver tracks on glass substrate. Applied Physics a–Materials Science & Processing. 2013;111:593–600.

[73] Jang Y, Tambunan IH, Tak H, Nguyen VD, Kang T, Byun D. Non-contact printing of high aspect ratio Ag electrodes for polycrystalline silicone solar cell with electrohydrodynamic jet printing. Applied Physics Letters. 2013;102.

[74] Ferrer I, Svedin J. A 60 GHz image rejection filter manufactured using a high resolution LTCC screen printing process. 33rd European Microwave Conference Proceedings. 2003;1–3:423–425.

[75] Lim SC, Kim SH, Yang YS, Lee MY, Nam SLY, Bin Ko J. Organic thin-film transistor using high-resolution screen-printed electrodes. Japanese Journal of Applied Physics. 2009;48.

[76] Okamura H, Kayanoki M, Takada K, Nakajiri H, Muramatsu K, Yamashita M, Shirai M. High-resolution resist for screen printing: application to direct fabrication of Ag circuit. Polymers for Advanced Technologies. 2012; 23:1151–1155.

[77] Akahoshi H, Murakami K, Wajima M, Kawakubo S. A new fully additive fabrication process for printed wiring boards. IEEE Transactions on Components Hybrids and Manufacturing Technology. 1986;9:181–187.

[78] Dubey GC. Screens for Screen Printing of Electronic Circuits. Microelectronics and Reliability. 1974;13:203–207.

[79] Bogensch A, Krahl PH. Metal-containing screen printing mixtures for electronic circuits Metall. 1968,1968; 22:595–&.

[80] Kear FW. Screening – in printed circuit production. Photo Chemical Machining–Photo Chemical Etching. 1970;5:8.

[81] Booth CL, Cox JJ, Woodman RP, Geary JE, McMunn CW. Low cost, screen printed hermetic package for integrated circuits. American Ceramic Society Bulletin. 1971;50:757.

[82] Ikegami S, Yamashita T. J. Screen printed cds-cdte solar-cell. Journal of Electronic Materials. 1979;8:705–705.

[83] Nakayama N, Matsumoto H, Nakano A, Ikegami S, Uda H, Yamashita T. Screen printed thin-film cds-cdte solar-cell. Japanese Journal of Applied Physics. 1980;19:703–712.

[84] Kuribayashi K, Matsumoto H, Uda H, Komatsu Y, Nakano A, Ikegami S. Preparation of low resistance contact electrode in screen printed cds/cdte solar-cell. Japanese Journal of Applied Physics Part 1–Regular Papers Short Notes & Review Papers. 1983;22:1828–1831.

[85] Cheek GC, Mertens RP, Vanoverstraeten R, Frisson L. Thick-film metallization for solar-cell applications. IEEE Transactions on Electron Devices. 1984;31:602–609.

[86] Matsumoto H, Kuribayashi K, Uda H, Komatsu Y, Nakano A, Ikegami S. Screen-printed cds/cdte solar-cell of 12.8-percent efficiency for an active area of 0.78 Cm2. Solar Cells 1984;11:367–373.

[87] Nakano A, Ikegami S, Matsumoto H, Uda H, Komatsu Y. Long-term reliability of screen printed cds/cdte solar-cell modules. Solar Cells. 1986;17:233–240.

[88] Ikegami S. Cds/cdte solar-cells by the screen-printing sintering technique – fabrication, photovoltaic properties and applications. Solar Cells. 1988; 23:89–105.

[89] Shaheen SE, Radspinner R, Peyghambarian N, Jabbour GE. Fabrication of bulk heterojunction plastic solar cells by screen printing. Applied Physics Letters 2001;79:2996–2998.

[90] Krebs FC, Alstrup J, Spanggaard H, Larsen K, Kold E. Production of large-area polymer solar cells by industrial silk screen printing, lifetime considerations and lamination with polyethyleneterephthalate. Solar Energy Materials and Solar Cells 2004;83:293–300.

[91] Krebs FC, Jorgensen M, Norrman K, Hagemann O, Alstrup J, Nielsen TD, Fyenbo J, Larsen K, Kristensen J. A complete process for production of flexible large area polymer solar cells entirely using screen printing – first public demonstration. Solar Energy Materials and Solar Cells. 2009;93:422–441.

[92] Golovanov V, Solis JL, Lantto V, Leppavuori S. Different thick-film methods in printing of one-electrode semiconductor gas sensors. Sensors and Actuators B–Chem. 1996;34:401–406.

[93] Bao ZN, Feng Y, Dodabalapur A, Raju VR, Lovinger AJ. High-performance plastic transistors fabricated by printing techniques. Chemistry of Materials. 1997;9:1299–1301.

[94] Futakuchi T, Tanino K, Adachi M, Kawabata A. Preparation of Pb(Mg1/3Nb2/3)O-3-PbTiO3 dielectric thick films. 1st 1997 Iemt/Imc Symposium. 1997;122–126.

[95] Xi XM, Brandt L, Matijasevic G, Fu S, Gandhi P, Baxter D, Owings G. Metal-containing polymer-based composites for resistor and thermistor applications. 1998 International Symposium on Microelectronics. 1998;3582:453–458.

[96] Yao K, Zhu WG, Yao W. Thick-film capacitors prepared from sol-gel derived barium titanate glass-ceramics. Journal of the Korean Physical Society. 1998;32:S1172–S1175.

[97] Burnside S, Winkel S, Brooks K, Shklover V, Gratzel M, Hinsch A, Kinderman R, Bradbury C, Hagfeldt A, Pettersson H. J. Deposition and characterization of screen-printed porous multi-layer thick film structures from semiconducting and conducting nanomaterials for use in photovoltaic devices. Journal of Material Science – Materials in Electronics. 2000;11:355–362.

[98] Vincenzi D, Butturi MA, Guidi V, Carotta MC, Martinelli G, Guarnieri V, Brida S, Margesin B, Giacomozzi F, Zen M, Pignatel GU, Vasiliev AA, Pisliakov AV. Development of a low-power thick-film gas sensor deposited by screen-printing technique onto a micromachined hotplate. Sensors and Actuators B–Chemical. 2001;77:95–99.

[99] Filippini D, Fraigi L, Aragon R, Weimar U. Sensors and Actuators B–Chem. 2002;81:296–300.

[100] Borland W, Doyle M, Dellis L, Renovales O, Majumdar D. Embedding ceramic thick-film capacitors into printed wiring boards. Materials Integration Packaging Issues High–Frequency Devices II. 2005;833:143–151.

[101] Stojanovic BD, Foschini CR, Pavlovic VB, Varela JA. Barium titanate screen-printed thick films. Ceramics International. 2002;28:293–298.

[102] Stojanovic BD, Foschini CR, Pejovic VZ, Pavlovic VB, Varela JA. Electrical properties of screen printed BaTiO3 thick films. Journal of the European Ceramic Society. 2004;24:1467–1471.

[103] Huang XQ, Ge XD, Zhang YH, Lu Z, Xu JH, Chen KF, Dong DW, Liu ZG, Miao JP, Su WH. Screen-printed thin YSZ films used as electrolytes for solid oxide fuel cells. Journal of Power Sources. 2006;159:1048–1050.

[104] Zhang D, Hu WF, Meggs C, Su B, Price T, Iddles D, Lancaster MJ, Button TW. Fabrication and characterisation of barium strontium titanate thick film device structures for microwave applications. Journal of the European Ceramic Society. 2007;27:1047–1051.

[105] Wang H, Xiang F, Zhang MH, Sun X, Yao X. Preparation and dielectric tunability of bismuth-based pyrochlore dielectric thick films on alumina substrates. Ceramics International. 2008;34:925–928.

[106] Kim CH, Shin DY, Lee Y. Performance characterization of screen printed radio frequency identification antennas with silver nanopaste. Thin Solid Films. 2009;517:6112–6118.

[107] Koh JH, Ham YS. Ferroelectrics. The dielectric characteristics of screen printed srtio(3)-epoxy composite thick films on the cu plate pcb substrates. 2009;382:85–91.

[108] Koh JH, Moon SH. Screen printed znbo doped bst thick film interdigital capacitors for the microwave applications. Ferroelectrics. 2009; 383:133–139.

[109] Gutierrez CA, Meng E. Low-cost carbon thick-film strain sensors for implantable applications. Journal of Micromechanics and Microengineering. 2010;20.

[110] Koh JH, Kim SH. The microwave properties of Li doped 0.7(Ba,Sr)TiO(3)-0.3MgO thick film interdigital capacitors on the alumina substrates. Microelectronic Engineering. 2010;87:79–82.

[111] Jung SB, Kim JW, Lee YC, Kim KS. High frequency characteristics of printed cu conductive circuit. Journal of Nanoscience and Nanotechnology. 2011;11:537–540.

[112] Yun SW, Koh JH. Influence of cuo addition on dielectric properties of (ba,sr)tio(3) thick films. Journal of the Korean Physical Society. 2011;58:585–589.

[113] Stadlober B, Zirkl M, Sawatdee A, Helbig U, Krause M, Scheipl G, Kraker E, Ersman PA, Nilsson D, Platt D, Bodo P, Bauer S, Domann G. An all-printed ferroelectric active matrix sensor network based on only five functional materials forming a touchless control interface advanced materials. 2011;23:2069–2074.

[114] Kittila M, Hagberg J, Jakku E, Leppavuori S. Direct gravure printing (DGP) method for printing fine-line electrical circuits on ceramics. IEEE Transactions on Electronics Packaging Manufacturing. 2004;27: 109–114.

[115] Kang H, Kitsomboonloha R, Jang J, Subramanian V. High-performance printed transistors realized using femtoliter gravure-printed sub-10 mu m metallic nanoparticle patterns and highly uniform polymer dielectric and semiconductor layers. Advanced Materials. 2012;24:3065–3069.

[116] Kitsomboonoha R, Morris SJS, Rong XY, Subramanian V. Femtoliter-scale patterning by high-speed, highly scaled inverse gravure printing. Langmuir. 2012; 28:16711–16723.

[117] Voigt MM, Mackenzie RCI, King SP, Yau CP, Atienzar P, Dane J, Keivanidis PE, Zadrazil I, Bradley DDC, Nelson J. Gravure printing inverted organic solar cells: The influence of ink properties on film quality and device performance. Solar Energy Materials and Solar Cells. 2012;105:77–85.

[118] Voigt MM, Mackenzie RCI, Yau CP, Atienzar P, Dane J, Keivanidis PE, Bradley DDC, Nelson J. Gravure printing for three subsequent solar cell layers of inverted structures on flexible substrates. Solar Energy Materials and Solar Cells. 2011;95:731–734.

[119] Hambsch M, Reuter K, Stanel M, Schmidt G, Kempa H, Fügmann U, Hahn U, Hübler AC. Uniformity of fully gravure printed organic field-effect transistors. Materials Science and Engineering. 2010;B 170:93–98.

[120] Choi Y, Kim GH, Jeong WH, Kim HJ, Chin BD, Yu JW. Characteristics of gravure printed InGaZnO thin films as an active channel layer in thin film transistors. Thin Solid Films. 2010;518:6249–6252.

[121] Kaihovirta NJ, Tobjork D, Makela T, Osterbacka R. Low-voltage organic transistors fabricated using reverse gravure coating on prepatterned substrates. Advanced Engineering Materials. 2008;10:640–643.

[122] Kopola P, Aernouts T, Guillerez S, Jin H, Tuomikoski M, Maaninen A, Hast J. High efficient plastic solar cells fabricated with a high-throughput gravure printing method. Solar Energy Materials and Solar Cells. 2010;94:1673–1680.

[123] Yang JL, Vak D, Clark N, Subbiah J, Wong WWH, Jones DJ, Watkins SE, Wilson G. Organic photovoltaic modules fabricated by an industrial gravure printing proofer. Solar Energy Materials and Solar Cells. 2013;109:47–55.

[124] Tekoglu S, Hernandez–Sosa G, Kluge E, Lemmer U, Mechau N. Gravure printed flexible small-molecule organic light emitting diodes. Organic Electronics. 2013;14:3493–3499.

[125] Kopola P, Tuomikoski M, Suhonen R, Maaninen A. Gravure printed organic light emitting diodes for lighting applications. Thin Solid Films. 2009;517:5757–5762.

[126] Jung M, Kim J, Noh J, Lim N, Lim C, Lee G, Kim J, Kang H, Jung K, Leonard AD, Tour JM, Cho G. All-printed and roll-to-roll-printable 13.56-mhz-operated 1-bit rf tag on plastic foils. IEEE Transactions on Electron Devices. 2010;57:571–580.

[127] Reuter K, Kempa H, Deshmukh KD, Katz HE, Hubler AC. Full-swing organic inverters using a charged perfluorinated electret fabricated by means of mass-printing technologies. Organic Electronics. 2010;11:95–99.

[128] Hubler AC, Schmidt GC, Kempa H, Reuter K, Hambsch M, Bellmann M. Three-dimensional integrated circuit using printed electronics. Organic Electronics. 2011;12:419–423.

[129] Vig AL, Makela T, Majander P, Lambertini V, Ahopelto J, Kristensen A. J.. Roll-to-roll fabricated lab-on-a-chip devices. Journal of Micromechanics and Microengineering. 2011; 21:035006.

[130] Park H, Kang H, Lee Y, Park Y, Noh J, Cho G. Fully roll-to-roll gravure printed rectenna on plastic foils for wireless power transmission at 13.56 MHz. Nanotechnology. 2012;23.

[131] Hrehorova E, Rebros M, Pekarovicova A, Bazuin B, Ranganathan A, Garner S, Merz G, Tosch J, Boudreau R. Gravure printing of conductive inks on glass substrates for applications in printed electronics. Journal of Display Technology. 2011;7:318–324.

[132] Sung D, Vornbrock AD, Subramanian V. Scaling and Optimization of Gravure-Printed Silver Nanoparticle Lines for Printed Electronics IEEE Transactions on Components and Packaging Technologies. 2010;33:105–114.

[133] Noh J, Yeom D, Lim C, Cha H, Han J, Kim J, Park Y, Subramanian V, Cho G. Scalability of roll-to-roll gravure-printed electrodes on plastic foils. IEEE Transactions on Electronics Packaging Manufacturing. 2010;33:275–283.

[134] De la Fuente Vornbrock AD, Ding JM, Sung D, Tseng HY, Subramanian V. Printing and scaling of metallic traces and capacitors using a laboratory-scale rotogravure press. Flexible Electronics & Displays Conference and Exhibition. 2009;54–60 8.

[135] Voigt MM, Guite A, Chung DY, Khan RUA, Campbell AJ, Bradley DDC, Meng FS, Steinke JHG, Tierney S, McCulloch I, Penxten H, Lutsen L, Douheret O, Manca J, Brokmann U, Sonnichsen K, Hulsenberg D, Bock W, Barron C, Blanckaert N, Springer S, Grupp J, Mosley A. Polymer field-effect transistors fabricated by the sequential gravure printing of polythiophene, two insulator layers, and a metal ink gate. Advanced Functional Materials. 2010;20:239–246.

[136] Schmidt MBGC, Meier B, Hambsch M, Reuter K, Kempa H, Hübler AC. Modified mass printing technique for the realization of source/drain electrodes with high resolution. Organic Electronics. 2010;11:5.

[137] Makela T, Jussila S, Kosonen H, Backlund TG, Sandberg HGO, Stubb H. Utilizing roll-to-roll techniques for manufacturing source-drain electrodes for all-polymer transistors. Synthetic Metals 2005;153:285–288.

[138] Kaihovirta N, Makela T, He XH, Wikman CJ, Wilen CE, Osterbacka R. Printed all-polymer electrochemical transistors on patterned ion conducting membranes. Organic Electronics 2010;11:1207–1211.

[139] Hösel M, Søndergaard RR, Angmo D, Krebs FC. Comparison of fast roll-to-roll flexographic, inkjet, flatbed, and rotary screen printing of metal back electrodes for polymer solar cells. Advanced Engineering Materials. 2013;15:995–1001.

[140] Vena A, Perret E, Tedjini S, Tourtollet GEP, Delattre A, Garet F, Boutant Y. Design of chipless RFID tags printed on paper by flexography. IEEE Transactions on Antennas and Propagation. 2013;61:5868–5877.

[141] Lo CY, Huttunen OH, Hiitola–Keinanen J, Petaja J, Fujita H, Toshiyoshi H. MEMS-controlled paper-like transmissive flexible display. Journal of Microelectromechanical Systems. 2010;19:410–418.

[142] Kempa H, Hambsch M, Reuter K, Stanel M, Schmidt GC, Meier B, Hubler AC. Complementary ring oscillator exclusively prepared by means of gravure and flexographic printing. IEEE Transactions on Electron Devices. 2011;58:2765–2769.

[143] Bois C, Blayo A, Chaussy D, Vincent R, Mercier AG, Nayoze C. Catalyst layers for PEMFC manufactured by flexography printing process: performances and structure. Fuel Cells. 2012;12:199–211.

[144] Deganello D, Cherry JA, Gethin DT, Claypole TC. Patterning of micro-scale conductive networks using reel-to-reel flexographic printing. Thin Solid Films. 2010;518:6113–6116.

[145] Faddoul R, Reverdy–Bruas N, Blayo A, Haas T, Zeilmann C. Optimisation of silver paste for flexography printing on LTCC substrate. Microelectronics Reliability 2012;52:1483–1491.

[146] Zielke D, Hubler AC, Hahn U, Brandt N, Bartzsch M, Fugmann U, Fischer T, Veres J, Ogier S. Polymer-based organic field-effect transistor using offset printed source/drain structures. Applied Physics Letters. 2005;87.

[147] Reuter K, Kempa H, Brandt N, Bartzsch M, Huebler AC. Influence of process parameters on the electrical properties of offset printed conductive polymer layers. Progress in Organic Coatings. 2007;58:312–315.

[148] Leppavuori S, Vaananen J, Lahti M, Remes J, Uusimaki A. A novel thick-film technique, gravure offset printing, for the realization of fine-line sensor structures. Sensors and Actuators a–Physical. 1994;42:593–596.

[149] Hagberg J, Leppavuori S. Method for the manufacture of high quality gravure plates for printing fine line electrical circuits. Device and Process Technologies for Mems and Microelectronics 1999;3892:313–320.

[150] Lahti M, Lantto V. Gravure-offset-printing technique for the fabrication of solid films. Applied Surface Science. 1999;142.

[151] Lahti M, Lantto V. J. Passive RF band-pass filters in an LTCC module made by fine-line thick-film pastes. European Ceramic Society. 1997–2000, 2001;21.

[152] Markku L. Gravure offset printing for fabrication of electronic devices and integrated components in LTCC modules. Faculty of Technology, Department of Electrical and Information Engineering, Infotech Oulu, University of Oulu, Oulu, 2008.

[153] Pudas M, Hagberg J, Leppavuori S. Gravure offset printing of polymer inks for conductors. Progress in Organic Coatings. 2004; 49:324–335.

[154] Lee TM, Noh JH, Kim I, Kim DS, Chun S. J. Reliability of gravure offset printing under various printing conditions. Journal of Applied Physics. 2010;108.

[155] Lee TM, Lee SH, Noh JH, Kim DS, Chun SJ. The effect of shear force on ink transfer in gravure offset printing. Journal of Micromechanics and Microengineering. 2010;20.

[156] Pudas M, Hagberg J, Leppavuori S. J. Printing parameters and ink components affecting ultra-fine-line gravure-offset printing for electronics applications. Journal of the European Ceramic Society. 2004;24:2943–2950.

[157] Noh JH, Kim I, Park SH, Jo J, Kim DS, Lee TM. A study on the enhancement of printing location accuracy in a roll-to-roll gravure offset printing system. International Journal of Advanced Manufacturing Technology 2013;68:1147–1153.

[158] Lee TM, Noh JH, Kim CH, Jo J, Kim DS. Development of a gravure offset printing system for the printing electrodes of flat panel display. Thin Solid Films. 2010;518:3355–3359.

[159] Hahne P, Hirth E, Reis IE, Schwichtenberg K, Richtering W, Horn FM, Eggenweiler U. Progress in thick-film pad printing technique for solar cells. Solar Energy Materials and Solar Cells. 2001;65:399–407.

[160] Krebs FC. Pad printing as a film forming technique for polymer solar cells. Solar Energy Materials and Solar Cells. 2009;93:484–490.

[161] Mooring L, Karousos NG, Livingstone C, Davis J, Wildgoose GG, Wilkins SJ, Compton RG. Evaluation of a novel pad printing technique for the fabrication of disposable electrode assemblies. Sensors and Actuators B–Chem. 2005;107:491–496.

[162] Merilampi SL, Bjorninen T, Ukkonen L, Ruuskanen P, Sydanheimo L. Characterization of UHF RFID tags fabricated directly on convex surfaces by pad printing. International Journal of Advanced Manufacturing Technology. 2011;53:577–591.

[163] Filoux E, Lou–Moeller R, Calle S, Lethiecq M, Levassort F. Optimised properties of high frequency transducers based on curved piezoelectric thick films obtained by pad printing process. Advances in Applied Ceramics 2013;112:75–78.

[164] Lee TM, Hur S, Kim JH, Choi HC. EL device pad-printed on a curved surface. Journal of Micromechanics and Microengineering. 2010;20.

[165] Prime K, Whitesides G. Self-assembled organic monolayers: model systems for studying adsorption of proteins at surfaces. Science. 1991;252:1164–1167.

[166] Wang Y, Lieberman M. Growth of ultrasmooth octadecyltrichlorosilane self-assembled monolayers on SiO2Langmuir. 2003;19:1159–1167.

[167] Laibinis PE, Whitesides GM, Allara DL, Tao YT, Parikh AN, Nuzzo RG. Comparison of the structures and wetting properties of self-assembled monolayers of n-alkanethiols on the coinage metal surfaces, copper, silver, and gold. Journal of the American Chemical Society. 1991;113:7152–7167.

[168] Chinga–Carrasco G. J. Exploring the multi-scale structure of printing paper – a review of modern technology. Journal of Microscopy–Oxford. 2009;234:211–242.

[169] Osterbacka R, Tobjork D. Paper electronics. Advanced Materials. 2011;23:1935–1961.

[170] Samyn P, Van Erps J, Thienpont H, Schoukens G. Paper coatings with multi-scale roughness evaluated at different sampling sizes. Applied Surface Science. 2011;257:5613–5625.

[171] Kim YH, Moon DG, Han JI. Organic TFT array on a paper substrate. IEEE Electron Device Letters. 2004;25:702–704.

[172] Bollstrom R, Maattanen A, Tobjork D, Ihalainen P, Kaihovirta N, Osterbacka R, Peltonen J, Toivakka M. A multilayer coated fiber-based substrate suitable for printed functionality. Organic Electronics. 2009;10:1020–1023.

[173] Tracton AA, editor. *Coatings Technology: Fundamentals, Testing, and Processing Techniques*. Boca Raton: CRC Press, 2006.

[174] Krebs FC. Fabrication and processing of polymer solar cells: A review of printing and coating techniques. Solar Energy Materials and Solar Cells. 2009;93:394–412.

[175] Helgesen M, Carle JE, Krebs FC. Slot-die coating of a high performance copolymer in a readily scalable roll process for polymer solar cells. Advanced Energy Materials. 2013;3:1664–1669.

[176] Stutzmann N, Friend RH, Sirringhaus H. Self-aligned, vertical-channel, polymer field-effect transistors. Science, 2003;299:1881–1884.

[177] Hendriks CE, Smith PJ, Perelaer J, Van den Berg AMJ, Schubert US. "Invisible" silver tracks produced by combining hot-embossing and inkjet printing. Advanced Functional Materials. 2008;18:1031–1038.

[178] Perelaer J, Hendriks CE, Reinhold I, Eckardt R, van Osch THJ, Schubert US. Inkjet printing of conductive silver tracks in high resolution and the (alternative) sintering thereof. NIP 24, Digital Fabrication 2008: 24th International Conference on Digital Printing Technologies, Technical Program and Proceedings. 2008;697–701.

[179] Cui Z. *Nanofabrication, Principles, Capabilities and Limits*. Springer: 2008.

[180] Koch N, Vollmer A, Elschner A. Influence of water on the work function of conducting poly(3,4-ethylenedioxythiophene)/poly(styrenesulfonate). Applied Physics Letters. 2007;90.

[181] Perelaer J, Abbel R, Wunscher S, Jani R, van Lammeren T, Schubert US. Roll-to-roll compatible sintering of inkjet printed features by photonic and microwave exposure: from non-conductive ink to 40% bulk silver conductivity in less than 15 seconds. Advanced Materials. 2012;24:2620–2625.

[182] Kang SJ. *Sintering: Densification, Grain Growth and Microstructure*. Butterworth Heinemann: 2005.

[183] Durr H, Pilz R, Eleser NS. Rapid tooling of EDM electrodes by means of selective laser sintering. Computers in Industry. 1999;39:35–45.

[184] Chung WH, Hwang HJ, Lee SH, Kim HS. In situ monitoring of a flash light sintering process using silver nano-ink for producing flexible electronics. Nanotechnology. 2013;24.

[185] Park SH, Jang S, Lee DJ, Oh J, Kim HS. J. Two-step flash light sintering process for crack-free inkjet-printed Ag films. Micromechanics and Microengineering. 2013;23.

[186] Hwang HJ, Chung WH, Kim HS. In situ monitoring of flash-light sintering of copper nanoparticle ink for printed electronics. Nanotechnology. 2012;23.

[187] Perelaer J, Klokkenburg M, Hendriks CE, Schubert US. Microwave flash sintering of inkjet-printed silver tracks on polymer substrates. Advanced Materials. 2009;21:4830–4834.

[188] Sangermano M, Chiolerio A, Marti G, Martino P. UV-cured acrylic conductive inks for microelectronic devices. Macromolecular Materials and Engineering. 2013;298:607–611.

[189] Kanai K, Miyazaki T, Suzuki H, Inaba M, Ouchi Y, Seki K. Effect of annealing on the electronic structure of poly(3-hexylthiophene) thin film. Physical Chemistry Chemical Physics 2010;12:273–282.

[190] Conboy JC, Olson EJC, Adams DM, Kerimo J, Zaban A, Gregg BA, Barbara PF. Impact of solvent vapor annealing on the morphology and photophysics of molecular semiconductor thin films. Journal of Physical Chemistry B. 1998;102:4516–4525.

[191] Yang YW, Wang CH, Cheng YC, Su JW, Fan LJ, Huang PY, Chen MC. Origin of high field-effect mobility in solvent-vapor annealed anthradithiophene derivative. Organic Electronics. 2010;11:1947–1953.

[192] Chaabane RB, Ltaief A, Dridi C, Rahmouni H, Bouazizi A, Ouada HB. Study of organic thin film transistors based on nickel phthalocyanine: effect of annealing. Thin Solid Films 2003;427:371–376.

[193] Dickey KC, Anthony JE, Loo YL. Improving organic thin-film transistor performance through solvent-vapor annealing of solution-processable triethylsilylethynyl anthradithiophene. Advanced Materials. 2006;18:1721–1726.

[194] Hong AH, Kang JM, Lim T, Kim JH, Choi JS, Kim YM. Gate dielectric integrity of all organic thin film transistor and annealing effect. AD'07: Proceedings of Asia Display. 2007;1–2:1696–1699.

[195] Liu JY, Zhang R, Osaka I, Mishra S, Javier AE, Smilgies DM, Kowalewski T, McCullough RD. Transistor paint: environmentally stable n-alkyldithienopyrrole and bithiazole-based copolymer thin-film transistors show reproducible high mobilities without annealing. Advanced Functional Materials. 2009;19:3427–3434.

[196] Zen A, Pflaum J, Hirschmann S, Zhuang W, Jaiser F, Asawapirom U, Rabe JP, Scherf U, Neher D. Effect of molecular weight and annealing of poly (3-hexylthiophene)s on the performance of organic field-effect transistors. Advanced Functional Materials. 2004;14:757–764.

[197] Li G, Yao Y, Yang H, Shrotriya V, Yang G, Yang Y. "Solvent annealing" effect in polymer solar cells based on poly(3-hexylthiophene) and methanofullerenes. Advanced Functional Materials. 2007;17:1636–1644.

[198] Li G, Shrotriya V, Yao Y, Yang Y. Investigation of annealing effects and film thickness dependence of polymer solar cells based on poly(3–hexylthiophene). Journal of Applied Physics. 2005;98,4:043754.

5

Printed Thin Film Transistors

Jianwen Zhao

5.1 Introduction

Since the transistor was invented at Bell Laboratories by a team of physicists led by William Shockley, John Bardeen, and Walter Brattain in 1947, the microelectronics industry based on transistors has experienced more than 60 years of continuous growth and become the foundation of all modern electronics and related industrial sectors. A transistor generally consists of five parts: a source electrode, a drain electrode, a gate electrode, an active layer (semiconductor), and a dielectric layer. The semiconductor active layer is connected to the source electrode and the drain electrode. The dielectric layer is positioned between the semiconductor active layer and the gate electrode. A transistor has at least three terminals (also called a triode), source, drain and gate electrodes, which connect to an external circuit to act as an amplifier, switch, oscillator or frequency converter. The transistors we encounter every day are predominantly made from inorganic semiconducting materials, most famously, silicon. Because it requires expensive thin film deposition and patterning processes, the cost of silicon transistor technology is prohibitively high.

The desire for large area, flexible and low cost electronics has stimulated the development of a new category of transistors, which are made from solution-based conductor, semiconductor and dielectric materials. These materials, as well as their printing technologies, have been introduced in previous chapters. The present chapter focuses on how solution-based materials and printing processes can be utilized for making thin-film transistors. The working principle of thin-film transistors, particularly the most widely used field-effect transistors (FET), will be introduced. Then the characteristics of organic thin-film transistors (OTFTs) and inorganic thin-film transistors (ITFTs) will be described, together with the issues related to materials, device structures and printing processes.

Printed Electronics: Materials, Technologies and Applications, First Edition. Zheng Cui, Chunshan Zhou, Song Qiu, Zheng Chen, Jian Lin, Jianwen Zhao, Changqi Ma and Wenming Su.
© 2016 Higher Education Press. All rights reserved. Published 2016 by John Wiley & Sons Singapore Pte. Ltd.

5.2 Types of Transistors

Transistors can be divided into unipolar and bipolar or ambipolar transistors according to the type of charge transport carrier they use. A unipolar transistor, that is an n-type or p-type, is a transistor in which electrons (in an n-channel transistor) or holes (in a p-channel transistor) are mobile inside the conducting channel. Bipolar or ambipolar transistors use both holes and electrons for conduction. They can be represented by the transfer characteristics curve, which is the variation of drain current (I_d) corresponding to gate-source voltage (V_{gs}) while the drain-source voltage (V_{ds}) is constant. It can be used to identify the polarity of transistors. Figure 5.1 represents the typical transfer characteristic curves of p-type, n-type and ambipolar transistors, respectively.

A field-effect transistor (FET) is a transistor that uses the gate voltage to control the drain current, resulting in the output current being proportional to the input voltage (in the linear region). This operation is controlled by an electric field generated by the input gate voltage, called the "field effect". In general, FETs are divided into junction FETs (JFETs) and insulated gate FETs (IGFETs). The JFET has a long channel of semiconductor material which is doped with n- and p-dopants. Contacts between the semiconductor layer and the source and drain electrodes show ohmic contact characteristics. As there is a p-n junction on one or both sides of the channel, this type of transistor is called JFET. An IGFET has its gate input electrically insulated from the conduction channel. The most common type of IGFET used in logic circuits is the metal oxide semiconductor FET (MOSFET). Although a MOSFET is also a voltage controlled FET, it differs from a JFET. A MOSFET has a "metal oxide" gate electrode, which is insulated from the main semiconductor (n-channel or p-channel) by a thin layer of silicon dioxide. This insulated metal gate electrode can be regarded as a capacitor. The isolated gate makes the input resistance of MOSFET extremely high, almost infinite.

Both the p-channel and the n-channel MOSFETs have two modes of operation, enhancement mode and depletion mode, depending on whether the transistor is at on-state or off-state with zero gate voltage. Enhancement-mode MOSFETs are at on-state with zero gate voltage, whereas depletion-mode MOSFETs are at off-state when gate voltage is zero. All the MOSFET types and working modes are summarized in Figure 5.2.

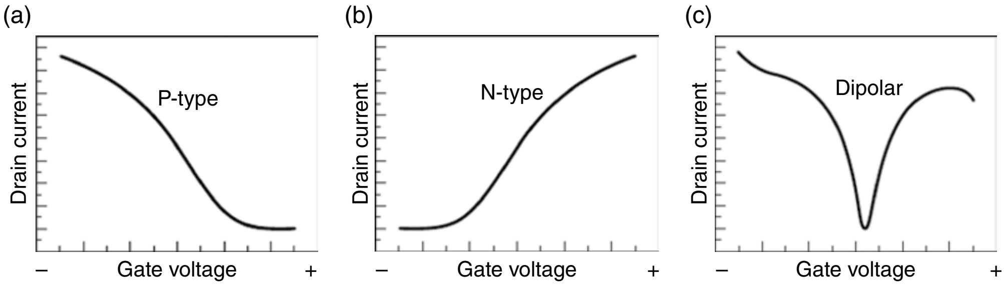

Figure 5.1 Typical transfer characteristics for (a) p-type, (b) n-type, and c) ambipolar transistors

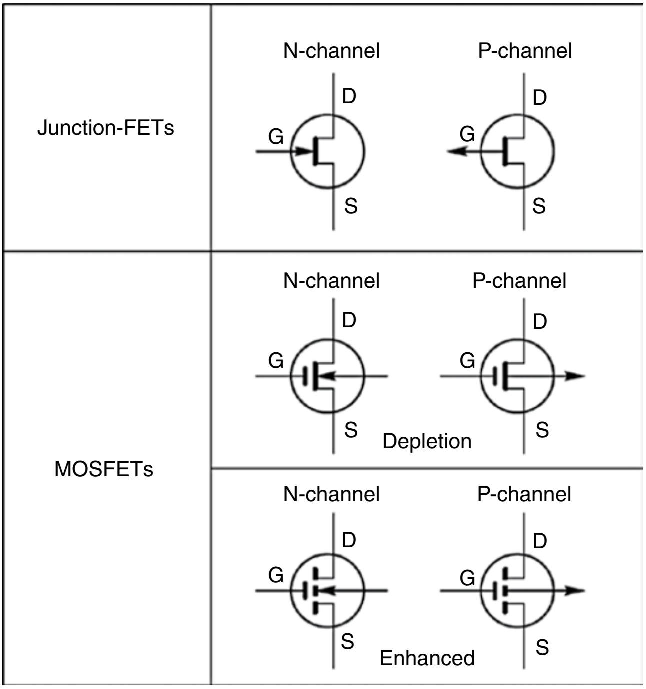

Figure 5.2 Different types of FETs

5.3 Working Principles of Transistors

5.3.1 Basic Mechanism of MOSFETs

Figure 5.3 shows a schematic structure of an n-channel enhancement-mode MOSFET, where S, D, and G represent source, drain and gate electrodes, respectively. It is fabricated by forming the source and drain regions with n-doping (N^+). A thin silicon dioxide layer is then deposited on top of the channel, which insulates the doping channel from the gate electrode. In an n-channel enhancement-mode transistor, the conductive channel does not exist when no bias voltage is applied to the gate. When a positive gate-source voltage is applied, an electron inversion layer is created at the interface between the insulating oxide and the semiconductor, forming a conductive channel. With the increase of gate voltage, electrons are attracted and cumulate near the gate to counter the doping ions. When the gate voltage increases to a certain value, a region called the depletion region, which is free of mobile carriers, is formed. The corresponding gate voltage is called the threshold voltage. Further increasing the gate-source voltage causes more electrons to be attracted to the gate and a conductive channel is established from source to drain. This phenomenon is called inversion.

When the gate voltage is less than threshold voltage, an inversion layer cannot be formed at the interface of a silicon dioxide and n-doping silicon substrate. Even if a voltage is applied to the source and drain electrodes, there is no current flow from source to drain. When the gate voltage exceeds the threshold voltage, an inversion layer will be formed beneath the dielectric layer, and an electron conduction channel is formed. In this case, the voltage applied to the

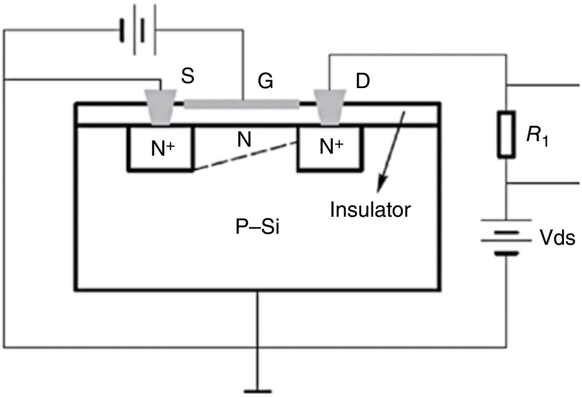

Figure 5.3 Schematic diagram of the working principle of an n-type MOSFET

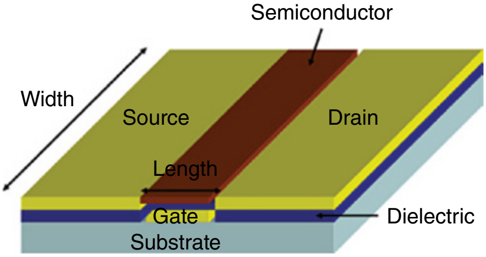

Figure 5.4 Schematic structure of a TFT

source/drain electrode will induce electrons flowing from source electrode to drain electrode. The source/drain current has a close relationship with the channel thickness, which is controlled by the gate voltage. The current increases with the increase of gate voltage. A small change in gate voltage can lead to a large change of source/drain current, which is called amplification. The signal voltage input to the gate electrode is amplified in the form of source/drain current output. When a resistor R_L is externally connected to the transistor, voltage amplification is observed. Therefore, transistors are frequently used as amplifiers. Some transistor circuits are current amplifiers when the external load is a small resistor. Otherwise, voltage amplification can be achieved when the external load is a large resistor [1–3].

A thin-film transistor (TFT) is also an FET. It is basically a MOSFET, with some differences as compared to silicon MOSFET. The structure of a TFT is shown in Figure 5.4. TFTs can be divided into two types, according to whether the semiconducting material is inorganic or organic. The working principle of organic thin-film transistors (OTFTs) is similar to that of inorganic TFTs. However, mechanism of carrier transport in inorganic semiconductors is different from that of organic semiconductors. It is well known that the atoms in an inorganic semiconductor are held together by strong covalent bonds, which create large conduction and valance bandwidths. Inorganic semiconductors always show high charge carrier mobility. For example, the mobility of silicon can be up to 10^3 $cm^2V^{-1}s^{-1}$. However, for organic semiconductor materials, the intermolecular interaction is mainly weak van der Waals forces, which in general have little effect on the properties of intra-molecules. Hence, the width of the valence and conduction bands of organic semiconductors is narrower than that of inorganic semiconductors. The band-transport model can no longer describe an organic semiconductor. Charge carrier transport in organic semiconductors generally occurs by charge hopping between localized states and π-electron cloud overlaps in molecules with π-conjugate systems. Therefore, electrical properties of inorganic TFTs are significantly different from those of OTFTs.

5.3.2 Charge Carriers and Carrier Mobility

In order to better understand the behavior of TFTs, some characteristics of semiconductor materials are first introduced. There are two types of charge carrier in a semiconductor: negatively charged electrons and positively charged holes. As the concentrations of electrons and holes are relatively low in an intrinsic semiconductor, doping of impurity elements is commonly used to increase the carrier concentration. A semiconductor doped by electron-deficient boron (B) is called a p-type semiconductor due to the existence of a large number of holes. In contrast, using electron-rich phosphorus (P) or arsenic (As) as a doping agent, a semiconductor can change to n-type. In p-type and n-type semiconductors, holes and electrons are called majority carriers. Correspondingly, their opposites are called minority carriers. Generally, there are two driving forces that cause carriers to move in a semiconductor, that is electric field and concentration gradient. The carrier movements caused by electric field and concentration gradients are called drift and diffusion, respectively.

The motion of a carrier drifting in semiconductor materials is caused by an applied electric field. When an electric field E is applied in one direction, a force in the same direction is produced on holes, which acquire a drift velocity V_{dp} calculated by

$$V_{dp} = \mu_p E \tag{5.1}$$

Here, μ_p is a constant, called hole mobility and its unit is $cm^2V^{-1}s^{-1}$.

For electrons the drift velocity V_{dn} is calculated by

$$V_{dn} = -\mu_n E \tag{5.2}$$

Here, μ_n is electron mobility. Both μ_p and μ_n are critical parameters when deciding whether a semiconductor material is good enough for making TFTs.

5.3.3 Basic Parameters of TFT

5.3.3.1 Effective Mobility

In a standard MOSFET, drain current equation for an *n*-channel device in the linear region of operation ($V_{ds} < V_{gs} - V_t$) can be expressed as equation (5.3), where μ is a factor that relates the drain current (I_d) to the gate-drain voltages (V_{gs}) and the drain-source voltages (V_{ds}), the gate dielectric capacitance per unit area (C_{ox}), the threshold voltage (V_t), the channel width (W) and length (L) [1]. For *p*-channel MOSFETs, applied voltage polarities and current directions are reversed.

$$I_{ds} = \pm \frac{\mu C_i}{2} \times \frac{W}{L} \times \left[2\left(V_g - V_t\right) V_{ds} - V_{ds}^2 \right] \tag{5.3}$$

V_g: gate voltage $\mathrm{V_t}$: threshold voltage of CMOS transistor;

$C_i = \frac{\varepsilon_0 \varepsilon_{SiO_2}}{d_i}$: the gate dielectric capacitance per unit area;

ε_0: vacuum permittivity $8.85\times10^{-14}\,\mathrm{F}/cm)$;

ε_{SiO_2} : dielectric constant of $\mathrm{SiO_2}$; $\mathrm{d_i}$: thickness of dielectric layer;

W: channel width; L : channel length;

μ: effective mobility.

When V_{ds} is far less than the value of $V_{gs}-V_t$, the standard MOSFET drain-current equation for an *n*-channel device in the linear region of operation is changed to:

$$I_{ds} = \mu C_i \times \frac{W}{L} \times \left(V_g - V_t\right) V_{ds} \tag{5.4}$$

In the saturation region of operation ($V_{ds} \geq V_{gs}-V_t$), the standard equation is changed to:

$$I_{ds} = \frac{\mu C_i}{2} \times \frac{W}{L} \times \left(V_g - V_t\right)^2 \tag{5.5}$$

Therefore, if the values of drain current, gate voltage and threshold voltage, channel length and channel width, and device capacitance are all known, the effective mobility of TFTs can be calculated from the equations (5.4) and (5.5). However, parasitic capacitance may appear when a TFT operates in a saturation region, resulting in overestimation of the mobility. Therefore, the mobility of a TFT in linear and in saturation regions are different. It has been demonstrated that the effective mobility calculated from the equation (5.5) (in saturation region) is generally larger than that calculated from the equation (5.4) (in linear region). Hence, to avoid the overestimation of the mobility, the equation (5.4) is commonly used to calculate the mobility of TFTs. The equation (5.4) can be changed to

$$\mu = 10^4 \times \left(\frac{dI_d}{dV_g}\right) \times \frac{L}{W} \times \frac{1}{C_{ox} V_{ds}} \tag{5.6}$$

If silicon dioxide is used as the dielectric layer and its thickness is 300 nm, C_{ox} is calculated to be 1.15×10^{-4} F/m^2. The equation (5.6) can be reduced to

$$\mu = 10^4 \times \left(\frac{dI_d}{dV_g}\right) \times \frac{L}{W} \times \frac{1}{1.15\times10^{-4} V_{ds}} \tag{5.7}$$

Equation (5.7) is commonly used to calculate the TFT mobility. From the slope of transfer curve (dI_d/dV_g) and known channel length, channel width and gate voltage, the effective mobility can be calculated.

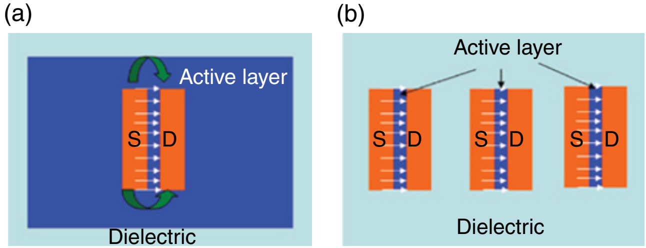

Figure 5.5 Schematics of carrier transport in active layers

However, when the semiconductor layer in a TFT is formed by spin coating, drop-casting, dip coating or spray-coating methods, its transfer curve cannot represent the true characteristics of the semiconducting layer inside the channel. As illustrated in Figure 5.5a, the spin-coated semiconductor layer is not confined inside the channel. Carrier movement can occur both inside and outside the channel. In this case, the calculated mobility is always larger than the actual value, especially for devices with small channel length to width ratio. To avoid this overestimation, either a large channel length to width ratio is made or patterned etching is performed to remove all the semiconductor material outside the channel, as illustrated in Figure 5.5b. If the semiconductor material can be printed, it can also be confined within the channel and the above-mentioned error can be avoided.

5.3.3.2 Operating Voltage

Operating voltage is the voltage required to switch a TFT from off state to on state. It should be low to reduce power consumption. Good gate dielectric with high capacitance can significantly reduce the operating voltage. The example shown in Figure 5.6a is a printed top-gate TFT, using organic semiconducting material P3HT as the active layer, printed ion gel as the dielectric layer and printed PEDOT:PSS as the top gate electrode. Its operating voltage is as low as ±1V, as shown in Figure 5.6b [4]. T. J. Marks reported using high-capacitance ultra-thin aluminum oxide as the dielectric material in metal oxide TFTs and achieved low operating voltage (Figure 5.7) [5].

5.3.3.3 Device Capacitance

Gate dielectric capacitance can be calculated by the following equation (5.8):

$$C_i = \frac{\varepsilon_0 \varepsilon_r}{d_i} \tag{5.8}$$

There are two ways to increase the capacitance, either by using high-k dielectric materials or reducing the thickness of dielectric layer. It has been demonstrated that a thin layer of high-κ gate dielectric, such as hafnium oxide (HfO_x) or aluminum oxide, can lead to a high gate capacitance, and the device shows low operation voltage and small hysteresis. Using a

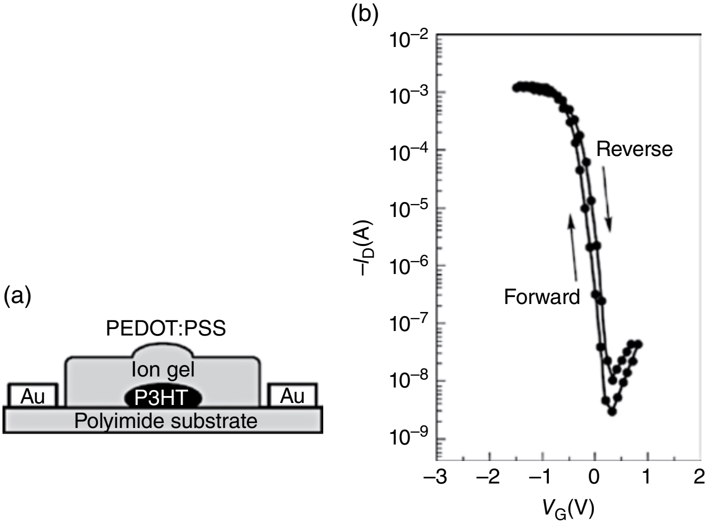

Figure 5.6 (a) Schematic of printed top-gate TFTs and (b) typical transfer curve of printed TFTs using ion gel as dielectric layer (Reprinted from [4] with permission from Nature publishing group)

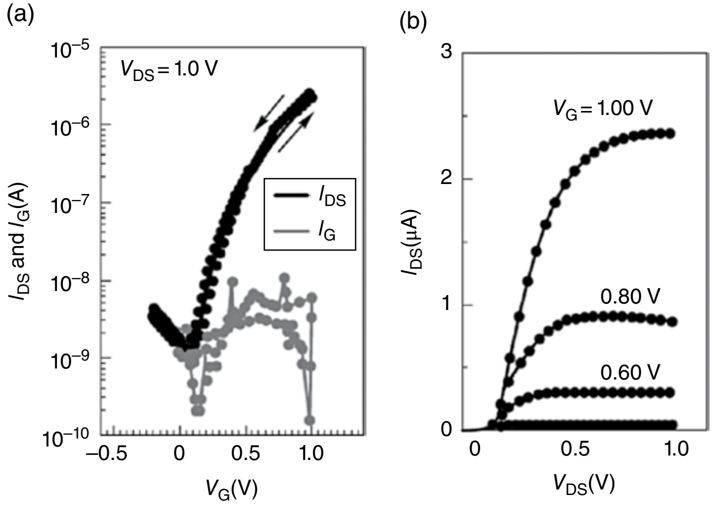

Figure 5.7 (a) Transfer characteristics in a combustion-processed In_2O_3 TFT; and (b) its output characteristics (Reprinted from [5] with permission from Nature publishing group)

thick ion gel dielectric layer can also achieve high capacitance (the very high polarization is obtained due to the transference of mobile ions in the gel dielectric layer in response to the applied voltages), and greatly reduce the operation voltage. Other techniques include using a cross-linked ultra-thin organic polymer layer or self-assembled molecular monolayer to achieve high capacitance.

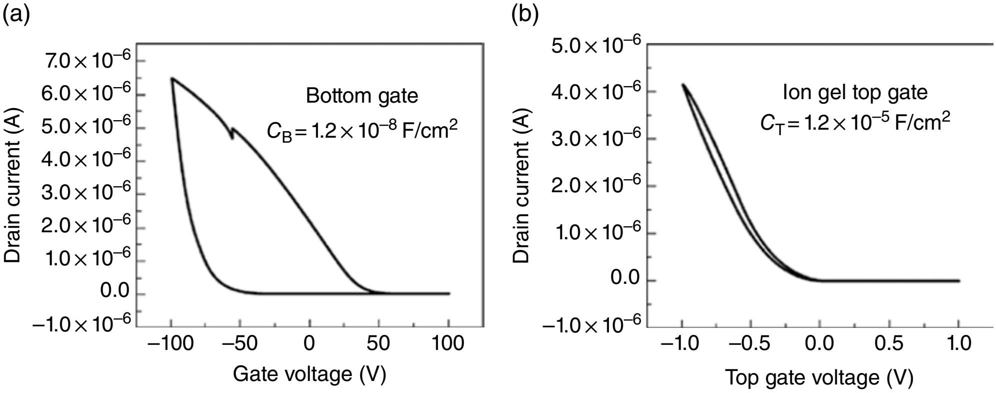

Figure 5.8 Typical transfer curves of (a) bottom-gate and (b) top-gate printed SWCNT TFTs (using ion gel as the dielectric layer)

For comparison, Figure 5.8 shows the transfer curves of two TFTs; one is bottom-gate and the other is top-gate. The top-gate TFT uses high capacitance ion gel as dielectric layer on SiO_2/Si substrates [6]. The device capacitance of bottom-gate and top-gate TFTs are 1.2×10^{-8} F/cm^2 and 2×10^{-5} F/cm^2, respectively. The resulted operating voltages are in the ranges of +60 to -100 V for the bottom-gate TFT and ±1 V for the top-gate TFT, demonstrating how critical is the device capacitance to the device operating voltage.

5.3.3.4 Threshold Voltage (V_t)

The threshold voltage (V_t) is the gate-source voltage at which the conducting channel of the TFT just begins to connect the source and drain of the transistor. V_t can be derived from the linear region of the I_D vs V_{gs} curve at small drain voltages ($V_{ds} << V_{gs} - V_t$), which is the voltage when extrapolating the curve to $I_d=0$ as shown in Figure 5.9. Also shown in Figure 5.9 is the plot of I_D vs V_{gs} for a printed single-walled carbon nanotube (SWCNT) TFT on silicon dioxide substrate where the V_t is about 16.5 V. Alternatively, the threshold voltage can be extracted from the saturation region $I_d^{1/2}$ vs V_{gs}.

Threshold voltage has a close relationship with the thickness of the dielectric layer, electrode and semiconductor work function, and so on [7]. Applying self-assembled monolayers such as octadecyltrichlorosilane (OTS) or organophosphate to the gate dielectric before deposition of the semiconductor layer helps to reduce the V_t. Employing a high capacitance gate dielectric can also reduce the V_t. Furthermore, V_t can be tuned by electron or hole doping and changing the ratio of channel width to channel length. The threshold voltage of solution-processed TFTs is usually large due to the high degree of trapped charge in semiconducting thin film.

When chemical or biological molecules are adsorbed or immobilized on semiconducting material surfaces, the threshold voltage of TFTs will change. Therefore, TFTs are often used as sensors to detect chemical and biological molecules. Figure 5.10 shows the typical transfer curves of SWCNT TFTs before and after immobilizing probe ss-DNA and complementary target ss-DNA. It is evident that the threshold voltage of SWCNT TFTs has

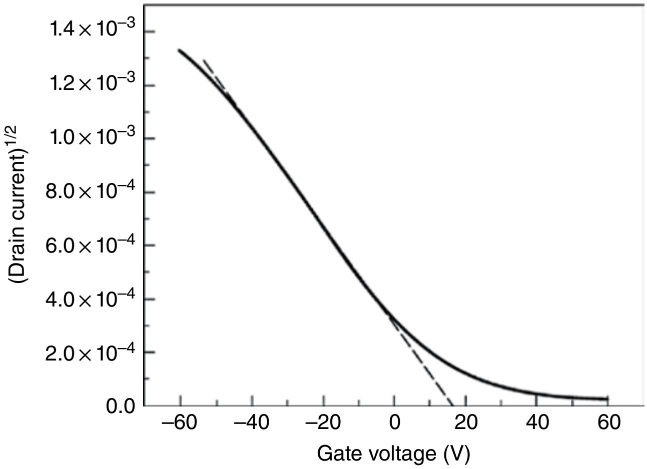

Figure 5.9 $I_d^{1/2}$-V_g curve of printed SWCNT TFT. (Vt is about 16.5V)

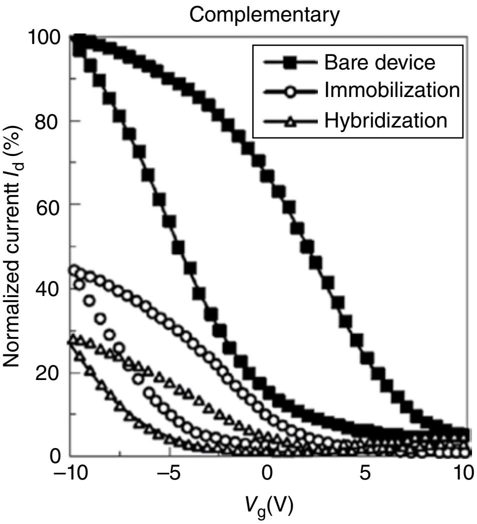

Figure 5.10 Transfer curves of TFTs based on CVD SWCNT networks immobilized probe ss-DNA and hybridized with complementary target ss-DNA. (Reprinted from [8] with permission from American Chemistry Society)

changed after reacting with probe ss-DNA and target ss-DNA due to p-doping by ss-DNA [8]. For sensor applications, the semiconductor material should be highly sensitive to changes in environment. This feature, however, becomes a disadvantage for electronic circuit applications (such as for logic circuits or for OLED driving circuits), which require long-term stability. Proper protection of the semiconductor channel will be needed to improve the TFT stability.

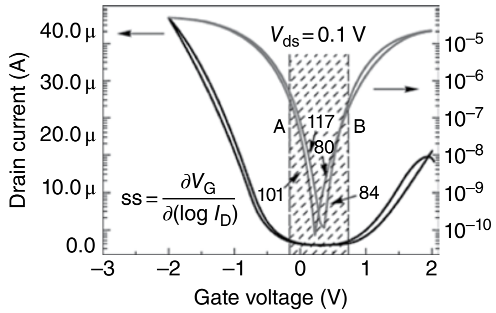

Figure 5.11 The subthreshold swings of printed SWCNT TFTs. AB represents the subthreshold region. 117, 101, 80 and 84 are SS for p-type and n-type transistors. (Reprinted from [9] with permission from The Royal Society of Chemistry)

5.3.3.5 Subthreshold Swing (SS)

The SS is an important feature of a TFT. In the subthreshold region (the shaded AB area in Figure 5.11) the drain current shows exponential increase with the gate voltage. The logarithmic drain current and gate-drain voltage shows an approximate linear relation when drain and source voltages are fixed. Its slope is called the subthreshold slope. A steeper subthreshold slope exhibits a faster inversion from off to on state. In general, the maximum subthreshold slope is named as subthreshold swing (SS). A small SS is desirable since fewer gate voltage changes are required to change the transistor from off to on state. The SS can be calculated by the following equation:

$$SS = \mathrm{In}(10)\frac{kT}{q}\left(1 + \frac{C_d}{C_{ox}}\right) \tag{5.9}$$

Here, C_d and C_{ox} are depletion layer capacitance and gate-oxide capacitance, respectively.

As shown in the equation (5.9), the SS is determined by the inverse ratio of gate capacitance (C_{ox}) to depletion layer capacitance (C_d). In general, high concentrations of impurities in the interface between an active layer and dielectric layer, and small gate capacitance will lead to large SS. Using high-purity semiconductor materials and high-capacitance dielectric can greatly decrease the SS value of printed TFTs [9].

5.3.3.6 On/off Current Ratio (I_{on}/I_{off})

On/off current ratio is another important parameter of TFT. It is defined as the ratio of drain current in a saturation region (I_{on}) to drain current at zero gate voltage (I_{off}) with fixed source-drain voltage. I_{on} can be calculated by the following equations in the linear and saturation region, respectively.

In the linear region,

$$I_{on} = \frac{WC_i}{2L}\mu\left(V_g - V_T - \frac{V_{ds}}{2}\right)V_{ds} \tag{5.10}$$

In the saturation region,

$$I_{on} = \frac{WC_i}{2L}\mu\left(V_g - V_T\right)^2 \tag{5.11}$$

In the pinch-off region (off state), I_{off} can be expressed as:

$$I_{off} = q\left(n\mu_e + p\mu_p\right)\frac{Wd}{L}V_{ds} \tag{5.12}$$

Here, q, n, μ_e, p, μp, W, d and L represent charge, electron density, electron mobility, hole density, hole mobility, channel length, channel width and thickness of active layer, respectively.

Transistors must have high on/off ratio and low operating voltage. For example, to control OLED or LED lighting, the on/off ratio of TFTs in driving circuits should be at least 10^5.

5.3.3.7 Hysteresis

Hysteresis refers to short-term reversible shifts that result from looping in the measured transfer characteristics, which depends on the sweeping direction of bias voltages. The typical hysteresis is represented by the transfer curves in Figure 5.8a where the forward and backward sweeping of bias voltage do not produce the same transfer characteristics. It has been demonstrated that the magnitude of hysteresis increases with the decrease of gate sweeping frequency, indicating that slowly moving charge species cause the hysteretic behavior. Some reported that hysteresis in TFTs is mainly caused by absorbates, such as oxygen, water and other impurities in active materials and dielectric materials. Therefore, hysteresis can be eliminated or decreased by removing the impurities in the active layer or dielectric layers. Using ion gel and other hybrid nanomaterials with high capacitance as dielectric materials can also effectively eliminate or reduce the hysteresis, as can be seen by a comparison of Figure 5.8b with Figure 5.8a. Figure 5.12 shows typical transfer curves of printed top-gate SWCNT TFTs using 50 nm HfO_2 as the dielectric layer. The printed top-gate TFT exhibits small hysteresis. Self-assembling a monolayer on the device substrate is another useful method to effectively

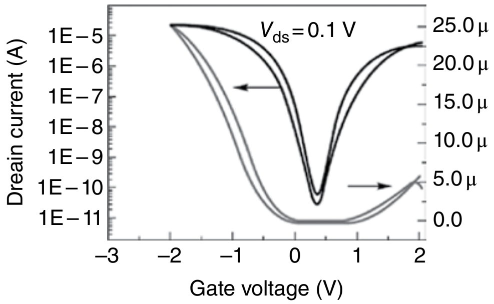

Figure 5.12 Transfer curves of printed top-gate SWCNT TFTs

reduce or eliminate the hysteresis. Generally, solution-processed TFTs have large hysteresis due to absorbed impurities on substrates and in active layers. Reduction or elimination of TFT hysteresis is one of the key research topics in the field of printed thin-film transistors.

5.3.3.8 Transconductance (g_m)

In FETs, especially MOSFETs, g_m is defined as the change of drain current induced by a small change of gate voltage when the source-drain voltage is fixed. The g_m for MOSFET can be expressed as follows

$$g_m = \frac{\Delta I_d}{\Delta V_g} \tag{5.13}$$

Typical values of g_m for a small-signal FET are in the range of 1 to 30 millisiemens. When transistors operate in the linear and saturation region with small source-drain voltage, g_m can be expressed as equation (5.14)

$$g_m = \frac{\partial I_{ds}}{\partial V_g} = \frac{\mu WC}{L} V_{ds} \tag{5.14}$$

5.3.3.9 Stability

Most organic TFTs are not stable in their ambient state due to their sensitivity to oxygen, water and light, whereas inorganic TFTs based on metal oxides (ZnO or IGZO) or carbon nanotubes show good stability in atmosphere.

5.4 Structures and Fabrication of TFTs

5.4.1 Structures of TFTs

A thin-film transistor consists of a source electrode, drain electrode, gate electrode, semiconductor active layer and dielectric layer. Depending on the location of gate electrode, there are four different layer structures concerning a TFT, as shown in Figure 5.13.

Bottom-gate structure is the most commonly used TFT structure that is used to evaluate the electrical properties of semiconducting materials. As the chemical and physical properties of some active layer materials, such as some of the organic semiconducting materials, are unstable in air, the electrical properties of these active materials will be degraded when dielectric layers are deposited on top by a solution process, sputtering methods, atomic layer deposition, thermal evaporation, and so on. The bottom-gate structure together with top encapsulation can avoid this problem. Silicon dioxide is an excellent dielectric material and heavily doped silicon can serve as the bottom-gate electrode, respectively.

Top-gate TFTs generally exhibit high mobility, low operating voltage and small hysteresis due to high induced electric fields. The fabrication process for a top-gate transistor is, however, more complicated than for a bottom-gate TFT. The fabrication process also tends to

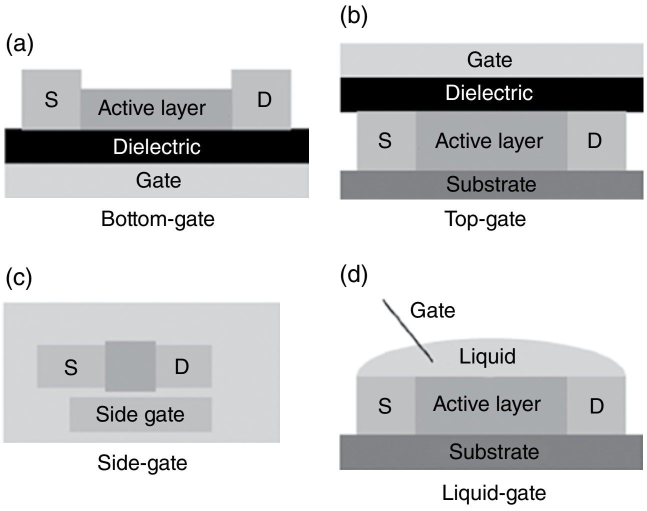
(a)
S
Active layer
D
Dielectric
Gate
Bottom-gate
(b)
Gate
Dielectric
S
Active layer
D
Substrate
Top-gate
(c)
S
D
Side gate
Side-gate
(d)
Gate
Liquid
S
Active layer
D
Substrate
Liquid-gate

Figure 5.13 Basic layer structures of TFT: (a) bottom-gate; (b) top-gate; (c) side-gate; (d) liquid-gate

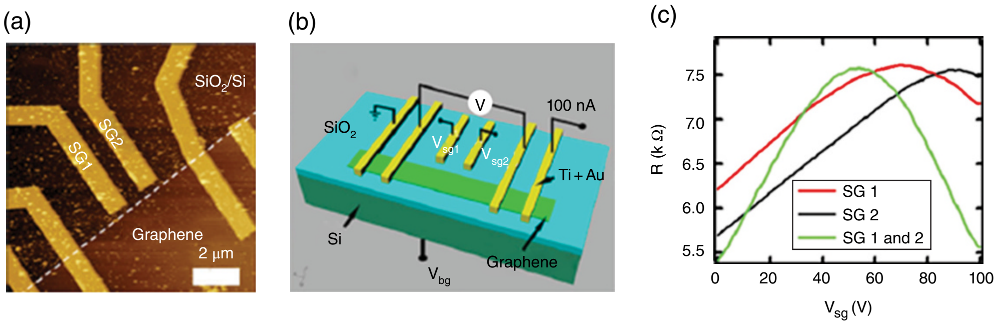

Figure 5.14 Side-gate graphene transistor (a) and (b), and curves of electrical properties (c) (Reprinted from [10] with permission from AIP publishing LLC)

introduce defects or impurities in the active layers during the deposition of the dielectric layer, resulting in deterioration of electrical properties. Despite the difficulty, top-gate TFTs are widely used to construct more complicated functional circuits because of their inherently low operating voltage and small hysteresis.

Compared to top-gate and bottom-gate TFTs, the structure of a side-gate TFT is simpler. Figure 5.14 shows the structure of a two side-gate graphene transistor and transfer characteristics [10]. However, side-gate TFTs have low mobility and on/off ratio due to the poor tuning ability of side-gate configuration.

Liquid-gate TFT is a special type of transistor that uses liquid, such as liquid ions, aqueous, and solvents as the dielectric materials, and tunes the TFT electrical properties by electrochemical reaction. They have wide applications in the field of biosensor/chemical sensors, drug screening, and so on [11, 12].

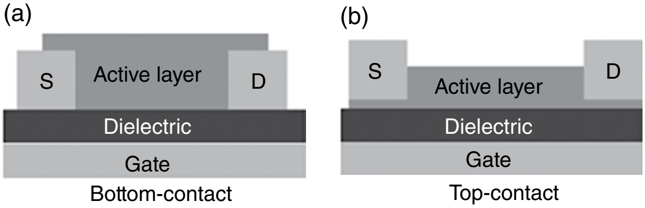

Figure 5.15 (a) Bottom-contact and (b) top-contact thin-film transistor structures

In addition to the four basic configurations of TFTs shown in Figure 5.13, the bottom-gate TFT can also have two different layer structures according to how the source and drain electrodes contact to the active layer. They are the bottom-contact and top-contact structures, as illustrated in Figure 5.15.

For bottom-contact TFTs, the source and drain electrodes are fabricated on the dielectric layer first, then the deposition of active materials (Figure 5.15a). The source and drain electrodes are in contact with the active layer at the bottom. As for the top-contact TFTs, active materials are deposited first, then the deposition of source and drain electrodes, so that they contact the active layer at top (Figure 5.15b). Both bottom-contact and top-contact TFTs have their own advantages and disadvantages. Top-contact TFTs have better contact between source/drain electrodes and the active layer than bottom-contact TFTs; moreover, the area of electrical field introduced by the gate electrode in a top-contact transistor is larger than that of a bottom-contact transistor, resulting in higher on current. Furthermore, the dielectric layer in top-contact TFTs can be modified physically or chemically without the interference of source/drain electrodes, which helps to tune the morphologies, structures and density of active materials, resulting in improved TFT mobility. However, when making top-contact TFTs, the electrode materials can easily diffuse into the active layer, causing leakage and low on/off ratio.

The advantage of a bottom-contact TFT is its simple fabrication process. In particular, when using silicon wafer as the substrate, thermally grown or chemical vapor deposition of SiO_2 on the silicon wafer can be used as the dielectric layer while the heavily doped highly conductive silicon substrate can act as the gate electrode. The source and drain electrodes arrays can be made either by printing or conventional photolithographical patterning. However, the contact between the semiconductor active layer and source/drain electrodes is not as good as that of top-contact TFT.

In general, bottom-gate TFTs, whether they are top-contact or bottom-contact, always have the semiconductor active layer exposed to the environment. These TFTs are less stable for electronic circuits because water and oxygen molecules can affect the charge transport in the TFTs. On the other hand, this property can be used to make sensors where semiconductor materials become the sensing materials. Recently, various chemical biosensors based on bottom-gate/bottom-contact TFTs have been developed, including gas sensors, DNA sensors, photon sensors, pressure sensors, and so forth.

5.4.2 Characteristics of TFTs

Depending on the semiconductor materials used, TFTs can be divided into two groups, organic and inorganic TFTs. The organic field-effect transistor, also called OFET or OTFT, uses organic semiconducting materials as active materials. Compared to traditional inorganic semiconductors, organic semiconductor materials are generally of low mobility and poor stability in an ambient environment. P-type organic semiconductors are better than n-type organic semiconductor materials because n-type organic semiconductors are more easily oxidized when exposed to oxygen. Other problems for OTFTs are high operating voltage and low switching speed.

Despite the drawbacks, OTFTs have some unique advantages, such as suitability for flexible substrates, good solubility for solution processes and potentially low cost to fabricate. OTFTs have been pursued by the academic research community and industry since the first OTFT was reported in 1986. In nearly three decades of research, the mobility of OTFTs have increased by more than 5 orders of magnitudes. For example, the mobility of pentacene (organic small molecular semiconductors) OTFTs was only 0.002 $cm^2V^{-1}s^{-1}$ in 1992 and it reached 5 $cm^2V^{-1}s^{-1}$ in 2003. OTFTs based on organic small molecular semiconductors and organic single crystalline semiconductors show higher mobility than those of polymeric semiconductors. The mobility of single crystal pentacene OTFTs was reported at up to 35–58 $cm^2V^{-1}s^{-1}$ [13]. Chapter 2 of this book provides more information about organic electronic materials.

The advantages of inorganic TFTs compared to OTFTs are high mobility and high environmental stability. For example, the transistors constructed from individual single-walled carbon nanotubes achieved mobility as high as 10^4 $cm^2V^{-1}s^{-1}$. Even random carbon nanotube network TFTs can have mobility up to 100 $cm^2V^{-1}s^{-1}$. TFTs made from metal oxide semiconductors such as In-Ga-Zn-O (IGZO) have achieved mobility of more than 100 $cm^2V^{-1}s^{-1}$ with high on/off ratio (up to 10^4) and low operating voltage (±1 V) [7]. Nanoscale inorganic materials, such as nanoparticles, nanowires, nanoflakes or nanocrystals, disperse well both in organic solvent or aqueous liquid, with the aid of sonication and surfactants. Hence, most of the inorganic materials, whether conductors, semiconductors or dielectrics, can be made into inks, opening the possibility of fabricating TFTs by the printing process. Chapter 3 of this book provides more information about inorganic electronic materials.

5.4.3 Fabrication of TFTs

5.4.3.1 Fabrication of Electrodes

Electrode materials should have high conductivity and a small Schottky barrier at the interface with a semiconductor layer, which means their work functions should match that of inorganic semiconductors or a HOMO/LUMO level for organic semiconductors. Metallic materials, such as Al, Ag, Ti, Cr, Mo, W, Ta, Au, Pd, Pt, Ni, are commonly used electrode materials. Other materials, such as CNT, graphene, graphene oxide, organic conducting materials (PEDOT:PSS), can also act as electrode materials. Some electrode fabrication techniques are listed as follows.

5.4.3.1.1 Conventional Microfabrication

Au, Cr and Ti are the most commonly used metallic electrode materials. They can be deposited by DC magnetic sputtering, thermal or electron beam evaporation as thin films and subsequently patterned by photolithography and etching, which is a subtractive process. Alternatively, electrodes can be fabricated by an additive process called "lift-off", which starts with the patterning of a photoresist layer and then depositing a metal thin film. After dissolving

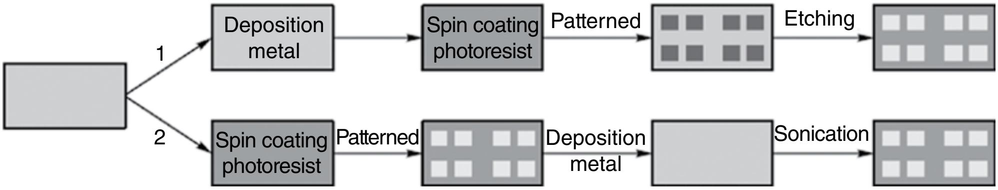

Figure 5.16 Subtractive (1) and additive fabrication (2) processes of source and drain electrode arrays on substrates

the photoresist, patterned metal electrodes remain on the substrate [14]. Figure 5.16 shows the schematics of both subtractive and additive processes. Generally, the adhesion force between a gold electrode and a substrate are not strong in the additive process. Gold electrodes are easily peeled off when sonication is performed. To increase the adhesion force, a thin layer of Ti or Cr is normally deposited first as an adhesion layer.

5.4.3.1.2 Spray Coating, Spin Coating and Langmuir–Blodgett (LB) Techniques

Spray coating or spin coating is a simple and non-patterning method to fabricate electrodes, active layers and dielectric layers. The thickness and uniformity of thin films can be controlled by tuning the spin speed, the concentrations of inks and the surface properties of substrates. LB film deposition technique is another method to deposit films with molecular accuracy.

Fu et al. [15] fabricated all-carbon TFTs on PET substrates by spray coating conductive carbon nanotubes as the electrodes. Li, et al. reported spin coating graphene oxide (rGO) to make source and drain electrodes for all-carbon TFTs [16]. The fabrication process is shown in Figure 5.17. A homogeneous reduced graphene oxide (rGO) thin film was first spin coated on a silicon wafer covered with silicon dioxide. The rGO electrodes were patterned by using a hard plastic or bamboo stick to scratch the rGO film. A catalyst was then selectively deposited on the rGO electrodes. The substrate was placed into a quartz tube furnace to grow SWCNTs in the device channel to form the final TFT.

GO thin film and CNT thin film can be fabricated on substrates by the LB technique [17, 18]. GO was then reduced at a high temperature to become rGO electrodes after lithographic patterning, from which organic TFTs were fabricated using patterned rGO as source and drain electrodes (Figure 5.18 and 5.19).

5.4.3.1.3 Printing

Spray coating or spin coating can only deposit blanket film. To make electrodes, the film needs to be patterned. Printing can directly deposit conductive solutions, or inks, as patterns. Chapter 4 of this book has introduced many printing techniques. Here only a few techniques that were reported to make electrodes are described.

Inkjet printing is the most commonly used printing method to make patterned electrodes with a variety of conductive inks. At the authors' Printable Electronic Research Center, silver electrode arrays and simple oscillators were fabricated on both rigid and flexible substrates by inkjet printing [19]. Haruya Okimoto et al. fabricated all-carbon transistors via inkjet printing in 2010 [20]. Aurore Denneulin [21] used a mixture of SWCNTs and PEDOT:PSS to fabricate high-performance SWCNT hybrid electrodes. A variation of inkjet printing is aerosol jet printing, which offers better resolution and high tolerance on inks. Cho et al. [22] and

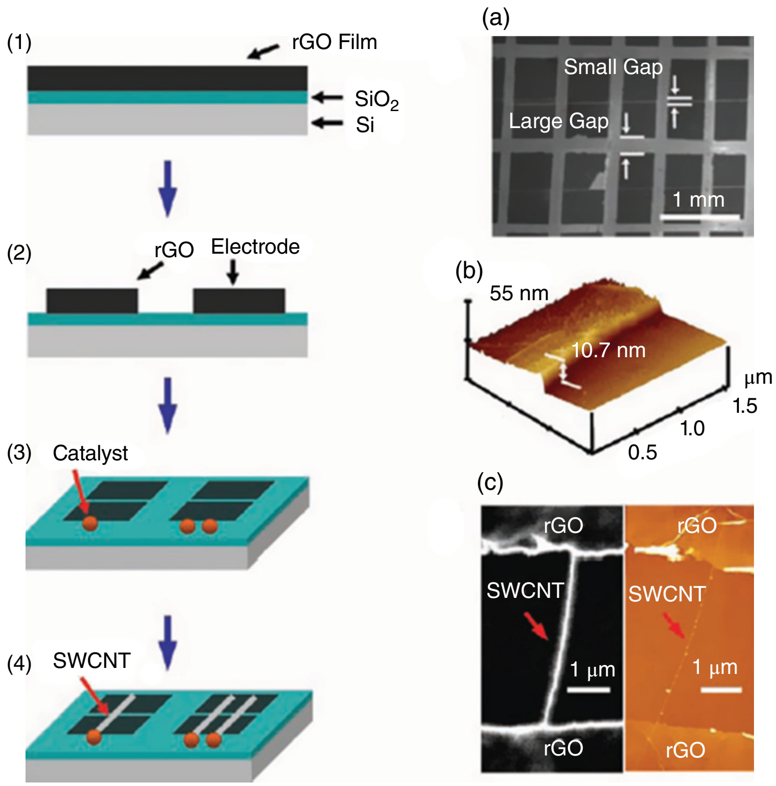
(1)
rGO Film
SiO2
Si
(2)
rGO
Electrode
(3)
Catalyst
(4)
SWCNT
(a)
Small Gap
Large Gap
1 mm
(b)
55 nm
10.7 nm
µm
1.5
1.0
0.5
(c)
rGO
SWCNT
1 µm
rGO
rGO
SWCNT
1 µm
rGO

Figure 5.17 Schematic illustration of the experimental procedures for fabrication of SWCNT TFTs with patterned rGO as source and drain electrodes. (1) Preparation of rGO film on SiO_2. (2) Creation of electrode patterns in rGO film by scratching. (3) Deposition of a catalyst in selected positions on the substrate. (4) Controlled growth of CNTs to bridge rGO electrodes by CVD. (a) SEM image of patterned rGO electrodes generated by scratching method. (b) 3D AFM image of the edge of a typical rGO electrode. The measured thickness of rGO film is 10.7 nm. (c) SEM (left) and AFM (right) images of a fabricated all-carbon device, i.e. an individual CNT–rGO device. (Reprinted from [16] with permission from John Wiley & Sons Singapore Pte Ltd)

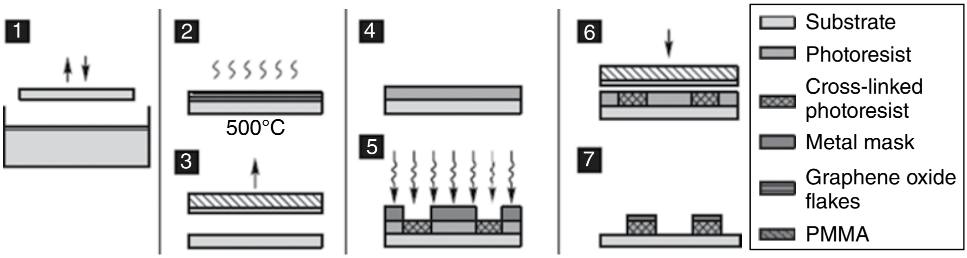
1
2
500°C
3
4
5
6
7
Substrate
Photoresist
Cross-linked photoresist
Metal mask
Graphene oxide flakes
PMMA

Figure 5.18 Interlayer lithography patterning of GO electrodes. A thin film (4 nm) of GO flakes is formed on a glass substrate by a Langmuir–Blodgett dip coating technique (1). The GO is partially reduced by annealing (2). Transfer of the conductive ultra-thin GO layer by lamination onto exposed SU8-2 photoresist (4, 5) with the help of a thin poly (methyl methacrylate) (PMMA) backing layer (3, 6). Immersion in a developer removes PMMA and UV cross-linking photoresist (7), resulting in patterned GO electrodes with underlying cross-linked SU8 interlayer photoresist. (Reprinted from [17] with permission from John Wiley & Sons Singapore Pte Ltd)

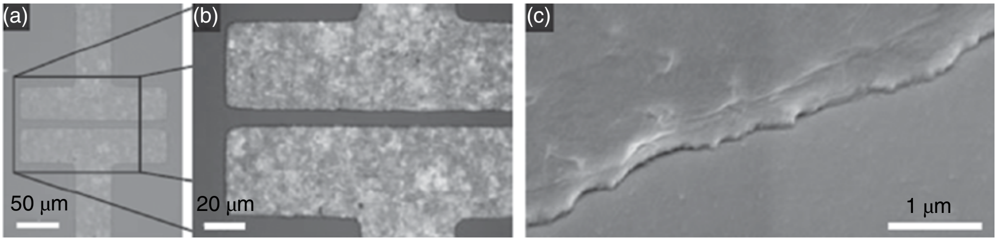

Figure 5.19 Patterned GO source and drain electrodes for thin-film transistors. (a) & (b) Optical microscopy images of patterned GO electrodes with a 10μm channel length. (c) Scanning electron microscopy image of the patterned electrode edge, taken at an angle of ≈30°. (Reprinted from [18] with permission from John Wiley & Sons Singapore Pte Ltd)

Vaillancourt et al. [23] fabricated high-performance top-gate organic and inorganic TFTs on flexible substrates using aerosol jet printing of gold and silver electrodes as source, drain and gate electrodes, and the printed TFTs showed excellent electrical properties.

Although inkjet printing is much easier to use and flexible for pattern designs, it is best suited for small batch fabrication and laboratory experiments. For large scale manufacturing, roll-to-roll printing is the ideal printing technique. In 2010, Jung et al. reported that flexible and all-printed RFID were successfully fabricated on PET substrates by roll-to-roll gravure printing [24].

The above printing processes are all based on transferring inks to substrates, which is a "wet" process. There is another type of printing, which is a "dry" process and often called "transfer printing". It is based on transferring a ready-made film from one substrate to another substrate. The method has been widely used to transfer graphene films to make TFTs. It is well known that graphene is one of the ideal electrode materials due to its extremely high carrier mobility. In order to fabricate graphene transistors or electrode arrays, graphene grown on copper, nickel and Pt substrates by CVD should be transferred to other substrates. Some works have demonstrated TFTs based on transferring CVD graphene electrodes [25, 26].

All the aforementioned techniques have their advantages and disadvantages. Conventional microfabrication techniques are complicated and expensive but can produce high quality electrodes, such as high conductivity, strong adhesion force with substrates and good uniformity. They are still widely used in printed electronics for making electrodes. Other techniques such as spin coating, spray coating and printing, although simple and low cost, have issues of low resolution, weak adhesion force and high surface roughness, which can compromise the performance of TFTs. However, both the printing technologies and ink materials have been advancing rapidly in recent years. It is expected that printing will be used more in future for TFTs and large-area flexible electronics applications.

5.4.3.2 Fabrication of Active Layer

An active layer acts as the channel for charge carriers and has the most influence on the performance of TFTs. Many organic and inorganic semiconductors have been used as active materials in TFTs. These materials may have considerably different physical and chemical properties. Therefore, the fabrication of the active layer is more diverse compared to fabrication

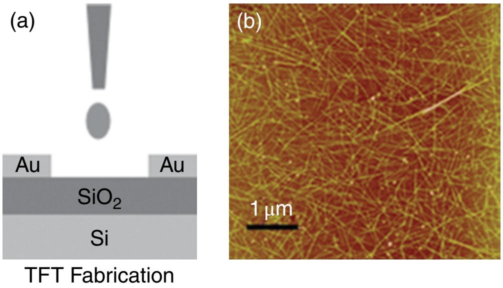

Figure 5.20 (a) Fabrication process of SWCNT TFTs by drop casting; (b) AFM image of SWCNT network

of other parts of a TFT. Currently, techniques such as spin coating, spraying, drop casting, CVD, sputtering, and printing methods, have all been employed to deposit the active layer. The techniques are different from the fabrication of electrodes and are described below.

5.4.3.2.1 Drop Casting

Many groups used this method because it is simple and does not need expensive apparatus. Figure 5.20a illustrates the fabrication process of SWCNT TFTs by drop casting and Figure 5.20b shows an AFM image of SWCNT network. Semiconductor SWCNT inks were dropped by a micro injector in the channel between source and drain electrodes, followed by drying at room temperature and rinsing with suitable solvents. The procedure was repeated until the of TFT is high enough to reach a desired level [26].

As shown in Fig. 5.20b, SWCNT films are homogeneous and the length of SWCNTs is in the range from 1 to 3 µm. The TFTs show high on/off ratio ($>10^5$) and high on current (up to 1×10^{-4} A) [27]. However, the drop casting method cannot deposit the semiconducting materials precisely in the channel between the source and drain electrodes. "Spillover" of SWCNTs can give rise to large leakage currents and overestimation of the mobility of TFTs.

5.4.3.2.2 Vacuum Thermal Evaporation

For organic TFTs based on small organic semiconductor molecules, the active layer is generally deposited by vacuum thermal evaporation. When the organic material is heated in vacuum, it evaporates and condenses on the surface of substrate because the lower temperature of substrate than that of evaporating source. Homogeneous organic thin film can be achieved at the vacuum below 10^{-3} pa. Other factors to control the film quality are evaporation rate and film thickness during the evaporation process.

5.4.3.2.3 Micromolding in Capillary

Micromolding in capillary (MIMIC) is a simple and useful method to fabricate 3D micro/nano structures of polymers and ceramics. This technique can also be used to pattern active layers in TFTs. Figure 5.21 shows a schematic of graphene oxide (GO) patterning by the MIMIC method. A patterned polydimethylsiloxane (PDMS) stamp with capillary channels is put on the substrate and a drop of GO aqueous solution is then placed at one end of the

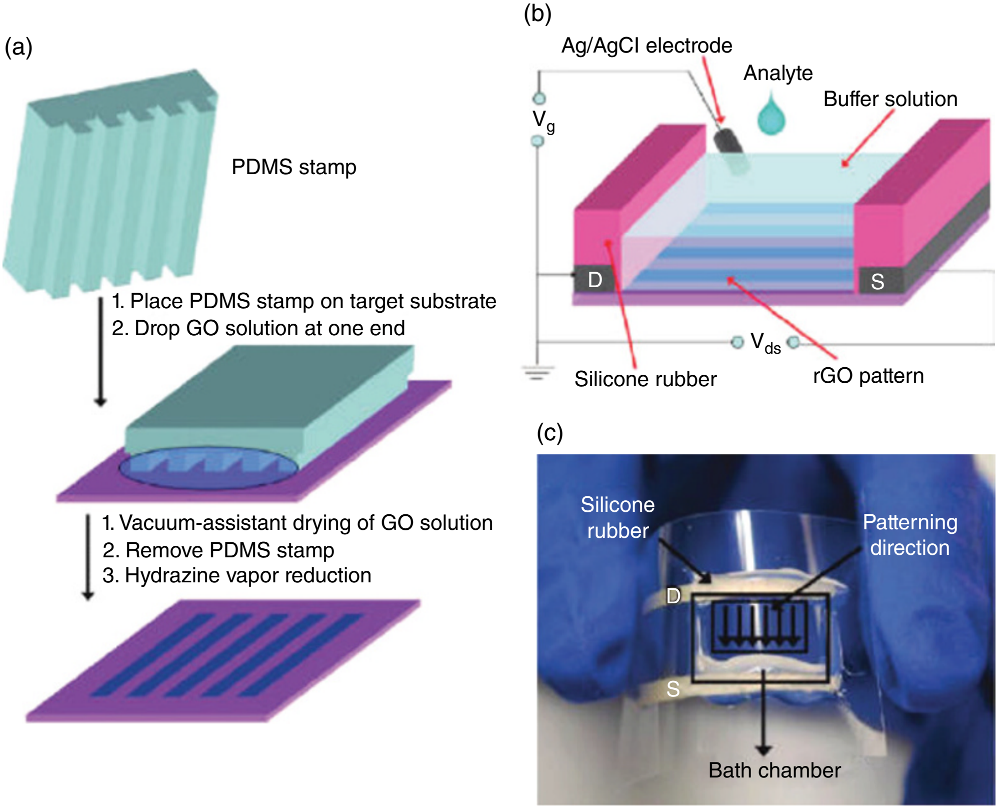
(a)
PDMS stamp
1. Place PDMS stamp on target substrate
2. Drop GO solution at one end
1. Vacuum-assistant drying of GO solution
2. Remove PDMS stamp
3. Hydrazine vapor reduction
(b)
Ag/AgCl electrode
Analyte
Buffer solution
V_g
D
S
V_{ds}
Silicone rubber
rGO pattern
(c)
Silicone rubber
Patterning direction
D
S
Bath chamber

Figure 5.21 (A) Schematic illustration of patterning GO films by MIMIC and reduction of the patterned GO films. (B) Schematic illustration of the experimental setup of front-gate FET for sensing application. (C) Photograph of rGO based sensing device on PET film. (Reprinted from [28] with permission from American Chemistry Society)

PDMS stamp, which is then sucked into the channels by capillary force. The substrate is then put into a vacuum oven for 30 minutes to dry. After peeling off the PDMS stamp, a GO pattern is formed on the substrate. TFTs made in this way have been used to detect hormonal catecholamine molecules and their dynamic secretion from living cells and showed good sensitivity [28].

5.4.3.2.4 Stamping Transfer

Stamping transfer is also an effective technique to construct active layers. SWCNT thin films, silicon nanowires, gallium arsenide and gallium nitride nanowires can be transferred by patterned stamps from one substrate to another substrate. For example, the SWCNT network was first deposited by a solution processing method such as spin coating, then transferred to the surface of another substrate using a patterned PDMS as the stamp [29]. The same method has been used to transfer silicon, GaN and GaAs nanowires as the active layers of TFTs, showing good performance [30].

5.4.3.2.5 Sputtering Deposition

Sputtering is mainly used to deposit metal oxide semiconductors such as ZnO and IGZO. Although metal oxide semiconductors can be solution-processed, the sputtered metal oxide layers gives much better electrical property and therefore is the main technique for making the active layers. More detailed information about metal oxide semiconductors has been given in Chapter 3 of this book.

5.4.3.2.6 Fabrication of Aligned Active Layers

The performance of TFTs can be improved significantly when semiconducting materials of active layers are highly oriented or aligned. There are some techniques that help to construct oriented or aligned semiconducting thin films.

1. Alignment of organic semiconductor crystal. With the help of an external force, the crystalline state of some organic semiconductors in liquid phase can be aligned along a specific direction during solvent evaporation. As shown in Figure 5.22a, hexa (4-dodecylphenyl) hexa-peri-hexabenzocoronene (HBC-PhC12) was aligned along the channel with the aid of applied high magnetic field. It can be seen in Figure 5.22b that the performance of devices was best when HBC-PhC12 crystalline orientation was parallel to channels [31]. A solution-sheared process is another approach to orientate the active layer. As shown in Figure 5.23, when a constant shear force was applied along the surface of an organic semiconductor solution in the horizontal direction or a vertical direction, aligned organic crystal thin films can be obtained, which have a significantly enhanced mobility of TFTs [32].
2. Alignment of SWCNTs in liquid phase. Currently, several approaches have been developed to create the alignment of SWCNTs in liquid phase. One method is to first make narrow channels on the substrate surface. The patterned substrate is then immersed into SWCNT solutions and slowly pulled out to form aligned SWCNT along the channels (Figure 5.24) [33]. When blowing the patterned substrate in certain direction while the solvent evaporates, it also helps to achieve the alignment of SWCNTs [34]. Dielectrophoresis

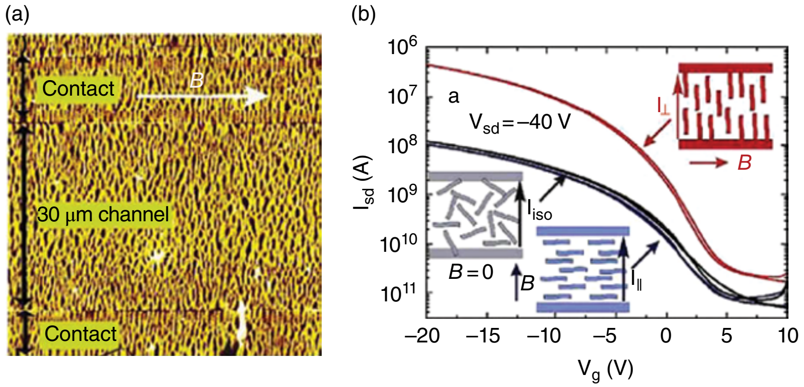

Figure 5.22 (a) Atomic force microscopy (AFM) images of magnetically aligned HBC-PhC$_{12}$-based field-effect transistors. (b) Electrical performance of a typical magnetically aligned HBC-PhC$_{12}$-based FETs and unaligned FETs (Reprinted from [31] with permission from American Chemistry Society)

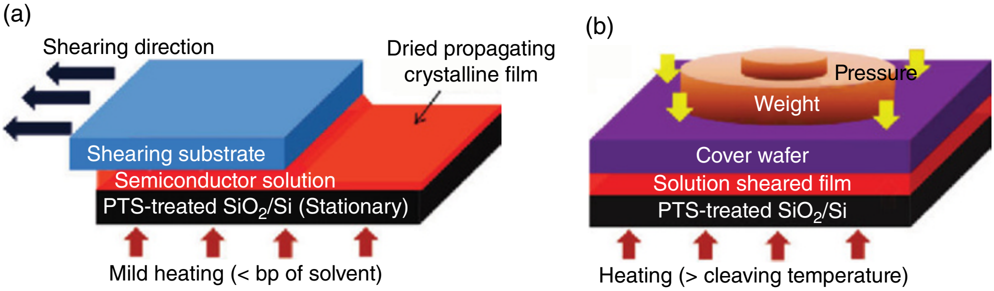
(a)
Shearing direction
Dried propagating crystalline film
Shearing substrate
Semiconductor solution
PTS-treated SiO2/Si (Stationary)
Mild heating (< bp of solvent)
(b)
Pressure
Weight
Cover wafer
Solution sheared film
PTS-treated SiO2/Si
Heating (> cleaving temperature)

Figure 5.23 Schematic diagrams for (a) solution shearing and (b) pressure-assisted thermal cleavage to construct alignment of organic semiconducting films (Reprinted from [32] with permission from American Chemistry Society)

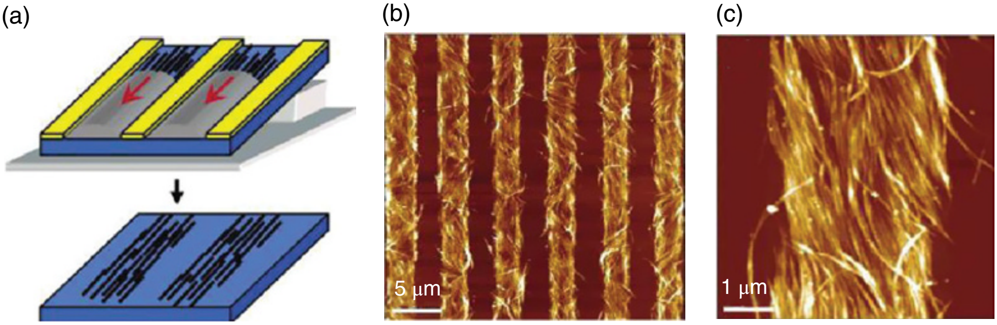

Figure 5.24 (a) Schemes for the tilted-drop fabrication of a thin film on an amine-terminated SAM surface micropatterned with photoresist polymer stripes. (b) and (c) are AFM topographical images of SWCNT films showing axially oriented, densely packed SWCNT bundles (Reprinted from [33] with permission from American Chemistry Society)

(DEP) is another effective method to produce aligned SWCNT arrays and Figure 5.25 shows different densities of aligned SWCNT arrays by tuning the concentrations of SWCNT solution [35]. Cao et al. reported in 2013 that the aligned high density arrays of SWCNTs by Langmuir–Schaefer technique. The fabrication process and SWCNT morphologies are shown in Figure 5.26 [36].

5.4.3.3 Fabrication of Dielectric Layers

The dielectric layer is no less important than the active layer in a TFT. The physical and chemical properties of the dielectric layer, such as thickness, surface roughness, dielectric constant, defects, all have strong influences on the threshold voltage, on current, effective mobility and the subthreshold slope of a TFT. For example, operating voltage and threshold voltage can be substantially reduced when using a dielectric layer of high capacitance. How to make a good dielectric layer is one of the important research areas in the field of printed electronics. The following are some of common techniques to make dielectric layers.

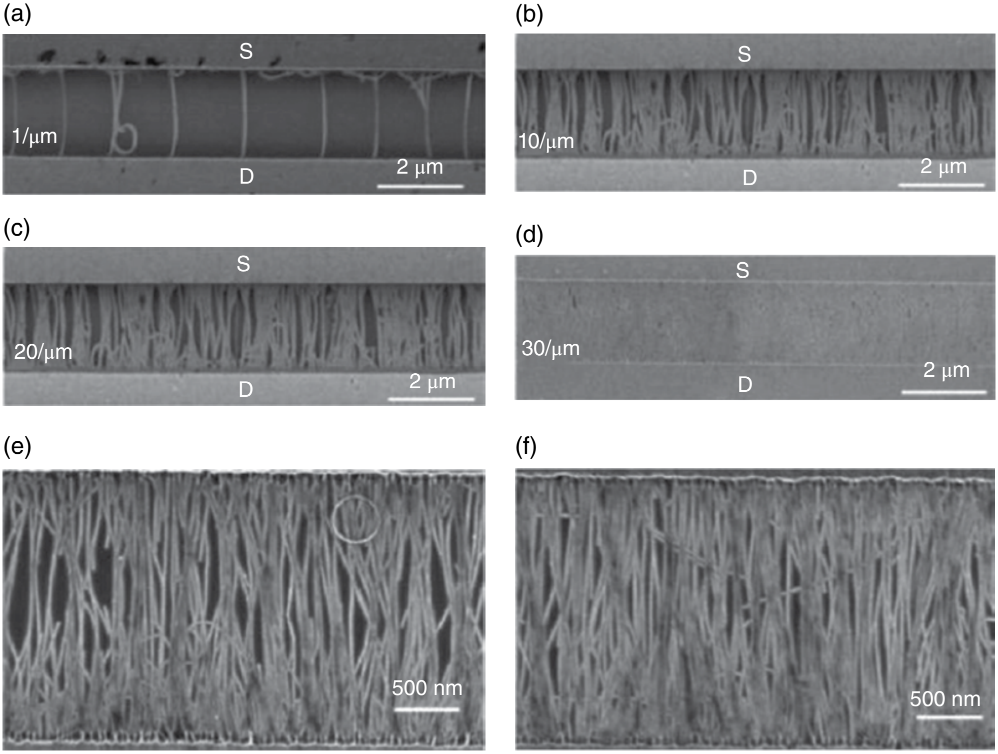

Figure 5.25 Scanning electron microscopy (SEM) image for a typical DEP assembly with varying SWCNT density: (a) ~1 SWCNT per µm, (b) 10 SWCNT per µm, (c) 20 SWCNT per µm, (d) 30 SWCNT per µm, (e) and (f) show magnified images of (c) and (d). For this assembly, L =2 µm and W =25 µm. (Reprinted from [35] with permission from American Chemistry Society)

5.4.3.3.1 Oxidation

Silicon dioxide is the most commonly used dielectric material in TFTs. Silicon dioxide can be formed by dry or wet oxidation of silicon wafers, which can produce a dielectric layer with dense film structure and smooth surface morphology. The thickness of silicon dioxide can be controlled by tuning the oxidation conditions. Normally 300 nm thick silicon dioxide is good enough for most TFTs.

5.4.3.3.2 Atomic Layer Deposition

Atomic layer deposition (ALD) can produce high quality dielectric film with high dielectric constant (high-k). The commonly encountered dielectric films in TFTs deposited by ALD are HfO_x and Al_2O_x thin films. The thickness of films can be controlled in atomic scale due to its self-limiting surface reaction process. Thin films deposited by ALD are more homogeneous than those deposited by other methods. However, ALD techniques have some insurmountable disadvantages. The dielectric films obtained by ALD normally have a high fixed charge, high interface state density and high interface stress. In addition, oxygen in the dielectric layer can diffuse to the active layer easily, resulting in degradation of TFTs. In general, ALD is still a good method to deposit a dielectric layer because of its high degree of quality and thickness control.

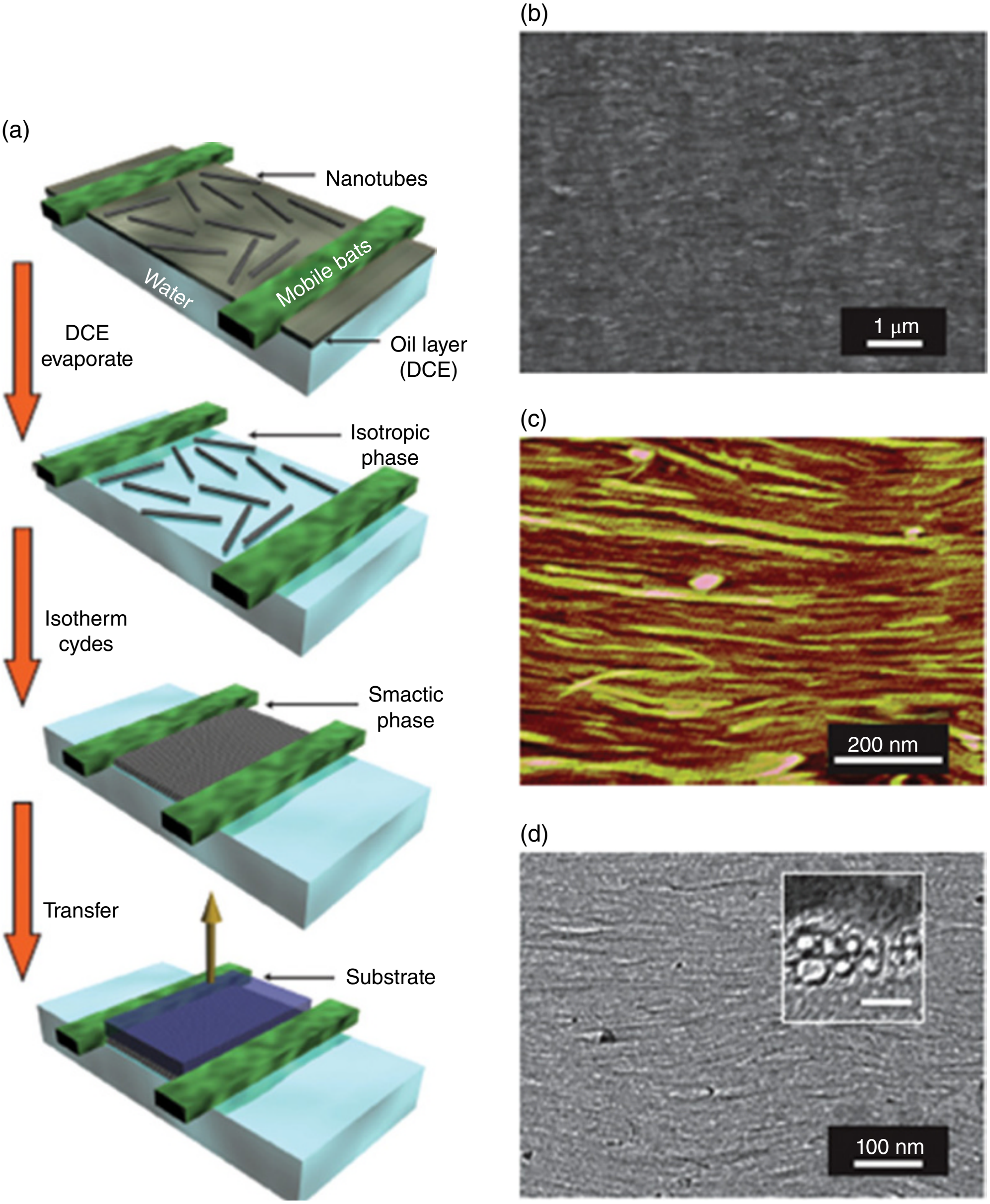
(a)
Nanotubes
Water
Mobile bats
DCE evaporate
Oil layer (DCE)
Isotropic phase
Isotherm cydes
Smactic phase
Transfer
Substrate
(b)
1 μm
(c)
200 nm
(d)
100 nm

Figure 5.26 Assembly and microscopic characterizations of full-coverage aligned arrays of SWCNTs. (a) Schematic illustration of the Langmuir–Schaefer assembly process. SEM (b), AFM (c) and top-view TEM (d) images of aligned nanotube arrays transferred onto solid substrates. Inset to (d): high-resolution cross-sectional TEM image (scale bar, 5 nm). (Reprinted from [36] with permission from Nature publishing group)

5.4.3.3.3 Spin Coating or Dip Coating

Spin coating is simple and some groups have investigated the electrical properties of spin-coated PVP and HAD thin films as dielectric layers. The structures of PVP and HAD are illustrated in Figure 5.27. Good performances of both organic and inorganic TFTs have been demonstrated using PVP and HAD as dielectric layers. Figure 5.28 displays the electrical characteristics of TFTs based on pentacene, FCuPc, semiconducting SWCNTs (sc-SWCNTs) and other semiconductor materials, all of which show low operating voltage and high on/off ratios [37], confirming PVP and HAD as the high-performance dielectric inks for printed TFTs.

Dip coating is another simple technique to prepare thin films, which is often used to coat sol-gel-type dielectric materials. A dip coating process can be performed in five stages: immersion, stir up, deposition, pulling and evaporation. In order to obtain a homogeneous coating, the viscosity of sol-gel should be controlled in the range of 2–5×10^{-2}P; at the same time, the pulling speed should be in the range of 1–20 cm min^{-1}. The film thickness depends on the concentration and viscosity of sol-gel and pulling speed.

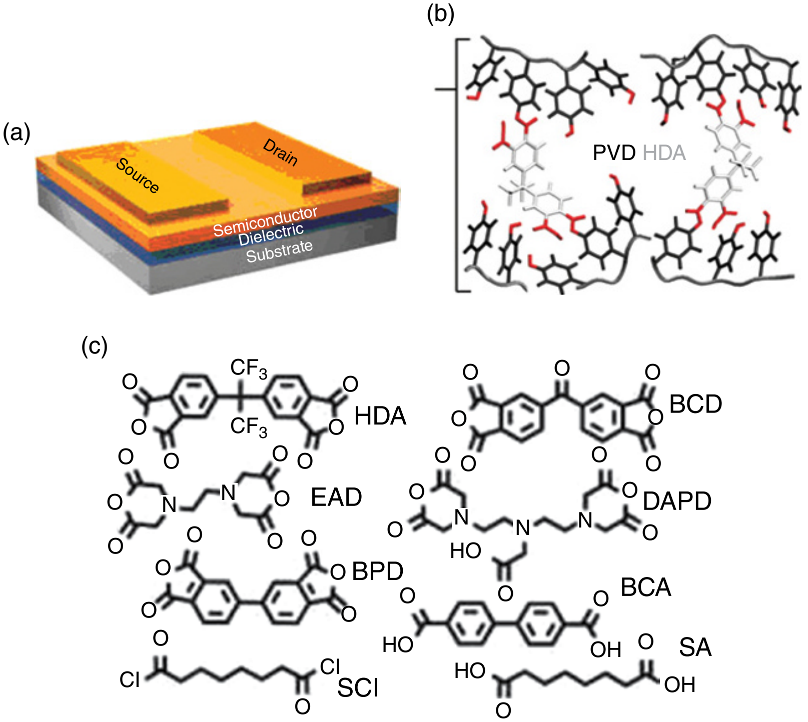

Figure 5.27 Schematic of an organic thin-film transistor (a) with the molecular structure of the cross-linked PVP with HDA (b). The molecular structure of a variety or dianhydrides and bifunctional carboxylic acids and acylchlorides (c). (Reprinted from [37] with permission from American Chemistry Society)

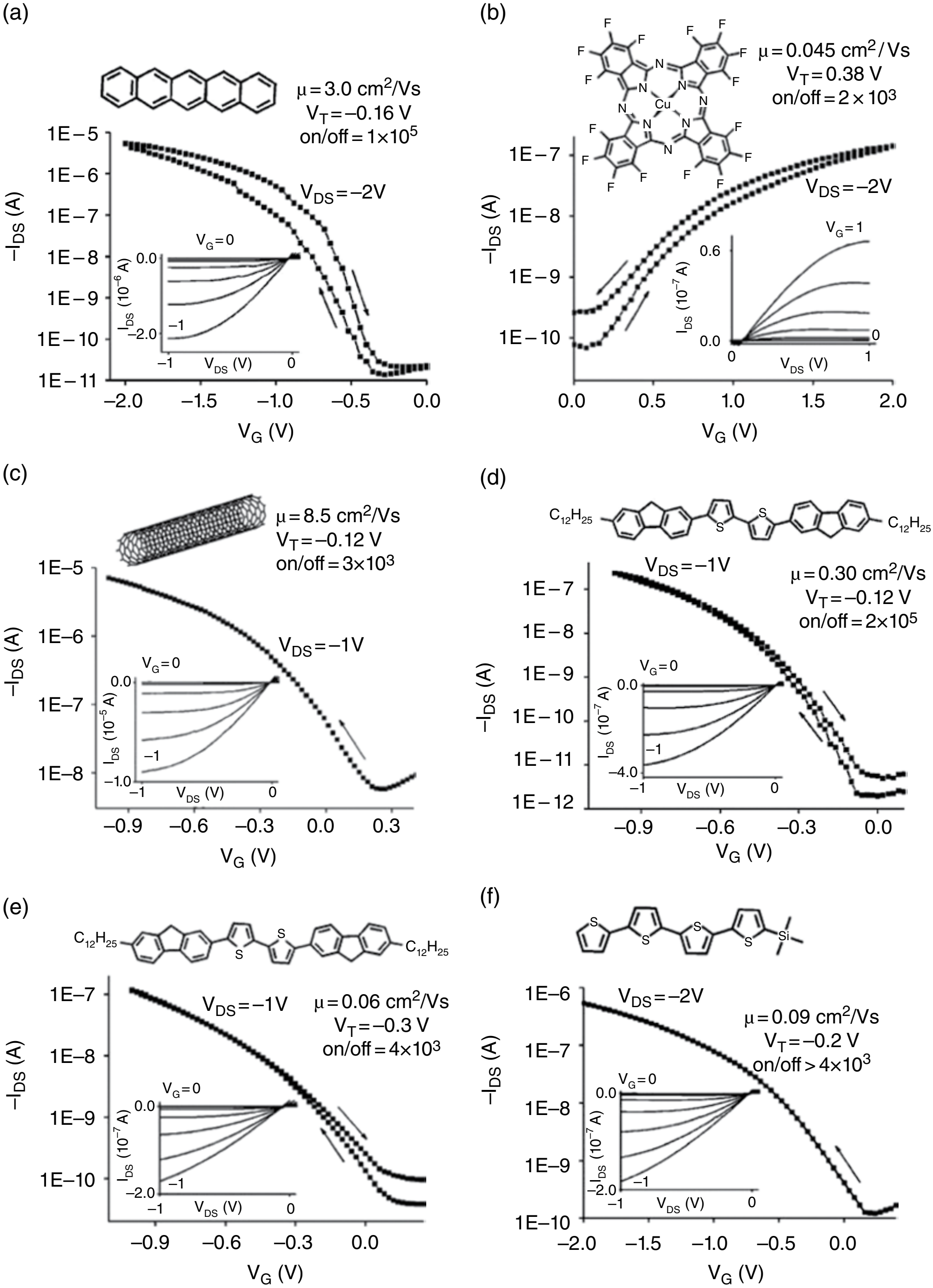

Figure 5.28 Transfer and output (inset) characteristics of thin-film transistors with PVP–HDA as the dielectric layer for pentacene (a), FCuPc (b), sorted SWCNT networks (c), DDFTTF (d), DDFTTF on PET/ITO substrates (e), and solution-processed TTMS (f). (Reprinted from [37] with permission from American Chemistry Society)

5.4.3.3.4 Magnetron Sputtering

Magnetron sputtering deposition is a physical deposition of thin films. In the magnetron sputtering process, a target plate is bombarded by energetic ions to free target atoms, which then deposit on a substrate as a thin film. Ta_2O_5 can be deposited by DC magnetron sputtering as a dielectric layer at room temperature with a high-purity Ta as target material under an argon/oxygen atmosphere.

5.4.3.3.5 Self-assembly

Self-assembly of a monolayer on top of a dielectric layer can improve its dielectric property and enhance the performance of a TFT. Phosphonates and silane have been used to modify metal oxides and silicon dioxide substrates and electrical properties of both inorganic and organic TFTs were significantly improved [38]. Acton et al. reported that TFTs showed low operating voltage (1–2 V), high on/off ratio ($>10^5$), small hysteresis and low subthreshold swing (60 mV/dec) after modification with a monolayer on substrate surfaces [39].

5.4.3.3.6 Printing

Solution-type dielectric materials can be deposited by printing, as is done for electrode and active layers. The printing processes can be inkjet printing, aerosol jet printing, screen printing, gravure printing and transfer printing. There has been some work demonstrating the fabrication of dielectric layers by aerosol jet printing of ion gel [4] and other work has demonstrated roll-to-roll printing of (PMMA/$BaTiO_3$ hybrid dielectric materials [24]. It is reported that transfer printing of PDMS is another method to make the dielectric layer [40].

5.5 Fully Printed TFTs

As described previously, electrodes, a dielectric layer and an active layer can all be fabricated by printing techniques. TFTs by inkjet printing (including aerosol jet printing), roll-to-roll gravure printing, and transfer printing have been reported [4, 24, 41]. However, making TFTs entirely by printing is still in its early stage of development. It is far from mature enough to be an industrial technology. In order for the printed TFTs to be useful for simple logic circuits or other electronic applications, they need to be further improved by developing new materials and optimized printing methods. This section describes some of the major issues related to fully printed TFTs.

5.5.1 Printability of Electronic Materials

To achieve fully printed TFTs, conductive materials, dielectric materials and semiconducting materials should all be soluble, printable and stable. Preparations of printable inks including conductive inks, dielectric inks and semiconductor inks are the first step towards fully printed TFTs. The processes for making printable organic and inorganic electronic inks have been introduced in Chapters 2 and 3 of this book. In this section, the printability issue is explained by the example of sc-SWCNT ink and printed TFTs.

It has been demonstrated that sc-SWCNT with a large diameter is one of the most ideal semiconductor materials for TFTs. Although there are several commercial SWCNTs, the as-synthesized SWCNTs are not suitable for thin film transistors because of the undesired presence of metallic nanotubes mixed with semiconducting nanotubes. In order to overcome this issue, various approaches to selectively remove or eliminate metallic species in commercial SWCNTs have been investigated, including dielectrophoresis; selective oxidation; aromatic extraction; surfactant extraction; amine extraction; surface alignment; removal of nanotube bundles; selective polymer wrapping; gel chromatography; selective chemical functionalization; density gradient ultracentrifugation (DGU); and the cycloadditive method, as has been described in Chapter 3.

Different kinds of printable SWCNT inks can be obtained by tuning types of solvent and viscosity of sorted sc-SWCNTs or purified sc-SWCNTs solution. For example, SWCNTs were dispersed well in DMF with the aid of sonication. After centrifugation, as-prepared SWCNT inks can be directly used to fabricate SWCNT TFTs by inkjet printing and aerosol jet printing. As DMF is toxic, many groups focus on developing water-based or low-toxic solvent-based SWCNT inks. At the authors' Printable Electronic Research Center, several water-based and solvent-based high performance printable sc-SWCNT inks have been developed. Printed TFTs have been realized and applied to make inverters and OLED driving circuits, all of which showed excellent properties.

Although some polymers and inorganic materials show very low solubility in organic solvents and water, their precursors or oligomers can dissolve well in some solvents or water. These kinds of solutions can also be used as printable electronic inks to fabricate electronic devices because the precursors or oligomers can be converted to target compounds by annealing, IR or UV irradiation or other treatments. For example, oligomers of PMMA thin films are firstly deposited by spin coating or printing, and then cross-linked PMMA can be obtained after UV irradiation. The PMMA thin films show good dielectric property.

Though most electronic materials disperse well in some solvents with the aid of appropriate physical and chemical treatments, not all solutions or suspensions can meet the printing requirements. Moreover, film-forming ability and impurities in thin films also affect the electrical properties of printed TFTs. The preparation of high quality printable electronic inks is still a main challenge to fabricating high performance fully printed TFTs.

5.5.2 Influence of Surface Morphology

Surface morphology of electrodes, active layers and dielectric layers, such as roughness, uniformity and continuity, is closely related to the electrical properties of printed TFTs. Figure 5.29 shows the morphologies of active layer for a group of TFTs, which were deposited by spin coating, inkjet printing, and brush painting. The organic semiconductor ink was core-expanded naphthalene diimide fused with 2-(1,3-dithiol-2-ylidene) malonitrile groups (NDI2ODDTYM2) [19]. The bottom-gate TFTs by spin coating and brush painting exhibited high electron mobility of 0.25-0.5 $cm^2V^{-1}s^{-1}$. However, Inkjet-printed devices with the same dielectric, substrate, and source/drain electrodes showed lower mobility (0.08-0.30 $cm^2V^{-1}s^{-1}$). This was probably due to the rough surface of thin film created by inkjet printing [19].

5.5.3 Interface Effect of Printed TFTs

As shown in Figure 5.30, four interfaces are encountered in a printed TFT: interfaces between semiconductor and electrode (interface 1); between semiconductor and semiconductor if the

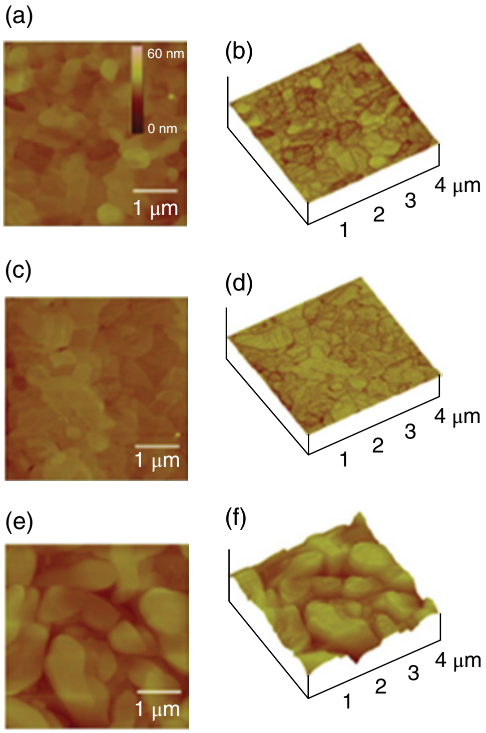
(a)
60 nm
0 nm
1 μm
(b)
1
2
3
4 μm
(c)
1 μm
(d)
1
2
3
4 μm
(e)
1 μm
(f)
1
2
3
4 μm

Figure 5.29 AFM images of NDI2OD-DTYM2 films by different solution processes. (a) Top view and (b) surface plot of thin film deposited by spin coating. (c) Top view and (d) surface plot of thin film deposited by brush painting. (e) Top view and (f) surface plot of thin film deposited by inkjet-printing. (Reprinted from [19] with permission from John Wiley & Sons Singapore Pte Ltd)

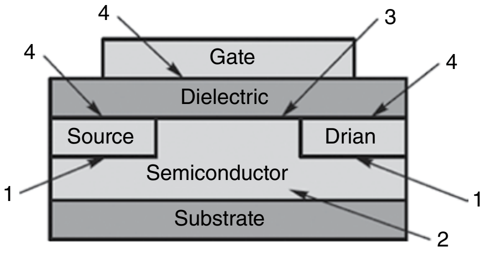
4
4
3
4
Gate
Dielectric
Source
Drian
Semiconductor
Substrate
1
1
2

Figure 5.30 A diagram of 4 interfaces in TFTs. 1–4 represent the semiconductor–electrode (interface 1), semiconductor–semiconductor (interface 2), semiconductor–dielectric (interface 3), and dielectric–electrode (interface 4)

semiconductor layer is made of individual sc-SWCNTs (interface 2); between semiconductor and dielectric (interface 3); and between dielectric and electrode (interface 4). The properties of these interfaces have decisive effects on the electrical properties of printed TFTs. For example, if the surface energies of the gate electrode and the dielectric layer do not match, the contact between these layers will be poor, resulting in poor control of charge transport, and usually a high gate voltage is required. The surface energy of the dielectric layer can be significantly reduced by treatment of oxygen plasma, which improves the binding force between electrodes and dielectric layers [42]. The interface properties of electrode/semiconductor, semiconductor/semiconductor and semiconductor/dielectric are even more important because carrier injection and carrier transportation take place at these three interfaces. They are discussed in detail below.

5.5.3.1 Effect of Semiconductor/Dielectric Interface

Accumulation and transportation of carriers take place at the interface of semiconductor/dielectric and in the region of the semiconductor adjacent to the dielectric layer. It has a key role in electrical properties of TFTs, such as operating voltage, hysteresis, mobility and on/off ratio. If there are defects and carrier trapping states at the interfaces of semiconductor/dielectric, these will lead to the degradation of charge transport in the TFT. Defects and carrier trapping states can be effectively eliminated by surface functionalization. In the case of a printed SWCNT TFT, the functionalization of a silicon dioxide substrate surface by APTES, OTS, CTS and BTS silane cross-linkers or simply putting the substrate in vacuum oven at 200 °C for 2 h could significantly improve the binding of SWCNTs with the substrate and reduce the charge trapping states. Furthermore, APTES-functionalized substrates can help to form aligned SWCNT thin film and improve the mobility and on/off ratio of SWCNT TFTs. The result is shown in Figure 5.31, where SWCNT TFTs fabricated on APTES-functionalized silicon dioxide substrates have high on/off ratio and mobility [43].

It has been reported by the authors' Printable Electronics Research Center that the wettability properties of dielectric layers are also important to TFTs [44]. Figure 5.32 illustrates the typical AFM images of SWCNT thin film on substrates with different treatments. The density

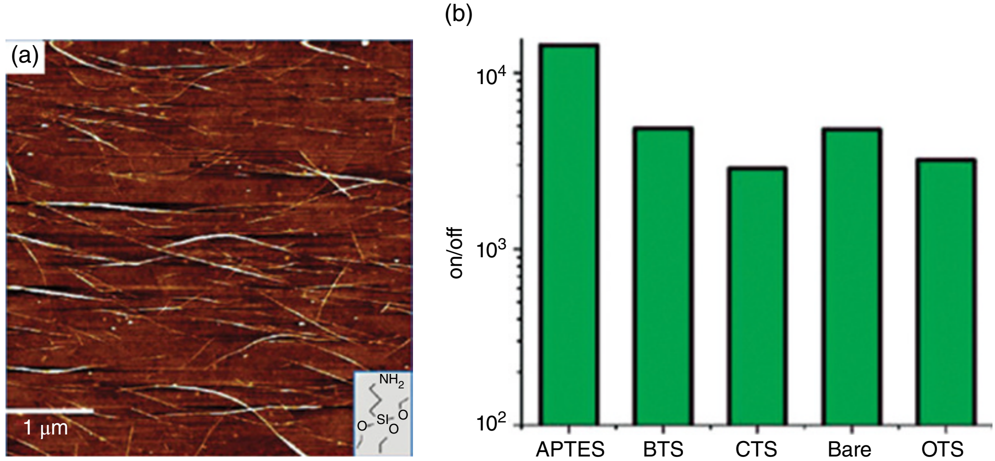

Figure 5.31 (a) AFM images of SWCNTs on amine-functionalized substrates and (b) Histogram of on/off ratio of SWCNT TFTs fabricated on different molecular functionalized substrates. (Reprinted from [43] with permission from American Chemistry Society)

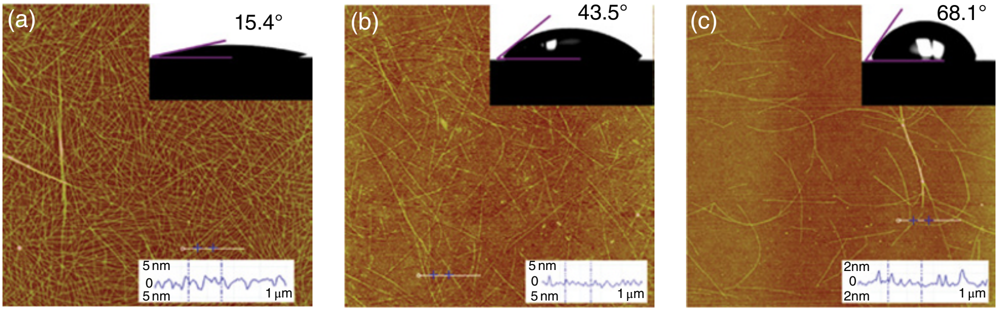

Figure 5.32 Typical AFM image of sorted SWCNTs in the device channels with different treatments. a) oxygen plasma treatment for 1 min, b) without any treatment, and c) annealing at 200°C for 1 h. (Reprinted from [44] with permission from American Chemistry Society)

of SWCNTs in the channels depends on the hydrophilic/hydrophobic property of the substrates. Oxygen plasma treated substrates resulted in higher density of SWCNTs. It is estimated to be about 35, 8, and 3 SWCNTs per μm^2 for oxygen plasma treated, untreated and annealed substrates, respectively.

Surface modification is also one of the commonly used methods to improve the electrical properties of organic TFTs. For example, when dielectric layers are modified by Octadecyltrichlorosilane (OTS), the mobility of OTFTs based on pentacene can increase from 0.02 to 1.03 and 0.63 $cm^2V^{-1}s^{-1}$, respectively [45]. This is due to the change of morphology of pentacene after modification with PhTMs and OTS. The sizes of pentacene crystal grain have been observed to change from 170 nm to 380 nm when substrates are modified with OTS. The density of grain boundary and trapping density decreases with the increase of grain size, resulting in better carrier transportation in the channel. Generally, modification or functionalization of dielectric layers by self-assembly or treated by oxygen plasma can effectively eliminate or decrease carrier trapping states at the interfaces for printed organic and inorganic TFTs.

5.5.3.2 Effect of Semiconductor/Semiconductor Interface

For SWCNT-based TFTs, each carbon nanotube is an individual semiconductor. When dispersed in an ink, tube-to-tube junctions create the semiconductor/semiconductor interface. In order to prepare printable SWCNT inks, surfactants, polymers and other additives have to be added to increase the solubility and stability of SWCNTs. However, all of them can reduce the mobility of printed TFTs due to the increase of tube-to-tube junction resistance. Therefore, it is always necessary to have a moderate post-processing to reduce tube-to-tube junction resistance. The authors' Printable Electronics Research Center reported that PDMS (Dow Corning® 3140) could significantly improve the electrical properties of SWCNT TFTs [46]. Figure 5.33 shows the typical transfer curves of SWCNT TFTs before and after PDMS coating. The silicon dioxide nanoparticles in PDMS neutralizes the surfactants in SWCNT thin film, which reduces the tube-to-tube junction resistance. As a result, the mobility of SWCNT TFTs increases by three to four times and hysteresis is also reduced. For OTFTs, there are interfaces between organic crystal grains. Aligned and large-size organic crystal grains always have

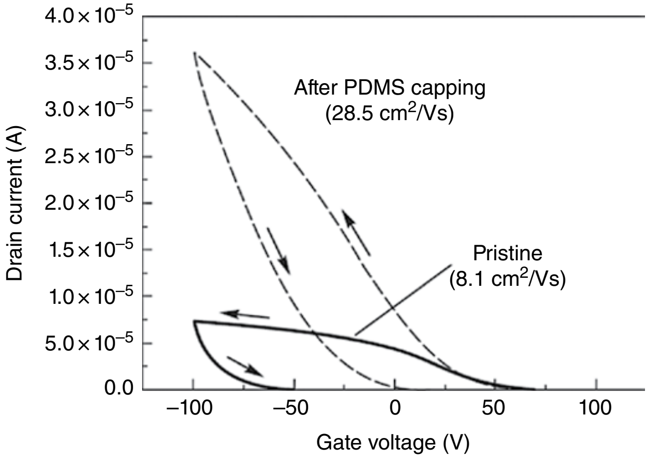

Figure 5.33 Typical transfer curves of SWCNT TFTs before and after PDMS coating. (Reprinted from [46] with permission from American Chemistry Society)

higher mobility than those of disordered and small-size organic crystal grains, because the former has lower density of grain boundaries and fewer defects.

5.5.3.3 Effect of Semiconductor/Electrode Interface

There is always an energy barrier, called the Schottky barrier, when a metal is in contact with a semiconductor, which is the result of difference between the work functions of metal and the electron affinity of semiconductor. Generally, Schottky barriers show rectifying characteristics, that is, electrons only flow in one direction. When the Schottky barrier is very low, the metal-semiconductor contact is called ohmic contact where electronics can flow easily in both directions between the semiconductor and metal. A Schottky barrier is undesirable in a TFT because it reduces the efficiency of charge injection from electrode to semiconductor. Electrical performance of TFTs can be significantly enhanced when the contacts between metals and semiconductors are ohmic contacts.

In organic TFTs, the flow of charge carriers is a process of electron injection to the LUMO level and hole injection to the HOMO level of an organic semiconductor. To facilitate the process, two different types of metal electrodes are needed as charge injection electrodes. For n-type TFTs, low work function materials (Al, Ca) are used as the electrodes. For p-type TFTs, high work function materials (Au, Cu, Cr, CNT, graphene and ITO) are used as the electrodes.

The work function of metal electrodes can be tuned by doping or surface modification. For example, the mobility of a TFT can increase from 0.2 to 0.55 $cm^2V^{-1}s^{-1}$ when its gold electrodes are modified by pentafluorobenzene thiol (PFBT), changing the work function of gold electrode from 5.1 to 4.77 eV [19]. The modification also increased the grain size of organic crystals (NDI2OD–DTYM2) as shown in Figure 5.34. For inorganic TFTs, electrode modification is also helpful. For example, it has been demonstrated that the performance of SWCNT TFTs can be enhanced by modifying a gold electrode with self-assembled thiol to reduce its work function [19].

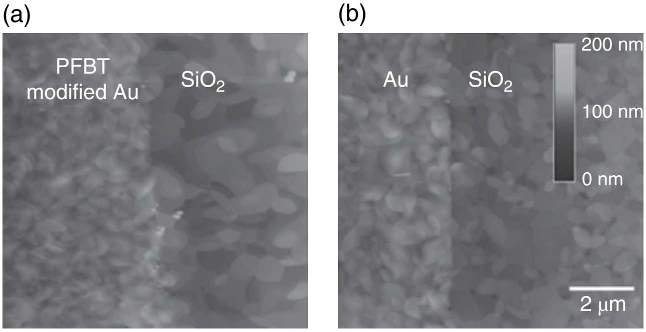

Figure 5.34 AFM images of NDI2OD–DTYM2 thin film by a solution process. (a) Devices using PFBT modified gold electrodes as source/drain electrodes and (b) devices using bare gold electrodes as source/drain electrodes (Reprinted from [19] with permission from John Wiley & Sons Singapore Pte Ltd)

5.5.4 Effect of Channel Length

Channel length (L), as defined in Figure 5.4, is an important parameter of TFTs. The operating frequency of TFTs is proportional to $1/L^2$. Short channels are favorable not only for high frequency applications but also for high-density integration. However, the channel length is not "the shorter the better". When the channel length is in the same dimension as the depletion-layer width of source and drain junction, the vertical electrical field generated by gate voltage can no longer control the charge flow in the channel, no matter how high the voltage. The TFT can no longer establish an off state by gate voltage. This is the so-called short-channel effect. It has been demonstrated that the ratio of channel length to dielectric layer thickness should be more than 10 in order to suppress or eliminate the short-channel effects, in other words, the vertical electric field should be at least 10 times higher than the lateral electric field [47]. Therefore, in order to reduce the channel length, the thickness of dielectric layer should also be reduced. On the other hand, if the channel is too long the lateral electric field along the channel will not be high enough and the carrier drift velocities will not reach their saturation levels. Printed TFTs generally belong to long-channel devices due to the current low-resolution printing techniques. The short-channel effect is not observed in printed TFTs.

For TFTs made by printing SWCNT inks, the channel length can dramatically affect the mobility and on/off ratio, particularly in the presence of metallic species in the ink. Wang et al. found that mobility of printed TFTS with 95% sc-SWCNTs ink decreased when increasing the channel length, whereas the mobility of TFTs with in-situ directly CVD grown SWCNTs increases as the channel length increases [48]. The reason for the difference is related to the length of SWCNTs. In the sc-SWCNT ink the sc-SWCNT length is in the range of 1–2 μm, so the TFT mobility depends on the percolative transport through SWCNT networks. As the channel length increases, more tube-to-tube junctions are introduced into the conduction path, leading to a decrease in the mobility of the TFT. For the directly grown SWCNTs that are a mixture of semiconducting and metallic carbon nanotubes and have much longer length (more than 20 μm), short channel normally results in low on/off ratio because the inevitable existence of metallic nanotubes in the ink easily forms a conductive path that deteriorates the off state, as the simulation and experiments in Figure 5.35 show, where separated nanotubes are high

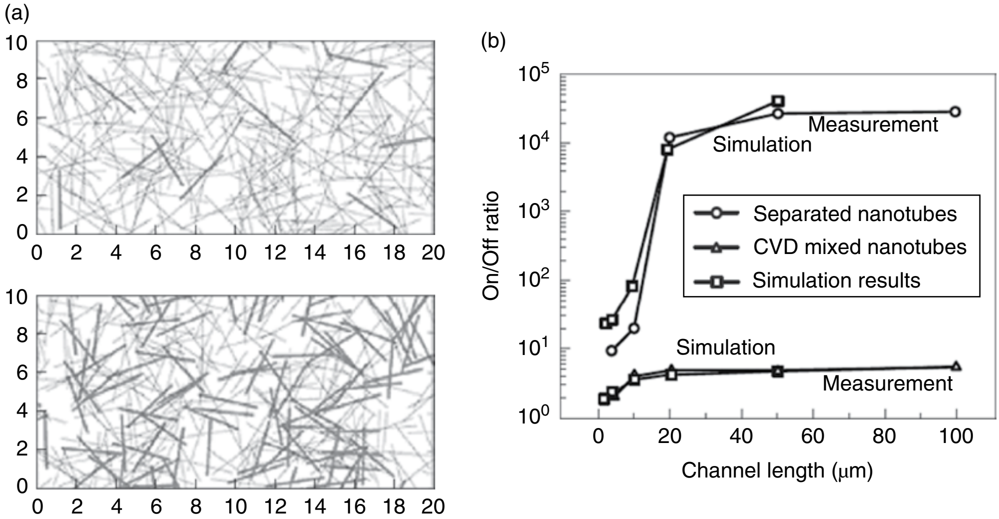

Figure 5.35 Simulation of nanotube thin-film percolation network. (a) Randomly generated nanotube percolation networks of separated nanotubes (top) and mixed nanotubes (bottom) for devices with L=10 μm and W=20 μm. The dark and light lines represent metallic and semiconducting nanotubes, respectively. (b) Comparison between the simulation data derived from the percolation network and measurement data (Reprinted from [48] with permission from American Chemistry Society)

purity semiconducting nanotubes and mixed nanotubes are the mixture of semiconducting and metallic carbon nanotubes. For a longer channel, the influence of metallic nanotubes becomes less dominant. Using longer and high purity SWCNTs as well as removing the impurities can significantly improve the electrical properties of printed SWCNT TFTs.

5.5.5 *Summary of Issues in Printing TFTs*

Printed TFTs have a long way to go before becoming mature and usable in practical electronic circuits. Printing as a manufacturing technique is inherently inferior to a conventional microfabrication process in terms of resolution, accuracy, structure complexity and quality. As a consequence, the performances of TFTs made by printing are impossible to match those made by conventional processes at present. In order to catch up, further research and development in ink materials, printing processes and structural optimization are needed. Some of the major issues related to improvement of printed TFTs are summarized in the following.

5.5.5.1 Printable Inks and Printing Processes

The performance of printed TFTs is largely dependent on the intrinsic electrical properties of materials and properties of printable inks. Once a good electronic material is selected, developing stable and printable ink to keep its intrinsic properties to the maximum becomes the key factor. For example, in order to formulate an ink, surfactants, solvents or carrier liquids are always required. Sonication or ball milling is sometimes needed to help to achieve better dispersion of nanomaterials-based electronic inks. Generally, film quality becomes better with increasing amount of additives in printable inks. However, these additives are hazardous to charge transport, which have to be removed in various post-process steps, such as post-printing washing, annealing, etc. The contradictory aims of good dispersion in inks and good electrical properties in printed TFTs need to be balanced carefully.

The properties of thin films are also affected by the preparation methods. Large-area homogeneous thin films are easier to obtain by spin coating than by inkjet printing due to fast evaporation of solvent. Inkjet printing of organic small molecular TFTs showed poor electrical properties due to the formation of poor crystalline of compounds. Other techniques have been developed to ratify the problem. For example, by designing special channel structures inkjet printed organic ink can form crystals preferentially along the channel [49].

5.5.5.2 Printed Electrodes

Unlike sputtering deposited or thermal evaporation deposited electrodes, printed electrodes are easily peeled off when rinsing with water or solvents or during annealing process, which is a major cause of failures for printed TFTs. Substrate surface modification, ink modification with adhesive components and optimized annealing are among the methods which have been employed to improve the binding between electrodes and substrates. Poor printing resolution is another problem that makes it difficult to print small electrodes with high accuracy. Recently, electrohydrodynamic jet printing has been developed which can print much finer features than conventional inkjet printing [50, 51]. Another new hybrid printing technique has been developed at the Authors' Printable Electronics Research Center, which combines nanoimprinting with embedded silver nanoparticles ink and has achieved fine resolution of conductive patterns while at the same time improving the adhesion of conductive material to substrate [52]. Chapter 4 of this book provides further information about printing technology.

5.5.5.3 Printed Dielectric Thin Films

High performance printed dielectric is also important for fully printed TFTs. Using high-k and ultra-thin dielectric layers is crucial to reduce the operating voltage of printed TFTs. Ion gel is regarded as one of the most important printable dielectric inks. For example, printed TFTs using a high capacitance ion gel as a dielectric layer showed high on current, low operation voltage and small hysteresis [4, 41, 52]. However, ion gel can diffuse into the active layer of TFTs, which can destroy the TFTs. The device capacitance is related to the thickness of dielectric layers and dielectric constants. Currently, there are some printable organic dielectric inks, but the printed layer is too thick and the dielectric constant is low. In addition, solvents in organic dielectric inks are likely to dissolve the active layer. Although inorganic dielectric materials have a high dielectric constant and low leakage currents, good printable inorganic inks have rarely been reported due to their instability of dispersion and poor quality of printed films.

5.6 Advances in Printed TFTs

With the advance in new materials and printing technologies, some novel and high performance printed TFTs have been achieved. In this section, some novel printed TFTs are introduced, including printed inorganic (SWCNT TFTs, metal oxide TFTs, metal dichalcogenide and graphene TFTs) and OTFTs.

5.6.1 *Printed Inorganic TFTs*

5.6.1.1 SWCNT TFTs

The performances of printed or solution-processed sc-SWCNT TFTs, in particular with the use of polymer-sorted large diameter sc-SWCNTs inks and commercial high-purity sc-SWCNT inks, have been greatly improved in the last few years. Several groups, such as Zhou, Frisbie, Hersam and Javey et al., have reported considerable progress in printed SWCNT TFTs [53–66]. In particular, the authors' Printable Electronics Research Center recently reported printed SWCNT TFTs with mobility as high as 40 $cm^2V^{-1}s^{-1}$ and on/off ratio up to 10^7 [44, 67–69].

The key factor of the success is the highly efficient and high purity sorting of semiconducting SWCNTs. It is found that many polymers, such as P3DDT, PFO-BT, PFO-DBT, F8T2 and other polymer derivates, have the ability to selectively sort large-diameter sc-SWCNTs from commercial arc discharge SWCNTs that contain a large proportion of metallic SWCNTs. As-prepared and sorted sc-SWCNT solutions can be directly used as inks to print TFTs by inkjet or aerosol jet printers and the printed TFTs displayed excellent electrical properties, as shown in Figure 5.36 [44, 67–69].

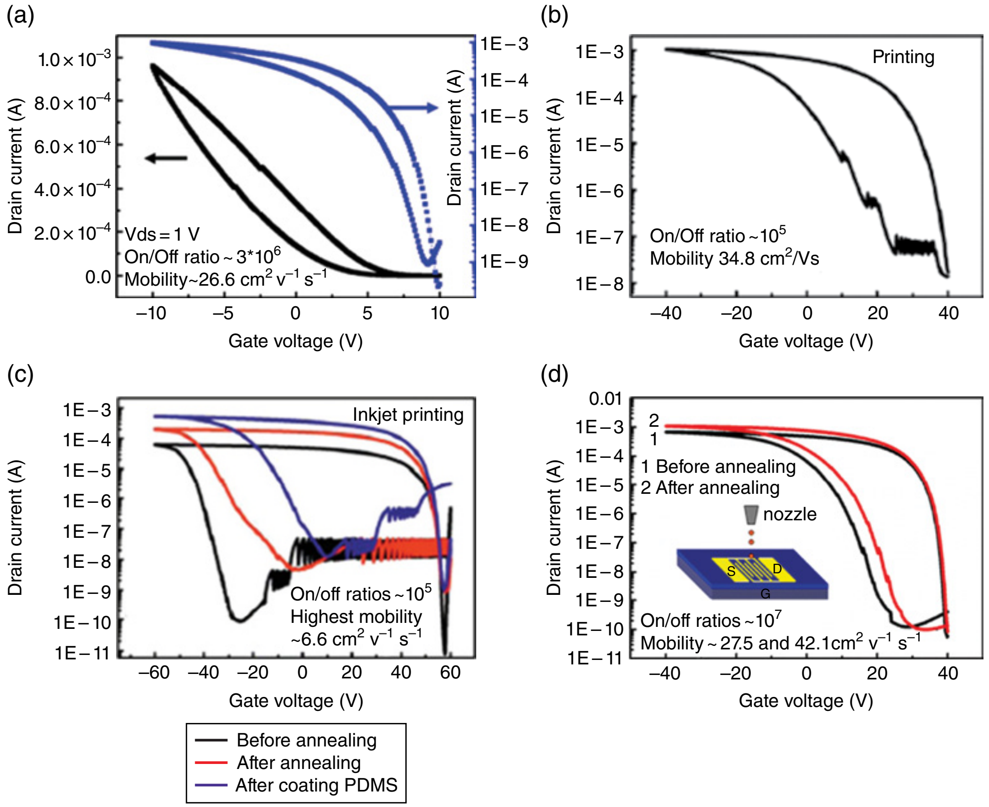

Figure 5.36 Typical transfer curves of printed TFTs based on sc-SWCNTs sorted by (a) PFO-BT, (b) PFO-BDT, (c) P3DDT and (d) F8T2 sorted sc-SWCNT TFTs. (Reprinted from reference [67, 68] with permission from The Royal Society of Chemistry); (reprinted from [44, 69] with permission from American Chemistry Society)

With these printed working TFTs, simple circuits such as inverters and oscillators have been constructed. Figure 5.37 illustrates the input–output and gain characteristics of printed inverters. The voltage gain of the printed inverter has reached 118 with a working frequency of 10 Hz [68]. Figure 5.38 shows printed ring oscillators based on printed amipolar transistors. The output frequency of ring oscillators has reached 25 kHz at V_{dd} of 2.6 V [70]. However, printed inverters and ring oscillators need to be encapsulated or measured in vacuum because n-type transistors are sensitive to water and oxygen.

5.6.1.2 Metal Oxide TFTs

The most prominent development in TFT technology is the emergence of metal oxide TFTs. Metal oxides are inexpensive, nontoxic and environmentally stable inorganic semiconductors. Most of the metal oxides, such as ZnO, In_2O_3, SnO_2, and their binary, ternary or quaternary metal oxides are n-type semiconductors, whereas most SWCNT TFTs and organic TFTs are p-types. Metal oxide TFTs are superior in performance as compared to other TFTs, with

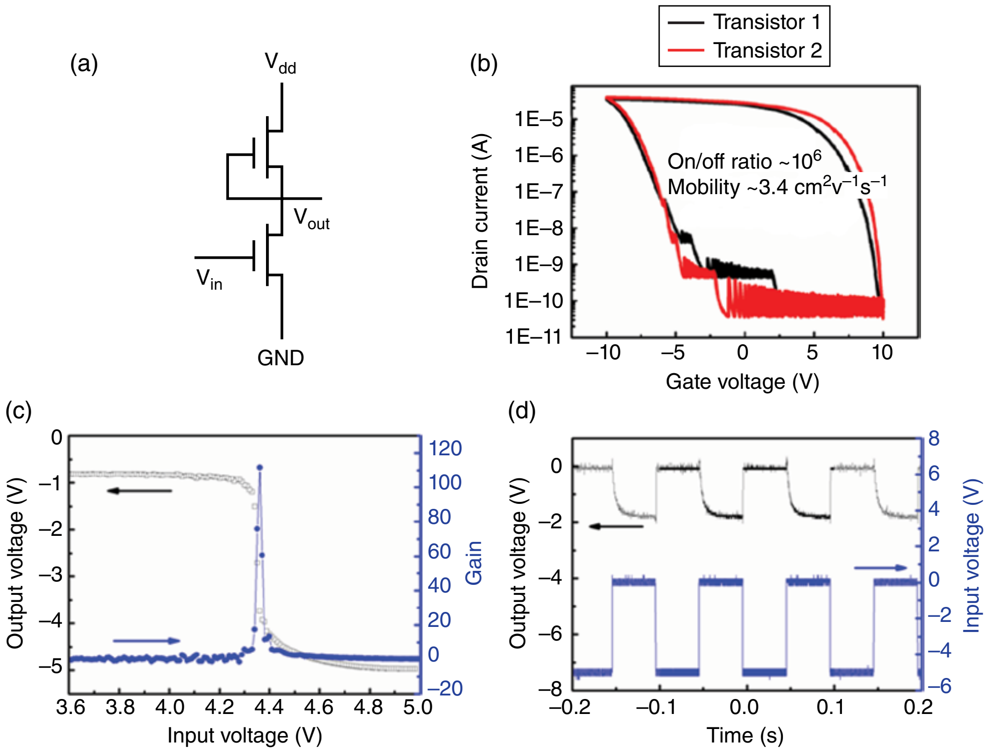

Figure 5.37 (a) The symbol of the inverter; (b) Transfer curves of two transistors in the inverter on glass substrates (Vds=2 V); (c) Input–output and gain characteristics of an inverter at V_{dd}=5 V. The value of gain is 112. (d) The input and output characteristics of a SWCNT inverter at 10 Hz. (Reprinted from [68] with permission from The Royal Society of Chemistry)

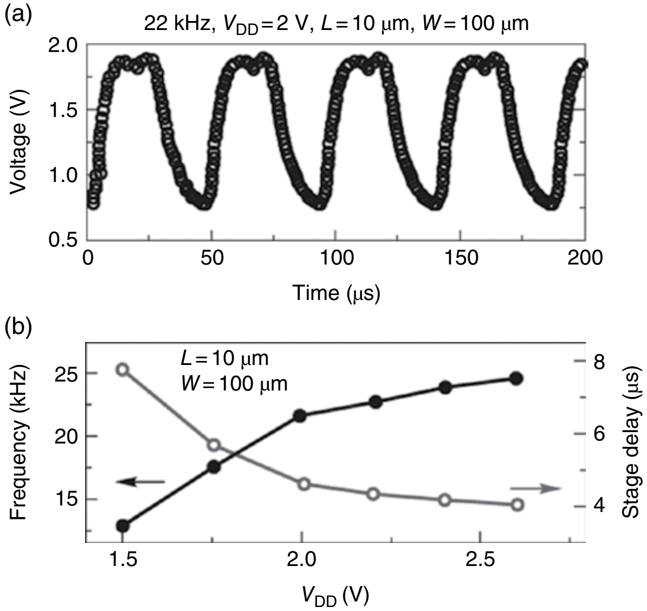

Figure 5.38 Printed five-stage SWCNT ring oscillators employing high capacitance ion gel gate dielectrics. (a) The output signal of a SWCNT ring oscillator with a frequency of 22 kHz and stage delays of 4.5 μs at V_{DD} = 2 V. The TFTs have a channel length of 10 μm, a channel width of 100 μm, and an ion gel dielectric with thickness of 1.2 μm. (b) Frequency and stage delay times of the ring oscillator as functions of supply voltage V_{DD} (Reprinted from reference [70] with permission from American Chemistry Society)

mobility up to 100cm^{2}V^{-1}s^{-1}, on/off ratio up to 10^9 and little or no hysteresis. However, the best performing metal oxide TFTs are made by vacuum sputtering of metal oxide thin film. Solution-processed or printed metal oxide TFTs lag far behind.

In general, solution-processed or printed n-type metal oxide TFTs can be made using either their nanoparticle solutions or oxide precursors. However, annealing at a high temperature (more than 300° C) is needed for the precursor-based method, which limits its application in flexible electronics. Some reported metal oxide materials, solution deposition methods and charge transport mobilities of their TFTs are listed in Table 5.1 [71].

Printed multi-component oxide TFTs can have mobility as high as 30 cm^{2}V^{-1}s^{-1} when the transistors are annealed at the temperatures of 500 to 600°C. At low annealing temperatures, the mobility decreases drastically. When using an electrochemical gate with a high-capacitor, TFTs based on metal oxide nanoparticles can be inkjet-printed at room temperature and show good performance with mobility around 1 cm^{2}V^{-1}s^{-1} and low operating voltages [71]. Developing printable and low temperature metal oxide inks will be an area of intensive research in the next few years. It is believed that the mobility of printed metal oxide TFTs will be improved and the processing temperature will be greatly decreased.

Table 5.1 Metal oxide TFTs, materials, solution deposition methods, process temperatures and mobilities

Transistor channel		Compound symbol	Processing method	T(°C)	$\mu(cm^2V^{-1}s^{-1})$	dielectric
Oxide precursors	Multi-components oxide	IZTO	Printed	600	30	SiO_2
		IZO	Spin coated	600	16.1	SiO_2
		IZO	Printed	600	7.4	SiO_2
		ZTO	Spin coated	500	28	SiO_2
		ZTO	Printed	500	1	SiO_2
		ZTO	Printed	500	0.5	SiO_2
		IZO	Spin coated	300	0.5	SiO_2
		IGZO	Spin coated	250	0.006	SiO_2
		IZO	Spin coated	200	0.03	SiO_2
		IZO	Spin coated	225	0.32	SiO_2
		ZTO	Spin coated	225	0.29	SiO_2
	Single-component oxides	In2O3	Spin coated	200	0.81	SiO_2
		ZnO	Spin coated	325	0.045	SiO_2
		ZnO	Printed	150	0.006	SiO_2
Oxide nano-particles		ZnO	Spin coated	150	0.008	SiO_2
		In2O3	Printed	25(RT)	0.8	SiO_2
		In2O3	Printed	25(RT)	0.26	SiO_2

5.6.1.3 Metal Dichalcogenide and Graphene TFTs

Two-dimensional (2D) materials, such as graphene and metal dichalcogenide (MoS_2, WS_2, and so on) have attracted increasing attention due to their high charge mobility (graphene ~200 000 $cm^2V^{-1}s^{-1}$), flexibility and stretchability, and excellent optical and mechanical properties. These 2D materials can be isolated by micromechanical exfoliation of corresponding bulk materials. For large-scale production there are CVD methods and liquid phase exfoliation processes. Among them, liquid phase exfoliation is suitable for making printable 2D inks. Layered materials such as graphite, MoS_2, WS_2, $MoSe_2$, $MoTe_2$, $TaSe_2$, $NbSe_2$, $NiTe_2$ and BN can be exfoliated by chemical wet dispersion followed by sonication in aqueous liquids or organic solvents. A monolayer or a few layers of 2D materials can be extracted after centrifugation. Some of the 2D materials have been explored for printable TFTs.

Li et al. and Orrisi et al. have demonstrated that graphene suspensions prepared by liquid phase exfoliation in DMF and N-methylpyrrolidone can serve as printable inks to make TFTs, as shown in Figure 5.39 [72]. Smooth, straight and long graphene lines around 80μm wide were achieved on both plastic substrates (Figure 5.39a) and silicon wafers (Figure 5.39d) by inkjet printing. The fabrication process was reliable and reproducible. However, the printed graphene TFTs showed very low on/off ratio (1.25) and low mobility ($0.12cm^2V^{-1}s^{-1}$). Orrisi also used graphene solutions to make printed TFTs and the mobility and on/off ratio of printed graphene TFTs were improved to 95 $cm^2V^{-1}s^{-1}$ and 10 after annealing at 170° C, as shown in Figure 5.40 [73].

Although pristine graphene has extremely high carrier mobility, the very low on/off ratio for graphene-based TFTs is because graphene is a semi-metal material with zero band gap. Thus,

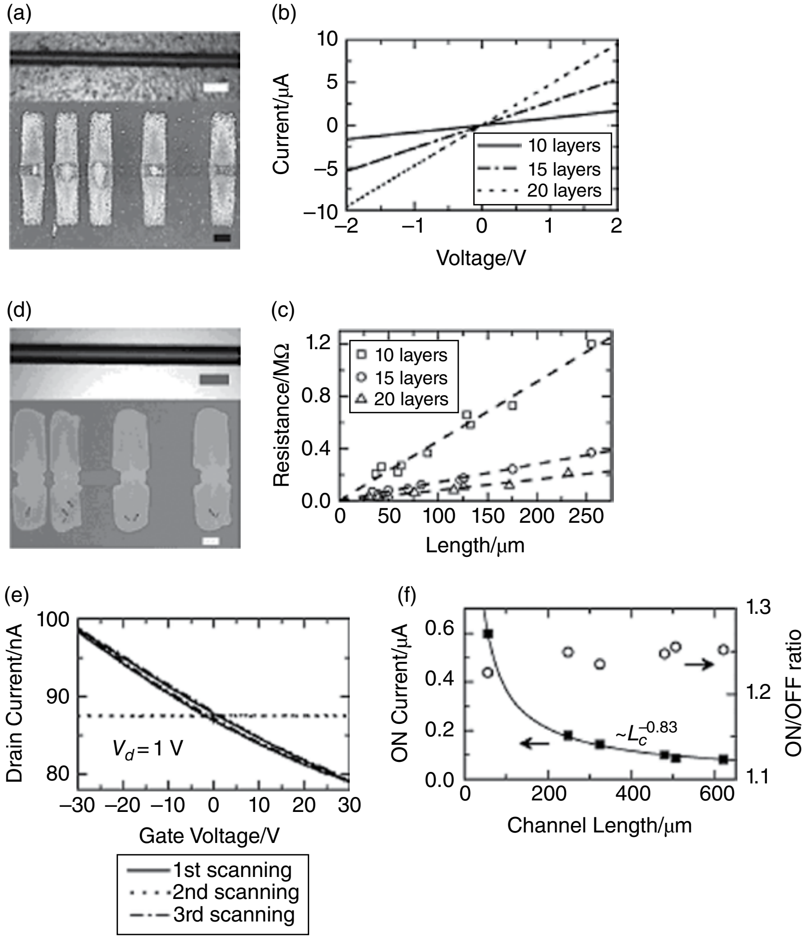

Figure 5.39 Inkjet printed graphene narrow-line resistors on Kapton and TFTs on Si wafer. (a) Optical images of as-printed 15-layers graphene lines (upper) and the final resistors with vertical silver electrodes on Kapton (lower). (b) Current-voltage curves of the printed line resistors of about 250μm long and with different printing layers. (c) Resistance versus length for resistors with different printing layers. (d) Optical images of as-printed six-layer graphene lines (upper) and the final TFTs with vertical silver source/drain electrodes on a silicon wafer (lower). (e) Transfer characteristics of a six-layer TFT with channel length about 480μm. For each scanning, gate voltage increases from -30 V to 30 V and then goes back to -30 V. For the second scanning, the gate cable is not connected. (f) Dependence of on current and on/off current ratio on channel length for six-layer graphene TFTs. All scale bars are 100μm. (Reprinted from [72] with permission from John Wiley & Sons Singapore Pte Ltd)

it is not suitable as an active material in TFTs. Currently, many groups have been trying to open the band gap by doping boron or nitrogen and organic molecules. Other 2D metal dichalcogenides are being pursued because they have similar properties as graphene but with a non-zero band gap. These 2D metal dichalcogenides, such as BN, MoS_2 and WS_2, can be extracted by liquid phase exfoliation methods [74]. TEM images of extracted 2D metal

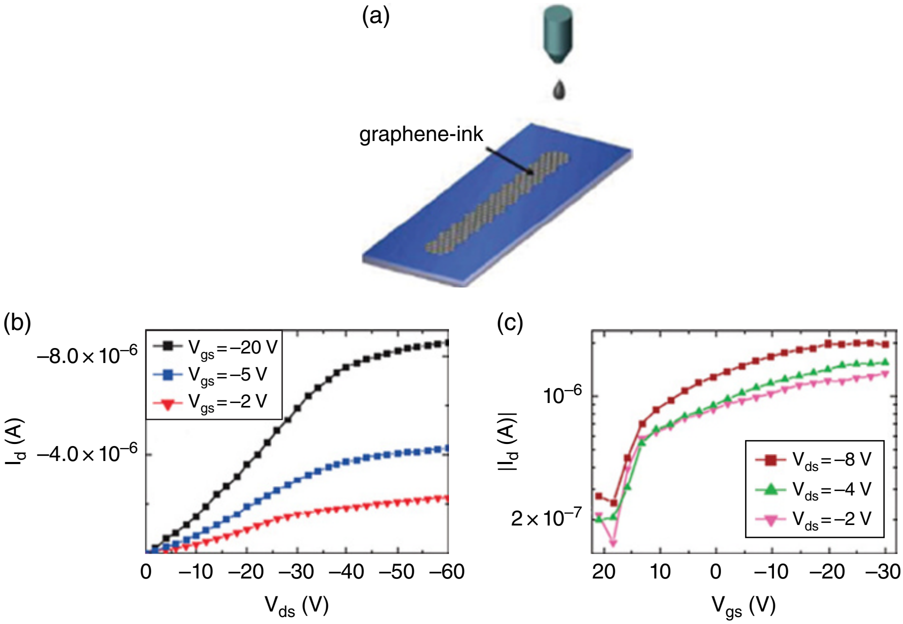

Figure 5.40 (a) Printed graphene thin films on Si/SiO_2; and (b) and (c) The typical electrical properties of a printed graphene transistor. (Reprinted from [73] with permission from American Chemistry Society)

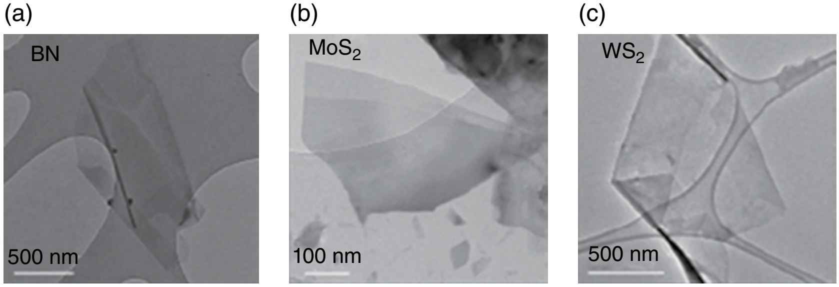

Figure 5.41 Low resolution TEM images of (a) BN, (b) MoS_2, and (c) WS_2, respectively. (Reprinted from [74] with permission from John Wiley & Sons Singapore Pte Ltd)

dichalcogenides nanosheets are shown in Figure 5.41. Generally, a pristine monolayer or few layers of 2D metal dichalcogenides show n-type characteristics with high mobility and a high on/off ratio, whereas solution-processed 2D metal dichalcogenides exhibit p-type conduction and low mobility due to defects generated during ink preparation.

Solution-processed WS_2 TFTs exhibit high mobility (electron and hole mobility up to ~20 and 90 $cm^2\ V^{-1}s^{-1}$) and high on/off ratios (~10^4) with ambipolar characteristics when using ion liquids as liquid gates. The TFT and its transfer curves are shown in Figure 5.42 [75]. It is interesting to note that the subthreshold slopes for both electrons and holes are very steep and off-state currents are extremely low. Figure 5.42 also reveals the width of the band gap of WS_2.

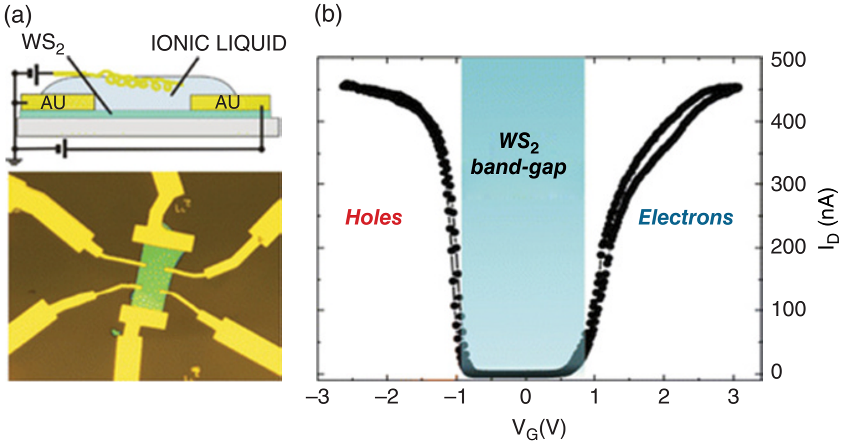

Figure 5.42 (a) Optical image, and (b) Transfer characteristics of a WS_2 ionic liquid-gated FET measured at Vd = 0.1 V. (Reprinted from [75] with permission from American Chemistry Society)

While the solution-processed WS_2 TFTs exhibit ambipolar characteristics, 2D metal dichalcogenides by micromechanical exfoliation always shows n-type conduction and much higher mobility and on/off ratio. TFTs made by a single sheet of MoS_2 show mobility as high as 1090 $cm^2V^{-1}s^{-1}$ and an on/off ratio of 10^7 [76]. TFTs made by a CVD grown bilayer MoS_2 were used to construct five-stage ring oscillators [77]. The ring oscillator worked at 1.6MHz, making them the suitable candidates for high-speed electronics.

5.6.2 Printed Organic TFTs

Although the mobility of OTFTs by solution process are generally in the range of 0.1–1 $cm^2V^{-1}s^{-1}$, organic semiconductors are still regarded as important semiconductor ink materials due to their solution processability and printability. There are two types of organic semiconductor materials: organic polymeric semiconductors and organic small-molecule semiconductors. Semiconducting polymers are suitable for spin coating or printing in solution form, whereas small molecule materials are usually deposited by thermal evaporation or vapor phase deposition. With the advances of new material formulations and printing technologies, both polymeric and small-molecule semiconductors can now be made into printable inks to fabricate OTFTs. Currently, various printing methods including aerosol jet printing, flexographic printing, gravure printing, screen printing, inkjet printing, have been developed to fabricate polymer and small-molecule OTFTs.

In 2009, Yan et al. reported high-performance n-type NDI2OD-T2 OTFTs via gravure printing. Mobility and on/off ratio were 0.85 $cm^2V^{-1}s^{-1}$ and 10^7 [78]. Figure 5.43 displays the morphologies of gravure printed thin films using semiconductor inks with different viscosities. It was evident that the crystal morphologies changed with the viscosity of inks. Figure 5.43b shows the AFM images of P(NDI2OD-T2) films by different printing methods on PET/Au substrates. Gravure-printed and spin-coated thin films showed fiber-like morphologies and are comparably smooth, leading to excellent properties of OTFTs (Figure 5.43c and d).

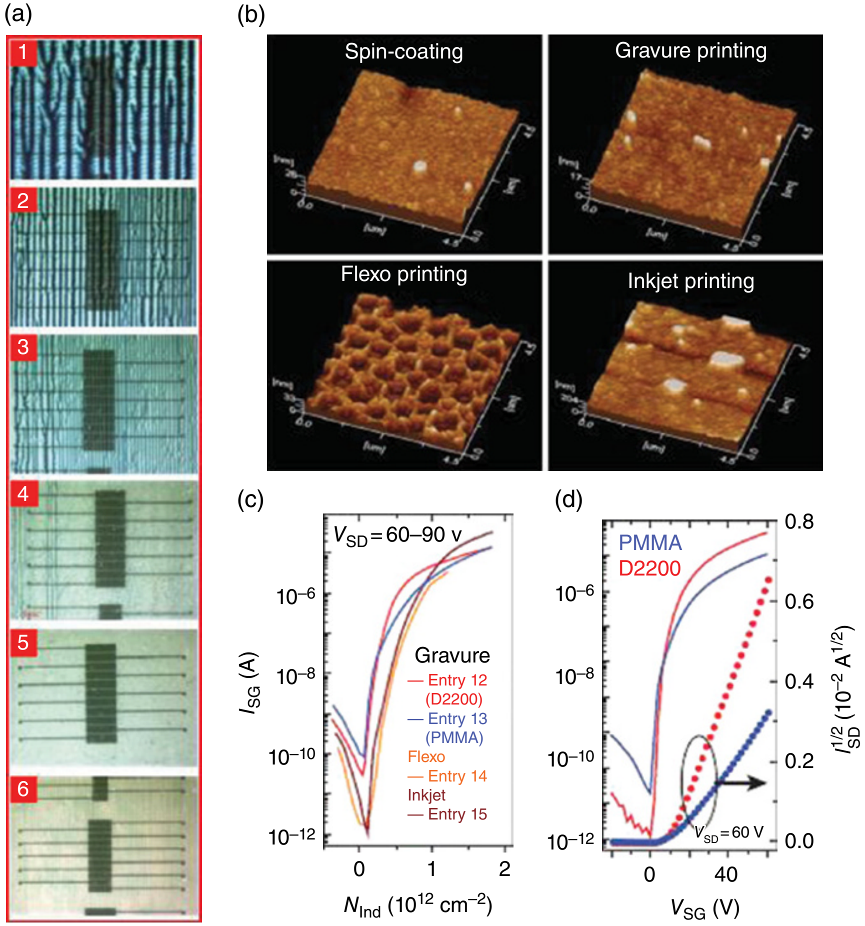

Figure 5.43 P(NDI2OD-T2) film morphologies and TGBC TFT performance using various solution-processing techniques on PET/Au substrates (L550 mm, W51 000 mm.) (a) Optical images of P(NDI2OD-T2) films with underlying Au source/drain contacts gravure-printed from a 2% w/w polymer DCB-CHCl3 50-50 v/v solution and using printing disks with decreasing gravure cell depth/volume ratio (depth D in mm, volume V in mlm22). The optimized film morphology corresponds to image 5. (b) Atomic force microscopy (AFM) images of spin-coated and printed films ("flexo" indicates "flexographic"). (c) Representative TFT transfer plots of current versus carrier density (Nind) of various gravure-, flexo-, and inkjet-printed TGBC devices. (d) TFT transfer plot of current versus VSG for representative TGBC TFTs with gravure-printed semiconductor and dielectric layers. (Reprinted from [78] with permission from Nature publishing group)

Organic small molecule semiconductors are normally not suitable for printing because they can quickly form crystals while being solution processed. However, it is undeniable that organic small molecule semiconductors are far better in terms of charge transport mobility than their polymeric counterparts. One of the hot research areas in recent years in organic semiconductors is to make organic small molecule semiconductors printable while maintaining their superior charge transport ability. In 2011, Minemawari et al. reported inkjet-printed

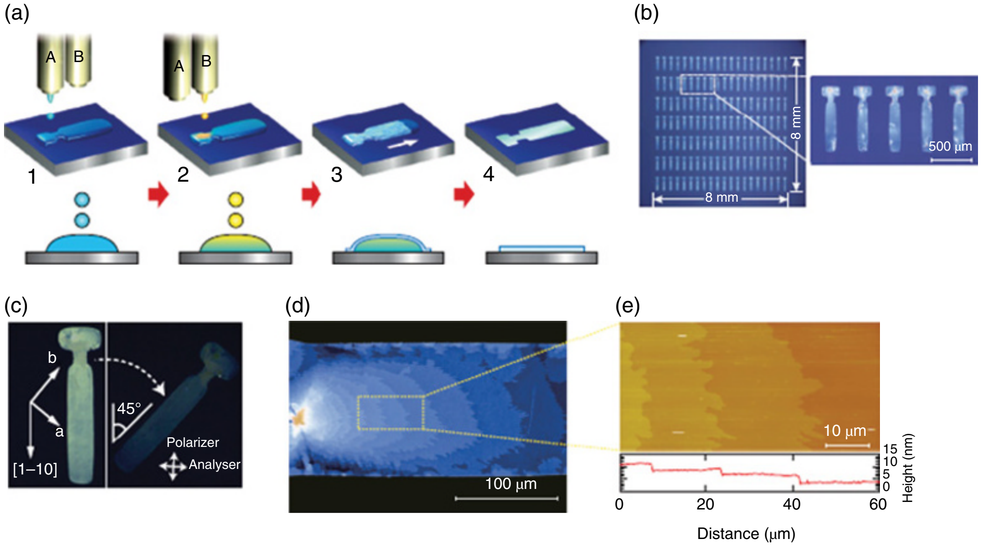

Figure 5.44 Inkjet printing of organic single-crystal thin films. (a) Schematic of the process. Antisolvent ink (A) is first inkjet-printed (step 1), and then solution ink (B) is overprinted sequentially to form intermixed droplets confined to a predefined area (step 2). Semiconducting thin films grow at liquid-air interfaces of the droplet (step 3), the solvent fully evaporates (step 4). (b) Micrographs of a 2037 array of inkjet-printed C8-BTBT single-crystal thin films. (c) Crossed Nicols polarized micrographs of the film. (d) Expanded micrograph of the film, showing stripes caused by molecular-layer steps. (e) Atomic-force microscope image and the height profile (below) showing the step-and-terrace structure on the film surfaces. (Reprinted from [49] with permission from Nature publishing group)

small molecule OTFTs with mobility as high as 31.3 $cm^2V^{-1}s^{-1}$ [49]. They managed to obtain a highly oriented single crystal of an organic semiconductor along the OTFT channel by controlling the channel configuration and solvent vaporization rate, as well as using an in-situ chemical reaction process. The printing process and single crystal morphologies are shown in Figure 5.44. The OTFTs have average mobility of 16.4 $cm^2V^{-1}s^{-1}$ and on/off ratio of 10^7.

5.7 Basics of Printed Logic Circuits

Constructing logic circuits by printed TFTs is the next step in printed electronics development. With the advances in semiconductor inks and printing processes, some of the printed TFTs are good enough to be used for making simple logic circuits and works in this area are already ongoing [53, 61, 62, 70, 79, 80]. Logic circuits are typically made of PMOS, NMOS, pseudo-PMOS/pseudo-NMOS transistors and CMOS transistors. These design approaches use only one type of transistor, which are well suited for printed TFTs because majority of printed TFTs are either n-type or p-type transistors due to the natures of their relevant semiconductor ink materials. To help readers to get familiar with the basics of logic circuits, some simple circuit types such as NOR and OR gates, inverter, oscillator, flip flop, and particularly the driving circuits for backplane of flat panel displays, will be introduced.

(a)

A	B	C = AB
0	0	1
0	1	0
1	0	0
1	1	0

(b)

A	B	C = AB
0	0	1
0	1	1
1	0	1
1	1	0

Figure 5.45 Truth tables of NOR and NAND gates. A and B represent the input variables, and C represents the output

5.7.1 NAND and NOR Gates

When two transistors are connected in series or parallel, they form NAND or NOR gates, which are the basic elements of a logic circuits. Series transistors only allow the device to be pulled up when all outputs are on. Parallel transistors allow the output to be pulled up when any of the transistors are on. The NAND and NOR operations have two input logic variables, A and B. The relationships of inputs and outputs of NAND and NOR operations are listed in the following truth tables in Figure 5.45. AB is 1 only if A and B are both 0 in the NOR gates, whereas AB is 1 if A or B (or both) are 0 in the NAND gate. Sun et al. reported simple logic circuits made from transfer printed SWCNT TFTs [80]. Figure 5.46 presented SWCNT NOR and NAND gates fabricated on flexible substrate. As shown in Figure 5.46d and h, NOR and NAND gates operated by a clock (CLK) signal at 100 Hz showed clear logic outputs with large voltage swings.

5.7.2 Inverter

The inverter is the simplest logic gate from which more complicated logic gates can be constructed. The basic function of an inverter is to output a high voltage at the input of a low voltage and vice versa. Two transistors are needed to form an inverter and their configurations are shown in Figure 5.47 [46]. The transistors can be either single type (PMOS or NMOS) or complementary type (CMOS). Compared to NMOS or PMOS inverters, CMOS inverters are of high noise immunity and low static power consumption because one transistor is always off. Part-printed or full-printed high performance inverters based on inorganic or organic TFTs have been successfully fabricated [19, 20, 46, 53, 61, 62]. Figure 5.48 illustrates the structure and electrical properties of a printed SWCNT inverter. The voltage gain can reach to 58 [41].

5.7.3 Ring Oscillator

A ring oscillator is a metastable device that consists of an odd number of inverters and the output of each inverter is connected to the input of next one. The output of the last inverter is fed back to the first one. As the result, an oscillation occurs due to the positive feedback loop. A ring oscillator has a certain oscillating frequency because each stage has its delay time. The frequency (f) depends on the number of stages (n) and the delay time of each inverter (t) as equation (5.15):

$$f = \frac{1}{2nt} \tag{5.15}$$

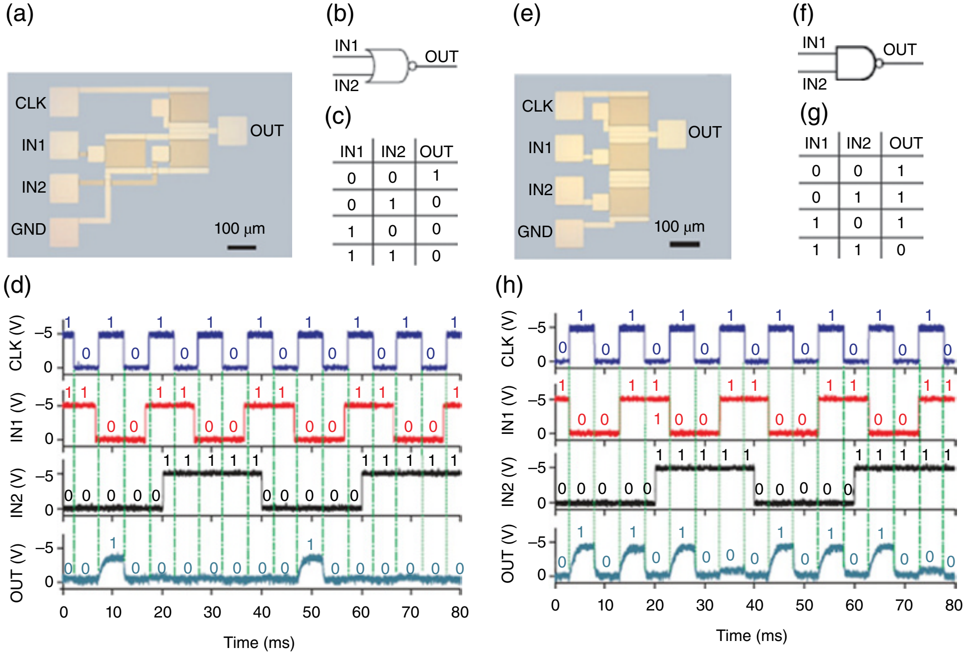

(c)

IN1	IN2	OUT
0	0	1
0	1	0
1	0	0
1	1	0

(g)

IN1	IN2	OUT
0	0	1
0	1	1
1	0	1
1	1	0

Figure 5.46 Logic gates based on SWCNTs on a flexible substrate. (a)–(d) represented the NOR gate optical image, circuit symbol, truth table and input–output characteristics. (e)–(h) are the NAND gate optical image, circuit symbol, truth table and input–output characteristics (Reprinted from [79] with permission from Nature publishing group)

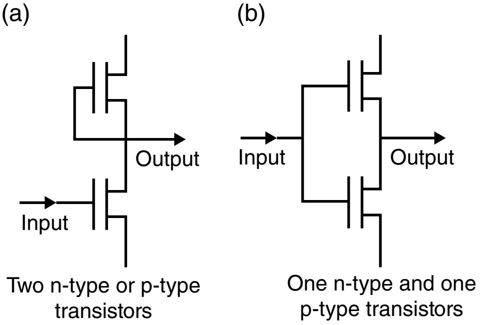
(a)
Output
Input
Two n-type or p-type transistors
(b)
Input
Output
One n-type and one p-type transistors

Figure 5.47 Two symbols of the inverters

Sun et al. reported successful fabrication of a 21-stage SWCNT ring oscillator on a flexible substrate. Figure 5.49 shows the optical image, equivalent circuit diagram and the oscillation waveform for the 21-stage ring oscillator [79]. A series of 21 inverters were connected and an additional output buffer inverter was integrated. When V_{dd} was −3V, the oscillator began oscillating spontaneously. The oscillating frequency reached 3.0 kHz for V_{dd} of −5V and the delay time of each inverter was 7.9 ms. There have been other reported full-printed and part-printed ring oscillators [18, 41].

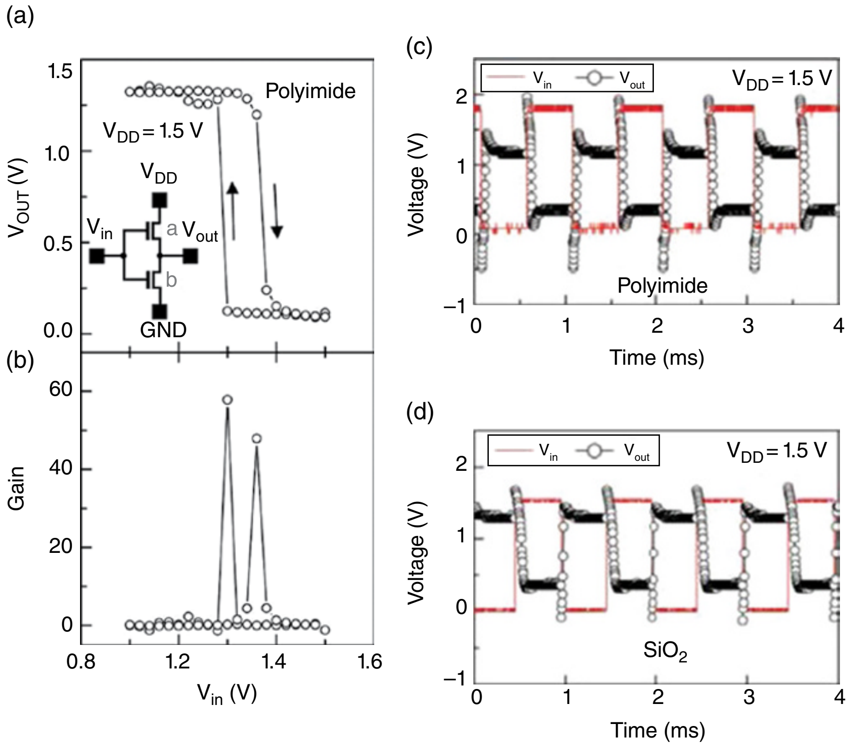

Figure 5.48 Electrical characterization of printed inverters based on ambipolar ion gel-gated CNT transistors. (a) Input–output characteristics of a CNT inverter printed on polyimide substrate. The inset shows the circuit diagram of the inverter based on two identical ambipolar CNT TFTs. (b) Maximum inverter gain is 58 at V_{DD} =1.5 V. (c) Dynamic response of an inverter on polyimide substrate acquired with V_{DD} = 1.5 V. (d) Inverter printed on SiO_2 substrate, where input voltage ranges from 0 to 1.6 V, with V_{DD} =1.5 V. (Reprinted from [41] with permission from American Chemistry Society)

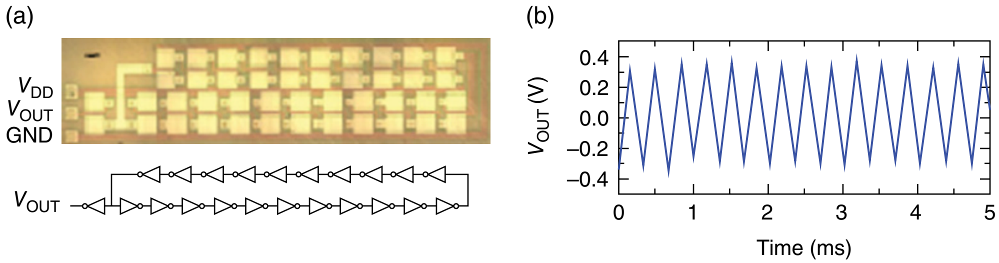

Figure 5.49 21-stage all-carbon ring oscillator. (a) The optical image and equivalent circuit diagram (scale bar, 100 mm). (b) Oscillation waveform. (Reprinted from [80] with permission from Nature publishing group)

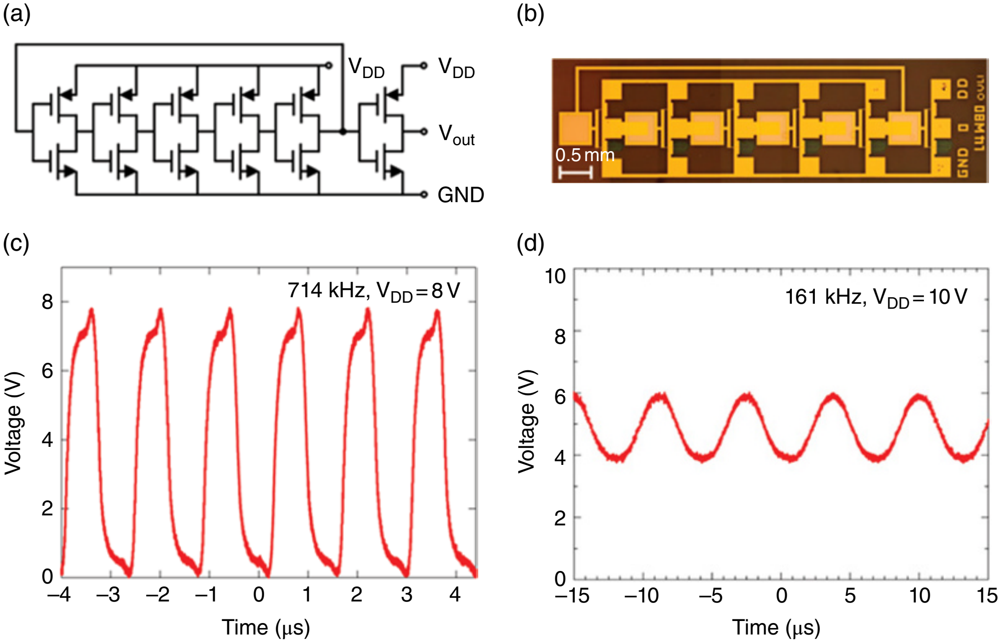

Figure 5.50 (a) Circuit diagram of a five-stage ring oscillator circuits. The last stage is a buffer stage. (b) Optical micrograph of the five-stage ring oscillator circuits. (c) The output signal of CMOS ring oscillator circuits based on p-type SWCNT TFTs and n-type metal oxide TFTs. The oscillation frequency is 714 kHz at Vdd = 8 V. (d) The output signal of ring oscillator circuits based on ambipolar TFTs. (Reprinted from [62] with permission from American Chemistry Society)

CMOS circuits can be constructed by carbon nanotube/metal oxide hybrid complementary circuits because of their p-type and n-type characteristics [44, 62]. As shown in Figure 5.50, the frequency and delay time per stage can reach 714 kHz and 140 ns. Although the performance of these printed ring oscillators are not yet comparable to those of silicon oscillators, they are on the path for further improvements and may in the future find their places in practical applications.

5.7.4 *Flip-flop*

A flip-flop is a circuit that serves as a delay or one bit memory because of its two stable states. It changes from one state to the other state when it is triggered by external signals. The state retention property can be used to make memories and more complicated digital circuitries. A flip-flop can be implemented using a NAND gate as the basic element. Figure 5.51 shows a master–slave delay flip-flop consisting of eight NAND and two NOT gates on a flexible substrate [80]. The circuit consists of two gated delay latches connected in a series, where the slave latch changes the state in response to a change in the master latch. The input–output characteristics (Fig. 5.51e) shows that the master–slave delay flip-flop was triggered on the rising edge of the CLK signal. The master–slave delay flip-flop was the first sequential logic circuit based on SWCNT TFTs [79, 80]. Roll-to-roll printed flexible flip-flops were also successfully fabricated in 2011 [24].

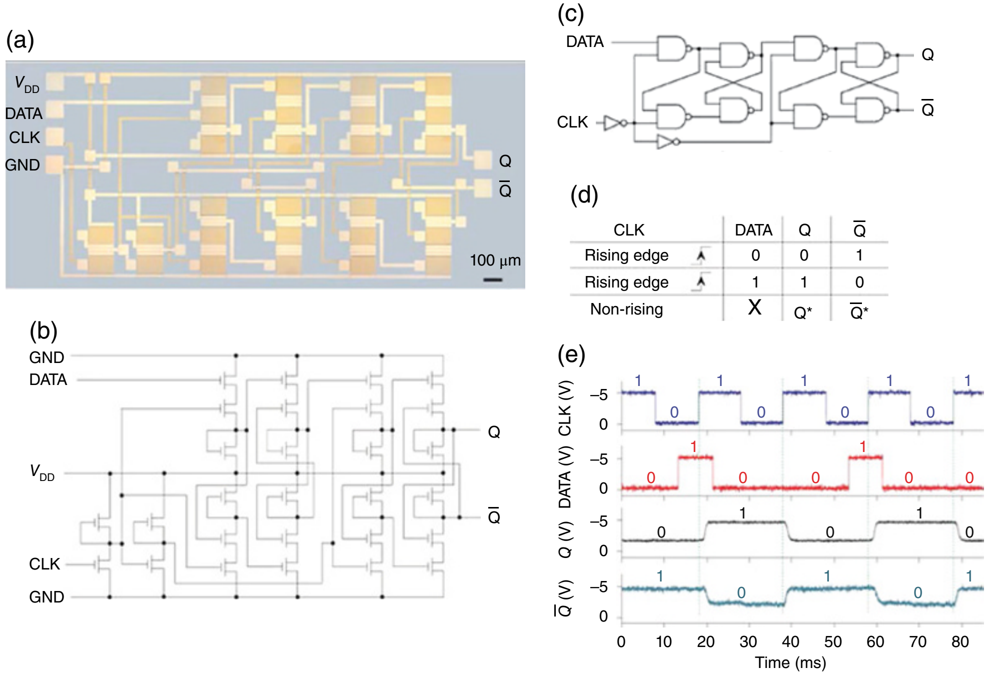
(a)
V_{DD}
DATA
CLK
GND
Q
$\overline{Q}$
100 μm
(b)
GND
DATA
V_{DD}
CLK
GND
Q
$\overline{Q}$
(c)
DATA
CLK
Q
$\overline{Q}$
(d)
(e)
CLK (V)
DATA (V)
Q (V)
$\overline{Q}$ (V)
−5
0
Time (ms)
0 10 20 30 40 50 60 70 80
1 0 1 0 1 0 1 0 1
0 1 0 0 1 0 0
0 1 0 1 0
1 0 1 0 1

CLK	DATA	Q	$\overline{Q}$
Rising edge	0	0	1
Rising edge	1	1	0
Non-rising	X	Q*	$\overline{Q}$*

Figure 5.51 Delay flip-flops on a flexible substrate. (a) An optical micrograph; (b) and (c) circuit symbol; (d) Truth table; and (e) Input–output characteristics of the device. In the truth table, "X" denotes a "don't care" condition and "*" denotes "no change" in output. The master–slave delay flip-flop is triggered on the rising edge of the CLK signal. (Reprinted from [79] with permission from Nature publishing group)

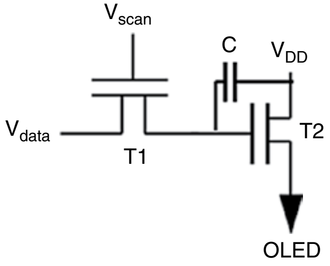
V_{scan}
C
V_{DD}
V_{data}
T1
T2
OLED

Figure 5.52 Diagram of an OLED driving circuit with a storage capacitor

5.7.5 Backplane Driving Circuits for Display

Passive and active matrix TFT driving circuits are widely used as backplanes for flat panel displays. TFTs made by low temperature polycrystalline silicon (LTPS), amorphous-Si, organic semiconductors, SWCNTs, nanowires and metal oxides have all been employed to fabricate the backplanes for driving liquid crystal displays (LCD) and organic light-emitting diodes (OLEDs). As shown in Figure 5.52, the elementary circuit to drive a pixel consists of one switching transistor (T1), at least one driving transistor (T2), and one storage capacitor (C) that maintains the line pixel states. Each pixel is controlled by a scan line, a data line, V_{dd} line and a common cathode line.

Backplane TFTs made of polysilicon and amorphous silicon require vacuum sputtering, lithographic patterning and acidic etching, which is complex and the investment in manufacturing equipment is high, driving up the cost of display. Recently, TFTs based on solution-processable metal oxides attracted great attention due to the low cost process and low waste of materials. However, solution-processed metal oxide TFTs exhibited poor electrical properties without high temperature annealing and have to be made on a glass substrate. SWCNT TFTs have the advantage of low temperature and solution-based processes.

Many works have demonstrated that SWCNT TFTs made by solution process such as inkjet printing showed high uniformity, high on/off ratio, high on current, excellent mobility, low operation voltage, room temperature processing compatibility. AMOLED driving circuits based on SWCNT TFTs on both glass and flexible substrates have been reported by Zhou's groups and Javey's groups [57, 58, 64–66]. The schematic diagram and optical image of one pixel of the SWCNT-based AMOLED display are shown in Figure 5.53a and b.

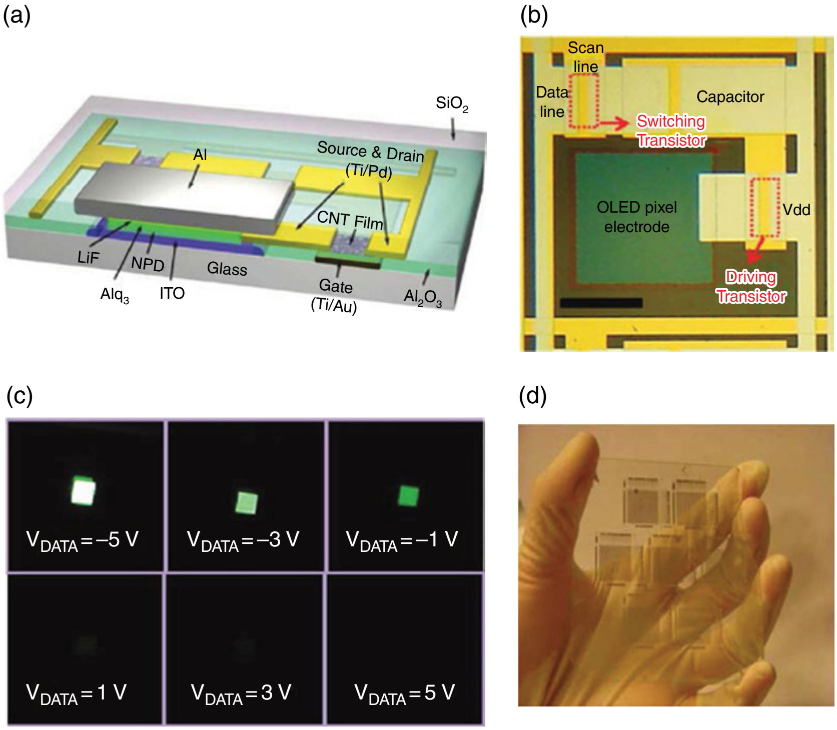
(a)
SiO2
Source & Drain (Ti/Pd)
Al
CNT Film
LiF
NPD
Glass
Alq3
ITO
Gate (Ti/Au)
Al2O3
(b)
Scan line
Data line
Capacitor
Switching Transistor
OLED pixel electrode
Vdd
Driving Transistor
(c)
VDATA = −5 V
VDATA = −3 V
VDATA = −1 V
VDATA = 1 V
VDATA = 3 V
VDATA = 5 V
(d)

Figure 5.53 (a) Schematic diagram showing one pixel of integrated AMOLED. Each pixel consists of two semiconducting nanotube TFTs, one capacitor, and one OLED. (b) Optical micrograph of a AMOLED pixel. (c) Photographs showing OLED light output under various VDATA voltages. (d) Photograph of 7 AMOLED chips fabricated on glass substrate. (Reprinted from [57] with permission from American Chemistry Society)

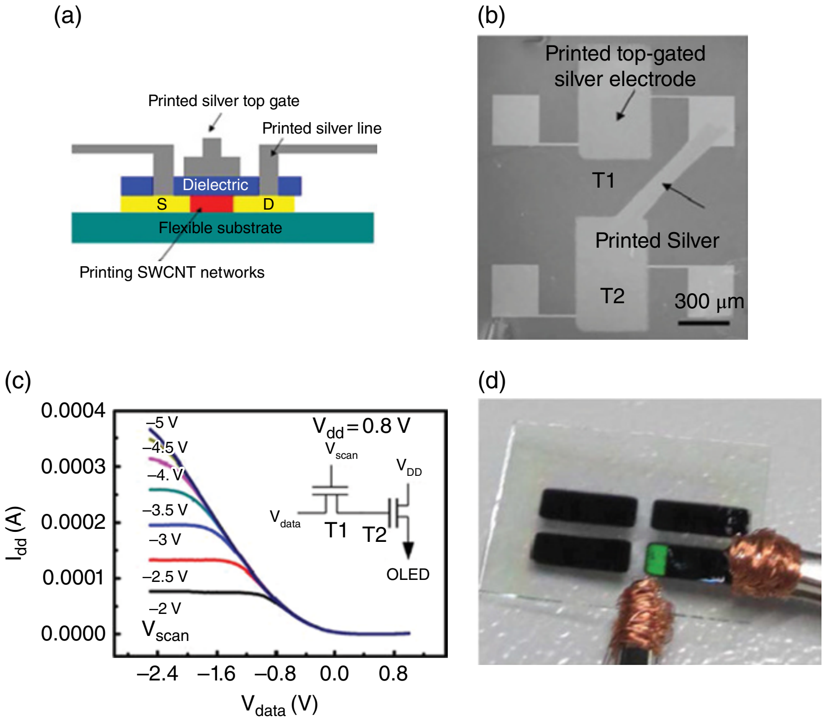

Figure 5.54 (a) Schematic of printed top gate TFT; (b) Printed OLED driving circuit; (c) Typical current output characteristic of OLED driving circuits without external OLED; and (d) Optical image of single pixel OLED (Reprinted from [67] with permission from The Royal Society of Chemistry)

Each pixel driving circuit consists of two SWCNT TFTs and one capacitor. The lighting intensity of an OLED can be controlled by changing the voltage of the switching transistors, shown in Figure 5.53c.

In 2014, the authors' Printable Electronics Research Center also demonstrated printed flexible SWCNT TFTs for OLED pixel driving circuits. Figure 5.54a is the schematic structure of printed top-gate TFT on PET substrates. Two top-gate TFTs are connected with printed silver lines (as shown in Figure 5.54b). The OLED driving circuit exhibits on/off ratio up to 10^4 and output current up to 3.5×10^{-4} A at V_{scan}= -4.5 V and V_{dd}= 0.8 V (in Figure 5.54c). The printed driving circuit has the ability to control the light emission of an OLED pixel (Figure 5.54d).

5.8 Summary

With the advances in new semiconducting materials and novel printing technologies, different types of printed TFTs can be easily fabricated. However, the performance of printed TFTs is still not good enough for practical application. In the authors' experience, the following measures should be taken in order to further improve printed TFTs.

1. Preparation of high-performance printable inks. For example, using high-purity sc-SWCNTs with a large diameter as printed inks can achieve higher mobility and small hysteresis TFTs. Using high-k or high-capacitance dielectric inks to reduce the operating voltage. Low operating voltage and small hysteresis of printed TFTs are both very important parameters to construct high-performance logic circuits. Since it is difficult to obtain an ultrathin dielectric layer by printing methods, some high-k or high-capacitance inks need to be developed.
2. Improvement on interfaces, such as the interface between printed semiconducting materials and substrates or dielectric layers, and the interface between printed electrodes and substrates (dielectric layers). For example, substrates should be modified with functionalized groups, such as amine-groups, to eliminate or decrease the trapping density, and increase the interaction force between semiconductors and dielectric layers, which is beneficial to decrease the operating voltage and hysteresis of printed TFTs. Improvement on the binding force between printed electrode and substrates (dielectric layer), especially the printed top-gate or bottom-gate electrode and the dielectric layer, is needed. If the adhesion force of gate electrode and dielectric layer is not strong, printed TFTs exhibit will have poor performance, such low on/off ratio, instability, high operation voltage and low on currents, due to poor gate tuning ability. It is necessary to modify the surface properties of substrates and also to use better conductive inks to increase the binding force between electrodes and substrates.
3. There are optimum channel lengths for printed TFTs. Previous experience shows that mobility and working frequency for printed SWCNT TFTs increase as the channel length decreases. However, with a decrease in channel length, on/off ratios also decrease due to some metallic species and impurities in SWCNT thin films. Therefore, printed TFTs can exhibit high on/off ratios and mobility when selecting an optimal channel length.

As a result of the advancements in new materials, novel printing technologies and other processing technologies, the performance of partly or fully-printed TFTs will be further improved. The practical applications of these printed TFTs are already on the horizon and will expand in the years to come.

References

[1] Chen J. *Analogue Integrated Circuits: Principle, Design and Applications (in Chinese).* 1st ed. Hefei: Chinese University of Science and Technology, 1997.

[2] Chen X, Zhang Q. *Principle and Design of Transistors (in Chinese).* 2nd ed. Beijing: Publishing House of Electronics Industry, 2006.

[3] Shi M, Wu G. *Physics of Semiconductor Devices (in Chinese).* 3rd ed. Xi'an: Publishing House of Xi'an Jiaotong University, 2008.

[4] Cho JH, Lee JY, Xia Y, Kim B, He YY, Renn MJ, Lodge TP, Frisbie CD. Printable ion-gel gate dielectrics for low-voltage polymer thin-film transistors on plastic [J]. Nature Materials. 2008;7:900–906.

[5] Kim MG, Kanatzidis MG, Facchetti A, Marks TJ. Low-temperature fabrication of high-performance metal oxide thin-film electronics via combustion processing [J]. Nature Materials. 2011;10:382–388.

[6] Zhao JW, Lin J, Chen Z, Cui Z. Fabrication and characterization of thin-film transistors based on printable functionalized SWCNTs [C]. NSTI Nanotechnology Conference & Expo. Nanotech. 2011;1:192-195. Boston, US.

[7] Yamaguchi K, Takamiya S, Minami M, Doge Y, Nishide Y, Osuga H, Uno K, Tanakaa, I. Crystallinity improvement of benzodithiophene-dimer films for organic field-effect transistors [J]. Appl.Phys.Lett. 2008; 93:043302.

[8] Gui EL, Li LJ, Zhang K, Xu Y, Dong X, Ho X, Lee PS, Kasim J, Shen ZX, and Rogers JA. DNA Sensing by field effect transistors based on networks of carbon nanotubes [J], J. Am. Chem. Soc. 2007;129:14428–14431.

[9] Wong WS, Salleo A (eds.). *Flexible Electronics: Materials and Applications. Electronic Materials: Science & Technology [M].* New York: Springer Science Business Media. 2009;322–323.

[10] Tian JF, Jauregui LA, Lopez G, Cao H, and Chen YP. Ambipolar graphene field transistors by local metal side gates [J]. Appl.Phys.Lett. 2010;96:263110–3.

[11] Dong X, Shi YM, Huang W, Chen P, and Li LJ. Electrical detection of DNA hybridization with single-case specificity using transistors based on CVD-grown graphene sheets [J], Adv. Mater. 2010; 22:1649–1654.

[12] Pui TS, Sudibya HG, Luan X, Zhang Q, Ye F, Huang Y, Chen P. Non-invasive detection of cellular bioelectricity based on carbon nanotube devices for high-throughput drug screening [J], Adv. Mater. 2010;22:3199–3203.

[13] Jurchenscu OD, Baas J, Palstra, TTM. Effect of impurities on the mobility of single crystal pentacene [J]. Appl. Phys. Lett., 2004;84(16): 3061–3064.

[14] Zheng Cui. *Nanofabrication: Principles, Capabilities and Limits*. (Chapter 6: Nanoscale Pattern Transfer). Springer: 2008.

[15] Fu D, Lim H, Shi Y, Dong X, Mhaisalkar S, Chen Y, Moochhala S, Li LJ. Differentiation of gas molecules using flexible and all-carbon nanotube devices [J]. J. Phys. Chem. C, 2008;112(3): 650–653.

[16] Li B, Cao X, Ong H, Cheah J, Zhou X, Yin Z, Li H, Wang J, Boey F, Huang W, Zhang H. All-carbon electronic devices fabricated by directly grown single-walled carbon nanotubes on reduced graphene oxide electrodes [J]. Adv. Mater. 2010;22:3058–3061.

[17] Wöbkenberg PH, Eda G, Leem D-S, de Mello JC, Bradley DD, Chhowalla M, Anthopoulos TD. Reduced graphene oxide electrodes for large area organic electronics [J]. Adv. Mater. 2011;23:1558–1562.

[18] Allen R, Fuller GG and Bao Z. Aligned SWNT films from low-yield stress gels and their transparent electrode performance. ACS Appl. Mater. Interfaces, 2013;5(15):7244–7252.

[19] Zhao Y, Di C, Gao X, Hu Y, Guo Y, Zhang L, Liu Y, Wang J, Hu E, Zhu D. All-solution-processed, high-performance n-channel organic transistors and circuits: toward low-cost ambient electronics [J]. Adv. Mater. 2011:23:2448–2453.

[20] Okimoto H, Takenobu T, Yanagi K, Miyata Y, Shimotani H, Kataura H, Iwasa Y. Tunable carbon nanotube thin-film transistors produced exclusively via inkjet printing [J], Adv. Mater. 2010;22:3981–3986.

[21] Denneulin A, Bras J, Carcone F, Neuman C, Blayo A. Impact of ink formulation on carbon nanotube network organization within inkjet printed conductive films [J]. Carbon. 2011;49:2603–2614.

[22] Cho JH, Lee J, Xia Y, Kim BS, He Y, Renn MJ, Lodge TP, Daniel FC. Printable ion-gel gate dielectrics for low-voltage polymer thin-film transistors on plastic [J], Nature Materials, 2008;7:900–906.

[23] Vaillancourt J, Zhang H, Vasinajindakaw P, Xia H, Lu X, Han X, Janzen DC, Shih WS, Jones CS, Stroder M, Chen MY, Subbaraman H, Chen RT, Berger U, Renn M. All ink-jet-printed carbon nanotube thin-film transistor on a polyimide substrate with an ultrahigh operating frequency of over 5 GHz [J], Appl. Phys. Lett. 2008;93:243301–3.

[24] Jung M, Kim J, Noh J, Lim N, Lim C, Lee G, Kim J, Kang H, Jung K, Leonard AD, Tour JM, Cho G. All-printed and roll-to-roll-printable 13.56-MHz-operated 1-bit RF tag on plastic foils [J], IEEE Transactions on electron devices. 2010;57(3):571–580.

[25] Yu WJ, Lee SY, Chae SH, Perello D, Han GH, Yun M, and Lee YH. Small hysteresis nanocarbon-based integrated circuits on flexible and transparent plastic substrate [J]. Nano Lett. 2011;11:1344–1350.

[26] Lee WH, Park J, Sim SH, Jo SB, Kim KS, Hong BH, Cho K. Transparent flexible organic transistors based on monolayer graphene electrodes on plastic [J], Adv. Mater. 2011;23:1752–1756.

[27] Zhao JW, Lee CW, Han XD, Chan-Park MB, Chen P, Li LJ. Solution-processable semiconducting thin-film transistors using single-walled carbon nanotubes chemically modified by organic radical initiators [J], Chem. Comm. 2009;46:7182–7184.

[28] He Q, Sudibya HG, Yin Z, WuS, Li H, Boey F, Huang W, Chen P, Zhang H. Centimeter-long and large-scale micropatterns of reduced graphene oxide films: fabrication and sensing applications [J]. ACS Nano, 2010;4 (6):3201–3208.

[29] Li X, Zhu Y, Cai W, Borysiak M, Han B, Chen D, Piner RD, Colombo L, Ruoff RS. Transfer of large-area graphene films for high-performance transparent conductive electrodes [J], Nano Lett. 2009;9(12): 4359–4363.

[30] Ahn JH, Kim HS, Lee KJ, Jeon S, Kang SJ, Sun Y, Nuzzo RG, Rogers JA. Heterogeneous three-dimensional electronics by use of printed semiconductor nanomaterials [J]. Science. 2006;314:1754–1757.

[31] Shklyarevskiy IO, Jonkheijm P, Stutzmann N, Wasserberg D, Wondergem HJ, Christianen PCM, Schenning APHJ, de Leeuw DM, Tomovic Z, Wu J, llen KM, Maan JC. High anisotropy of the field-effect transistor mobility in magnetically aligned discotic liquid-crystalline semiconductors [J]. J. Am. Chem. Soc. 2005;127:16233–16237.

[32] Oh JH, Lee WY, Noe T, Chen WC, Konemann M, Bao Z. Solution-shear-processed quaterrylene diimide thin-film transistors prepared by pressure-assisted thermal cleavage of swallow tails [J]. J. Am. Chem. Soc. 2011;133:4204–4207.

[33] Ko H, Tsukruk VV. Liquid-crystalline processing of highly oriented carbon nanotube arrays for thin-film transistors [J], Nano Lett. 2006;6(7):1443–1448.

[34] Li S, Liu N, Chan-Park MB, Yan Y, Zhang Q. Aligned single-walled carbon nanotube patterns with nanoscale width, micron-scale length and controllable pitch. Nanotechnology. 2007;18:455302.

[35] Shekhar S, Stokes P, Khondaker SI. Ultrahigh density alignment of carbon nanotube arrays by dielectrophoresis [J]. ACS Nano. 2011;5(3):1739–1746.

[36] Cao Q, Han S, Tulevski GS, Zhu Y, Lu DD, Haensch W. Arrays of single-walled carbon nanotubes with full surface coverage for high-performance electronics. Nature Nanotechnology. 2013;8:180–186.

[37] Roberts ME, Queralto N, Mannsfeld SCB, Reinecke BN, Knoll W, Bao Z. Cross-linked polymer gate dielectric films for low-voltage, organic transistors [J]. Chem. Mater. 2009;21:2292–2299.

[38] Aeton O, Ting G, Ma H, Ka JW, Yip HL, Tueker NM, Jen AKY. σ-∏ phosphonics acid organic monolayer/sol-gel hafnium oxide hybrid dielectrics for low voltage organic transistors on plastic [J]. J Mater Chem. 2009;19:7929–7936.

[39] Acton O, Hutchins D, Árnadóttir L, Weidner T, Cernetic N, Ting GG, Kim TW, Castner DG, Ma H, Jen AKY. Spin-cast and patterned organophosphonate self-assembled monolayer dielectrics on metal-oxide-activated Si [J]. Adv. Mater. 2011;23(16):1899–1902.

[40] Sundar VC, Zaumseil J, Podzorov V, Menard E, Willett RL, Someya T, Gershenson ME, Rogers JA. Elastomeric transistor stamps: reversible probing of charge, transport in organic crystals [J]. Science. 2004;303:1644–1646.

[41] Ha M, Xia Y, Green AA, Zhang W, Renn MJ, Kim CH, Hersam MC, Frisbie CD. Printed, sub-3V digital circuits on plastic from aqueous carbon nanotube inks [J]. ACS Nano. 2010;4(8):4388–4395.

[42] Di C, Liu Y, Yu G, Zhu D. Interface engineering: an effective approach toward high-performance organic field-effect transistors [J]. Acc. Chem. Res. 2009;42(10):1573–1583.

[43] Vosgueritchian M, LeMieux MC, Dodge D, Bao Z. Effect of surface chemistry on electronic properties of carbon nanotube network thin film transistors [J]. ACS Nano. 2010;4(10):6137–6145.

[44] Liu Z, Zhao J, Xu W, Qian L, Nie S, Cui Z*. Effect of surface wettability on electrical properties of printed carbon nanotube thin-film transistors on SiO_2/Si substrates. ACS Applied Materials and Interfaces. 2014;ASAP, DOI:10.1021/am502168x.

[45] Yuan GC, Xu Z, Gong C, Qin QJ, Zhi ZS, Shi JS, Zhang FJ, Zhao SL, Xu N, Li CM. High performance organic thin film transistor with phenyltrimethoxysilane-modified dielectrics. Appl. Phys. Lett. 2009;94:153308.

[46] Zhao J, Zhang W, Xu Y, Li L. Mobility enhancement in carbon nanotube transistors by screening charge impurity with silica nanoparticles. The Journal of Physical Chemistry C. 2011;115:6975–6979.

[47] Chen Y, Shih I. Scaling down of organic thin film transistors: short channel effects and channel length-dependent field effect mobility [J]. J Mater Sci. 2009;44:280–284.

[48] Wang C, Zhang JL, Ryu K, Badmaev A, De Arco LG, Zhou CW. Wafer-scale fabrication of separated carbon nanotube thin-film transistors for display applications [J]. Nano Lett. 2009;9(12):4285–4291.

[49] Minemawari H, Yamada T, Matsui H, Tsutsumi J, Haas S, Chiba R, Kumai R, Hasegawa T. Inkjet printing of single-crystal films. Nature. 2011;475:364–367.

[50] Barton K, Mishra D, Alleyne A, Ferreira P, Rogers J. Control of high-resolution electrohydrodynamic jet printing. Control Engineering Practice. 2011;19:1266–1273.

[51] Sutanto E, Shigeta K, Kim YK, Graf PG, Hoelzle DJ, Barton KL, Alleyne AG, Ferreira, PM, Rogers JA. A multimaterial electrohydrodynamic jet (E-jet) printing system. J. Micromech. Microeng. 2012;22:045008.

[52] Zhao J, Gao Y, Gu W, Wang C, Lin J, Chen Z, Cui Z. Fabrication and electrical properties of all-printed carbon nanotube thin film transistors on flexible substrates. Journal of Materials Chemistry. 2012;22:20747–20753.

[53] Chen H, Cao Y, Zhang J, Zhou C. Large-scale complementary macroelectronics using hybrid integration of carbon nanotubes and IGZO thin-film transistors. Nature Communication. 2014;DOI:10.1038/ncomms5097.

[54] Zhang J, Gui H, Liu B, Liu J, Zhou C. Comparative study of gel-based separated arcdischarge, HiPCO, and CoMoCAT carbon nanotubes for macroelectronic applications. Nano Research. 2013;6(12):906–920.

[55] Zhang J, Wang C, Zhou C. Rigid/flexible transparent electronics based on separated carbon nanotube thin-film transistors and their application in display electronics. ACS Nano. 2012;6(8):7412–7419.

[56] Wang C, Badmaev A, Jooyaie A, Bao M, Wang KL, Galatsis K, Zhou C. Radio frequency and linearity performance of transistors using high-purity semiconducting carbon nanotubes. ACS Nano. 2011;5(5):4169–4176.

[57] Zhang J, Fu Y, Wang C, Chen P, Liu Z, Wei W, Wu C, Thompson ME, Zhou C. Separated CNT macroelectronics for active matrix OLED display. Nano Lett. 2011;11(11):4852–4858.

[58] Chen P, Fu Y, Aminirad R, Wang C, Zhang J, Wang K, Galatsis K, Zhou C. Fully printed separated carbon nanotube thin-film transistor circuits and its application in organic light emitting diode control. Nano Lett. 2011;11(12):5301–5308.

[59] Zhang J, Wang C, Fu Y, Che Y, Zhou C. Air-stable conversion of separated carbon nanotube thin-film transistors from p-type to n-type using atomic layer deposition of high-κ oxide and its application in CMOS logic circuits. ACS Nano. 2011;5(4):3284–3292.

[60] Wang C, Zhang J, Zhou C. Macroelectronic integrated circuits using high-performance separated carbon nanotube thin-film transistors. ACS Nano. 2010;4(12):7123–7132.

[61] Geier ML, Prabhumirashiv PL, McMorrow JJ, Xu W, Seo JT, Everaerts K, Kim CH, Marks TJ, Hersam MC. Subnanowatt carbon nanotube complementary logic enabled by threshold voltage control. Nano Lett. 2013; 13(10):4810–4814.

[62] Kim B, Jang S, Geier ML, Prabhumirashi PL, Hersam MC, Dodabalapur A. High-speed, inkjet-printed carbon nanotube/zinc tin oxide hybrid complementary ring oscillators, Nano Lett. 2014;14(6):3683–3687.

[63] Ha TJ, Kiriya D, Chen K, Javey A. Highly stable hysteresis-free carbon nanotube thin-film transistors by fluorocarbon polymer encapsulation, ACS Applied Materials & Interfaces. 2014;6(11):8441–8446.

[64] Takahashi T, Yu Z, Chen K, Kiriya D, C. Wang C, Takei K, Shiraki H, Chen T, Ma B, Javey A. Carbon nanotube active-matrix backplanes for mechanically flexible, visible light and x-ray imagers. Nano Letters. 2013;13(11):5425–5430.

[65] Lau PH, Takei K, Wang C, Ju Y, Kim J, Yu Z, Takahashi T, Cho G, Javey A. Fully-printed, high performance carbon nanotube thin-film transistors on flexible substrates. Nano Letters. 2013;13(8):3864–3869.

[66] Wang C, Takei K, Takahashi T, Javey, A. Carbon nanotube electronics-moving forward. Chem. Soc. Rev. 2013;42:2592–2609.

[67] Xu W, Zhao J, Qian L, Su W, Zhou L, Zheng C. Sorting of large-diameter semiconducting carbon nanotube and printed flexible driving circuit for organic light emitting diode (OLED). Nanoscale,]. 2014;6(3):1589–1595.

[68] Wang C, Qian L, Xu W, Nie S, Gu W, Zhang J, Zhao J, Lin J, Zheng Chen, Zheng C. High performance thin-film transistors based on regioregular poly(3-dodecylthiophene)-sorted large diameter semiconducting single-walled carbon nanotubes. Nanoscale. 2013;5:4156–4161.

[69] Qian L, Xu W, Fan X, Wang C, Zhang J, Zhao, J, Zheng C. Electrical and photoresponse properties of printed thin-film transistors based on poly(9,9-dioctylfluorene-co-bithiophene) sorted large-diameter semiconducting carbon nanotubes, The Journal of Physical Chemistry C. 2013;117:18243–18250.

[70] Ha M, Seo J, Prabhumirashi PL, Zhang W, Hersam MC, Frisbie CD. Aerosol jet printed, low voltage, electrolyte gated carbon nanotube ring oscillators with sub-5 μs stage delays, Nano Lett. 2013;13(3):954–960.

[71] Dasgupta S, Kruk R, Mechau N, Hahn H. Inkjet printed, high mobility inorganic-oxide field-effect transistors processed at room temperature. ACS Nano. 2011;5(12):9628–9638.

[72] Li J, Ye1 F, Vaziri S, Muhammed M, Lemme MC, Östling M. Efficient Inkjet Printing of Graphene. Adv. Mater. 2013;25:3985–3992.

[73] Torrisi F, Hasan T, Wu W, Sun Z, Lombardo A, Kulmala TS, Hsieh GW, Jung S, Bonaccorso F, Paul PJ, Chu D, Ferrari AC. Inkjet-printed graphene electronics, ACS Nano. 2012;6:2992–3006.

[74] Coleman JN, Lotya M, et al. Two-dimensional nanosheets produced by liquid exfoliation of layered materials. Science. 2011;331–568.

[75] Braga D, Lezama IG, Berger H, Morpurgo AF. Quantitative determination of the band gap of WS_2 with ambipolar ionic liquid-gated transistors. Nano Lett. 2012;12:5218–5223.

[76] Lembke D, Kis A. Breakdown of high-performance monolayer MoS2 transistors. ACS Nano. 2012;6(11): 10070–10075.

[77] Wang H, Yu L, Lee Y-H, Shi Y, Hsu A, Chin ML, Li L-J, Dubey M, Kong J, Palacios T. Integrated circuits based on bilayer MoS_2 transistors. Nano. Lett. 2012;12:4674–4680.

[78] Yan H, Chen Z, Zheng Y, Newman C, Quinn JR, Dötz F, Kastler M, Facchetti A. A high-mobility electron-transporting polymer for printed transistors. Nature. 2009;457:679–686.

[79] Sun DM, Timmermans MY, Tian Y, Nasibulin AG, Kauppinen EI, Kishimoto S, Mizutani T, Ohno Y. Flexible high-performance carbon nanotube integrated circuits [J]. Nature Nanotechnology. 2011;6:156–161.

[80] Sun DM, Timmermans MY, Kaskela A, Nasibulin AG, Kishimoto S, Mizutani T, Kauppinen EI, Ohno Y. Nat. Commun. 2013;4:2302.

[81] Spencer RR, Ghausi MS. *Design Basis of Electronic Circuits (in Chinese)*. 1st ed. Beijing: Publishing House of Electronics Industry, 2005.

6

Printed Organic Thin Film Solar Cells

Changqi Ma

6.1 Introduction

6.1.1 Solar Energy and its Utilization

Energy is one of the key necessities for human activities. The rapid increase in population is speeding up the consumption of conventional fossil fuel resources. On the one hand, overexploitation of resources and use of fossil fuels have caused environmental pollution and ecological destruction. On the other hand, the limited fossil fuel resources will inevitably lead to a shortage of energy supply in the future. The development of renewable energies has been considered the best form of energy from a sustainability point of view. Renewable energy sources include wind, hydropower, wave and tidal, geothermal and solar, among which solar is the most sustainable and clean energy source.

There are different ways to use solar energy, including photosynthesis in plants (chemical conversion of solar energy); water splitting into hydrogen and oxygen by solar; concentrated solar thermal power; water heating; and solar cell battery, which converts solar energy to electricity directly based on the photovoltaic effect of semiconductors. Solar cells have been considered as the most feasible way to use solar energy [1]. Where there is sunshine, there is the possibility to generate solar power. Therefore, solar cells can be used in a variety of applications, from a huge solar power station to a portable battery charger.

Although solar energy is advantageous over other energy sources, it currently makes up only a tiny proportion in global energy consumption. In 2009 the percentage of solar power in the world total energy consumption is only 0.16% [2]. The reason for this situation is the high cost of solar cells, which make it a much less favorable energy source compared to conventional fossil fuels. Reducing the cost of solar cells is recognized as the most urgent step towards the full utilization of solar energy.

Printed Electronics: Materials, Technologies and Applications, First Edition. Zheng Cui, Chunshan Zhou, Song Qiu, Zheng Chen, Jian Lin, Jianwen Zhao, Changqi Ma and Wenming Su.
© 2016 Higher Education Press. All rights reserved. Published 2016 by John Wiley & Sons Singapore Pte. Ltd.

6.1.2 Classification of Solar Cells

Depending on the semiconductors used, solar cells can be divided into four main categories: (1) Silicon solar cells; (2) Inorganic compound thin-film solar cells; (3) Organic dye-sensitized solar cells; (4) Organic thin-film solar cells based on oligomeric or polymeric semiconductors [3,4].

Silicon solar cells include single-crystal silicon solar cells, polysilicon solar cells and amorphous silicon thin-film solar cells [5,6]. A single-crystal silicon solar cell has the highest power conversion efficiency (PEC) up to 25% [7]. However, due to the difficulties in getting high quality single crystal, the cost of a single crystal-based silicon solar cell is rather high. The cost of polysilicon solar cells is lower because polysilicon materials are more readily available. The power conversion efficiency of the polysilicon solar cell, however, is lower than single-crystal silicon solar cells, typically less than 20%. As the cost of amorphous silicon thin-film solar cells has become less, this has attracted much attention in the last few years. The power conversion efficiency of amorphous silicon solar cells is typically 8–10%, which is much lower than that of crystal silicon solar cells [7]. Overall, due to the costliness of high purity silicon material as well as high energy consumption to manufacture the solar cells, widespread use of silicon-based solar cells is limited.

Inorganic compound based thin-film solar cells, including GaAs, CdTe, and $Cu_2InGaSe_4$, have developed very fast in the last few years for their relatively less material consumption, low cost and good device performance (PEC can be as high as 20%) [7,8]. However, this type of solar cell requires a high process temperature. Meanwhile, indium and gallium are rare earth metals, which increase the cost of final product. Furthermore, arsenic, gallium and cadmium are all toxic metals and environmentally hazardous, and may cause poisoning during production and use. Thin-film inorganic compound solar cells might not be the ideal alternative for silicon solar cells.

Organic dye-sensitized solar cells (DSSC) are the kind of photochemical cells that are typically composed of microporous inorganic semiconducting film, organic dyes (photosensitizer), redox electrolyte, counter electrode, and conductive substrate [9,10]. The most widely used inorganic semiconductor in DSSC is nanocrystalline TiO_2. High temperature sintering usually forms 5–10 μm thick TiO_2 film. Organic dyes are attached to a TiO_2 surface by covalent chemical bonds. In addition, liquid electrolyte is needed to support the electron cycles during the photon-induced electron generation. Compared to traditional silicon solar cells, the advantages of DSSC include low cost of manufacturing and ease of preparing organic dyes. Power conversion efficiency of DSSC can be over 10% [11], whereas the cost is typically 1/5–1/10 that of silicon solar cells. The use of TiO_2 and noble metal-based organic dye, such as ruthenium and osmium complexes, could be a problem for large-scale application of DSSC. In addition, the liquid electrolyte may cause problems for DSSCs due to the penetration of organic solvent [12]. Development of solid (or quasi-solid) state electrolytes attracts much attention, and could be beneficial for the large scale application of DSSCs [13].

Organic thin-film solar cells based on organic semiconductors are the latest developed technology and has shown great potential [14,15]. Compared to inorganic semiconductors, organic materials can be easily synthesized in large scale, which in principle can reduce the cost of solar cells. Unlike DSSCs, organic thin-film solar cells are solid devices, which are easy to process and to handle. In addition, organic semiconductors show good compatibility with flexible plastic substrates, making it suitable for large-scale roll-to-roll production, which can potentially lower the cost significantly. Very recently, organic thin-film solar cell has successfully passed the strict IEC-61646 environmental chamber tests, which proved that organic thin-film solar cells can be stable enough for real application [16]. Overall, organic thin-film solar cells are low in cost, light in weight, easy to produce, flexible and bendable, and they have become the hotly pursued new energy technology in the last few years [17].

6.1.3 A Brief History of Organic Thin-Film Solar Cells

The history of organic thin-film solar cell research can be traced back to the 1950s. Kearns and Calvin (1958) reported the first organic solar device using laminated organic thin films containing magnesium phthalocyanine (MgPc) and oxidized tetramethyl *p*-phenylenediamine (TMΦD) as the photoactive layer [18]. Results showed that solar conversion effect was dependent on the oxidation of TMΦD, which indicated the photon-induced electron transfer between MgPc and TMΦD. A high open circuit voltage of 200 mV was measured. The thickness of the organic film was around 100 μm. Due to the low conductivity of organic compounds, the internal resistance was too high to yield good efficiency. In 1986, Tang et al. prepared a high efficiency organic thin-film solar cell using copper phthalocyanine (CuPc) as electron donor and perylene tetracarboxylic derivative (PV) as electron acceptor (Figure 6.1) [19]. In this case, both organic compounds were deposited by thermal evaporation and the thicknesses of these films were limited to 25 and 45 nm, respectively. The greatly reduced film thickness decreased the internal resistance of the device and high solar power conversion efficiency around 1% was achieved under light illumination at 750 W/m^2.

In 1992, Sariciftci et al. confirmed the ultrafast photon-induced electron transfer process from conjugated polymer to fullerene C_{60}, and the consequent formation of stable charge separated species [20], which became the ground work for all modern polymer solar cells. In 1995, Yu et al. made the first polymer solar cell by the spin coating method [21]. In this

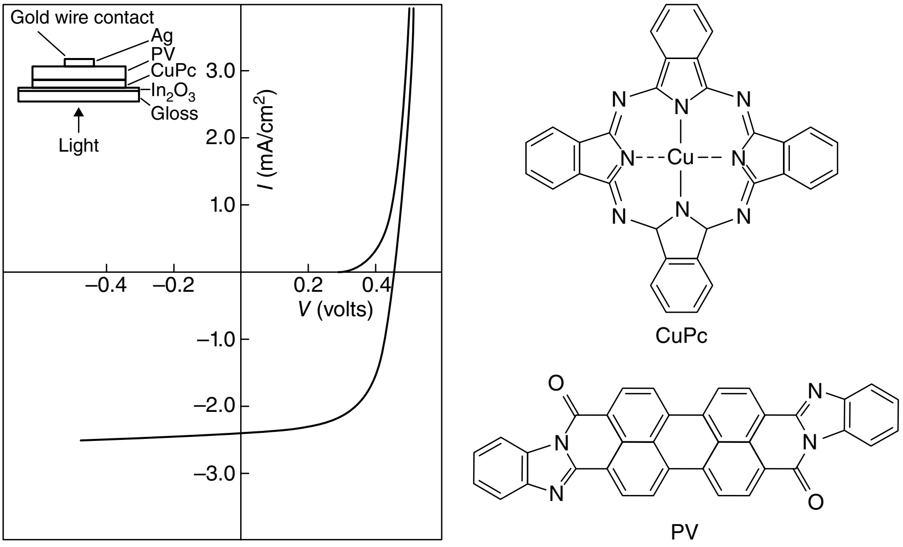

Figure 6.1 Tang's OPV device structure and output performance (left), chemical structure of CuPc and PV. (Reprinted from ref. [19] with permission from AIP Publishing LLC)

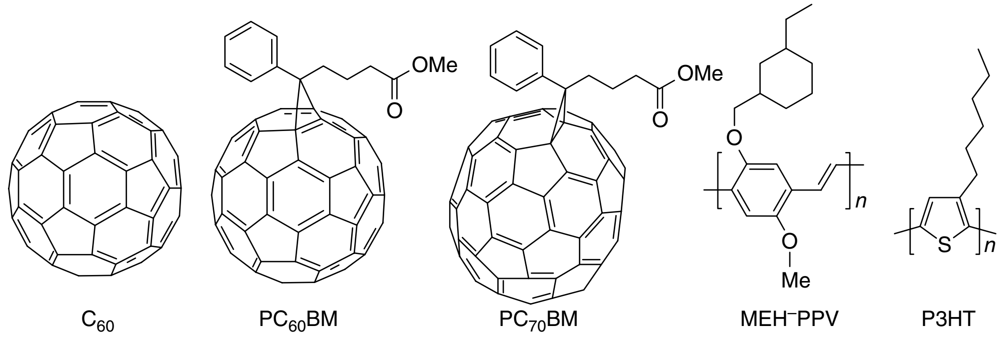

Figure 6.2 Chemical structures of organic semiconductors in polymer solar cells

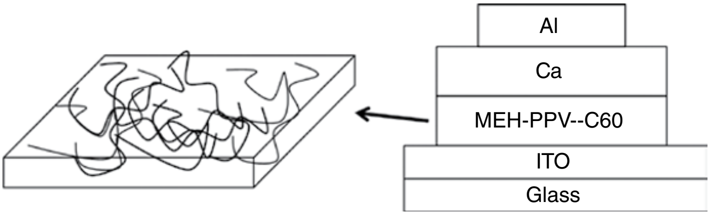

Figure 6.3 Device structure of the first MEH-PPV:C60 based polymer solar cell

pioneering work, the authors used conjugated poly[2-methoxy-5-(2'-ethyl-hexyloxy)phenylenevinylene] (MEH-PPV) (see Figure 6.2) as the electron donor and soluble fullerene derivative phenyl-C_{61}-butyric acid methyl ester ($PC_{61}BM$) as the electron acceptor. The photoactive layer was fabricated by spin coating a mixture of these two materials in an organic solvent. The authors claimed that within this thin polymer film there was a phase separation between donor and acceptor, forming a so-called heterojunction structure. The electron donor and acceptor were connected to each other, forming a net-like structure. A polymer solar cell with a sandwich structure (see Figure 6.3) was fabricated. In this device, the formation of nanoscale donor and acceptor domains created a large donor–acceptor interface, which dramatically increased the charge separation efficiency. Although the power conversion efficiency was not high and the working mechanism was not clear at that time, this work proved the possibility of making solar cells based on solution processing, which opened a new field in novel solar cell technology.

In the next phase of polymer solar cell development, the choice of solvents for thin-film deposition [22], the use of high performance p-type conjugated poly(3-hexylthiphene) (P3HT) [23] and n-type fullerene derivative $PC_{71}BM$ (Figure 6.2) [24], the post thermal annealing of photoactive layer [23], and the introduction of low-band-gap polymer [25], were all considered as the key milestones. With these results, the general relations among materials, device structure and device performance, and the working principles were getting more and more understood. Today, the single junction organic solar cell has achieved efficiency of 9.4% [26], and almost 12% efficiency has been reported for multi-junction tandem solar cells [27,28]. Furthermore, large-scale organic solar cell modules have reached an efficiency of 6.8% [7], showing promising future of their applications (Figure 6.4).

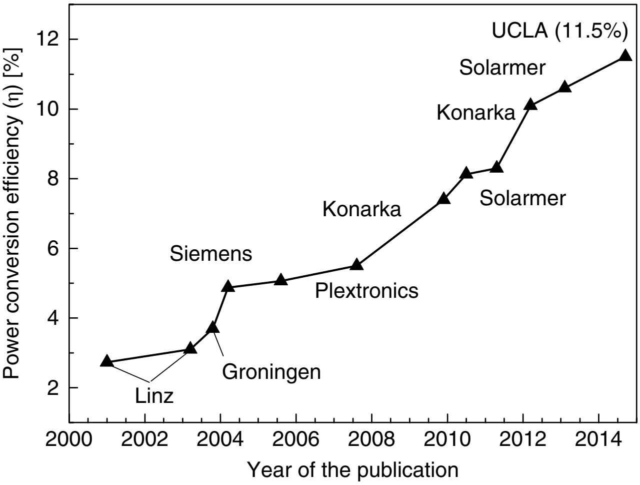

Figure 6.4 Efficiency development of the organic thin-film solar cell

With the steady increase of efficiency over the years, issues that limit the industrialization of organic solar cells, including lifetime and large-scale manufacturing of organic solar cells have attracted more and more attention [29,30]. The most recently emerged printed electronics provide a new thinking for organic solar cells. Since organic semiconductors have excellent compatibility with flexible substrates and can be solution processed, printing would be the most cost-efficient way to mass-produce solar cells. The combination of organic solar cells with printed electronics leads to a new research area: printable organic solar cell technology, which involves material science, solid-state physics, semiconducting devices and printing engineering. In this chapter, the principles, structures and fabrication of printable organic solar cells will be discussed, together with its current status and challenges. The future prospect of this new technology will also be analyzed.

6.2 Working Principles and Characterization of Organic Solar Cells

6.2.1 *Physical Processes*

Unlike inorganic semiconductors, which generate mobile charge carriers (electrons and holes) upon light illumination, organic semiconductors can only generate strongly bounded electron-hole pairs, so called excitons, by Coulomb interaction. The binding energies for these electron-hole pairs are typically of tenths of eV, which makes it very difficult to dissociate into free charge carriers [31,32]. In order to dissociate the electron–hole pair (exciton) into free charge carriers, p-n heterojunctions are usually introduced by using electron donor (p-type semiconductor) and electron acceptor (n-type semiconductor) in organic solar cells. The basic physical processes of an organic solar cell include the following five steps [32] (as illustrated Figure 6.5):

1. Photon absorption and exciton generation: Photons with energy above the optical band gap of the organic semiconductor are absorbed by the molecules. Electrons move from the highest occupied molecular orbital (HOMO) energy level to the lowest unoccupied

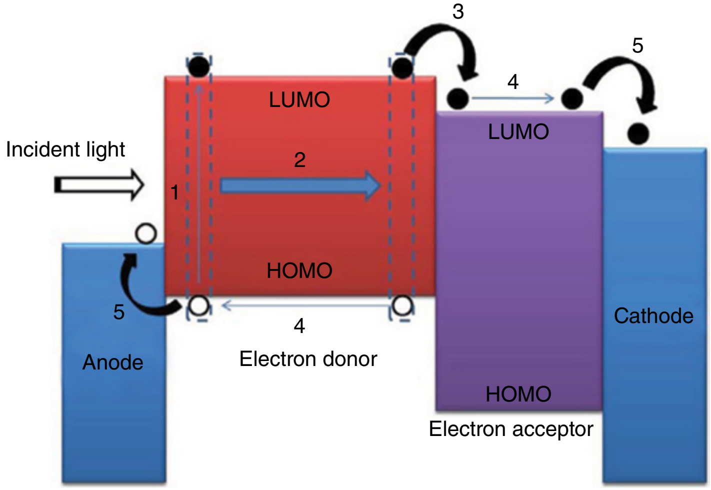

Figure 6.5 The five steps associated with organic solar cells operation: (1) photon absorption and exciton generation; (2) diffusion of exciton; (3) exciton dissociation and charge carrier generation; (4) charge transport; (5) charge carries extraction and current generation

molecular orbital (LUMO) energy level, and consequently generate high energy electron–hole pairs bonded by Coulomb attraction, called excitons.

2. Diffusion of excitons: The excitons can diffuse freely within their lifetime. One of the major problems that influences device performance is the annihilation of excitons during the diffusion process.
3. Exciton dissociation and charge carrier generation: When the exciton diffuses to the donor–acceptor interface, intermolecular electron transfer between donor and acceptor occurs if the LUMO energy level of the donor is higher than that of the acceptor, which creates a cation of the donor and an anion of the acceptor. The high energy exciton is then dissociated into charge carriers.
4. Charge transport: After dissociation, the free electrons and holes move via acceptor and donor pathways towards the cathode and anode, respectively. During the movement, the free electrons and holes can potentially be quenched or recombined, which is another key factor causing poor device performance.
5. Charge carriers extraction and current formation: The electrons and holes are finally collected by their corresponding electrodes and consequently an electrical current flow is generated.

6.2.2 *Basic Structure*

An organic solar cell typically consists of multilayer structures, in which a photoactive layer is sandwiched between two electrodes (Figure 6.6). The photoactive layer is where the aforementioned five physical processes take place, that is photon absorption and creation of excitons, diffusion of excitons, dissociation of charge carriers at D/A interface, charge transport, and extraction of charge carriers [33].

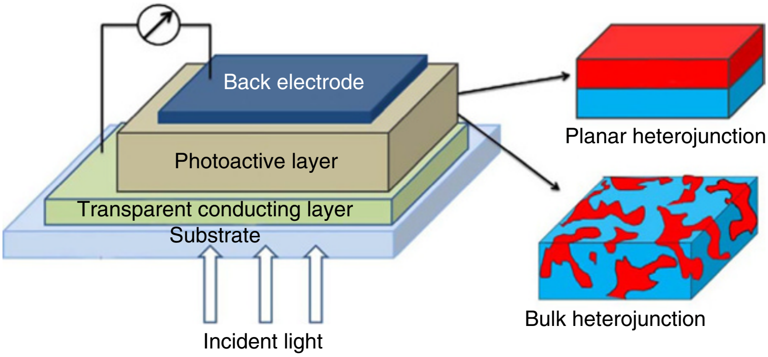

Figure 6.6 Typical device configuration of organic solar cells: planar heterojunction solar cell and bulk heterojunction solar cell

Within the photoactive layer there are electron donor and electron acceptor materials. Depending on the layer structure between the donor and acceptor, organic solar cells can be divided into two types: planar heterojunction solar cell (PHJ), and bulk heterojunction solar cell (BHJ). In a PHJ cell, the donor and acceptor layers are sequentially stacked layer by layer, whereas in a BHJ cell, the electron donor and acceptor materials form interpenetrating network morphology with a phase separation at nanoscale (Figure 6.6). As the diffusion length of excitons for most organic semiconductors is only about 4~20 nm [34–36], the donor or acceptor layers cannot be too thick, which adversely reduces the photon absorption length and thus leads to low quantum efficiency. The relatively small D/A interface area is also a limiting factor of charge dissociation efficiency in planar heterojunction. In contrast to a PHJ cell, the nanoscale interlacing network of donor and acceptor in a BHJ cell decreases the distance between donor and acceptor, and consequently reduces the necessary diffusion length for the excitons as well as increases the effective D/A interfacial area. Both factors would be beneficial to the device performance. It has been proved that charge dissociation efficiency in a BHJ solar cell can reach to 100% [37,38]. However, because the donor and acceptor phases in a BHJ solar cell are not vertically continuously distributed, recombination of a free electron and hole cannot be suppressed during the charge transport process, which could affect the device performance as well.

In general, bulk heterojunction photoactive layers can be deposited in solution process with a mixed solution of donor and acceptor [39] and the nanoscale phase separation occurs spontaneously during the thin-film deposition. However, it is more difficult to deposit organic layers by solution process in a layer-by-layer manner, because the solvent of each newly deposited layer might destroy the pre-deposited organic layer. Nevertheless, with careful selection of solvents, planar heterojunction solar cells can be fabricated [40–42].

With better understanding of the physical processes in organic solar cells, various functional materials that can facilitate charge transport and extraction in organic light emitting diodes (OLED) have also been applied to organic solar cells to improve device performance. Multilayered organic solar cells with different charge injection or blocking layers were developed [43,44]. In addition, novel device structures, such as tandem cells [45–47], inverted solar cells, and so forth [48,49] were also developed to broaden the range of spectra response and to improve the device stability. These novel device structure concepts will be described in detail in Section 4 of this chapter.

6.2.3 Characterization

Although the working principle of organic solar cells is different from that of inorganic solar cells, the characterization of an organic solar cell is similar to that of an inorganic one, that is a current-voltage sweeping curve (I-V) and spectrum response (SR).

6.2.3.1 I-V Characteristics

The current-voltage curve (I-V) is generally used to characterize an organic solar cell. In the dark, the solar cell should act as a simple diode, and the ideal factor of this cell can be evaluated (Figure 6.7). Under illumination, the whole I-V characteristics curve moves to the 3rd and 4th quadrants. Several important parameters, including open circuit voltage (V_{OC}), short circuit current (I_{SC}), fill factor (FF), maximum power point (P_{max}), and power conversion efficiency (η) can be derived from the I-V characteristics.

The open-circuit voltage (V_{OC}) is the maximum voltage at zero current. The V_{OC} is the voltage difference between heterojunction interfaces on the open circuit condition under light illumination. In an organic solar cell, the V_{OC} is linearly dependent on the HOMO level of the donor and the LUMO level of the acceptor. Considering the voltage loss at various interfaces, the V_{OC} can be estimated using an empirical equation as follows:

$$V_{\mathrm{OC}} = \left(E^{A}_{LUMO} - E^{D}_{HOMO} - 0.3eV\right)/\,e\left(\mathrm{V}\right) \tag{6.1}$$

where E^{A}_{LUMO} and E^{D}_{HOMO} are the LUMO energy level of the acceptor and the HOMO energy level of the donor.

The short-circuit current (I_{SC}) is the maximum current through the solar cell under light illumination when the bias voltage across the cell is zero. I_{SC} is directly related to the number of charge carriers generated within the photoactive layer. Therefore, I_{SC} depends on the efficiencies of three steps: photon absorption, exciton dissociation and charge transport.

Fill factor (FF) is defined as the ratio of maximum power to the product of V_{OC} and I_{SC} as in the following equation:

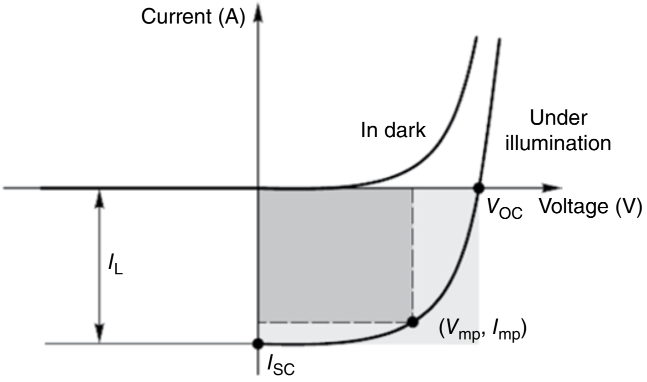

Figure 6.7 Typical I-V characteristics of organic solar cells

$$\mathrm{FF} = \frac{p_{max}}{V_{OC} \cdot I_{SC}} = \frac{V_{max} \cdot I_{max}}{V_{OC} \cdot I_{SC}} \tag{6.2}$$

where $P_{\max}$ is the maximum power of a solar cell, $I_{\max}$, and $V_{\max}$ are the corresponding current and voltage at the maximum power point. As shown in figure 6.7, FF is the area ratio of the rectangle with a length of $V_{\max}$ and a width of $I_{\max}$ to the large rectangle with a length and width of V_{OC} and I_{SC}, respectively. A good solar cell usually has an FF of 60–65%.

Power conversion efficiency (η) is defined as the ratio of $P_{\max}$ to the input solar power, which can be written as

$$\eta = \frac{p_{max}}{p_{in}} = \frac{V_{max} \cdot I_{max}}{p_{in}} = \frac{V_{OC} \cdot I_{SC} \cdot FF}{p_{in}} \tag{6.3}$$

It is worth mentioning that the above parameters are usually measured at 25° C under the illumination of AM1.5G, which has a standard light intensity of 100 mW/cm^2.

6.2.3.2 Spectrum Response

Spectrum response is another important parameter that describes the quality of a solar cell. Spectrum response defines the current collection efficiency at the electrode per number of incident photons on the solar cell area at a given wavelength. Spectrum response is sometimes also defined as the quantum efficiency (QE). Depending on the types of input light, the quantum efficiency can be further divided into external quantum efficiency (EQE) and internal Quantum Efficiency (IQE).

External Quantum Efficiency (EQE) is the number ratio of collected carriers to all the incident photons, whereas the Internal Quantum Efficiency (IQE) is the number ratio of collected carriers to the photons absorbed by the cell. Therefore, IQE excludes the light that has not been absorbed by the cell; for example, photon loss due to light transmission or reflection. A study of IQE is useful for understanding the intrinsic performance of a cell.

In organic solar cells, only photons with energy larger than the band-gap of an organic semiconductor can be absorbed to generate electron–hole pairs, while photons with lower energy cannot be used. The spectra response range of the solar cell is therefore determined by the band-gap of organic semiconductors. Figure 6.8 shows the I-V characteristics of P3HT:PC$_{61}$BM solar cell. From the I-V curve, the performance parameters have been calculated to be V_{OC} of 0.60 eV, I_{SC} of 12.5 mA/cm^2, FF of 59%, and power conversion efficiency (η) of 4.5%. From the EQE spectra of the P3HT:PC$_{61}$BM solar cell and the absorption spectrum of P3HT, the offset of spectra response of the P3HT:PC$_{60}$BM cell is found to center at about 675 nm (optical band-gap of 1.85 eV), which is consistent with the offset of absorption spectrum. Since the absorption of PC$_{61}$BM is very weak in the visible range, the photon response of a polymer:fullerene blend solar cell is primarily determined by the electron donor materials.

6.2.4 *The Main Factors Influencing Device Performance*

According to the working principle of organic solar cells (see section 6.2.1), one can conclude that the loss of efficiency in an organic solar cell is caused by optical losses, exciton losses due to insufficient transport of exciton, non-radiative recombination losses, and charge carrier

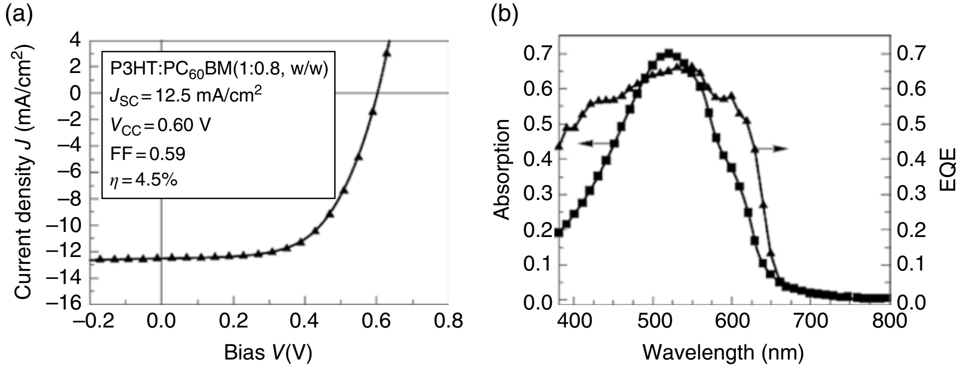

Figure 6.8 (a) I-V characteristics of a typical P3HT:$PC_{61}BM$ based organic solar cells. (b) EQE of the P3HT:$PC_{61}BM$ solar cells and the absorption spectrum of P3HT films

collection losses due to insufficient motilities. Several microscopic models have been developed to give some insight into the above causes.

6.2.4.1 Photon Absorption Ability of Organic Semiconductors

In accordance with the physical process of organic solar cells, only photons with energy greater than the band-gap of the organic semiconductor can be absorbed and subsequently generate electron–hole pairs. Therefore, the photocurrent generated by the organic solar cell is directly related to the photon absorption ability, which is characterized by:

1. Molar extinction coefficient. For a given film thickness, the higher the molar extinction coefficient, the more photons the organic semiconductor can absorb. In an organic solar cell, the thickness of photoactive layer is usually limited due to the low charge carrier mobility of organic semiconductors. Thus, the molar extinction coefficient can provide important information about the light absorption ability of organic semiconductors.
2. Mismatch between the absorption spectrum of an organic semiconductor and the solar radiation spectrum. Most organic semiconductors have a large band-gap (~2 eV) and narrow absorption width. Figure 6.9 shows the AM 1.5G solar spectrum and the absorption spectrum of the commonly used P3HT donor. It is found that the absorption spectrum of P3HT covers from 400 to 700 nm, which is not matched with the condensed energy range of the solar spectrum (500~900 nm). This means that better light harvesting organic semiconductors via lowering the optical band-gap.

6.2.4.2 Energy Level Arrangement of Donor and Acceptor

In organic solar cells, it is found that open circuit voltage (V_{OC}) is linearly dependent on the HOMO level of the donor and the LUMO of the acceptor (equation 6.1) [50]. Thus, V_{OC} is directly related to the energy levels of the donor and the acceptor. Figure 6.10 is a schematic diagram showing how the device performance depends on the energy levels arrangement of donor and acceptor. For an ideal organic solar cell, the difference between the donor HOMO

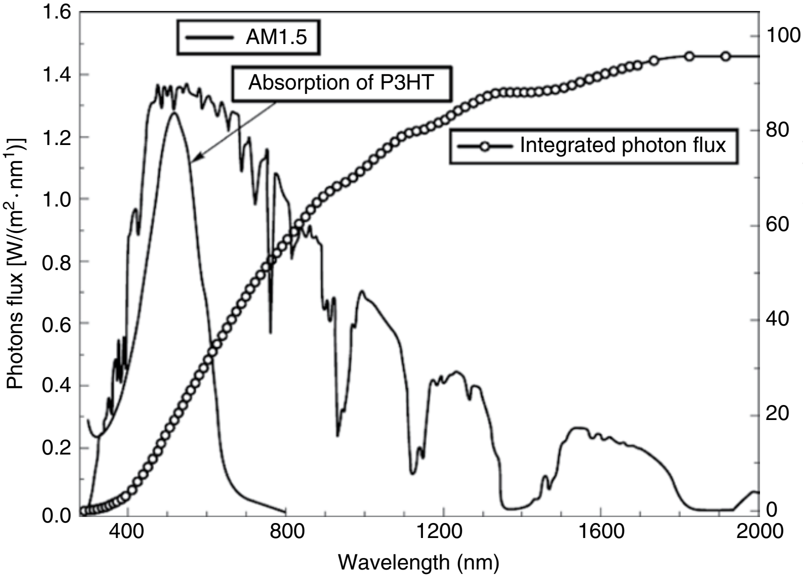

Figure 6.9 AM 1.5G solar spectrum, the resulting cumulative intensity, and the absorption spectrum of P3HT

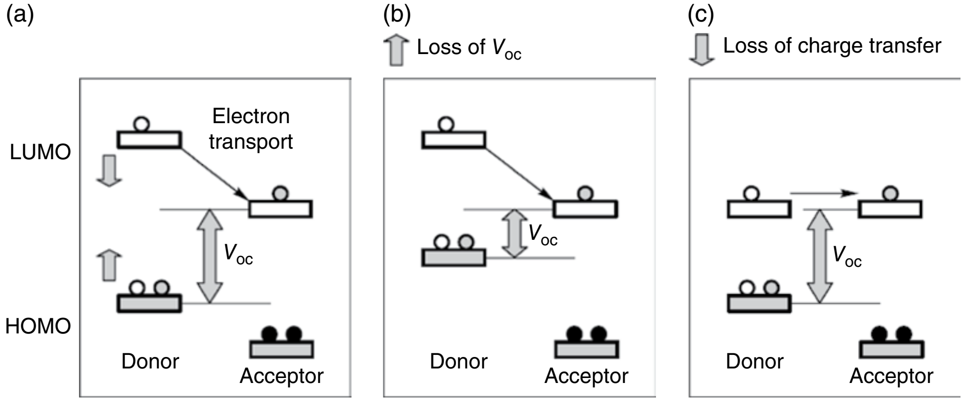

Figure 6.10 The dependence of device performance on the energy level arrangement of donor and acceptor

and the acceptor LUMO should be large enough to obtain a high V_{OC}; on the other hand, a driving force of more than 0.30 eV (energy difference between the LUMO of donor and the HOMO of acceptor) is required to achieve efficient electron transfer (Figure 6.10a). An increase in the HOMO level of the donor will lead to a lower V_{OC} (Figure 6.10b), whereas a decrease in the LUMO level of the donor will lead to insufficient electron transfer between donor and acceptor (Figure 6.10c). So, besides the reduction of the band-gap, the donor and acceptor materials for high efficiency organic solar cells must be designed to optimize the D/A

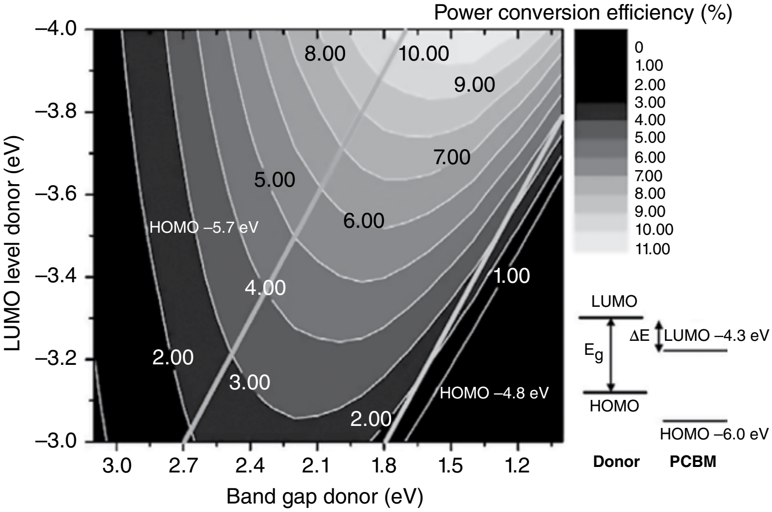

Figure 6.11 The calculated energy-conversion efficiency vs. the band gap and the LUMO level of donor in the polymer:PCBM blend solar cells. (Reprinted from ref. [51] with permission from John Wiley and Sons)

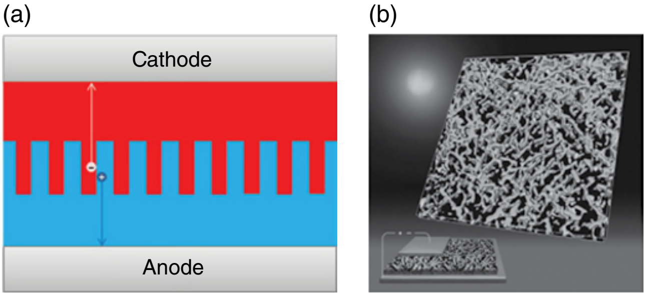

Figure 6.12 (a) Schematic diagram of an ideal structure of BHJ solar cell. (b) Morphology images of P3TH:PCBM obtained by 3D reconstruction of TEM (Reprinted from reference [60] with permission from John Wiley and Sons)

combination with matched HOMO and LUMO levels. Scharber et al. investigated the relationship between the energy conversion efficiency of a polymer:$PC_{61}BM$ BHJ solar cell and the LUMO level of the donor, and demonstrated that efficiency of more than 10% should be achievable with donor materials having an optical band-gap of 1.4–1.5 eV and a HOMO energy level of –5.4 eV (Figure 6.11) [51].

6.2.4.3 Morphology of Photoactive Layer

The energy conversion efficiency of solar cells is significantly dependent on the nanoscale morphology of photoactive layer. Figure 6.12 shows the schematic diagram of an ideal nanophase separation structure of the photoactive layer in a BHJ solar cell, in which the donor and acceptor connect to an anode and cathode, respectively, to minimize the charge recombination losses. Meanwhile, the donor and acceptor form an interpenetrating network morphology, where the interface distance is less than the exciton diffusion length. This is beneficial for efficient charge separation. Additionally, such a nanoscale interlacing network increases the D/tA interfacial area enormously, resulting in improved device performance.

However, due to the fact that the nanostructure forms spontaneously during the deposition of the photoactive layer, it is quite a challenge to design or to have exact control of the nanoscale morphology. Important studies showed some general relationships between film processing conditions and the final film morphology [52–54]. It is found that solvents [25,55], ratios between donor and acceptor [56], thermal annealing [57,58] or solvent annealing [59] of the photoactive layer are all influential on the formation of nanoscale morphology of the photoactive layer and, hence, on the energy conversion efficiency of solar cells. Such understanding of the underlying structure–property relationship can serve as a guide for making better organic solar cells.

Current experimental methods have limitations in the study of film morphology. The commonly used atomic force microscope (AFM) can only investigate the surface morphology. Recently, a three-dimensional transmission electron microscope (3D-TEM) was developed to investigate the 3D morphology with a nanometer resolution [60,61]. 3D-TEM can provide the information of donor and acceptor distribution in the photoactive layer. Oosterhout et al. (2009) quantitatively analyzed the distribution of the D/A interface area and the distribution of minimum space distance. They found the correlation between the 3D morphology and device performance was based on the distribution of exciton quenching that resulted from the charge carrier dissociation and transport [62].

In contrast to BHJ solar cells, it is relatively simple to study the influence of film morphology on energy conversion efficiency in planar heterojunction (PHJ) solar cells where the donor and acceptor are sequentially stacked. However, it was found that the donor and acceptor molecules diffused into and mixed with each other during operation. The device performance ended up largely correlated with the micro-heterojunction at the D/A interface of PHJ solar cells [40,42]. Up to now, there are only a few reports on the investigation of morphology–performance correlation for PHJ solar cells due to the difficulties in fabrication of PHJ solar cells by solution processing and the lack of methods for 3D morphology study.

Overall, the device performance is impacted by various factors, such as the molecular weight of the donor [63,64], the charge carrier mobility of organic semiconductors [65] and the interface between different layers [66–68]. To obtain a high efficiency solar cell, all the aspects, including the combination of donor and acceptor materials, device structure optimization and thin-film morphology control should be considered carefully.

6.3 Materials for Organic Solar Cells

Depending on their functions in a solar cell, the materials used in organic solar cells can be classified as transparent substrate, electrode, semiconductors and other functional materials. Every material has to perform well in order to facilitate the maximum power generation in the external circuit. In addition, their compatibility with solution processing needs to be considered as well, in order to facilitate the low cost manufacturing of solar cells.

6.3.1 Transparent Substrate

In a typical organic solar cell, the photoactive layer is sandwiched between two electrodes. One is low-work-function metal, such as aluminum or calcium, and the other should be transparent to allow sunlight through. Besides the high transparency, the adhesiveness to organic conducting thin film and the compatibility with solution-processing methods also need to be considered when selecting a transparent substrate. Glass is the most commonly used transparent substrate in organic solar cells due to its excellent transparency and chemical stability. However, the rigidity and brittleness of glass have been identified as significant disadvantages for use in continuous roll-to-roll processes. On the other hand, polymeric materials are highly compatible with roll-to-roll processing for their flexibility. Therefore, a number of polymers have gained considerable attention as promising flexible substrate materials for organic solar cells, due to their flexibility, bendability, light weight and transparency [69]. The polymeric materials that have been used in organic solar cells as transparent substrates include polyethylene terephthalate (PET) [70–74], polyethylene naphthalate, (PEN) [75–77], polycarbonate (PC) [78–81], poly(4,4′-oxydiphenylene-pyromellitimide, Kapton), polyethersulfone (PES) [82–84], poly-L-lactide (PLLA) [85], and so forth.

6.3.2 Transparent Conductive Electrode

A transparent conductive electrode is a thin-film electrode with high transparency and high conductivity. Different types of transparent conductive electrodes, including transparent conductive oxide film, conductive polymer film, metal grid, carbon nanotube films or graphene films, have been developed for organic solar cells.

6.3.2.1 Metal Oxide Film

Of all the above-mentioned transparent conductive electrodes, metal oxide is the most commonly used electrode, typically the indium tin oxide (ITO) film [68]. First, the sputtering deposition of ITO is a mature technology. The film thickness, conductivity and optical transparency can be accurately controlled. More importantly, ITO has excellent charge transport properties. Apart from ITO glass, ITO coated plastic films are also widely used in organic solar cell devices, such as PET/ITO [70–73], PEN/ITO [75,77]. Although ITO film has many advantages, the limited indium resource on earth can cause the fluctuation in the cost of indium. The price of indium has been increasing in the last few years since the rapid rise in demand of touch panels in mobile phones and tablet computers. ITO substrates have become an important cost factor in organic solar cells [86]. Moreover, the toxicity and mechanical rigidity of indium would also be a problem for large-scale application. In response to demand, other transparent metal oxide thin films are emerging as interesting materials for organic solar cells [87,88]. These metal oxide thin films include fluorine doped tin oxide (SnO2:F, FTO) [89–91], aluminum doped ZnO film (ZnO:Al, AZO) [92–94] and titanium oxide (TiO2) [95]. They have shown performances comparable to ITO and could be suitable candidates to replace ITO film.

6.3.2.2 Conductive Polymer Film

Poly(3,4-ethylenedioxythiophene):polystyrene sulfonate (PEDOT:PSS) composite film is the most promising conductive polymer which has been well investigated due to its good environmental stability, good optical transparency and reasonably high conductivity (above 1400 $S{\cdot}cm^{-1}$)[96]. Figure 6.13 displays the structures of PEDOT and PSS. PEDOT is prepared from ethylenedioxythiophene (EDOT) monomers and is not soluble in water due to its rigid polymer chain. By using polystyrenesulfonate sodium (PSS) as supporting electrolyte during the polymerization of EDOT, the resulting polymers can be dispersed in water, offering the possibility for solution processing. The PEDOT:PSS film can be easily deposited, for example, by spin coating, screen printing and ink-jet printing [97–99]. In organic solar cells, the PEDOT:PSS film can be used as hole extraction material to modify the interfacial property between the active layer and ITO [100].

6.3.2.3 Thin Metal Film and Metal Grid

When the thickness of a metal thin film is less than 20 nm, its absorbance and reflection are greatly reduced. Therefore, these ultrathin metal films usually show good optical transparency and can be used as transparent conductive electrodes in organic solar cells [101–103]. It should be noted that metal deposition follows an island growing model, which means the first few nanometers of meal film might not be continuous. Therefore, when the thickness of metal film is too thin, it might significantly impact on the conductivity. To keep the best balance between transparency and conductivity, the thickness of the metal electrode is usually around 15 nm, which yields a sheet resistance around 10 Ω/sq. [104].

In recent years, a conductive polymer combined with a metal grid has emerged as a practical alternative to the transparent conductive electrode. Tvingstedt and Inganäs (2007) used the lithographic method to pattern silver grids with width of 20–40 μm, spacing of 100–800 μm, and thickness of 100 nm. The light transmittance and sheet resistance of silver grids are

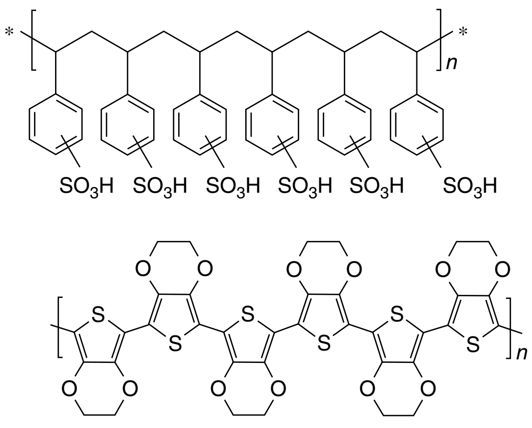

Figure 6.13 The structures of poly(3,4-ethylenedioxythiophene) (PEDOT) and polystyrenesulfonate (PSS)

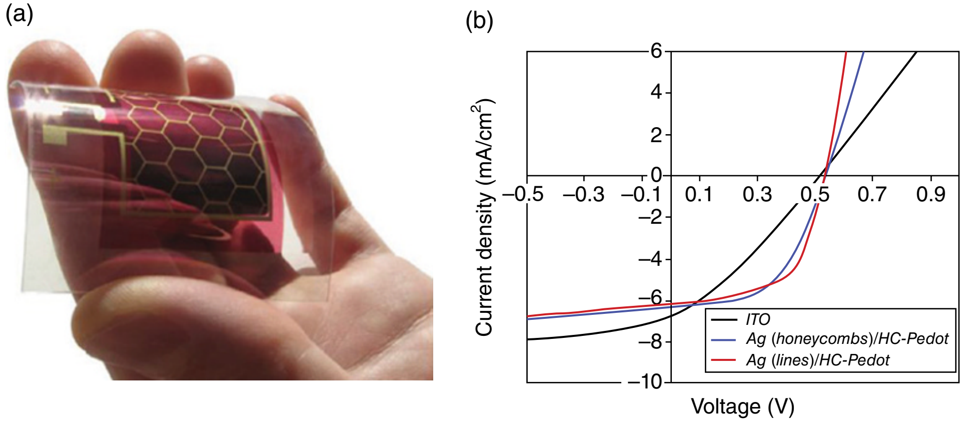

Figure 6.14 (a) Flexible organic thin film solar cell device with areas of 2×2 cm^2. (b) Current density-voltage (*J*-*V*) curves. (Reprinted from reference [106] with permission from Elsevier)

85% and 0.5 Ω/sq., respectively. Compared to conventional ITO film, silver grids demonstrate better light transmittance in wavelength beyond 800 nm. When used in organic solar cells, a thin film of PEDOT:PSS is required on top of silver grids.[105] Galagan and coworkers reported a honeycomb grid electrode with a line width of 160 μm and line spacing of 5 mm by screen printing on top of PEN film. With an additional layer of high conductivity PEDOT:PSS, the resulting electrode has a sheet resistance of 1 Ω/sq., and an average light transmittance of 70%. Large-area organic solar cells (2.0 × 2.0 cm^2) were fabricated on this type of electrode and high fill factors (ca. 53%) and power conversion efficiency (1.9%) were achieved, which is almost two times higher than that fabricated on an ITO/PEDOT:PSS electrode (Figure 6.14) [106].

Very recently, the authors' Printable Electronics Research Center (PERC) reported using PET/Ag grid as transparent electrode to fabricate ITO-free flexible organic solar cells. Unlike the printed silver grid electrode developed by Galagan et al., the Ag-grid electrode developed by PERC has much finer honeycomb structure. The width of the Ag line is around 3 μm and the diagonal length is around 130 μm. Because of its fine metal grids, these PET/Ag-grids have excellent transparency of more than 85% with low sheet resistance of less than 5 Ω/sq. A layer of highly conductive PEDOT:PSS (Hereaus PH1000) on the top of Ag-grid is added to increase the charge collection efficiency. Flexible organic solar cell using this PET/Ag-grid as the electrode, and P3HT:PCBM as the photoactive layer, achieved a PCE of 1.36% (Figure 6.15) [107]. When using high performance conjugated polymer, PTB7, as the donor, the highest power conversion efficiency of 5.85% was achieved for a large-area flexible polymer solar cell [108].

In another work, Hany et al. reported on a semi-transparent flexible electrode based on metal and polymer fibers woven into a mesh. The conductivity and transmittance are dependent on the ratio of metal wires to polymer fibers. Solar cells using blends of P3HT:PC_{61}BM as the photoactive layer have reached PCEs of 2.2% with a ratio of 3:1 between polymer fibers and metal wires for the electrode, which is comparable to cells with ITO/glass (Figure 6.16) [109]. This type of electrode is compatible with roll-to-roll printing process.

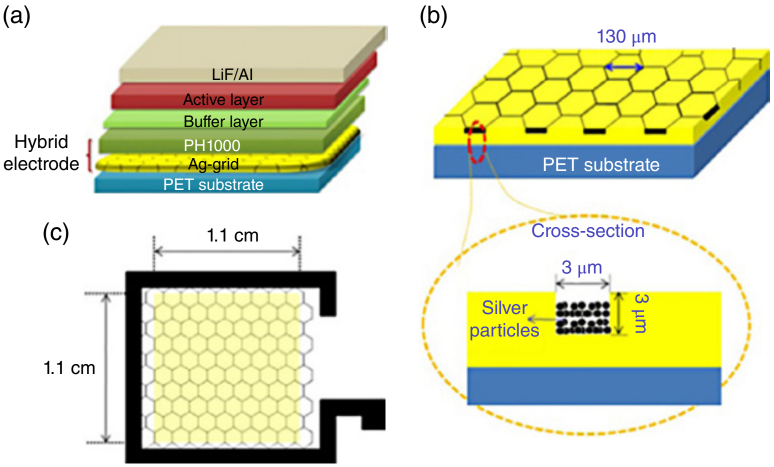
(a)
LiF/Al
Active layer
Buffer layer
PH1000
Ag-grid
PET substrate
Hybrid electrode
(b)
130 μm
PET substrate
Cross-section
3 μm
Silver particles
3 μm
(c)
1.1 cm
1.1 cm

Figure 6.15 (a) Schematic of device structure. (b) Ag grid deposited PET substrate. (c) Top view of the device with 1.1 × 1.1 cm^2 area. (Reprinted from reference [107] with permission from Elsevier)

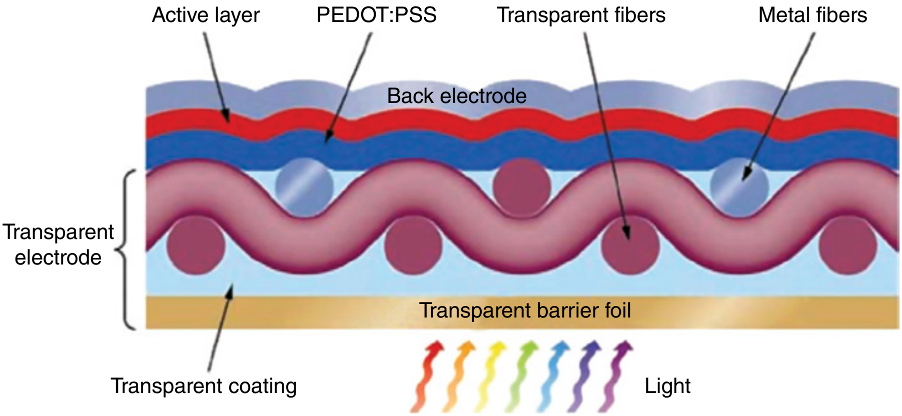
Active layer
PEDOT:PSS
Transparent fibers
Metal fibers
Back electrode
Transparent electrode
Transparent barrier foil
Transparent coating
Light

Figure 6.16 Schematic of an organic thin-film OPV device fabricated by interwoven of metal and polymer. (Reprinted from reference [109] with permission from John Wiley and Sons)

6.3.2.4 Carbon-rich Materials

More recently, it was found that carbon-rich materials, such as carbon nanotube (CNT) and graphene are particularly useful for transparent conductive films [110,111]. As demonstrated by Barnes et al. carbon nanotube-based thin film has a sheet resistance of 60 Ω/sq., which is comparable to those of ITO films [110]. Although thicker CNT films are generally more efficient in reducing the resistance, they are also less transparent (Figure 6.17) [111]. Therefore, the key issue for carbon nanotube or graphene transparent conductive films is the balance between transparency and sheet resistance. However, the rather high sheet resistance may make them difficult in large scale application.

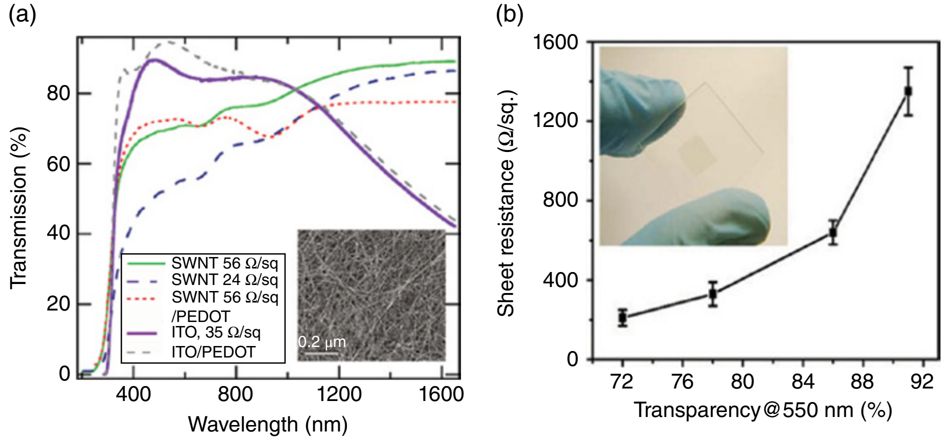

Figure 6.17 (a) The transmittance of carbon nanotube film and ITO/glass (inset: the TEM image of carbon nanotube film. (Reprinted from reference [110] with permission from AIP Publishing LLC) (b) Sheet resistance versus transmittance of graphene film. (Reprinted from reference [111] with permission from AIP Publishing LLC)

In summary, significant progresses have been made in developing transparent conductive electrodes in the last few years. Although most of research labs are still using ITO as the transparent electrode, novel transparent conductive materials with a remarkable combination of high electrical conductivity, optical transparency and low cost should be available in the near future. The development of high quality transparent electrodes will also push the organic solar cell technology closer to practical applications.

6.3.3 Organic Semiconductor Materials

As mentioned before, the most important component of an organic solar cell is the photoactive layer. For most of the conventional organic solar cells, blends of *p*-type (electron donor) and *n*-type (electron acceptor) organic semiconductors are used as the photoactive layer. The main task in developing organic semiconductors is to find the appropriate donor and acceptor combination to reduce the energy losses for each process (Figure 6.5) thereof to improve the power conversion efficiency. The categories and properties of organic semiconductors have been reviewed in Chapter 2. In this section, a general introduction to the organic semiconductors for use in organic solar cells will be given according to their functionalities.

6.3.3.1 *p*-Type Organic Semiconductors

Poly(2-methoxy-5-(2′-ethylhexyloxy)-1,4-phenylene vinylene (MEH-PPV) was the first and the most popular *p*-type conjugated polymer used in organic solar cells in the early research on polymer solar cells (from 1995 to 2003). PPV derivatives have high molecular weight and good film forming ability [21,39]. The maximum absorption wavelength of PPV derivatives is positioned between 450–580 nm, which is not ideal for sunlight conversion. Devices based on PPV derivatives exhibited low PCEs (around 2–3.5%) [24].

Furthermore, PPV derivatives suffer from poor photochemical stability owning to the chemical reactive double bonds on the main chain [112].

The breakthrough in this area was the discovery of poly(3-hexylthiophene) (P3HT) for bulk heterojunction organic solar cells, made by Padinger et al. in 2003 [23]. Regioregular P3HT has since evolved to become a ubiquitous material for organic electronic devices, due to its easy preparation, red-shifted absorption spectrum, stronger intermolecular interactions, and higher charge carrier mobility (10^{-4}–10^{-2} $cm^2 \cdot V^{-1} \cdot s^{-1}$) (Figure 6.18). The improved performance of P3HT is ascribed to the tendency of forming semicrystalline lamellar microstructures after thermal annealing [58]. Introduction of NiOx for hole injection led to a high PCE of 5.2% [113]. Despite good device performance, P3HT is a wide band-gap donor material (1.85 eV, 670 nm) and thus only absorbs the light at a wavelength less than 670 nm, which accounts for only 44% of the total solar spectrum. Taking the energy losses into account, such as the energy loss of high energy exciton splitting and the energy loss during charge transportation, the short circuit current of a P3HT:$PC_{61}BM$ solar cell is usually limited to 12.8 mA/cm^2, which limits the PEC to less than 6% [114]. However, by incorporating a new acceptor with a higher LUMO level, such as indene-C_{60} bisadduct (ICBA, see Figure 6.23), the highest achieved efficiency for a P3HT-based solar cell was 6.48% [115,116]. Nevertheless, P3HT shows reasonable photovoltaic performance in an organic solar cell and has been widely used as a model polymeric semiconductor for printing processing [117] and investigation of solar cell stability [118].

In order to gain higher power conversion efficiency, p-type semiconductors with reduced optical band-gap is the aim for the development of novel organic solar cell materials. With this aim, several novel low band-gap polymers have been developed, and the device performance was increased to more than 8% for a single junction solar cell [119,120]. Figure 6.19 shows the chemical structure of some low band-gap *p*-type polymers. For more information about conjugated polymers for use in organic solar cells, the interested reader is referred to the relevant review articles [119,120].

The low band-gap copolymer (poly(4,4-dialkyl-cyclopenta[2,1-*b*:3,4-*b′*]-dithiophene-*alt*-2,1,3-benzothiadiazole) (PCPDTBT) was designed with a 4,4-dialkyl-cycolpentadithiophene (CPDT) as an electron-rich segment alternating with electron-deficient benzothiadiazole (TBT) unit along the conjugation chain. The optical band gap of PCPDTBT is around1.40 eV [25,121], which is ideal for polymer solar cells [51]. The fully conjugated donor–acceptor block structure is beneficial to the red-shift of absorption spectrum. In an early report, BHJ solar cells based on PCPDTBT as the donor and $PC_{71}BM$ as the acceptor achieved PCE of 3.5% [121,122]. By using a high boiling point organic solvent as an additive, which promotes the crystallization of polymer, a high PCE of 5.5% was latterly achieved [25].

Similar to PCPDTBT, poly[[9-(1-octylnonyl)-9*H*-carbazole-2,7-diyl]-2,5-thiophenediyl-2,1,3-benzothiadiazole-4,7-diyl-2,5-thiophenediyl] (PCDTBT) was developed as another donor material for organic solar cells. Solar cells based on PCDTBT:$PC_{71}BM$ have achieved a PCE as high as 6.1% by an optimized device structure [123]. It has a backbone consisting of repeating carbazole and benzothiadiazole units through the alternative electron push–pull connection, resulting in an optical band-gap of 1.90 eV. Replacing the CPDT unit in PCPDTBT with a carbazole unit, the PCDTBT has a lower HOMO energy level of −5.5 eV, which increases the V_{OC} of the final device. Poly[(4,4′-bis(2-ethylhexyl)dithieno[3,2-*b*:2′,3′-*d*]silole)-2,6-diyl-alt-(2,1,3-benzothiadiazole)-4,7-diyl] (PSBTBT), which consists of dithienosilole and benzothiadiazole as the electron donor and the electron acceptor unit, respectively,

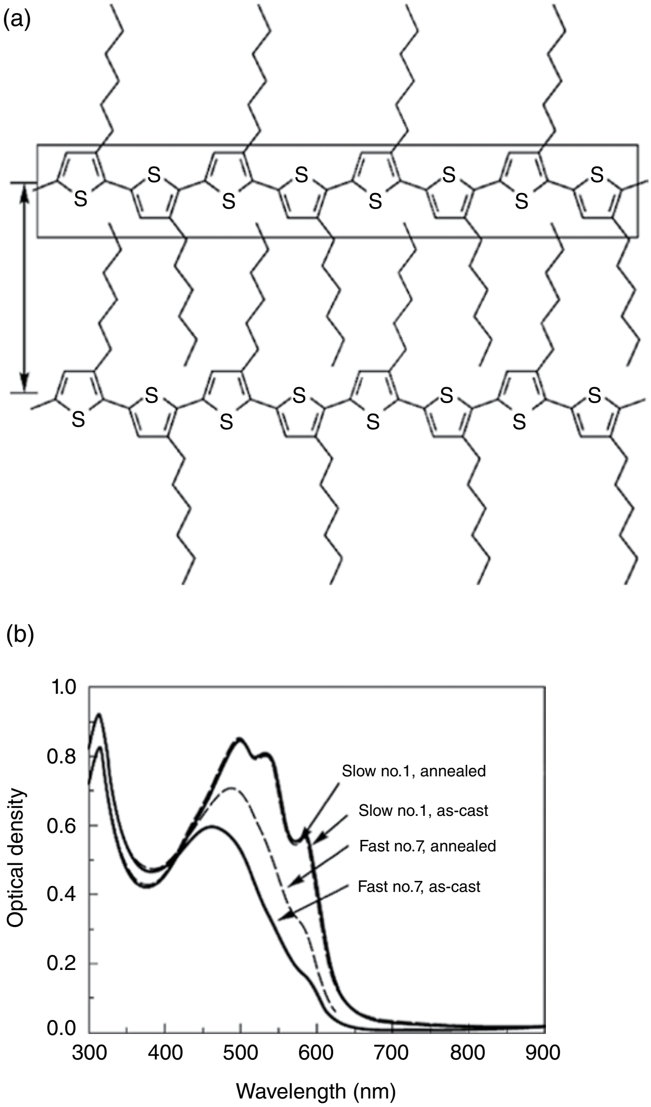

Figure 6.18 (a) Schematic diagram of π-π interactions of P3HT, and (b) the UV–Vis spectra of P3HT thin film at different deposition condition. (Reprinted from reference [59] with permission from Nature Publishing Group)

and contributes to a high PCE of 5.1% [124]. A new alternating copolymer of dithienosilole and thienopyrrole-4,6-dione (PDTSTPD) has both a low band gap of 1.73 eV and a deep HOMO energy level of −5.57 eV. When blended with $PC_{71}BM$, it exhibited a PCE of 7.3% in a conventional single junction solar cell devices [125].

A series of conjugated copolymers based on alternating thieno[3,4-*b*]thiophene and benzodithiophene units was prepared by Liang et al. (2009) (the chemical structure of the representative copolymer PTB7 is shown in Figure 6.19 above [126,127]. It is believed that in these polymer

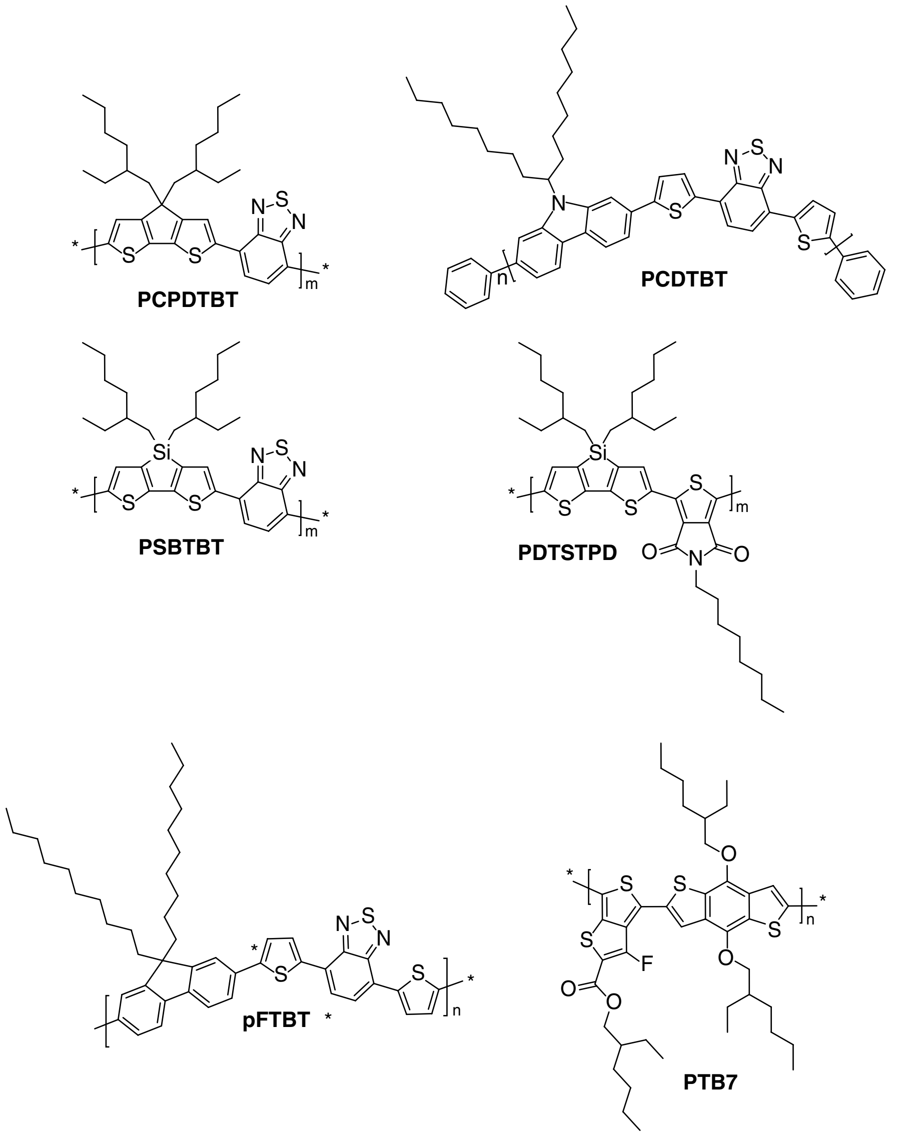

Figure 6.19 Representative low band-gap conjugated polymers

backbones the thieno[3,4-*b*]thiophene unit is coplanar to the benzodithiophene unit, which leads to an extended π-conjugation system. Meanwhile, the thieno[3,4-*b*]thiophene unit stabilizes the quinoidal structure of the conjugated backbone, and consequently results in a low band gap of 1.6 eV [128]. With that, copolymers thieno[3,4-*b*]thiophene and benzodithiophene have been considered as one of the best conjugated polymer for BHJ solar cells and PCEs up to 7% have been reported for conventional single junction solar cell. By using a polymer electrolyte (PFN) as the electron buffer layer, efficiency of 9.2% has been achieved, which is the highest for a single junction polymer solar cell [129].

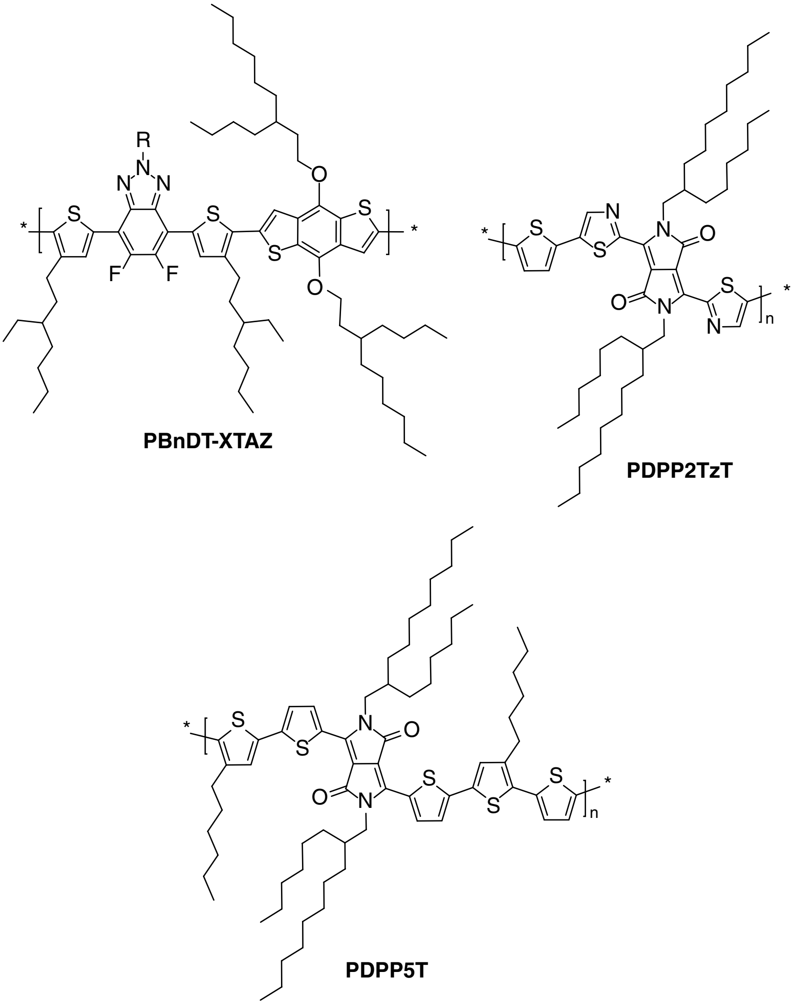

PBnDT-XTAZ

PDPP2TzT

PDPP5T

Figure 6.19 (Continued)

Price et al. (2011) recently developed a new polymer PBnDT-FTAZ by incorporating benzodithiophene (BnDT) as the donor and fluorinated benzotriazole (FTAZ) as the acceptor units, respectively [130]. The introduction of two fluorine atoms into PBnDT-FTAZ provides the polymer with a relatively low-lying HOMO energy level (~ −5.4 eV). Enhanced V_{OC} (~0.75 V) was achieved for a PBnDT-FTAZ:PC$_{61}$BM-based solar cell. It should be noted that BHJ cells based on PBnDT-FTAZ:PCBM exhibit a high efficiency of 7.2% even with an active layer thickness up to 1 μm, which enables the fabrication by conventional printing processes [130].

Diketopyrrolopyrrole (DPP) is a widely used industrial dye with high molar extinction coefficient (10^5 M^{-1}cm^{-1}). Its facile synthesis, ease of structural modification, broad absorption spectrum and high carrier mobility (up to 1.95 cm^2·V^{-1}·s^{-1}) [131] enable it as an attractive acceptor segment in the D–A conjugated polymers [132–135]. Power conversion efficiencies of more than 7% and 9% have been reported for a single junction and tandem solar cells, respectively [136–139]. Very recently, Li et al. (2014) developed a new DPP-containing copolymer PDPP2TzT, in which a thiazole unit is introduced to replace the thiophene unit [140]. Due to the electronegativity of the imine nitrogen group, PDPP2TzT has lower HOMO and LUMO energy levels, and this copolymer can serve as an electron acceptor in a BHJ solar cell. A high PCE of 2.9% was obtained for an all-polymer solar cell using PDPP5T:PDPP2TzT blended film as the photoactive layer [140].

Besides good performance in organic solar cells, polymeric semiconductors have other advantages such as high molecular weight and excellent processability. However, their drawbacks are the regioregularity issues, wide molecular weight distribution, low purity, batch to batch inconsistency of property, and so on, which sometimes leads to poor reproducibility in large scale manufacturing. As alternatives to conjugated polymers, some moderate or small molecules with defined structures and molecular weights have been developed for organic solar cells [141,142]. Much effort has been devoted into the design and synthesis of new π-conjugated backbones in this respect, including DPP-containing small molecular derivative $DPP(TBFu)_2$ [143], linear thiophene-derivatives DCAO7T [144,145], dendritic thiophene-derivatives (DOTs) [146,147], and triphenylamine star-shaped derivatives [148] (Figure 6.20). Very recently, new small molecules like p-SIDT(FBTTh2)2 [149] and DR3TBDTT [150] show excellent performance in organic solar cells. A high PCE of more than 8% has been achieved, showing a very promising future for these small molecular semiconductors [151,152].

6.3.3.2 *n*-Type Organic Semiconductors

For the acceptor in organic solar cells, fullerene derivatives [6,6]-phenyl-C_{61}-butyric acid methyl ester ($PC_{61}BM$) are the most widely used material (see Figure 6.2 above). $PC_{61}BM$ offers the advantages of high electron mobility (10^{-3} $cm^2 \cdot V^{-1} \cdot s^{-1}$), low LUMO energy level (~ –4.1 eV) [153] and good solubility in organic solvents. Owing to their high symmetry, C_{60} derivatives show weak absorption in the visible light region and have only limited contribution to a photon-generated current in solar cells. In contrast, a C_{70} derivatives [6,6]-phenyl-C_{71}-butyric acid methyl ester ($PC_{71}BM$) show much intensive visible light absorption (Figure 6.21) [24] Meanwhile, $PC_{71}BM$ has HOMO/LUMO energy levels and electron transport ability similar to $PC_{61}BM$. Therefore, $PC_{71}BM$ has been widely used in the lab to make a high efficiency solar cell. Up to now, most of the record efficiencies of organic solar cells are using $PC_{71}BM$ as the electron acceptor. However, the high price of C_{70} derivatives may limit its widespread application.

According to the empirical equation 6.1, V_{OC} and the consequent PCE of an organic solar cell is dependent on the LUMO energy level of the acceptor. For example, $PC_{61}BM$ has a LUMO energy level of –4.1 eV, which is around 1.0 eV lower than that of P3HT (–3.1 eV). Such a LUMO energy difference (1.0 eV) is good for intermolecular electron transfer. However, this energy difference means a large energy loss during the electron transfer process, and it therefore causes a low open circuit voltage. In order to further improve the open circuit voltage, it is important to design new acceptor materials with higher LUMO energy levels. Blom et al. firstly reported the preparation and electrochemical properties of bis-$PC_{61}BM$. The result showed that $PC_{61}BM$ bis-adduct has a LUMO level 0.1 eV higher than the monosubstituted $PC_{61}BM$. A higher V_{OC} of 0.73 V was obtained in the devices based on P3HT:bis-$PC_{61}BM$,

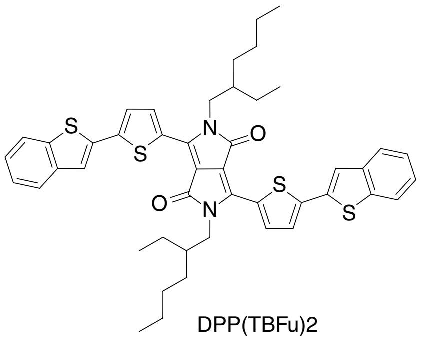

DPP(TBFu)2

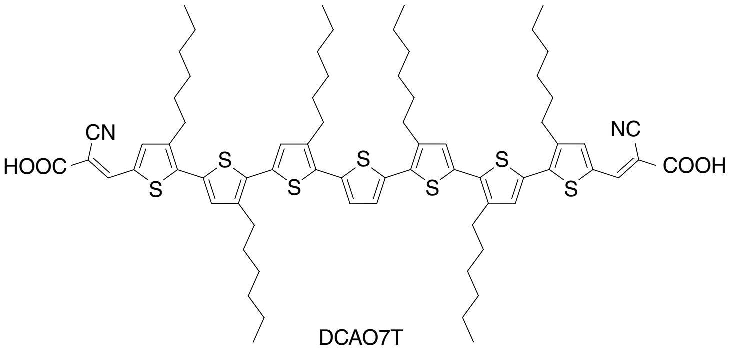

DCAO7T

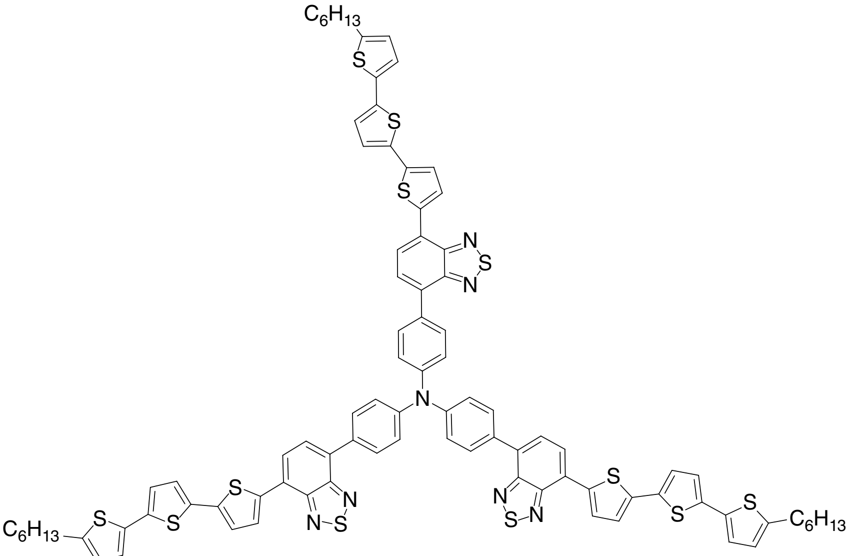

S(TPA-BT-HTT)

Figure 6.20 New p-type organic semiconductors with moderate to low molecular weight and defined molecular structures

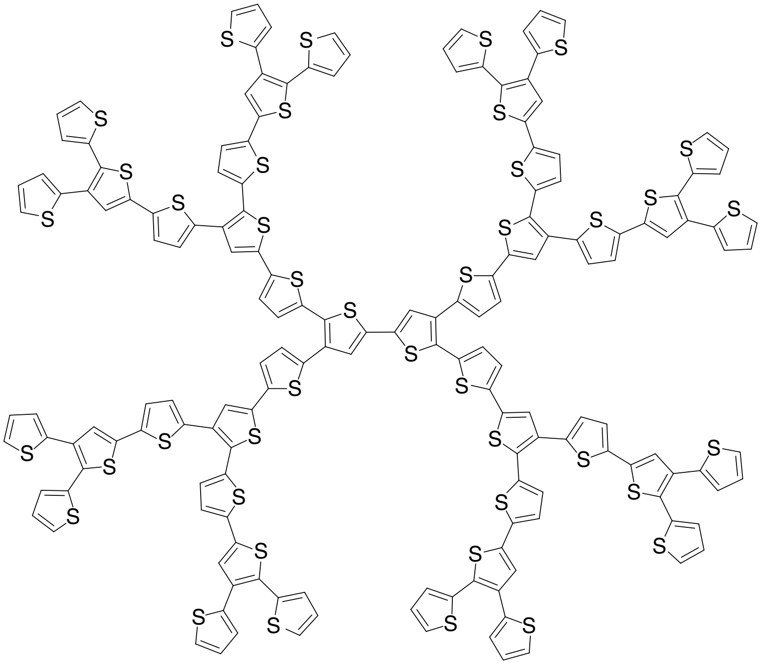

DOT-42T

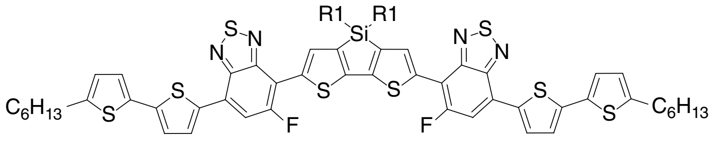
R1
R1
Si
C6H13
C6H13
F
F

R = 2-ethylhexyl

p-SIDT(FBTTh2)2

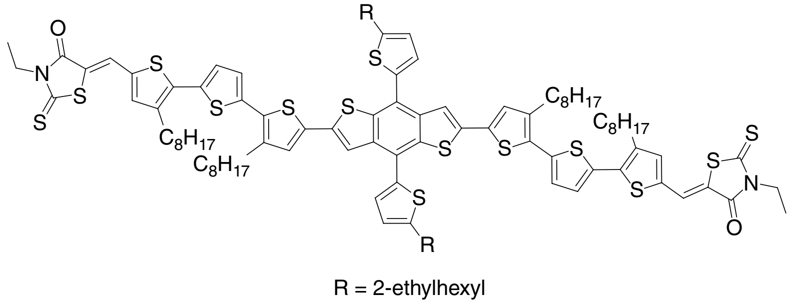
R
R
C8H17
C8H17
C8H17
C8H17

R = 2-ethylhexyl

DR3TBDTT

Figure 6.20 (Continued)

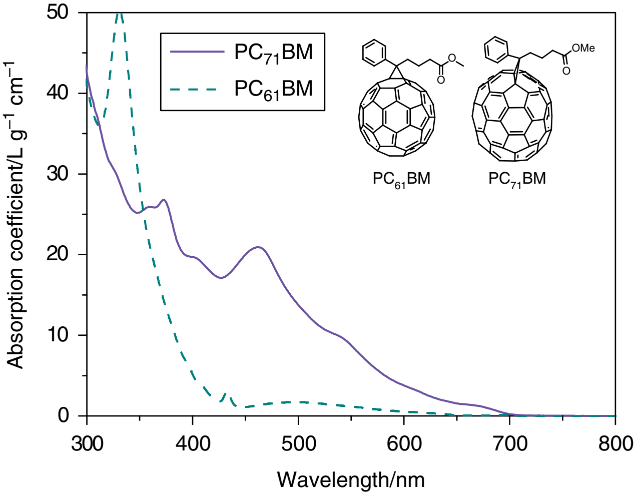

Figure 6.21 The chemical structures and absorption spectra of $PC_{61}BM$ and $PC_{71}BM$

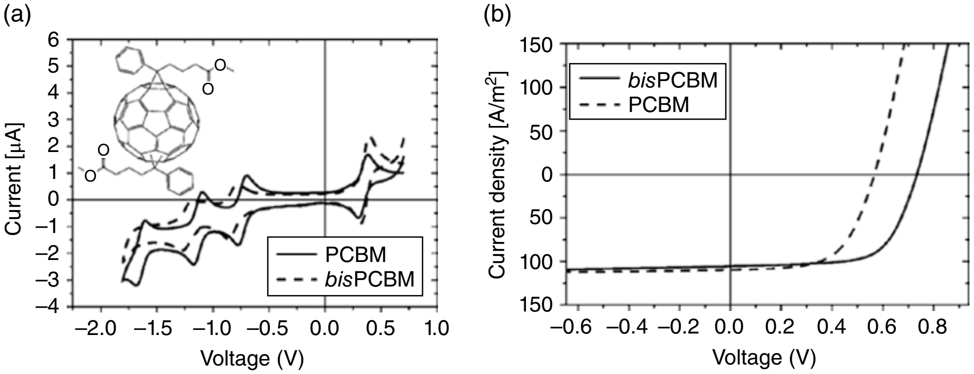

Figure 6.22 (a) Cyclic voltammograms of $PC_{61}BM$ and bis-$PC_{61}BM$. (b) The comparison of solar cell performances of $PC_{61}BM$ and bis-$PC_{61}BM$. (Reprinted from reference [154] with permission from John Wiley and Sons)

which is 0.15 V of increase when compared to that of P3HT:$PC_{61}BM$-based device (Figure 6.22) [154]. Recently, He et al. reported the indene-C_{60} bisadduct (ICBA, Figure 6.23), which has similar LUMO energy as bis-$PC_{61}BM$ [115]. The PSC based on P3HT:ICBA exhibited a higher open circuit voltage of 0.84 eV and was able to achieve a PCE of 6.5% [116].

Besides the above mentioned fullerene derivatives, several other substitutive fullerene derivatives (Figure 6.23) were also synthesized, such as bis(dimethylphenylsilylmethyl)[60] fullerenes (SIMEF) [42], methanofullerene derivatives (ThCBM) [155], as *n*-type conductor materials to apply to organic solar cells. Perylene diimide [156] and its copolymer with oligothiophene were also developed as electron acceptors for organic solar cells [157–159]. Although the device performance was far worse than that based on fullerene derivatives, Brunetti et al. found out that 9,9′-bifluorenylidene (9,9′-BF) could be used as the acceptor to fabricate organic solar cells [160].

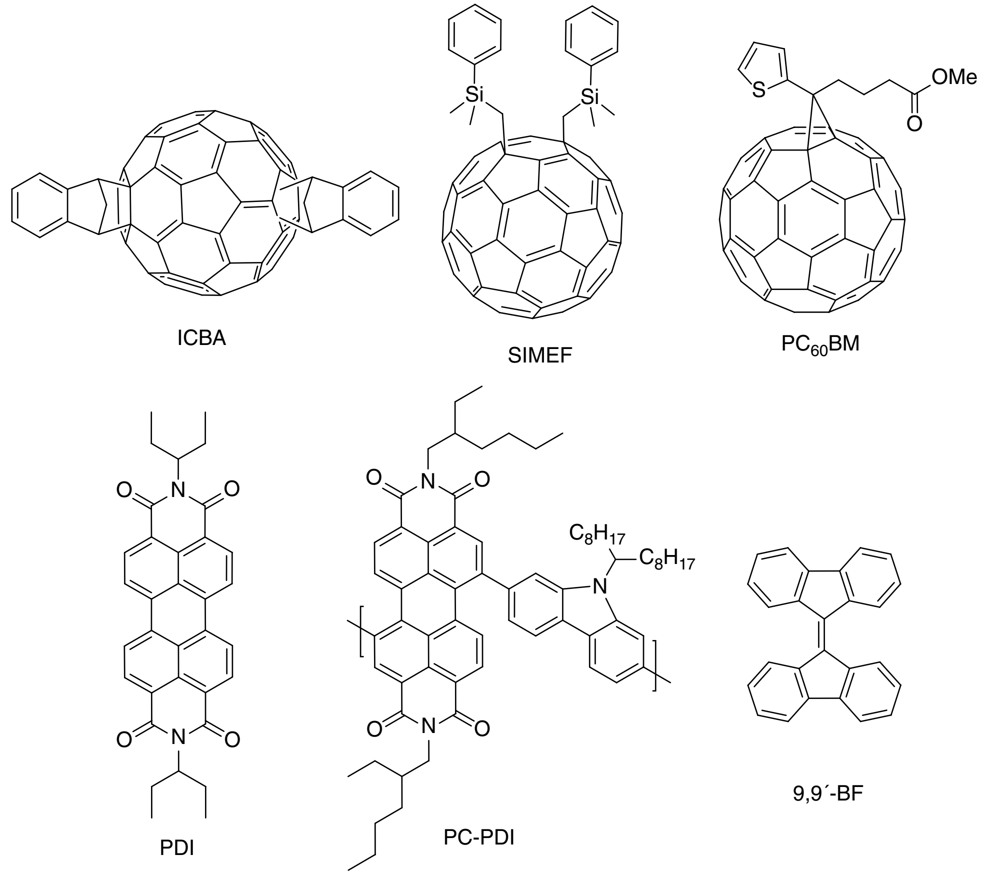

Figure 6.23 The structures of other n-type conductors

6.3.4 *Inorganic Semiconductors*

Inorganic semiconductors can also be used in organic solar cells. In the case of dye-sensitized solar cells (DSSC), *p*-type inorganic semiconductors are usually used as dyes to harvest light [161,162]. In organic solar cells, *n*-type inorganic materials are usually used to blend with *p*-type conjugated polymers [163]. The *n*-type inorganic semiconductors include CdSe [164–166], ZnO [62,167], TiO_2 [168,169] and $CuInSe_2$ [170]. In order to obtain good solution processability, inorganic semiconducting materials are generally in nanoparticle form and these nanoparticles are dispersed in solvent for further use. PPV or P3HT is usually used as the p-type polymer, since these two polymers are well studied. The PCE of hybrid polymer solar cells ranges from 1%–3% and is inferior to that of organic BHJ solar cells using fullerene as the acceptor. Owing to the large electron density difference between inorganic and organic materials, the nanostructure and nanomorphorlogy of organic/inorganic hybrid film can be fully characterized by three-dimensional TEM [62,169]. Figure 6.24 shows the 3D-TEM image of hybrid film of P3HT and ZnO. Phase separation takes place in thin films and results in exciton quenching. For thicker films (~100 nm), homogeneous phase separation is formed between P3HT and ZnO. These effects are significantly amplified on the performances of the devices [62].

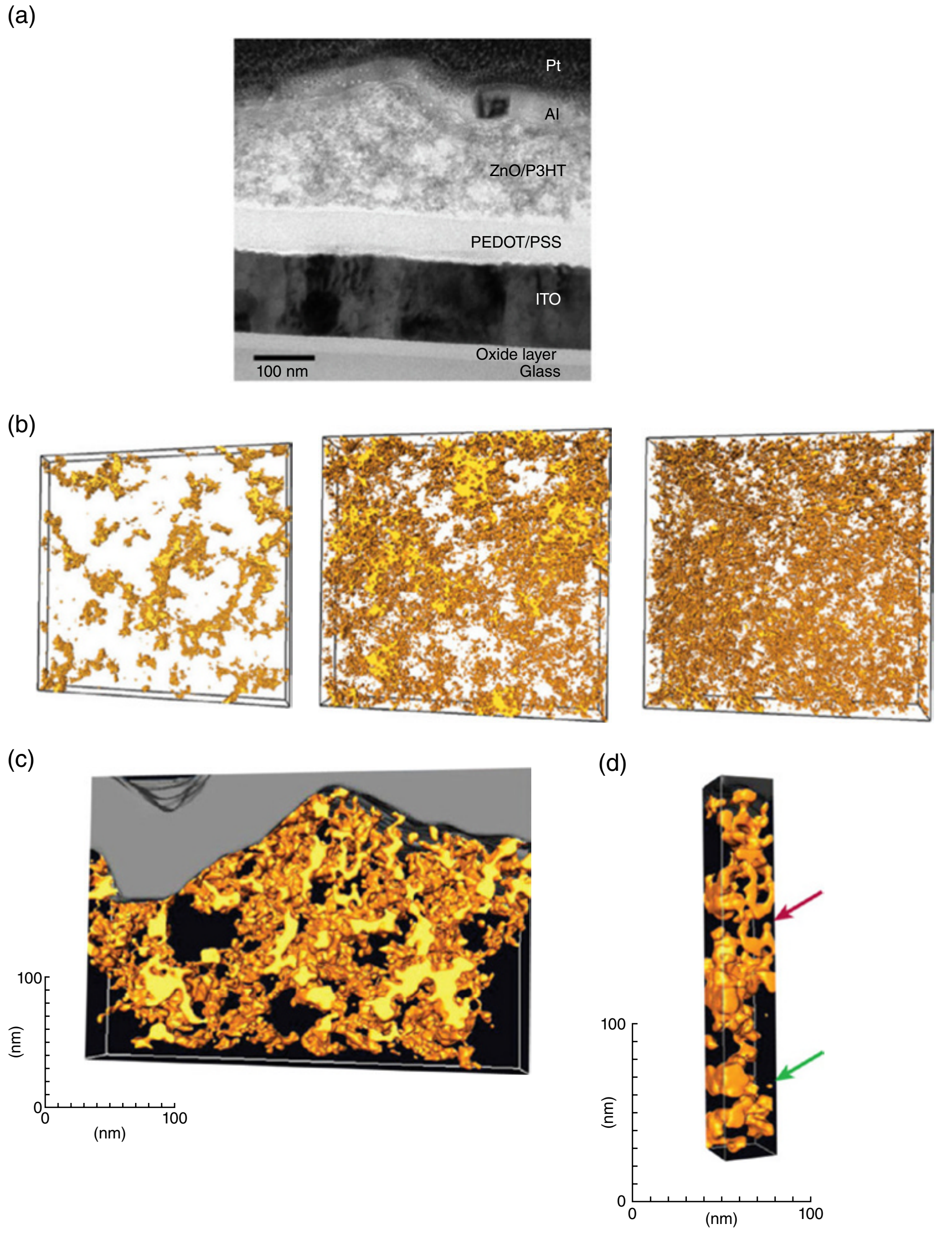
(a)
Pt
Al
ZnO/P3HT
PEDOT/PSS
ITO
Oxide layer
Glass
100 nm
(b)
(c)
100
(nm)
0
0
100
(nm)
(d)
100
(nm)
0
0
(nm)
100

Figure 6.24 (a) Scanning electron micrograph of a cross-section of P3HT:ZnO solar cell. (b–d) Three dimensional morphology images of P3HT:ZnO with thicknesses of 57 nm (b), 100 nm (c) and 167 nm (d). Yellow: ZnO; transparent: P3HT. (Reprinted from reference [230] with permission from Elsevier) (Reprinted from reference [62] with permission from Nature Publishing Group)

6.3.5 Other Functional Materials

The interface properties between an electrode and an active layer play a critical role in tuning device performance. Auxiliary buffer layers, such as a hole extraction layer, electron injection layer and exciton blocking layer are generally used to improve the efficiency and stability of organic solar cells by eliminating the energy barriers at the interface and enhancing the electron/hole injection efficiency [66,171,172]. PEDOT:PSS is widely used as an interface modification layer in organic electronics. The work function of PEDOT:PSS is about −5.2 eV, which matches very well with ITO [173,174]. PEDOT:PSS can reduce the hole injection barrier, smooth the ITO interface and avoid the shorts. However, PEDOT:PSS suffers from poor device lifetime due to its acidity and hygroscopic nature; MoO_3 (−5.3 eV) [175], V_2O_5 (−4.7 eV) [175], and NiOx [113] were also introduced as the hole extraction materials to improve the performance of polymer solar cells.

LiF/Al is the most commonly used cathode in organic solar cells. It is recognized that a thin layer of LiF (1 nm) will increase the open circuit voltage due to the formation of a dipole layer between Al and LiF. Gao et al. reported that a high PCE can be obtained from a LiF doped C_{60} as the cathode buffer layer. The advantage of this layer is that it can efficiently block the holes in the device [176]. The other cathode modified materials include ZnO [177,178], TiO_2 [123], and so on.

6.4 Inverted and Tandem Organic Solar Cells

6.4.1 Inverted Organic Solar Cells

Conventional organic solar cells with the architecture of ITO/PEDOT:PSS/organic photoactive layer/LiF/Al usually suffer from serious physical and chemical degradation problems. In this type of device architecture, a transparent ITO electrode and a metal Al act as anode and cathode, respectively. It has been proved that oxygen can diffuse into the active layer through pinholes and the boundaries of aluminum thin film [179], resulting in device degradation. In addition, the hygroscopic and acidic nature of PEDOT:PSS has also been considered a factor in causing the low stability of organic solar cells [180]. In order to increase the stability of organic solar cells, the inverted device geometry with the layer sequence of ITO/electron transport layer/active layer/hole transport layer/metal electrode was developed (Figure 6.25) [48]. In the inverted structure, the ITO is used as the cathode, while high work function metals, that is Ag and Au, were used as the anode; thus the chemical oxidation degradation of metal electrode was suppressed. Besides its better ambient stability, the inverted device architecture is regarded to be more suitable for large-scale printing processes such as vacuum-free Ag electrode coating or printing deposition. With these two advantages, much effort has been devoted to inverted organic solar cells in the last few years.

In inverted solar cells, several *n*-typed semiconductors, such as zinc oxide (ZnO) [181–183] and titanium oxide (TiO_x), [184,185] are used as the electron buffer layer to improve the electron extraction efficiency. Lin et al. (2011) [183] induced composite TiO_x nanotube and ZnO as an electron transport layer (Figure 6.26). Due to the excellent electron transport ability of the TiO_x nanotube, a PCE of 5.6% was obtained for the P3HT:ICBA cell, which is 1.2% higher than the device without a TiO_x nanotube.

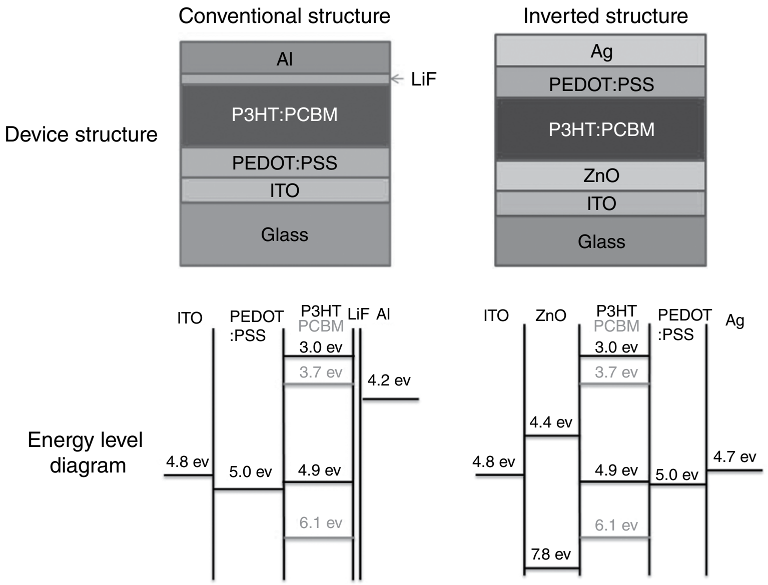
Conventional structure
Inverted structure
Device structure
Al
LiF
P3HT:PCBM
PEDOT:PSS
ITO
Glass
Ag
PEDOT:PSS
P3HT:PCBM
ZnO
ITO
Glass
Energy level diagram
ITO
PEDOT :PSS
P3HT PCBM
LiF
Al
3.0 ev
3.7 ev
4.2 ev
4.8 ev
5.0 ev
4.9 ev
6.1 ev
ITO
ZnO
P3HT PCBM
PEDOT :PSS
Ag
3.0 ev
3.7 ev
4.4 ev
4.8 ev
4.9 ev
5.0 ev
4.7 ev
6.1 ev
7.8 ev

Figure 6.25 Device structure of the conventional and inverted P3HT-based solar cells, and the schematic diagrams of the energy level

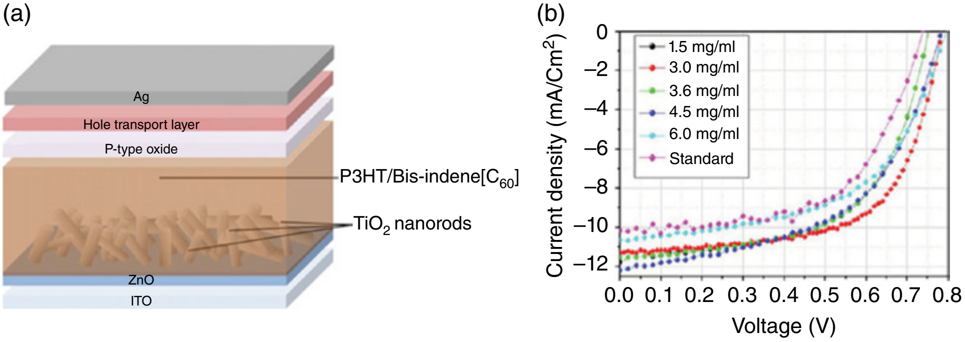

Figure 6.26 (a) Inverted solar cell with TiO_x nano-tube and ZnO electron transport layer. (b) J-V characteristics of the inverted solar cell. (Reprinted from reference [183] with permission from Elsevier)

On the anode side, a conventional hole buffer layer is the solution-processed PEDOT:PSS [48] and vacuum deposited metal oxide, such as molybdenum trioxide (MoO_3) [49], vanadium oxide (V_2O_5) [186], tungsten trioxide (WO_3) [187], or nickel oxide (NiO) [188]. Recently, solution-processed metal oxide hole buffer layers were also developed to make it more compatible with the printing process. Inverted cells using solution-processed V_2O_5 hole buffer layer was reported by Huang et al. [189]. The work function of V_2O_5 was 4.7 eV, and thus provided good Ohmic contact to organic materials with large HOMO energies and improved the hole extraction efficiency at the interface of organic materials and Ag electrode. As a result, a significant improvement of PCE was achieved compared with a device without a buffer layer (3.56% vs. 2.52%).

6.4.2 *Tandem Organic Solar Cells*

One of the reasons for low efficiencies of organic solar cells is the rather narrow absorption band of organic photoactive materials. Another inherent limitation is the low charge carrier mobility of organic semiconductors. In order to ensure that the separated charge can reach the electrode before they recombine again, the thickness of the photoactive layer has to be thin. However, this will unfortunately lead to insufficient light absorption, and consequently limit the PCE of a single organic solar cell [51]. This can be overcome by using tandem structured solar cells, where more than one cell is stacked together. In tandem organic solar cells, the sub-cells are electrically connected in a series, or in parallel through transparent intermediate electrodes [45,47]. Other approaches for tandem solar cells include mechanical stacking, folded reflective orientation, and self-passivation structures.

Kim et al. [190] reported solution-processed tandem solar cells with PCDTBT:$PC_{61}BM$ and P3HT:$PC_{71}BM$ as the back and front sub-cell, respectively. As shown in the EQE spectra, the absorption spectra of P3HT and PCDTBT were almost complementary. In the tandem solar cell, the two sub-cells were connected through a transparent TiO_x layer and a highly conductive hole transport layer, poly(3,4-ethylenedioxylenethiophene)-polystylene sulfonic acid (PEDOT:PSS). The TiO_x layer and PEDOT:PSS acted as the electron layer and the hole transport layer in each sub-cell. Meanwhile, electrons from the first cell recombined with holes from the second cell at the TiO_x-PEDOT:PSS interface. Thus, the V_{OC} of the series tandem solar cell reached 1.24 eV, which was nearly the sum of the V_{OC} of the two sub-cells. However, the J_{SC} of the series tandem cell was limited by the smaller J_{SC} of the two sub-cells.

As mentioned above, in series tandem solar cells, the J_{SC} of tandem cells is determined by the smaller current generated in either the front or the back cell. Therfore, it is critical to optimize the J_{SC} through varying the thickness of the two sub-cells. Recently, Janssen et al. (2010) reported a tandem solar cell comprising a wide (pFTBT) and a small (pBBTDPP2) band gap polymer electode donor mixed with a $PC_{61}BM$ electron acceptor. They used optical simulation results and internal quantum efficiency (IQE) of the single cells to find the best thin film conbination [191]. This is very helpful for the optimization of organic tandem solar cells.

In summary, much effort has gone into proving that enhanced PCE can be achieved by using tandem structure. However, how to balance the photocurrent of each sub-cell by varying the thickness of the photoactive layer of each sub-cells is still a big challenge [192,193].

6.4.3 *Inverted Tandem Organic Solar Cells*

Tandem solar cells with an inverted structure combine the advantages of the wide spectra response range of tandem cells with the long-term stability and better compatibility for printing processing of inverted cells [194–196]. Early inverted tandem cells were not all solution processed. Sun et al. (2010) [197] reported P3HT:$PC_{61}BM$-based inverted tandem cells with evaporated MoO_3/Al/Ag/ Ca as the intermediate electrode (Figure 6.27). The V_{OC} for the cell with the MoO_3/Ca intermediate layer was much smaller than the V_{OC} summation of two sub-cells, while the V_{OC} of the cell using MoO_3/Ag/Ca or MoO_3/Ag/Al/Ca reached 1.19 eV, equal to the sum of the V_{OC} of two sub-cells. This result indicated that it is crucial for the energy match between the intermediate layer and the organic photoactive materials in organic tandem solar cells. Similarly, Chou et al. (2011) [194] reported P3HT:$PC_{61}BM$ and PSBTBT:$PC_{71}BM$ BHJ-based inverted tandem cell with a solution-processed ZnO-d layer and

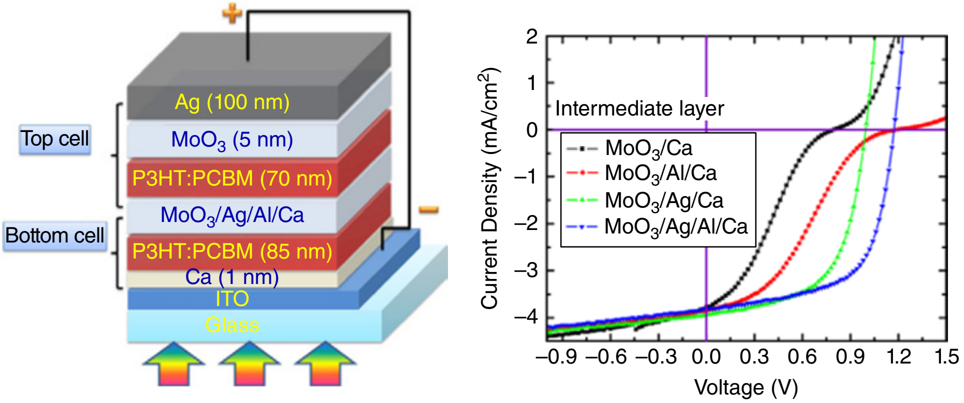

Figure 6.27 (a) Device structure of an inverted tandem solar cell with MoO_3/Ag/Al/Ca as the intermediate electrode. (b) The J-V characteristics of inverted tandem solar cells with different intermediate layers. (Reprinted from reference [197] with permission from AIP Publishing LLC)

an evaporated MoO_3/Al layer as the intermediate layer (Figure 6.28). The high transparency as well as the physical and chemical compatibility of ZnO-d and MoO_3/Al intermediate layers lead to a high performance device with a V_{OC} of 1.20 V, a J_{SC} of 7.84 mA/cm^2, an FF of 54% and a PCE of 5.1%.

Since these intermediate layers were fabricated by vacuum evaporation, the above mentioned inverted tandem cells are not compatible with printing. The challenges in fabricating inverted tandem cells by a solution process include surface wettability and the possible washing away of the underlying layer by the top layer. Recently, Yang et al. (2011) developed a semi-transparent intermediate layer by combining a modified PEDOT:PSS hole transport layer with a ZnO electron transport layer [198]. The modified PEDOT:PSS layer was physically robust enough to prevent the destruction of the bottom layer during subsequent solution processes, even with the slow drying solvents such as chlorobezene (CB) and dichlorobenzene (DCB). An inverted tandem cell with a P3HT:ICBA front cell and a PSBTBT:PCBM back cell gave a V_{OC} of 1.47 V, a J_{SC} of 7.6 mA/cm^2, an FF of 63%, and a PCE of 7.0%. By using a new copolymer poly[2,7-(5,5-bis-(3,7-dimethyloctyl)-5H-dithieno[3,2-b:2',3'-d]pyran)-alt-4,7-(5,6-difluoro-2,1,3-benzothia diazole)] (PDTP-DFBT), which has a small band gap of 1.38 eV, high charge carrier mobility, and a deep HOMO energy level, Yang et al. reported an inverted tandem cell with a PCE of 10.6% [199], which was the record PCE for organic solar cells (Figure 6.29). Very recently, by using a triple-junction structure, a PCE of 11.5% was achieved by the same research group, which is the highest PCE for a solution-processed organic solar cell [28].

6.5 Fabrication Methods

Since the discovery of conductive polymers in 1977, many efforts have been devoted to developing new conductive polymers and their applications. Polymers have the advantages of low cost, light weight and ease of chemical modification. Polymers are also compatible with plastic substrate, which makes them suitable for roll-to-roll processing. Based on the new class of polymers, printed organic photovoltaic has become one of the printed electronics disciplines where printing is the primary fabrication technique [30]. Detailed introduction on printing technologies, processing

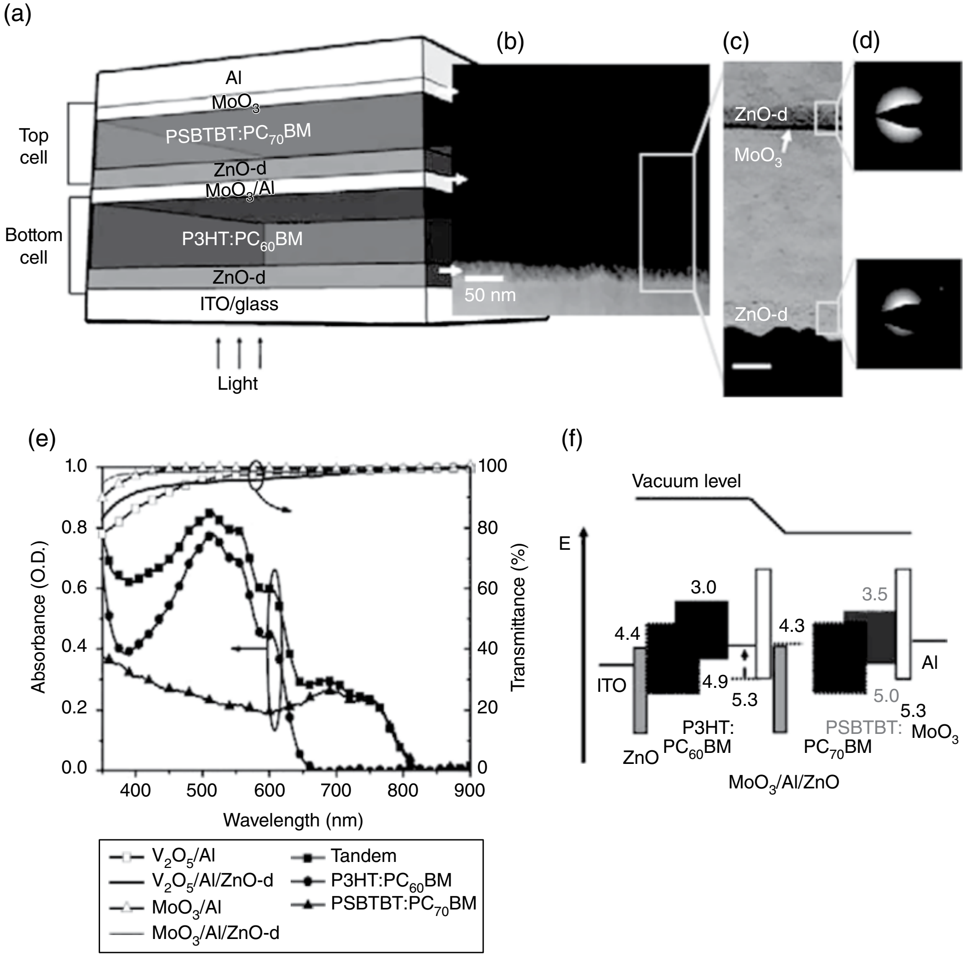

Figure 6.28 (a) Device structure of an inverted organic tandem solar cell; (b) SEM and (c) TEM images of the intermediate layer. (d) TEM image of the ZnO-d film; (e) Absorption spectra of reference films and the transmittance spectra of the intermediate layers; (f) Energy level diagram of the tandem cell. (Reprinted from reference [194] with permission from John Wiley and Sons)

and equipment have been described in Chapter 4 of this book. In this chapter, only printing methods for making organic solar cells in laboratory are introduced.

6.5.1 Spin Coating

Spin coating is the most widely used device fabrication method in organic solar cells. Spin coating involves the application of a liquid to a flat substrate, followed by high-speed rotation of the substrate. The excess liquid is ejected and only a thin film is left on the substrate (Figure 6.30) [30,200]. There are several advantages regarding the spin coating. Firstly, it is a simple film-forming technique and no expensive equipment is needed. Secondly, the thickness, morphology and surface topography of the film from a particular material in a given

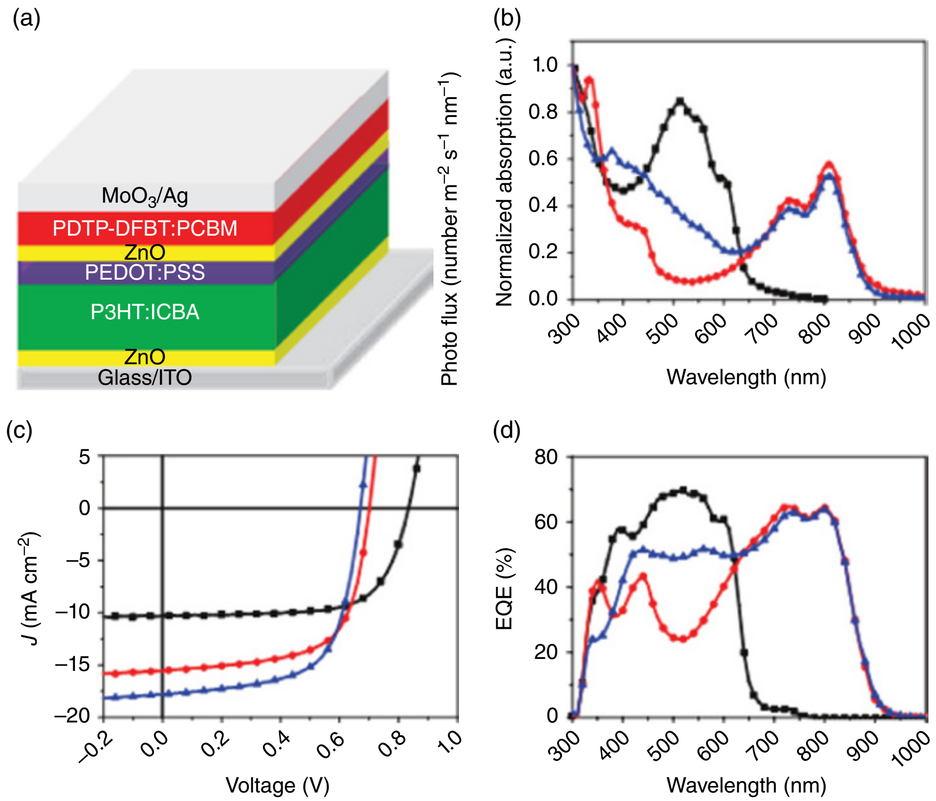

Figure 6.29 (a) Device structure of an inverted tandem cell structure; (b) Absorption spectra of a P3HT:ICBA and PDTP-DFBT:$PC_{61}BM$ and PDTP-DFBT:$PC_{71}BM$ blend; (c) J-V characteristics of the single and tandem cells; and (d) EQE of P3HT:ICBA, PDTP-DFBT:$PC_{61}BM$, PDTP-DFBT:$PC_{71}BM$-based single cells. (Reprinted from reference [199] with permission from Nature Publishing Group)

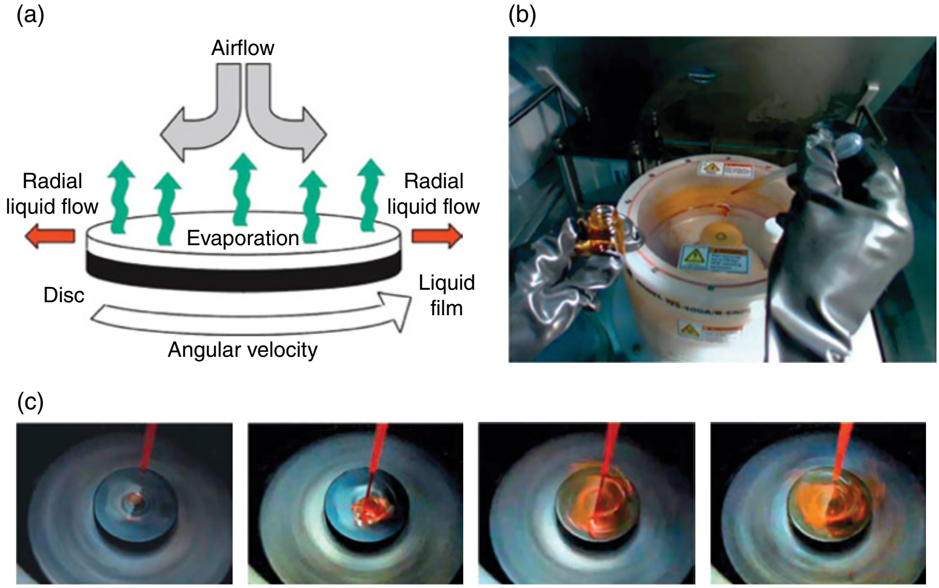
(a)
Airflow
Radial
liquid flow
Radial
liquid flow
Evaporation
Disc
Liquid
film
Angular velocity
(b)
(c)

Figure 6.30 (a) Schematic illustration of spin coating. (b) A photograph of a typical spin coator. (c) High-speed images showing the film formation process, from left to right, photos at 17, 100, 137, and 180 ms. (Reprinted from reference [30] with permission from Elsevier)

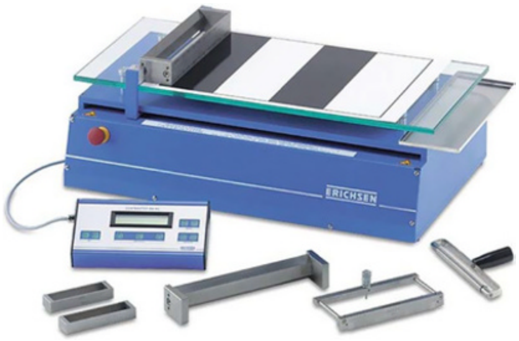

Figure 6.31 A picture of laboratory scaled doctor blading machine

solvent at a given concentration is homogenous and highly reproducible. Thirdly, it is a fast film-forming technique. However, spin coating also has some disadvantages, such as large wastage of polymer materials since most of the liquid is ejected during spin coating; it is also a non-patterning process and is not roll-to-roll (R2R) compatible.

6.5.2 Doctor Blading

Doctor blading is another widely used film-formation technique for producing organic solar cells (Figure 6.31). In the doctor blading process, a line drop of polymer solution is placed on a substrate underneath the doctor blade. When a constant movement of the blade relative to the substrate is established, the polymer solution spreads over the substrate and forms a thin film upon drying [201–203]. The thickness of dry polymer film is controlled by regulating the gap between the blade and the substrate, as well as being dependent on surface tension and viscosity of the polymer solution. A hot plate is always configured to regulate the drying rate of the coated solution and hence the thickness of the final film. Unlike the spin-coating technique, the waste for doctor blade coating can be minimized to less than ~5%. In addition, doctor blading can be easily transferred to an R2R coating line. However, with doctor blading patterning is not possible. Compared to spin coating where the wet film formation is fast, solvent evaporation in doctor blading is relatively slow, which may lead to aggregation or crystallization of certain polymer materials. Therefore, it is necessary to optimize the solution, moving speed and other parameters to obtain a high quality thin film [204,205].

6.5.3 Screen Printing

Screen printing has been widely used in the silicon solar cell industry to print silver electrodes for charge collection. Polymer solar cells fabricated by screen printing technique was reported in 2001 by Shaheen et al. In the report, an MDMO-PPV:PCBM-based organic solar cell was fabricated and power conversion efficiency of 4.3% was achieved when the solar cell was illuminated with a monochromatic light of 488 nm with a light intensity of 27 mW/cm^2 [206]. Since screen printing requires high viscosity and low volatility ink, early studies on solar cell fabrication using screen printing were focused on a PPV:PCBM blend solution [207–210]. This is because PPV-polymer usually has high molecular weight (up to 100,000 Da), and it is possible

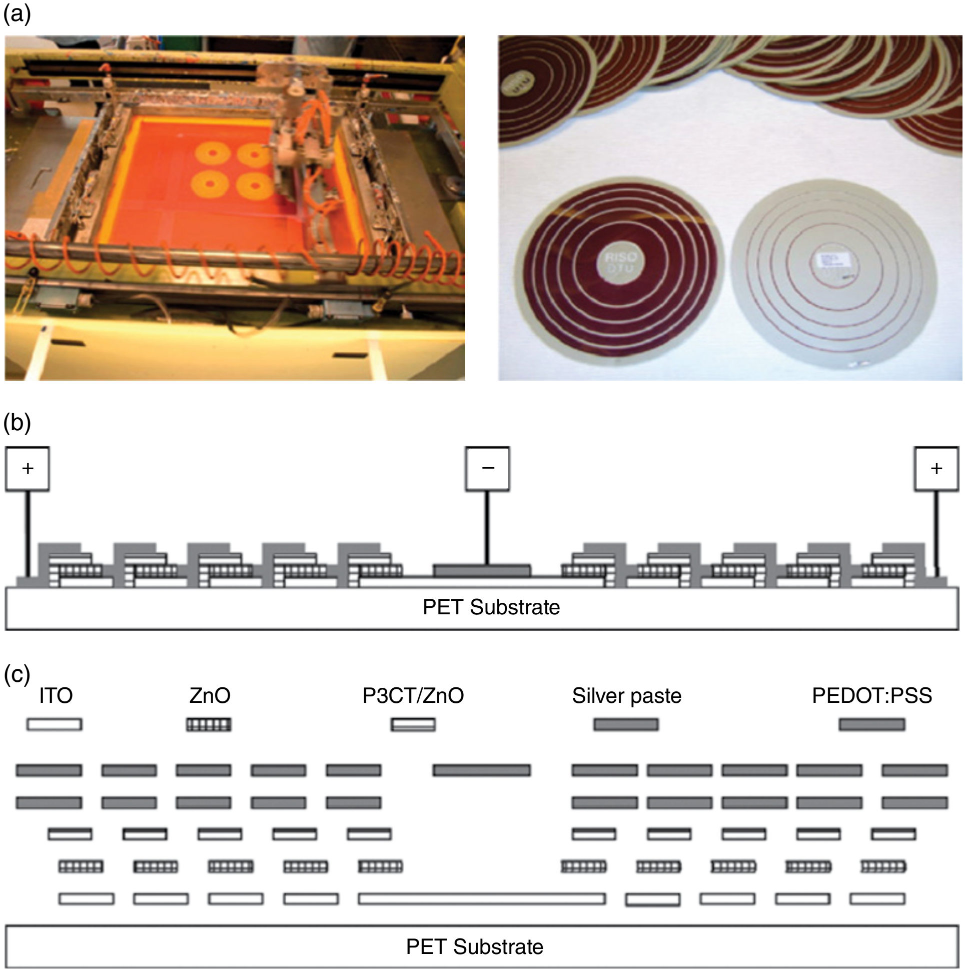

Figure 6.32 (a) Organic solar cell fabricated by screen printing, (b) completed organic solar cells, (c) device structure. (Reprinted from reference [213] with permission from Elsevier)

to make a highly viscous polymer solution. Recently, more efforts were focused on screen printing of P3HT-based solar cells. Unlike spin coating method, the solvent dries much slower during screen printing process; thus phase separation and device performance are highly dependent on the vapor pressure of the solvent. It is also critical to choose a suitable solvent for screen printable polymer inks. In the case of a P3HT:PCBM blend of inks, Zhang et al. compared the morphology of films prepared by screen printing with different organic solvents (chloroform, toluene, chlorobenzene, and 1,2-dichlorobenzene), and demonstrated that thin film prepared from chloroform solution showed the lowest surface roughness. Consequently, the highest PCE of 4.23% was obtained by the screen printing from chloroform [211]. Krebs et al. reported a series of all screen-printed organic solar cells based on P3CT:ZnO (Figure 6.32) [212,213]. Although the efficiency is rather low in these devices, the results confirmed that screen printing can be a viable technique to make organic solar cells.

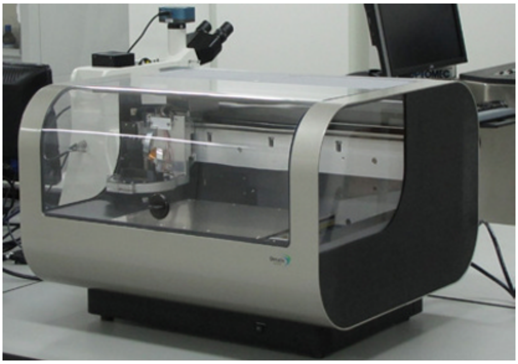

Figure 6.33 A picture of Dimatix DMP-2831 ink jet printer

6.5.4 Inkjet Printing

Inkjet printing is a non-contact printing technique with much higher resolution than screen printing. Inkjet printer nozzles are usually made of ceramic, which offers excellent corrosion resistance against organic solvents. Figure 6.33 shows a desktop inkjet printer from Dimatix. Generally, inks for inkjet printing are of low viscosity and high volatility. Appropriate additives are generally added to obtain high surface tension in order to easily generate a stream of droplets. Hoth et al. systematically investigated the morphology and performance of a P3HT:PCBM device fabricated by inkjet printing from different solvent mixtures, and demonstrated that morphologies and interfacial properties of inkjet printed films are dependent on the constituents of solvent mixture [214,215]. A mixture of 68% *o*-dichlorobenezene (oDCB) and 32% of 1,3,5-trimethylbenzene resulted in uniform polymer:fullerene blend films and a high PCE of 3.5% was achieved for P3HT:PCBM solar cells [216]. In addition, Aernouts et al. demonstrated that a solvent mixture of 50% tetrahydronaphthalene and 50% chlorobenzene (CB) is also good for polymer inks [217]. The disadvantage of inkjet printing is probably the rather slow printing speed. Thus, it is uncertain whether inkjet printing will ever play an important role in large scale production of organic solar cells. Nevertheless, the high printing resolution enables inkjet printing to prepare complex patterned films.

6.5.5 Other Thin Film Deposition Techniques

Other thin film deposition techniques suitable for organic solar cell preparation include: gravure printing [218–220], spray coating [221–224], or even brush painting [225]. The reported device performances, however, were not comparable to that by spin coating technique.

6.6 Roll-to-roll Processing

Although various printing methods have been employed to fabricate organic solar cells in the laboratory, these methods are not suitable for mass manufacturing. In fact, most laboratory-scale devices are ITO-glass-based and have a small active area (less than 1 cm^2). These cells can be made by separate step-by-step processes, including substrate cleaning, surface

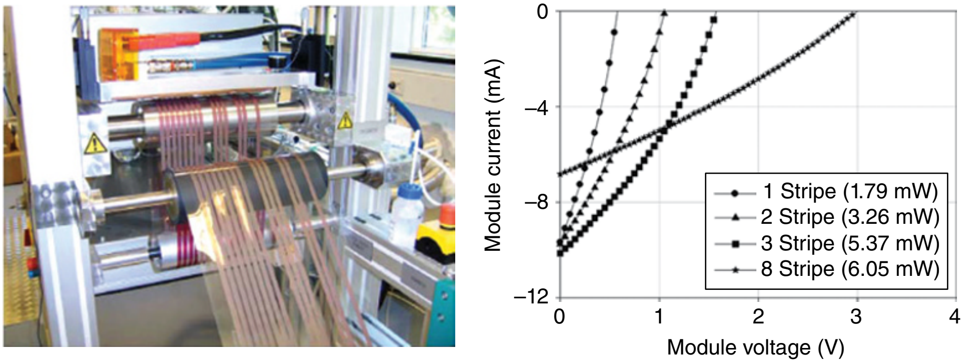

Figure 6.34 (a) Solar cells on the rewinding side of film. (b) J-V curves for the modules device prepared by slot-die coating. (Reprinted from reference [226] with permission from Elsevier)

treatment, thin film deposition, solvent drying, and device capsulation. In contrast, roll-to-roll (R2R) processing is the most suitable method for mass production of organic solar cells. However, before one can transfer the laboratory results to industrial scale R2R processing, many aspects, such as flexible substrate, ink formulation, device structure patterning, module structure design, should be studied carefully. Investigations on R2R processing of organic solar cells on medium size substrate (20–35 cm wide) would be very helpful to gain important knowledge for further scale-up.

Krebs et al. reported the preparation of PET/ITO/ZnO/P3MHOCT:ZnO/PEDOT:PSS/Ag organic solar cell modules using R2R methods. Their R2R processes include knife-over-edge coating, slot-die coating and screen printing (Figure 6.34) [226]. Furthermore, they developed a light-induced thermocleavage method in their R2R fabrication line, leading to an improved PCE of 0.2% for a polythiophene:ZnO based device [227]. In addition, they prepared an inverted P3HT:PCBM solar cell by the R2R process and demonstrated that the highest conversion of a large area device (120 cm^2) could reach to 2.1%, which is quite good for such a large area solar cell [228].

A cost analysis of an organic solar cell was carried out by Krebs et al. Their results indicated that the flexible ITO substrate accounted for 55% of the materials cost and 30% of the overall module cost in R2R processing of organic solar cells [86]. Therefore, ITO-free flexible electrodes are of high interest in the field of low-cost organic solar cell technology. In 2009, Krebs et al. reported a new R2R process to prepare an inverted organic solar cell with a structure of PEN/Ag/ZnO/P3HT:PCBM/PEDOT:PSS/Ag-grid [229]. In this work, the silver ink was slot-die coated on PEN substrate as the back electrode and then dried in a hot air oven at 130°C. Other layers, except for the Ag-grid, which was deposited by screen printing, were deposited by slot-die coating. Although the process was not highly efficient, the work demonstrated a true R2R printing of organic solar cells.

Generally, the sheet resistance of ITO is greater than 10 Ω/sq. To reduce the current losses from ITO substrate, large area organic solar cells are always comprised of a number of small cells that are connected in series or in parallel. With this configuration, it is difficult to deposit the photoactive layer and metal electrodes accurately at different steps of printing process. To solve the problem, Krebs et al. developed the Kapton/Cu/TiO$_x$ substrate-based monolithic device

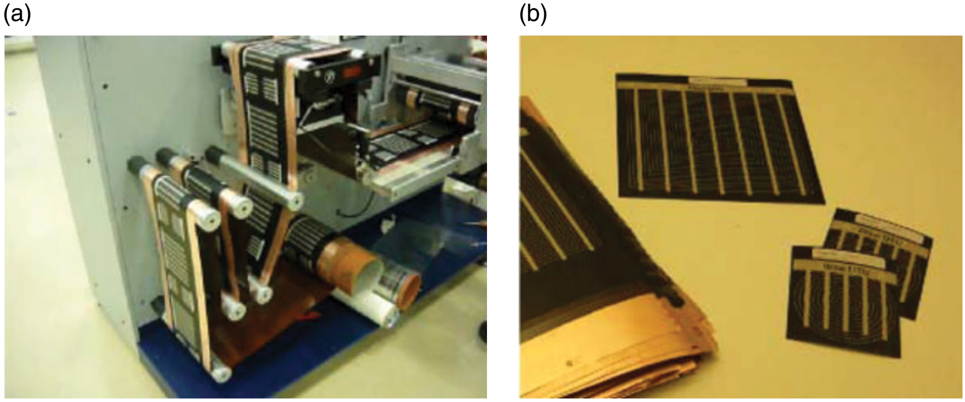

Figure 6.35 (a) Organic solar cell with PET/Cu/Ti back electrodes. (b) Pictures of the device. (Reprinted from reference [230] with permission from Elsevier)

(Figure 6.35). The innovation made it possible to prepare a solar module without patterning due to the excellent conductivity of Cu. However, there were two disadvantages: (1) the obtained PCE was low (0.3%), which might be originated from the high work function of Cu; and (2) the TiO_x layer was prepared by vacuum deposition and oxidized at high temperature [230].

6.7 Printable Perovskite Solar Cells

During the preparation of this manuscript, a new type of organic–inorganic hybrid solar cell based on methylammonium lead halide perovskite material was developed, which shows high power conversion efficiency and excellent solution-processability [231,232]. The perovskite solar cell was first reported in 2009, where methylammonium lead bromide nanocrystals were used as a sensitizer in DSSC [233]. Although the power conversion efficiency was reported to be around 3–4%, this pioneering work opened up a new type of solar cell technology. To date, the PCE of 19.3% was reported in the literature [234], and efficiency of 17.9% was confirmed by the National Renewable Energy Laboratory (NREL) [235]. Most importantly, perovskite solar cells can be fabricated using a low-temperature solution process, either a one-step [236] or a two-step [237] process. Along with this, perovskite solar cells based on flexible substrate was also reported [238]. All these features enable this new type of solar cell to be well compatible with the roll-to-roll printing process, and hence potentially reduce the cost of solar energy conversion significantly. It is still at a very early stage for perovskite solar cells to be considered practical; however, one would expect that low cost perovskite solar cells fabricated by printing technology will be on the market in the near future.

6.8 Summary and Outlook

After two decades of development in organic solar cell technology, much progress has been achieved, especially in organic semiconducting materials and device structure optimization. To date, the lab-scale organic solar cells have achieved efficiency more than 8%, which is approaching that of amorphous silicon thin-film solar cells. However, before the organic solar cell can be commercially viable, there is still a great challenge to overcome in increasing the device performance, including power conversion efficiency, long-term stability and reduction of manufacturing cost. At the moment, many research institutions, including the Holst research center in the Netherlands, IMEC research center in Belgium, Denmark National Renewable Energy research Center, NREL of USA, and VICOSC of Australia, have endeavored to develop printable organic solar cells. Technological breakthroughs in device efficiency, production cost and the lifetime of organic solar cells will be achievable in the foreseeable future, which will eventually bring the organic solar cells to the market place. Flexible organic solar cells will become a common feature in our daily life.

References

[1] Ni M, Leung MK, Sumathy K. Progress on solar cell research. Renew. Energy Resources. 2004;2*:* 9–11.

[2] “Renewable Energy Policy Network for the 21st Century” *Renewables 2010 Global Status Report* 2011, http://www.ren21.net/REN21Activities/Publications/GlobalStatusReport/GSR2010/tabid/5824/Default.aspx.

[3] Parida B, Iniyan S, Goic R. A review of solar photovoltaic technologies. Renew. Sust. Energy Rev. 2011;15(3):1625–1636.

[4] Wolden CA, Kurtin J, Baxter JB, Repins I, Shaheen SE, Torvik JT, Rockett AA, Fthenakis VM, Aydil ES. Photovoltaic manufacturing: Present status, future prospects, and research needs. J. Vac. Sci. Technol. A. 2011;29(3):030801.

[5] Wenham SR, Green MA. Silicon solar cells. Prog. Photovoltaics Res. Appl. 1996;4(1):3–33.

[6] Huang Q, Lin J, Wei C, Yao R. Progress in application of silicon solar cell. Develop. Appl.Mater. 2009;24(6):93–96.

[7] Green MA, Emery K, Hishikawa Y, Warta W, Dunlop ED. Solar cell efficiency tables (version 43). Prog. Photovoltaics Res. Appl. 2014;22(1):1–9.

[8] Wang Y, Liu X, Chen T, Jiang C, Wang R. Recent progress of thin film solar cells. Semicond. Optoelectronics. 2008;2:151–157.

[9] O’Regan B, Grätzel M. A low-cost, high-efficiency solar cell based on dye-sensitized colloidal TiO2 films. Nature. 1991;353(6346):737–740.

[10] Clifford JN, Martinez-Ferrero E, Viterisi A, Palomares E. Sensitizer molecular structure-device efficiency relationship in dye sensitized solar cells. Chem. Soc. Rev. 2011;40(3):1635–1646.

[11] Yella A, Mai C-L, Zakeeruddin SM, Chang S-N, Hsieh C-H, Yeh C-Y, Grätzel M, Molecular engineering of push–pull porphyrin dyes for highly efficient dye-sensitized solar cells: The role of benzene spacers. Angew. Chem. Int. Ed. 2014;53(11):2973–2977.

[12] Yang L, Xin G, Wu L, Ma T. Flexible dye-sensitized solar cells. Prog. Chem. 2009;21(10): 2242–2249.

[13] Zhang Y, Zhu J, Dai S. Recent research development on solid state and quasi-solid state electrolyte for dye-sensitized solar cells. Chemistry. 2010;73(12):1059–1065.

[14] Mi B, Gao Z, Deng X, Huang W. Progress on organic thin film solar cell materials and devices. Sci. China B. 2008;38(11):957–975.

[15] Brabec C, Dyakonov V, Scherf U. Organic Photovoltaics: materials, device physics, and manufacturing technologies. Weinheim: Wiley-VCH Verlag, GmbH&Co, 2008.

[16] Yan F, Noble J, Peltola J, Wicks S, Balasubramanian S. Semitransparent OPV modules pass environmental chamber test requirements. Sol. Energy Mater. Sol. Cells. 2013;114(0):214–218.

[17] Lipomi DJ, Tee BCK, Vosgueritchian M, Bao Z. Stretchable Organic Solar Cells. Adv. Mater. 2011;23(15):1771–1775.

[18] Kearns D, Calvin M. Photovoltaic effect and photoconductivity in laminated organic systems. J. Chem. Phys. 1958;29(4):950–951.

[19] Tang CW. Two-layer organic photovoltaic cell. Appl. Phys. Lett. 1986;48(2):183–185.

[20] Sariciftci NS, Smilowitz L, Heeger AJ, Wudl F. Photoinduced electron transfer from a conducting polymer to buckminsterfullerene. Science. 1992;258:1474–1476.

[21] Yu G, Gao J, Hummelen JC, Wudl F, Heeger AJ. Polymer photovoltaic eells: enhanced efficiencies via a network of internal donor–acceptor heterojunctions. Science. 1995;270(5243): 1789–1791.

[22] Shaheen SE, Brabec CJ, Sariciftci NS, Padinger F, Fromherz T, Hummelen JC. 2.5% efficient organic plastic solar cells. Appl. Phys. Lett. 2001;78(6):841–843.

[23] Padinger F, Rittberger RS, Sarififtci NS. Effects of postproduction treatment on plastic solar cells. Adv. Funct. Mater. 2003;13(1):85–88.

[24] Wienk MM, Kroon JM, Verhees WJH, Knol J, Hummelen JC, van Hal PA, Janssen RAJ. Efficient methano[70] fullerene/MDMO-PPV bulk heterojunction photovoltaic cells. Angew. Chem. Int. Ed. 2003;42(29): 3371–3375.

[25] Peet J, Kim JY, Coates NE, Ma WL, Moses D, Heeger AJ, Bazan GC. Efficiency enhancement in low-bandgap polymer solar cells by processing with alkane dithiols. Nat. Mater. 2007;6:497–500.

[26] Ye L, Zhang S, Zhao, Yao H, Hou J. Highly efficient 2D-conjugated benzodithiophene-based photovoltaic polymer with linear alkylthio side chain. Chem. Mater. 2014;26(12):3603–3605.

[27] You J, Chen C-C, Hong Z, Yoshimura K, Ohya K, Xu R, Ye S, Gao J, Li G, Yang Y. 10.2% power conversion efficiency polymer tandem solar cells consisting of two identical sub-cells. Adv. Mater. 2013;25(29): 3973–3978.

[28] Chen C-C, Chang W-H, Yoshimura K, Ohya K, You J, Gao J, Hong Z, Yang Y. An efficient triple-junction polymer solar cell having a power conversion efficiency exceeding 11%" *Adv. Mater.* 2014;DOI:10.1002/adma.201402072.

[29] Jørgensen M, Norrman K, Krebs FC. Stability/degradation of polymer solar cells. Sol. Energy Mater. Sol. Cells. 2008;92 (7):686–714.

[30] Krebs FC. Fabrication and processing of polymer solar cells: A review of printing and coating techniques. Sol. Energy Mater. Sol. Cells. 2009;93(4):394–412.

[31] Mihailetchi VD, Koster LJA, Hummelen JC, Blom PWM. Photocurrent generation in polymer-fullerene bulk heterojunctions. Phys. Rev. Lett. 2004:93(21):216601.

[32] Blom PWM, Mihailetchi VD, Koster LJA, Markov DE. Device physics of polymer:fullerene bulk heterojunction solar cells. Adv. Mater. 2007;19(12):1551–1566.

[33] Yang X, Loos J. Toward high-performance polymer solar cells: The importance of morphology control. Macromolecules. 2007;40(5):1353–1362.

[34] Halls JJM, Pichler K, Friend RH, Moratti SC, Holmes AB. Exciton diffusion and dissociation in a poly(p-phenylenevinylene)/C[sub 60] heterojunction photovoltaic cell. Appl. Phys. Lett. 1996;68(22):3120–3122.

[35] Pettersson LAA, Lucimara SR, Inganäs O. Modeling photocurrent action spectra of photovoltaic devices based on organic thin films. J. Appl. Phys. 1999;86:487–496.

[36] Theander M, Yartsev A, Zigmantas D, Sundström V, Mammo W, Andersson MR, Inganäs O. Photoluminescence quenching at a polythiophene/C60 heterojunction. Phys. Rev. B. 2000;61 (19):12957.

[37] Janssen RAJ, Sariciftci NS, Heeger AJ. Photoinduced absorption of conjugated polymer/C[sub 60] solutions: Evidence of triplet-state photoexcitations and triplet-energy transfer in poly(3-alkylthiophene). J. Chem. Phys. 1994;100(12):8641–8645.

[38] Brabec CJ, Zerza G, Cerullo G, De Silvestri S, Luzzati S, Hummelen JC, Sariciftci S, Tracing photoinduced electron transfer process in conjugated polymer/fullerene bulk heterojunctions in real time. Chem. Phys. Lett. 2001;340(3–4):232–236.

[39] Brabec CJ, Sariciftci NS, Hummelen JC. Plastic solar cells. Adv. Funct. Mater. 2001;11(1):15–26.

[40] Lee KH, Schwenn PE, Smith ARG, Cavaye H, Shaw PE, James M, Krueger KB, Gentle IR, Meredith P, Burn PL. Morphology of all-solution-processed “bilayer” organic solar cells. Adv. Mater. 2011;23(6):766–770.

[41] Alam MM, Jenekhe SA. Efficient solar cells from layered nanostructures of donor and acceptor conjugated polymers. Chem. Mater. 2004;16(23):4647–4656.

[42] Matsuo Y, Sato Y, Niinomi T, Soga I, Tanaka H, Nakamura E. Columnar structure in bulk heterojunction in solution-processable three-layered p-i-n organic photovoltaic devices using tetrabenzoporphyrin precursor and silylmethyl[60]fullerene. J. Am. Chem. Soc. 2009;131(44):16048–16050.

[43] Meyer J, Hamwi S, Kröger M, Kowalsky W, Riedl T, Kahn A. Transition metal oxides for organic electronics: Energetics, device physics and applications. Adv. Mater. 2012;24(40):54085427.

[44] Duan C, Zhong C, Huang F, Cao Y. In Interface Engineering for High Performance Bulk-Heterojunction Polymeric Solar Cells, *Vol.* (Ed. W. C. H. Choy), pp.43–79. London: Springer, 2013.

[45] Ameri T, Dennler G, Lungenschmied C, Brabec CJ. Organic tandem solar cells: A review. Energy Environ. Sci. 2009;2(4):347–363.

[46] Siddiki MK, Li J, Galipeau D, Qiao Q. A review of polymer multijunction solar cells. Energy Environ. Sci. 2010;3(7):867–883.

[47] Sista S, Hong Z, Chen L-M, Yang Y. Tandem polymer photovoltaic cells – current status, challenges and future outlook. Energy Environ. Sci. 2011;4(5):1606–1620.

[48] Hau S K, Yip H-L, Jen AKY. A review on the development of the inverted polymer solar cell architecture. Poly. Rev. 2010;50(4):474–510.

[49] Zhang F, Xu X, Tang W, Zhang J, Zhuo Z, Wang J, Wang J, Xu Z, Wang Y. Recent development of the inverted configuration organic solar cells. Sol. Energy Mater. Sol. Cells. 2011;95(7):1785–1799.

[50] Brabec CJ, Cravino A, Meissner D, Sariciftci NS, Fromherz T, Rispens MT, Sanchez L, Hummelen JC. Origin of the open circuit voltage of plastic solar cells. Adv. Funct. Mater. 2001;11(5):374–380.

[51] Scharber MC, Mühlbacher D, Koppe M, Denk P, Waldauf C, Heeger AJ, Brabec CJ. Design rules for donors in bulk-heterojunction solar cells–towards 10% energy-conversion efficiency. Adv. Mater. 2006;18(6)789–794.

[52] Li G, Shrotriya V, Yao Y, Huang J, Yang Y. Manipulating regioregular poly(3-hexylthiophene) : [6,6]-phenyl-C61-butyric acid methyl ester blends-route towards high efficiency polymer solar cells. J. Mater. Chem. 2007;17(30):3126–3140.

[53] Chen L-M, Hong Z, Li G, Yang Y. Recent progress in polymer solar cells: manipulation of polymer: Fullerene morphology and the formation of efficient inverted polymer solar cells. Adv. Mater. 2009:21(14–15):1434–1449.

[54] Gao Y, Ma T. Bulk heterojunction polymer solar cells. Prog. Chem. 2011;23(5):991–1013.

[55] Yao Y, Hou J, Xu Z, Li G, Yang Y. Effects of solvent mixtures on the nanoscale phase separation in polymer solar cells. Adv. Funct. Mater. 2008;18(12):1783–1789.

[56] van Duren JKJ, Yang X, Loos J, Bulle-Lieuwma CWT, Sieval AB, Hummelen JC, Janssen RAJ. Relating the morphology of poly(p-phenylene vinylene)/methanofullerene blends to solar-cell performance. Adv. Funct. Mater. 2004;14(5):425–434.

[57] Ma W, Yang C, Gong X, Lee K, Heeger AJ. Thermally stable, efficient polymer solar cells with nanoscale control of the interpenetrating network morphology. Adv. Funct. Mater. 2005;15:1617–1622.

[58] Yang X, Loos J, Veenstra SC, Verhees WJH, Wienk MM, Kroon JM, Michels MAJ, Janssen RAJ. Nanoscale morphology of high-performance polymer solar cells. Nano Lett. 2005;5(4):579–583.

[59] Li G, Shrotriya V, Huang J, Yao Y, Moriarty T, Emery K, Yang Y. High-efficiency solution processable polymer photovoltaic cells by self-organization of polymer blends. Nat. Mater. 2005;4(11):864–868.

[60] van Bavel S, Veenstra S, Loos J. On the importance of morphology control in polymer solar cells. Macromol. Rapid Commun. 2010;31(21):1835–1845.

[61] van Bavel SS, Loos J. Volume organization of polymer and hybrid solar cells as revealed by electron tomography. Adv. Funct. Mater. 2010;20(19):3217–3234.

[62] Oosterhout SD, Wienk MM, van Bavel SS, Thiedmann R, Koster LJA, Gilot J, Loos J, Schmidt V, Janssen RAJ. The effect of three-dimensional morphology on the efficiency of hybrid polymer solar cells. Nat. Mater. 2009;8:818–824.

[63] Brinkmann M, Rannou P. Effect of molecular weight on the structure and morphology of oriented thin films of regioregular poly(3-hexylthiophene) grown by directional epitaxial solidification. Adv. Funct. Mater. 2007; 17(1):101–108.

[64] Moet DJD, Lenes M, Kotlarski JD, Veenstra SC, Sweelssen J, Koetse MM, de Boer B, Blom PWM. Impact of molecular weight on charge carrier dissociation in solar cells from a polyfluorene derivative. Org. Electron. 2009;10(7)1275–1281.

[65] Mozer AJ, Ma C-Q, Wong WWH, Jones D, Bäuerle P, Wallace GG. The effect of molecule size and shape on charge transport, recombination and free charge generation in all-thiophene dendrimer:fullerene bulk heterojunctions. Org. Electron. 2010;11(4):573–582.

[66] Wu J, Cheng D, Shen X, Yu Z. Electrode modification research of organic solar cells. Electronics & Packaging 2010;10(10):38–43.

[67] Potscavage W J, Sharma A, Kippelen B. Critical interfaces in organic solar cells and their influence on the open-circuit voltage. Acc. Chem. Res. 2009;42(11):1758–1767.

[68] Armstrong NR, Veneman PA, Ratcliff E, Placencia D, Brumbach M. Oxide contacts in organic photovoltaics: Characterization and control of near-surface composition in indium-tin oxide (ito) electrodes. Acc. Chem. Res. 2009;42(11):1748–1757.

[69] Brown TM, Zardetto VZ, Reale A, Di Carlo A. Substrates for flexible electronics: a practical investigation on the electrical, film flexibility, optical, temperature, and solvent resistance properties. J. Polym. Sci., Part B: Polym. Phys. 2011;49(9):638–648.

[70] Bradley DDC, Huang J, Wang X, Kim Y, deMello A J, Demello JC. High efficiency flexible ITO-free polymer/fullerene photodiodes. Phys. Chem. Chem. Phys. 2006;8(33):3904–3908.

[71] Krebs FC, Biancardo M, Winther-Jensen B, Spanggard H, Alstrup J. Strategies for incorporation of polymer photovoltaics into garments and textiles. Sol. Energy Mater. Sol. Cells. 2006;90(7–8): 1058–1067.

[72] Kim HK, Jeong JA, Choi KH, Jeong SW, Kang JW. Characteristics of flexible ito electrodes grown by continuous facing target roll-to-roll sputtering for flexible organic solar cells. Electrochem Solid St. 2009;12(5): H169–H172.

[73] Kim HK, Choi KH, Jeong JA, Kang JW, Kim DG, Kim JK, Na SI, Kim DY, Kim SS. Characteristics of flexible indium tin oxide electrode grown by continuous roll-to-roll sputtering process for flexible organic solar cells. Sol. Energy Mater. Sol. Cells. 2009;93(8):1248–1255.

[74] Kim HK, Park YS, Jeong SW, Cho WJ. Highly flexible indium zinc oxide electrode grown on PET substrate by cost efficient roll-to-roll sputtering process. Thin Solid Films. 2010;518(11):3071–3074.

[75] Fonrodona M, Escarré J, Villar F, Soler D, Asensi JM, Bertomeu J, Andreu J. PEN as substrate for new solar cell technologies. Sol. Energy Mater. Sol. Cells. 2005;89(1):37–47.

[76] Rhee SW, Kim JM, Thiyagarajan P. Deposition of Al-doped ZnO films on polyethylene naphthalate substrate with radio frequency magnetron sputtering. Thin Solid Films. 2010;518(20):5860–5865.

[77] Chang HJ, Gong SC, Jang SK, Ryu SO, Jeon H, Park HH. Post annealing effect of flexible polymer solar cells to improve their electrical properties. Curr. Appl. Phys. 2010;10(4):E192E196.

[78] Jung YS, Choi HW, Kim KH, Park SJ, Yoon HH. Properties of AZO thin films for solar cells deposited on polycarbonate substrates. J. Korean Phys. Soc. 2009;55(5):1945–1949.

[79] Kim D. Deposition of indium tin oxide films on polycarbonate substrates by direct metal ion beam deposition. Appl. Surf. Sci. 2003;218(1–4):70–77.

[80] Lin Y-S, Weng M-S, Chung T-W, Huang C. Enhanced surface hardness of flexible polycarbonate substrates using plasma-polymerized organosilicon oxynitride films by air plasma jet under atmospheric pressure. Sur. Coating Tech. 2011;205(13–14):3856–3864.

[81] Ye ZZ, Gong L, Lu JG. Transparent and conductive Ga-doped ZnO films grown by RF magnetron sputtering on polycarbonate substrates. Sol. Energy Mater. Sol. Cells. 2010;94(6):937–941.

[82] Kim HK, Park YS, Choi KH. Room temperature flexible and transparent ITO/Ag/ITO electrode grown on flexile PES substrate by continuous roll-to-roll sputtering for flexible organic photovoltaics. J. Phys. D Appl. Phys. 2009;42(23):235109.

[83] Park Y-S, Kim H-K. Flexible indium zinc oxide/Ag/indium zinc oxide multilayer electrode grown on polyethersulfone substrate by cost-efficient roll-to-roll sputtering for flexible organic photovoltaics. J. Vac. Sci. Technol. A. 2010;28:41–47.

[84] Heo G-S, Yuji-Matsumoto, Gim I-G, Park J-W, Kim G-Y, Kim T-W. Deposition of amorphous zinc indium tin oxide and indium tin oxide films on flexible poly(ether sulfone) substrate using RF magnetron co-sputtering system. Jpn. J. Appl. Phys. 2010;49:035801.

[85] Strange M, Plackett D, Kaasgaard M, Krebs FC. Biodegradable polymer solar cells. Sol. Energy Mater. Sol. Cells. 2008;92(7):805–813.

[86] Krebs FC, Tromholt T, Jorgensen M. Upscaling of polymer solar cell fabrication using full roll-to-roll processing. Nanoscale. 2010;2(6):873–886.

[87] Kumar A, Zhou C. The race to replace tin-doped indium oxide: which material will win? ACS Nano. 2010;4(1):11–14.

[88] Inganas O. Organic photovoltaics: Avoiding indium. Nat. Photon. 2011;5(4):201–202.

[89] Baek WH, Choi M, Yoon TS, Lee HH, Kim YS. Use of fluorine-doped tin oxide instead of indium tin oxide in highly efficient air-fabricated inverted polymer solar cells. Appl. Phys. Lett. 2010;96(13):133506.

[90] Shin WS, Kim JR, Cho JM, Lee AR, Chae EA, Park JU, Byun WB, Lee SK, Lee JC, So WW, Yoo S, Moon SJ. Improvement of the performance of inverted polymer solar cells with a fluorine-doped tin oxide electrode. Curr. Appl. Phys. 2011;11(1):S175–S178.

[91] Qin P, Fang G, Sun N, Fan X, Zheng Q, Chen F, Wan J, Zhao X. Organic solar cells with p-type amorphous chromium oxide thin film as hole-transporting layer. Thin Solid Films. 2011;519(13):4334–4341.

[92] Kim SW, Ihn SG, Shin KS, Jin MJ, Bulliard X, Yun S, Choi YS, Kim Y, Park JH, Sim M, Kim M, Cho K, Kim TS, Choi D, Choi JY, Choi W. ITO-free inverted polymer solar cells using a GZO cathode modified by ZnO. Sol. Energy Mater. Sol. Cells. 2011;95(7):1610–1614.

[93] Park H-K, Kang J-W, Na S-I, Kim D-Y, Kim H-K. Characteristics of indium-free GZO/Ag/GZO and AZO/Ag/AZO multilayer electrode grown by dual target DC sputtering at room temperature for low-cost organic photovoltaics. Sol. Energy Mater. Sol. Cells. 2009;93(11):1994–2002.

[94] Park J-H, Ahn K-J, Park K-I, Na S-I, Kim H-K. An Al-doped ZnO electrode grown by highly efficient cylindrical rotating magnetron sputtering for low cost organic photovoltaics. Journal of Physics D: Applied Physics. 2010;43(11):115101.

[95] Park J-H, Kim H-K, Lee H, Lee H, Yoon S, Kim C-D. Highly transparent, low resistance, and cost-efficient Nb:TiO2/Ag/Nb:TiO2 multilayer electrode prepared at room temperature using black Nb:TiO2 target. Electrochem. Solid State Lett. 2010;13(5):J53–J56.

[96] Kim YH, Sachse C, Machala ML, May C, Müller-Meskamp L, Leo K. Highly conductive PEDOT:PSS electrode with optimized solvent and thermal post-treatment for ITO-free organic solar cells. Adv. Funct. Mater. 2011;21(6):1076–1081.

[97] Na S-I, Kim S-S, Jo J, Kim D-Y. Efficient and flexible ITO-free organic solar cells using highly conductive polymer anodes. Adv. Mater. 2008;20(21):4061–4067.

[98] Hau SK, Yip H-L, Zou J, Jen AKY. Indium tin oxide-free semi-transparent inverted polymer solar cells using conducting polymer as both bottom and top electrodes. Org. Electron. 2009;10(7):1401–1407.

[99] Zhou Y, Li F, Barrau S, Tian W, Inganäs O, Zhang F. Inverted and transparent polymer solar cells prepared with vacuum-free processing. Sol. Energy Mater. Sol. Cells. 2009;93(4):497500.

[100] Hu Z, Zhang J, Hao Z, Zhao Y. Influence of doped PEDOT:PSS on the performance of polymer solar cells. Sol. Energy Mater. Sol. Cells. 2011;95(10):2763–2767.

[101] Berredjem Y, Bernede JC, Djobo SO, Cattin L, Morsli M, Boulmokh A. On the improvement of the efficiency of organic photovoltaic cells by the presence of an ultra-thin metal layer at the interface organic/ITO. Eur Phys J-Appl Phys. 2008;44(3):223–228.

[102] Koeppe R, Hoeglinger D, Troshin PA, Lyubovskaya RN, Razumov VF,Sariciftci NS. Organic solar cells with semitransparent metal back contacts for power window applications. ChemSusChem. 2009;2(4):309–313.

[103] Ghosh DS, Betancur R, Chen TL, Pruneri V, Martorell J. Semi-transparent metal electrode of Cu-Ni as a replacement of an ITO in organic photovoltaic cells. Sol. Energy Mater. Sol. Cells. 2011;95(4):1228–1231.

[104] Lee K-S, Kim I, Yeon CB, Lim JW, Yun SJ, Jabbour GE. Thin metal electrodes for semitransparent organic photovoltaics. ETRI Journal. 2013;35(4):587–593.

[105] Tvingstedt K, Inganäs O. Electrode grids for ITO free organic photovoltaic devices. Adv. Mater. 2007; 19(19):2893–2897.

[106] Galagan Y, Rubingh JE, Andriessen R, Fan C-C, Blom P, Veenstra SC, Kroon J, ITO-free flexible organic solar cells with printed current collecting grids. Sol. Energy Mater. Sol. Cells. 2011:95(5):1339–1343.

[107] Li Y, Mao L, Gao Y, Zhang P, Li C, Ma C, Tu Y, Cui Z, Chen L. ITO-free photovoltaic cell utilizing a high-resolution silver grid current collecting layer. Sol. Energy Mater. Sol. Cells. 2013;113:85–89.

[108] Mao L, Chen Q, Li Y, Li Y, Cai J, Su W, Bai S, Jin Y, Ma C-Q, Cui Z, Chen L. Flexible silver grid/PEDOT:PSS hybrid electrodes for large area inverted polymer solar cells. Nano Energy. 2014;10:259–267.

[109] Kylberg W, de Castro FA, Chabrecek P, Sonderegger U, Chu BT-T, Nüesch F, Hany R. Woven electrodes for flexible organic photovoltaic cells. Adv. Mater. 2011;23(8):1015–1019.

[110] Barnes TM, Bergeson JD, Tenent RC, Larsen BA, Teeter G, Jones KM, Blackburn JL,van de Lagemaat J. Carbon nanotube network electrodes enabling efficient organic solar cells without a hole transport layer. Appl. Phys. Lett. 2010;96(24):243309.

[111] Wang Y, Chen X, Zhong Y, Zhu F, Loh KP. Large area, continuous, few-layered graphene as anodes in organic photovoltaic devices. Appl. Phys. Lett. 2009;95(6):063302.

[112] Chambon S, Rivaton A, Gardette J-L, Firon M. Photo- and thermo-oxidation of poly(p-phenylene-vinylene) and phenylene-vinylene oligomer. Polymer Degradation and Stability. 2011;96(6):1149–1158.

[113] Irwin MD, Bruce Buchholz D, Hains AW, Chang RPH, Marks TJ. p-Type semiconducting nickel oxide as an efficiency-enhancing anode interfacial layer in polymer bulk-heterojunction solar cells. Proc. Natl. Acad. Sci. 2008;105(8):2783–2787.

[114] Dennler G, Scharber M C, Brabec CJ. Polymer-fullerene bulk-heterojunction solar cells. Adv. Mater. 2009;21(13):1323–1338.

[115] He Y, Chen H-Y, Hou J, Li Y. Indene−C60 bisadduct: A new acceptor for high-performance polymer solar cells. J. Am. Chem. Soc. 2010;132(4):1377–1382.

[116] Zhao G, He Y, Li Y. 6.5% Efficiency of polymer solar cells based on poly(3-hexylthiophene) and indene-C_{60} bisadduct by device optimization. Adv. Mater. 2010;22(39):4355–4358.

[117] Peet J, Senatore ML, Heeger AJ, Bazan GC. The role of processing in the fabrication and optimization of plastic solar cells. Adv. Mater. 2009;21(14–15):1521–1527.

[118] Peters CH, Sachs-Quintana IT, Mateker WR, Heumueller T, Rivnay J, Noriega R, Beiley ZM, Hoke ET, Salleo A, McGehee MD. The mechanism of burn-in loss in a high efficiency polymer solar cell. Adv. Mater. 2012;24(5):663–668.

[119] Zhan X, Zhu D. Conjugated polymers for high-efficiency organic photovoltaics. Polym. Chem. 2010;1(4): 409–419.

[120] Cheng Y-J, Yang S-H, Hsu C-S. Synthesis of conjugated polymers for organic solar cell applications. Chem. Rev. 2009;109(11):5868–5923.

[121] Mühlbacher D, Scharber M, Morana M, Zhu Z, Waller D, Gaudiana R, Brabec C. High photovoltaic performance of a low-bandgap polymer. Adv. Mater. 2006;18(21):2884–2889.

[122] Zhu Z, Waller D, Gaudiana R, Morana M, Muhlbacher D, Scharber M, Brabec C. Panchromatic conjugated polymers containing alternating donor/acceptor units for photovoltaic application. Macromolecules. 2007;40(6):1981–1986.

[123] Park SH, Roy A, Beaupre S, Cho S, Coates N, Moon JS, Moses D, Leclerc M, Lee K, Heeger AJ. Bulk heterojunction solar cells with internal quantum efficiency approaching 100%. Nat. Photonics. 2009;3(5): 297–302.

[124] Hou J, Chen H-Y, Zhang S, Li G,Yang Y. Synthesis, characterization, and photovoltaic properties of a low band gap polymer based on silole-containing polythiophenes and 2,1,3-benzothiadiazole. J. Am. Chem. Soc. 2008;130(48):16144–16145.

[125] Chu T-Y, Lu J, Beaupré S, Zhang Y, Pouliot J-R m, Wakim S, Zhou J, Leclerc M, Li Z, Ding J, Tao Y. Bulk heterojunction solar cells using thieno[3,4-c]pyrrole-4,6-dione and dithieno[3,2-b:2′,3′-d]silole copolymer with a power conversion efficiency of 7.3%. J. Am. Chem. Soc. 2011;133(12):4250–4253.

[126] Liang Y, Feng D, Wu Y, Tsai S-T, Li G, Ray C, Yu L. Highly efficient solar cell polymers developed via fine-tuning of structural and electronic properties. J. Am. Chem. Soc. 2009;131(22):7792–7799.

[127] Liang Y, Xu Z, Xia J, Tsai S-T, Wu Y, Li G, Ray C, Yu L. For the bright future – bulk heterojunction polymer solar cells with power conversion efficiency of 7.4%. Adv. Mater. 2010;2 (20):E135–E138.

[128] Liang Y, Yu L. A new class of semiconducting polymers for bulk heterojunction solar cells with exceptionally high performance. Acc. Chem. Res. 2010;43(9),1227–1236.

[129] He Z, Zhong C, Su S, Xu M, Wu H, Cao Y. Enhanced power-conversion efficiency in polymer solar cells using an inverted device structure. Nat. Photonics 2012;6(9)591–595.

[130] Price SC, Stuart AC, Yang L, Zhou H, You W. Fluorine substituted conjugated polymer of medium band gap yields 7% efficiency in polymer-fullerene solar cells. J. Am. Chem. Soc. 2011;133(12):4625–4631.

[131] Zhang H, Glasbeek M, Vekemans JAJM, Meijer EW. Hierarchical growth of chiral self-assembled structures in protic media. J. Am. Chem. Soc. 2000;122(26):6175–6182.

[132] Bronstein H, Chen Z, Ashraf RS, Zhang W, Du J, Durrant JR, Shakya Tuladhar P, Song K, Watkins SE, Geerts Y, Wienk MM, Janssen RAJ, Anthopoulos T, Sirringhaus H, Heeney M, McCulloch I. Thieno[3,2-b]thiophene−diketopyrrolopyrrole-containing polymers for high-performance organic field-effect transistors and organic photovoltaic devices. J. Am. Chem. Soc. 2011;133(10):3272–3275.

[133] Bürckstümmer H, Weissenstein A, Bialas D, Würthner F. Synthesis and characterization of optical and redox properties of bithiophene-functionalized diketopyrrolopyrrole chromophores. J. Org. Chem. 2011;76(8):2426–2432.

[134] Wienk MM, Turbiez M, Gilot J, Janssen RAJ. Narrow-bandgap diketo-pyrrolo-pyrrole polymer solar cells: the effect of processing on the performance. Adv. Mater. 2008;20(13):25562560.

[135] Bijleveld JC, Zoombelt AP, Mathijssen SGJ, Wienk MM, Turbiez M, de Leeuw DM, Janssen RAJ. Poly(diketopyrrolopyrrole−terthiophene) for ambipolar logic and photovoltaics. J. Am. Chem. Soc. 2009; 131(46):16616–16617.

[136] Li W, Roelofs WSC, Wienk MM, Janssen RAJ. Enhancing the photocurrent in diketopyrrolopyrrole-based polymer solar cells via energy level control. J. Am. Chem. Soc. 2012;134:13787-13795. (Copyright (c) 2014 American Chemical Society (ACS). All Rights Reserved.)

[137] Hendriks KH, Li W, Wienk MM, Janssen RAJ. Band gap control in diketopyrrolopyrrole-based polymer solar cells using electron donating side chains. *Adv. Energy Mater.* 2013.

[138] Li W, Furlan A, Hendriks KH, Wienk MM, Janssen RAJ. Efficient tandem and triple-junction polymer solar cells. J. Am. Chem. Soc. 2013;135(15):5529–5532.

[139] Li W, Hendriks KH, Furlan A, Roelofs WSC, Wienk MM, Janssen RAJ. Universal correlation between fibril width and quantum efficiency in diketopyrrolopyrrole-based polymer solar cells. J. Am. Chem. Soc. 2013;135(50): 18942–18948.

[140] Li W, Roelofs WSC, Turbiez M, Wienk MM, Janssen RAJ. Polymer solar cells with diketopyrrolopyrrole conjugated polymers as the electron donor and electron acceptor. *Adv. Mater.* 2014;DOI:10.1002/adma.201305910.

[141] Boudreault P-LT, Najari A, Leclerc M. Processable low-bandgap polymers for photovoltaic applications. Chem. Mater. 2011;23(3):456–469.

[142] Walker B, Kim C, Nguyen T-Q. Small molecule solution-processed bulk heterojunction solar cells. Chem. Mater. 2011;23(3):470–482.

[143] Walker B, Tamayo AB, Dang X-D, Zalar P, Seo JH, Garcia A, Tantiwiwat M, Nguyen T-Q. Nanoscale phase separation and high photovoltaic efficiency in solution-processed, small-molecule bulk heterojunction solar cells. Adv. Funct. Mater. 2009;19(19):3063–3069.

[144] Liu Y, Wan X, Yin B, Zhou J, Long G, Yin S, Chen Y. Efficient solution processed bulk-heterojunction solar cells based a donor-acceptor oligothiophene. J. Mater. Chem. 2010;20(12):2464–2468.

[145] Liu Y, Wan X, Wang F, Zhou J, Long G, Tian J, You J, Yang Y,Chen Y. Spin-coated small molecules for high performance solar cells. Adv. Energy Mater. 2011;1(5):771–775.

[146] Ma C-Q, Fonrodona M, Schikora MC, Wienk MM, Janssen RAJ, Bäuerle P. Solution-processed bulk-heterojunction solar cells based on monodisperse dendritic oligothiophenes. Adv. Funct. Mater. 2008; 18(20):3323–3331.

[147] Ma C-Q. Conjugated dendritic oligothiophenes for solution-processed bulk heterojunction solar cells. Frontiers of Optoelectronics in China 2011;4(1):12–23.

[148] Shang H, Fan H, Liu Y, Hu W, Li Y, Zhan X. A solution-processable star-shaped molecule for high-performance organic solar cells. Adv. Mater. 2011;23(13):1554–1557.

[149] Love JA, Nagao I, Huang Y, Kuik M, Gupta V, Takacs CJ, Coughlin JE, Qi L, van der Poll TS, Kramer EJ, Heeger AJ, Nguyen T-Q, Bazan GC. Silaindacenodithiophene-based molecular donor: morphological features and use in the fabrication of compositionally tolerant, high-efficiency bulk heterojunction solar cells. J. Am. Chem. Soc. 2014;136(9):3597–3606.

[150] Zhou J, Zuo Y, Wan X, Long G, Zhang Q, Ni W, Liu Y, Li Z, He G, Li C, Kan B, Li M, Chen Y. Solution processed and high performance organic solar cells using small molecules with benzodithiophene unit. J. Am. Chem. Soc. 2013;135(23):8484–8487.

[151] Chen Y, Wan X, Long G. High performance photovoltaic applications using solution-processed small molecules. Acc. Chem. Res. 2013;46(11):2645–2655.

[152] Coughlin JE, Henson ZB, Welch GC, Bazan GC. Design and synthesis of molecular donors for solution-processed high-efficiency organic solar cells. Acc. Chem. Res. 2013;47(1):257–270.

[153] Hummelen JC, Knight BW, LePeq F, Wudl F, Yao J, Wilkins CL. Preparation and characterization of fulleroid and methanofullerene derivatives. J. Org. Chem. 1995;60(3)532–538.

[154] Lenes M, Wetzelaer G-JAH, Kooistra FB, Veenstra C, Hummelen JC, Blom PWM, Fullerene bisadducts for enhanced open-circuit voltages and efficiencies in polymer solar cells. Adv. Mater. 2008;20(11):2116–2119.

[155] Popescu LM, van 't Hof P, Sieval AB, Jonkman HT, Hummelen JC. Thienyl analog of 1-(3-methoxycarbonyl) propyl-1-phenyl-[6,6]-methanofullerene for bulk heterojunction photovoltaic devices in combination with polythiophenes. Appl. Phys. Lett. 2006;89(21):213507–213503.

[156] Kamm V, Battagliarin G, Howard IA, Pisula W, Mavrinskiy A, Li C, Müllen K, Laquai F. Polythiophene:perylene diimide solar cells – the impact of alkyl-substitution on the photovoltaic performance. Adv. Energy Mater. 2011;1(2):297–302.

[157] Zhan X, Tan Z, Domercq B, An Z, Zhang X, Barlow S, Li Y, Zhu D, Kippelen B, Marder SR. A high-mobility electron-transport polymer with broad absorption and its use in field-effect transistors and all-polymer solar cells. J. Am. Chem. Soc. 2007;129(23):7246–7247.

[158] Zhou E, Cong J, Wei Q, Tajima K, Yang C, Hashimoto K. All-polymer solar cells from perylene diimide based copolymers: material design and phase separation control. Angew. Chem. Int. Ed. 2011;50(12):2799–2803.

[159] He Y, Li Y. Photovoltaic materials in polymer solar cells. Prog. Chem. 2009:21(11):23032318.

[160] Brunetti FG, Gong X, Tong M, Heeger AJ, Wudl F. Strain and Hückel aromaticity: driving forces for a promising new generation of electron acceptors in organic electronics. Angew. Chem. Int. Ed. 2009;49(3): 532–536.

[161] Tada H, Fujishima M, Kobayashi H. Photodeposition of metal sulfide quantum dots on titanium(iv) dioxide and the applications to solar energy conversion. Chem. Soc. Rev. 2011;40(7):4232–4243.

[162] Kamat PV, Tvrdy K, Baker DR, Radich JG. Beyond photovoltaics: semiconductor nanoarchitectures for liquid-junction solar cells. Chem. Rev. 2010;110(11):6664–6688.

[163] Zhou Y, Eck M, Kruger M. Bulk-heterojunction hybrid solar cells based on colloidal nanocrystals and conjugated polymers. Energy Environ. Sci. 2010;3(12):1851–1864.

[164] Huynh WU, Dittmer JJ, Alivisatos AP. Hybrid nanorod-polymer solar cells. Science. 2002;295(5564): 2425–2427.

[165] Sun B, Marx E, Greenham NC. Photovoltaic devices using blends of branched CdSe nanoparticles and conjugated polymers. Nano Lett. 2003;3(7):961–963.

[166] Dayal S, Kopidakis N, Olson DC, Ginley DS, Rumbles G. Photovoltaic devices with a low band gap polymer and CdSe nanostructures exceeding 3% efficiency. Nano Lett. 2009;10(1):239–242.

[167] Beek WJE, Wienk MM, Janssen RAJ. Efficient hybrid solar cells from zinc oxide nanoparticles and a conjugated polymer. Adv. Mater. 2004;16(12):1009–1013.

[168] Wu M-C, Lo H-H, Liao H-C, Chen S, Lin Y-Y, Yen W-C, Zeng T-W, Chen Y-F, Chen C-W, Su W-F. Using scanning probe microscopy to study the effect of molecular weight of poly(3-hexylthiophene) on the performance of poly(3-hexylthiophene):TiO2 nanorod photovoltaic devices. Sol. Energy Mater. Sol. Cells. 2009;93(6–7): 869–873.

[169] Li S-S, Chang C-P, Lin C-C, Lin Y-Y, Chang C-H, Yang J-R, Chu M-W, Chen C-W. Interplay of Three-dimensional morphologies and photocarrier dynamics of polymer/TiO2 bulk heterojunction solar cells. J. Am. Chem. Soc. 2011;133(30):11614–11620.

[170] Arici E, Hoppe H, Schäffler F, Meissner D, Malik MA, Sariciftci NS. Morphology effects in nanocrystalline $CuInSe_2$-conjugated polymer hybrid systems. Appl. Phys. A: Mater. Sci. Proc. 2004;79(1):59–64.

[171] Ma H, Yip H-L, Huang F, Jen AKY. Interface engineering for organic electronics. Adv. Funct. Mater. 2010;20(9):1371–1388.

[172] Po R, Carbonera C, Bernardi A, Camaioni N. The role of buffer layers in polymer solar cells. Energy Environ. Sci. 2011;4(2):285–310.

[173] Groenendaal LB, Friedrich J, Freitag D, Pielartzik H, Reynolds JR. Poly(3,4-ethylenedioxythiophene) and its derivatives: past, present and future. Adv. Mater. 2000;12(7):481–494.

[174] Perepichka IF, Perepichka DF. Handbook of Thiophene-Based Materials, p. 910. Chichester: John Wiley & Sons.

[175] Shrotriya V, Li G, Yao Y, Chu C-W,Yang Y. Transition metal oxides as the buffer layer for polymer photovoltaic cells. Appl. Phys. Lett. 2006;88(7):073508–073503.

[176] Gao D, Helander MG, Wang Z-B, Puzzo DP, Greiner MT, Lu Z-H. C60:LiF blocking layer for environmentally stable bulk heterojunction solar cells. Adv. Mater. 2010;22(47):5404–5408.

[177] Cheun H, Fuentes-Hernandez C, Zhou Y, Potscavage WJ, Kim S-J, Shim J, Dindar A, Kippelen B. Electrical and optical properties of ZnO processed by atomic layer deposition in inverted polymer solar cells. J. Phys. Chem. C 2010;114(48):20713–20718.

[178] Saarenpaa H, Niemi T, Tukiainen A, Lemmetyinen H, Tkachenko N. Aluminum doped zinc oxide films grown by atomic layer deposition for organic photovoltaic devices. Sol. Energy Mater. Sol. Cells. 2010;94(8):1379–1383.

[179] Norrman K, Larsen NB, Krebs FC. Lifetimes of organic photovoltaics: Combining chemical and physical characterisation techniques to study degradation mechanisms. Sol. Energy Mater. Sol. Cells. 2006;90(17):2793–2814.

[180] Toshihiro Y, Tetsuya T, Jun S, Jun T,Yuji Y. Effect of buffer layers on stability of polymer-based organic solar cells. Jpn. J. Appl. Phys. 2010;49(1S):01AC02.

[181] Hau SK, Yip H-L, Baek NS, Zou J, O'Malley K, Jen AK-Y. Air-stable inverted flexible polymer solar cells using zinc oxide nanoparticles as an electron selective layer. Appl. Phys. Lett. 2008;92(25):253301.

[182] Krebs FC, Fyenbo J, Jorgensen M. Product integration of compact roll-to-roll processed polymer solar cell modules: methods and manufacture using flexographic printing, slot-die coating and rotary screen printing. J. Mater. Chem. 2010;20(41):8994–9001.

[183] Lin Y-H, Yang P-C, Huang J-S, Huang G-D, Wang I-J, Wu W-H, Lin M-Y, Su W-F, Lin C-F. High-efficiency inverted polymer solar cells with solution-processed metal oxides. Sol. Energy Mater. Sol. Cells. 2011;95(8): 2511–2515.

[184] Schmidt H, Flügge H, Winkler T, Bülow T, Riedl T, Kowalsky W. Efficient semitransparent inverted organic solar cells with indium tin oxide top electrode. Appl. Phys. Lett. 2009;94(24):243302.

[185] Kuwabara T, Sugiyama H, Kuzuba M, Yamaguchi T, Takahashi K. Inverted bulk-heterojunction organic solar cell using chemical bath deposited titanium oxide as electron collection layer. Org. Electron. 2010;11(6): 1136–1140.

[186] Zilberberg K, Trost S, Meyer J, Kahn A, Behrendt A, Lützenkirchen-Hecht D, Frahm R, Riedl T. Inverted organic solar cells with sol–gel processed high work-function vanadium oxide hole-extraction layers. Adv. Funct. Mater. 2011;21(24):4776–4783.

[187] Stubhan T, Li N, Luechinger NA, Halim SC, Matt GJ, Brabec CJ. High Fill Factor Polymer Solar Cells Incorporating a Low Temperature Solution Processed WO3 Hole Extraction Layer. Adv. Energy Mater. 2012;2(12):1433–1438.

[188] Yu W, Shen L, Ruan S, Meng F, Wang J, Zhang E, Chen W. Performance improvement of inverted polymer solar cells thermally evaporating nickel oxide as an anode buffer layer. Sol. Energy Mater. Sol. Cells. 2012;98(0): 212–215.

[189] Huang J-S, Chou C-Y, Liu M-Y, Tsai K-H, Lin W-H, Lin C-F. Solution-processed vanadium oxide as an anode interlayer for inverted polymer solar cells hybridized with ZnO nanorods. Org. Electron. 2009:10(6):1060–1065.

[190] Kim JY, Lee K, Coates NE, Moses D, Nguyen T-Q, Dante M, Heeger AJ. Efficient tandem polymer solar cells fabricated by all-solution processing. Science. 2007;317(5835):222–225.

[191] Gilot J, Wienk MM, Janssen RAJ. Optimizing polymer tandem solar cells. Adv. Mater. 2010;22(8):E67–E71.

[192] Gilot J, Wienk MM, Janssen RAJ. Measuring the current density – voltage characteristics of individual subcells in two-terminal polymer tandem solar cells. Org. Electron. 2011;12(4):660–665.

[193] Min Nam Y, Huh J, Jo W H. A computational study on optimal design for organic tandem solar cells. Sol. Energy Mater. Sol. Cells. 2011;95(4):1095–1101.

[194] Chou C-H, Kwan WL, Hong Z, Chen L-M, Yang Y. A Metal-oxide interconnection layer for polymer tandem solar cells with an inverted architecture. Adv. Mater. 2011;23(10):1282–1286.

[195] Ajuria J, Etxebarria I, Cambarau W, Munecas U, Tena-Zaera R, Jimeno JC, Pacios R. Inverted ITO-free organic solar cells based on p and n semiconducting oxides. New designs for integration in tandem cells, top or bottom detecting devices, and photovoltaic windows. Energy Environ. Sci. 2011;4(2):453–458.

[196] Puetz A, Stubhan T, Reinhard M, Loesch O, Hammarberg E, Wolf S, Feldmann C, Kalt H, Colsmann A, Lemmer U. Organic solar cells incorporating buffer layers from indium doped zinc oxide nanoparticles. Sol. Energy Mater. Sol. Cells. 2011;95(2):579–585.

[197] Sun XW, Zhao DW, Ke L, Kyaw AKK, Lo GQ, Kwong DL. Inverted tandem organic solar cells with a MoO3/Ag/Al/Ca intermediate layer. Appl. Phys. Lett. 2010;97(5):053303.

[198] Yang J, Zhu R, Hong Z, He Y, Kumar A, Li Y, Yang Y. A robust inter-connecting layer for achieving high performance tandem polymer solar cells. Adv. Mater. 2011;23(30):3465–3470.

[199] You J, Dou L, Yoshimura K, Kato T, Ohya K, Moriarty T, Emery K, Chen C-C, Gao J, Li G, Yang Y. A polymer tandem solar cell with 10.6% power conversion efficiency. Nat. Commun. 2013;4:1446.

[200] Norrman K, Ghanbari-Siahkali A, Larsen NB. Studies of spin-coated polymer films. Annu. Rep. C. 2005;101: 174–201.

[201] Padinger F, Brabec CJ, Fromherz T, Hummelen JC, Sariciftci NS. Fabrication of large area photovoltaic devices containing various blends of polymer and fullerene derivatives by using the doctor blade technique. Opto-Electron Rev. 2000;8(4):280–283.

[202] Byun W-B, Lee SK, Lee J-C, Moon S-J, Shin WS, Bladed organic photovoltaic cells. Curr. Appl. Phys. 2011;11(1, Supplement 1):S179–S184.

[203] Chang Y-H, Tseng S-R, Chen C-Y, Meng H-F, Chen E-C, Horng S-F, Hsu C-S. Polymer solar cell by blade coating. Org. Electron. 2009;10(5):741–746.

[204] Sanyal M, Schmidt-Hansberg B, Klein MFG, Colsmann A, Munuera C, Vorobiev A, Lemmer U, Schabel W, Dosch H, Barrena E. In situ x-ray study of drying-temperature influence on the structural evolution of bulk-heterojunction polymer–fullerene solar cells processed by doctor-blading. Adv. Energy Mater. 2011;1(3): 363–367.

[205] Sanyal M, Schmidt-Hansberg B, Klein MFG, Munuera C, Vorobiev A, Colsmann A, Scharfer P, Lemmer U, Schabel W, Dosch H, Barrena E. Effect of photovoltaic polymer/fullerene blend composition ratio on microstructure evolution during film solidification investigated in real time by x-ray diffraction. Macromolecules. 2011;44(10)3795–3800.

[206] Shaheen SE, Radspinner R, Peyghambarian N, Jabbour GE. Fabrication of bulk heterojunction plastic solar cells by screen printing. Appl. Phys. Lett. 2001;(79):2996–2998.

[207] Aernouts T, Vanlaeke P, Poortmans J, Heremans PL. *Proc. SPIE* (Strasbourg, France). 2004:252–260.

[208] Krebs FC, Alstrup J, Spanggaard H, Larsen K, Kold E. Production of large-area polymer solar cells by industrial silk screen printing, lifetime considerations and lamination with polyethyleneterephthalate. Sol. Energy Mater. Sol. Cells. 2004;83(2–3):293–300.

[209] Sakai J, Fujinaka E, Nishimori T, lto N, Adachi J, Nagano S, Murakami K. *Photovoltaic Specialists Conference, 2005. Conference Record of the Thirty-first IEEE*. 2005:125–128.

[210] Krebs FC, Spanggard H, Kjær T, Biancardo M, Alstrup J. Large area plastic solar cell modules. Mat Sci Eng B-Solid. 2007;138(2):106–111.

[211] Zhang B, Chae H, Cho SM. Screen-Printed polymer:fullerene bulk-heterojunction solar cells. Jpn. J. Appl. Phys. 2009;48:020208.

[212] Jørgensen M, Hagemann O, Alstrup J, Krebs F C, "Thermo-cleavable solvents for printing conjugated polymers: Application in polymer solar cells. Sol. Energy Mater. Sol. Cells. 2009;93(4):413–421.

[213] Krebs FC, Jørgensen M, Norrman K, Hagemann O, Alstrup J, Nielsen TD, Fyenbo J, Larsen K, Kristensen J. A complete process for production of flexible large area polymer solar cells entirely using screen printing – First public demonstration. Sol. Energy Mater. Sol. Cells. 2009;93(4):422–441.

[214] Hoth CN, Choulis SA, Schilinsky P, Brabec CJ. High photovoltaic performance of inkjet printed polymer:fullerene blends. Adv. Mater. 2007;19(22):3973–3978.

[215] Hoth CN, Schilinsky P, Choulis SA, Brabec CJ. Printing highly efficient organic solar cells. Nano Lett. 2008;8(9):2806–2813.

[216] Hoth CN, Choulis SA, Schilinsky P, Brabec CJ. On the effect of poly(3-hexylthiophene) regioregularity on inkjet printed organic solar cells. J. Mater. Chem. 2009;19(30):5398–5404.

[217] Aernouts T, Aleksandrov T, Girotto C, Genoe J, Poortmans J. Polymer based organic solar cells using ink-jet printed active layers. Appl. Phys. Lett. 2008;92:033306-033303.

[218] Ding JM, de la Fuente Vornbrock A, Ting C, Subramanian V. Patternable polymer bulk heterojunction photovoltaic cells on plastic by rotogravure printing. Sol. Energy Mater. Sol. Cells. 2009;93(4):459–464.

[219] Kopola P, Aernouts T, Guillerez S, Jin H, Tuomikoski M, Maaninen A, Hast J. High efficient plastic solar cells fabricated with a high-throughput gravure printing method. Sol. Energy Mater. Sol. Cells. 2010;94(10): 1673–1680.

[220] Voigt MM, Mackenzie RCI, Yau CP, Atienzar P, Dane J, Keivanidis PE, Bradley DDC, Nelson J. Gravure printing for three subsequent solar cell layers of inverted structures on flexible substrates. Sol. Energy Mater. Sol. Cells. 2011;95(2):731–734.

[221] Park S-E, Hwang J-Y, Kim K, Jung B, Kim W, Hwang J. Spray deposition of electrohydrodynamically atomized polymer mixture for active layer fabrication in organic photovoltaics. Sol. Energy Mater. Sol. Cells. 2011;95(1): 352–356.

[222] Tedde SF, Kern J, Sterzl T, Fürst J, Lugli P, Hayden O. Fully Spray Coated Organic Photodiodes. Nano Lett. 2009;9(3):980–983.

[223] Kim JS, Chung WS, Kim K, Kim DY, Paeng KJ, Jo SM, Jang SY. Performance Optimization of polymer solar cells using electrostatically sprayed photoactive layers. Adv. Funct. Mater. 2010;20(20):3538–3546.

[224] Girotto C, Moia D, Rand BP, Heremans P. High-performance organic solar cells with spray-coated hole-transport and active layers. Adv. Funct. Mater. 2011;21(1):64–72.

[225] Kim S-S, Na SI, Jo J, Tae G, Kim DY. Efficient polymer solar cells fabricated by simple brush painting. Adv. Mater. 2007;19(24):4410–4415.

[226] Krebs FC. Polymer solar cell modules prepared using roll-to-roll methods: Knife-over-edge coating, slot-die coating and screen printing. Sol. Energy Mater. Sol. Cells. 2009;93(4):465–475.

[227] Krebs FC, Norrman K. Using light-induced thermocleavage in a roll-to-roll process for polymer solar cells. ACS Appl. Mater.Interfaces. 2010;2(3):877–887.

[228] Krebs FC, Gevorgyan SA, Alstrup J. A roll-to-roll process to flexible polymer solar cells: model studies, manufacture and operational stability studies. J. Mater. Chem. 2009;19(30):5442–5451.

[229] Krebs FC. All solution roll-to-roll processed polymer solar cells free from indium-tin-oxide and vacuum coating steps. Org. Electron. 2009;10(5):761–768.

[230] Krebs FC. Roll-to-roll fabrication of monolithic large-area polymer solar cells free from indium-tin-oxide. Sol. Energy Mater. Sol. Cells. 2009;93(9):1636–1641.

[231] Snaith HJ. Perovskites: The emergence of a new era for low-cost, high-efficiency solar cells. J. Phys. Chem. Lett. 2013;4(21):3623–3630.

[232] Park N-G. Organometal perovskite light absorbers toward a 20% efficiency low-cost solid-state mesoscopic solar cell. J. Phys. Chem. Lett. 2013;4:2423–2429.

[233] Kojima A, Teshima K, Shirai Y, Miyasaka T. Organometal halide perovskites as visible-light sensitizers for photovoltaic cells. J. Am. Chem. Soc. 2009;131(17);6050–6051.

[234] Zhou H, Chen Q, Li G, Luo S, Song T-b, Duan H-S, Hong Z, You J, Liu Y,Yang Y. Interface engineering of highly efficient perovskite solar cells. Science. 2014;345(6196):542–546.

[235] http://www.nrel.gov/ncpv/images/efficiency_chart.jpg.
[236] Ball JM, Lee MM, Hey A, Snaith HJ. Low-temperature processed meso-superstructured to thin-film perovskite solar cells. Energy Environ. Sci. 2013;6(6):1739–1743.
[237] Burschka J, Pellet N, Moon S-J, Humphry-Baker R, Gao P, Nazeeruddin MK, Gratzel M. Sequential deposition as a route to high-performance perovskite-sensitized solar cells. Nature 2013;499:316–319.
[238] Docampo P, Ball JM, Darwich M, Eperon GE, Snaith HJ. Efficient organometal trihalide perovskite planar-heterojunction solar cells on flexible polymer substrates. Nat. Commun. 2013;4:2761.

7

Printed Organic Light Emission and Display

Wenming Su

7.1 Introduction

The twenty-first century is the information era, when owning information has become the most valuable assets for a nation, an organization or an individual. Processing or distributing information cannot be realized without an information carrier, that is, a display. While a display device was just an icing on the cake 30 years ago, nowadays, various types of electronic display have become one of the indispensible parts of daily life, ranging from mobile phones, TVs, computer screens and instrument monitors to advertising billboards, traffic signs, and so forth. With the explosive spread of Internet and mobile communication in the last decade, electronic displays have gained ever-increasing importance and the associated industry has become a global pillar industry in the twenty-first century.

Electronic display experienced several generations of evolution, from the first generation of cathode-ray tube (CRT) to the second generation of liquid crystal display (LCD) and plasma display panel (PDP), together with laser display and E-ink display. The organic light-emitting diode (OLED) is the latest device that offers thin, lightweight and better color quality of display. With its self-light emission capability, the OLED also promises to revolutionize the lighting industry with large area and free form lighting panels.

Though OLED technology has been developed over 20 years, the OLED display has only drawn worldwide interest since 2007 when technology breakthroughs in lifetime and backplane driving circuitry took place. Compared to a traditional liquid crystal display, OLED offers the advantages of self-emitting light; better color rendering; wide viewing angle; fast response; energy saving; simple in structure; light and thin; low temperature resistance; anti-knocking; and it can be fabricated on flexible substrate, and by printing, and so on. It has been hailed as the third generation display after LCD, sometimes called "dreamy display". Since 2009, OLED display has become a fast growing industry and is expected to

Printed Electronics: Materials, Technologies and Applications, First Edition. Zheng Cui, Chunshan Zhou, Song Qiu, Zheng Chen, Jian Lin, Jianwen Zhao, Changqi Ma and Wenming Su.

© 2016 Higher Education Press. All rights reserved. Published 2016 by John Wiley & Sons Singapore Pte. Ltd.

exceed 40 billion dollars by 2020. There are already commercial products available, such as mobile phones and TVs with OLED as display panels. OLED lighting is potentially another game changer for lighting industry.

7.1.1 Overview of Lighting and Display

Light is one of the most common phenomena in nature. Light emission is a form of energy release by certain matter that absorbs external energy and converts into light. Atoms in some materials can be excited to a high energy state by external energy such as photon illumination or an electrical field. When they return to their original stable low state, they give out energy in the form of electromagnetic waves (luminescence), which can be visible or invisible. According to the excitation modes, luminescence is divided into photoluminescence (PL), electroluminescence (EL), cathode ray luminescence (CL), X ray luminescence, high energy particle luminescence, chemical luminescence, bioluminescence, and so on. Visible luminescence is an electromagnetic wave with a wavelength of 400–700 nm.

The human eye can see not only light but also distinguish the color of light. The ability to distinguish color originates from three photoreceptor cone cells in the eye, which are very sensitive to red, green and blue. In addition, they each have different relative spectra of vision, called brightness vision and dark vision. Based on these characteristics, the colorimetry is established, which divides the light into three components, red, green and blue. The ratio of the three luminous fluxes determines the total color sensitivity of the human eye. Therefore, by adjusting the ratio of red, green and blue luminous fluxes, any color can be created, which forms the basis of color display.

The first electronic display was the oscillographic tube invented in 1907. The working principle of this device is that mica substrate coated with phosphor powder is excited by electron beams from gas discharge. In the 1920s, cathode ray tubes (CRT) were developed, which became the foundation of television. In 1950, CRT-based color picture tubes were developed and along came television broadcasting. Though CRT display is colorful, with high brightness and fast response, it requires high working voltage, is big, heavy and energy-consuming. The breakthrough in liquid crystal research in the mid-1980s led to the invention of liquid crystal display (LCD). LCD needs low working voltage, is energy saving, flicker-free, thin and light. It quickly dominated the display market, from TV to instrument display panels. By the late 90s, CRT display was completely replaced by LCD.

Liquid crystal molecule is the fourth state of material that has both the fluidity of liquid and the properties of crystal. It does not emit light itself but acts as a light valve in an LCD. The basic components of an LCD panel include a backlighting unit, liquid crystal cells and optical filters. The liquid crystal cell, which acts as a switch controlling the transmission of backlight in the display, is composed of liquid crystal molecules sandwiched between two polarizer plates. The liquid crystal molecules become ordered under an electronic field and change into a twist angle with the change of applied voltage. Combining with the polarizers, the luminous flux of backlight can be controlled by applied voltage to display images. Full color display is realized by employing three color filters on each pixel. From the above process one can conclude that the utilization of backlight is very poor. About 2/3 of the backlight is lost when light passes through the optical filter and another 50% is lost through the polarizers, together with the loss occurring through the opening rate, liquid crystal optical rotation rate and optical membrane module. The total backlight utilization in LCD is less than 10%. The backlight used in LCD for full color display was realized with a cold cathode fluorescent lamp (CCFL) combined with diffusion foil. In recent years CCFL has been gradually replaced by light emitting diode (LED).

7.1.2 Overview of Organic Light Emitting Diodes (OLEDs)

The first organic electroluminescence phenomenon was discovered by Bernanose et al. in mid-1920s [1]. They observed light emission from a piece of organic anthracene single crystal when 400V voltage was applied on both sides of the crystal. Pope et al. [2] also observed the electroluminescence phenomenon of anthracene in 1963. Williams et al. obtained organic electroluminescence with a quantum efficiency of 5% in 1970. However, most of the organic electroluminescent materials were from single crystals of anthracene, acridine and phenazine, which had a small emission area, needed high driving voltage, and had very low efficiency. In 1982, Vincett et al. [3] tried vacuum evaporation of organic anthracene crystal to deposit 50 nm thick film as well as vacuum evaporation of thin metal film serving as a semi-transparent anode. They observed bright light emission under 30V voltage, but the electron injection and stability were poor as the result of poor film quality. The external quantum efficiency was only 0.03–0.06%. In the same year, Tang et al. built a device by using a transparent ITO glass as both substrate and anode, a layer of Ag as the cathode, a 100 nm thick CuPc as the electron transport layer and a resin containing triphenyl fluorescent pigment as the emission layer. They obtained 170 cd/m^2 luminance at 30V, which was a great step forward in organic electroluminescence. In 1985, Tang and Vanslyke adopted 75 nm thick 1,1–Bis(4–di–p–tolyaminophenyl) cyclohexane as a hole transport layer and Alq3 as emission layer and electron transport layer, to improve the luminance to 1700 cd/m^2 at 20V and 340 cd/m^2 at 15V with quantum efficiency of 0.58%. In 1987, they reported using TPD as the hole transport layer, Alq3 as the emission layer and Mg:Ag alloy as the cathode, which achieved luminance of >1000 cd/m^2 and efficiency of 1.5 lm/W at driving voltage of ~10V [4]. This work was considered as the milestone of OLED development and triggered worldwide interest in this technology. In 1988, C. Adachi of Kyushu University in Japan proposed multi-layer configuration [5]. They introduced a hole transport layer and an electron transport layer between the emission layer and the anode/cathode and further improved device performance, as well as expanding the selection of organic materials and electrodes. In 1990, Burroughes et al. at Cambridge University successfully developed a polymer OLED [6], which expanded organic material from small molecules to polymers. Later, Braun and Heeger, from California University, fabricated a polymer OLED with a soluble PPV derivative of MEH-PPV by the spin coating method [7]. Gustafsson et al. made a flexible polymer OLED with a threshold voltage of 2–3 V and quantum efficiency exceeded 1% [8]. In 1998, Baldo et al. developed phosphorescent OLED, which could have 100% theoretical inner quantum efficiency [9]. In 2001 Adachi et al. reported a blue OLED with nearly 100% inner quantum efficiency [10]. As for white lighting OLED, Sun et al. fabricated white OLED with power efficiency of 37.6 lm/w in 2006 [11]. Zhou et al. improved the mobility of organic materials by an order of magnitude by doping the carrier transport layer to P and N type, respectively [12], which lowered the operation voltage to about 3V and further improved power efficiency, making the OLED lighting more practical. In 2006, Konica Minolta in Japan successfully realized white OLED lighting with an efficiency of 64 lm/W and half-life period of about 10000 h under initial light

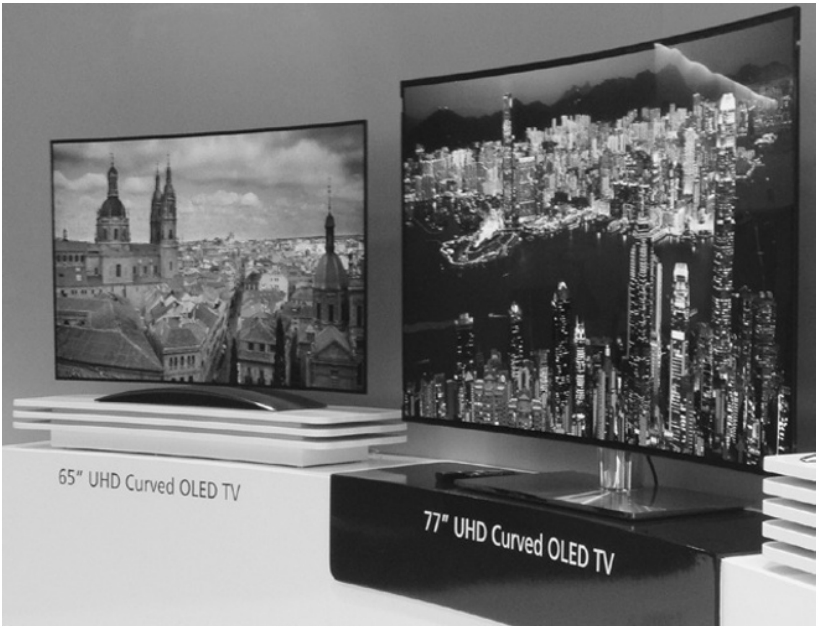

Figure 7.1 Super large curved OLED TVs shown at the 2014 Display Week Exhibition

of 1000 cd/m^2. In 2008, the efficiency reported by UDC reached to 102 lm/W which far exceeded the efficiency of incandescent light (15 lm/W) and traditional fluorescent light (80–100 lm/W). The latest record of efficiency was achieved by NEC at 156 lm/W in 2014.

The rapid improvement in efficiency has led the OLED into display applications. There are two types of OLED display: passive matrix OLED (PMOLED) display, which only displays still images or signs; and active matrix OLED (AMOLED), which can display video frequency images such as TVs. AMOLED requires a matrix of transistors as backplane driving circuitry, which is similar to the backplane for LCD display. Because of its high energy efficiency, better color saturation, thinness and flexibility, OLED display is considered to be the third generation display after LCD display. Sony developed the first OLED TV (11 inch) in July 2008, which marked the start of OLED for display. LG demonstrated a 31-inch OLED TV prototype in September 2010. By 2014, more than 65 inch large size OLED TVs were demonstrated at the Dsiplay Week exhibition (Figure 7.1). Today, many companies and research organizations are developing OLED for display applications. Production lines have been built and OLED display has entered the mobile phone and TV market, which exceeded one billion dollars.

7.2 Mechanism of Organic Light Emission

Organic light-emitting diodes (OLEDs) are charge carriers (holes and electrons) injection induced luminance devices. Under the influence of an electric field, the holes and electrons inject from the anode and cathode, respectively. They combine to form excitons within the organic layers where they decay to the ground state and release radiation in the form of photons (Figure 7.2).

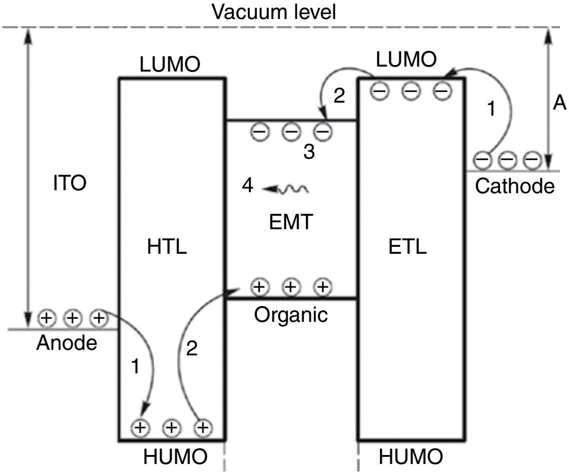

Figure 7.2 Working mechanisms of OLEDs

Light emitting from the OLEDs involves five processes:

(i) Injection of holes and electrons.
(ii) Transport of holes and electrons into the emitting layer.
(iii) Combination of the holes and electrons into excitons.
(iv) Migration of the excitons under the external electric field and transfer of their energy to emissive molecules to make them excited.
(v) The excited molecules return to their ground states and release energy as electroluminescence. The color of the light depends on the energy difference between the excited state and ground state of excitons.

7.2.1 Charge Injection and Transport

Under the applied voltage, charge carriers (holes and electrons) inject from the anode and cathode of OLED through the hole transport layer (HTL) and electron transport layer (ETL) and meet in the emitting layer (EMT), respectively. The current in OLED is determined by the interface property of the electrodes and the organic layers. For example, the barrier from the ITO anode to HTL can hinder the hole injection. In order to reduce the injection barrier, UV-O_3 or O_2 plasma treatment is often used to increase the work function of ITO. Recently, the authors' Printable Electronics Research Center has found that it is the O_3 that increases the work function of ITO, not the UV; whereas the UV light irradiation is actually detrimental to the OLED performance. As for the injection barrier, a buffer layer is normally employed to decrease the barrier between the anode and the hole transport layer. Generally, the injection barrier should not be higher than 0.4 eV, otherwise it will degrade the OLED performance.

The manner of charge transport in OLED is described as a hopping process; electrons or holes hop from molecule to molecule, due to the fact that organic materials in OLED are not crystalline but amorphous and have no conduction bands. For electron transport, the organic molecular system should be electron deficient, using, for instance, nitrogen-containing arenes or phosphine oxide derivatives, which facilitates electron reception; whereas the hole transport materials normally are rich in electrons, like arylamine derivatives, which facilitate electron donation. The charge mobility of electron transport materials is about 1~3 orders lower than that of hole transport materials. Therefore, improving the charge mobility, especially the electron mobility of the organic materials, is very important to the OLED performance.

7.2.2 Exciton Formation and Light Emission

Under the influence of an electric field, a positive charge (holes) and a negative charge (electrons) from the anode and cathode move towards each other by Coulomb attraction force to form "electron–hole pairs", namely the excitons. If organic molecules are excited but the electron spin direction did not change ($S = 0$), then it is called a singlet state. If the spin direction has changed ($S = 1$), then it is a triplet state. The singlet state is immune to the external magnetic field, while the triplet state will be divided into three energy states.

In electroluminescent devices, singlet and triplet excitons are formed simultaneously and the triplet energy is lower than that of singlet excitons. Theoretically, the number of triplet excitons is three times as much as the singlet excitons. When the excited state decays to ground state it gives out photons, called fluorescence or phosphorescence. Depending on the exciton's state, the photon emission of singlet decay is called fluorescence, whereas the photon emission of triplet decay called phosphorescence. Studies on fluorescence and phosphorescence have found that almost all the electroluminescence of organic molecules follow Kasha's rules, by which the fluorescence is corresponding to the S1 state to the ground state and the phosphorescence is corresponding to the T1 to the ground state. The fluorescence and phosphorescence from the decay of excited S2, S3, T2, T3 are usually observed only in gaseous phase. The electron spinning states are asymmetrical in triplet state due to the different spin directions. The repulsive force between the electrons is smaller than the electrons in the excited state, which causes the triplet energy lower than that of the singlet.

7.2.3 Characterization of OLED Performance

The performance of OLED is characterized by luminous efficacy, quantum efficiency, color and lifetime.

7.2.3.1 Luminous Efficacy

For display and lighting, the luminous efficacy is normally defined by the current efficiency (cd A^{-1}) and luminous power efficiency (lm W^{-1}), respectively. The current efficiency indicates the light-emitting ability of a material, while the power efficiency defines the energy consumption of device.

The current efficiency is expressed as:

$$\eta_L = \frac{A \times L}{I_{OLED}} \left(\text{cd A}^{-1}\right) \tag{7.1}$$

where A is the active area of device (m^{-2}), L is the luminance (cd.m^{-2}), I_{OLED} is the current (A).

The power efficiency is expressed as:

$$\eta_P = \frac{L_P}{I_{OLED} \times V}\left(\text{lm W}^{-1}\right) \tag{7.2}$$

where L_P is luminous efficiency (light comes from the front side), V is voltage. As for the light emits from one side (1 lm = π × 1 cd), η_P can be expressed as:

$$\eta_P = \frac{\pi \times \mathrm{A} \times \mathrm{L}}{I_{OLED} \times V} = \frac{\pi \times L}{\frac{I_{OLED}}{\mathrm{A}} \times V} = \frac{\pi \times L}{J \times V} \tag{7.3}$$

where J is current density (A m^{-2}).

The relationship between current efficiency and power efficiency can be expressed as:

$$\eta_P = \frac{\pi\eta_L}{\mathrm{V}} \tag{7.4}$$

7.2.3.2 Quantum Efficiency

Quantum efficiency is the ratio of emitted photons to injected charges. Quantum efficiency is usually expressed separately as internal quantum efficiency (η_{int}) and external quantum efficiency (η_{ext}). Internal quantum efficiency is the ratio of emitted photons to injected electrons in the emitting layer, which indicates the luminance and charge transport properties of material itself. External quantum efficiency is the ratio of emitted photons from the direction of observation to injected electrons, which is the summary of internal quantum efficiency and many factors influencing the efficiency, such as output coupling of light. It reflects more accurately the overall performance of OLED.

7.2.3.3 Color

The theory of full color display was introduced in section of 7.1.1 using three primary colors. In 1931, Commission Internationale Ed I'eclairage (CIE) set a technical standard for the measurement of color, namely CIE 1931. CIE defines all the visible light in the x, y, z coordinate system (x: red component; y: green component and z: blue component). This system is very complicated and not easy to understand. In practice, the chromaticity value is only related to the wavelength and color purity, rather than intensity. By normalizing the x, y and z values, the only thing one needs to consider is the ratio of the three primary colors. Since $x + y + z = 1$, the chromaticity diagram can be described as a two-dimensional diagram, as shown in Figure 7.3. Each specific color corresponds to a specific point in the diagram. For pure white light, the coordinate is the point E ($x = y = z$). The three primary colors are represented by three points in the diagram. A triangular area covered by connecting the three points in the diagram represents the colors that can be produced by combining the three primary colors. Therefore, the larger the triangular area, the more colorful it displays. For a good red color, the coordinate should be larger than (0.65, 0.35). As for blue color, the value of (x, y) should be smaller than (0.16, 0.16). The color coordinate can be calculated from the luminescent spectral, or directly measured by spectrometers such as PR655 or CS2000.

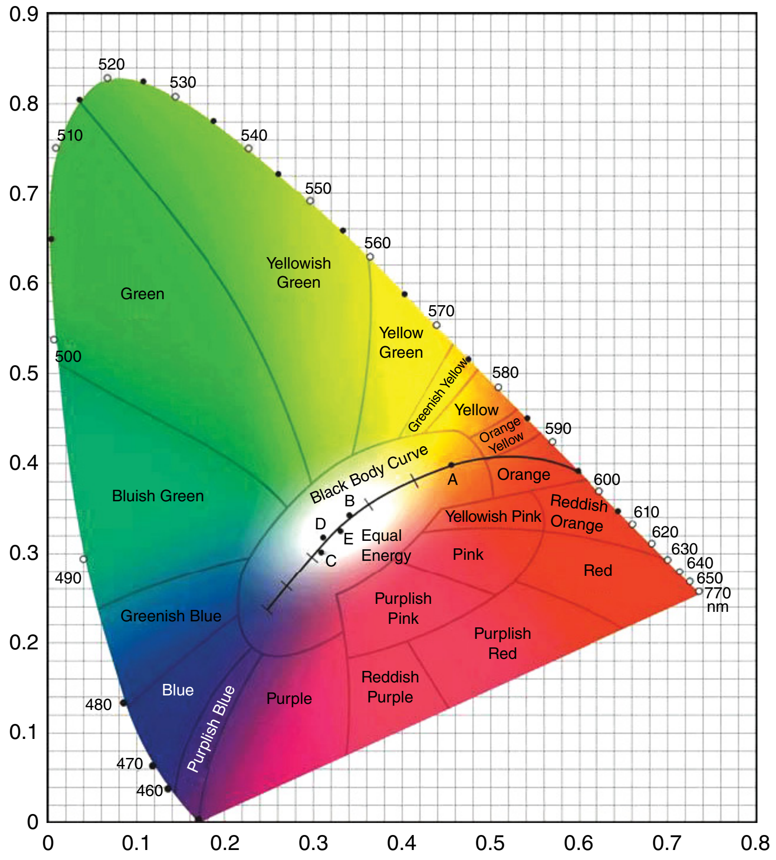

CIE1931 chromaticity diagram
all possible color coordinates (x,y) are on or inside horseshoe curve
Pure colors line on the curve, where as the white point has the coordinates (1/3, 1/3)

Figure 7.3 Chromaticity coordinates of CIE 1931. Reprinted from ref. [13] with permission from Nature Publishing Group

7.2.3.4 Three Primary Colors

To realize high efficiency, most OLEDs use phosphorescent materials as emitters for red, green and blue colors. However, the development of phosphorescent materials for the three primary colors is not at the same stage of maturity. The green phosphorescent material is well developed with satisfactory performance. The red and blue phosphorescent material, especially the blue, is less well developed. In particular, the poor efficiency and lifetime of blue material has become the bottleneck. For example, the power efficiency of full phosphorescent white OLED has exceeded 120 lm W^{-1}. Because of the short lifetime of blue materials, to achieve long lifetime of white OLED lighting is quite a challenge. Changing the blue phosphorescent emitter to a blue fluorescent emitter can increase the lifetime but efficiency is decreased. Therefore, the efficiency and lifetime of the blue system is critical for the display and lighting of OLEDs.

As for high purity single color OLEDs, several requirements should be considered.

(i) A narrower emission spectrum is beneficial for color purity.
(ii) Confinement of excitons within the emitting layer is important. If the excitons migrate to the neighboring layers, it will cause strayed emission, leading to bad color purity.
(iii) A good match of energy levels between layers is needed.

7.3 Structures and Materials of OLED

7.3.1 Small Molecular OLED

7.3.1.1 Typical Structure

An OLED consists of three basic functional layers between the anode and cathode: a hole transport layer, photon emitting layer and electron transport layer. As many emitter materials have charge transport ability as well, the charge transport layer may not be needed; some OLEDs have only single layer or two layers. Figure 7.4 shows the typical OLED structure with different functional layers [7,14,15] where the HIL and EIL are added to improve the charge injection. Another promising method to increase the charge injection is through chemical doping to form a p-i-n junction. Figure 7.5 shows the structure and energy levels of p-i-n OLEDs. By doping F4-TCNQ in a hole transport layer, Pfeiffer et al. [16] successfully increased the hole transport mobility by several orders of magnitude, which greatly improved the OLED performance [12,17]. They also tried n-doping but did not obtain satisfactory results [18,19]. By using p-i-n structure, the turn-on voltage can be lowered to 2.5 V, high luminance of 1000 and 10000 cd m^{-2} can be achieved at 2.9 and 5.2 V [20,21], respectively. This doping system effectively increases the charge transport abilities of organic materials, and it also works for organic sensing, OPVs and so forth, although short lifetime is still an issue.

7.3.1.2 Electrode Materials

Organic electroluminescence begins with the charge injection. The property of electrode material is important for the injection. Stossel et al. investigated the influence of cathode with work function ranging from 2.6 to 4.7 eV [22,23]. As the work function decreases, the current

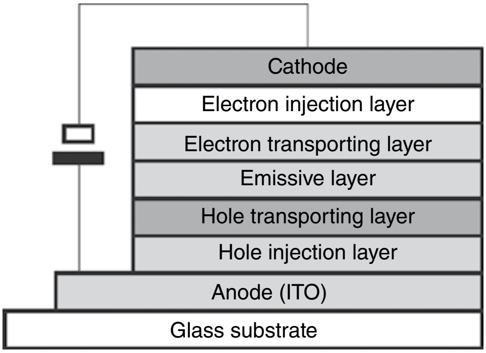

Figure 7.4 Typical OLED structure. Reprinted from ref. [7] with permission from Elsevier S.A.

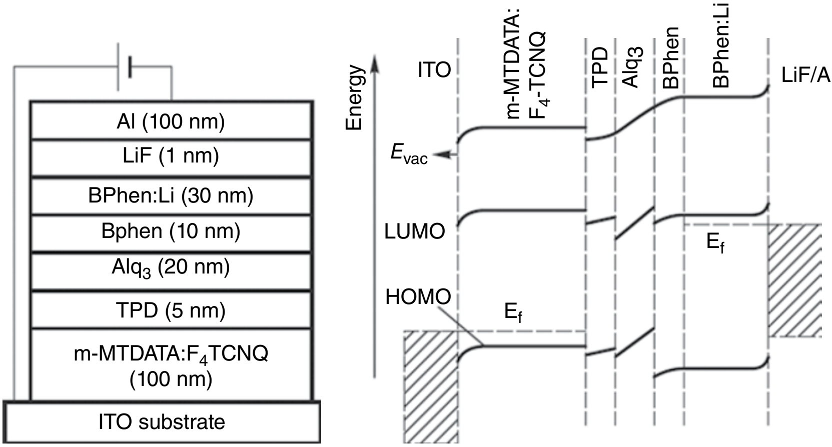

Figure 7.5 Structure and energy level of p-i-n devices. Reprinted from ref. [21] with permission from AIP Publishing LLC

density increases, but the efficiency becomes unchanged at the work function below 3.6 eV. They believed this is caused by the reaction of active metals with the organic materials. In order to prevent the reaction, low work function alloys such as Mg: Ag alloy [24] and Li/Al alloy [25] were invented. Nowadays, Li/Al are widely used as a cathode material because of its simple deposition process (without co-deposition). For most polymer light-emitting diodes, Ca is usually used as the cathode. Since Ca is easily oxidized, several procedures are needed to prevent the formation of CaO thin film [26–30].

Indium tin oxide (ITO) is usually used as the anode, which has a transmittance of over 80% at the wavelength of 400–1000 nm and the forbidden energy band at 3.75 eV [31]. There are several surface treatment methods to increase the work function of ITO, such as UV-O_3 treatment [32], SAMs coating [33,34], plasma treatment [35–38] and acid treatment [8,39,40]. Other anode materials including polymer [41], and Si-based material [42–44] have also been investigated. In addition, transparent oxide semiconductors such as Al_2O_3: Zn is also attracting interest [45,46].

Apart from aforementioned treatment to the ITO surface, adding a buffer layer can also help to increase the hole injection (HIL). The HOMO level of the buffer layer should be between the Fermi level of ITO and the HOMO level of the hole transport material. The commonly used HIL materials include CuPc [47,48], Pt [49], and C [50]. A buffer layer, such as Al_2O_3 [51,52], LiF [53–55], or CsF [56,57], is also used at the cathode side to increase electron injection (EIL). In some cases, a self-assembled monolayer is employed as an organic buffer layer to prevent the formation of black spot [6].

7.3.1.3 Fabrication Process

OLEDs are traditionally fabricated in a vacuum deposition system with multi-heating sources as in the picture shown in Figure 7.6. The vacuum system consists of a mechanical pump and a molecular pump which can create a vacuum at 10^{-4}~10^{-5} Pa. The thermal evaporation sources include metal electrode sources and organic material sources. Typically, 6~12 sources for organic materials evaporation are needed. The more sources there are, the more complicated

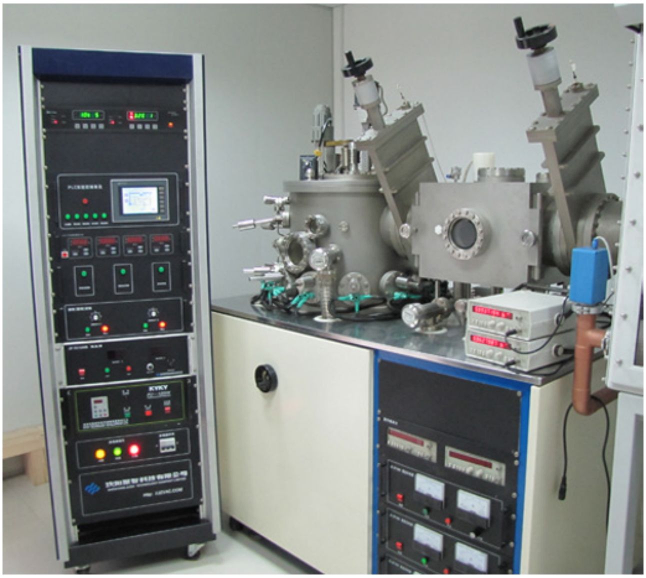

Figure 7.6 High vacuum multi-source thermal deposition systems

devices can be made, including white OLEDs. Tungsten wire or a tantalum boat heater is usually used to evaporate cathode electrode materials, such as Mg: Ag alloy (9:1), LiF/Al and Al/Li. LiF/Al electrode is more widely used for its simplicity. ITO glass is usually used both as the substrate and as the anode. It is recommended that the sheet resistance of ITO should be around 10~30 Ω/sq. To pattern the ITO anode, photoresist or transparent adhesive tape is used for selective protection. FeCl3 – HBr, FeCl3 – HCl or HCl solution with Zn powder is used for etching. Thorough cleaning of ITO glass is also very important for OLED fabrication.

The OLED fabrication starts with substrate cleaning in acetone and isopropanol (or ITO detergent) separately under ultrasonic agitation, then the substrate is washed with plenty of deionized water and any secondary contaminations should be avoided. After cleaning, the substrate undergoes oxygen plasma treatment for 5 minutes or in a UV-O_3 chamber for 15 minutes before putting it into the vacuum deposition chamber. When the chamber pressure reduces to about 5×10^{-4} Pa, the deposition of organic materials begins in the sequence of the hole transport layer, emitting layer and electron transport layer, respectively. The deposition rate is controlled at 2 ~ 3 Å s^{-1}. For the emitting layer, two or three heating sources are needed for co-deposition. For a certain doping concentration, the evaporation rates are controlled at a specific ratio by separate detectors. For LiF buffer layer and Al cathode, the deposition rates are controlled at 0.5 and 10 Å s^{-1}. The thickness of the film is monitored with a quartz microbalance detector. For laboratory experiments, the active area of device is usually 2 mm × 2 mm or 3 mm × 3 mm. Generally, a device with a small active area has a higher efficiency than a large one. Electroluminescent spectral (EL) and CIE coordinates can be measured by PR655 (USA), MPF-4 (Japan), CS2000 (Japan), and so on. Together with a KEITHLEY 2400 source meter, the Luminance-current-voltage (L-I-V) characteristics can be obtained.

For OLED display devices, the fabrication process is the same. The above processes can be regarded for a single color OLED. For a color display panel, the emitter layer for three primary colors should be deposited separately. In this case, a shadow mask is used for separate deposition and positioning. First, the blue emitting layer is deposited, then the green emitting layer and the red emitting layer. The three emitting layers are side by side at the same plane.

7.3.2 Polymer OLEDs

Polymer light emitting diode (PLED) has attracted wide attention since it was first reported by Holmes et al. of Cambridge University [6,7,58,59]. The classic PLED consists of ITO, polymers and anode (Figure 7.7). The polymers include a charge transport layer [60,61] and an emitter layer. Compared to small molecular OLED, PLED has a simple device structure and can be fabricated by spin coating, which is suitable for large scale manufacturing at low cost. The performance of PLEDs is comparable to small molecular OLEDs. Table 7.1 lists the performance data of red, green and blue PLEDs, reported in 2010 [62,63].

7.3.3 General OLED Materials

The key to the success of OLED and PLED is the rapid progress in functional organic electroluminescent materials, including charge injection materials, charge transport materials and emitter materials. The charge transport materials should have suitable HOMO and LUMO levels for charge injection, good transport ability for shortening the response time, lowering the operating voltage and decreasing the heat. The emitter materials should have high luminous efficiency and high color purity. All the materials should have good chemical stability.

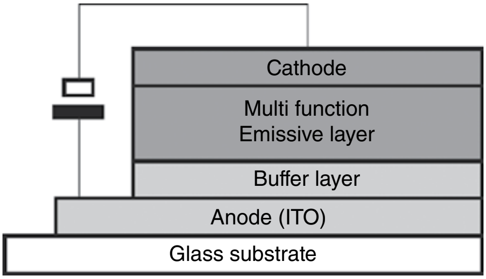

Figure 7.7 Typical PLED structure. Reprinted from reference [60] with permission from AIP Publishing LLC

Table 7.1 Performance of PLED*

	Red		Green		Blue	
Current efficiency (cd/A)	11	31	28	50	9	6
color (CIE)	X=0.67	X=0.63	X=0.35	X=0.30	X=0.14	X=0.15
	Y=0.32	Y=0.37	Y=0.60	Y=0.63	Y=0.22	Y=0.14
lifetime (Kh)	200	350	200	140	34	21
Voltage (V)	6.0	5.7	4.4	6.0	5.0	5.0

* measured under 1000 cd/m^2 (Data from Cambridge Display Technology Ltd.)

7.3.3.1 Charge Injection Materials

To date, a p-i-n structure is commonly employed to increase the charge injection. Materials such as $SbCl_5$ [64], $FeCl_3$ [65], iodine [66], tetra(fluoro)-tetra(cyano) quinodimethane (F_4-TCNQ) [17] and tris (4-bromophenyl) aminium hexachloroantimonate (TBAHA) [67] doping into the hole transport materials can work as hole injection layers. Doping 3% F_4-TCNQ into NPB is a popular p-type doping. Because the HOMO level of NPB is close to the LUMO level of F_4-TCNQ, the electrons on the HOMO level can jump to the LUMO level. Under this condition, free holes are formed in the hole transport layer, and the hole transport ability is greatly improved [68]. Also p-type doping can make the energy band bend so that the holes can inject by a tunneling mode and near perfect ohm contact can be formed [69].

7.3.3.2 Charge Transport Materials

Aromatic amine derivatives like N, N′-diphenyl- N, N′-bis(3-methylphenyl)-1, 1′-4, 4′-diamine (TPD), 4, 4′-bis[N-(1-napthyl)-N-phenyl-amino]-biphenyl (NPB) and spiro-NPB (Germany, Covion Co.) are the mostly used hole transport materials (Figure 7.8). Polymers such as poly (dioxyethylene thienylene) (PEDOT:PSS), poly(9-vinyl carbazole) (PVK) are used as the hole transport materials in PLED.

To date, electron transport materials with good performance are rare. Tis (8-hydroxyquinoline) aluminum (Alq_3, Eastman Kodak) is usually used as the electron transport materials and also

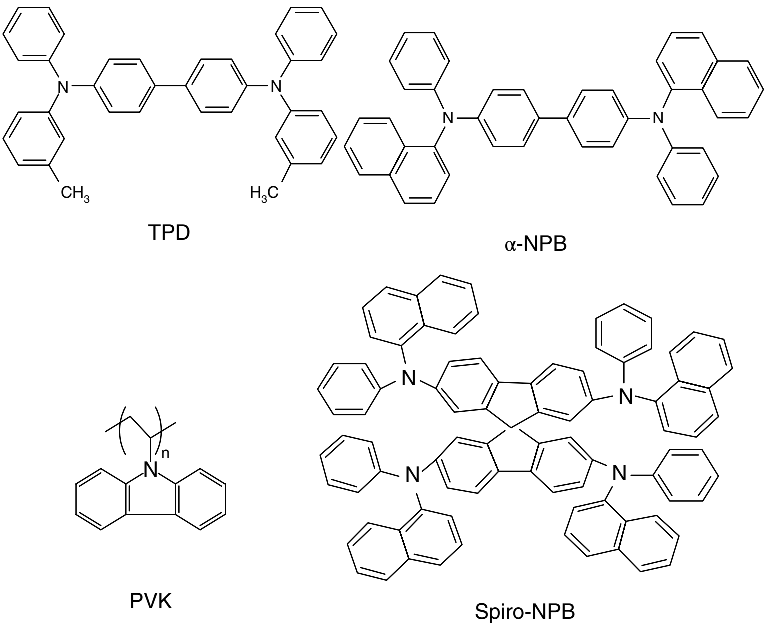

Figure 7.8 Molecular structure of common hole transport materials

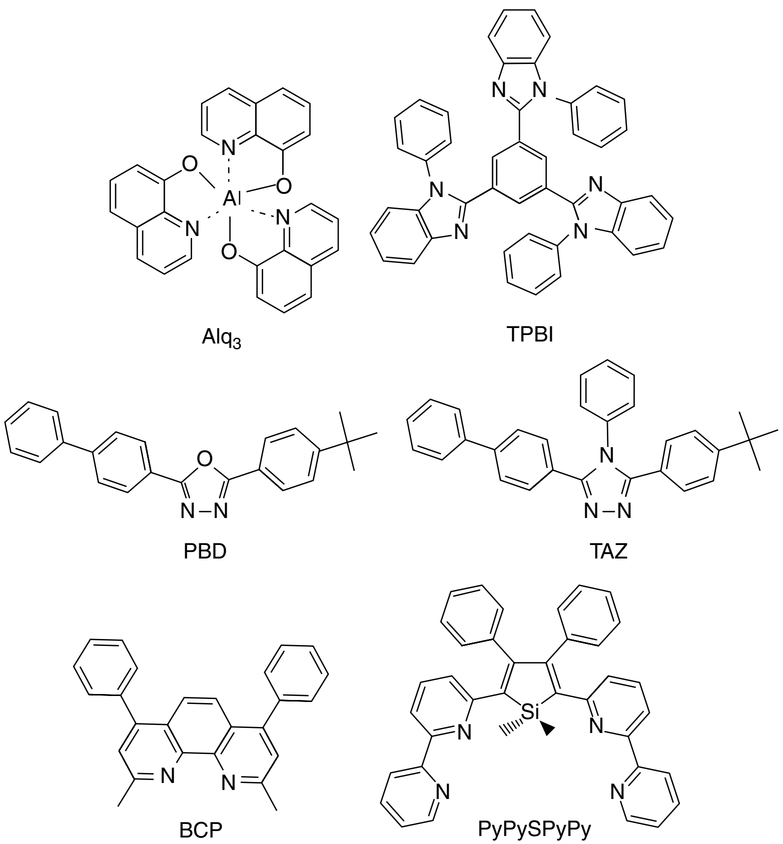

Figure 7.9 Molecular structures of common electron transport materials. (Adopted from [70] with courtesy)

good emitters. 1,2,4-triazoles (TAZ), 2, 4-(biphenyl)-5-(4-tert-butylphenyl)-1, 3, 4-oxadiazole, 2,9-dimethyl-4,7-diphenyl-1,10-phenanthroline (BCP) and 1,3,5-tris(N-phenylbenz imidazole-2-yl)benzene (TPBi) are the electron transport materials with hole block ability. In addition, the Chisso company developed a novel electron transport material, PyPySPyPy, which showed better stability and higher electron mobility than Alq$_3$ [70]. Poly (2,7-(9,9-dioctofluorene)-alt-5,5-(4′,7′-di-thienylbenzo [c] [1,2,5] thiadiazole)) (PFO-DBT) is the polymer electron transport material (Figure 7.9).

7.3.3.3 Emitter Materials

In terms of luminous efficiency, phosphorescent emitter is the best candidate because of its high efficiency. Classic green emitters include Ir(ppy)$_3$ and Ir(ppy)$_2$(acac). PtOEP and iridium complexes are for red emitters [71,72]. FIrpic is the mostly used blue emitter [73] (Figure 7.10).

In PLEDs, the emitting layer is made by doping emitter materials into polymer, such as PVK [74,75], which is the same as in the small molecular OLEDs.

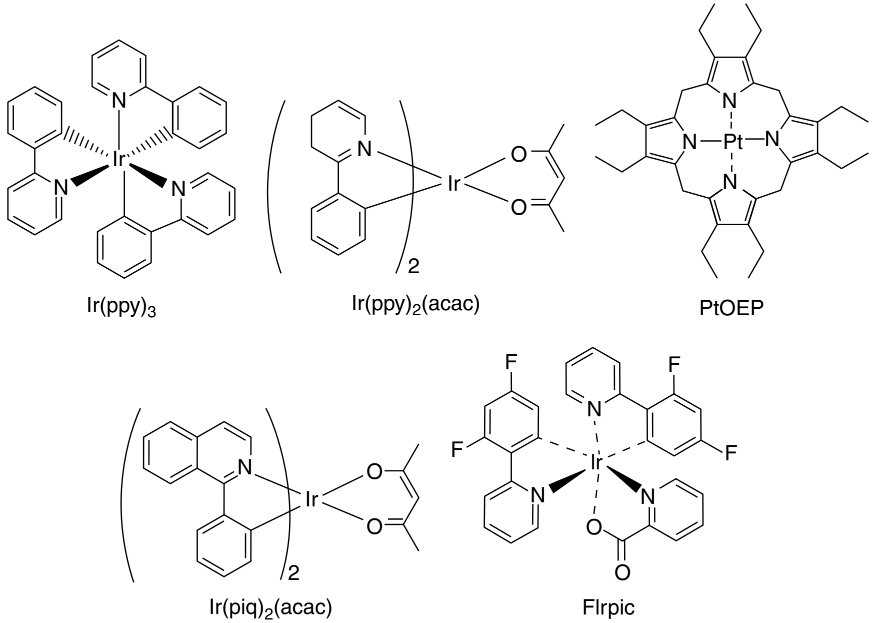

Ir(ppy)$_3$ Ir(ppy)$_2$(acac) PtOEP

Ir(piq)$_2$(acac) FIrpic

Figure 7.10 Molecular structure of typical phosphorescence materials. (Adopted from [73] with courtesy)

7.3.4 Soluble OLED Materials

By making the OLED materials soluble, traditional printing can be employed to print OLED lighting or display, which can greatly reduce the cost (equipment cost and material cost). To convert OLED materials into printable inks, several problems need to be solved. First, OLED materials based on either polymers or small molecules must be soluble. One way is to attach side chains like alky chains and ether chains to OLED material molecules to increase the solvability. However, these side chains usually reduce the ability of molecular charge transport and luminous efficiency. Second, the ink must have good film-forming property, for which the volatility of solvents in the ink should be controllable. Mixed solvents are usually used in OLED inks to manipulate the volatility of solvents, for instance, xylene, chlorobenzene or dichloromethane. As there is more than one compound in the inks, for example, LUMATION * 1304 has the emitter polyfluorene, hole and electron transport material [76], this may cause problems in ink stability, molecular crystallization, precipitation or other detrimental effects.

An OLED always consists of multifunctional layers. In traditional OLED fabrication by thermal evaporation, there are no problems in depositing multiple layers. When depositing soluble OLED inks by printing or coating, solvents in different inks can affect each other. The intermixing of solvents can cause damage to each functional layer. One way to solve the problem is to use orthogonal solvents, such as water-soluble and oil-soluble inks, and they do not intermix when printing them on top of each other. For example, water-soluble PEDOT:PSS and LUMATION * 1304 in xylene can be printed successively without damaging each other. As for printing multi solvent inks, the solvents contained in each ink should be different in polarity. Inks containing thermal or UV monomers can also be used for printing deposition, by which each of the printed films can be solidified by heating or UV exposure without disturbing the next printed layer [77]. Combining correctly formulated OLED inks with a suitable drying process, multi-layer OLEDs can be fabricated by solution processes.

7.3.4.1 Printable Polymer OLEDs

Since a group from Cambridge University observed electroluminescence (EL) in a conjugated polymer in 1989, polymer OLED (PLED) materials were regarded as appropriate candidates to allow manufacturing techniques such as inkjet printing to be used for the fabrication of large sized OLED devices. PLEDs show not only red, green, and blue (RGB) emissions but also white color emissions, which are essential for various applications. As a typical PLED structure consists only of an anode, a hole injection layer, an emissive layer, and a cathode, the fabrication process is simple and low cost. Over the last 25 years, Sumitomo Chemical Co. Ltd in Japan, Covion in Germany, Dow Chemical in the US, and Cambridge Display Technology (CDT) in the UK, have all invested in the development of polymer OLED materials; while HP, Panasonic and DuPont were developing printing technologies to print PLED devices. As the results of intensive R&D, PLEDs with high EQE of 5~10% and a long operating lifetime of over several tens of thousands of hours have been achieved [78].

PLED technologies are advancing particularly fast in recent years. DuPont and Cambridge Display Technology now (a subsidiary of Sumitomo Chemicals) have developed three primary colors (red, green and blue) phosphorescent polymers with lifetimes up to a million hours. Printed prototype display panels have been successfully demonstrated. Based on Sumitomo's PLED materials, Panasonic accomplished a 55-inch PLED TV panel prototype in 2013, using an inkjet printing method and Sumitomo Chemical demonstrated printed PLED lighting panels in 2014.

The main issue regarding PLED for high volume manufacturing is the poor consistency in the material properties from batch to batch in polymer synthesis and purification, because the large molecule size and weight distribution of polymers are difficult to control in different batch processes compared to small molecular OLED materials. This issue has hindered its widespread application and large scale manufacturing.

7.3.4.2 Printable Small Molecular OLEDs

OLEDs based on organic small molecules have a longer development history than polymer OLEDs. Vacuum evaporation is the main method to form layers of OLED and many technical improvements have been made in this area.

Recently, soluble small molecule materials have received much attention and many material companies have reported or press-released their progress in this area. Merck, DuPont and Plextronics have focused on making soluble small molecular OLED materials for some years. The small molecular OLED inks from Merck have been used to make white OLEDs by Novaled. The company is also working closely with other companies to develop printable small molecular OLEDs. Soluble small molecular materials enable high throughput and low cost roll-to-roll or inkjet printing process to be used for making OLED display and lighting panels. AUO in Taiwan has demonstrated a 65-inch printed OLED display panel based on Merck's soluble small molecular OLED materials in 2014.

State-of-the-art OLEDs always have a multilayer structure to ensure higher efficiencies and longer lifetimes [79]. As small molecular OLED inks are solvent-based solutions [80], when creating a multilayer OLED by printing, it is important to prevent intermixing and erosion between layers. This can usually be achieved by using orthogonal solvents for each ink so that they do not mix when depositing one upon another [81], as has been described in Section 7.3.4.

7.3.4.3 Cross-linking Materials for Printable OLEDs

Besides orthogonal solvent processing a well-established approach to prepare solvent-based multilayer devices is the chemical functionalization of organic semiconductors with reactive moieties so that they can be solidified by thermal polymerization and/or cross-linking [82]. The molecular structure of typical cross-linking hole transport materials is shown in Figure 7.11. Cross-linking is believed to be a promising technique to develop a printable multilayer OLED with efficiency and lifetime close to an evaporated multilayer device. Thermally initiated dimerization of benzocyclobutene has been used by Fréchet and co-workers to cross-link HTMs [83]. There are also reports on a thermally cross-linkable host material, DV-CBP, that incorporates two vinylbenzyl ether groups as cross-linking groups and 4,40-bis(carbazol-9-yl)biphenyl (CBP) as an optoelectroactive backbone for solution-processed multilayer OLEDs [84]. An X-Ir complex cross-linkable with host has also been proved [85].

At the authors' Printable Electronics Research Center (PERC), some cross-linking type bipolar host, electron transport materials, and even TADF materials have been developed as shown in Figure 7.12. The strategy at PERC is to introduce soluble groups with some cross-linking moiety such as styrene into the high performance and vacuum thermal evaporated small molecular OLED materials, making them cross-linkable.

All the styryl, including monomer, are soluble and can be spin coated or printed, then thermally cross-linked to resist solvent. For example, bipolar host materials of A,B,C, are dissolved in THF (5mg/ml), then spin coated and cured at 70°C for 30 minutes, cross-linked at 180°C for 60 minutes and rinsed by DCM, CHCl3 and Acetone. The absorption spectra of the double-styrene-containing compounds before and after the rinsing process were identical, indicating that the cross-linked film of DV-CBP is completely resistant to the solvent, as the results shown in Figure 7.13, which were obtained at the authors' Printable Electronics Research Center (PERC). It was also found that their optical and electric characteristics had not changed before and after cross-linking. The cross-linking approach will facilitate the realization of printing OLED with multilayer architectures.

7.4 White Lighting OLEDs

7.4.1 White Light Emission Mechanism

White light is a mixture of multicolor (red, green and blue) lights. Therefore, white lighting OLEDs are made of multicolor OLEDs. For example, Figure 7.14 illustrates four types of white lighting OLED configurations.

In Figure 7.14a the white OLED is made of a single emissive layer with multiple color dopants; In Figure 7.14b the white OLED is made of R, G, B doped multiple emissive layers, or a blue emissive layer and two fluorescent phosphor layers (red and green), and white is

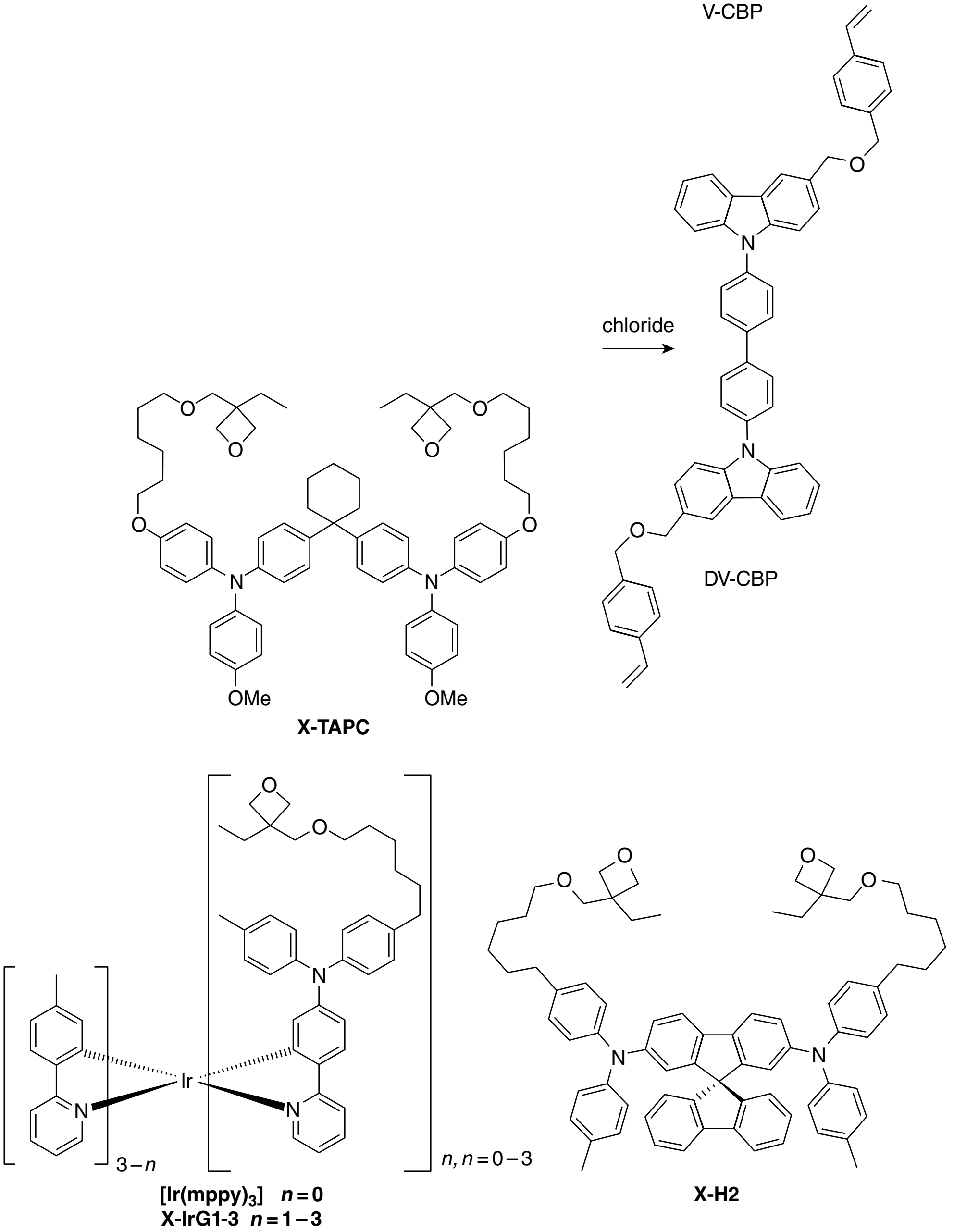
V-CBP
chloride
DV-CBP
X-TAPC
[Ir(mppy)3] n = 0
X-IrG1-3 n = 1 − 3
3 − n
n, n = 0 − 3
X-H2

Figure 7.11 Molecular structure of typical crosslinking hole transport materials. (Adopted from [82–85] with courtesy)

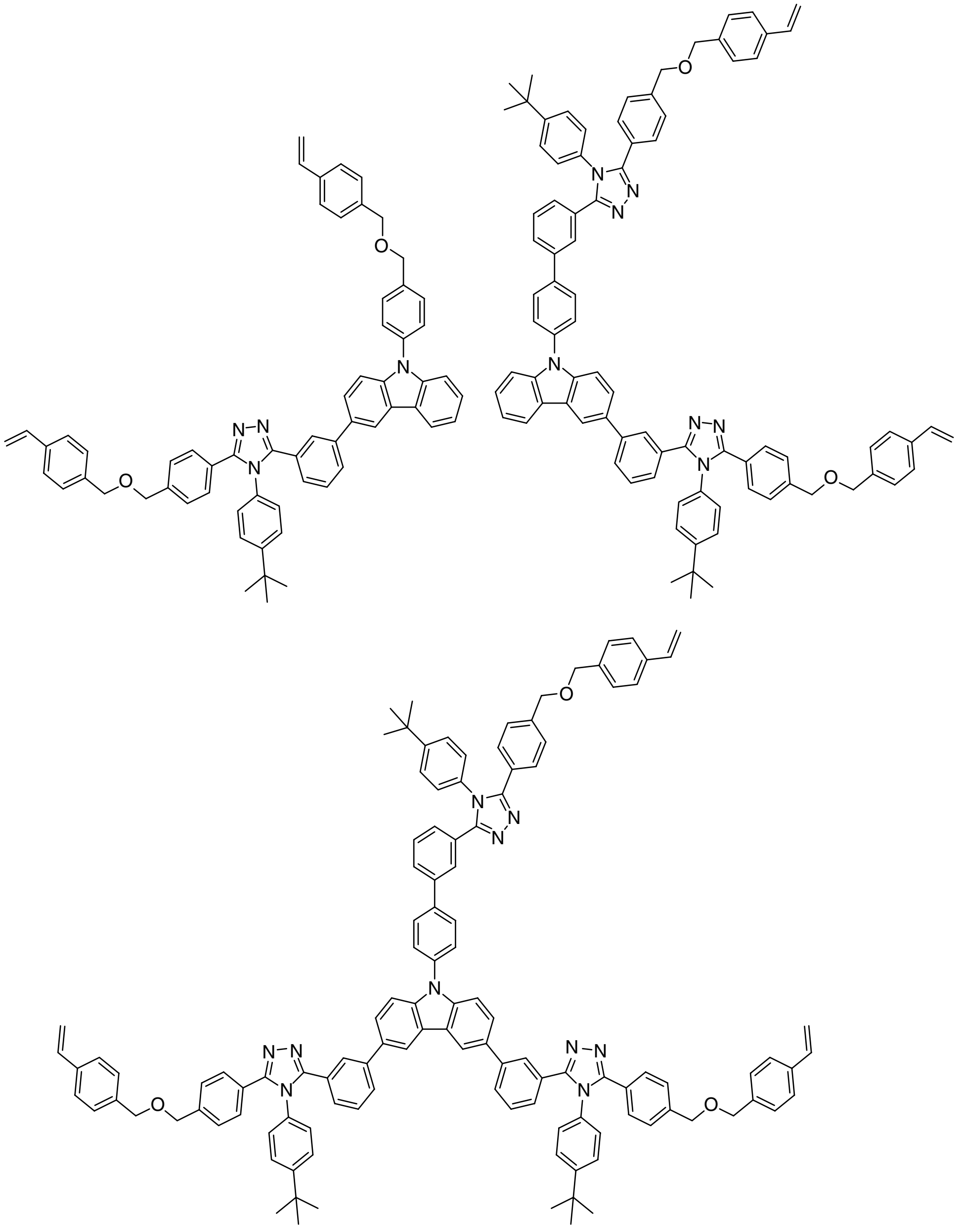

Bilolar host material

Figure 7.12 Molecular structure of cross-linking materials developed at PERC

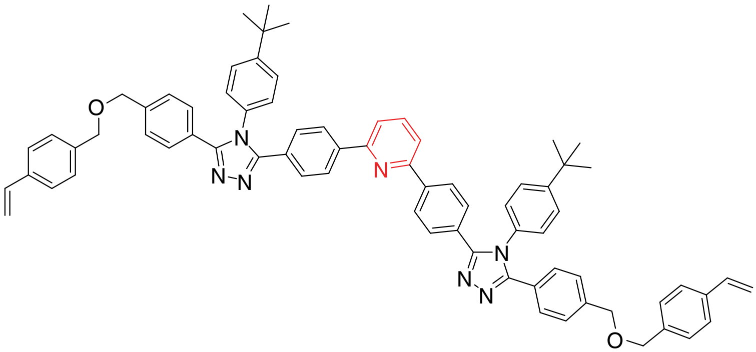

26PyTAZOSM

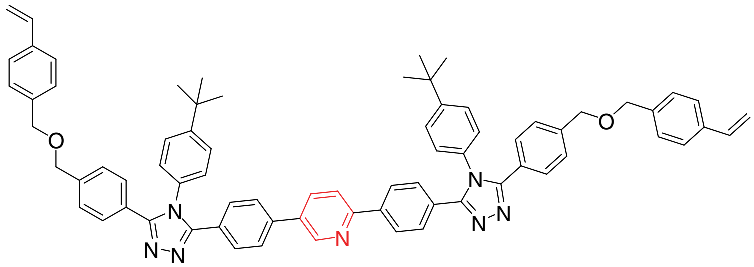

25PyTAZOSM

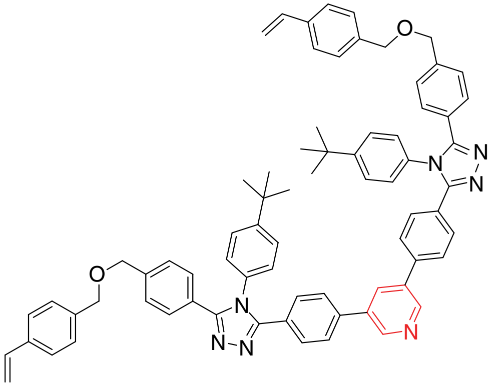

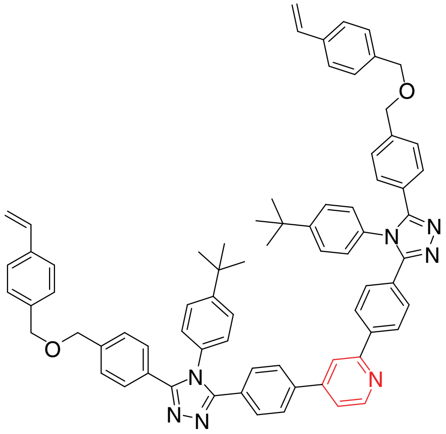

35PyTAZOSM **24PyTAZOSM**

Electron transport materials

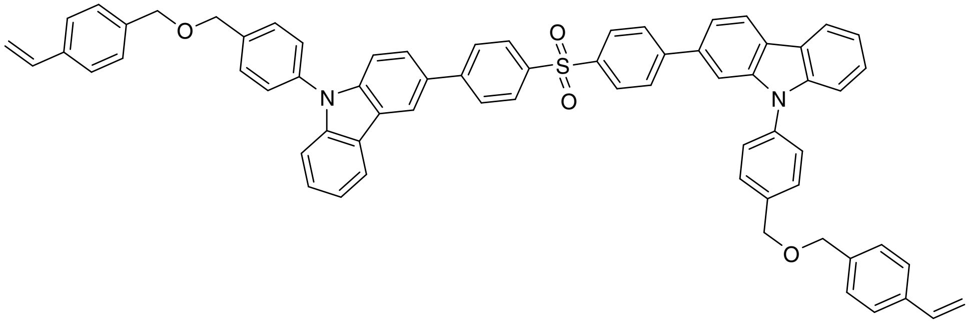

Blue TADF material

Figure 7.12 (Continued)

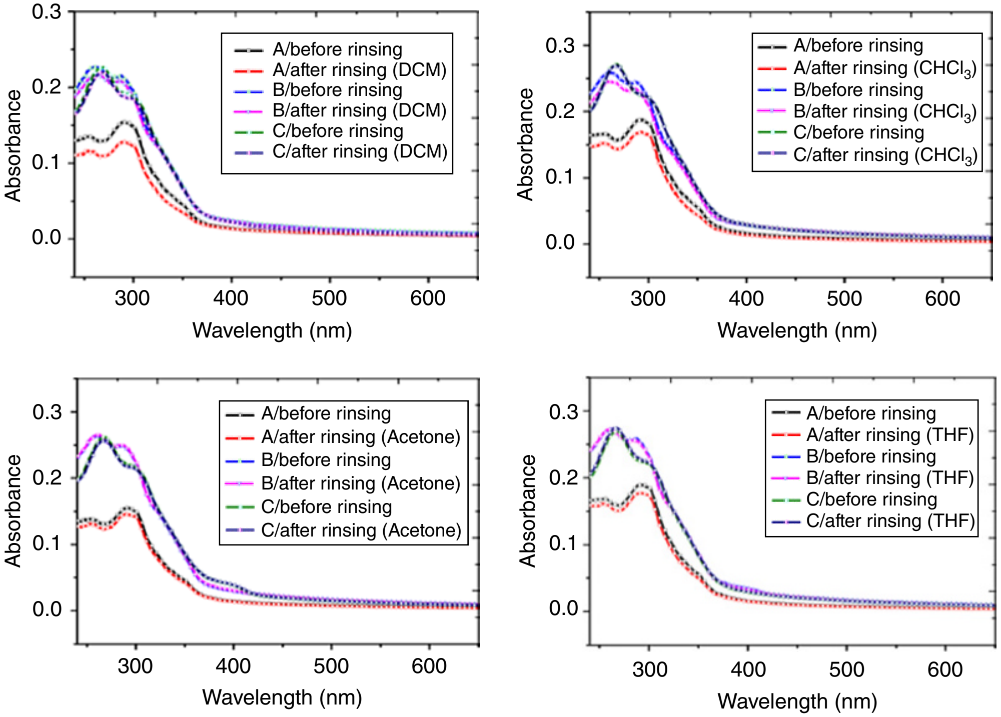

Figure 7.13 Absorption spectra of DV-CBP films after spin coating, cross-linking and rinsing with DCM, CHCl3, Acetone and THF

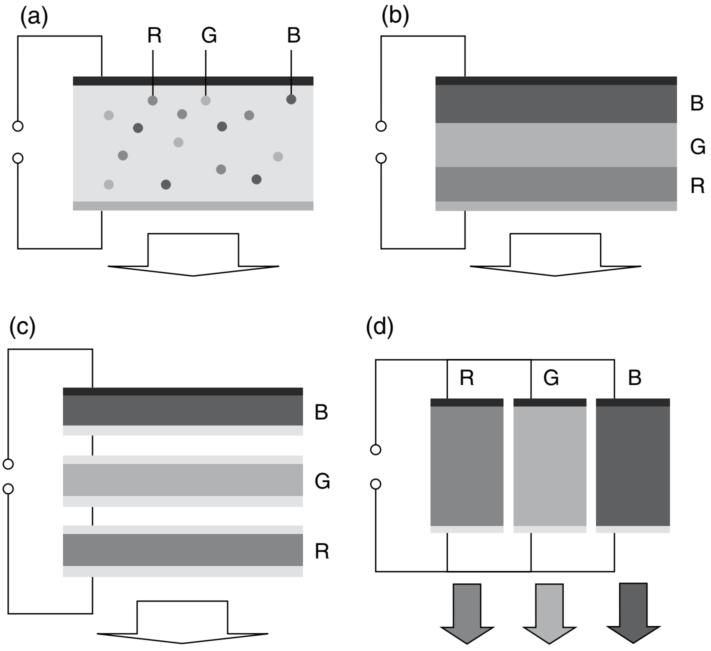

Figure 7.14 Configurations of white OLED [86]. (Reprinted from reference [86] with permission from Wiley-VCH Verlag Gmbg & CO. KGaA)

generated by down conversion mechanism. In Figure 7.14c/d, the three primary colors emissive layers are stacked vertically (tandem structure) or horizontally with each layer emitting relevant color light and the three primary color light are mixed to form white light. The structure in Figure 7.14d is mainly used in full color display instead of white lighting.

A simple guidance for synthesizing white light by color mixing is to use the CIE 1931 coordinate (Figure 7.3). Connecting any two points in the coordinate with a straight line, if the line is across the white zone, then the mixing of these two colors can generate white light. In 2002, Forrest et al. created white OLEDs by using a sky-blue phosphorescent emitter (FIrpic) and a red phosphorescent emitter [$Btp_2Ir(acac)$]. The coordinate was (0.35, 0.36), the CRI rendering index was 50 and the external quantum efficiency was only 3.8%. Though the white OLED structure was simple, the low color rendering index (CRI) and low efficiency were not suitable for lighting. Nowadays, white OLEDs usually employ a three colors emissive structure, which has high CRI and high efficiency.

Besides the color mixing to form white light, a single material that can emit white light has been reported. By attaching phosphorescent emitters to polymers, the Wang group (Changchun Institute of Applied Chemistry, Chinese academy of sciences) obtained series of stable white light emitting polymers [87,88]. In 2007, Konica Minolta reported a white OLED with high power efficiency of 64 lm W^{-1} at the luminance of 1000 cd m^{-2}. The device was fabricated with a new blue phosphorescent emitter and light output coupling structures. UDC developed a white OLED with the power efficiency over 100 lm W^{-1}, but the exact structure is unknown. In 2009, the Leo group reported a white OLED with the power efficiency as high as 124 lm W^{-1} [89].

Although white OLEDs with multiple emissive layers have high efficiencies, the complicated device structure poses some challenges. For example, the exciton combination zone may drift with the applied bias, which can cause the change of color in light emission. To prevent the combination zone from drifting, hole-blocking layers have been introduced to confine the excitons within the emitting layer. However, the introduction of a hole-blocking layer will increase the operating voltage. White light obtained from the down conversion is based on blue emissive layer and fluorescent phosphor layers (Figure 7.14b). They have a simple structure and stable white color, which is not affected by applied bias or the device lifetime. By using red and green fluorescent phosphors, these devices have a very high CRI. But this white light device is quite dependent on the efficiency and lifetime of the blue OLEDs. The patents related to the down conversion OLED are mostly owned by Fuji Film Japan in the field of display and some in the field of lighting. The performance of blue OLEDs have been improved greatly in recent years. Franky So's group reported a power efficiency of blue OLEDs over 50 lm W^{-1} in 2008, and they are aiming to achieve over 100 lm W^{-1} [90]. With the progress in high efficiency blue OLEDs, this type of white light OLED is developing very fast because of its simplified device structure and low cost.

7.4.2 Important Parameters

7.4.2.1 CRI

For lighting applications, particularly for the backlight in a flat panel display, the color rendering index (CRI) is a very important parameter. The CRI defines how well colors are rendered by a lighting source in comparison to a standard light, that is, incandescent light or daylight. The higher the CRI, the wider the white spectrum and the better the quality of white light.

If a white light is short of certain wavelength, chromatic aberration occurs. The bigger the chromatic aberration is, the smaller the color rendering index will be. The CRI of a standard incandescent light is defined as 100, which is the benchmark for all light sources. By measuring the deviation of eight standard colors emitted from a light source under the same color temperature, the CRI can be calculated. For normal lighting, the CRI of a light source should be higher than 80. Blue-yellow-based white OLEDs are not good enough for lighting. The three primary colors-based white OLEDs have CRI of about 85, which can be used for lighting or backlight. Because the choices of OLED emitter materials are huge, which greatly helps to optimize the emission spectrum, CRI of above 95 are relatively easy to achieve.

7.4.2.2 Efficiency and Light Extraction

Besides CRI, luminous efficacy is another important parameter for lighting. Lighting consumes 22% of global energy. Therefore, energy-saving in lighting is important for a green society. The efficiency of an incandescent light bulb is about 16 lm W^{-1}, which is very low. A fluorescent lamp has efficiency of 60 ~ 80 lm W^{-1} but a short lifetime. The Hg in fluorescent tubes is a big threat to the environment. In the past decade, incandescent lighting has been gradually phased out and fluorescent lamps are being replaced by semiconductor light emitting diodes (LEDs). Since 2000, the US government has invested over 50 million dollars in the National Semiconductor Lighting Project, which aims to increase the efficiency of LED lighting to 150 lm W^{-1}.

Compared to LED lighting, OLEDs have not only high power efficiency but also higher CRI than LED. To date, the highest power efficiency of white OLEDs is over 140 lm W^{-1} and their internal quantum efficiency is approaching 100% [72]. The structure of white OLEDs is the same as small molecule OLEDs for display applications, but using phosphorescent emitters is the key to obtain high efficiencies. For high CRI white light, the emitting layer should at least contain three primary colors. Phosphorescent doping separately in emitter layers is better than doping in the same layer. The former can avoid the interference of excitons and has higher efficiency. An interlayer using bipolar materials like CBP thin film is proved effective to increase the efficiency [11].

Since OLEDs are surface-emitting devices, total reflection of light wave inside the device seriously affects the light output. In this case, the external quantum efficiency can be only 1/5 of the internal quantum efficiency. Therefore, improving light output coupling (extraction) becomes absolutely necessary. Generally, the differences in the refractive index at the organic materials/ITO, ITO/glass and glass/air interfaces are the cause of low light output efficiency. The reflection at the glass/air interface can be reduced by forming micro prisms on the surface of glass [91]. When there is a micro prisms array with period of 25 μm, a 42% increase of light extraction efficiency is observed [92]. To reduce the reflection at the ITO/glass interface, optical micro cavities can be used, which increases the light extraction efficiency by 40%. Other methods include the introduction of low-index aerogel materials, which can achieve 1.8 times of enhancement [93], and nanoimprinted photonic crystals, which can achieve a 50% enhancement [94]. In 2008, Sun et al. in Princeton University reported low-index SiO_2 grid on ITO surface (organic materials/ITO interface) (Figure 7.15), which led to 1.3 times of enhancement [95]. This periodic grid structure seemed to be the most promising technology for light extraction, which can be made by photolithography and etching, nanoimprinting or conventional inject printing, depending on the dimension of grids.

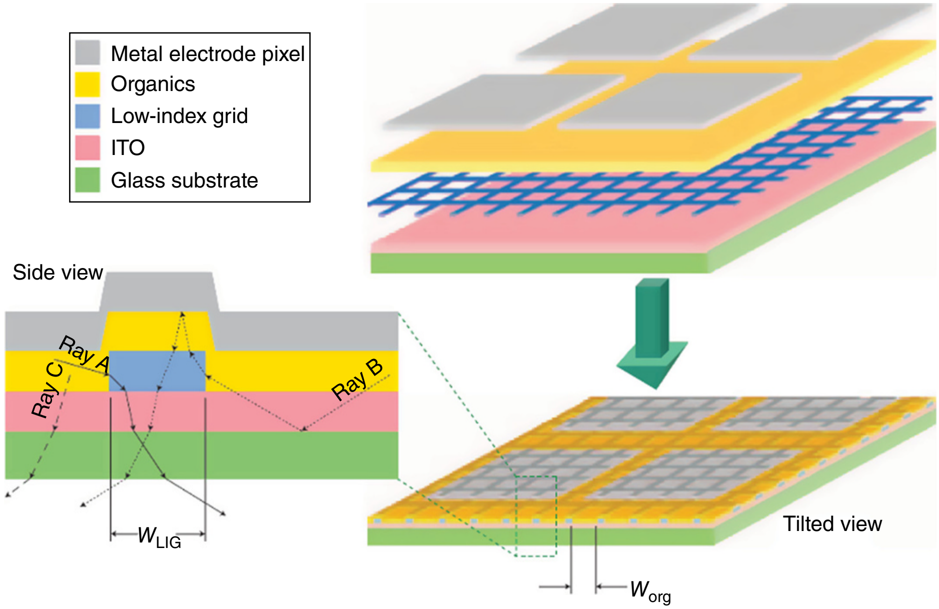
Metal electrode pixel
Organics
Low-index grid
ITO
Glass substrate
Side view
Ray A
Ray B
Ray C
W_{LIG}
Tilted view
W_{org}

Figure 7.15 Embedded SiO_2 LIG structure for light out-coupling. (Reprinted from reference [95] with permission from Nature Publishing Group)

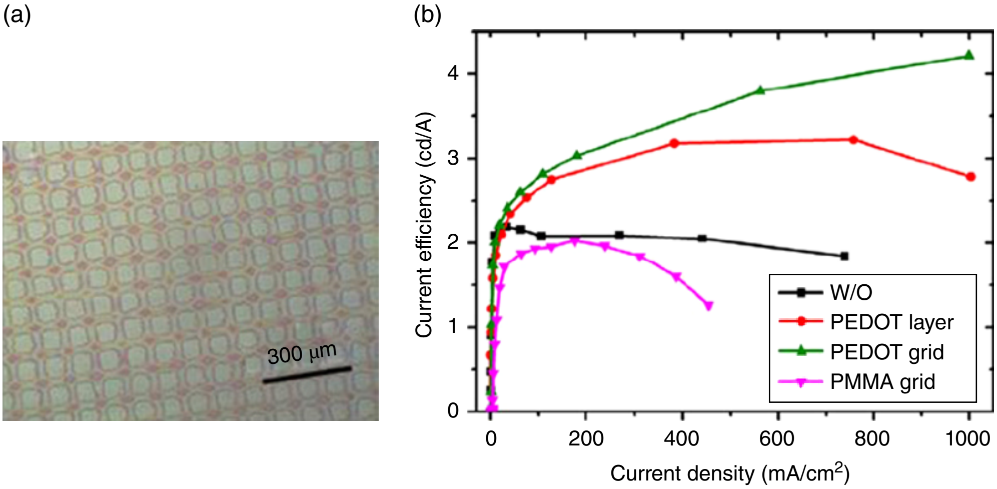

Figure 7.16 (a) Optical microscope images of the AJ printed PEDOT: PSS grid, and (b) Current efficiency–current density characteristics for the devices. (Reprinted from ref. [96] with permission from IOP Publishing)

Such a light out-coupling structure can also be fabricated by printing. At the authors' Printable Electronics Research Center (PERC), a simple printing process has been developed, which employs an aerosol jet printer to print PEDOT:PSS grids on the ITO anode [96], as shown in Figure 7.16a. The printed conductive grid helped to increase the OLED efficiency to 1.92 times higher than a conventional device without light extraction structure (Figure 7.16b).

7.4.2.3 Lifetime

The issue of lifetime was once the bottleneck during the early development of OLEDs, because the organic materials in OLED are very sensitive to moisture and oxygen. With the advances in encapsulation technology, which will be introduced in Chapter 8 of this book, the lifetime issue has been successfully resolved. Small-sized OLEDs for display are now in high volume production and widely used in mobile phones. For display, the average luminance required for an OLED is about 200 cd m^{-2}, which is relatively low compared to a lighting application that requires luminance higher than 1000 cd m^{-2}. High luminance requires high electric current and the stability of organic materials under constant high electric current for a long period is a serious issue, because OLEDs decay very quickly at high current. Choosing organic materials with high glass temperatures, reducing the charge injection barrier, improving the interface, and so on, are all important for improving the lifetime. Research on the lifetime of OLED lighting is mainly carried out by industry and is very rarely reported in literatures. In 2009, Eastman Kodak demonstrated a fluorescent white OLED with a lifetime of over 10000 h at the starting luminance of 1000 cd m^{-2}. In 2011, Novaled reported PIN-OLED with a lifetime of 100000 h and efficiency of 60 lm W-1 at the luminance of 1000 cd m^{-2} [97]. The above results from industry demonstrated that the lifetime of OLEDs for lighting is no longer an issue.

7.4.3 Investment in OLED Lighting

In the past decade, funding on OLED science and technology research has been huge. The US government has invested \$74.7 million in the National Semiconductor Lighting Project, which is mainly on solid-state lighting, including LEDs and OLEDs. Based on the distribution of funding (\$74.7 million), 25 of 51 projects are OLEDs with total funding of \$36.9 million. The remaining 26 projects are for LEDs. As the OLEDs projects amount 49.4% of the total project research, the US government is determined to push the OLED technology to industrialization.

In Europe, the EU (European Union) started the OLLA program (OLEDs for Lighting) in 2004 and finished in 2008. With the participation of 15 companies and research institutions from Austria, France, Germany, the United Kingdom, Netherlands and Belgium, the aim was to develop white OLEDs having a lifetime of more than 10000 h and power efficiency of 50.7 lm W^{-1} at initial luminance of 1000 cd m^{-2}. At the end of 2008, EU proposed a new project named “OLED100. Eu”. The goals of this project include efficiency of 100 lm W^{-1}; lifetime of over 100000 h; area of 100 cm × 100 cm; and a cost of lower than 100 Euros per square meter. Philips recently made commercially available a white OLED panel of 100 × 100 mm that offers 300 lumens, 50 lm/W, 10,000 hours’ lifetime and is only 1.4 mm thick. In the last few years, the EU OLED lighting projects are focusing more on the development of printable and flexible OLED materials and devices; for example, the ENAB-SPOLED project aims to use solution-based OLED materials to enable high performing and cost competitive OLEDs; the Phebe project aims to develop and commercialize TADF OLED emitters; and the Flex-o-Fab project is a new €11.2-million project that aims to have R2R production of flexible OLEDs within six years. In Korea, LG Chem have supplied commercial 320 × 320 mm OLED lighting panels since 2014. These lighting panels are 0.88 mm thick, efficiency of 100 lm/W, CRI of over 90 and with output of 800 lm - 1,200 lm, although they are very expensive. LG Chem has also produced flexible panels based on flexible glass substrate and are developing "truly bendable" panels on plastic substrates. In China, Nanjing First O-Lite has set up gen-1 manufacturing line of OLED lighting panels, with efficiency reaching 50 lm/w and has supplied OLED lighting installations inside China (Figure 7.17). In 2013, the company improved its OLED lighting module efficiency to 111.7 lm/W.

In Japan, Panasonic announced that they developed a OLED lighting device with 128 lm/W efficiency in 2011. In March 2013, NEC Lighting announced that they developed a device that has an efficiency of 156 lm/W, which is the world's most efficient OLED to date. Konica Minolta started mass producing flexible OLED lighting panels in 2015 in what is probably the world's most advanced OLED fabrication, a roll-to-roll manufacturing fabrication that has the capacity to produce a million flexible and color-tunable OLED panels every month.

UBI Research forecasts that the OLED lighting market will reach 82 million in 2015 as shown in Figure 7.18, and grow quickly till 2020 – when it will reach $4.7 billion. IDTechEx forecasts a $200 million panel market in 2019 and will grow to $1.9 billion in 2025, while Cintelliq expects OLED lighting starts to compete with LED lighting in 2016.

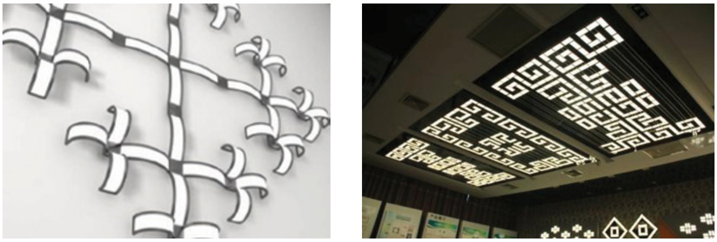

Figure 7.17 OLED lighting panels developed by First-O-Lite in China. Adapted from DOE with permisison

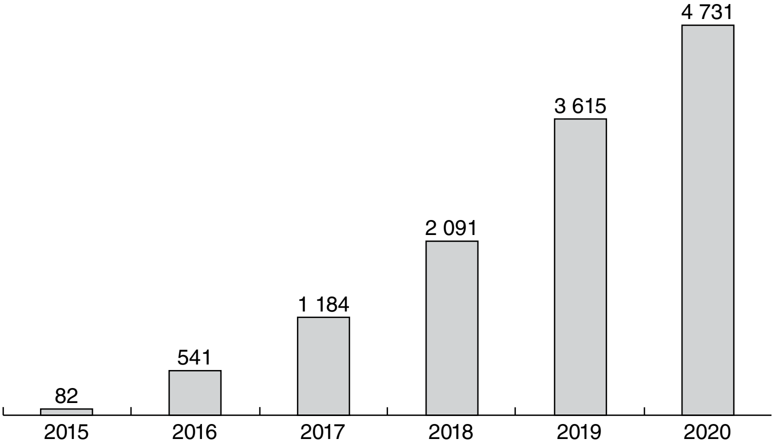

Figure 7.18 Forecasted market growth of OLED lighting (UBI Research, unit: USD$ million). Adapted from UBI Research with permission

7.5 Fabrication of OLED by Printing

The key reason that prevents the widespread use of OLEDs is the cost. In flat panel displays and lightings, OLED technology is still 5–10 times more expensive compared to LCD display and LED lighting. The high production cost is due to the vacuum deposition process for making OLED panels, which not only needs expensive equipment but is also a great waste of OLED materials, not to mention its high consumption of energy. To lower the cost, printable OLED becomes a very interesting research direction in recent years [98]. The idea of printing electroluminescent devices came from the work of printing polymer light-emitting device (PLED) reported by Burroughes et al. in 1990 [6]. With suitable light-emitting materials in solution forms that have been introduced in Section 7.3.4 of this chapter, a wide range of coating/printing processes can be employed for making OLEDs, including spin coating or slot die coating [6,7,99,100], inkjet printing [74,100–102], screen printing [103,104], aerosol printing, gravure printing, flexographic printing, and so forth. Comprehensive descriptions on printing technologies have been presented in Chapter 4 of this book. This section will only introduce the printing methods relevant to making OLEDs.

7.5.1 Spin and Slot Die Coating

Spin coating (Figure 7.19a) is the simplest solution process for making OLEDs. In 2003, Müller et al. reported solution-processed organic light-emitting devices by spin coating [100]. First, the hole injection layer PEDOT was span on the ITO substrate and annealed at 120°C. Second, the red, green and blue polymers were dissolved in toluene (15 mg mL^{-1}), which were then spun on PEDOT. Finally, a metal cathode was deposited by vacuum deposition. The spin coating technique is only used in laboratory for making small size OLEDs and the material utilization is very low, which increases the cost of production, especially for expensive materials. Slot die coating (Figure 7.19b) only coats the material where it is needed and large size substrates, especially flexible substrate, can be coated. Patterning is not possible with spin coating but may be possible for large size patterns with selective slot die coating, which restricts these two techniques so they are only suitable for making OLED lighting panels, not for displays.

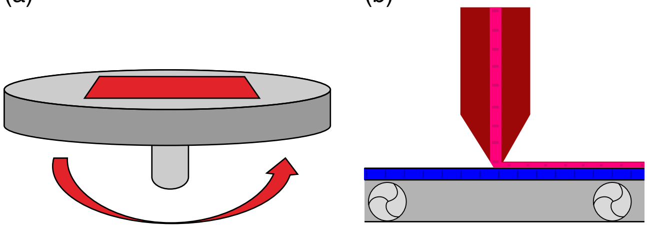

Figure 7.19 Spin coating (a) and Slot die coating (b) to deposit soluble OLED materials

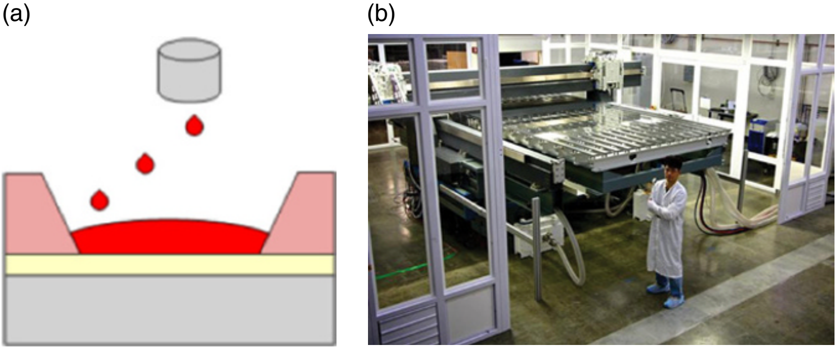

Figure 7.20 (a) The principle of Inkjet printing and (b) Industrial scale inkjet printer marketed by Kateeva of USA for making OLED display panels. (Adopted from web with courtesy to its origin)

7.5.2 Inkjet Printing

Inkjet printing combines both material coating and patterning and the working principle is basically the same as an office inkjet printer but with much higher precision. Due to the need for printed electronics, many inkjet printer manufacturers have developed professional printers. Now the commercial printer can print a line width of 20μm and a speed of 20 m.min^{-1} with ink viscosity ranging from 10 to 20 cP [105]. Inkjet printing can deposit ink material in precise locations, which is essential for making color pixels in OLED display (Figure 7.20a). In 1998, Hebner et al. printed hole transport material (PVK) and emitters in chloroform solutions on a flexible ITO substrate by a Canon PJ-1080 printer [74]. After the deposition of cathode Mg/ Ag (10: 1) in vacuum, red, green and blue devices are obtained. Bharathan et al. printed PEDOT in specific area with a MEH-PPV (poly[2-methoxy-5-28-ehtylhexloxy-1, 4-phenylene vinylene]) buffer layer and made an OLED graphic logo [101]. In recent years, inkjet printing has been used for making large size OLED TVs, with the demonstration of a 55-inch printed OLED TV by Panasonic in 2013 and a 65-inch printed OLED TV by AUO of Taiwan. Figure 7.20b shows an inkjet printer for making 8.5 generation OLED display panels, indicating that large scale inkjet printing of OLED display has become possible.

7.5.3 Screen Printing

Screen printing uses a woven mesh to support an ink-blocking stencil to print patterns (Fig. 7.21a). The stencil mask has patterns in the form of open areas that can let ink or other printable materials through the mesh onto a substrate. A blade or squeegee moves across the screen stencil, forcing or pumping ink through the mesh openings. In comparison with spin coating and inkjet printing, screen printing is of high printing speed, large area printing and continuous printing, which makes it very suitable for industrial scale production. However, traditional screen printing is of low resolution in the range of 50–100μm and requires high viscosity of ink (>1000 mPa.s).

Screen printing was mostly employed for coating some of the layers in OLEDs. For example, Pardo et al. used a 4 × 12 inch nylon stencil mask to coat TPD: polycarbonate (1: 1) chloroform ink as the hole transport layer on ITO substrate [103]. Birnstock et al. printed PEDOT on ITO substrate by a semiautomatic screen printer with the stencil of 350 cm × 350 cm, such as the one shown in Figure 7.21b. The emitter layer and cathode (Ca/Ag) were deposited by thermal evaporation in vacuum [104].

7.5.4 *Roll-to-roll Printing*

Roll printing [106] is a contact printing technique that includes gravure printing (Figure 7.22), flexographic printing, gravure offset printing, and so on. The resolution of roll printing varies from 20μm to 50μm. The most significant feature of roll printing is the high speed and high throughput when in roll-to-roll (R2R) mode. In conventional printing industry, R2R printing can print on more than 1m wide flexible sheet at the speed of more 100m per minute. R2R printing has been used in making flexible OLED lighting and display. Figure 7.23 shows the

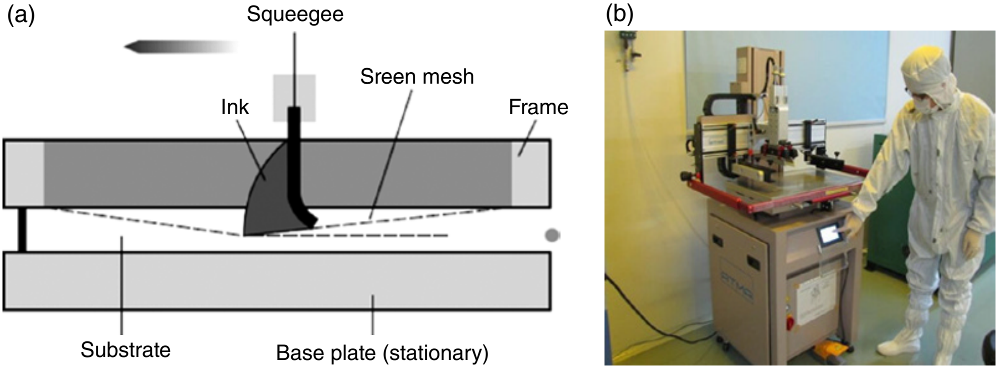
(a)
Squeegee
Sreen mesh
Ink
Frame
Substrate
Base plate (stationary)
(b)

Figure 7.21 Schematic of screen printing (a) and a screen printer (b)

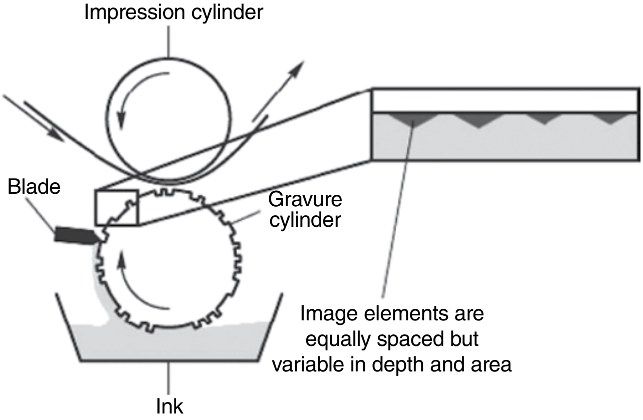
Impression cylinder
Blade
Gravure cylinder
Image elements are equally spaced but variable in depth and area
Ink

Figure 7.22 OLED display fabricated by roll-to-roll printing. (Adopted from [106] with courtesy)

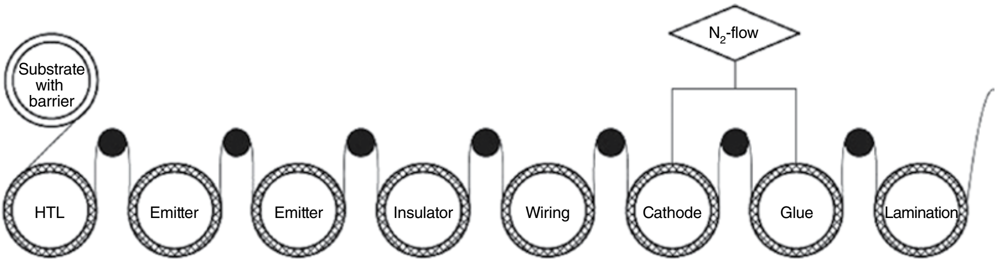

Figure 7.23 Fabrication of OLED by roll-to-roll printing process. Adopted from web with courtesy to its origin. Reproduced with permission from ref. [107] with permission from Hast Jukka

schematic process by R2R printing for making OLED lighting devices, which is realized at the Holst Center of The Netherlands.

In addition to the above printing techniques, laser printing [108,109] and electric spray printing [110] are also reported. More information can be found in Chapter 4 of this book.

7.5.5 Current Status of the Printed OLED Industry

The OLED industry is most active in Asia, with Samsung and LG in South Korea playing the key roles, focusing on OLED display for mobile phones and TVs. Sony and Panasonic in Japan, AUO and CMO in Taiwan, and Visionox in China have also been active in OLED technology for many years. The biggest commercial success of OLED is in mobile phone display, which is dominated by Samsung. In the last two years, OLED TVs began to emerge on the market, with LG as the main driver of the technology. The most noticeable development in OLED industry is the rise of Chinese players. Since 2013, several production lines for AMOLED display panels have been built and a few more are planned to be built. China is rapidly becoming the largest OLED producer in the world.

So far the manufacturing of OLED is dominated by vacuum deposition process. The high manufacturing cost due to the vacuum process and high waste of materials due to the thermal evaporation deposition make the OLED display much less competitive compared with LCD display. Manufacturing OLED by printing is a promising route to reduce the cost. The industry began to seriously consider printed OLED in the last few years, with Panasonic first demonstrating their inkjet-printed 55-inch OLED TV in 2013 and AUO demonstrating their 65inch inkjet-printed OLED TV in 2014. In January 2015, Japan announced the formation of an industrial alliance (JOLED) to develop printable OLED. Since 2014, South Korea has also had a national R&D program on printable flexible display.

In fact, development on printable OLED goes as far back as 2007, when General Electric (GE) in the US and Konica Minolta in Japan jointly developed printable OLED materials and the printing process for OLED lighting. In 2010, GE demonstrated a printed flexible OLED lighting sheet (Figure 7.24) from its pilot production line with a yield of over 90%. DuPont reported printable polymer emitters with the lifetime reaching thousands to millions of hours. However, the industrialization of printable OLED lighting is slow because the cost and performance of printable OLED lighting still cannot compete with solid-state LED lighting. Further improvements for both printable OLED display and lighting are needed.

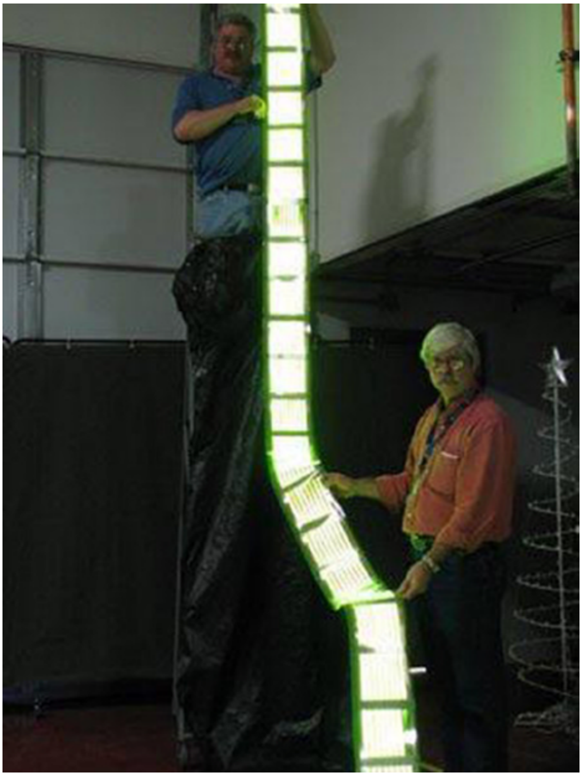

Figure 7.24 R2R printed OLED lighting sheet manufactured by GE. (Adopted from web with courtesy to its origin)

7.6 Summary

Since the report of a double layer structure of OLED by Vanslyke and Tang in 1987, the technologies for both OLED display and lighting are advancing very rapidly. OLED offers the advantages of self-luminance, better color rendering, a wide viewing angle, fast response, and they are also energy saving, simple in structure, light and thin, low temperature resistant, anti-knocking, and can be fabricated on flexible substrate and by printing.

In the OLED industry, Samsung and LG in South Korea are the pioneers focusing on OLED display for mobile phones and TVs. Currently, AMOLEDs are widely used in small size display, such as smart phones and digital cameras, which are dominantly produced by Samsung. With its nearly 100% inner quantum efficiency, better color saturation, high contrast ratio of more than 1000000:1,thinness and lightness, the OLED display is considered to be the third generation display technology after LCD display. LG began mass production of its 55-inch OLED TV in 2014, the AMOLED display market is expected to exceed $20 billion by 2022, according to the forecast made by Display Search in 2014.

Besides display, OLEDs are surface-emitting lighting devices. Compared to LED, OLEDs have not only high power efficiency but also higher CRI (over 90) than LED. To date, the highest power efficiency of white OLEDs is over 150 lm W^{-1} and several companies already offer OLED lighting panels, including Philips, Osram, LG Chem, Konica Minolta and others. LG Chem has commercially supplied 320 × 320 mm OLED lighting panels since 2014, and the company is investing 200 billion won ($184 million) to install a fifth-generation production line that can fabricate OLEDs about eight times larger than the current OLED panels.

However, the cost has been the key factor that prevents OLEDs from widespread use. In flat panel displays and lightings, OLED technology is 5–10 times more expensive compared to LCD display and LED lighting, due to the use of vacuum deposition process for making OLED panels, which not only needs expensive equipment but is also a great waste of OLED materials. To lower the cost, developing printable OLEDs has become a global focus in recent years, especially with the additional advantage of being flexible for printed OLEDs, which can greatly expand their application areas.

Printable OLEDs are based on either polymer or small molecular materials. For a polymer OLED, the poor consistency of OLED material property from batch to batch is a critical issue. Soluble small molecules are becoming more competitive technology as compared with polymers. The performance of solution-processed OLEDs is close to vacuum evaporated OLEDs. The major challenge in printing OLEDs is to deposit multilayers. When depositing soluble OLED inks by printing or coating, the solvent in each of the inks can affect the others. The intermixing of solvents can cause damage to each functional layer, consequently decreasing the efficiency. Adding an interface layer, or making each layer cross-linkable, is believed to be the two most promising techniques to facilitate printable multilayer OLED with comparable efficiency and lifetime. As for the printing methods, many printing processes, such as inkjet printing and roll-to-roll printing (gravure, flexographic, gravure offset or slot die) are all applicable to printing OLEDs. Printed OLEDs are believed to be the future if OLEDs are to become dominant in the lighting and display market.

References

[1] Bernanose A. The mechanism of organic electroluminescence. J. Chim. Phys. 1955;52:396.
[2] Pope M, Magnante P, Kallmann PHP. Journal of Chemical Physics. 1963;38:2042.
[3] Vincett PS, Barlow WA, Hann RA, Roberts GG. Electrical conduction and low voltage blue electroluminescence in vacuum-deposited organic films. Thin Solid Films. 1982;94:171.
[4] Tang CW, Vanslyke SA. Organic electroluminescence diodes. Applied Physics Letters. 1987;51:913.
[5] Adachi C, Tokito S, Tsutsui T, Saito S. Electroluminescence in organic films with three-layer structure. Japanese Journal of Applied Physics. 1988;27:L269.
[6] Burroughes JH, Bradley DDC, Brown AR, Marks RN, Mackay K, Friend KRH, Burn PL, Holmes AB. Light-emitting diodes based on conjugated polymers. Nature 1990;347:539.
[7] Braun D, Heeger AJ. Electroluminescence from light-emitting-diodes fabricated from conducting polymers. Thin Solid Films. 1992;216:96–8.
[8] Gustafsson G, Cao Y, Treacy GM, Klavetter F, Colaneri N, Heeger AJ. Flexible Light-emitting-diodes made from soluble conducting polymers. Nature. 1992;357:477.
[9] Baldo MA, O'Brien DF, You Y, Shoustikov A, Sibley S, Thompson ME, Forrest SR. Highly efficient phosphorescent emission from organic electroluminescent devices. Nature. 1998;395:151.
[10] Adachi C, Baldo MA, Thompson ME, Forrest SR. Nearly 100% internal phosphorescence efficiency in an organic light-emitting device. Journal of Applied Physics. 2001;90:5048.
[11] Sun YR, Giebink NC, Kanno H, Ma BW, Thompson ME, Forrest SR. Management of singlet and triplet excitons for efficient white organic light-emitting devices. Nature. 2006;440:908.
[12] Zhou X, Pfeiffer M, Blochwitz J, Werner A, Nollau A, Fritz T, Leo K. Very-low-operating-voltage organic light-emitting diodes using a p-doped amorphous hole injection layer. Applied Physics Letters. 2001; 78:410.

[13] Sun CY, Wang XL, Zhang X, Qin C, Li P, Su ZM, Zhu DX, Shan GG, Shao KZ, Wu H, Li J. Efficient and tunable white-light emission of metal–organic frameworks by iridium-complex encapsulation. Nature Communications. 2013;4:2717.

[14] Harding MJ, Poplavskyy D, Choong VE, Campbell AJ, So F. Effects of solution-processed polymer interlayers on hole injection and device performance of polymer light-emitting diodes. Organic Electronics. 2008;9:183.

[15] Niu YH, Liu MS, Ka JW, Jen AKY. Thermally crosslinked hole-transporting layers for cascade hole-injection and effective electron-blocking/exciton-confinement in phosphorescent polymer light-emitting diodes. Applied Physics Letters. 2006;88.

[16] Pfeiffer M, Beyer A, Fritz T, Leo K. Controlled doping of phthalocyanine layers by cosublimation with acceptor molecules: A systematic Seebeck and conductivity study. Applied Physics Letters. 1998;73:3202.

[17] Blochwitz J, Pfeiffer M, Fritz T, Leo K. Low voltage organic light emitting diodes featuring doped phthalocyanine as hole transport material. Applied Physics Letters. 1998;73:729.

[18] Nollau A, Pfeiffer M, Fritz T, Leo K. Controlled n-type doping of a molecular organic semiconductor: Naphthalenetetracarboxylic dianhydride (NTCDA) doped with bis(ethylenedithio)-tetrathiafulvalene (BEDT-TTF). Journal of Applied Physics. 2000;87:4340.

[19] Werner AG, Li F, Harada K, Pfeiffer M, Fritz T, Leo K. Pyronin B as a donor for n-type doping of organic thin films. Applied Physics Letters. 2003;82:4495.

[20] Kido J, Matsumoto T. Bright organic electroluminescent devices having a metal-doped electron-injecting layer. Applied Physics Letters. 1998:73:2866.

[21] Huang JS, Pfeiffer M, Werner A, Blochwitz J, Leo K, Liu SY. Low-voltage organic electroluminescent devices using pin structures. Applied Physics Letters 2002;80:139.

[22] M. Stossel, J. Staudigel, F. Steuber, J. Simmerer, A. Winnacker, Impact of the cathode metal work function on the performance of vacuum-deposited organic light emitting-devices. Applied Physics a-Materials Science & Processing 1999, 68, 387.

[23] Stossel M, Staudigel J, Steuber F, Blassing J, Simmerer J, Winnacker A, Neuner H, Metzdorf D, Johannes HH, Kowalsky W. Electron injection and transport in 8-hydroxyquinoline aluminum. Synthetic Metals. 2000;111:19.

[24] Wang JF, Kawabe Y, Shaheen SE, Morrell MM, Jabbour GE, Lee PA, Anderson J, Armstrong, NR, Kippelen B, Mash EA, Peyghambarian N. Exciplex electroluminescence from organic bilayer devices composed of triphenyldiamine and quinoxaline derivatives. Advanced Materials. 1998;10;230.

[25] Haskal EI, Curioni A, Seidler PF, Andreoni W. Lithium-aluminum contacts for organic light-emitting devices. Applied Physics Letters. 1997;71:1151.

[26] Braun D, Heeger AJ, Kroemer H. Improved efficiency in semiconducting polymer light-emitting-diodes. Journal of Electronic Materials. 1991;20:945.

[27] Braun D, Heeger AJ. Visible-light emission from semiconducting polymer diodes. Applied Physics Letters. 1991;58:1982.

[28] Gao Y, Park KT, Hsieh BR. X-ray photoemission investigations of the interface formation of ca and poly(p-phenylene vinylene). Journal of Chemical Physics. 1992;97:6991.

[29] Gao Y, Park KT, Hsieh BR. Interface formation of ca with poly(p-phenylene vinylene). Journal of Applied Physics. 1993;73:7894.

[30] Jeglinski SA, Amir O, Wei X, Vardeny ZV, Shinar J, Cerkvenik T, Chen W, Barton TJ. Symmetric light emitting devices from poly(p-di ethynylene phenylene) (p-di phenylene vinylene) derivatives. Applied Physics Letters. 1995;67:3960.

[31] Wu CC, Wu CI, Sturm JC, Kahn A. Surface modification of indium tin oxide by plasma treatment: An effective method to improve the efficiency, brightness, and reliability of organic light emitting devices. Applied Physics Letters. 1997;70:1348.

[32] Hatton RA, Day SR, Chesters MA, Willis MR. Organic electroluminescent devices: enhanced carrier injection using an organosilane self assembled monolayer (SAM) derivatized ITO electrode. Thin Solid Films. 2001;394:292.

[33] Appleyard SFJ, Day SR, Pickford RD, Willis MR. Organic electroluminescent devices: enhanced carrier injection using SAM derivatized ITO electrodes. Journal of Materials Chemistry 2000;10:169.

[34] Mason MG, Hung LS, Tang CW, Lee ST, Wong KW, Wang M. Characterization of treated indium-tin-oxide surfaces used in electroluminescent devices. Journal of Applied Physics. 1999;86:1688.

[35] Milliron DJ, Hill IG, Shen C, Kahn, Schwartz AJ. Schwartz, Surface oxidation activates indium tin oxide for hole injection. Journal of Applied Physics. 2000;87:572.

[36] Choi B, Yoon H, Lee HHH. Surface treatment of indium tin oxide by SF6 plasma for organic light-emitting diodes. Applied Physics Letters. 2000;76:412.

[37] Hung LS. Organic electroluminescent device with a non-conductive fluorocarbon polymer layer. *US6208077-B1*, 2001.

[38] Nuesch F, Rothberg LJ, Forsythe EW, Le QT, Gao YL. A photoelectron spectroscopy study on the indium tin oxide treatment by acids and bases. Applied Physics Letters.1999;74:880.

[39] Le QT, Nuesch F, Rothberg LJ, Forsythe EW, Gao YL. Photoemission study of the interface between phenyl diamine and treated indium-tin-oxide. Applied Physics Letters. 1999;75:1357.

[40] Ganzorig C, Kwak KJ, Yagi K, Fujihira M. Fine tuning work function of indium tin oxide by surface molecular design: Enhanced hole injection in organic electroluminescent devices. Applied Physics Letters. 2001;79:272.

[41] Parker ID, Kim HH. Fabrication of polymer light-emitting-diodes using doped silicon electrodes. Applied Physics Letters. 1994;64:1774.

[42] Tada K, Yokota Y, Kobashi K, Yoshino K. Characteristics of heterojunction utilizing conducting polymer and diamond film on Si. Japanese Journal of Applied Physics. 1997;36:L1678.

[43] Bsiesy A, Nicolau YF, Ermolieff A, Muller F, Gaspard F. Electroluminescence from N(+)-type porous silicon contacted with layer-by-layer deposited polyaniline. Thin Solid Films. 1995;255:43.

[44] Jiang X, Wong FL, Fung MK, Lee ST. Aluminum-doped zinc oxide films as transparent conductive electrode for organic light-emitting devices. Applied Physics Letters. 2003;83:1875.

[45] Kim H, Horwitz JS, Kim WH, Qadri SB, Kafafi ZH. Anode material based on Zr-doped ZnO thin films for organic light-emitting diodes. Applied Physics Letters. 2003;83:3809.

[46] Forsythe EW, Abkowitz MA, Gao YL, Tang CW. Influence of copper phthalocynanine on the charge injection and growth modes for organic light emitting diodes. Journal of Vacuum Science & Technology a-Vacuum Surfaces and Films. 2000;18:1869.

[47] Hill IG, Kahn A. Combined photoemission/in vacuo transport study of the indium tin oxide/copper phthalocyanine/N,N′-diphenyl-N,N′-bis(l-naphthyl)-1,1′ biphenyl-4,4″ diamine molecular organic semiconductor system. Journal of Applied Physics. 1999;86:2116.

[48] Shen YL, Jacobs DB, Malliaras GG, Koley G, Spencer MG, Ioannidis A. Modification of indium tin oxide for improved hole injection in organic light emitting diodes. Advanced Materials. 2001;13:1234.

[49] Gyoutoku A, Hara S, Komatsu T, Shirinashihama M, Iwanaga H, Sakanoue K. An organic electroluminescent dot-matrix display using carbon underlayer. Synthetic Metals. 1997;91:73.

[50] Li F, Tang H, Anderegg J, Shinar J. Fabrication and electroluminescence of double-layered organic light-emitting diodes with the Al_2O_3/Al cathode. Applied Physics Letters. 1997;70:1233.

[51] Tang H, Li F, Shinar J. Bright high efficiency blue organic light-emitting diodes with Al_2O_3/Al cathodes. Applied Physics Letters. 1997;71:2560.

[52] Hung LS, Tang CW, Mason MG. Enhanced electron injection in organic electroluminescence devices using an Al/LiF electrode. Applied Physics Letters. 1997;70:152.

[53] Jabbour GE, Kippelen B, Armstrong NR, Peyghambarian N. Aluminum based cathode structure for enhanced electron injection in electroluminescent organic devices. Applied Physics Letters. 1998;73:1185.

[54] Kido J, Iizumi Y. Fabrication of highly efficient organic electroluminescent devices. Applied Physics Letters. 1998;73:2721.

[55] Fujikawa H, Mori T, Noda K, Ishii M, Tokito S, Taga Y. Organic electroluminescent devices using alkaline-earth fluorides as an electron injection layer. Journal of Luminescence. 2000;87-9:1177.

[56] Lee CH. Enhanced efficiency and durability of organic electroluminescent devices by inserting a thin insulating layer at the Alq(3)/cathode interface. Synthetic Metals. 1997: 91:125.

[57] Kanai H, Ichinosawa S, Sato Y. Effect of aromatic diamines as a cathode interface layer. Synthetic Metals. 1997;91:195.

[58] Kraft A, Grimsdale AC, Holmes AB. Electroluminescent conjugated polymers - Seeing polymers in a new light. Angewandte Chemie-International Edition. 1998;37: 402.

[59] Salbeck J. Electroluminescence with organic compounds. Berichte Der Bunsen-Gesellschaft-Physical Chemistry Chemical Physics. 1996;100:1667.

[60] Kim JS, Friend RH, Grizzi I, Burroughes JH. Spin-cast thin semiconducting polymer interlayer for improving device efficiency of polymer light-emitting diodes. Applied Physics Letters. 2005;87.

[61] Yoshioka Y, Jabbour GE. Inkjet printing of oxidants for patterning of nanometer-thick conducting polymer electrodes. Advanced Materials. 2006;18:1307.

[62] Cambridge Display Technology Home Page. Available online: http://www.cdtltd.co.uk (accessed on 10 Febuary 2011).

[63] Cambridge Display Technology Status. Available online: http://www.cdtltd.co.uk/technology/status/ (accessed on 10 February 2011).

[64] Ganzorig C, Fujihira M. Improved drive voltages of organic electroluminescent devices with an efficient p-type aromatic diamine hole-injection layer. Applied Physics Letters. 2000;77:4211.

[65] Romero DB, Schaer M, Zuppirolim L, Cesar B, Francois B. Effects of doping in polymer light-emitting-diodes. Applied Physics Letters. 1995;67:1659.

[66] Huang F, MacDiarmid AG, Hsieh BR. An iodine-doped polymer light-emitting diode. Applied Physics Letters. 1997;71:2415.

[67] Yamamori A, Adachi C, Koyama T, Taniguchi Y. Doped organic light emitting diodes having a 650-nm-thick hole transport layer. Applied Physics Letters. 1998;72:2147.

[68] Maennig B, Pfeiffer M, Nollau A, Zhou X, Leo K, Simon P. Controlled p-type doping of polycrystalline and amorphous organic layers: Self-consistent description of conductivity and field-effect mobility by a microscopic percolation model. Physical Review B. 2001;64.

[69] Blochwitz J, Fritz T, Pfeiffer M, Leo K, Alloway DM, Lee PA, Armstrong NR. Interface electronic structure of organic semiconductors with controlled doping levels. Organic Electronics. 2001;2:97.

[70] Murata H, Kafafi ZH, Uchida M. Efficient organic light-emitting diodes with undoped active layers based on silole derivatives. Applied Physics Letters. 2002;80:189.

[71] Lamansky S, Djurovich P, Murphy D, Abdel-Razzaq F, Lee HE, Adachi C, Burrows PE, Forrest SR, Thompson ME. Highly phosphorescent bis-cyclometalated iridium complexes: Synthesis, photophysical characterization, and use in organic light emitting diodes. Journal of the American Chemical Society. 2001;123:4304.

[72] Adachi C, Baldo MA, Forrest SR, Lamansky S, Thompson ME, Kwong RC. High-efficiency red electrophosphorescence devices. Applied Physics Letters. 2001;78:1622.

[73] Holmes RJ, Forrest SR, Tung YJ, Kwong RC, Brown JJ, Garon S, Thompson ME. Blue organic electrophosphorescence using exothermic host-guest energy transfer. Applied Physics Letters. 2003;82:2422.

[74] Hebner TR, Wu CC, Marcy D, Lu MH, Sturm JC. Ink-jet printing of doped polymers for organic light emitting devices. Applied Physics Letters. 1998;72:519.

[75] Singh M, Kondou T, Chae H, Froehlich JD, Li S, Mochizuki A, Jabbour GE. Mater. Res. Soc. Fall Meeting. 2008:G13:7.

[76] Kram SL, Marshall WB, Obrien JJ, Pickering TA,Wu W. Composition for preparing ink comprises blend of luminescent polymer having specific weight average molecular weight, and viscosity modifier having specific luminescent emission maximum and containing no exocyclic conjugated double bonds. *US2006197059-A1; US7517472-B2*.

[77] Rehmann N, Ulbricht C, Koehnen, Zacharias AP, Gather MC, Hertel D, Holder E, Meerholz K, Schubert US. Advanced device architecture for highly efficient organic light-emitting diodes with an orange-emitting crosslinkable iridium(III) complex. Advanced Materials. 2008;20:129.

[78] Sekine C, Tsubata Y, Yamada T, Kitano M, Doi S. Recent progress of high performance polymer OLED and OPV materials for organic printed electronics. Science and Technology of Advanced Materials. 2014;15.

[79] Xiao L, Chen Z, Qu B, Luo J, Kong S, Gong Q, Kido J. Recent progresses on materials for electrophosphorescent organic light-emitting devices. Advanced Materials. 2011;23:926.

[80] Zhong C, Duan C, Huang F, Wu H, Cao Y. Materials and devices toward fully solution processable organic light-emitting diodes. Chemistry of Materials. 2011;23:326.

[81] Morteani AC, Dhoot AS, Kim JS, Silva C, Greenham NC, Murphy C, Moons E, Cina S, Burroughes JH, Friend RH. Barrier-free electron-hole capture in polymer blend heterojunction light-emitting diodes. Advanced Materials. 2003;15:1708.

[82] Zuniga CA, Abdallah J, Haske W, Zhang Y, Coropceanu I, Barlow S, Kippelen B, Marder SR. Crosslinking using rapid thermal processing for the fabrication of efficient solution-processed phosphorescent organic light-emitting diodes. Advanced Materials. 2013;25:1739.

[83] Ma B, Lauterwasser F, Deng L, Zonte CS, Kim BJ, Frechet JMJ. New thermally cross-linkable polymer and its application as a hole-transporting layer for solution processed multilayer organic light emitting diodes. Chemistry of Materials 2007;19:4827.

[84] Aizawa N, Pu Y.-J, Sasabe H, Kido J. Thermally cross-linkable host materials for enabling solution-processed multilayer stacks in organic light-emitting devices. Organic Electronics. 2013;14:1614.

[85] Liaptsis G, Hertel D, Meerholz K. Solution processed organic double light-emitting layer diode based on crosslinkable small molecular systems. Angewandte Chemie-International Edition. 2013;52:9563.

[86] Gather MC, Koehnen A, Meerholz K. White Organic Light-Emitting Diodes. Advanced Materials. 2011;23:233.

[87] Liu J, Zhou QG, Y, Cheng X, Geng YH, Wang LX, Ma DG, Jing XB, Wang FS. White electrolumineseence from a single-polymer system with simultaneous two-color emission: Polyfluorene as the blue host and a 2,1,3-benzothiadiazole derivative as the orange dopant on the main chain. Advanced Functional Materials 2006;16:957.

[88] Tu GL, Mei CY, Zhou QG, Cheng YX, Geng YH, Wang LX, Ma DG, Jing XB, Wang FS. Highly efficient pure-white-light-emitting diodes from a single polymer: Polyfluorene with naphthalimide moieties. Advanced Functional Materials. 2006;16:101.

[89] Reineke S, Lindner F, Schwartz G, Seidler N, Walzer K, Luessem B, Leo K. White organic light-emitting diodes with fluorescent tube efficiency. Nature. 2009;459:234.

[90] Chopra N, Lee J, Zheng Y, Eom S.-H, Xue J, So F. High efficiency blue phosphorescent organic light-emitting device. Applied Physics Letters. 2008;93.

[91] Carr WN. Photometric figures of merit for semiconductor luminescent sources operating in spontaneous mode. Infrared Physics. 1966;6:1.

[92] Wei MK, Lin HY, Lee JH, Chen KY, Ho YH, Lin CC, Wu CF, Lin HY, Tsai JH, Wu TC. Efficiency improvement and spectral shift of an organic light-emitting device with a square-based microlens array. Optics Communications. 2008;281:5625.

[93] Tsutsui T, Yahiro M, Yokogawa H, Kawano K. Doubling coupling-out efficiency in organic light-emitting devices using a thin silica aerogel layer. Advanced Materials. 2001;13:1149.

[94] Jeon S, Kang JW, Park HD, Kim JJ, Youn JR, Shim J, Jeong JJH, Choi DG, Kim KD, Altun AO, Kim SH, Lee YH. Ultraviolet nanoimprinted polymer nanostructure for organic light emitting diode application. Applied Physics Letters. 2008;92.

[95] Sun Y, Forrest SR. Enhanced light out-coupling of organic light-emitting devices using embedded low-index grids. Nature Photonics. 2008;2:483.

[96] Zhou L, Zhuang JY, Song MS, Su WM, Cui Z. Enhanced performance for organic light-emitting diodes by embedding an aerosol jet printed conductive grid, Journal of Physics D-Applied Physics. Journal of Physics D-Applied Physics. 2014;47.

[97] http://www.novaled.com/news/2011_07_13_pr.html

[98] OE-A roadmap for prganic and printed electronics. Organic Electronics Association (OE-A) 2013.

[99] Pschenitzka F, Sturm JC. Three-color organic light-emitting diodes patterned by masked dye diffusion. Applied Physics Letters. 1999;74:1913.

[100] Muller CD, Falcou A, Reckefuss N, Rojahn M, Wiederhirn V, Rudati P, Frohne H, Nuyken O, Becker H, Meerholz K. Multi-colour organic light-emitting displays by solution processing. Nature. 2003;421:829.

[101] Bharathan J, Yang Y. Polymer electroluminescent devices processed by inkjet printing: I. Polymer light-emitting logo. Applied Physics Letters. 1998;72:2660.

[102] Chang SC, Liu J, Bharathan J, Yang Y, Onohara J, Kido J. Multicolor organic light-emitting diodes processed by hybrid inkjet printing. Advanced Materials. 1999;11:734.

[103] Pardo DA, Jabbour GE, Peyghambarian N. Application of screen printing in the fabrication of organic light-emitting devices. Advanced Materials. 2000;12:1249.

[104] Birnstock J, Blassing J, Hunze A, Scheffel M, Stossel, Heuser MK, Wittmann G, Worle J, Winnacker A. Screen-printed passive matrix displays based on light-emitting polymers. Applied Physics Letters. 2001; 78:3905.

[105] http://www.dimatix.com/

[106] Lee ST, Lee JY, Kim MH, Suh MC, Kang TM, Choi YJ, Park JY, Kwon JH, Chung HK, Baetzold J, Bellamann E, Savvateev V, Wolk M, Webster S. SID 02 Digest Society for Information Display, San Jose, CA 2002, 784.

[107] Hast J. Roll-to-roll printing of organic light emitting diodes (OLED) in 3rd Chinese Printed Electronics Symposium, 13th September 2012, Suzhou, China.

[108] Lee JY, Lee ST. Laser-induced thermal imaging of polymer light-emitting materials on poly(3,4-ethylene-dioxythiophene): Silane hole-transport layer. Advanced Materials. 2004;16:51.

[109] Ju J, Yamagata Y, Higuchi T. Thin-Film Fabrication Method for Organic Light-Emitting Diodes Using Electrospray Deposition. Advanced Materials. 2009;21:4343.

[110] Park J, Jacobson JM. All printed bistable reflective displays: Printable electrophoretic ink and all printed metal-insulator-metal diodes. In *Flat-Panel Display Materials-1998*, Vol. 508, p. 211 (Eds: G. N. Parsons, C. C. Tsai, T. S. Fahlen, C. H. Seager), 1998.

8

Encapsulation Technology for Organic Electronic Devices

Wenming Su

8.1 Introduction

Most electronic devices need encapsulation (or packaging). For inorganic electronic devices such as integrated circuit chips, encapsulation is needed to protect the chips from external physical or chemical damages. For organic electronic devices, such as organic light-emitting diodes (OLED), organic photovoltaic devices (OPV), and organic thin-film transistors (OTFT), encapsulation is used not only to prevent external damage but also prolong to the lifetime of organic devices, because most organic semiconductor materials tend to decay and lose their electronic properties upon contact with even tiny traces of water and oxygen. The permeable trace of water is measured by water vapor transition rate (WVTR) in g/m^2/d (gram per square meter area per day). For organic electronic devices, the WVTR should be less than 10^{-4}–10^{-6}g/m^2/d, which is an extremely small amount to be allowed to penetrate through the encapsulation. Therefore, the encapsulation requirement in organic electronics is more stringent than conventional packaging for inorganic electronic devices.

There are generally two types of encapsulation; one involves using a glass lids technique by which organic materials are encapsulated between two glass lids and only the edge of glass lids need to be well sealed with UV glue to stop water and oxygen permeation; the other involves thin-film encapsulation, particularly for flexible organic electronics where organic materials are deposited on flexible plastic substrates. Compared to glass, plastic thin film is permeable to water and oxygen molecules. A barrier layer is required for the entire surface of plastic film, not just the edge. The encapsulation for flexible organic electronics is much more difficult.

In this chapter, the aging mechanism of organic electronic materials will be analyzed, together with the requirements of encapsulation for organic electronic devices. Different encapsulation techniques will be introduced, with particular emphasis on thin-film encapsulation. The characterization of encapsulation properties for various barrier formation processes will be described, together with an overview of the current status in thin-film encapsulation technology worldwide and its future development trends.

Printed Electronics: Materials, Technologies and Applications, First Edition. Zheng Cui, Chunshan Zhou, Song Qiu, Zheng Chen, Jian Lin, Jianwen Zhao, Changqi Ma and Wenming Su.
© 2016 Higher Education Press. All rights reserved. Published 2016 by John Wiley & Sons Singapore Pte. Ltd.

8.2 Aging of Organic Electronic Devices

Device aging is the decay of device property and performance over a period of time. Device aging is generally divided into natural aging and unnatural aging [1]. The so-called natural aging refers to the decay caused by the change of basic properties of material and structure in a device, while changes other than these are usually classified as unnatural aging. Water and oxygen attacks are considered to be the most important cause of unnatural aging. Other factors, such as temperature and electrochemical process can also lead to unnatural aging. Macroscopically, the signs of aging are: dark spots appearing in the emission surface and a decrease in light emission intensity, efficiency and lifetime for OLED; a decrease in electric current and lifetime in the case of OPV, and a sharp decrease of on/off ratio in OTFT.

8.2.1 Characteristics and Mechanisms of Aging

The study of OLED aging was early and relatively mature, due to the long history of OLED development. The short lifetime of OLED caused by aging has been a great challenge for its industrialization. Eastman Kodak proposed a calculation method for OLED lifetime, which is the time needed for decay to half of the luminance from its initial intensity. The lifetime of early OLED was very short, from only a few minutes to a few hours. The aging starts with the formation of black spots in the luminescence area. Figure 8.1 illustrates the evolution of black spots with time. The black spots lead to gradual decrease of luminescence area, a decrease in luminance intensity, to complete failure.

Factors causing the formation of dark spots are analyzed as follows.

1. Effect of substrate and electrode roughness. If the roughness of the substrate or electrode surface is too large or there are sharp spikes on the surface, local discharge will occur when applying voltage on the device, leading to a high local current and the generation of large amount of heat, even causing short circuit and breakdown of the device. Excessive heat may result in the crystallization of organic material, electrochemical change at the interface and finally material peel-off from the electrode. Peeling from the electrode will lead to complete failure of the electrons injection. As a result, a dark spot is generated at these locations [2,3]. As the total thickness of the function layers deposited on the electrode surface is only about 100 nm, the surface roughness of substrate or electrode should be ideally less than 1 nm.
2. Effect of particle contamination. Particle contamination is another important cause of the generation of dark spots. The fabrication of OLED demands strict cleanliness on the

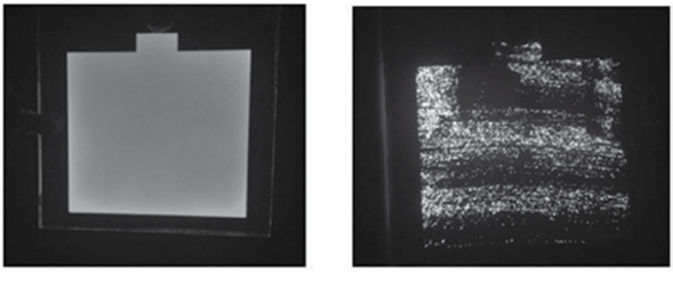

Figure 8.1 Evolution of dark spots in OLED with time. (Experimental results at the authors' Printable Electronics Research Center)

substrate. Small residual particles on the substrate surface, falling dust during loading or particles generated in fabrication equipment, will result in dark or bright spots in OLED. Low conductivity particles will cause local insulation of the device, which stops the local current flow from anode to cathode, generating black spots. High conductivity particles will lead to a locally high current, generating bright spots. Big particles on the surface will result in locally thinner or discontinued film, consequently resulting in black spots. Moreover, the particles may cause cracks in the organic layer during deposition. The subsequent deposition of a metal electrode layer can penetrate through the organic layer, leading to a short circuit between cathode and anode.

3. Effect of water and oxygen attack. The cathodes of OLED and OPV are often made of LiF/Al, Ca, Ag, or alloy of Li-Al and Mg-Ag. These materials are relatively active and will be oxidized or eroded by water when exposed to air for long time, forming insulating layers that will seriously affect charge injection or collection, eventually deteriorating the efficiency and lifetime of device.

In OLED, Al often works as a cathode and will react with water under moisture conditions and consequently deteriorate. The existence of an electronic current will accelerate the reaction. The dark spots generated after Al deterioration is a serious problem and related to the environmental moisture and the time of year. For example, in winter when the weather is dry, the lifetime of unencapsulated device may reach several hours, while in summer when the weather is humid, black spots will be observed in only a few minutes and the lifetime of device may be less than an hour.

In addition, some functional materials are also very sensitive to oxygen and water. For example, the n-type material in OTFT is oxidizable, P3HT in OPV is deliquescent with moisture; the functional layers can react with each other electrochemically at the interface with the assistance of water molecules. All the above processes accelerate the aging of devices [4]. Figure 8.2 compares the aging of OTFT and OLED with and without encapsulation. The encapsulation helps to extend the lifetime significantly.

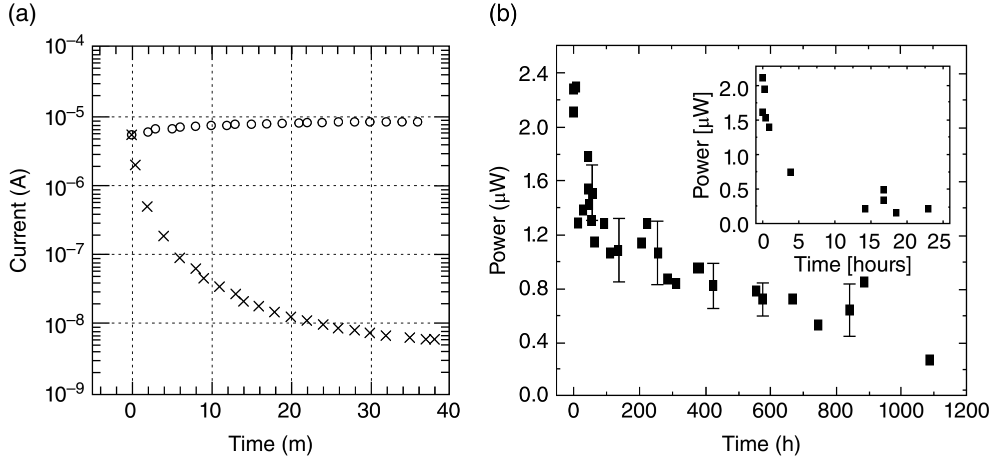

Figure 8.2 (a) Decay curve of conductivity of C60 based OTFT under 30 V driving voltage, line x represent unencapsulated device while line o represents encapsulated devices [5] Reprinted from ref. [5] with permission from AIP Publishing LLC; (b) Lifetime of encapsulated OLED, the insert represents unencapsulated OLED device. (Reprinted from reference [4] with permission from AIP Publishing LLC)

The aging mechanism of OPV and OTFT is similar to that of OLED. However, the sensitivity to water and oxygen in OPV and OTFT is far lower than that of OLED. The encapsulation requirement for OPV and OTFT is far less stringent than for OLED, which can be several orders of magnitude less demanding in encapsulation. Then there is the question as to why there is such a difference, considering they are based on similar organic semiconductor materials, Alhough there is still no reasonable explanation to this question, it is believed that the differences in working voltage and current result in the different reaction rate of a metallic electrode with water and oxygen. For example, the working current and voltage of OLED is 20mA·cm^{-2} and 5-8 V, while the photon generated current and voltage of OPV are only about a few mA·cm^{-2} and less than 1V. The current flow through gate electrodes of OTFT or electrodes in OPV is very small. The electrochemical corrosions to the electrodes of OPV or OTFT by water/oxygen are relatively slower than OLED.

8.2.2 Requirements for Organic Electronics Encapsulation

The purpose of encapsulations is to protect and extend the lifetime of organic electronic devices. As ambient water and oxygen are the main causes of rapid aging in organic electronic devices, preventing water and oxygen from permeating into the devices is the first consideration of encapsulation [6]. Experimental studies indicated that the total permeating rate of substrate and encapsulated layer to water vapor should be lower than 5×10^{-6} g·m^{-2}·d^{-1} and to oxygen lower than 10^{-3} g·m^{-2}·d^{-1} [4],in order for an OLED to reach a working life of more than 1×10^{4} h [4]. For OPV the encapsulation requirement at water permeating rate of 10^{-4}–10^{-5} g·m^{-2}·d^{-1} would be adequate. The requirement for OTFT encapsulation is even less stringent, allowing water

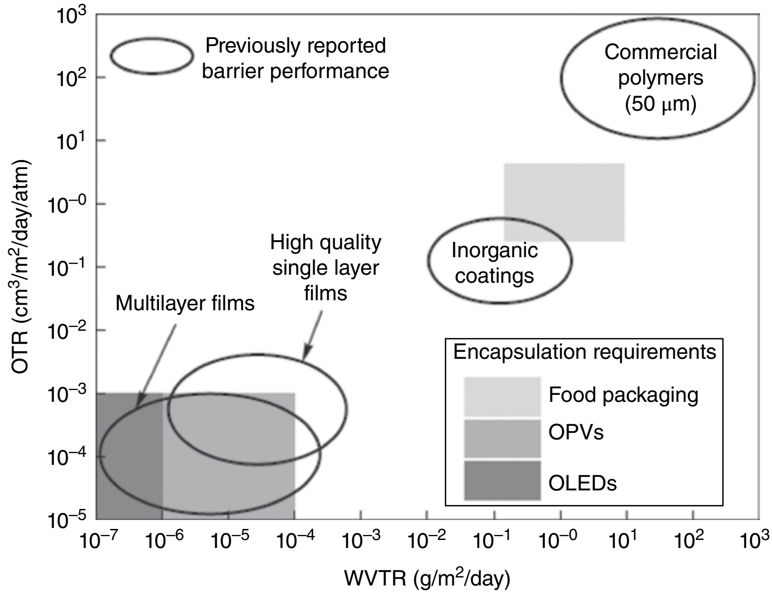

Figure 8.3 Techniques required of OLED, OPV and conventional food packaging to water/oxygen permeability requirements and their blocking ability under different encapsulating technique [7]. (Adapted from [7] with courtesy)

permeating rate at 10^{-2}–10^{-3} $g{\cdot}m^{-2}{\cdot}d^{-1}$. Figure 8.3 is a chart showing different types of encapsulation methods and their relevant water (horizontal axis) and oxygen (vertical axis) permeation rates [7,8]. The various gray rectangular regions represent the required range of water/oxygen permeating rate for different applications such as food packaging, OPV and OLED. The oval circles represent different encapsulation methods and their water/oxygen barrier performance. One can conclude from the chart that OLED has the highest requirement on blocking water/oxygen permeation, and only multilayer barrier films can meet the barrier requirement.

When choosing a suitable encapsulation method, the process compatibility must be considered during encapsulation. As most organic materials have a glass transition temperature (Tg), above which the organic materials begin to crystallize, the temperature to encapsulate OLED should not exceed 100°C. OPV and OTFT differ from OLED in that they usually need a high annealing temperature to achieve better performance. They can be encapsulated at a relatively wide range of temperatures, which its substrate can withstand. Generally, the optimum encapsulating temperature for flexible organic electronic devices is between 100 and 130°C, no higher than 150°C. Other factors such as the light transmittance of a encapsulation layer should also be a consideration for OLED and OPV, as both require high transmission of light in and out of the device.

8.3 Principle of Encapsulation

8.3.1 Water/oxygen Penetration Mechanism through Thin Films

The penetration of water/oxygen through thin films can be described in the following two steps: adsorption of water/oxygen on one side of film and the subsequent diffusion into the film to emerge on the other side of film. The pressure and concentration gradients of water/oxygen is the driving force for penetration. The penetrability (P) of single layer film is the product of a solubility coefficient (S) and a diffusion coefficient (D), where S and D are the intrinsic properties of material [9]:

$$P = S{\cdot}D \tag{8.1}$$

The unit of penetration rate for oxygen is $cm^3{\cdot}m^{-2}{\cdot}d^{-1}$ and the unit of water vapor transmission rate (WVTR) is $g{\cdot}m^{-2}{\cdot}d^{-1}$. They are defined under certain temperature and moisture conditions. The above process can also be described by Fick's law of diffusion. According to Fick's law, the penetration flux (J) is proportional to concentration gradient $\bigtriangledown(c)$:

$$J = -D{\cdot}\triangledown(c) \tag{8.2}$$

Where the concentration c is linearly related to partial pressure, $c{=}S\triangle P$, according to Henry's law of gas transport. The penetration flux is then expressed in the following equation:

$$J = DS(P_0 - P_1)/L \tag{8.3}$$

where L is the length the water/oxygen penetrates through, that is, the film thickness. The penetration delay time of a single layer film can be deduced by the time derivative of the above equation [10]. Equation (8.3) indicates the relationship among the penetration delay time, film thickness and diffusion coefficient. The penetration delay time for multilayer film can be calculated by summarizing each single layer and assuming that the penetration flux is the same for each single layer in the multilayer film. The above analysis is assumed under an ideal condition. The real process is much more complicated. Nevertheless, it indicates that the amount of water/oxygen that has penetrated into the device is related to the penetration delay time which is related to film thickness, namely the length that water/oxygen penetrates through.

8.3.2 Organic/inorganic Multilayer Encapsulation

The sensitive nature of organic electronic devices to water and oxygen determines that the encapsulated structure must have excellent water/oxygen blocking behavior, which is the key property of flexible thin-film encapsulation. Normal plastic film cannot effectively block the penetration of water and oxygen, because the intertwining of long molecular chains with each other, together with the dynamical changing of crystal structure, makes water/oxygen molecules penetrate quickly along the gap of polymer molecular chains. The WVTR of single layer polymer encapsulation is about 1–40 $g \cdot m^{-2} \cdot d^{-1}$ [4,11,12].

The closely packed crystal grain structure of inorganic film is better suited for blocking water/oxygen molecule penetration. A thin layer of inorganic material on a polymer film can enhance the barrier capability to 10–100 times. However, the barrier capability is very much dependent on the quality of the inorganic film, which is closely related to its growth method. For example, even for the same film thickness, the compactness, surface pinhole, defect density, surface morphology and roughness vary greatly with different growth methods such as sputtering, thermal evaporation, plasma-enhanced chemical vapor deposition (PECVD) and atomic layer deposition (ALD). Water/oxygen penetrate mainly through pinholes and defects in inorganic film, so the encapsulating film must be uniform and compact; the diameter and amount of defect or pinhole should be extremely low if unavoidable.

SiO_x and SiN_x are the commonly used inorganic encapsulation films. The compactness of SiO_x and SiN_x films are much higher by PECVD than by sputtering or thermal evaporation. However, the film deposited by PECVD still contains nanoscale pinholes caused by loosely packed crystal grains, as shown in Figure 8.4 [9,12,13–15]. Although the film deposited by PECVD is generally compact, once a defect is formed during growth it will propagate and duplicate, creating a perforation channel through the film rather than disappearing with the increase of film thickness.

The AFM image of SiO_x deposited by PECVD is shown in Figure 8.5a–c. The porosity due to loosely packed crystal grains is clearly visible, which easily forms the water/oxygen penetration channel, as illustrated in Figure 8.5d, considering the size of water/oxygen molecules (0.33 nm for water and 0.32 nm for oxygen). To block these channels, organic/inorganic alternating multilayer film structures have been developed.

The idea of an organic/inorganic alternating multilayer film structure is to use organic material to fill up the pinholes in the inorganic layer, as well as to dislocate the pinholes in inorganic layer, which can significantly increase the diffusion length and penetration delay time of water/oxygen. The multilayer thin-film encapsulation is schematically illustrated in Figure 8.6 and encapsulation experiments carried out at the authors' Printable Electronics Research Center (PERC) has proved that using the alternating multilayer film structure, the blocking capability improves to 3–4 order of magnitudes, which meets the requirement of OLED encapsulation.

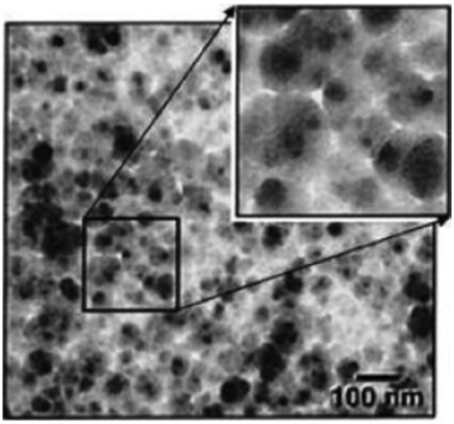

Figure 8.4 TEM image of SiOx grown by PECVD. (Reprinted from reference [14] with permission from the American Chemical Society)

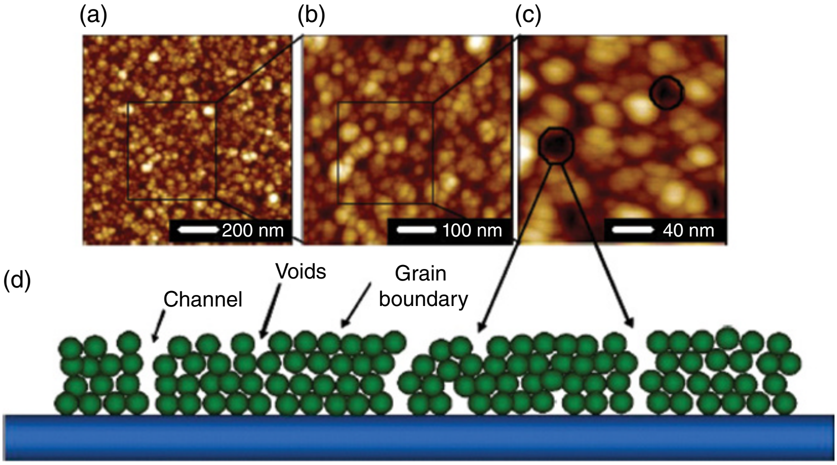

Figure 8.5 AFM images of SiOx grown on glass substrate by PECVD method; the images of figure (a), (b) and (c) represent pinholes observed under different resolutions, while (d) represents porosity of the SiOx film. (Reprinted from reference [14] with permission from the American Chemical Society)

8.3.3 Measurement of Encapsulation Property

How to measure the water/oxygen penetration rate plays the key role in designing high quality encapsulating film structures and optimizing film deposition processes. However, it is still a challenge to measure WVTR as low as $10^{-6}g \cdot m^{-2} \cdot d^{-1}$ for OLED encapsulation. There are only a few types of commercially available water/oxygen measurement instruments. Mocon is the main provider of these types of instruments on market at present with the models Permatran-W 3/33 and the Aquatran model 2. Figure 8.7a is Mocon's Permatran-W instrument and Figure 8.7b illustrates the principle of water/oxygen penetration measurement [16].

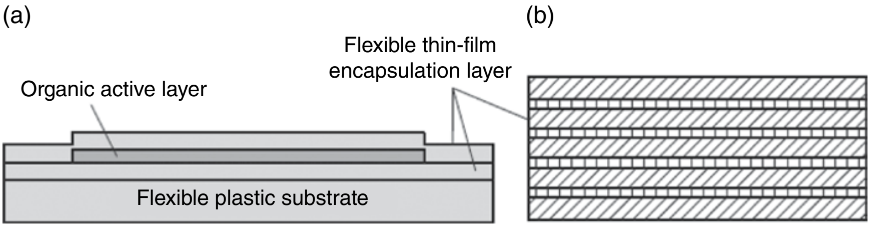
(a)
(b)
Flexible thin-film encapsulation layer
Organic active layer
Flexible plastic substrate

Figure 8.6 (a) Schematic of flexible thin-film encapsulation of organic electronics, and (b) Structures of transition organic/inorganic alternating multilayer encapsulation

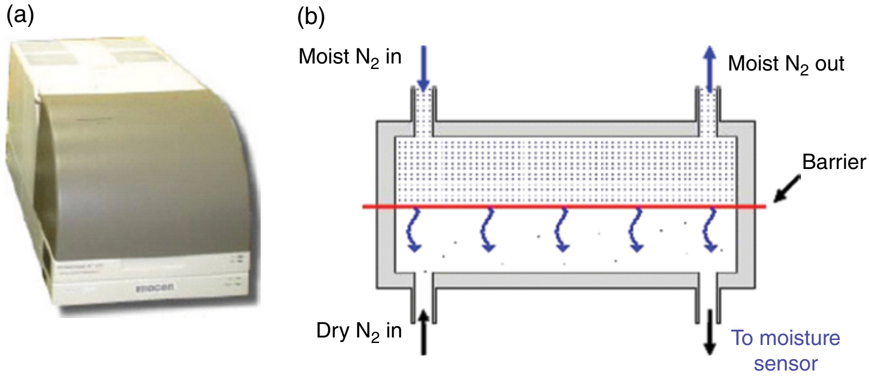

Figure 8.7 (a) Permatran-W water/oxygen penetration measurement instrument from Mocon and (b) The measurement principle. (Adopted from [16] with courtesy)

The sample to be measured is located between the dry and wet chamber. The dry chamber side is ventilated with nitrogen, while the wet chamber side is ventilated with wet nitrogen or placed with a wet sponge. Water from the wet chamber penetrates into the dry chamber via the sample film and arrives at the water sensor, which is an infrared sensor that generates an electronic signal by detecting the adsorption of infrared by water molecules. The electronic signal is proportional to the concentration of water. This measurement method is simple and fast, but has a detection limit of about 5×10^{-5} $g\cdot m^{-2}\cdot d^{-1}$ to water, which is not quite enough to measure the required WVTR of 10^{-6} $g\cdot m^{-2}\cdot d^{-1}$for OLED encapsulation.

A simple method to detect water/oxygen penetration in OLED encapsulation is the Ca film erosion measurement. Ca is an active metal and will react with water and oxygen in the following processes:

$$2Ca + O_2 = 2CaO$$

$$Ca + 2H_2O = Ca(OH)_2 + H_2$$

As reported in literature [14], less than 5% percent of the penetrated oxygen can react with Ca. Therefore, the method is mainly for evaluating the penetration of water rather than the penetration of oxygen. Since water and oxygen react with Ca simultaneously during the Ca erosion detection, the WVTR measured is not purely for water but an effective WVTR.

Quantification of Ca erosion is performed by measuring the conductivity of Ca film. Figure 8.8a shows the schematic of an experimental setup and Figure 8.8b shows the conductivity changes over the time. The effective WVTR can be calculated from the change of conductivity as a function of time using equation (8.4):

$$WVTR\left[\mathrm{g}/\mathrm{m}^2/day\right] = 2\delta_{Ca} \times \rho_{Ca} \times \frac{dG_s}{dt} \times \frac{M\left(H_2O\right)}{M\left(Ca\right)} \times \frac{Ca\_Area}{Window\_Ares} \tag{8.4}$$

where n is 2 for double molecule reaction, δc_a is resistivity coefficient ($3.4 \times 10^{-8} \Omega \cdot \mathrm{m}$), G is the conductivity of Ca, which is linearly dependent on time, and d(G)/dt is a constant. M (H_2O) and M (Ca) is the molecular weight of H_2O and Ca, respectively.

Another method to estimate the WVTR from Ca film erosion is by observing optical changes in Ca film, which becomes transparent after reaction with water. The degree of transparency is related to the content of H_2O reacted with the film, as shown in Figure 8.9. By comparing and analyzing the ratio of the transparent region (erosion region), the amount of water penetrated and penetration rate can be estimated. The detection limit of this method can reach $10^{-7} \mathrm{g} \cdot \mathrm{m}^{-2} \cdot \mathrm{d}^{-1}$ as reported [14,18]; despite this, large errors may occur because the transparent and non-transparent regions are difficult to quantify. Nevertheless, it is a popular method used in OLED application due to its simplicity.

The uncertainty in quantifying WVTR is the fact that local property of Ca film will change after absorbing water/oxygen, which has an effect on the transparency of film. Therefore, the transparency may not be linearly dependent on the amount of water absorbed. If the mass change of Ca film can be precisely weighed after absorbing water, it may be possible to work

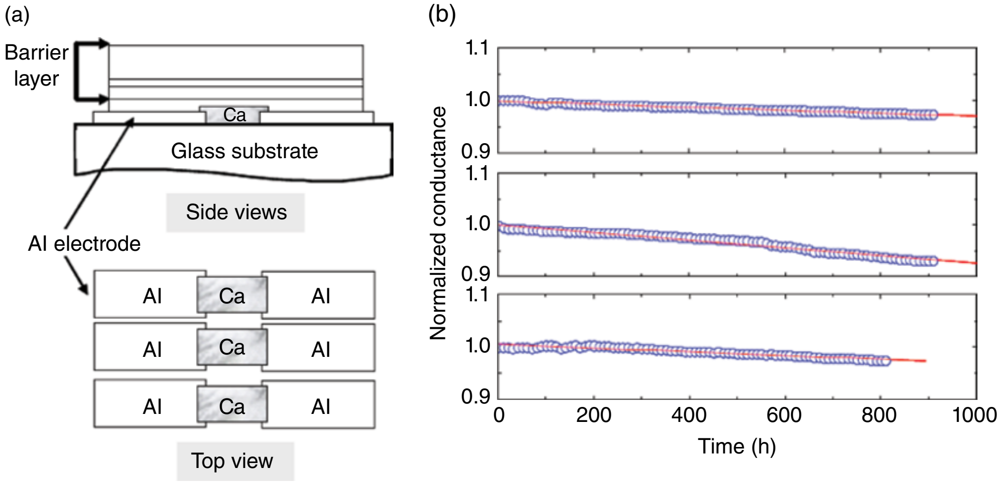

Figure 8.8 Ca erosion method to measure water penetration. (a) Schematic of experimental setup, and (b) Normalized curve of conductivity change with time [17]. (Reprinted from reference [7] with permission from AIP Publishing LLC)

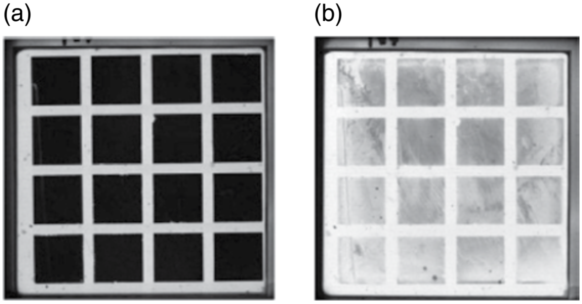

Figure 8.9 Water penetration measured by the optical change of Ca film (a) before water erosion and (b) after water erosion. (Adopted from [17] with courtesy)

out the amount of water absorbed, hence the accurate value of WVTR can be evaluated. However, the change of mass is very minute, usually in nanogram range, which is difficult to weigh even with a microbalance. A new weighing method has been developed at the authors' Printable Electronics Research Center to precisely quantify the WVTR, based on the principle of quartz microbalance. The measurement procedure is firstly to deposit a layer of Ca film at the center of a quartz monitor crystal and put the quartz crystal into a chamber similar to the one shown in Figure 8.7b. Instead of measuring the penetrated water by an infrared sensor, the Ca coated quartz crystal is used to absorb the penetrated water. The increased mass of quartz crystal due to the absorbed water in the Ca film can be detected precisely by a quartz microbalance, which detects the change of vibration frequency caused by the mass change of the quartz crystal. A frequency change as small as 0.1Hz can be detected, which corresponds to a mass change of 0.1ng, and is good enough to quantify the WVTR for OLED encapsulation.

8.4 Thin-film Encapsulation Technology

Commercial OLED lighting and display panels use glass or metal lids and edge seal with epoxy to encapsulate, in combination with desiccants such as CaO or BaO sealed inside, to prolong the lifetime of OLEDs [4,18,19]. However, this method is costly and has low throughput. Moreover, epoxy sealing is insufficient to block water/oxygen penetration without the aid of desiccants (or getter). Glass lids also increase the panel thickness, making the lighting or display unit heavy, and it cannot be used for flexible lighting and display devices. For flexible devices, the glass substrate and top glass lid can be replaced by plastic films. However, the plastic films must have water/oxygen blocking ability.

Thin-film encapsulation (TFE) can significantly reduce the thickness, saving about 50% of the encapsulation cost, is fully compatible with flexible organic electronics and can be integrated into OLED or OPV fabrication processes. Figure 8.10 compares three types of encapsulations for OLED. Considering that flexible OLEDs and OPVs represent the future trend in development with great market potential, thin-film encapsulation technology will be in high demand. Even the conventional rigid OLEDs or OPVs can be benefit from TFE technology with reduced weight, simplified process and lower cost.

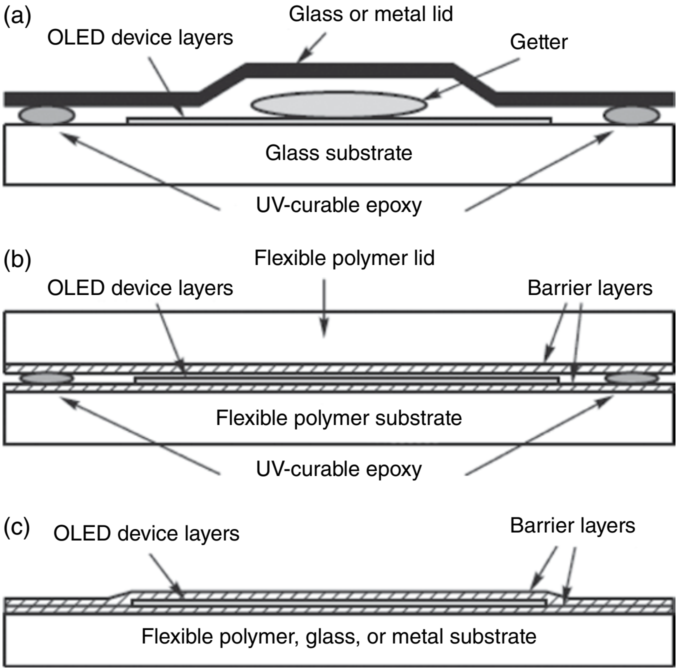
(a)
OLED device layers
Glass or metal lid
Getter
Glass substrate
UV-curable epoxy
(b)
Flexible polymer lid
OLED device layers
Barrier layers
Flexible polymer substrate
UV-curable epoxy
(c)
OLED device layers
Barrier layers
Flexible polymer, glass, or metal substrate

Figure 8.10 Methods of OLED encapsulation: (a) Traditional rigid encapsulation; (b) Flexible encapsulation, and (c) Thin-film encapsulation. (Reprinted from reference [4] with permission from AIP Publishing LLC)

8.4.1 History of Thin-film Encapsulation

Encapsulation is widely used in various fields, such as food packaging, drug capsules, medical equipment coating, and electronic packaging. Encapsulation materials are divided into rigid and soft types. The most popular encapsulation material is paper and plastic. Plastic thin-film encapsulation is thin, lightweight, transparent, easily shapeable, insulating, as well as wet and acid/alkali resistant, and so forth. However, conventional plastic thin films have limited ability to block water and oxygen, as described in previous sections of this chapter.

In the mid twentieth century, researchers found that depositing a thin layer of inorganic film on plastic surface under vacuum conditions could significantly improve the water/oxygen blocking ability [20,21]. Initially, they only deposited aluminum on the surface of plastic film, which is like aluminum kitchen foil but much thinner and flexible. In the 1980s, with increased demand such as transparency and suitability for microwave heating in food encapsulation, transparent thin oxides such as SiO_x, SiN_x and AlO_x were used as the barrier layer and soon gained importance [21–23]. Nowadays, coating oxide on plastic has become the mainstream thin-film encapsulation technology. Normal PET has the WVTR around $0.5 g \cdot m^{-2} \cdot d^{-1}$. A thin layer coating of oxide can improve the blocking ability of PET film over 100–1000 times.

8.4.2 Single Layer Thin-film Encapsulation

As aforementioned, a single layer oxide on PET can improve its blocking of water/oxygen significantly. However, the blocking ability is highly dependent on the quality of oxide layer. The quality of the oxide layer varies greatly with different deposition processes. Major deposition methods include physical vapor deposition (PVD), plasma-enhanced chemical vapor deposition (PECVD), atomic layer deposition (ALD) and plasma-enhanced atomic layer deposition (PEALD), with the PECVD and ALD-based Si-O-N and Al-O-N precursor systems being the widely used processes.

The most promising single layer encapsulation is Al_2O_3 deposited by ALD [12,24–26]. The film deposited by ALD is dense and has fewer defects. Moreover, it can evenly cover on the surface at a fairly low temperature. The WVTR of 25 nm Al_2O_3 deposited by ALD has reached 1.7×10^{-5} $g\cdot m^{-2}\cdot d^{-1}$ [27]. A pentancene/C_{60} activated OPV with 200 nm Al_2O_3 deposited by ALD can have lifetime of 6000 h [28]. A top emission OLED with a single layer of Al_2O_3 deposited at 100°C by ALD is reported to have a lifetime of 1000 h at 85°C with 85% humidity, which is the best result for a single layer encapsulation [29]. However, what restricts ALD from being widely adopted for encapsulations is its slow deposition rate (a few nanometers per minute), which is not the best choice for low cost and large-scale encapsulation.

The PECVD method is better than the ALD method because it has a fast deposition rate; 100 times faster than that of ALD. The commonly used material deposited with PECVD is SiO_x and SiN_x, and low temperature deposition is available with this method, which can meet the demands of organic electronic device encapsulation. Consequently, it receives great attention [30,31]. Huang et al. (2003) reported that the lifetime of OLED encapsulated with a single layer SiN_x is 600 h, while the lifetime of an unencapsulated device is only 6 h [32]. Recently, SiO_x:H film made by PECVD demonstrated better barrier property. The process uses HDMSO and O_2 gases as the precursors. The film contains SiO_2 and silicone and the lifetime of encapsulated OLED reached 7500 h at 65°C under 85% humidity [28].

Other single layer encapsulations are also reported besides the popular PECVD and ALD. For example, Jung, et al. reported tetratetracontane (TTC) encapsulated OTFT with lifetime at room temperature of about 40 days [33]; Cho, et al. reported the lifetime of OTFT encapsulated with SnO_2 deposited by IBAD [34]; others reported that by coating a layer of TiO_2 as a passivation layer [35], the lifetime of device based on P3HT and PCBM was improved to 500–2000h. Unfortunately, the above encapsulation technologies are still short of the 10000 h in lifetime required by industry.

8.4.3 Multilayer Thin-film Encapsulation

Multilayer film encapsulation is the combination of multiple single layer encapsulations. In the case of the double layer encapsulation process, the film consists of two different barrier layers with two different materials or deposition methods. Inorganic double layers such as Al_2O_3 and ZrO_2 structure deposited by ALD, or SiO_2/Al_2O_3 double layers, showed good barrier performance [36,37]. Due to the fact that the deposition rate of ALD is too slow, Kim et al. combined PECVD with ALD for fast deposition with PECVD and slow deposition with ALD of SiO_x film to encapsulate pentancene/C_{60} based OPV and obtained a lifetime of 6000 h, which achieved the WVTR of 10^{-5} $g\cdot m^{-2}\cdot d^{-1}$ examined by Ca film erosion method.

Multilayer film combining inorganic layers with organic layers has been widely used for encapsulation [4,38–42]. High performance encapsulation is achieved by blocking the water/oxygen penetration channels caused by the defects in inorganic layers with organic layers. As schematically shown in Figure 8.11, even the size and density of defects are similar in each inorganic layer, the water/oxygen penetration distance and time through the film is greatly increased because of the existence of organic interlayers. The organic/inorganic pair (dyad) can be stacked up. For more than three dyads of multilayer film, the water/oxygen blocking ability can be improved to 3–4 orders of magnitude and the WVTR can easily reach below 10^{-4} $g \cdot m^{-2} \cdot d^{-1}$. The exact blocking capability depends on the quality of the inorganic layer, the smoothness of the organic layer and the interface between organic and inorganic layers. The simulated result indicates that the thinner the organic layer the better on the basis that it forms for a uniform layer, while the number of the organic/inorganic pair (dyad) should be less than 5, as the WVTR shows no further improvement if the dyads exceed 5 [43].

Different inorganic/organic multilayer film structures have been proposed. Chen et al. reported a SiO_x/SiN_x/parylene layer structure and achieved WVTR of 2.5×10^{-7} $g \cdot m^{-2} \cdot d^{-1}$at room temperature under 45% humidity [40]. GE developed a gradient blocking structure by the PECVD method deposited at 55°C, as shown in Figure 8.12, where a flexible organic

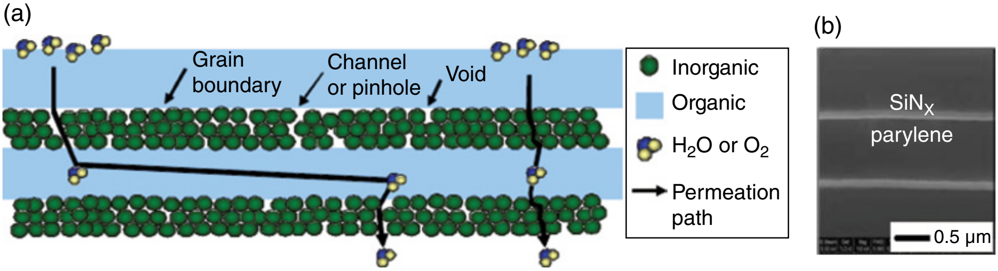

Figure 8.11 (a) Mechanism of the water/oxygen penetration path of a multilayer structure; (b) the cross-section image of multilayer composed of SiNx and parylene. (Reprinted from reference [43] with permission from Elsevier)

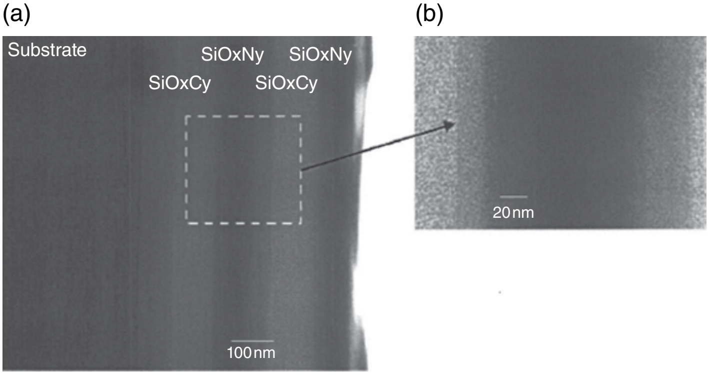

Figure 8.12 TEM image of a gradient barrier structure developed by GE. (Reprinted from reference [45] with permission from Elsevier BV)

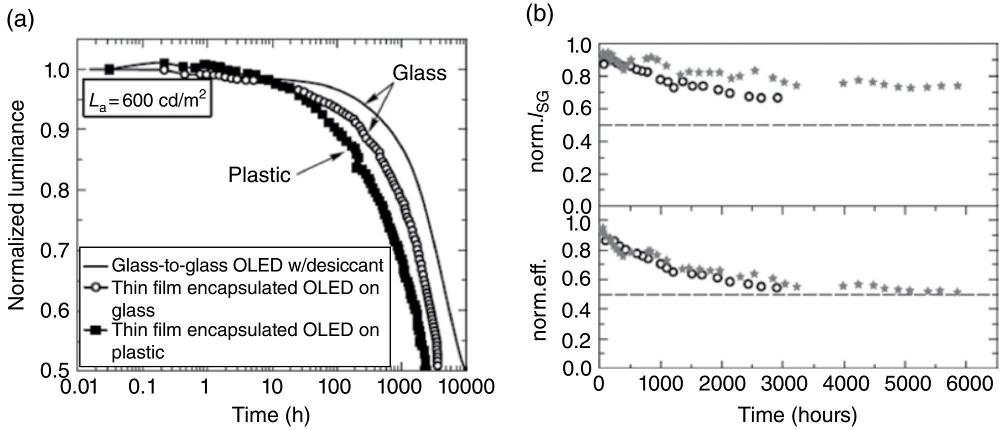

Figure 8.13 (a) Normalized lifetime of phosphorescence OLED encapsulated by traditional glass encapsulation with glass substrate, thin-film encapsulation with glass substrate, thin-film encapsulation with blocking plastics substrate (Reprinted from reference [42] with permission from AIP Publishing LLC); (b) Normalized lifetime of OPV encapsulated with thin film. (Reprinted from reference [45] with permission from AIP Publishing LLC)

silicon couplet SiO_xC_y was fabricated with organosilane in the process at Ar atmosphere with a pressure lower than 10 Pa, while the inorganic film of SiO_xN_y was fabricated in NH_3 and O_2 atmosphere with 2% silane (in He flue) under 100–500 Pa. The WVTR of this blocking structure reached 5×10^{-6}~5×10^{-5} $g{\cdot}m^{-2}{\cdot}d^{-1}$. A hybrid of Al_2O_3 by ALD and Parylene C by CVD is also an option to make an inorganic/organic multi-layer encapsulation.

The lifetime of organic electronic devices encapsulated with a multilayer structure can be improved, compared to those encapsulated with single-layer structure. Chwang et al. reported the lifetime of about 2500 h for multi-layer encapsulated flexible OLED, approaching the lifetime of same device encapsulated with traditional glass plate, as compared in Figure 8.13a [42]. The multilayer film is composed of 4–5 dyads of Al_2O_3/polycarbonate with a total thickness of about 5–7 μm. An MDMO-PPV device encapsulated with the above film gained a lifetime of 3000 h. A P3HT based OPV encapsulated with this structure gained a lifetime of 6000 h, as the lifetime curves shown Figure 8.13b [45].

8.4.4 Barix™ Thin-film Encapsulation

The first flexible organic/inorganic alternating encapsulation film structure was reported by Affinito et al. at Pacific Northwest National Laboratory in 1996 [46]. The deposition of the organic layer includes vapor condensation and film polymerization, by which liquid monomer is first vaporized under vacuum conditions and condensed over the surface of substrate, which is then cured under UV illumination to form a film. It was found that the surface of the film obtained from UV photo polymerized monomer under vacuum conditions was very smooth and almost defect-free, enabling a high quality inorganic layer (AlO_x) deposition over the organic layer. Repeating the organic and inorganic layer deposition, a multilayer film structure can be formed, as the cross-section shown in Figure 8.14a. Barix™ is the name given to this combination of inorganic/organic alternating layer structure and it is extremely effective in

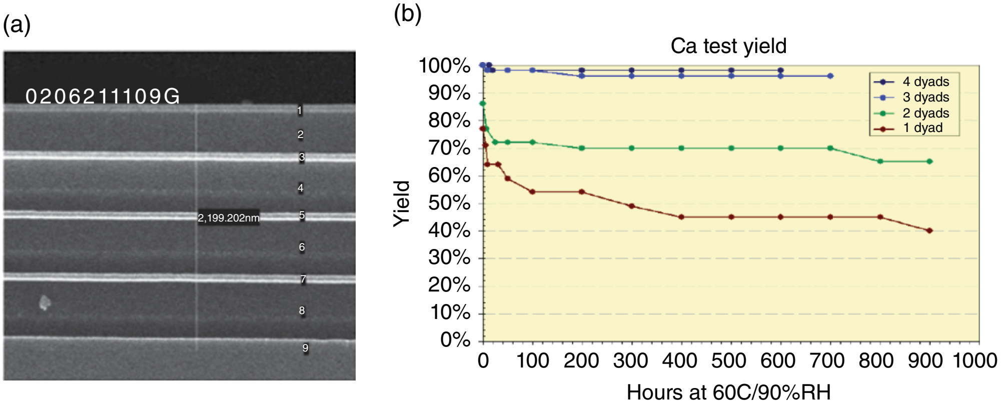

Figure 8.14 Barix™ encapsulation: (a) Multilayer structure with RF sputtering deposited AlOx and UV photopolymerized monomer; (b) Protection effect to Ca film with a different alternative layer structure. (Reprinted from reference [48] with permission from Elsevier Ltd)

blocking water vapor penetration. Figure 8.14b shows the Ca test results with different dyads of Barix encapsulation films. The WVTR of 4 dyads film was measured at 10^{-6} $g{\cdot}m^{-2}{\cdot}d^{-1}$ by Ca absorption test. The Barix™ technique was later commercialized by US company Vitex and it is now the most widely used technique in flexible film encapsulation.

Though very effective, Barix technology still faces great challenges. Defects in sputtered AlOx film are unavoidable. It is reported that Vitex has substituted sputtered AlOx by the PECVD process. Samsung is using Vitex's multilayer encapsulation technology currently, which is very slow and a panel has to enter the deposition chamber six times. In addition to the slow process, the cost of ownership is also a matter of concern. Even an R&D system can cost a few million US dollars. Encapsulation is a major factor in the overall cost of OLED manufacture and this cost is the primary hindrance to the widespread commercialization of OLED display and lighting.

8.4.5 Thin Film Deposition Methods

Good encapsulation relies on good quality of thin films. Considering the constraints imposed by the properties of organic electronic materials and flexible substrate materials, there are not many thin-film deposition methods that are suitable for depositing organic and inorganic thin films for the encapsulation purpose. The following are the most commonly used deposition methods.

8.4.5.1 PECVD

PECVD is a well-established high quality film deposition method. SiO_x and SiN_x films deposited by this technique are dense. The deposition rate is high and the adhesion to the substrate is good. There are plenty of literatures reporting on PECVD technology. However, conventional PECVD usually relies on high deposition temperature to achieve good quality films. The deposition temperature is usually around 300–500°C. Films deposited at temperatures

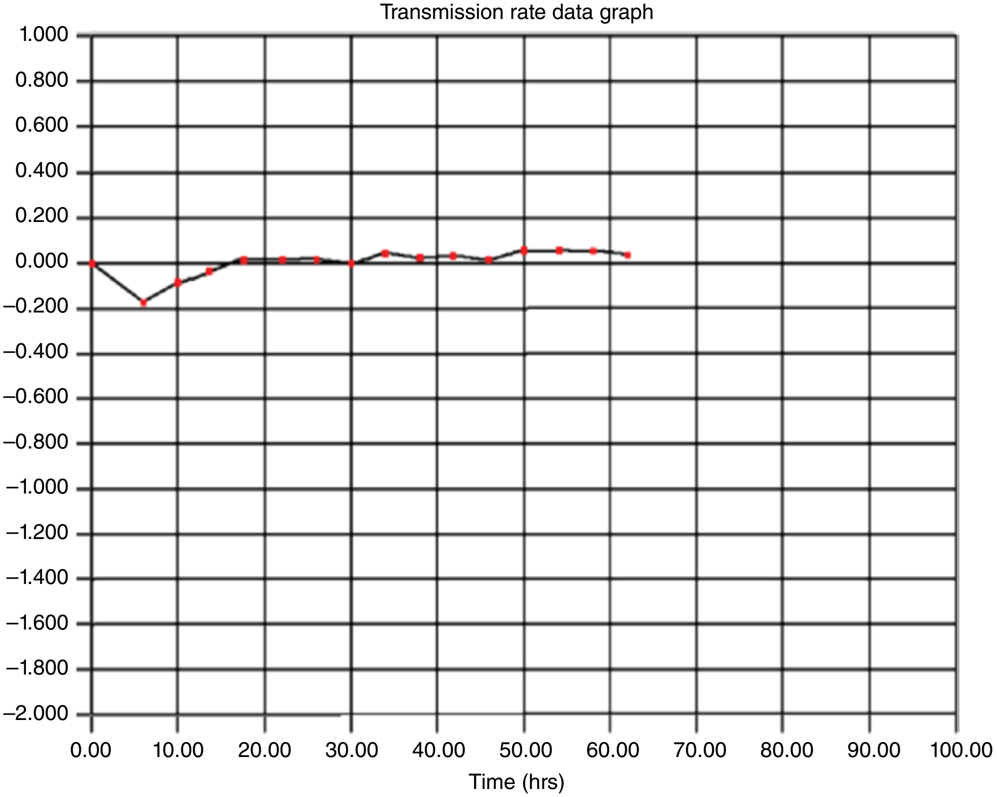

Figure 8.15 The WVTR of a 4 dyad $SiO_x/SiO_xC_yH_z$ structure on PET substrates at 3.6×10^{-5}g/m^2/day achieved at PERC

below 200°C are loose and have an abundance of defects. New PECVD technology with inductively coupled plasma, called ICP-PECVD, can solve this problem. The density of electrons generated by ICP can reach as high as 10^{11} and films deposited from ICP-PECVD are dense even at temperatures below 120°C. High density SiNx or SiNOx inorganic layers can be deposited with N_2 or NH_3 precursor gases. An organosilicon layer can be deposited with HMDSO or TEOS as precursor under Ar/He atmosphere. Both inorganic and organic layers can be deposited in the same plasma chamber by using different precursor gases. A composition gradient structure can also be obtained by adjusting the ratio of mixed gas dynamically.

The above process has been realized at the authors' Printed Electronic of Research Centre (PERC). By combining ICP-PECVD with HMDSO as precursor, inorganic and organic layers have been deposited in the same plasma chamber and the deposited layers have a gradient composition similar to those shown in Figure 8.12. WVTR of 3.6×10^{-5}g.m^{-2}.d^{-1} has been achieved at PERC with 4 dyads layer with thickness of 1.5 μm and the result is shown in Figure 8.15. Normally, the inorganic layer alone at such thickness is brittle and lacks flexibility. The new process blends the organic and inorganic hybrid materials in gradient, which ensures the blocking property as well as good flexibility.

8.4.5.2 ALD

An atomic layer deposition (ALD) is basically a chemical vapor deposition (CVD). Different from conventional CVD process, the precursor and reaction gases arrive at the substrate surface not simultaneously but alternatively in ALD process and react with each other to form the film. The deposition process is a switching between saturation adsorption and reaction processes. The switching of precursor and reaction gases is realized by fast mass flow controllers with the pulse about 0.015s. The film obtained by this method is very dense and almost defect-free. Considering that the reactivity of a precursor is related to temperature, although the film can be deposited at room temperature, a high reaction temperature can shorten the reaction time. For example, to react with a monolayer of water molecules takes 60s at 80°C, 40s at 150°C, 16s at 200°C, 10s at 250°C and 6 s at 300°C. The thickness (0.1 nm) of each atomic layer is almost irrelevant to temperature. The molecular bond length and angle together with the quality of films deposited at different temperatures are almost same. However, the lower the reaction temperature, the slower the complete desorption, and the longer the evacuation time to remove the residual molecules of the previous cycle. Incomplete removal of unreacted gases can lead to defects or low density film. In general, high temperature deposition is beneficial to completely remove the residuals and to obtain high quality film.

Because of its high quality film and highly conformable deposition, ALD technology is developing rapidly in recent years and has found applications in many fields. However, the deposition rate, which is only a few nanometers per minute, is a disadvantage for thin-film encapsulation. Plasma-enhanced ALD and fast ALD have recently been developed. For a similar quality of film, the deposition rate of fast ALD has improved an order of magnitude, though it is still slower than PECVD.

8.4.5.3 Parylene Deposition

Parylene deposition is a polymer coating developed by Union Carbide in the mid-1960s. It is a family of polymers derived from p-xylene. Parylene is divided into N, C, D and HT types, according to their molecular structures. Parylene can be deposited by vacuum chemical vapor deposition at room temperature and can be coated on the surfaces of various shapes, including sharp edge, inner part of the crack and inner surface, with uniform thickness ranging from 0.1 to 100 μm. The film is dense, transparent, pinhole-free and stress-free, additives-free and does not harm a coated surface. It also has excellent electric insulation property and protective property. It is one of the most effective moisture-proof, mold-proof, corrosion-preventing and salt-proof coatings.

C type parylene can be used as organic interlayers in multilayer film encapsulation, as it has a smooth surface and good adhesion. The deposition system is schematically shown in Figure 8.16. It is deposited at room temperature with a high deposition rate and has been used to form a protection layer in organic electronic encapsulation. For example, deposition of an organic layer by PECVD may damage the active layer in an organic electronic device because of the ion bombardment from plasma. Deposition of 300 nm parylene C as the first layer can avoid the damage as well as eliminate trace amounts of oxygen on metal electrode.

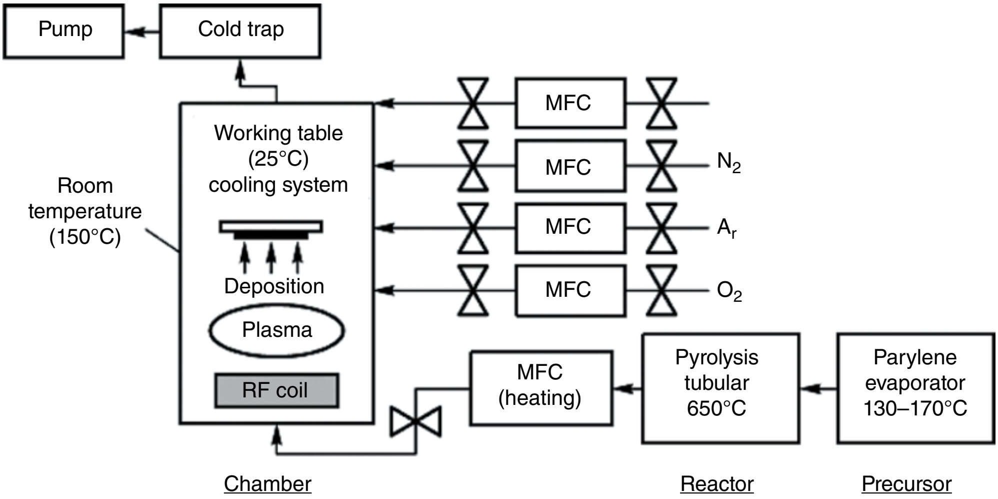

Figure 8.16 Schematic of a parylene CVD system. (Adopted from web with courtesy to its origin)

8.4.6 *Flexibility of Encapsulation Thin Film*

In addition to the water/oxygen blocking ability, the encapsulation layer should also have sufficient flexibility to avoid the occurrence of cracks when subject to bending. Normally, inorganic layers in encapsulation film lack the flexibility, not only because of the brittleness of inorganic material itself but also because of some internal stress built up during deposition, although they have the best water/oxygen blocking property. Once cracks are formed, the barrier property of an encapsulation layer will deteriorate rapidly.

The cracks are hardly detectable in the transparent thin film after it is bent and deformed, even with an optical microscope. An effective detection method is to deposit a thin layer of Ca between the substrate and encapsulation layer. If cracks happen after bending, the Ca layer at the location of the cracks will absorb water molecules and change its color to become visible under an optical microscope, as shown in Figure 8.17 [48].

To quantitatively define the flexibility of the encapsulation film, control bending is performed to measure at what bending radius the cracks occur in the film. Figure 8.18 shows an apparatus for the bending test. Grego et al. (2007) reported X-Y-θ bending tests performed on a 130 μm thick PEN film deposited with a single inorganic SiN_xO_y layer and with an organic/inorganic multilayer respectively [49]. Figure 8.19a is the principle of X-Y-θ bending and Figure 8.19b gives the test results, which are the crack density vs. bending radius. Experimental results revealed that the cracks occur when the bending radius of a single SiN_xO_y layer is about 7 mm, whereas the bending radius for the inorganic/organic composite layer is 5 mm, indicating that the addition of an organic polymer layer can improve the flexibility of encapsulation film. In practice, the bending property of an encapsulation film is measured by how many times it bends at a specific bending radius the film can endure before its water/oxygen blocking ability degrades.

Regarding film stress, there are mainly two types of stresses, compressive stress and tensile stress, when a thin film is subjected to bending, as illustrated in Figure 8.20. The outer surface

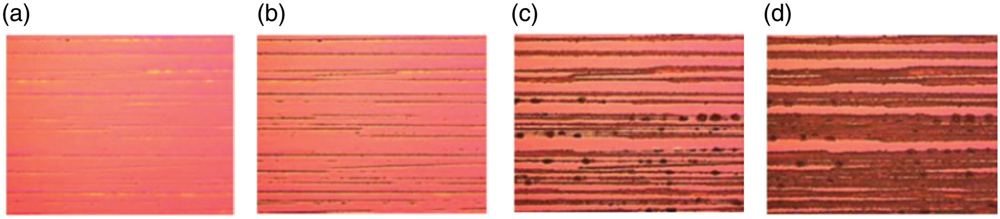

Figure 8.17 Optical image of Ca coated encapsulation film after rolling for (a) 1 minute, (b) 10 minutes, (c) 30 minutes and (d) 60 minutes, respectively. (Reprinted from reference [47] with permission from Elsevier S.A.)

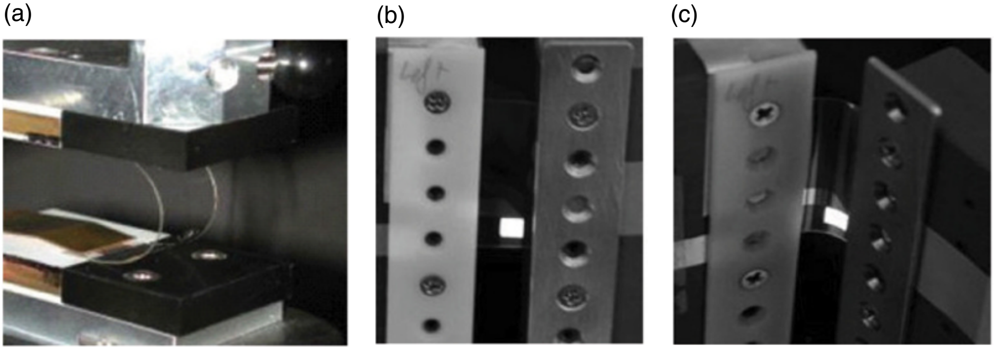

Figure 8.18 (a) Measurement apparatus of flexible structure based on two-point bending; (b) and (c) X-Y-θ bending of a flexible light emitting OLED. (Reprinted from reference [48] with permission from Elsevier S.A.)

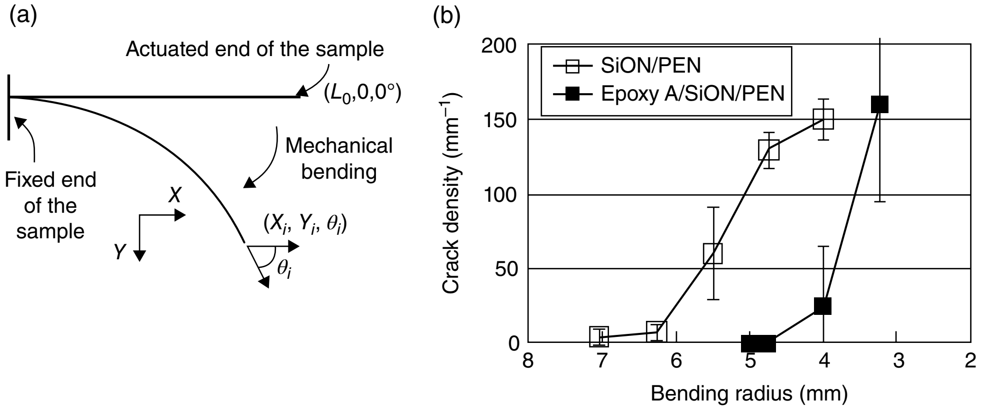

Figure 8.19 (a) Schematic of X-Y-θ bending measurement; (b) Comparison of flexibility tests for single inorganic layer and inorganic/organic composite layer of film. (Reprinted from reference [48] with permission from Elsevier S.A.)

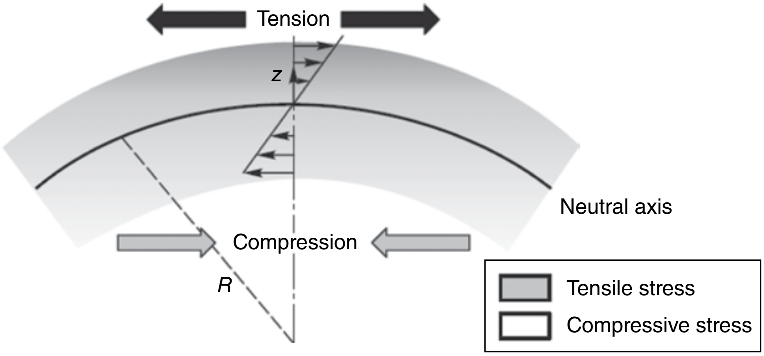

Figure 8.20 Schematic of stress condition of a bending thin film. (Reprinted from reference [48] with permission from Elsevier S.A.)

is stretched by tensile stress and the inner surface is squeezed by compressive stress, while leaving the central axis at minimum stress. For multilayer thin-film structures the distribution of stress should be taken into account to avoid possible damages due to bending.

8.4.7 Trends of Thin-film Encapsulation

There is a general consensus that the alternating organic/inorganic multilayer coating is the best option for thin-film encapsulation both for its barrier property and for its flexibility. However, one must pay attention to the fact that the encapsulation property is crucially related to the material used and how the material is coated for each layer. For inorganic materials, SiOx, SiNx and Al_2O_3 are widely used and the deposition methods include physical vapor deposition (PVD), chemical vapor deposition (CVD), plasma sputtering and atom layer deposition (ALD).

As most of the organic function layers of OLED and OPV have T_g lower than 150°C, any deposition methods should not cause the temperature of film to be higher than 120°C. ALD can deposit very dense film at low temperatures, however, at the expense of extremely slow deposition rate. For example, ALD takes about 10 minutes to grow a 1 nm thick Al_2O_3 layer at a reaction temperature of 80°C. Although ALD producers such as Beneq are developing a fast ALD system, its deposition rate still cannot compete with high plasma density PECVD, which can achieve high density pinhole-free thin film at a deposition rate of hundreds of nanometers per minute. In general, ICP-PECVD should be the first choice when considering encapsulation deposition techniques. ALD can be used as a supplementary method to deposit only tens of nanometers of a super high quality Al_2O_3 layer. As for the inorganic materials deposited by ICP-PECVD, SiNx or SiOxNy is better than SiOx.

A new development in encapsulation technology is the tera-barrier film developed by the Institute of Materials Research and Engineering (IMRE) in Singapore. With this method, the inorganic layer is deposited by PECVD. In between the inorganic layers, the organic layer is replaced by a layer of nanocrystals coating that can capture water/oxygen molecules and simultaneously repair defects in the inorganic layers. The WVTR of new film structure was reported to reach 10^{-6} $g.m^{-2}.d^{-1}$ [50]. Although attractive, the nanocrystals layer may reach saturation gradually if too many water molecules are absorbed with the accumulation of time, which would weaken its barrier property and shorten the lifetime of organic electronic devices.

8.5 Applications of Thin-film Encapsulation

8.5.1 Encapsulation of Flexible OLED

The previous sections have described various aspects of thin-film encapsulation technology. In this section, the gradient multilayer encapsulation process developed by GE [51] is introduced as an example to further explain how flexible OLED is made with encapsulation.

The gradient "multilayer" film encapsulation was briefly introduced in section 8.4.3. It is an organic/inorganic gradient structure (Figure 8.12) deposited by PECVD at 55°C with organosiloxane as a precursor. Different film structures can be obtained depending on the deposition atmosphere and precursors. Organosilicon SiO_xC_y is deposited under Ar atmosphere. An inorganic SiN_x or SiO_x layer is deposited with 2 % silane (in He gas flow) under mixture of NH_3 and O_2. The pressure and sputtering power in the deposition chamber should be kept constant when depositing the transition layer, while the composition gradient of the film is achieved by continuously adjusting the mass flow of each gas component. GE also developed a roll-to-roll PECVD thin-film encapsulation system, as shown in Figure 8.21, which was able to deposit a gradient encapsulation layer on an 8-inch flexible substrate. The system adopted a face down deposition strategy to avoid particles dropping on substrate. The system could achieve high quality encapsulation with WVTR down to10^{-5} $g \cdot m^{-2} \cdot d^{-1}$ [52].

Once the encapsulation layers are prepared, the flexible PET substrate which has the ITO transparent conductive layer on the other side can be used to make OLED. The fabrication processes are as follows. The substrate is first fixed on a frame to ensure easy handling

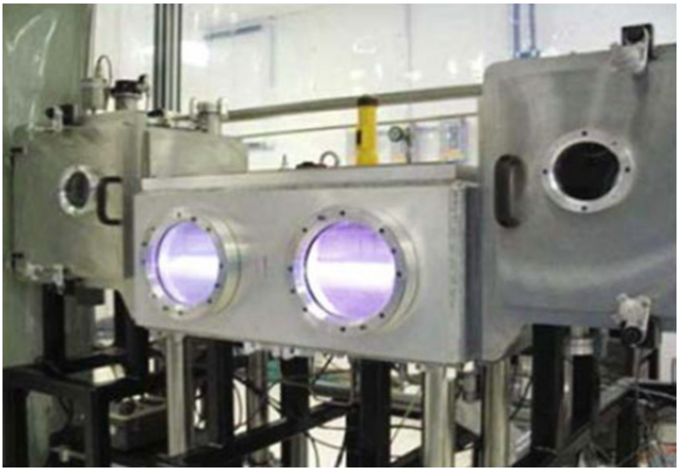

Figure 8.21 GE roll-to-roll gradient blocking layer PECVD equipment. (Reprinted from reference [51] with permission from Springer Science Business Media, LLC)

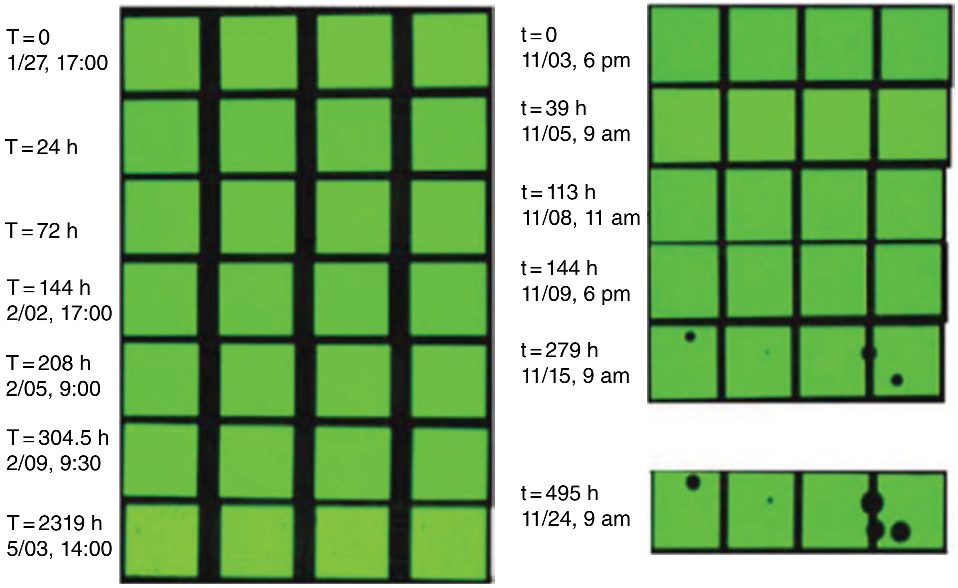

Figure 8.22 Lifetime measurement of light-emitting pixels from the UDC's OLED, (a) OLED on glass substrates, (b) OLED on GE barrier layer coated PC substrates. (Reprinted from reference [51] with permission from Springer Science Business Media, LLC)

during the batch process. The framed substrate is then washed with isopropanol, followed by ultrasonic treatment with alcohol for 10 minutes, and finally washed with deionized water and dried. The ITO layer is patterned by photolithography and etching to form OLED anode electrode. The functional layers of OLED are prepared by first coating a water-soluble PEDOT:PSS on the ITO anode and heated at 110°C; subsequently a polymer light-emitting material, LUMATION*1304, dissolved in xylene is coated to 70 nm thickness and heated for 10 minutes. The electron injection layer of NaF with a thickness of about 1 nm is vacuum deposited. Finally, an aluminum cathode electrode is deposited by vacuum thermal evaporation with the aid of a metal shadow mask. The device is encapsulated with an Al foil and sealed by acrylic adhesive in a glove box.

It has been proved that the encapsulation layer can endure the above OLED fabrication processes without causing any damages. Universal Display Corporation (UDC) fabricated a small molecular OLED with a flexible encapsulated PC substrate provided by GE under standard device fabrication process, and compared with the same OLED on a glass substrate. The measured lifetime results at 60°C and humidity of 85% are shown in Figure 8.22. Most of the light-emitting pixels are undamaged except individual dark spots; the lifetime of the device based on the PE substrate is about 80% of that based on glass substrate (Figure 8.23). These results confirm that the flexible water/oxygen blocking layer is compatible with both polymer and small molecular OLED fabrication processes.

At the authors' Printable Electronics Research Center, OLED encapsulation experiments were carried out using two different approaches, one with single layer Al_2O_3 thin film of 50 nm deposited by ALD and another with 3 dyads Al_2O_3 (50nm)/Parylene C (500nm) alternating

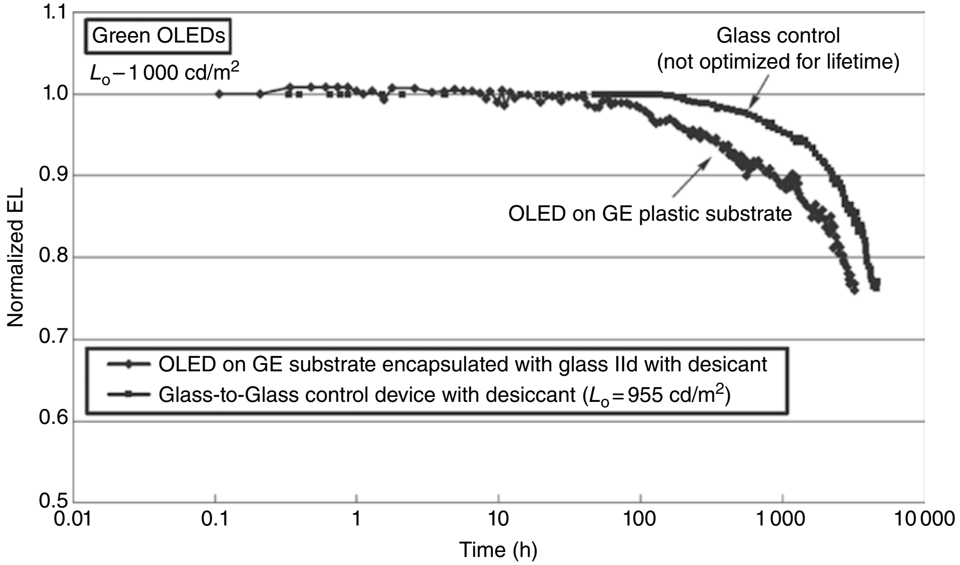

Figure 8.23 Comparison of lifetimes for glass and encapsulated plastic OLEDs. (Reprinted from reference [51] with permission from Springer Science Business Media, LLC)

barrier layers deposited by ALD and CVD. For comparison, an OLED with a glass lid for encapsulation (edge sealed by UV cured glue) was also fabricated. All three types of OLED devices were using ITO/glass as substrates and they were exposed to the atmosphere after deposition and before encapsulation. Figure 8.24 shows the lifetime test results by the visual images of their light emission. In the glass lid encapsulated OLED initial black spots started to grow in numbers over time (Figure 8.24a). In the single layer Al_2O_3 encapsulated device, an initial small black spot started to grow bigger and bigger over time (Figure 8.24b), which may come from a defect in the Al_2O_3 barrier layer during deposition. In the 3 dyads Al_2O_3 /Parylene C encapsulated OLED, no dark spots were observed throughout the entire test period (1000 h), proving that the organic/inorganic alternating multilayer barrier is the best encapsulation approach.

8.5.2 *Encapsulation of Flexible OPV*

Organic photovoltaic (OPV) is another major application requiring flexible encapsulation. Apart from the compatibility issue of an encapsulation layer with organic device fabrication processes, another concern is whether the water/oxygen blocking layer will bring an adverse effect to the device performance [8]. To investigate the effect, two types of multilayer encapsulation were performed on pentacene/C_{60} based OPV devices: the first layer in contact with the devices was SiO_x deposited by PECVD at 110°C, followed by parylene (CVD) and SiN_x(PECVD) alternating multilayers or Al_2O_3(ALD) and a C type parylene (CVD) hybrid. The OPV properties were obtained, based on the J-V of devices shown in Figure 8.25. The J-V curves were measured by Keithley amperemeter with a wide range Xe lamp (ASB-XE-175EX, CVI) as illumination source. The properties of OPV before and after multilayer encapsulation are shown in Table 8.1.

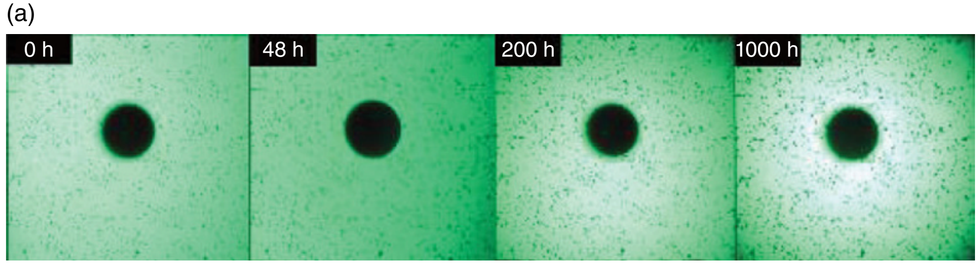

Glass lid encapsulation

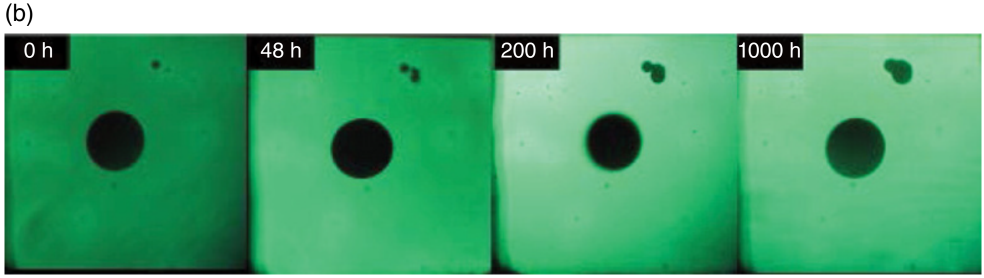

Single layer Al_2O_3 encapsulation

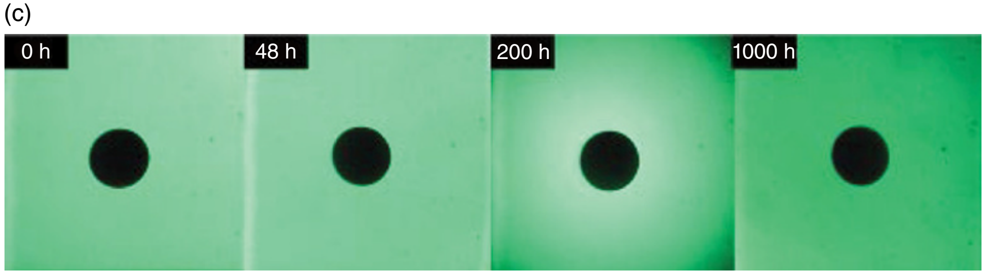

3 dyads alternating Al_2O_3/Parylene C encapsulation

Figure 8.24 OLED encapsulation experiments carried out at PERC

As seen in the Table 8.1, the V_{oc} of the encapsulated device increased slightly with the decrease of reverse saturation current density, which is consistent with the effect of annealing on J-V in OPV [24] caused by the PECVD deposition of the encapsulation layer at 110°C. As for the average efficiency of the nine group devices, the multilayer encapsulation showed detrimental effect.

For the hybrid of $Al_2O_3$and parylene C encapsulation, the number of layers were greatly reduced. Although the deposition rate of ALD is slower and the OPV is subjected to 110°C deposition temperature longer, there was no side effect caused by encapsulation observed besides the expected annealing effect, as is shown in Table 8.2.

Encapsulation has significant effect on the lifetime of OPV. For the pentacene/C_{60} OPV encapsulated by parylene (CVD) and SiN_x (PECVD) alternating multilayers, the lifetime curves are shown in Figure 8.26. The lifetime of unencapsulated OPV decaying to below 20% was 50 h and was totally dead after 8 days. The lifetime of one pair of SiN_x/parylene encapsulated device decaying to about 50% was 1000 h. With a further increase of the encapsulation pairs to two, the lifetime of the device improves two times. When the encapsulation pairs increased to three, the lifetime of the OPV device decaying to 90% was 7000 h. The

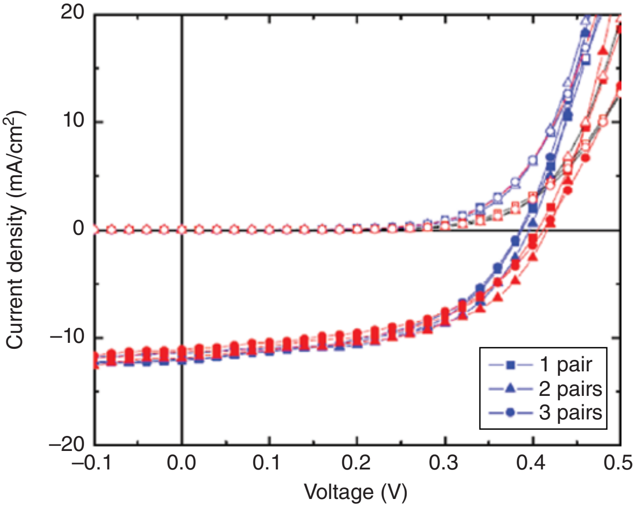

Figure 8.25 Optoelectronic properties of pentccene/C60 OPV before and after encapsulation. ○ represents dark current while ● represents light current. (Reprinted from reference [7] with permission from AIP Publishing LLC)

Table 8.1 Properties of OPV before and after multi-layer encapsulation

No. of layers (SiN_x/parylene)	Before encapsulation			
	η (%)	J_{SC} (mA/cm^2)	FF	V_{OC} (mV)
0 dyad	3.2 ± 0.0	11.6 ± 0.3	0.54 ± 0.01	387 ± 1
1 dyads	3.2 ± 0.0	11.6 ± 0.1	0.53 ± 0.01	385 ± 2
2 dyads	3.5 ± 0.1	12.7 ± 0.4	0.55 ± 0.01	399 ± 3
3 dyads	3.2 ± 0.1	11.9 ± 0.4	0.53 ± 0.01	385 ± 1
Average	3.4 ± 0.2	12.0 ± 0.7	0.54 ± 0.03	390 ± 4
No. of layers (SiN_x/parylene)	After encapsulation			
	η (%)	J_{SC} (mA/cm^2)	FF	V_{OC} (mV)
0 dyad	NA	NA	NA	NA
1 dyad	3.3 ± 0.0	11.1 ± 0.1	0.49 ± 0.01	407 ± 2
2 dyads	3.5 ± 0.1	11.8 ± 0.1	0.53 ± 0.01	410 ± 5
3 dyads	3.1 ± 0.1	11.1 ± 0.1	0.49 ± 0.01	408 ± 4
Average	3.3 ± 0.2	11.4 ± 0.5	0.52 ± 0.02	412 ± 7

corresponding Ca film measurement indicated that the WVTR of three pairs of encapsulation was $(7.3 \pm 0.5) \times 10^{-6}$ g·m^{-2}·d^{-1}.

The lifetimes of OPV devices encapsulated with $Al_2O_3$and C type parylene hybrid are shown in Figure 8.27. The results indicate that introducing high quality AlO_x dense film deposited by ALDenables the efficiency of encapsulated OPV to maintain nearly constant up

Table 8.2 Properties of OPV before and after hybrid encapsulation

No. of layers (SiN_x/parylene)	Before encapsulation			
	η (%)	J_{SC} (mA/cm^2)	FF	V_{OC} (mV)
w/o encapsulation	3.2 ± 0.0	11.6 ± 0.3	0.54 ± 0.01	387 ± 1
SiO_x/Al_2O_3/P	3.2 ± 0.0	10.4 ± 0.0	0.56 ± 0.01	392 ± 2
SiN_x/Al_2O_3/P	3.1 ± 0.1	10.4 ± 0.2	0.55 ± 0.01	394 ± 2
Average	3.2 ± 0.1	10.8 ± 0.4	0.55 ± 0.01	391 ± 3

No. of layers (SiN_x/parylene)	After encapsulation			
	η (%)	J_{SC} (mA/cm^2)	FF	V_{OC} (mV)
w/o encapsulation	NA	NA	NA	NA
SiO_x/Al_2O_3/P	3.3 ± 0.1	9.8 ± 0.1	0.53 ± 0.02	448 ± 2
SiN_x/Al_2O_3/P	3.5 ± 0.0	9.2 ± 1.0	0.54 ± 0.01	450 ± 7
Average	3.4 ± 0.1	9.5 ± 0.1	0.53 ± 0.01	449 ± 7

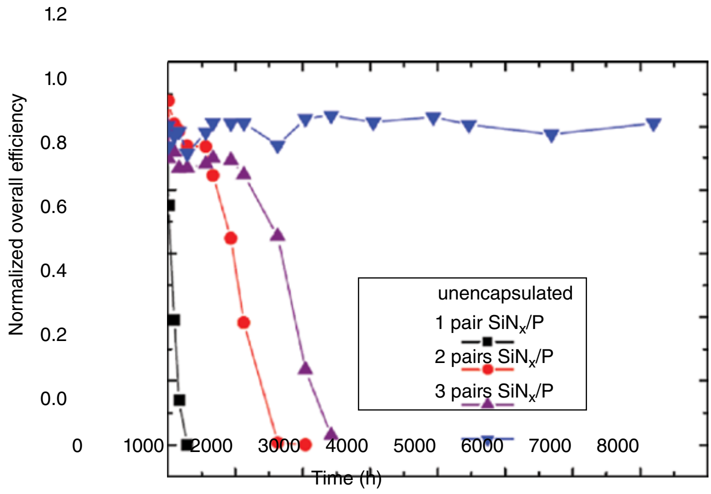

Figure 8.26 Lifetime of multilayer encapsulated pentccene/C60 OPV with different encapsulation units. (Reprinted from ref. [47] with permission from IEEE)

to 6000 h. However, the devices encapsulated with hybrid structures containing SiO_x started to decay after working for 7000 h. The reason for the decay was that a defect in the encapsulation layer generated after working over 6000 h. Water penetrated through the defect and accelerated the decaying process. It may be that a micro defect formed during the deposition of SiO_x and the interface adhesion strength is insufficient. The internal stress between soft

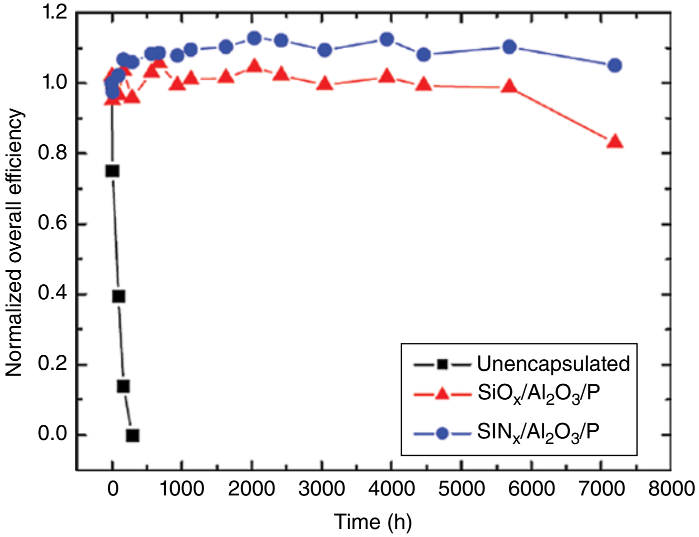

Figure 8.27 Lifetime of pentacene/C60 OPV encapsulated by hybrid structures. (Reprinted from reference [47] with permission from IEEE)

organic and rigid inorganic layers was built up after long time working, causing exfoliation and damaging the encapsulation.

The above results conclude that the efficiency and lifetime of a device encapsulated with SiN_x is better than that encapsulated with SiO_x. The reasons may due to the fact that the SiN_x film is denser than SiO_x film and has less defects than SiO_x film. It is also probably because an oxygen source is involved in the deposition process of SiO_x, which caused the slight degradation of device.

Generally, it is relatively easier to encapsulate OPV than to encapsulate OLED. Experimental results indicate that the encapsulation layer with a WVTR value of 10^{-5} $g{\cdot}m^{-2}{\cdot}d^{-1}$ will meet the demand of OPV encapsulation. The encapsulation process has no detrimental effects on the properties of OPV as long as the deposition temperature is controlled below 120°C. The inorganic film of SiN_x is more suitable for use in a water/oxygen blocking layer than SiO_x as far as the commonly used encapsulation method by PECVD is concerned. However, one must be aware that the CVD chamber for parylene deposition contains a certain amount of water/oxygen. If devices are encapsulated with CVD of parylene, the CVD chamber should be designed with water/oxygen removal measures, such as to have embedded CaO water-absorbent material. In addition, micro-sized defects generated during encapsulation can grow bigger with time and affect the encapsulation property in the later working life of the devices.

8.6 Summary

Organic electronic devices such as OLED, OPV and OTFT, whether made by vacuum deposition or solution deposition such as printing, cannot work or work longer without effective encapsulation to block water/oxygen. Accompanying the development of organic electronics, encapsulation technologies have evolved from traditional rigid cover plate encapsulation, rigid inorganic thin film encapsulation to the current flexible thin-film encapsulation. The encapsulation layer structures have advanced from the original single layer to a multilayer complex structure. Generally, a good encapsulation technology should have the temperature of blocking material deposition lower than 120°C, high water/oxygen blocking ability, be flexible, light, thin and low cost, which defines the direction of future development of this technology. The general consensus is that high density plasma PECVD is the best suitable process to deposit an inorganic SiOx or SiNx water/oxygen blocking layer, in terms of low deposition temperature, fast deposition rate and reasonably good quality of deposited layer. In addition, it is possible to deposit organic and inorganic alternating encapsulation layers in the same system.

The advantage of organic electronic devices such as OLED, OPV and OTFT is that they can be made on flexible substrates and may be possible to manufacture in roll-to-roll manner. Therefore, flexible encapsulation becomes an integral part of organic electronic manufacturing. Many companies worldwide have invested in flexible encapsulation technology and great progress has been made. The industry is further looking into simplifying the encapsulation process, increasing productivity and yield and lowering the cost of encapsulation, so that organic electronic devices can quickly enter the mass market.

References

[1] Aziz H, Popovic ZD. Chemistry of Materials. 2004;16:4522.
[2] Lee ST, Gao ZQ, Hung LS. Applied Physics Letters. 1999;75:1404.
[3] Popovic ZD, Aziz H, Hu NX, Hor AM, Xu G. Synthetic Metals. 2000;111:229.
[4] Lewis JS, Weaver MS. IEEE Journal of Selected Topics in Quantum Electronics. 2004;10:45.
[5] Aziz H, Popovic Z, Xie S, Hor AM, Hu NX, Tripp C, Xu G. Applied Physics Letters. 1998;72:756.
[6] Dennler G, Lungenschmied C, Neugebauer H, Sariciftci NS, Labouret A. Journal of Materials Research. 2005;20:3224.
[7] Kim N. Dissertation of Georgia Institute of Technology. 2009, 23.
[8] Roberts AP, Henry BM, Sutton AP, Grovenor CRM, Briggs GAD, Miyamoto, Kano TA, Y. Tsukahara M, Yanaka M. Journal of Membrane Science. 2002;208:75.
[9] Grank J. The mathematics of Diffusion. Clarendon University Press,1975.
[10] Henry BM, Dinelli F, Zhao FKY, Grovenor CRM, Kolosov OV, Briggs GAD, Roberts AP, Kumar RS, Howson RP. Thin Solid Films. 1999;355:500.
[11] Sang-Hee Ko P, Jiyoung O, Chi-Sun H, Jeong-Ik L,Yong Suk Y, Hye Yong C, Kwang-Yong K. ETRI Journal. 2005;27:545.
[12] Tropsha YG, Harvey NG. Journal of Physical Chemistry B. 1997;101:2259.
[13] Erlat AG, Spontak RJ, Clarke RP, Robinson TC, Haaland PD, Tropsha Y, Harvey YNG, Vogler EA. Journal of Physical Chemistry B. 1999:103:6047.
[14] Erlat AG, Wang BC, Spontak RJ, Tropsha Y, Mar YKD, Montgomery DB, Vogler EA. Journal of Materials Research. 2000;15:704.
[15] http://www.mocon.com/pdfperm/wvtrtestultrabarriers.pdf.
[16] Nisato G, Bouten PCP, Slikkerveer PJ, Bennett WD, Graff GL, Rutherford N, Wiese L. Proc. Int. Display Workshop/Asia Display. 2001;61:1435.
[17] Paetzold R, Winnacker A, Henseler D, Cesari V, Heuser K. Review of Scientific Instruments. 2003:74,:5147.
[18] Williams DJ, Rajeswaran G. Proc SPIE. 2003;5050:166–169.
[19] Tsukahara Y, Hieda S, Tanaka S, Takahashi H. ProcSoc Inform Display Symp Dig Tech Papers. 2003, 860.
[20] Jamieson EHH, Windle AH. Journal of Materials Science. 1983;18:64.
[21] Krug TG. Proceedings of the Society of Vacuum Coaters, 33rd Annual Technical Conference 1990, 163.
[22] Krug TG, Ludwig R, Steiniger G. Pro. Soc. Vacuum Coaters, 36th Annual Technical Conference 1993, 302.

[23] Chatham H. Surface & Coatings Technology. 1996;78:1.

[24] Potscavage WJ, Yoo S, Domercq B, Kippelen B. Applied Physics Letters. 2007;90.

[25] Park SHK, Oh J, Hwang CS, Lee JI, Yang YS, Chu HY. Electrochemical and Solid State Letters. 2005;8:H21.

[26] Ghosh AP, Gerenser LJ, Jarman CM, Fornalik JE. Applied Physics Letters. 2005;86.

[27] Carcia PF, McLean RS, Reilly MH, Groner MD, George SM. Applied Physics Letters. 2006;89.

[28] Mandlik P, Gartside J, Han L, Cheng IC, Wagner S, Silvernail JA, Ma RQ, Hack M, Brown JJ. Applied Physics Letters. 2008;92.

[29] Yoo S, Potscavage Jr. WJ, Domercq B, Han SH, Li TD, Jones SC, Szoszkiewicz R, Levi D, Riedo E, Marder SR, Kippelen B. Solid-State Electronics. 2007;51:1367.

[30] Leterrier Y. Progress in Materials Science. 2003;48:1.

[31] Sobrinho ASD, Latreche M, Czeremuszkin G, Klemberg-Sapieha JE, Wertheimer MR. Journal of Vacuum Science & Technology A .1998;16:3190.

[32] Huang WD, Wang XH, Sheng M, Xu LQ, Stubhan F, Luo L, Feng T, Wang, Zhang XFM, Zou SC. Materials Science and Engineering B-Solid State Materials for Advanced Technology. 2003;98,:248.

[33] Fenrych J, Reynhardt EC, Basson I. Powder Diffraction. 1997;12:49.

[34] Cho S, Lee K, Heeger AJ. Advanced Materials. 2009;21:1941.

[35] Felts JT. In Proceedings of the Society of acuum Coaters, 34th Annual Technical Conference, 1991; 99.

[36] Cros S, Firon M, Lenfant S, Trouslard P, Beck L. Nuclear Instruments & Methods in Physics Research Section B-Beam Interactions with Materials and Atoms. 2006;251:257.

[37] Lewis J, Grego S, Vick E, Temple D. In 4th Annual Flexible Displays and Microelectronics Conference, 2004.

[38] Weaver MS, Michalski LA, Rajan K, Rothman MA, Silvernail JA, Brown JJ, Burrows PE, Graff GL, Gross ME, Martin PM, Hall M, Mast E, Bonham C, Bennett W, Zumhoff M. Applied Physics Letters. 2002;81:2929.

[39] Chiang CC, Wuu DS, Lin HB, Chen YP, Chen TN, Lin YC, Wu CC, Chen WC, Jaw TH, Horng RH,.Surface & Coatings Technology. 2006;200:5843.

[40] Chen TN, Wuu DS, Wu CC, Chiang CC, Chen YP, Horng RH. Plasma Processes and Polymers. 2007:4:180.

[41] Weaver MS, Chwang AB, Rothman MA, Silvernail JA, Hack MM, Brown JJ, Burrows PE, Graff GL, Gross ME, Martin PM, Hall M, Mast E, Bonham CC, Bennett WD, Zumhoff M. In Proc. SPIE Int. Soc. Opt. Eng. 2002:;237, 4712.

[42] Chwang AB, Rothman MA, Mao SY, Hewitt RH, Weaver MS, Silvernail JA, Rajan K, Hack M, Brown JJ, Chu X, Moro L, Krajewski T, Rutherford N. Applied Physics Letters. 2003;83:413.

[43] Greener J, Ng KC, Vaeth KM, Smith TM. Journal of Applied Polymer Science. 2007;106:3534.

[44] Tsai-Ning C, Dong-Sing W, Chia-Cheng W, Cheng-Chung C, Yung-Pei C, Ray-Hua H. Plasma Processes and Polymers. 2007;4:180.

[45] Lungenschmied C, Dennler G, Neugebauer H, Sariciftci SN, Glatthaar M, Meyer T, Meyer A. Solar Energy Materials and Solar Cells. 2007;91:379.

[46] JAffinito JD, Gross ME, Coronado CA, Graff GL, Greenwell EN, Martin PM. Thin Solid Films. 1996;290:63.

[47] Kim N, Graham S. Thin Solid Films. 2013;547:57.

[48] Grego S, Lewis J, Vick E, Temple D. Thin Solid Films. 2007;515:4745.

[49] Yanaka M, Henry BM, Roberts AP, Grovenor CRM, Briggs GAD, Sutton AP, Miyamoto T, Tsukahara Y, Takeda N, Chater RJ. Thin Solid Films. 2001;397:176.

[50] Chua SJ, Ke LK, Ramadas SK, Senthil KR, Cai S. *WO2009126115-A1; AU2009234506-A1; EP2281420-A1; KR2011007166-A; TW201012648-A; US2011132449-A1; CN102057750-A; JP2011520216-W; JP5263849-B2; CN102057750-B; AU2009234506-B2; SG165601-A1; SG165601-B; TW430885-B1; US2014179040-A1; EP2281420-B1*.

[51] Ahmet GE, Yan M, Duggal AR. Springer Science+Business Media. 2009;433.

[52] Yan M, Erlat AG, Zhao R, Smith DJ, Scherer B, Jones C, Foust D, McConnelee PA, Feist TP, Duggal AR. In 6th Annual Flexible Displays and Microelectronics Conference, 2007.

9

Applications and Future Prospects of Printed Electronics

Zheng Cui

9.1 Introduction

Previous chapters have introduced various aspects of printed electronics, including materials, processes and equipment, the principles and fabrication of typical printed electronics devices, as well as encapsulation and packaging of printed electronics devices. It should be realized that the reason printed electronics has risen to its current status and drawn such wide attention is because of its very distinctive domain of applications.

As explained in Chapter 1, printed electronics, together with organic electronics, plastic electronics, flexible electronics, paper electronics, transparent electronics, textile electronics and wearable electronics, are in a class of electronics that is very different from silicon microelectronics. They represent a domain of applications that are distinctively of large size, flexible, low cost, and the manufacturing processes are of low energy consumption and less harmful to environment. These distinctive features can bring many novel and unexpected applications to our daily life, such as large outdoor signage displays and advertising boards made of printed flexible light-emitting panels; building-integrated thin-film solar cells, which are semi-transparent and can at the same time serve as sun shades; interactive displays that become part of shop windows; flexible sensors, displays and data processing circuits that are conformable to 3D objects, human skin or textiles. Their low cost means that these electronic products can enter the vast low-end consumer market. To enable these electronic products to be sold at low price, manufacturing them by printing is essential. Therefore, printed electronics is leading the way over other types of electronics in the development of large size, flexible and low cost electronic applications.

This chapter presents an overview of current applications for printed, organic, plastic and flexible electronics, as well as future potential applications of these classes of electronics. The challenges for printed electronics to realize its potentials are also reviewed. Prospects of future developments are predicted.

Printed Electronics: Materials, Technologies and Applications, First Edition. Zheng Cui, Chunshan Zhou, Song Qiu, Zheng Chen, Jian Lin, Jianwen Zhao, Changqi Ma and Wenming Su.

© 2016 Higher Education Press. All rights reserved. Published 2016 by John Wiley & Sons Singapore Pte. Ltd.

9.2 Application Areas of Printed Electronics

The inherent nature of large area, flexible and low cost of printed electronics opens many possibilities for variety of applications. Instead of going through each individual application, this book adopted the grouping method published by OE-A (Organic Electronics Association) [1]. OE-A is the largest international organization in the field of organic and printed electronics, with more than 230 members from academic and industry in 32 countries. The members are either actively involved in organic and printed electronics R&D or manufacturing, or are end users of the technology. Every two years, OE-A publishes a report based on the information and opinions gathered from its members, to review the progress of past two years in organic and printed electronics R&D, which are already in the market or close to market. Together with the report, there is a roadmap that predicts where the technologies are going and what would be the likely products on the market in the next 5–10 years. The OE-A report is a good benchmark for global development of organic and printed electronics.

The latest Organic and Printed Electronics Roadmap was published in July 2015 in the 6th edition of the OE-A report. In the roadmap, organic and printed electronics applications are defined in 5 groups: organic photovoltaic, flexible and OLED display, organic lighting, electronics and components, and integrated smart systems. Figure 9.1 is the 2015 edition of roadmap for organic and printed electronics.

It must be pointed out that the roadmap is not for printed electronics alone, but for organic, flexible and printed electronics together. As described earlier, organic and flexible electronics devices are not necessarily printable, particularly for organic electronics where vacuum deposition is still the dominant manufacturing process. The roadmap presents, therefore, a general picture of future development for the whole category of non-silicon electronics. To be able to manufacture them by printing is, of course, the key factor to make them large size, flexible and, most importantly, low cost. The following sections contain descriptions of each group of applications, the state-of-the-art in technology and future directions of development.

9.2.1 Organic Photovoltaic

The global photovoltaic industry has experienced huge turbulence in the last couple of years. The overcapacity problem of the silicon PV industry in China, coupled with reduced demand in the European solar energy market, has caused lower than expected pricing of solar cells. Closures and bankruptcies of PV companies have been frequently in the news. Organic solar cells are doomed in such a global scenario, because of its low solar conversion efficiency, even though they can be manufactured by printing. A well-known example is the closure of Konarka in 2012, which was the world's first company making OPV solar cells in mass production by printing. Figure 9.2 is Konarka's roll-to-roll printing of OPV solar cells.

While the silicon PV can easily achieve solar energy conversion efficiency of up to 20%, Konarka's mass produced OPV could only achieve efficiency of 3%. In the world of solar energy where pricing is benchmarked by dollar-per-watt, OPV cells are 10 times more expensive than silicon solar cells. At present, OPV can only compete in the portable energy source market with its light weight and flexible features. Printing can, of course, lower the cost. The printed organic polymer solar cell, however, has a lower efficiency than a vacuum deposited organic small molecular solar cell, which largely offsets its cost advantage. There are companies, such as Heliatek in Germany, which produce organic solar cells by vacuum

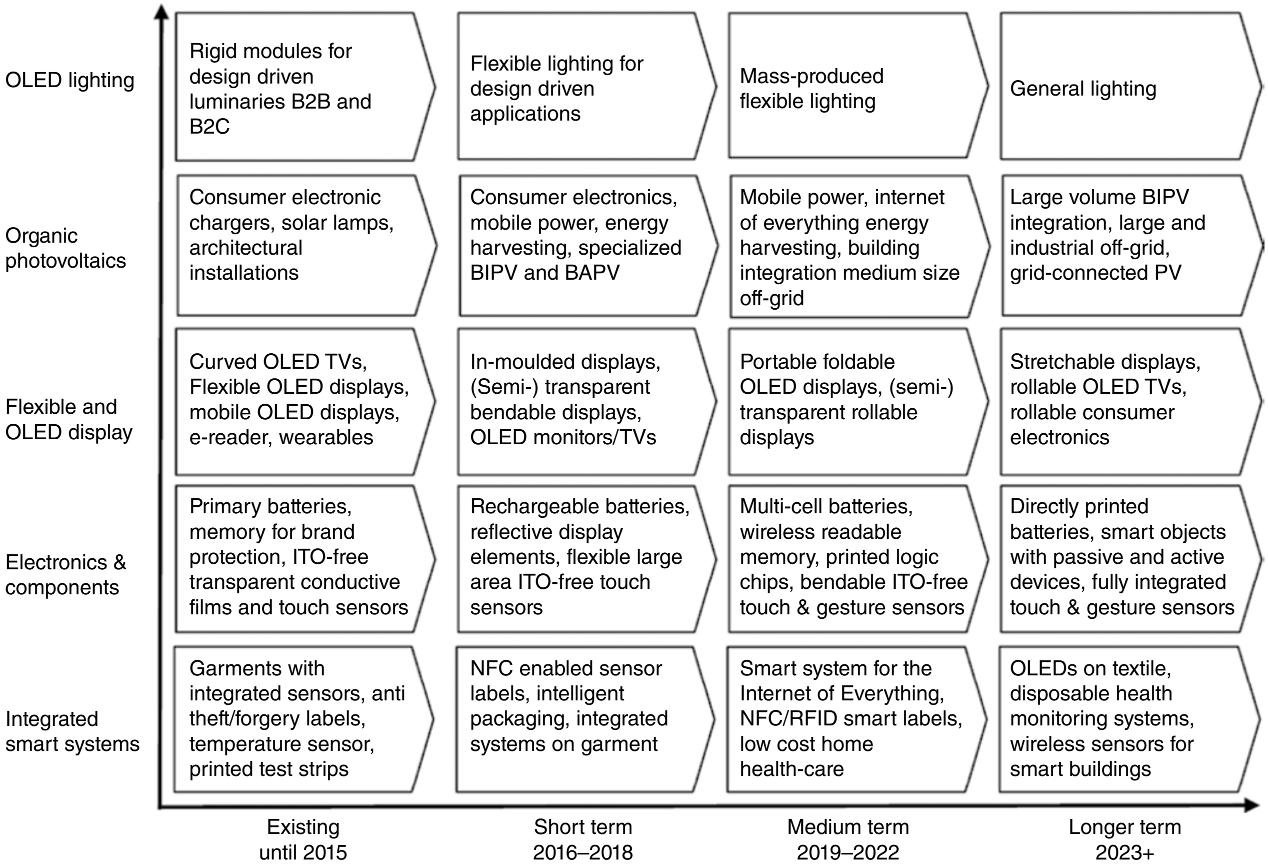

	Existing until 2015	Short term 2016–2018	Medium term 2019–2022	Longer term 2023+
OLED lighting	Rigid modules for design driven luminaries B2B and B2C	Flexible lighting for design driven applications	Mass-produced flexible lighting	General lighting
Organic photovoltaics	Consumer electronic chargers, solar lamps, architectural installations	Consumer electronics, mobile power, energy harvesting, specialized BIPV and BAPV	Mobile power, internet of everything energy harvesting, building integration medium size off-grid	Large volume BIPV integration, large and industrial off-grid, grid-connected PV
Flexible and OLED display	Curved OLED TVs, Flexible OLED displays, mobile OLED displays, e-reader, wearables	In-moulded displays, (Semi-) transparent bendable displays, OLED monitors/TVs	Portable foldable OLED displays, (semi-) transparent rollable displays	Stretchable displays, rollable OLED TVs, rollable consumer electronics
Electronics & components	Primary batteries, memory for brand protection, ITO-free transparent conductive films and touch sensors	Rechargeable batteries, reflective display elements, flexible large area ITO-free touch sensors	Multi-cell batteries, wireless readable memory, printed logic chips, bendable ITO-free touch & gesture sensors	Directly printed batteries, smart objects with passive and active devices, fully integrated touch & gesture sensors
Integrated smart systems	Garments with integrated sensors, anti theft/forgery labels, temperature sensor, printed test strips	NFC enabled sensor labels, intelligent packaging, integrated systems on garment	Smart system for the Internet of Everything, NFC/RFID smart labels, low cost home health-care	OLEDs on textile, disposable health monitoring systems, wireless sensors for smart buildings

Figure 9.1 OE-A roadmap of organic and printed electronics applications beyond 2015 (Reprinted from reference [1] with permission from OE-A)

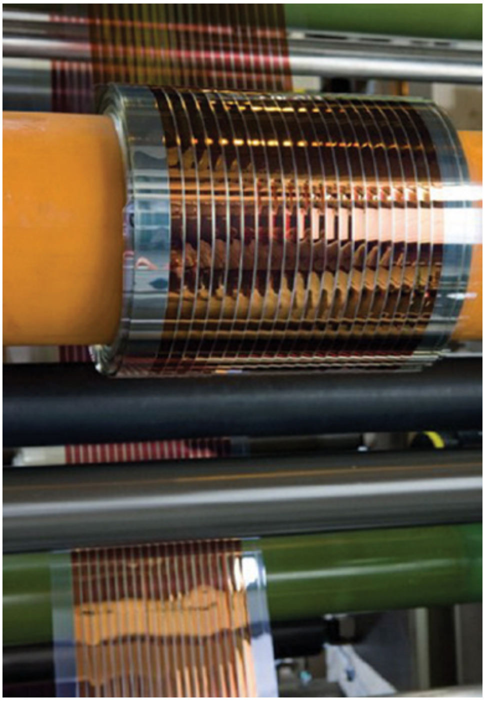

Figure 9.2 Roll-to-roll printing of organic solar cells. (Courtesy of Konarka)

deposition and can achieve cell efficiency of more than 10% [2]. Vacuum deposition of organic solar materials can also be done in roll-to-roll fashion, such as Heliatek's process, which can boost the throughput and lower the manufacturing cost. In the long run, printable OPV is still a cheap option for solar energy source. OPV can generate electricity in low light conditions. For example, in a room lighting condition, OPV generates twice as much electricity than a crystal silicon solar cell. The worldwide research into printable organic solar technology is still very active, as reviewed in Chapter 6. Apart from applications in portable solar energy sources, printable OPV can be integrated into buildings, such as the glass walls seen in many modern skyscrapers, and sunshades for windows. Recent progress in semi-transparent OPV solar cells opens up this new potential application.

When comparing different solar energy technologies, one should not ignore the energy payback factor. The energy payback is the length of time a solar cell takes to generate enough electricity to offset the electricity which has been consumed to manufacture the solar cell. Obviously, the higher the energy it takes to manufacture a solar cell the longer the energy payback time. Although some types of solar cell have high efficiency, the energy payback is also high, such as single crystal silicon solar cells. Printable OPV is low in efficiency, but the manufacturing process is simple and low temperature. The energy payback time can be potentially as short as one day [3].

OPV is not the only solar cell that can be manufactured by printing. The fairly old thin-film solar technology based on copper-indium-gallium-selenide (CIGS) can be printed or solution-processed as well. The Center for Solar and Hydrogen Energy Research in Germany (Zentrum für Sonnenenergie- und Wasserstoff-Forschung (ZSW) Baden-Württemberg) has studied screen printing of CIGS solar cells since 2010. They produced flexible CIGS solar cells on polyimide films (25 µm thick and 300mm wide) and achieved efficiency of 10.2% [4]. There was also a report of using inkjet printing to make CIGS solar cells and the inkjet-printed CIGS solar cell achieved efficiency of 5% [5]. However, one has to be aware that the current world record of CIGS solar cell efficiency is 20.8%, achieved by ZSW of Germany [6], using not printing but vacuum evaporation. Printed CIGS solar cells have a long way to catch up.

An important development in printed inorganic solar cell is Innovalight's nanosilicon inks. Innovalight, a start-up company in Silicon Valley in the US, developed a process that suspends silicon nanoparticles in a solution without congregation. By printing the silicon ink onto a conventional silicon solar cell substrate with proper annealing, it can boost 5 to 7% of conversion efficiency of an existing silicon solar cell [7]. This is not a completely new solar cell manufacturing technology, but an addition to existing silicon solar cell manufacturing processes. The silicon ink can be printed either by screen printing or inkjet printing, without adding too much to the existing manufacturing cost. In October 2011, DuPont acquired Innovalight and its silicon ink technology to become the new provider of silicon ink. The above examples show that printable photovoltaic is not confined to organic materials. Making inorganic materials printable may open up new avenues to advance photovoltaic technology.

The most amazing development in PV technology in the last few years has to be the newly emerged perovskite PV. With just over 2% in 2006, its power efficiency reached to 20.1% in late 2014. Figure 9.3 is the trajectory of efficiency improvement since the material was discovered for PV application [8]. As briefly overviewed in Chapter 6, the attraction of perovskite PV is its simple structure and the solar cells can potentially be manufactured by printing. The technology is far from mature yet. The stability issue has been a major obstacle to overcome.

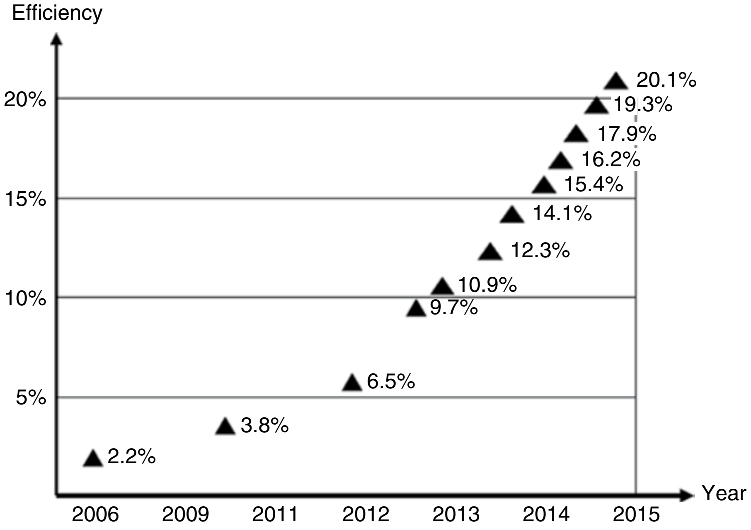

Figure 9.3 Efficiency improvement of perovskite solar cells (adopted from IDTechEx market report [8] with permission)

However, the prospect of achieving high efficiency, much higher than could ever be dreamed of for OPV, has drawn many researchers to this new technology; even those who have been working on OPV technology for many years. Though most of the R&D activities on perovskite PV technology are still largely confined to academic research, industries have started to pay attention to the technology. Venture capitals began to invest into startups. Before the perovskite PV can be viable as practical solar cells, some intermediate applications have been proposed. For example, the Oxford Photovoltaic, a spinoff company from Oxford University, is developing hybrid tandem solar cells combining a single crystal silicon solar cell with perovskite top layer. The hybrid system can significantly increase the utilization of sunlight spectrum and boost the power conversion efficiency [9].

9.2.2 *Flexible Display*

The most eye-catching development in display technology in recent years is the flexible display. In the 2013 Consumer Electronics Show, the big name companies in the display industry all demonstrated their flexible display products, from bendable mobile phones to rollable e-papers. According to the latest report from IHS Technology, a display market research firm, the market for flexible display panels will grow to \$1.3 billion by 2016 and reach \$67.7 billion by 2023. Figure 9.4 illustrates the trend of the flexible display market in the next 10 years [10]. In terms of volume, the production of flexible display panels will be 24 million by 2016 and as much as 17 billion by 2023, taking up a 25% share of the total display market.

A display panel consists of two basic parts: the front plane which is made of a pixel array and backplane which is an array of electronic driving circuits. In liquid crystal display (LCD), the pixel array is an array of cells containing liquid crystal material; in e-paper display, the pixels are e-ink cells containing charged micron-sized black and white spheres, which are not emitting light themselves but reflect ambient light. In the organic light-emitting diode (OLED)

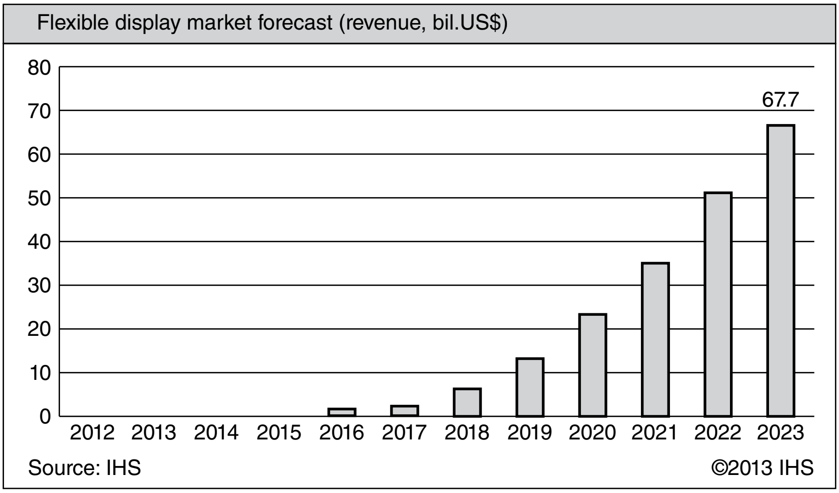

Figure 9.4 Market forecast for flexible display (Adopted from IHS report with permission from IHS)

display, the pixels are array of light emitting diodes. The backplane is an array of thin-film transistors (TFT), which switch on and off each pixel.

Making front plane flexible is fairly easy, as only a proper sealing of liquid crystal cells or e-ink cells is needed in a flexible assembly for LCD and e-paper. As for OLED, it is a thin-film structure that is inherently flexible on a flexible substrate. The difficult part is to make the backplane flexible. The current technology for making a backplane TFT array is based on either amorphous silicon (a-Si) or low temperature polycrystalline silicon (LTPS) technology. Both require high temperature processes and cannot be easily adapted to flexible plastic substrates. For example, to get good performance from TFTs, the LTPS needs a 450–600°C process temperature and a-Si needs a 300–350° C process temperature. At temperatures around 300° C, it may be possible to make the a-Si TFT on some high temperature plastic films such as polyimide. However, a-Si TFT has too low charge mobility. TFTs made of LTPS have a charge mobility exceeding 100 cm^2/Vs, whereas a-Si TFTs only have the mobility around 0.1 ~1 cm^2/Vs, which is unsuitable for active matrix OLED (AMOLED) displays.

For an AMOLED display, the charge mobility of the TFT should be at least greater than 5 cm^2/Vs. In recent years, a new class of semiconductor materials has been introduced to backplane technology, which is based on doped zinc oxide (ZnO) semiconductors, such as Zinc-Tin Oxide (ZTO), Indium-Zinc oxide (IZO) and Indium-Gallium-Zinc Oxide (IGZO) [11]. The key advantages of this type of oxide semiconductors are their high charge mobility (>10 cm^2/Vs) and low process temperature similar to that of a-Si. The process cost is also similar to that of a-Si, which is much lower than that of LTPS. These oxide semiconductor materials are also transparent, enabling to produce transparent display panels or other transparent electronics applications [12]. More detailed information about the oxide semiconductors can be found in Chapter 3 of this book. There is a growing trend to use the oxide semiconductors to replace LTPS for backplane in flat panel display industry. Although they can be deposited either by vacuum sputtering or printing onto flexible substrates to make flexible backplanes, printable oxide TFTs are normally inferior in performance and require high post-processing temperature [13].

Organic thin-film transistor (OTFT) seems perfectly placed to solve the problem. Organic semiconductor material can be printed on flexible substrates and require no high temperature process. Previously, OTFTs have only been used as backplane for e-paper display, because of their low charge mobility (<1 cm^2/Vs). The most prominent example is the e-paper display devices developed and mass manufactured by Plastic Logic, a company founded by Cambridge University professor Richard Friend whose group was the first in the world to make organic transistors by inkjet printing technique [14]. However, the advances in organic semiconductors are rapid in the last few years. Newly invented organic semiconductors have the charge mobility approaching those of oxide semiconductors, as compared in Figure 9.5. Their low process temperature and good flexibility make the OTFTs promising candidates for the backplane of flexible AMOLED display.

Making flexible backplane for flexible display is fairly straightforward, as long as the TFTs do not deteriorate when subject to bending. Making printed backplane is a completely different matter. As abovementioned, LTPS and a-Si are not printable. Oxide semiconductors though can be printable, do not show good properties unless undergoing high temperature annealing after printing deposition. The printable organic polymer semiconductor materials are not as good as organic small molecular materials, which are better to be deposited by vacuum evaporation. Moreover, the printing deposition does not have the fine resolution required for making the backplane TFT structures. Therefore, the backplanes in commercial display panels are not made by printing but by vacuum sputtering or evaporation, plus photolithographic patterning.

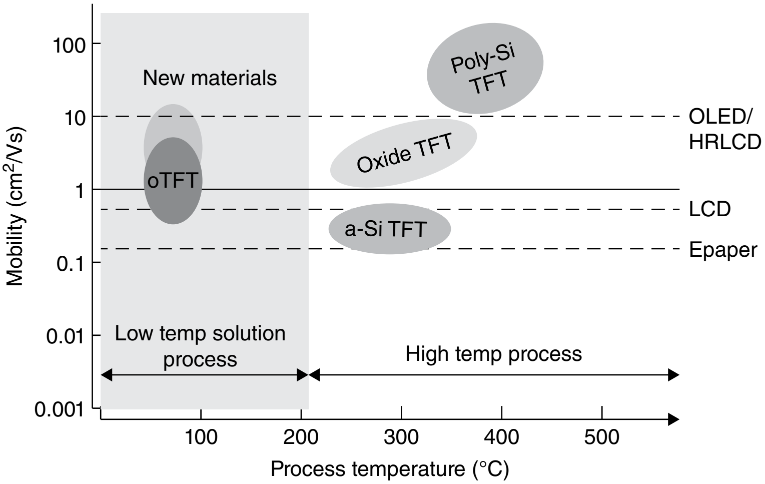

Figure 9.5 Comparison of organic semiconductor with a-Si, Oxide and poly-si for backplane TFTs (Adopted from [15] with permission)

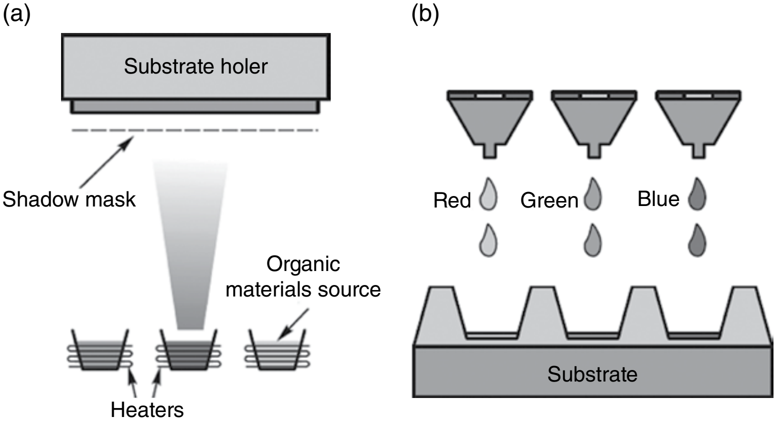

Figure 9.6 Comparison of depositing RGB materials by vacuum deposition through (a) a shadow mask and (b) by inkjet printing

However, the printing technique can still play a part in making flexible display panels. In fact, printing has already been employed for depositing color filter materials in LCD panel manufacturing. It is also a preferred technique for depositing OLED materials. Currently in OLED display panel manufacturing, red, green and blue (RGB) organic light emitting materials are deposited by vacuum evaporation through a fine metallic shadow mask, which has wasted 90% of the precious RGB materials. Using inkjet printing the RGB materials can be deposited with only the amount needed and precisely at each pixel location. Figure 9.6 illustrates the difference between shadow mask deposition and inkjet printing to deposit RGB materials. The cost saving will be huge. As the pixel size is normally 100 μm or bigger, the resolution capability of an inkjet printer can meet the requirement perfectly. Panasonic has been developing the inkjet-printing process for some years and demonstrated the world's first printed 55-inch OLED TV at the 2013 Consumer Electronics Show. AUO, a display panel manufacturer in Taiwan, demonstrated a 65-inch OLED TV made by inkjet printing at the 2014 Display Week conference [16]. A picture of the printed TV has been shown in Figure 1.10 at Chapter 1. It is anticipated that printing will be used more and more in future display panel manufacturing and will play a major role in manufacturing flexible displays. With future improvement in resolution and innovation in semiconductor ink materials, printing will also be used to make backplane TFT arrays.

9.2.3 Organic Lighting

Organic lighting, also called OLED lighting, is another area where the printing process can play a major role. Although the light emission mechanism is the same as OLED display, organic lighting is much simpler in device structure and fabrication process. The most important difference between OLED display and OLED lighting is that an OLED lighting panel does not need a backplane.

OLED lighting has many distinctive features compared to conventional lighting. It is a planar light source and can be tailored in any size according to designs and environment. It is a diffused light source instead of conventional point or line light source, posing no glare to human eyes. It can be flexible, translucent and highly decorative, as shown in Figure 9.7 where the purpose of OLED lights is not only for luminescence but also for decoration. In fact, the aesthetic nature of OLED lighting has drawn major interest from the interior design community. Many interior designers have used the features to create many interesting lighting designs.

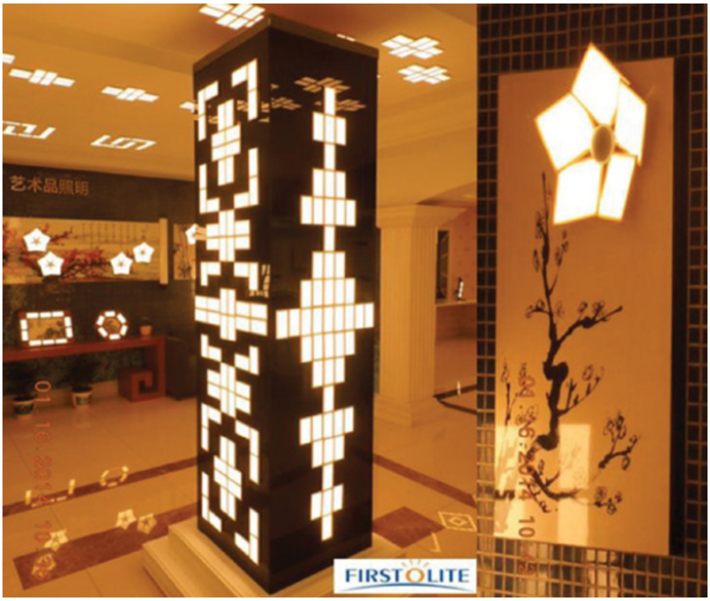

Figure 9.7 Decorative lighting by planar OLED light sources. (Adopted from Web with courtesy of First O-Lite Inc., Nanjing, China)

Industry has been developing OLED for lighting for over a decade and there has been steady progress over the years. The industry aimed to achieve luminous efficiency of 100 lm/W in order to compete with current fluorescent lamps (approx. 60-80 lm/W) or LED lighting fixtures (approx. 80 lm/W). The goal has been achieved at least at laboratory level, with the announcement of 114 lm/W for a light-emitting area of 1 cm^2 and 110 lm/W for a light-emitting area of 25 cm^2 by Panasonic in 2013 [17]. The efficiency at mass production level is not yet that high, currently at around 60 lm/W [18].

However, OLED lighting is facing fierce competition in a conventional lighting market where current light sources, particularly the LED, have much lower cost. According to Yole Development's report in 2012, the cost of per kilo luminance (klm) for OLED lighting source is 70 times higher than that of LED lighting source, at ~$352/klm. By industrial estimate and prediction, the cost of OLED lighting will come down, as the technology is getting more mature and demands are getting larger. However, LED lighting will be getting cheaper as well. By 2020, the cost of OLED lighting would still be 16 times higher than LED lighting (OLED at ~$13/klm vs. LED at ~$0.8/klm) [19]. With edge-lit technology, LED lighting can be planar and flexible as well, eating up the decorative lighting market where OLED lighting may have a competitive advantage.

To lower the manufacturing cost of OLED lighting panels, one obvious option is to use printing instead of a vacuum deposition process. Research and development on printing OLED has been going on for many years. Scientists at General Electric (GE) demonstrated roll-to-roll printed OLED on flexible substrate in 2008, as in the picture shown in Figure 9.8 [20]. In 2010, GE also collaborated with Konica Minolta and made their flexible white OLEDs with

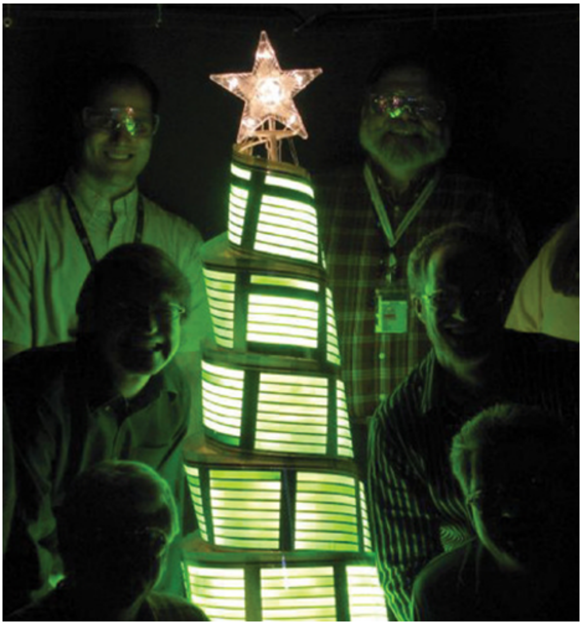

Figure 9.8 A Christmas tree made from a printed flexible OLED lighting sheet. (Adopted from Web with courtesy of GE)

an efficiency of 56 lm/w using solution-coatable materials in a roll-to-roll printing process [21]. Now, Konica Minolta is building the world's first factory for mass production of flexible OLED panels on plastic substrate by roll-to-roll printing [22]. Last year, DuPont demonstrated inkjet-printed OLED lighting panels and it was estimated that the cost of a 1000cm^2 OLED lighting panel could drop to $25 if adopting the printing approach [23].

Other cost cutting measures for OLED lighting include further improving the efficiency of solution-processed organic light emitting materials, replacing ITO by other low cost transparent conductive electrode materials, and finding low cost barrier film technology for encapsulation. On the equipment side, the startup company Kateeva in Silicon Valley in the US, has developed a new inkjet-printing machine, which is specially designed for OLED panel manufacturing and capable of printing on Gen-8.5 size (2200 x 2500 mm) substrates. Though OLED lighting is currently only suitable for the high-end decorative lighting market, with the maturing of technology it will eventually penetrate into the general lighting market, as predicted by the OE-A roadmap shown in Figure 9.1.

9.2.4 Electronics and Components

Although printing can be used for making solar cells, displays and lighting, as described in above sections, they are not exactly electronics. The general sense of "electronics" involves transistors, memories, power supplies and electric current carrying circuits. If printing technology is used in general electronics, it will have a much wider impact on industry, the economy and our daily life.

Transistors are at the heart of all electronics. Making transistors by printing has been a dream since organic electronics research started 30 years ago. Although organic polymer materials are inherently soluble and can be made into ink form, it was until the year 2000 when researchers at Cambridge University, UK, produced the first all-printed transistor [14]. However, printing organic transistors has remained as an interest of academic research and was not taken up by industry, because the solution form of organic polymer semiconductors has always been inferior in electric properties to organic small molecular semiconductors which can only be deposited by vacuum evaporation to make thin-film transistors. Figure 1.3 in Chapter 1 illustrated the evolution of the charge mobility of organic semiconductors over the past 25 years. Though both small molecule and polymer organic semiconductor materials were improving in charge mobility, the charge mobility of polymer semiconductors was always an order of magnitude lower than its small molecule counterpart. Printed organic TFTs are at best made into low-resolution display backplane, such as e-paper displays, which do not require high charge mobility.

The first commercial use of printed transistors was the 128-bit RFID tag, developed and commercialized in 2008 by Kovio, a US company. Kovio made the transistors by printing a special nanosilicon ink, which could achieve charge mobility exceeding 100 cm^2/Vs [24]. Figure 9.9 is part of Kovio's inkjet-printed RFID tag, showing arrays of printed transistors. The only drawback of the nanosilicon ink is its requirement of a high annealing temperature (>400°C). The transistors cannot be printed on plastic substrate but on thin stainless steel sheets in order to withstand such a high process temperature. Another successful example is the printing of carbon nanotube ink for transistors, which does not need high annealing temperature (<150°C) and therefore can be printed on flexible plastic substrates. RFID tags

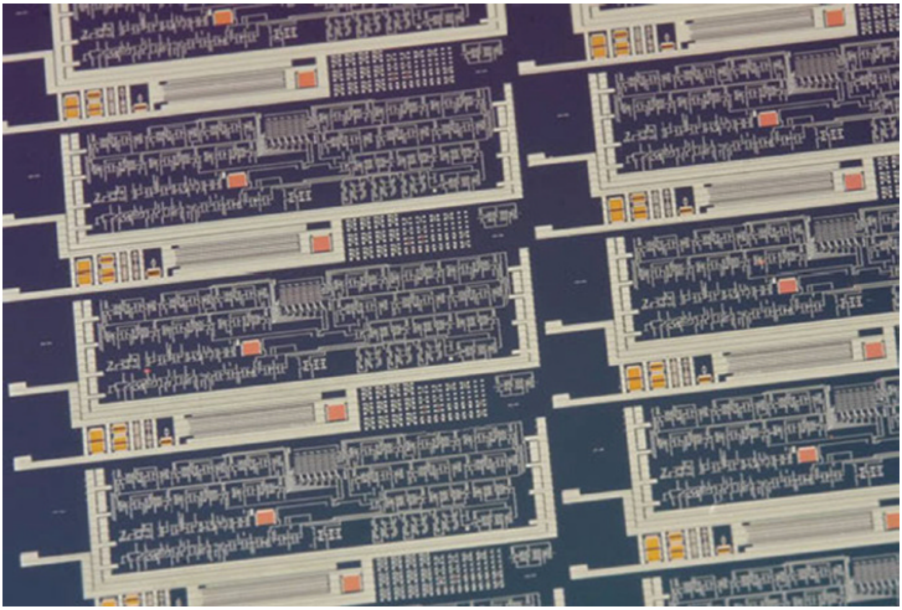

Figure 9.9 Kovio's inkjet-printed 128-bit RFID tag. (Adopted from Web with Courtesy of Kovio)

made by a roll-to-roll gravure printing process on plastic thin films have been demonstrated at Sunchon National University of Korea [25]. At the authors' Printable Electronics Research Center (PERC), a series of development work was carried out to separate semiconducting single-walled carbon nanotubes (SWCNTs) from commercial mixed as-grown SWCNTs [26,27]. Printable semiconductor SWCNTs inks were made and thin-film transistors with mobility over 40 cm^2/Vs have been fabricated by inkjet printing the inks on flexible plastic substrate [28], as shown in Figure 9.10.

Making RFID tags is an obvious application for printed transistors. The Internet of Things (IoT) is being accepted worldwide as the next big development of the Internet. The essence of IoT is to connect everything to everything else. At the heart of IoT are the sensors and communications. There will be a need for a lot of sensors; in fact, a trillion sensors are needed by 2023. That is the vision presented and discussed at the first Trillion Sensors (TSensors) Summit held at Stanford University in October 2013. A roadmap is being drawn up for a plan to meet this goal. That is not as crazy as it sounds. A trillion sensors society is actually not that far off. There are already about 3.5 billion sensors around us today—up from just 10 million in 2007. We know that we are already able to control TV, house lights, and air conditioning units from a smart phone or augmented reality devices like Google glass, or wearable electronics such as the Apple Watch. The sticky question is that if sensors are going into every home, every person and every object, who is going to pay for the trillion sensors, or who can afford the trillion sensors? The Summit came to the conclusion that if the trillion sensors goal is to be materialized it is not going be with silicon but something else far cheaper, say, far less than a dollar per sensor [29].

Printed electronics may realistically offer an answer to the trillion sensors question. With printed electronics, sensors can be printed onto plastics or papers in a high throughput

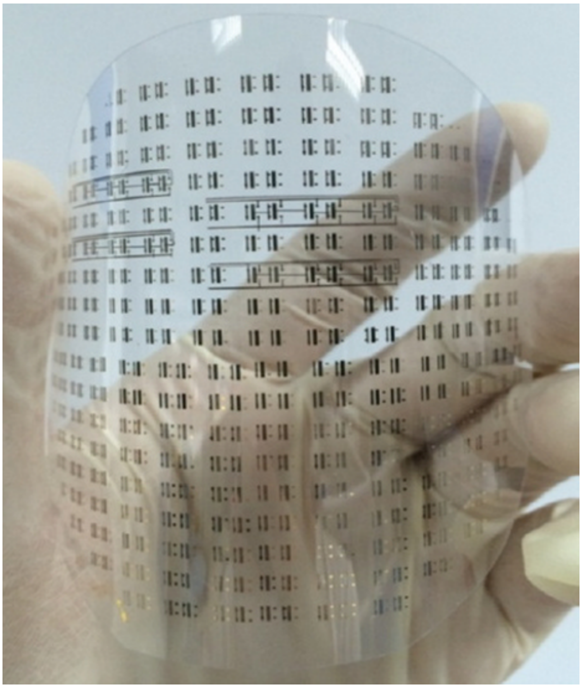

Figure 9.10 Inkjet printed thin-film transistors on flexible plastic substrate at PERC

roll-to-roll process, which can potentially lower the cost significantly. A considerable amount of R&D work has been carried out in the printable sensor area whether using organic or inorganic sensing materials [30–32]. However, the low cost promise of printed sensors has so far not been materialized. On the one hand, the printable sensing materials have not reached a performance level that can pose a real threat to the existing sensors industry. On the other hand, the infrastructures for mass production of existing sensors are already well established and so are their market shares. Printed sensors need a huge investment to establish such infrastructures to compete at the cost front with existing sensors. Taking the RFID tags as an example, a passive 96-bit EPC (Electronics Product Code) RFID tag nowadays costs from 7 to 15 US cents. That includes the silicon chip and antenna mounted on a flexible substrate. A previously mentioned company that produced printed silicon RFID tags was not been able to compete at this cost level and has recently gone out of business and been acquired by a Swedish company making printable memories. The South Korean university, which successfully demonstrated roll-to-roll printed RFID tags on plastic using carbon nanotube ink, also gave up on commercializing the printed tags and used the technology for something else. Although RFID tags based on organic transistors have been developed for many years [33,34], they have never made it into the commercial market because of the performance and stability issues. It is a tough business for fully printable RFID tags. Printed RFID tags are simply not ready yet to take on the challenge. Other type of sensors, such as bio and chemical sensors that do not need transistors and use only layers of sensing materials may stand a chance of getting into the sensors market, because they can be made by simple printing of sensing layers and potentially at a very low cost, for example, printed on paper such as the very successful glucose test strips [35,36].

Printed electronics implies not only printing transistors but also printing electrical circuits, which are simply conductive tracks on rigid or flexible substrates. A typical application is the printed circuit board (PCB). The PCB, as we know it, is in fact not printed, but patterned by photolithography and wet chemical etching. The fabrication process is not only complicated, wasting conductive materials, but also polluting the environment. China is the world's largest producer of PCBs, making up more than 40% of total global volume of PCBs. The discharge of acidic wastes and solvents from PCB manufacturing into the environment is so acute in China that the government has prohibited the building of new PCB factories in the densely populated coastal regions. Printed electronics offers the potential to solve this problem. Printing is an additive manufacturing process. No acidic etching is needed and no materials are wasted. However, the only conductive material that can be printed at present is silver, which is not cost competitive as compared to copper-based PCBs. Considerable efforts have been made to develop copper inks but this has not been very successful because copper is very prone to oxidation, particularly in the form of nanoparticles, and copper oxide (CuO) is a poor conductor. One solution is to print a thin layer of silver and build up the conductive material by electroless plating of copper afterwards, albeit a slightly complicated process. Printing circuits found its first successful application in making RFID antennas (Figure 9.11). Unlike PCBs that require a thick layer of conductive material for carrying a large electric current, a RFID antenna needs only a thin conductive layer. The high cost of silver can be tolerated as it does not need too much silver ink to print on. While the antennas made by printed silver ink may not be the cheapest on the market, their greener manufacturing process may win over users and attract government support.

Recent successful applications of printed electronics are in the making of transparent conductive films (TCFs). TCFs are thin-film materials that are both transparent and conductive.

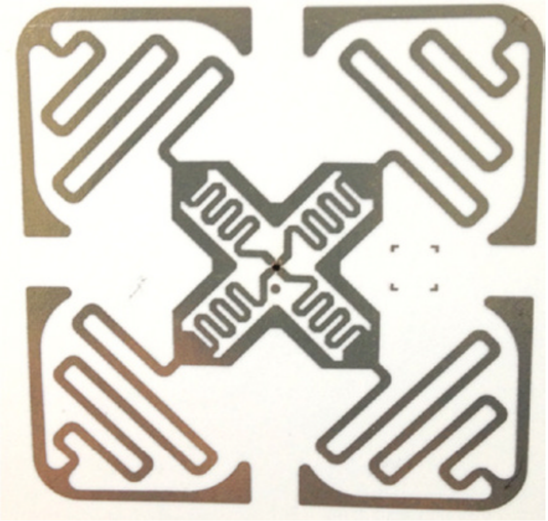

Figure 9.11 Printed silver RFID antenna with a silicon IC chip mounted in the center (produced at Beijing College of Communication, China)

Owing to the great popularity of iPhones and iPads, touch control has become an essential feature in all mobile phones and pad computers, and another trend is emerging whereby notebook computers are also adopting touch sensitive display to increase their usability. By estimate, touch control will be used in over 90% of all display panels by 2017. Currently, more than 95% of all touch panels rely on a transparent conductive material called ITO (indium-tin-oxide). Indium is a scarce mineral resource on earth and making ITO films is a costly process. Moreover, TCFs made from deposited ITO on flexible plastic thin film substrates are of relatively high sheet resistance (>100 Ω/sq.). This is fine for a small screen such as a mobile phone, but becomes an issue when applied to a large screen, such as those in notebook computers or TVs. High sheet resistance will reduce the touch sensitivity. The display industry and research community are racing to find alternative TCFs to replace ITO. The ITO replacement market is estimated to grow to $4 billion by 2020 [37]. New materials such as conductive polymers, carbon nanotubes (CNT), graphene, metal mesh (grid), metal nanowires (NW), have been proposed as alternatives for making TCFs. Among these alternatives, the metal mesh approach comes out as a clear winner because it offers the highest surface conductivity as well as maintaining low manufacturing cost, as the comparison shown in Figure 9.12 [38].

Most of the aforementioned materials need to be in ink form first and then coated onto a thin film or glass for subsequent patterning into touch panels. The printing method offers the possibility to perform coating of conductive material and patterning of touch electrodes at the same time, particularly with the metal mesh approach. The problem is that the resolution of the printing methods currently available is not high enough to make the metal mesh lines invisible. A new hybrid printing process has been developed at the authors' Printable Electronics Research Center to solve the problem [39]. The hybrid printing approach uses a master template that has all the patterns needed for a touch panel and imprints into a polymeric layer. A conductive material such as nanosilver ink is then filled into the imprinted trenches and sintered to become embedded conductive silver tracks. High resolution patterns (less than 3 μm line width for the mesh) can be made on the master template, which ensures the making of high resolution embedded silver lines on a substrate. TCFs made by the hybrid printing process have superior

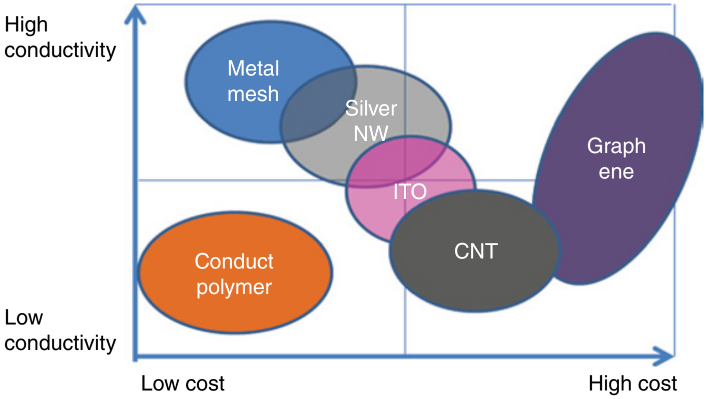

Figure 9.12 Comparison of different ITO replacement materials according their surface conductivity and manufacturing cost (Reprinted from [35] with permission)

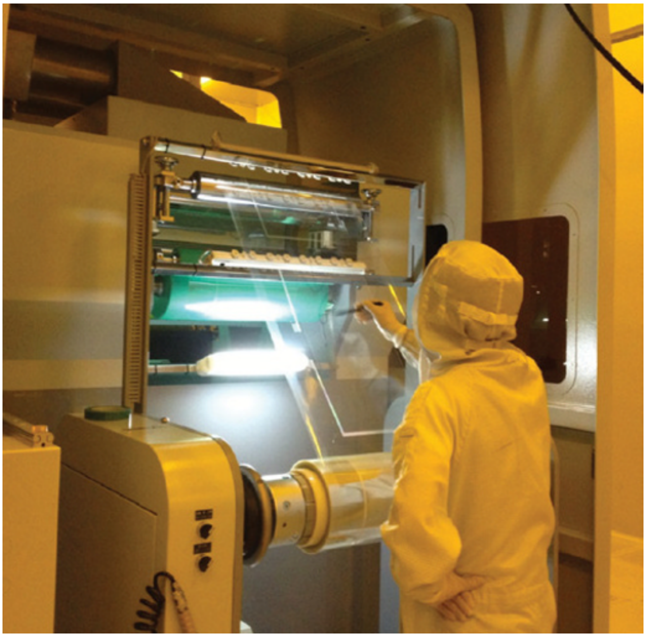

Figure 9.13 Roll-to-roll manufacturing transparent conductive films for touch panels at O-film

surface conductivity (sheet resistance <1Ω/sq.) and over 88% transparency. The low sheet resistance is particularly advantageous when the TCFs are used in large size touch panels, such as in a notebook computer or a TV screen. It increases the touch sensitivity considerably. Another big advantage of the hybrid printing process is that the manufacturing of TCFs for touch panels can be done in one continuous process in a roll-to-roll manner. The high throughput and high volume manufacturing has been realized by the touch panel manufacturer O-film Co. Ltd. in China. As shown in Figure 9.13, TCFs for touch panels are rolling out of the machine like printing newspapers. Other printing approaches for making metal mesh-based TCFs include direct gravure printing or inkjet printing, but they have not been able to match the resolution capability of the aforementioned hybrid printing approach.

9.2.5 Integrated Smart Systems

Individual devices and components can be fabricated by printing as described above. The end users or the market, however, need functional systems that not only have electronic components such as transistors and sensors but also have power supply and data communication. There are two approaches to integrated systems; all-printed integrated systems or a system integrated with printed devices or components.

It would be ideal if a smart system could be all printed. Previous attempts to make all-printed RFIDs either by printing nanosilicon ink or by printing carbon nanotube ink were not successful, because the all-printed RFIDs were not able to match the existing silicon chip RFIDs in terms of both performance and cost. As mentioned above, the RFID market is a

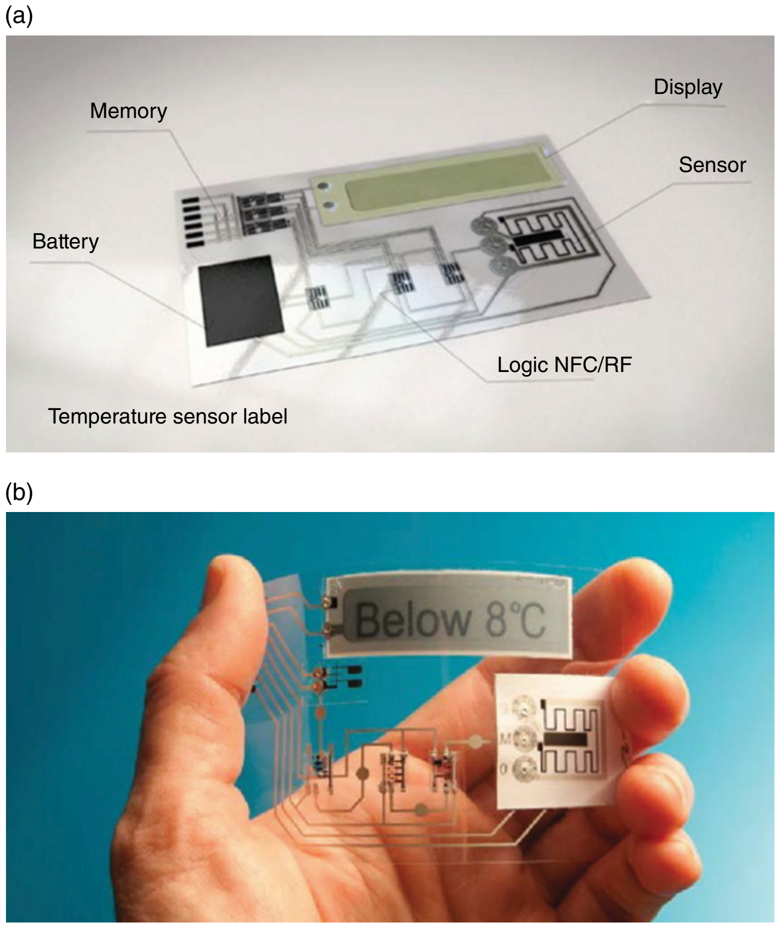

Figure 9.14 (a) Integration of various printed components for a temperature sensor tag, (b) a flexible and printed sensor tag. (Courtesy of Thin Film Electronics ASA)

highly competitive market. Other types of smart sensor systems, however, may be suitable for printing. A recent development by Thin-Film Electronics has shown some promises in that regard. The company, which previously developed printable thin-film memories and acquired Kovio in 2013, is now able to offer all-printed smart temperature sensor tags that integrates printed transistors for a logic, printed temperature sensor strip, a printed battery patch and an electrochromatic display to form a complete flexible sensor tag, as shown in Figure 9.14.

Although it is quite difficult to have everything printed for a smart system at present, to have some parts printed would be relatively easy and the system would still retain its thin, flexible and low cost features. Following the example of the above mentioned temperature sensor tag, a Chinese company, Kunshan Printed Electronics Co. Ltd., has developed similar tags, which integrates an existing RFID tag and temperature sensor chip with a printed paper battery [40]. It has all the characteristics of a wireless temperature sensor but is self-powered, thin and flexible. Another example is shown in Figure 9.15, where printed conductive tracks are combined

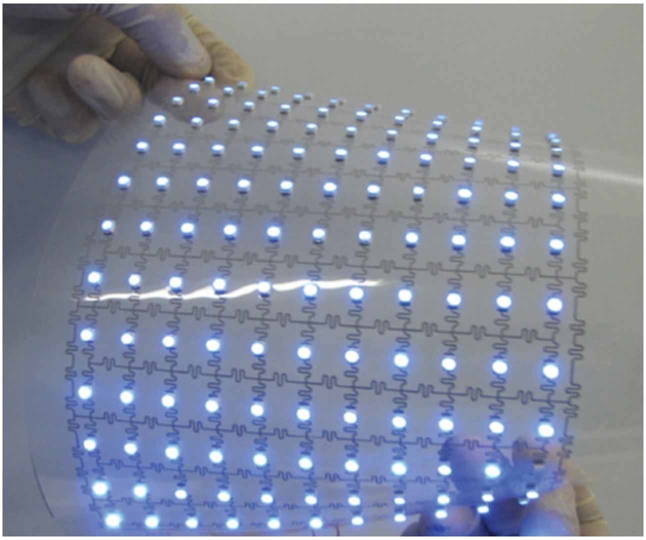

Figure 9.15 A flexible transparent LED luminary as an example of a printed electronics application

with surface mounted LEDs to form a flexible transparent luminary, made at the authors' Printable Electronics research Center [41]. Printing can provide extra freedom in the design and formation of integrated smart systems. As the roadmap shown in Figure 9.1 reveals, future smart textiles, intelligent packaging and smart labels will largely rely on printed electronics to achieve the required form factors and low cost mass manufacturing.

9.3 Challenges for Printed Electronics

Considering that organic electronics has only very limited success in the commercial world after more than two decades of research and development, printed electronics as a new field will have a long way to go before becoming a mainstream industrial technology. Although printing is a relatively mature technique, printing electronics, displays and photovoltaic still face many challenges, both scientific and technological. The newly published 6th edition of the OE-A report grouped the challenges into 4 areas: materials, processes, encapsulation and standards [1]. Based on the authors' own experience of working in various aspects of printed electronics, the following are the authors' opinions regarding the challenges that printed electronics faces in the four areas mentioned above in order to succeed in the commercial world.

9.3.1 Materials

Printable electronic materials are the foundation of printed electronics. Printable conductive materials are relatively mature. Silver has been the main conductor material for printing various electronic circuits. In recent years, nanosilver ink has enabled the sintering temperature to be lowered for printing conductive tracks on plastics and papers and has further enlarged its application scope. Other conductive materials, such as conductive polymers, carbon nanotubes and graphene, also have some success in printing conductive patterns. The main challenge is to develop low cost conductive materials such as copper and aluminum. Silver as a precious metal is not economical to make PCBs or RFID antennas. Copper and aluminum, however, are very easy to oxidize and attempts to make them into inks and printable have so far not been very successful.

Developing a high performance printable semiconductor, particularly with high charge mobility, is the biggest challenge for printed electronics. Charge mobility is a key figure-of-merit for a field-effect transistor and determines how fast a transistor can switch. Table 9.1 indicates the basic requirements for a transistor if it is to be used to drive display pixels in a backplane. For high end applications, the higher the better as far as charge mobility is concerned. For comparison, the current backplane transistors for flat panel display are based on amorphous silicon and polycrystalline silicon which have mobility of 1 and >100 cm^2/Vs, respectively.

Printing transistors has been the dream of researchers ever since the development of organic electronics started decades ago. A huge number of scientific research papers on organic semiconductors has been published and 726 organic compounds have been investigated and tested. Among them 55 were found to have charge mobility >1cm^2/Vs [42]. However, most of the organic semiconductors rely on vacuum evaporation to make transistors. Printable organic semiconductors are few and far between, and so far they only have commercial success in backplanes for e-paper display. In the last 5 years has seen the rise of inorganic printable semiconductors, including nanocrystal silicon, carbon nanotubes and transparent oxides. These inorganic nanomaterials are inherently of high charge mobility (>10cm^2/Vs) and the issues regarding these are mainly how to make these materials into ink forms and printable.

The major issue for organic semiconductors is their susceptibility to ambient oxygen and water molecules. Their charge transport property degrades rapidly as soon as they contact with oxygen and water molecules. Either the materials are improved to be more environmentally stable or good encapsulation is used, which will be discussed later. Research on new, stable organic semiconductors has made good progress in recent years, mostly in organic small molecular materials. Inorganic semiconductors do not have this problem. They have other issues regarding stability, mostly due to defects in the printed layers. When a transistor is working under applied voltage, the internal electric field can induce migration of material atoms or mechanical stress, causing gradual change of surface or interface electric characteristics.

Uniformity is another issue for solution-processed semiconductor materials. For organic semiconductors, only polymeric materials can achieve good uniformity when either spin coated or printed. Some organic small molecular materials can be in solution form and coated or printed. They do, however, tend to crystallize as soon as dried, forming preferential charge transport paths and resulting in non-uniform electric characteristics. Such property can be used to optimize an individual transistor. However, for a large array of transistors it becomes extremely difficult to control every transistor to have the same crystalline orientation. Inorganic nanomaterials also

Table 9.1 Minimum requirements on backplane transistors for different display devices

Display types	Mobility (uniformity)	On/off ratio	Working voltage
e-paper	0.05 cm^2/Vs (<30%)	10^5	+/− 30V
Passive matrix display	0.5 cm^2/Vs (<30%)	10^5	+/− 30V, +5V ~ −15V (LCD)
Active matrix display	5 cm^2/Vs (<3%)	10^6	+/− 10V

have the uniformity issue. As they are dispersed in solution, individual nanotubes or nanowires are in total random distribution in an ink. Such randomness remains when they are printed to form part of a device. This randomness may cause non-uniform electric characteristics of each device.

To print a transistor, there must be a layer of dielectric material to insulate the gate electrode. Unlike evaporation or sputtering deposition, printing normally cannot form a very thin film (<100 nm). For a thick layer of dielectrics, its dielectric constant must be high in order to have the same capacitance as a thin layer material. Those high dielectric materials such as $BaTiO_3$ nanoparticles are difficult to make into printable inks and difficult to form a pinhole-free film by printing. Some work has been done to mix $BaTiO_3$ nanoparticles with polymeric materials. Although the printability is improved, the dielectric constant is substantially reduced [43]. Therefore, the hybrid approach is commonly used when printing transistors, in which only semiconductor and electrodes are printed and the dielectric layer is usually formed by thermal or chemical vapor deposition or atomic layer deposition.

9.3.2 Printing Process and Equipment

Conventional printing is a well established process. Printing for electronics is different. Integrated circuits (IC) have set the standard for electronics. Printed electronics can never match up to that standard. State-of-the-art ICs have a minimum circuit dimension below 20 nm. So far, conventional printing can hardly go down to a micrometer. In the last few years, printing technology and equipment have progressed greatly in order to meet the requirements of printing transistors. Conventional inkjet printing normally has a resolution of 20–50 μm. The newly developed electrohydrodynamic (EHD) inkjet can print lines a micron wide. Gravure printing can now achieve resolution of below 10 μm. Even screen printing, which is normally above 100 μm, can now routinely print 30–50 μm lines. The challenge is to print even smaller features.

Apart from resolution, electronics such as transistors require multilayer printing. The challenge is how to accurately align each printed pattern. For inkjet printing, the alignment is relatively easy as movement in a work stage can be controlled with great accuracy. Most inkjet printers can achieve registration accuracy of 1 μm. The alignment or overlay of roll-to-roll (R2R) printing is much more difficult as it is a dynamic process. The best overlay accuracy for R2R printing is around 10 μm. For high speed R2R printing, inline electrical checkup is also a challenge. Without such inline checkup, process control and high yield are simply not possible.

Conventional printing is only concerned with visual effects. In printed electronics the electrical property of a printed device is the ultimate criteria, which is related to not only printing but also ink material, printing equipment, substrate and post processes. They are all correlated and need total optimization to achieve the best results: the printing equipment must be tailored to accommodate a particular ink material, or vice versa; the substrate has to be compatible to printed ink, printing equipment and post-printing sintering conditions, or vice versa.

9.3.3 Encapsulation

The largest applications of printed electronics will be in the areas of flexible display and thin-film solar cells. Unfortunately, both rely on organic materials, which as mentioned above are susceptible to oxygen and water molecules. If they are made on flexible plastic substrates, tight encapsulation of the printed layer is absolutely necessary. There are various solutions to tackle this problem. For example, different structures of barrier film have been developed, as described in Chapter 8. The process for making these barrier films is quite complicated. The main challenge in this area is to produce low cost and high throughput barrier films for encapsulation. On the other hand, the requirement for a barrier will be relaxed if more environmentally stable organic materials can be developed. That is why inorganic nanomaterials are preferred in printed electronics, because they do not have the environmental stability issue.

9.3.4 Design Methodology and Standardization

Printed electronics, although based on transistors, is different from traditional electronics where standard design tools are readily available to design functional circuits, because all the transistors in the circuits are made by a mature IC manufacturing technology with known characteristics. Printed transistors are different. There are no standard manufacturing processes. The uniformity is poor. There are only p-type transistors for one semiconductor material and n-type transistors for others. For example, organic semiconductor materials are best for p-type transistors. Semiconducting carbon nanotubes are also suitable for p-type transistors. Transparent oxide semiconductor materials, such as indium-gallium-zinc-oxide (IGZO), are only for n-type transistors. Although research works have demonstrated that it is possible to make other type transistors from these materials, the other type transistors are usually much poorer in performance. With single type of transistor, the conventional CMOS circuitry becomes impossible. One has to come up with different methodology to design the circuitry with all p-type or all n-type transistors.

Printed transistors are much larger than the transistors in an IC chip. The uniformity of electrical characteristics for printed transistors is also far poorer than the transistors in an IC chip. Therefore, it is advisable not to use a large number of transistors in a printed electronic system. With fewer transistors, the system function will be limited. For example, a HF (13,56 MHz) RFID should have at least 72000 transistors according to ISO18000EPC standard. It is easy to cram 72000 transistors in a grain sized IC chip, but impossible to print such a large number of transistors within a RFID tag that is only the size of a credit card. The maximum number of transistors that can be printed within this area by the current printing process is about 1000. So the printed RFID is in no way able to comply with the RFID tag standard. New standards specific to printed electronics need to be established.

Printed electronics is different from either the conventional printing industry or the conventional electronic industry. As a new industry, there are no standards available yet for printed electronics. A new standardization body, the IEC-TC119 committee, was established in 2012, with the aim of setting out standards for the industry. This is going to be a difficult task, as the industry itself is far from mature.

9.4 Summary and Outlook

It is no doubt that printed electronics is a disruptive technology. “Disruptive” meaning that it is not a continuation or extension of conventional electronics manufacturing, but a complete change in the way electronics are made. It is not an extension of media printing either, although it looks like conventional printing. Every new technology will take time to become accepted. Printed electronics shows much promise, such as low cost manufacturing of electronics in much larger sizes on flexible substrates. However, the success of this kind of printed electronic products in marketplace is not only about the technology itself but also about whether the product can meet a specific need and how it compares with existing technologies and products. In the last few years, we have seen some companies that were making printed electronic products fail. These companies tried to compete with the mature RFID tag industry and the silicon solar cell industry. Their printed electronic products were not better and cheaper; therefore, they did not sell on the market. Without profits from the market, these companies were not sustainable. We have also seen some printed electronic products that have succeeded. For example, the hybrid printed metal mesh transparent conductive films, developed by the authors' Printable Electronics Research Center, has been successfully implemented in large scale manufacturing (Figure 9.13) and entered the touch panel market with multimillion dollar sales. This particular technology is in direct competition with the mainstream ITO transparent conductive materials but has displayed better performance and lower manufacturing cost than ITO. That is what the markets expect and will embrace.

To deliver what the market needs requires considerable technological advances in printed electronics. The electronics industry has the much matured silicon microelectronics as a benchmark. They tend to compare printed electronics with silicon integrated circuits (IC) electronics. As has been described in previous chapters, printed electronics can never match the achievements of silicon microelectronics. However, the technology should strive to progress in that direction, namely to further improve charge mobility for printable semiconductors; to substantially improve power conversion efficiency of printable solar cells; to reduce as far as possible the printed feature dimensions of printing equipment, and so on. On the other hand, printed electronics should try not to compete directly with silicon microelectronics but to play its strength in large area, flexible and low cost manufacturing of electronics, to create a unique user experience in its products and to create new markets. The success of Apple's iPhone is a perfect example.

Looking into the future, printed electronics will prosper. In fact, printing as an alternative manufacturing technology will prosper not only in electronics but many other industrial sectors; for example, printing biomaterials and living cells has become popular in recent years. Printing combined with organic and inorganic electronic materials and flexible substrates will create new applications, new markets and new industries. With this great hope, we as scientists, technologists and engineers should face the challenges head on and make it happen. It is the authors' wish that this book will be of help in the process.

References

[1] Organic and Printed Electronics (Summary - OE-A Roadmap, 6th Edition). 2015.

[2] Guttowski A. HeliaFilm™ of Heliatek for BiPV. Printed Electronics Europe. 2014.

[3] Time for OPV to make headlines. OPE Journal. 2014;6:13.

[4] New development in the production of flexible thin-film solar cells. Press release, April 2011 (www.solar-consulting.de).

[5] Wang W, Su Y-W, Chang C-h. Inkjet printed chalcopyrite CIGS thin film solar cells. Solar Energy Materials and Solar Cells. 2011;95(9):2616.

[6] ZSW's thin-film solar PV cell of 20.8% efficiency sets world record. http://global.ofweek.com/news/, 10 Dec 2013.

[7] Silicon Ink Is Spot On, NREL Experiments Show. http://www.nrel.gov/news/, September 28, 2011.

[8] He X. Perovskite photovoltaics are a breath of fresh air. IDTechEX Market report, The rise of perovskite solar cells. 2015–2025, 2015.

[9] Case C. Critical Parameters Supporting the Case for Perovskite-based Solar Absorbers, in LOPEC 2015. 2015.

[10] Emerging Displays Report – Flexible Displays Technology IHS Technology, 2013.

[11] Fortunato E, Barquinha P, Martins R. Oxide Semiconductor Thin-Film Transistors: A Review of Recent Advances. Advanced Materials. 2012;24(2):2945–2986.

[12] Wager JF, Kesler DA, Presley RE. Transparent Electronics. New York: Springer, 2007.

[13] Chen Z, Wu XZ, Zhou T, et al. Printed low temperature metal oxide thin film transistors. in Proceedings of IEEE NEMES. 2014. Hawaii, USA.

[14] Sirringhaus H, Kawase T, Friend RH, Shimoda T, Inbasekaran M, Wu W, Woo EP. High-Resolution Inkjet Printing of All-Polymer Transistor Circuits. Science. 2000;290:2123–2126.

[15] Banach M. OTFT Technology: Enabling Transformational New Applications, in Printed Electronics Europe. 2014: Berlin.

[16] Chen P-Y, et al. 65-Inch Inkjet Printed Organic Light-Emitting Display Panel with High Degree of Pixel Uniformity, in Display Week. 2014;SID:396.

[17] Panasonic Develops World's Highest Efficiency White OLED for Lighting. Panasonic News (http://panasonic.co.jp/), 24 May 2013.

[18] Young, B. OLED technology and its impact on display and solid-state lighting market. In 3rd Annual China International OLED Summit Jan. 20–21, 2014. Shanghai.

[19] Bardsley JN OLED lighting: issues and challenges. in 3rd Annual China International OLED Summit Jan. 20–21, 2014. Shanghai.

[20] First-Ever OLED Christmas Tree (www.blogpcnews.com), 2008.

[21] White OLED Outlook Brightens with Efficiency Breakthrough. http://www.businesswire.com/, 2010.

[22] World first mass production of plastic substrate flexible OLED panels. Printed Electronics World (http://www.printedelectronicsworld.com/), 20 March 2014.

[23] DuPont Displays Develops Low-Cost Method of Printing OLED Panels. R&D Highlights, US Department of Energy (http://www1.eere.energy.gov/), 2013.

[24] O'Connor MC. Kovio Unveils Printed-Silicon HF RFID Chip Tag. RFID Journal, 2008. http://www.rfidjournal.com/article/view/4389.

[25] Jung M, et al. All-Printed and Roll-to-Roll-Printable 13.56-MHz-Operated 1-bit RF Tag on Plastic Foils. IEEE Transactions on Electron Devices. 2010;57(3):571–580.

[26] Xu W, et al. Sorting of large-diameter semiconducting carbon nanotube and printed flexible driving circuit for organic light emitting diode (OLED). Nanoscale. 2014;6(3):1589–1595.

[27] Wang C, et al. Selective silencing of the electrical properties of metallic single-walled carbon nanotubes by 4-nitrobenzenediazonium tetrafluoroborate. Journal of Materials Science. 2014;49:2064–2062.

[28] Zhao J, et al. Fabrication and electrical properties of all-printed carbon nanotube thin film transistors on flexible substrates. Journal of Materials Chemistry. 2012;22:20747–20753.

[29] Moyer B. Taking Sensors to a Trillion. Electronic Engineering Journal (http://www.eejournal.com/), November 4, 2013.

[30] Khan H.U, et al. In Situ, Label-Free DNA Detection Using Organic Transistor Sensors. Adv. Materials. 2010;22:4452–4456.

[31] Mannsfeld SCB, et al. Highly sensitive flexible pressure sensors with micro-structured rubber as the dielectric layer. Nature Materials. 2010;9:859–864.

[32] Zhang T, et al. Recent Progress in Carbon Nanotubes-based Gas Sensors. Nanotechnology. 2008;19:332001.

[33] Subramanian V, et al. Printed organic transistors for ultra-low-cost RFID applications. IEEE Transactions on Components & Packaging Technologies. 2005;28:742.

[34] Myny K, Van Winckel S, Steudel S. An Inductively-Coupled 64b Organic RFID Tag Operating at 13.56MHz with a Data Rate of 787b/s. in IEEE Solid-State Circuits Conference. 2008.

[35] Liana DD, Raguse B, Gooding JJ. Recent advances in paper-based sensors. Sensors. 2012;12:11505–11526.

[36] Soga T, et al. Inkjet-Printed Paper-Based Colorimetric Sensor Array for the Discrimination of Volatile Primary Amines. Anal. Chem. 2013;85(19):8973–8978.

[37] Colegrove J. ITO replacement market will grow to $4 billion by 2020. Information Display, 2013:4/13:44-45.

[38] ITO-replacement: non-ITO transparent conductor technologies, supply chain and market forecast report. May 2013, Touch Display Research Inc.

[39] Cui Z. Metal mesh for touch panels and beyond. In Printed Electronics Europe. April 2014.

[40] UHF Temperature Sensor tag. Kunshan Printed Electronics Co. Ltd. (http://www.ksfpe.com/), 2014.

[41] A printed LED luminary. Printable Electronics Research Center (http://www.perc-sinano.com/), 2014.

[42] Wang C, et al. Semiconducting π-conjugated xystems in field-effect transistors: A material odyssey of organic electronics. Chem. Rev. 2012:112:2208–2267.

[43] Wu XZ, Chen Z, Cui Z. Investigation of solution processable albumen-BaTiO3 nanocomposite and its application in high-k films. Compos Sci Technol. 2013:81(14):48–53.

Index

active layer, 33, 35, 37, 69, 90, 132, 145, 151, 156, 157, 163, 166, 172, 203, 229, 303
active-matrix organic light-emitting diode, 81, 83, 195, 254, 280, 322
aerosol jet printing, 80, 107, 111, 113, 161, 163, 172, 187
alignment, 16, 38, 115, 166, 335
ambipolar transistor, 23, 41, 146
AMOLED *see* active-matrix organic light-emitting diode
anilox cylinder, 122, 125
annealing, 2, 9, 10, 16, 36, 37, 54, 60, 66, 69, 70, 79, 88, 90, 95, 134, 135, 173, 180, 183, 204, 213, 291, 310, 320, 326
atomic layer deposition, 81, 132, 157, 168, 292, 298, 303

backplane driving circuits, 194
Barix™, 301
barrier film, 12, 292, 307, 326, 336
bottom-gate, 158
bulk heterojunction solar cells, 135

charge injection, 27, 177, 207, 255, 259, 262, 275, 289
charge mobility, 4, 5, 9, 17, 55, 184, 256, 322, 326, 334, 337
coating, 10, 21, 25, 40, 45, 47, 65, 76, 79, 86, 95, 106, 131–133, 151, 161, 170, 233, 260, 277, 282, 303, 306, 330
color rendering index, 272
compressive stress, 304–305
conjugated polymers, 24, 27, 39, 41, 48, 219, 221, 223, 227
corona treatment, 129

dark spots, 288, 308
desiccants, 296
dispersion, 10, 25, 55, 60, 72, 74, 88, 95, 120, 134, 180
doctor blading, 235
doping, 3, 24, 40, 55, 71, 80, 87, 107, 147, 153, 177, 185, 253, 259, 261, 273
drop casting, 40, 151, 164

effective mobility, 80, 149, 167
electrohydrodynamic jet printing, 107, 114, 180
electroluminescence, 253, 259, 266
electron acceptor, 24, 203, 218, 223
electron donor, 24, 203, 206, 209, 218
electron transport, 39, 41, 54, 65, 68, 74, 211, 223, 229, 232, 253, 259, 263–264, 267
embossing, 132
energy levels, 42, 210, 223, 259
exciton, 205

flexible display, 19, 280, 321, 335
flexible electronics, 10, 13, 43, 85, 316
flexible OPV, 309
flexographic printing, 115, 122, 131, 187, 277, 279
fullerene derivatives, 223, 226
fused aromatic compounds, 28

glove box, 308
graphene, 15, 18, 25, 55, 61, 72, 83, 86, 95, 158, 161, 180, 184, 217, 330
gravure offset, 12, 126, 279, 282

Printed Electronics: Materials, Technologies and Applications, First Edition. Zheng Cui, Chunshan Zhou, Song Qiu, Zheng Chen, Jian Lin, Jianwen Zhao, Changqi Ma and Wenming Su.

© 2016 Higher Education Press. All rights reserved. Published 2016 by John Wiley & Sons Singapore Pte. Ltd.

gravure plate, 118, 120, 126, 128
gravure printing, 12, 65, 72, 81, 107, 118, 121, 129, 163, 172, 187, 237, 277, 279, 329, 331, 335

highest occupied molecular orbit, 27, 31, 35, 42, 160, 177, 205, 206, 208, 210, 212, 223, 230, 232, 259, 260, 262
hole blocking, 272
hole mobility, 29, 33, 38, 43, 87, 91, 149, 156, 186
HOMO *see* highest occupied molecular orbit
hysteresis, 45, 71, 151, 156, 172, 176, 180, 197

IGZO *see* indium-gallium-zinc-oxide
indium-gallium-zinc-oxide, 66, 71, 95, 157, 166, 184, 322, 336
indium tin oxide, 8, 26, 55, 62, 67, 71, 78, 83, 129, 177, 204, 214, 216, 229, 238, 255, 260, 273, 308, 326, 330, 337
inkjet printing, 16, 26, 44, 47, 62, 81, 108, 111, 113, 161, 172, 180, 189, 195, 237, 266, 277, 320, 323, 327, 335
insulating materials, 44
inverted organic solar cells, 229
inverter, 81, 182, 190
ITO *see* indium tin oxide

lifetime, 37, 87, 205, 229, 240, 258, 262, 267, 272, 275, 280, 288, 296, 298, 308, 310, 313
light extraction, 273
logic circuits, 80, 146, 154, 172, 189, 197
lowest unoccupied molecular orbit, 27, 39, 42, 160, 177, 206, 208, 211, 219, 223, 255–256, 260, 262
low temperature polycrystalline silicon, 194, 322
LTPS *see* low temperature polycrystalline silicon
LUMO *see* lowest unoccupied molecular orbit

metal mesh, 60, 330, 331, 337
metal oxide, 15, 47, 54, 66, 68, 70, 90, 146, 157, 160, 166, 180, 182, 184, 193, 214, 230
morphology, 35, 44, 60, 107, 120, 134, 168, 173, 176, 188, 207, 212, 228, 233, 236, 292

nanocomposite, 93, 135
nanoimprint lithography, 133
nanosilver, 7, 330, 333
nanowires, 6, 15, 25, 54, 64, 66, 78, 95, 160, 165, 194–195, 330, 335
n-type, 146, 191
nucleation, 58, 72

OE-A, 6
OFETs *see* organic field-effect transistors
offset printing, 107, 125, 126, 279
OLED *see* organic light-emitting diode
on/off ratio, 27, 34, 37, 41, 45, 80, 156, 160, 164, 170, 175, 178, 181, 195, 334
OPVs *see* organic photovoltaics
organic field-effect transistors, 3, 18, 28, 33, 36, 38, 41, 111, 159
organic light-emitting diode, 4, 6, 62, 81, 194–195, 256, 258, 261, 264, 267, 275–276, 280, 288, 321, 324
  lighting, 252, 264, 275, 280, 296, 324
organic photovoltaics, 4, 9, 19, 21, 203, 217, 259, 287, 290, 296, 298, 306, 309, 312, 317
organic small molecule, 10, 27, 34, 48, 187, 188, 266
organic thin film transistors, 21, 37, 40, 44, 47, 145, 148, 160, 176, 187, 290, 298, 322
organosiloxane, 307
OTFT *see* organic thin film transistors

packaging, 49, 287, 297, 316, 333
pad printing, 127
parylene, 41, 299, 303, 308–309, 313
passive matrix OLED, 254
PCBM, 42, 47, 135, 216, 222, 230, 232, 236, 298
PCBs *see* printed circuit boards
PCE *see* power conversion efficiency
PECVD *see* plasma-enhanced chemical vapor deposition
perovskite solar cells, 239, 320
phosphorescence, 256, 265, 300
photolithography, 2, 8, 160, 273, 308, 329
P3HT, 35, 37, 39, 47, 110, 135, 151, 204, 209, 216, 219, 223, 226, 231, 236, 289, 298
planar heterojunction solar cells, 207
plasma-enhanced chemical vapor deposition, 292, 298, 301–302, 306, 310, 313
post processing, 10, 60, 107, 176, 322
power conversion efficiency, 216
printable OLEDs, 267, 282
printed circuit boards, 13, 329, 334
p-type, 146, 191

quantum dot, 55, 90

radio frequency identification, 7, 9, 13, 21, 28, 81, 87, 125, 128, 163, 326, 328, 331, 336
RFID *see* radio frequency identification
ring oscillator, 71, 81, 182, 187, 190, 193
roll-to-roll, 2, 16, 21, 81, 85, 95, 107, 119, 125, 135, 163, 172, 193, 214, 232, 237, 266, 276, 279–280, 307, 317, 331

screen printing, 13, 107, 116, 129, 187, 235, 278–279, 335
sheet resistance, 61, 65, 72, 79, 83, 86, 215, 217, 238, 261, 330
sintering, 2, 7, 16, 54, 60, 63, 91, 110, 134, 202, 333

small molecules, 10, 22, 27, 34, 42, 223, 253, 266–267, 282
solution-process, 5
spectrum response, 209
spin coating, 26, 40, 45, 47, 65, 79, 95, 131, 151, 161, 170, 180, 187, 203, 215, 233, 235, 253, 262, 271, 277
spray coating, 65, 79, 151, 161, 237
SS *see* subthreshold swing
subthreshold swing, 155, 172
surfactant, 10, 26, 54, 56, 61, 74, 85, 93, 95, 121, 160, 173, 179

tandem organic solar cells, 229, 231
tandem structure, 271–272
tensile stress, 304–306
TFT *see* thin-film transistor
thin film encapsulation, 287, 292, 296–307
thin-film transistor, 55, 66, 68, 70, 79, 81, 87, 92, 95, 148, 149, 157, 159, 163, 167, 172, 178, 181, 187, 196, 322
threshold voltage, 38, 44, 147, 149, 153, 167, 253
top-gate, 158, 196
touch panel, 8, 55, 65, 86, 214, 330, 337
transconductance, 79, 157
transparent conductive film, 8, 25, 55, 60, 64, 67, 73, 78, 111, 217, 318, 329, 331, 337
transparent conductive oxide, 55, 69, 71, 83, 214
transparent electrode, 25, 216
transparent oxide semiconductor, 18, 55, 66, 71, 260, 334

ultraviolet curing, 134

vacuum deposition, 6, 29, 44, 68, 71, 239, 260, 277, 280, 313, 317, 319, 323

water vapor transition rate, 287
work function, 34, 39, 40, 42, 55, 62, 81, 110, 129, 134, 153, 160, 177, 214, 229, 239, 255, 259–260
WVTR *see* water vapor transition rate

WILEY END USER LICENSE AGREEMENT

Go to www.wiley.com/go/eula to access Wiley's ebook EULA.